Heung Sik Kang
Sung Hwan Hong
Ja-Young Choi
Hye Jin Yoo

Oncologic Imaging
Soft Tissue Tumors

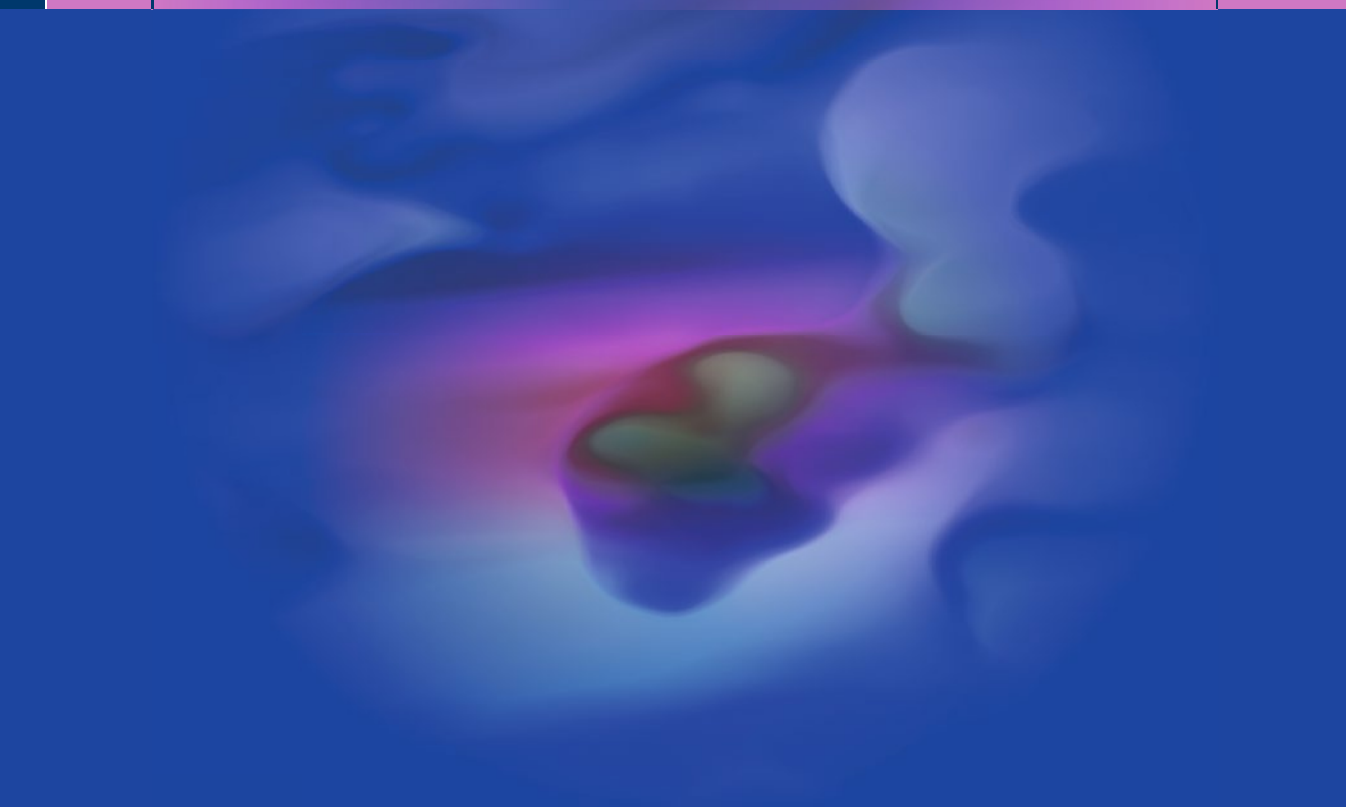

Springer

Oncologic Imaging: Soft Tissue Tumors

Heung Sik Kang • Sung Hwan Hong
Ja-Young Choi • Hye Jin Yoo

Oncologic Imaging: Soft Tissue Tumors

Springer

Heung Sik Kang, MD
Department of Radiology
Seoul National University College of Medicine
Seoul National University Bundang Hospital
Seongnam
Korea, Republic of (South Korea)

Ja-Young Choi, MD
Department of Radiology
Seoul National University Hospital
Seoul
Korea, Republic of (South Korea)

Sung Hwan Hong, MD
Department of Radiology
Seoul National University College of Medicine
Seoul National University Hospital
Seoul
Korea, Republic of (South Korea)

Hye Jin Yoo, MD
Department of Radiology
Seoul National University Hospital
Seoul
Korea, Republic of (South Korea)

ISBN 978-981-287-717-8 ISBN 978-981-287-718-5 (eBook)
DOI 10.1007/978-981-287-718-5

Library of Congress Control Number: 2017940416

Printed on acid-free paper

This Springer imprint is published by Springer Nature
The registered company is Springer Nature Singapore Pte Ltd.
The registered company address is: 152 Beach Road, #21-01/04 Gateway East, Singapore 189721, Singapore

To my coauthors, Sung Hwan Hong, Ja-Young Choi, and Hye Jin Yoo, for their passion, excellence, and cooperation.

And to my three lovely grandsons, wishing them a bright and prosperous future.

—Heung Sik Kang, MD

To all the teachers and colleagues who have brought me to this point.

And to my sweet wife, Yun Kyung, and daughter, Jisu, my buttress and love.

—Sung Hwan Hong, MD

To my colleagues and family.

And finally to my mentor, Professor Kang, for his new start.

—Ja-Young Choi, MD

To my colleagues without whom I would not be here.

To my family for their endless support.

And to my cute daughter, whose smile warms my heart with love.

—Hye Jin Yoo, MD

Preface

Diagnostic imaging of soft tissue tumors remains a challenge in musculoskeletal radiology. The difficulty can be attributed to the diversity of soft tissue tumors and the significant overlap in their imaging features. Moreover, confusion persists in the literature regarding the terminology of soft tissue tumors because their taxonomy has evolved over time.

Since the discovery of X-ray, radiologic examination has been widely used to assess bone tumors, whereas soft tissue tumor evaluation was not broadly possible until the introduction of magnetic resonance imaging (MRI) in the early 1980s. Since then, remarkable progress has been made in the imaging of soft tissue tumors. Today, MRI is indispensable in the management of patients with soft tissue tumors, and its utility continues to increase as newly developed technologies become clinically available. As a result, radiology now plays a pivotal role in the detection, diagnosis, and treatment planning of soft tissue tumors.

This book presents a wide range of radiologically illustrated soft tissue tumors classified according to the 2013 WHO classification for soft tissue tumor. Not only radiologists but also other specialists should become well versed in the imaging evaluation of soft tissue tumors, to allow a multidisciplinary approach to treatment. As a radiology textbook, this book aims to familiarize readers with both the imaging findings and pattern analysis of soft tissue tumors. We hope that it will allow readers to improve their understanding of soft tissue tumors and facilitate communication among physicians.

Seongnam, Korea, Republic of (South Korea) Heung Sik Kang
Seoul, Korea, Republic of (South Korea) Sung Hwan Hong
Seoul, Korea, Republic of (South Korea) Ja-Young Choi
Seoul, Korea, Republic of (South Korea) Hye Jin Yoo

Contents

Part III Practical Pearls in Diagnosis of Soft Tissue Tumors

Part I

General Considerations for the Diagnosis of Soft Tissue Tumors

Diagnostic Approach

1

1.1 Clinical Consideration

The vast majority of soft tissue masses that present to physicians are benign lesions. The incidence of benign soft tissue tumors is estimated to outnumber malignant tumors by a factor of at least 100 (Balach et al. 2011). Unlike their intraosseous counterparts, it is often not possible to establish a meaningful differential diagnosis for soft tissue tumors or reliably determine if they are benign or malignant. In these cases, knowledge of the soft tissue tumor's prevalence, along with the patient's age and the lesion's location, will allow a suitably ordered differential diagnosis (Kransdorf 1995). Embryonal rhabdomyosarcoma occurs most often in children under 10 years of age, while synovial sarcoma is most prevalent in adolescents and young adults. Most soft tissue sarcomas, including undifferentiated pleomorphic sarcoma, liposarcoma, and leiomyosarcoma, dominate in the elderly. The most common tumors in childhood and adolescence are, in order of prevalence, hemangioma, fibrous hamartoma, granuloma annulare, lipoblastoma, fibrosarcoma, and rhabdomyosarcoma. The most common tumors in adults are lipoma, liposarcoma, and myxofibrosarcoma (De Schepper and Bloem 2007).

Lesion locations include subcutaneous, perifascial, intramuscular, intermuscular, and intraarticular/periarticular. The lesion location is important for limiting the differential diagnosis (Walker et al. 2011a). For example, the majority of soft tissue myxomas are intramuscular, whereas myxoid liposarcomas are usually intermuscular lesions (Murphey et al. 2002). Certain tumors are known for their inherent predilections for specific locations, such as elastofibroma, which is typically found in the infrascapular or subscapular area. In a similar fashion, recognizing that a lesion arises from a specific structure (e.g., nerves, vessels, or tendons) can help in lesion characterization (Wu and Hochman 2009). A multifocal or an extensive lesion also limits diagnostic considerations to include angiomatous lesions, neurofibromatosis (NF), fibromatosis, lipomatosis, myxoma (Mazabraud syndrome), metastases, or lymphoma (Walker et al. 2011b).

Clinical history may be relevant in systemic or concomitant diseases, such as melanotic schwannoma in Carney syndrome (cardiac myxoma, spotty pigmentation, and endocrine overactivity), cavernous hemangioma in Maffucci syndrome (enchondromatosis), fibromatosis in Gardner syndrome (intestinal polyposis, osteomata), xanthoma in familial hypercholesterolemia, myxoma in Mazabraud syndrome (polyostotic fibrous dysplasia), amyloidoma in multiple myeloma and neurofibromata, and schwannomata in neurofibromatosis type II and schwannomatosis (De Schepper and Bloem 2007).

H.S. Kang et al., *Oncologic Imaging: Soft Tissue Tumors*, DOI 10.1007/978-981-287-718-5_1

1.2 Imaging Modalities

1.2.1 Radiography

Although the utility of radiographs in evaluating soft tissue lesions is rather limited, some radiographic findings help to detect or characterize soft tissue lesions. At radiography, lipoma or well-differentiated liposarcoma can be appreciated as a low-density mass. If radiography shows a soft tissue mass with multiple phleboliths, it is most likely hemangioma. A soft tissue mass with a central amorphous bone formation is suggestive of extraskeletal osteosarcoma, whereas a soft tissue lesion with peripheral shell-like mineralization is characteristic of myositis ossificans. The presence of multiple punctate or curvilinear calcifications is indicative of an extraskeletal chondroid tumor. Other examples of intratumoral mineralization include pilomatricoma, calcifying aponeurotic fibroma, gouty tophus, and synovial sarcoma. Localized cortical thickening or hyperostosis may occur adjacent to soft tissue hemangiomas or lipomas (Ly et al. 2003; Kim et al. 1999). Any tumor involvement with the adjacent bone may be better evaluated with radiography than with MR imaging. For example, long-term pressure erosion may be easily distinguished from an aggressive permeative destructive pattern on radiography, whereas it may be confusing on MR imaging (Manaster 2013).

1.2.2 Ultrasonography

Because of its safety, availability, feasibility, and cost-effectiveness, ultrasonography (US) is frequently used as the initial imaging technique in the evaluation of soft tissue masses. One of the primary roles of US is to determine whether a mass is a cyst or a solid tumor. Superficial soft tissue masses are particularly amenable to high-resolution US, which allows a detailed assessment of the distinguishing ultrasound characteristics that enable a specific tumor diagnosis based on recognized ultrasound appearances (Hung et al. 2014). Malignant tumors are usually hypoechoic and often are hypervascular, but the sonographic appearances of solid soft tissue tumors are otherwise usually nonspecific (Hwang and Panicek 2009). US is in most instances the primary imaging modality in the evaluation of soft tissue masses in children and is particularly useful in the diagnosis of vascular lesions (Navarro 2011). US is the most popular imaging modality for biopsies of soft tissue tumors. Sonographic guidance is suitable for targeting viable tissues, avoiding necrotic portions in soft issue tumors, and obviating the risk of neurovascular injury.

1.2.3 CT

Although MR imaging is preferred for evaluating soft tissue tumor imaging, there are distinguishing CT characteristics that can suggest a specific diagnosis, including the lesion's mineralization pattern, density, pattern of adjacent bone involvement, and degree and pattern of vascularity (Subhawong et al. 2010). CT remains superior to radiography and MR imaging in demonstrating soft tissue mineralization, and the mineralization pattern of soft tissue masses can be a clue for the histologic diagnosis. In myositis ossificans, for example, CT is more sensitive than MR imaging in detecting early-stage mineralization with zonal phenomenon. Lesion density can also suggest a histologic diagnosis, particularly in soft tissue masses containing fat density. CT is excellent in delineating the presence and pattern of bone involvement in soft tissue tumors, which are important factors during preoperative planning. CT has also become essential in radiation therapy, and the use of CT has resulted in greater precision in dose distribution, patient positioning, and 3D dose calculation (Pereira et al. 2014).

1.2.4 MR Imaging

MR imaging is the diagnostic modality of choice for soft tissue tumors due to the high tissue contrast and multiplanar capability. MR imaging is well suited for not only the diagnosis but also for the staging, preoperative planning, postsurgical evaluation, and post-therapy surveillance of soft tissue tumors. MR images can be particularly useful for characterizing benign lesions that do

not require imaging follow-up or biopsy, such as lipomas and ganglia. In cases where a soft tissue lesion is indeterminate based on the clinical and imaging features, a biopsy should be considered (Wu and Hochman 2009).

A combination of T1- and T2-weighted images is the mainstay of MR imaging of soft tissue tumors. Fat-suppression techniques are widely adopted to enhance the dynamic ranges and sensitivity of fast spin echo T2-weighted images and gadolinium-enhanced T1-weighted images. A T2*-weighted gradient-echo sequence is helpful in the detection of blood products, such as hemosiderin. The administration of intravenous gadolinium chelates is used to distinguish cystic from solid components to identify viable and necrotic areas, to show the relative vascularity of tumors, and to delineate the true margin of tumors.

Most soft tissue tumors are T1 isointense or hypointense and T2 hyperintense in signal intensity. The presence of T1 hyperintensity or T2 hypointensity in soft tissue tumors is occasionally found and helpful in differential diagnosis when present. An intratumoral T1 hyperintensity is suggestive of fat, subacute hemorrhage, high proteinaceous fluid, or melanin. Fat-suppression techniques are helpful to distinguish fat from the other T1-hyperintense materials. T2-hypointense substances include calcifications/ossifications, hemorrhages, vascular signal voids, or collagenous tissues. The T2-hypointense element can be a clue of some benign soft tissue tumors such as tenosynovial giant cell tumor, fibromatosis, and desmoplastic fibroblastoma. However, various soft tissue sarcomas may also have T2-hypointense components. Fluid-containing lesions exhibit very high signal intensity on T2-weighted images, which allows the specific diagnosis of cystic masses, such as ganglion or bursitis. Myxoid tumors also exhibit very high signal on T2-weighted images because of their high water content. Contrast enhancement is helpful to differentiate these bright T2-weighted signal intensity lesions. Contrast-enhanced MR images also show the vascularity of soft tissue tumors. Although malignant lesions are apt to show rapid and greater enhancement, the presence of contrast enhancement does not distinguish benign from malignant tumors.

1.3 Benign Versus Malignant

MR imaging provides clear advantages in terms of differential diagnosis of soft tissue tumors. There is, however, much controversy regarding the value of MR imaging in the differentiation of benign and malignant soft tissue tumors. MR imaging differentiation between benign and malignant tumors is complicated by the low prevalence of these lesions, the minimal experience of radiologists in non-dedicated hospitals, the ambiguous information on MR signal intensities, the highly variable histological findings, and the natural evolution of the lesions (Garcia-Gomez et al. 2004).

The definite malignant indicators are distant metastasis and adjacent organ invasion. The likelihood of malignancy also increases with the presence of tumor necrosis, neurovascular encasement, and bone invasion. The integrity of the deep fascia may also be a differential factor. The trend toward invasive behavior is greater in malignant than in benign tumors, and the destruction of the deep fascia on MR imaging can be a useful imaging finding in identifying malignant tumors (Liu et al. 2011).

Although benign tumors tend to be well delineated and some malignant tumors have ill-defined margins, several studies have concluded that the margin of a soft tissue mass on MR imaging is of no statistical relevance in predicting malignancy (De Schepper et al. 2000). In fact, most soft tissue tumors have well-defined margins regardless of whether they are benign or malignant. The administration of a contrast agent provides further information on the MR imaging characteristics of soft tissue tumors; however, it does not permit the discrimination between benign and malignant lesions when evaluated qualitatively. Dynamic contrast enhancement MR imaging can be used to differentiate malignant from benign soft tissue tumors (Tuncbilek et al. 2005).

In superficial soft tissue tumors, which are defined as masses located within the subcutaneous layer, the following various imaging features are known to be related to malignancy: lobulation, hemorrhage, necrosis, fascial edema, skin thickening, and skin contact. However, size was not found to be an important determining factor for malignancy, with a significant proportion of malignant

superficial sarcomas measuring less than 5 cm in maximal diameter (Calleja et al. 2012).

A study to assess the accuracy of MR imaging in predicting malignancy revealed that the absence of low signal intensity on T2-weighted images, a mean diameter greater than 33 mm, and a heterogeneous signal on T1-weighted images were the most sensitive indicators of malignant soft tissue tumors. MR imaging features with the highest specificity were evidence of necrosis, bone or neurovascular involvement, or metastases and a mean diameter greater than 66 mm (De Schepper et al. 1992).

A simplified systemic MR imaging approach has been proposed to help predict the benign or malignant nature of soft tissue tumors (Chung et al. 2012). The combination of the following three parameters arranged in order resulted in a higher diagnostic value for malignancy: signal intensity (heterogeneity on T2-weighted images), size (≥50 mm), and depth (deep relative to the superficial investing fascia).

1.4 Illustrations: Diagnostic Approach

1.4.1 Location of Soft Tissue Tumors

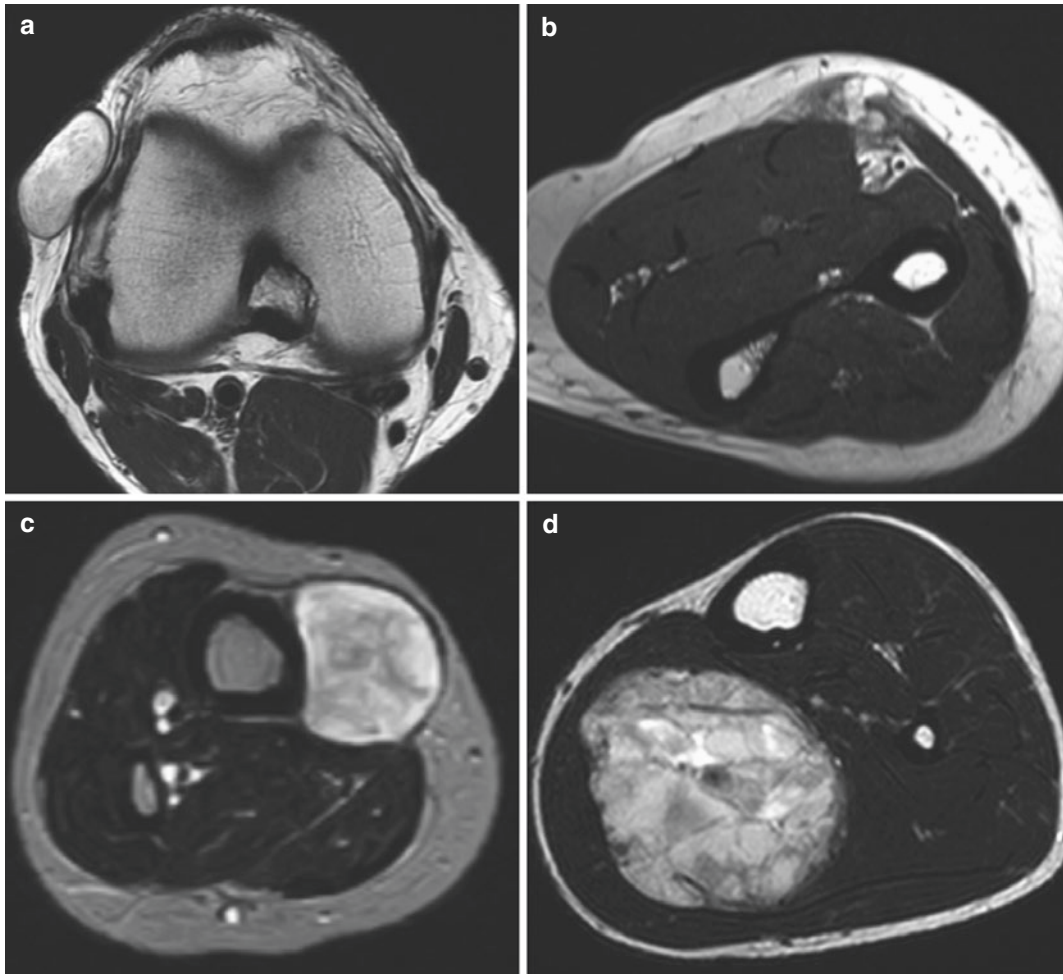

Fig. 1.1 Location of soft tissue tumors. Axial T2WIs show subcutaneous (**a**), perifascial (**b**), subfascial (**c**), and intramuscular (**d**) masses

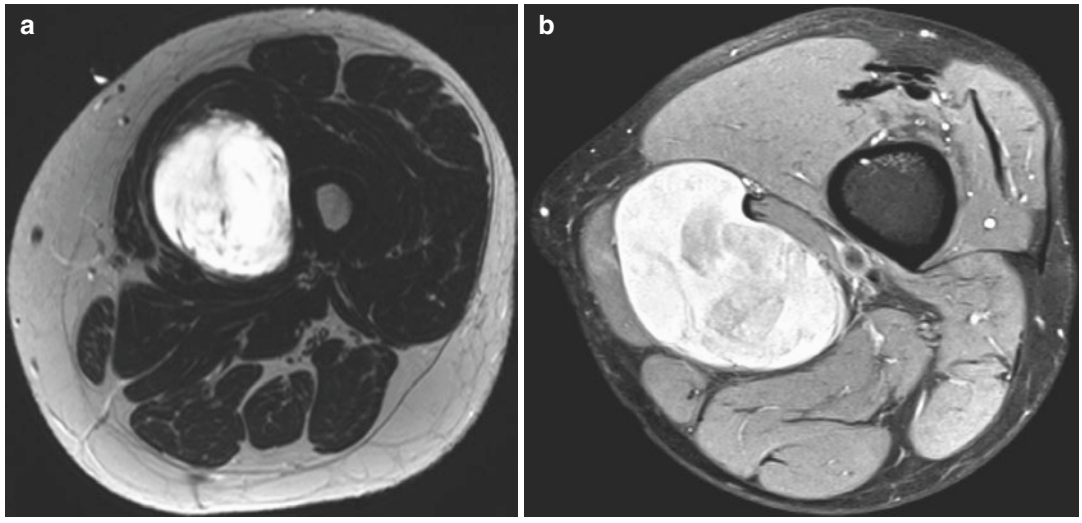

Fig. 1.2 Intra-versus intermuscular location. Axial T2WI (**a**) shows an intramuscular myxoma in the left vastus medialis. Axial FS PDWI (**b**) shows an intermuscular mass proven to be a myxoid liposarcoma in the left thigh

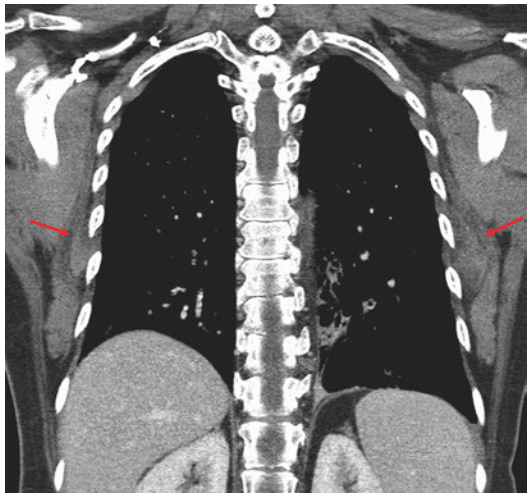

Fig. 1.3 Elastofibroma dorsi. There are bilateral symmetrical soft tissue masses (*arrows*) in the chest wall between the rib cage and serratus anterior. This tumor almost always arises in this very specific location

1.4.2 Soft Tissue Tumor in Clinical Syndrome

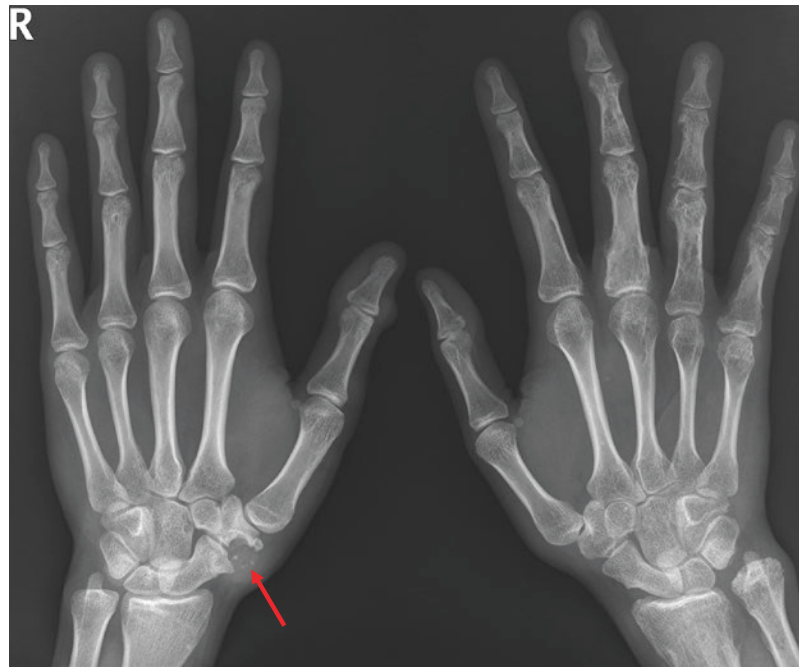

Fig. 1.4 Soft tissue hemangioma in Maffucci syndrome. AP radiograph of both hands shows multiple enchondromas in the left hand and wrist. There is a soft tissue hemangioma (*arrow*) with multiple calcific foci and adjacent bone erosions on the radial side of the right wrist

1.4.3 Radiographic Evaluation

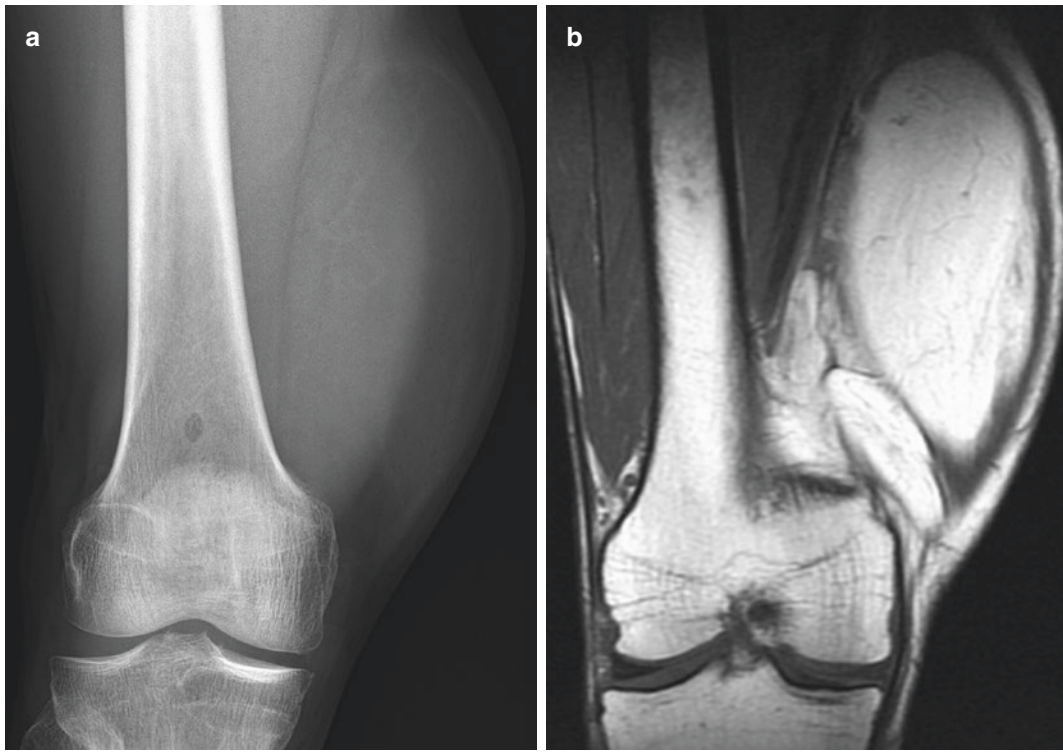

Fig. 1.5 Well-differentiated liposarcoma. AP radiograph of the right knee (**a**) shows a large soft tissue mass with low density indicating fat component. Coronal T1WI (**b**) shows a large fatty mass on the medial side of the right distal thigh

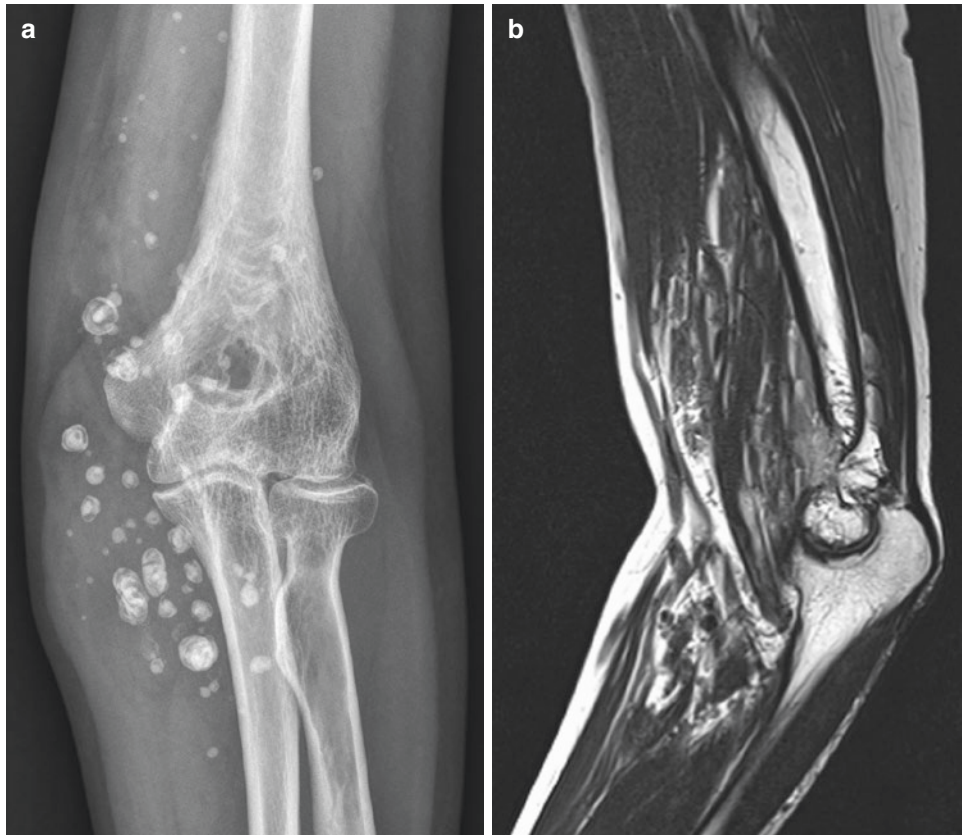

Fig. 1.6 Hemangioma. AP radiograph of the left elbow (**a**) shows a large soft tissue mass with numerous phleboliths. Sagittal T2WI (**b**) shows a complex and infiltrative soft tissue mass with multiple fluid-fluid levels on the left anterior elbow

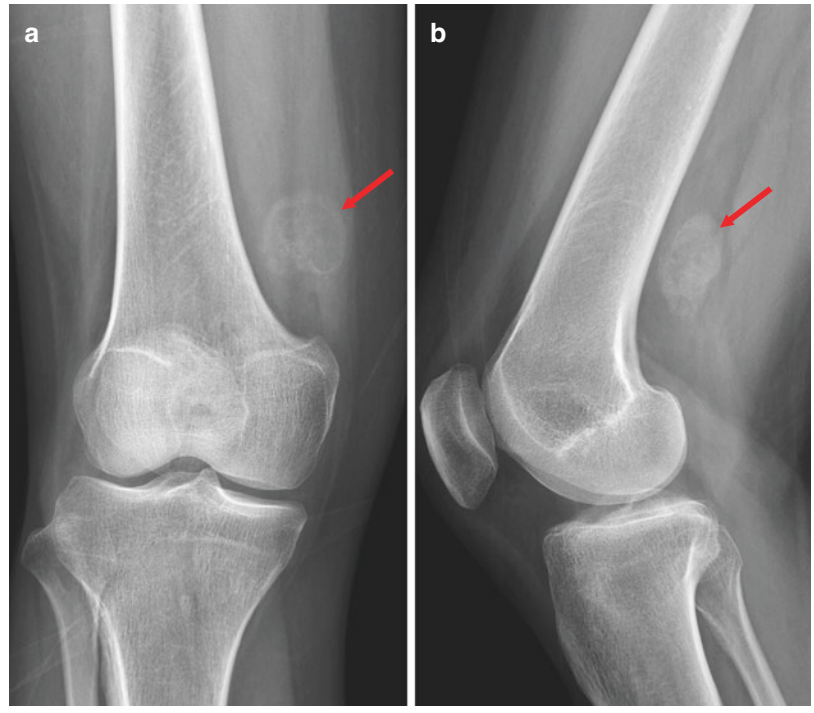

Fig. 1.7 Myositis ossificans. AP (**a**) and lateral (**b**) radiographs of the right knee show a mineralized soft tissue mass (*arrow*) on the posteromedial side of the right distal femur. The mineralization pattern is consistent with myositis ossificans, which exhibits a characteristic zonal phenomenon

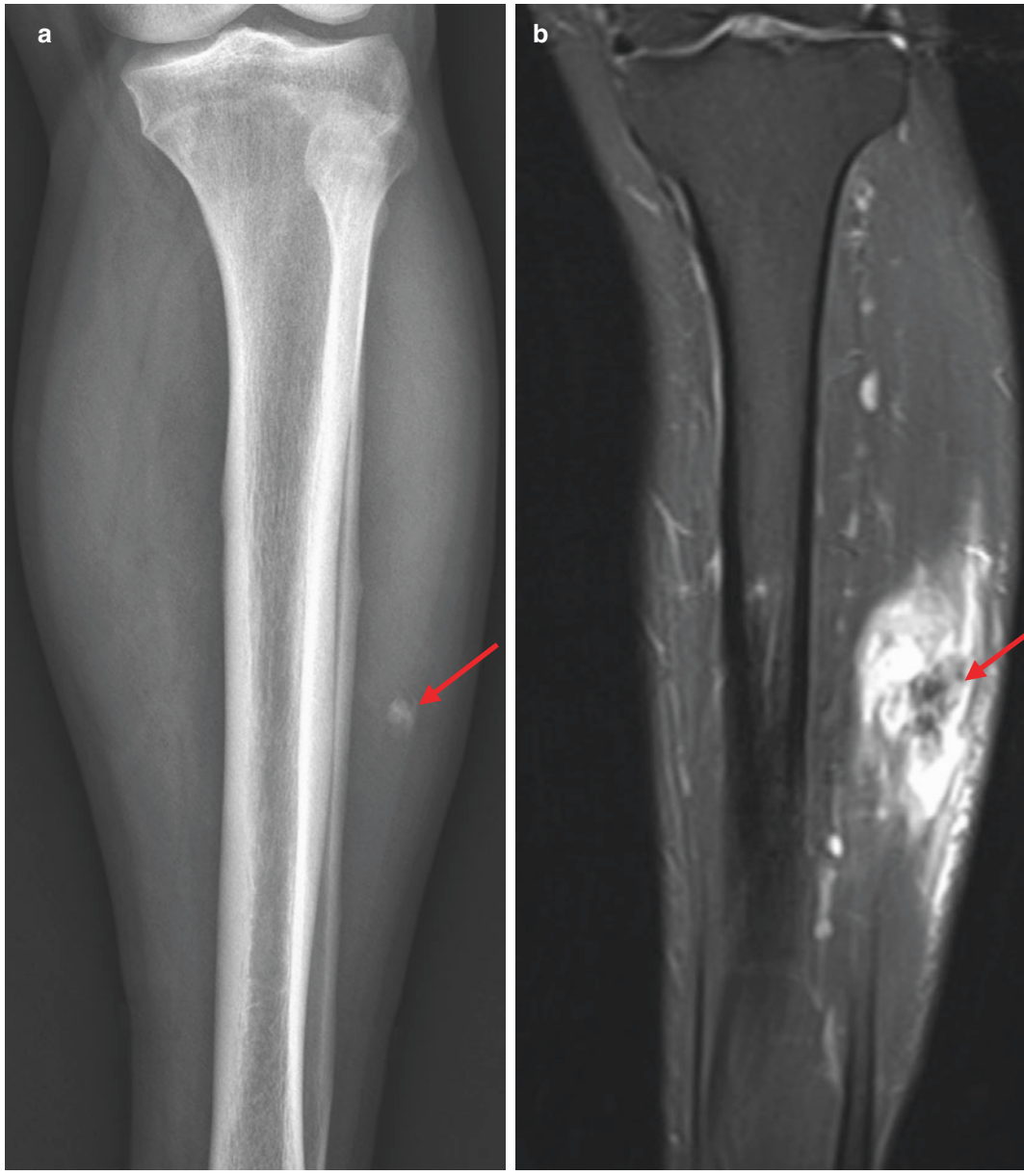

Fig. 1.8 Synovial sarcoma. AP oblique radiograph (**a**) shows a nonspecific calcification (*arrow*) on the lateral side of the left mid lower leg. Coronal postcontrast FS T1WI (**b**) shows a poorly demarcated enhancing soft tissue mass with a central low signal calcification (*arrow*), one of the well-known features of synovial sarcoma

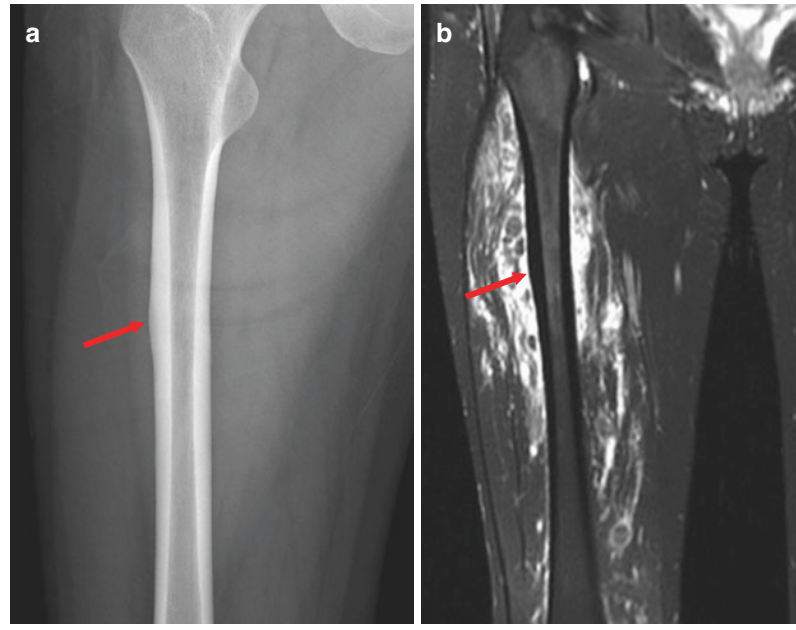

Fig. 1.9 Cortical hyperostosis adjacent to soft tissue hemangioma. AP radiograph of the right thigh (**a**) shows a segmental cortical thickening (*arrow*) on the lateral side of the right femur proximal diaphysis. Coronal FS T2WI (**b**) shows an extensive soft tissue hemangioma with cortical hyperostosis (*arrow*) in the right proximal femur

1.4.4 Sonographic Evaluation

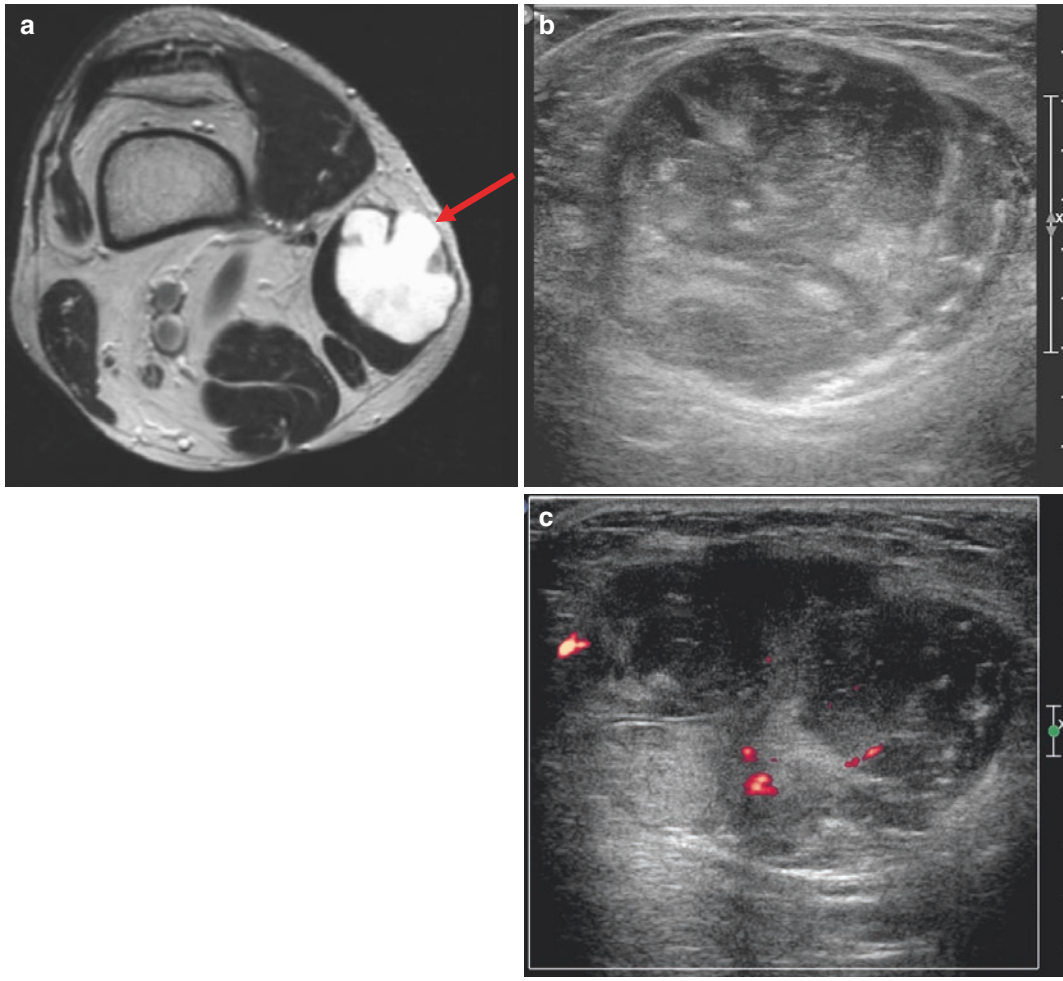

Fig. 1.10 Myxoid liposarcoma. Axial T2WI (**a**) shows a subfascial mass (*arrow*) of the right sartorius. The mass has a very high signal, which may suggest a cystic or myxoid nature. Transverse US (**b**) and power Doppler US (**c**) show complex internal echogenicity and intratumoral vascularity, indicating myxoid tissue rather than fluid content

1.4.5 CT Evaluation

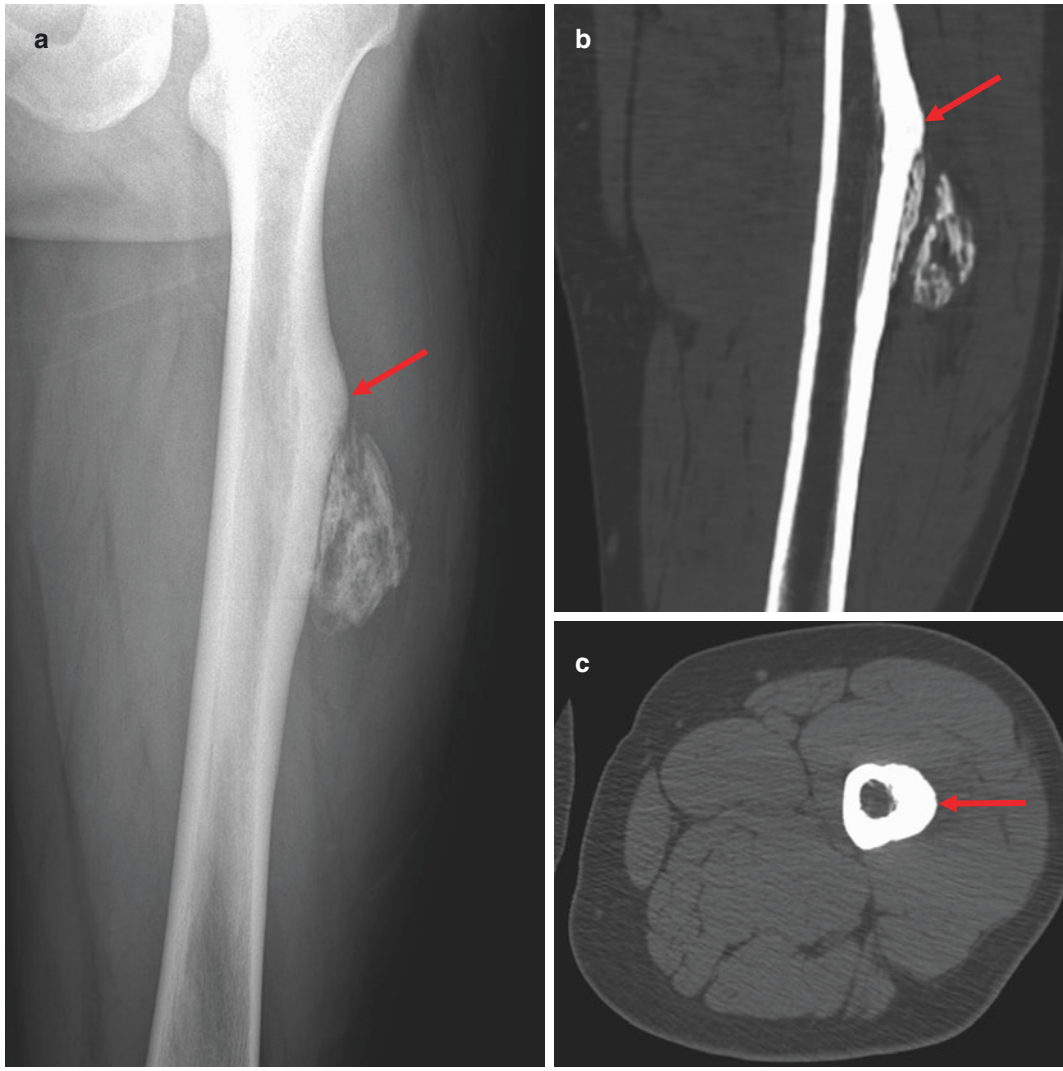

Fig. 1.11 Ossifying hemangioma. AP radiograph (**a**) shows cortical hyperostosis (*arrow*) of the left femur and a juxtacortical ossified mass. Coronal and axial CT images (**b**, **c**) clearly depict the extent of cortical change (*arrow*) and the internal architecture of the ossified mass

1.4.6 MR Imaging Evaluation

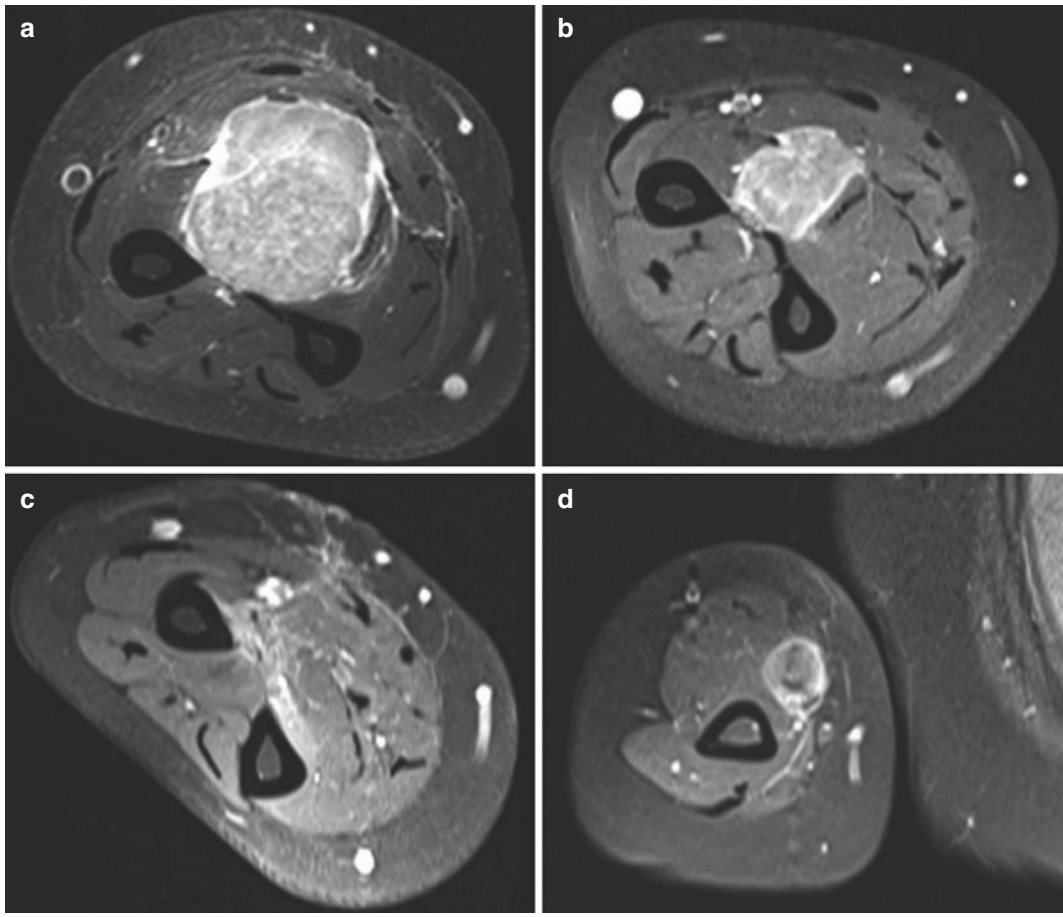

Fig. 1.12 Rhabdomyosarcoma. Axial postcontrast FS T1WI (**a**) shows a rhabdomyosarcoma in the anterior compartment of the right forearm. Axial postcontrast FS T1WI after neoadjuvant chemotherapy (**b**) shows a marked decrease in the size of the mass. Axial postcontrast FS T1WI at postoperative 3 months (**c**) shows postsurgical scar with no residual or recurred tumors. Axial postcontrast T1WI at postoperative 14 months (**d**) reveals a metastatic mass on the medial side of the right upper arm

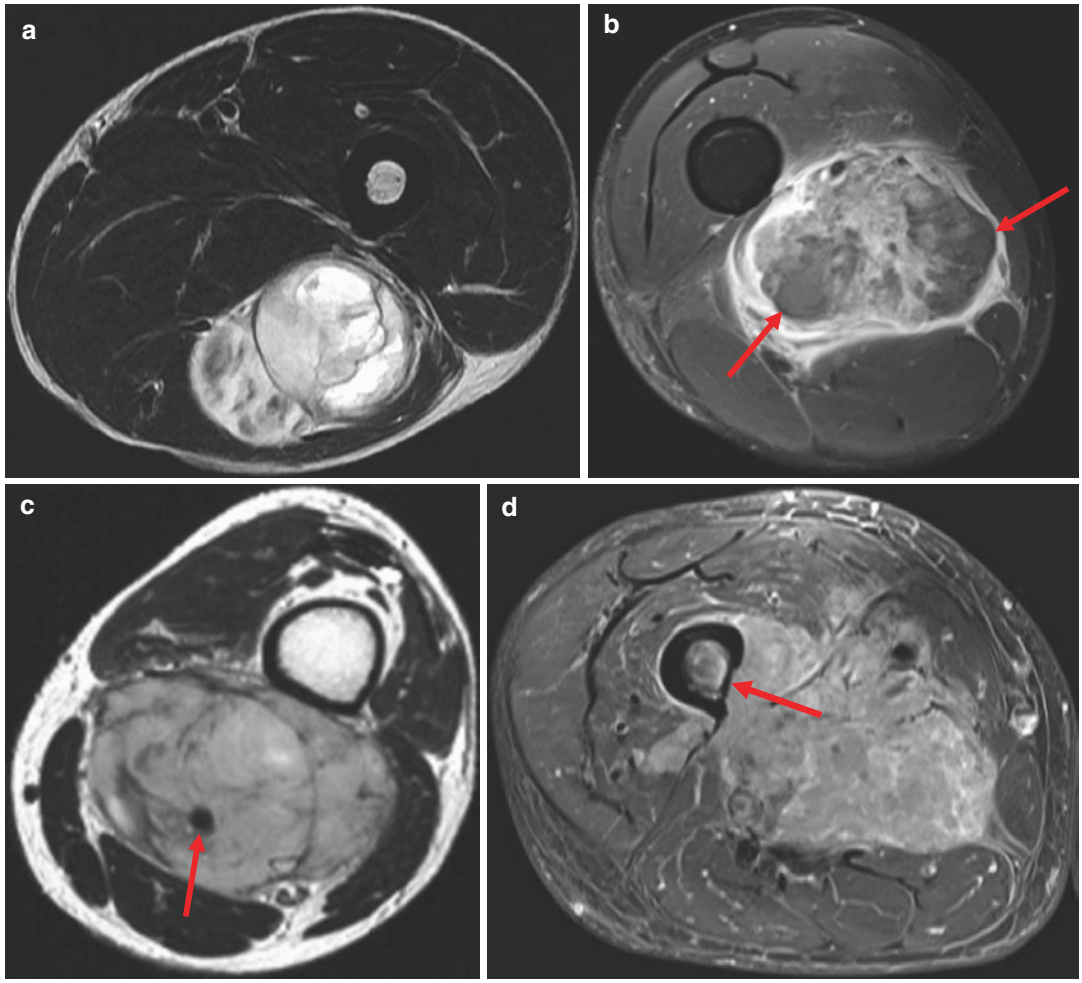

Fig. 1.13 MR predictors of malignant soft tissue tumor. Axial MR images show heterogeneity on T2WI (**a**, malignant peripheral nerve sheath tumor), necrotic changes (*arrows*) on postcontrast FS T1WI (**b**, extraskeletal Ewing sarcoma), popliteal artery encasement (*arrow*) (**c**, synovial sarcoma), and bone invasion (*arrow*) (**d**, undifferentiated pleomorphic sarcoma). All of these aggressive imaging features favor a diagnosis of malignant soft tissue tumor

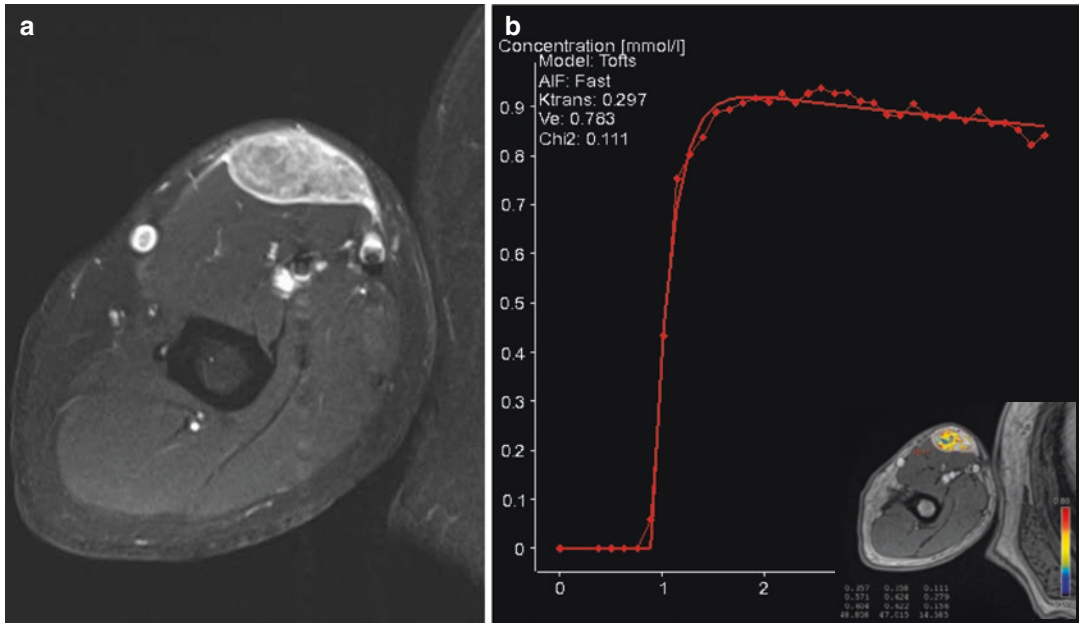

Fig. 1.14 Dynamic contrast-enhanced MRI. Axial post-contrast FS T1WI (**a**) shows a subfascial soft tissue mass with nonspecific heterogeneous enhancement in the right upper arm. Dynamic contrast-enhanced MRI (**b**) shows "rapid early enhancement followed by washout" enhancement pattern which is predictive of malignancy

References

Balach T, Stacy GS, Haydon RC. The clinical evaluation of soft tissue tumors. Radiol Clin N Am. 2011;49(6):1185–96. doi:10.1016/j.rcl.2011.07.005.

Calleja M, Dimigen M, Saifuddin A. MRI of superficial soft tissue masses: analysis of features useful in distinguishing between benign and malignant lesions. Skelet Radiol. 2012;41(12):1517–24. doi:10.1007/s00256-012-1385-6.

Chung WJ, Chung HW, Shin MJ, Lee SH, Lee MH, Lee JS, Kim MJ, Lee WK. MRI to differentiate benign from malignant soft-tissue tumours of the extremities: a simplified systematic imaging approach using depth, size and heterogeneity of signal intensity. Br J Radiol. 2012;85(1018):e831–6. doi:10.1259/bjr/27487871.

De Schepper AM, Bloem JL. Soft tissue tumors: grading, staging, and tissue-specific diagnosis. Top Magn Reson Imaging. 2007;18(6):431–44. doi:10.1097/rmr.0b013e3181652220.

De Schepper AM, De Beuckeleer L, Vandevenne J, Somville J. Magnetic resonance imaging of soft tissue tumors. Eur Radiol. 2000;10(2):213–23. doi:10.1007/s003300050037.

De Schepper AM, Ramon FA, Degryse HR. Statistical analysis of MRI parameters predicting malignancy in 141 soft tissue masses. RoFo. 1992;156(6):587–91. doi:10.1055/s-2008-1032948.

Garcia-Gomez JM, Vidal C, Marti-Bonmati L, Galant J, Sans N, Robles M, Casacuberta F. Benign/malignant classifier of soft tissue tumors using MR imaging. MAGMA. 2004;16(4):194–201. doi:10.1007/s10334-003-0023-7.

Hung EHY, Griffith JF, Hung Ng AW, Lee RKL, Lau DTY, Leung JCS. Ultrasound of musculoskeletal soft-tissue tumors superficial to the investing fascia. Am J Roentgenol. 2014;202(6):W532–40. doi:10.2214/AJR.13.11457.

Hwang S, Panicek DM. The evolution of musculoskeletal tumor imaging. Radiol Clin N Am. 2009;47(3):435–53. doi:10.1016/j.rcl.2008.12.002.

Kim JY, Jung SL, Park YH, Park SH, Kang YK. Parosteal lipoma with hyperostosis. Eur Radiol. 1999;9(9):1810–2. doi:10.1007/s003300050927.

Kransdorf MJ. Benign soft-tissue tumors in a large referral population: distribution of specific diagnoses by age, sex, and location. AJR Am J Roentgenol. 1995;164(2):395–402. doi:10.2214/ajr.164.2.7839977.

Liu L, Wu N, Ouyang H. Diagnostic value of delineating deep fascia in distinguishing between benign and malignant soft-tissue tumors in lower limbs using 3.0 T magnetic resonance imaging. J Magn Reson Imaging. 2011;33(1):173–9. doi:10.1002/jmri.22371.

Ly JQ, Sanders TG, Mulloy JP, Soares GM, Beall DP, Parsons TW, Slabaugh MA. Osseous change adjacent to soft-tissue hemangiomas of the extremities: correlation with lesion size and proximity to bone.

AJR Am J Roentgenol. 2003;180(6):1695–700. doi:10.2214/ajr.180.6.1801695.

Manaster BJ. Soft-tissue masses: optimal imaging protocol and reporting. AJR Am J Roentgenol. 2013;201(3):505–14. doi:10.2214/AJR.13.10660.

Murphey MD, McRae GA, Fanburg-Smith JC, Temple HT, Levine AM, Aboulafia AJ. Imaging of soft-tissue myxoma with emphasis on CT and MR and comparison of radiologic and pathologic findings. Radiology. 2002;225(1):215–24. doi:10.1148/radiol.2251011627.

Navarro OM. Soft tissue masses in children. Radiol Clin N Am. 2011;49(6):1235–59. doi:10.1016/j.rcl.2011.07.008.

Pereira GC, Traughber M, Muzic RF. The role of imaging in radiation therapy planning: past, present, and future. Biomed Res Int. 2014;2014:231090. doi:10.1155/2014/231090.

Subhawong TK, Fishman EK, Swart JE, Carrino JA, Attar S, Fayad LM. Soft-tissue masses and masslike conditions: what does CT add to diagnosis and management? AJR Am J Roentgenol. 2010;194(6):1559–67. doi:10.2214/AJR.09.3736.

Tuncbilek N, Karakas HM, Okten OO. Dynamic contrast enhanced MRI in the differential diagnosis of soft tissue tumors. Eur J Radiol. 2005;53(3):500–5. doi:10.1016/j.ejrad.2004.04.012.

Walker EA, Fenton ME, Salesky JS, Murphey MD. Magnetic resonance imaging of benign soft tissue neoplasms in adults. Radiol Clin N Am. 2011a;49(6):1197–217. doi:10.1016/j.rcl.2011.07.007.

Walker EA, Salesky JS, Fenton ME, Murphey MD. Magnetic resonance imaging of malignant soft tissue neoplasms in the adult. Radiol Clin N Am. 2011b;49(6):1219–34. doi:10.1016/j.rcl.2011.07.006.

Wu JS, Hochman MG. Soft-tissue tumors and tumorlike lesions: a systematic imaging approach. Radiology. 2009;253(2):297–316. doi:10.1148/radiol.2532081199.

Diagnostic Procedure 2

2.1 Anatomic Compartments

Compartmental spaces are confined anatomical areas that are separated by the fascia, interosseous ligaments, or bones (Bancroft et al. 2007). These separate compartments may act as natural barriers to tumor spread and limit the stage of a malignancy (Anderson et al. 1999; Bancroft et al. 2007). The tissues that can provide barriers include the synovium, capsule, articular cartilage of joints, cortical bone, periosteum, major fascial septa, tendinous origins, and insertions of muscles. In contrast, the fat, areolar tissue, and muscle are relatively poor barriers to tumor spread, and certain regions that are composed of these tissues are considered completely extracompartmental (Anderson et al. 1999).

2.1.1 Upper Extremity

2.1.1.1 Periscapular Region

The muscles and fasciae that cover the dorsal scapula are considered a compartment. They include the infraspinatus, teres minor, and rhomboid muscles; the supraspinatus muscle is in a separate compartment.

2.1.1.2 Upper Arm

There are two compartments in the upper arm as follows: anterior and posterior. The anterior compartment contains the biceps, brachialis, coracobrachialis, and brachioradialis muscles. The posterior compartment contains the triceps muscles.

2.1.1.3 Forearm

The forearm is divided into three compartments as follows: dorsal, volar, and mobile wad. The dorsal compartment contains the extensor muscles. The volar compartment contains the flexor muscles. The interosseous membrane separates the two compartments. The mobile wad comprises the extensor carpi radialis brevis, longus, and brachioradialis muscles.

2.1.1.4 Hand

There are multiple compact compartments in the hand and, therefore, several neurovascular bundles. For this reason, most lesions involving the hand region are considered extracompartmental.

2.1.1.5 Extracompartmental Spaces

Extracompartmental spaces of the upper extremity include the periclavicular region, axilla, antecubital fossa, wrist, and dorsum of the hand.

2.1.2 Pelvis

Individual bones or muscles in the pelvis are considered individual compartments. However, extracompartmental spread to adjacent tissues is frequently observed when pelvic lesions are large.

H.S. Kang et al., *Oncologic Imaging: Soft Tissue Tumors*, DOI 10.1007/978-981-287-718-5_2

2.1.3 Lower Extremity

2.1.3.1 Thigh

There are three compartments in the thigh as follows: anterior, posterior, and medial. The anterior compartment contains the iliotibial tract, tensor lata, rectus femoris, and vastus muscles. The vastus intermedius muscle is occasionally considered a separate fourth compartment. The posterior compartment contains the hamstring muscles (semimembranosus, semitendinosus, and biceps femoris) and the sciatic nerve. The medial compartment contains the gracilis and adductor muscles.

2.1.3.2 Lower Leg

The lower leg contains four compartments as follows: anterior, deep posterior, superficial posterior, and lateral. The anterior compartment contains the tibialis anterior, extensor digitorum longus, and extensor hallucis longus muscles, as well as the anterior tibial artery, vein, and deep peroneal nerve. The anterior compartment is separated from the deep posterior compartment by the interosseous membrane. The deep posterior compartment contains the tibialis posterior, flexor digitorum, and flexor hallucis longus muscles, with the posterior tibial and peroneal arteries and the tibial nerve. The superficial posterior compartment contains the gastrocnemius and soleus muscles and the sural nerve. The lateral compartment contains the peroneal muscles, with the common and superficial peroneal nerves.

2.1.3.3 Foot

The dorsum of the foot is considered extracompartmental. The sole of the foot is divided into three compartments as follows: medial, central, and lateral. The medial compartment contains the abductor hallucis and flexor hallucis brevis muscles. The central compartment contains the flexor digitorum brevis, quadratus plantae, lumbrical, and adductor hallucis muscles. The lateral compartment contains the abductor and short flexor muscles.

2.1.3.4 Extracompartmental Spaces

The inguinal region, femoral triangle, popliteal fossa, ankle, and dorsum of the foot are considered extracompartmental.

2.2 Imaging-Guided Percutaneous Biopsy

Percutaneous core needle biopsies of the musculoskeletal lesions are accurate and effective procedures and carry the advantages of decreased complications and cost compared with open biopsies (UyBico et al. 2012). However, there is a concern that tumor seeding and recurrence can occur along the needle track of percutaneous core needle biopsy because survival rates for patients who experience local recurrence of sarcomas are very low. If a percutaneous biopsy passes through tissues outside the planned incision plane, the orthopedic oncologic surgeon may alter the surgical plane to include the potentially contaminated tissue in the resection, which would require a wider irradiation field or increase the chance of local tumor recurrence at the biopsy site after the operation (Liu et al. 2007). A multicenter study conducted by the Musculoskeletal Tumor Society in 1996 showed that inappropriately performed biopsies of sarcomas led to unnecessary amputations in 5–8% of patients (Mankin et al. 1996). Therefore, it is strongly suggested that the biopsy of soft tissue sarcomas be performed along the plane of the planned incision for the definitive resection surgery, thereby avoiding needle penetration and contamination of uninvolved myofascial compartments (Liu et al. 2007). In general, biopsies of primary musculoskeletal sarcomas should be performed only at institutions with a multidisciplinary team, including orthopedic oncologic surgeons, and musculoskeletal radiologists and radiologists should consult with the surgeon to determine the safe biopsy route (Liu et al. 2007). An understanding of compartmental anatomy is, therefore, essential to safely biopsy suspected soft tissue sarcomas (Toomayan et al. 2005).

General principles for safe percutaneous biopsies include the following: (1) the shortest path between skin and the lesion should be chosen; (2) vital structures, such as neurovascular or joint structures, should be avoided; (3) the needle path must be in the same location where the incision for the definitive surgery will be made so that the needle path can be excised. The needle should not traverse an uninvolved compartment, joint, or neurovascular bundle; and (4) transverse surgical biopsy incisions should be avoided because further resection is required upon definitive longitudinal incision (Bancroft et al. 2007; Liu et al. 2007; UyBico et al. 2012). Several recommended needle paths for planning percutaneous needle biopsies of potential sarcomas have been proposed for specific regions. These biopsy guidelines are based on the standard surgical approaches used for limb salvage surgery of the extremities. Lesions in the upper arm should be biopsied through the anterior third of the deltoid muscle if possible. As the deltoid muscle is innervated by the axillary nerve from posterior to anterior, if the needle passes through the posterior portions of the deltoid muscle, which is then resected, the residual anterior deltoid muscle will be denervated after resection of the posterior portions of the muscle. In the pelvic region, the gluteal muscles should be preserved whenever possible because resection of these muscles will result in a poor functional outcome. In the lower extremity, the vital structures include the knee joint capsule, greater trochanteric bursa, vastus intermedius muscles, quadriceps tendon, tibial tubercle, peroneus brevis, peroneus longus distal tendons, and several neurovascular bundles. If a lesion is closely apposed to the femoral vessels, a medial approach is preferred because a medial incision facilitates vessel exploration. The hand and foot regions have such complex anatomies that it is necessary to discuss with a surgeon in planning a biopsy route (Anderson et al. 1999; UyBico et al. 2012). Knowledge of compartmental anatomy is important for optimal management of sarcomas and must be considered when planning and performing percutaneous needle biopsies. Radiologists performing needle biopsy for potential sarcomas should be aware of potential complications that can worsen the prognosis of patients and alter treatment plans (Bancroft et al. 2007).

2.3 Illustrations: Diagnostic Procedure

2.3.1 Anatomic Compartments

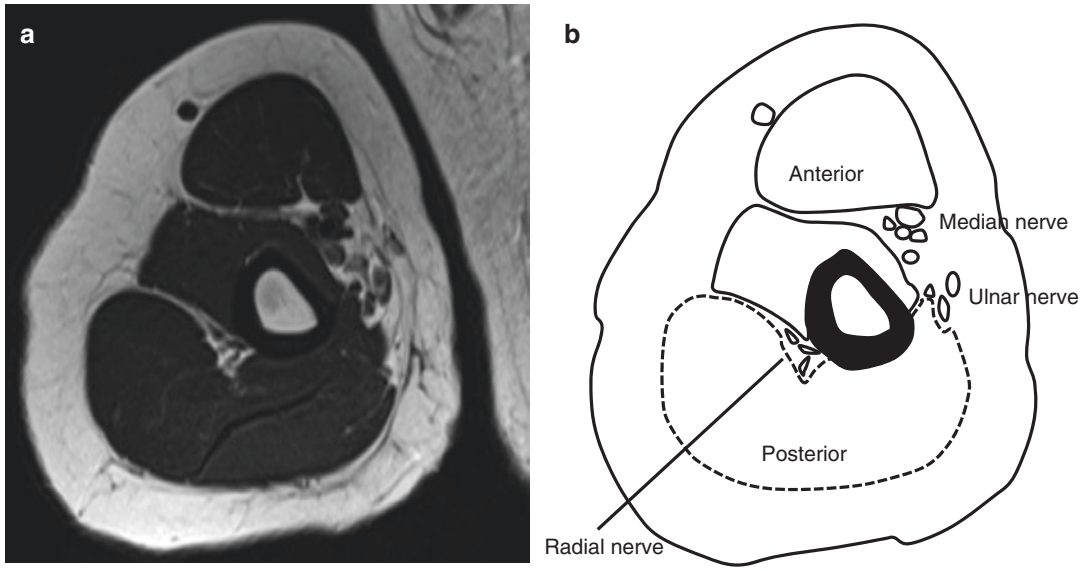

Fig. 2.1 The upper arm contains two compartments: anterior (*solid line*) and posterior (*dashed line*) in an axial T1-weighted image (**a**) and a diagrm (**b**)

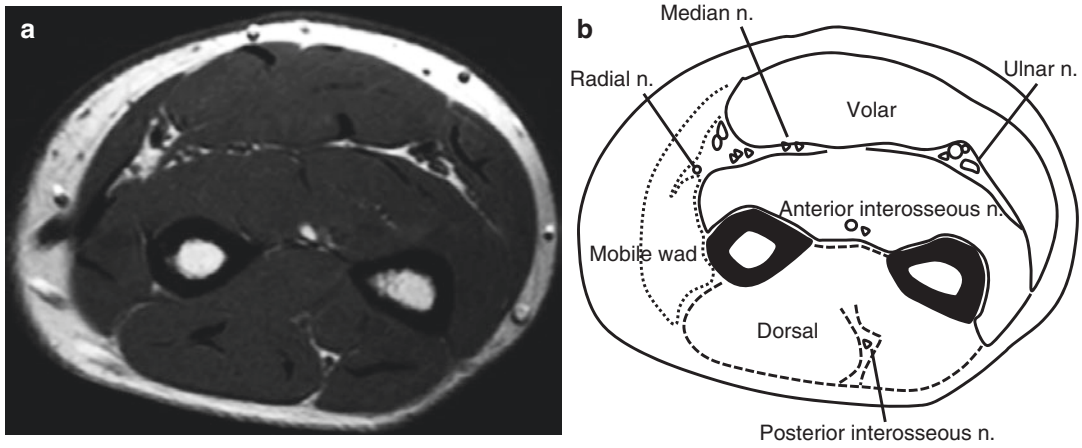

Fig. 2.2 The forearm contains three compartments: volar (*solid line*), dorsal (*dashed line*), and mobile wad (*dotted line*) in an axial T1-weighted image (**a**) and a diagrm (**b**)

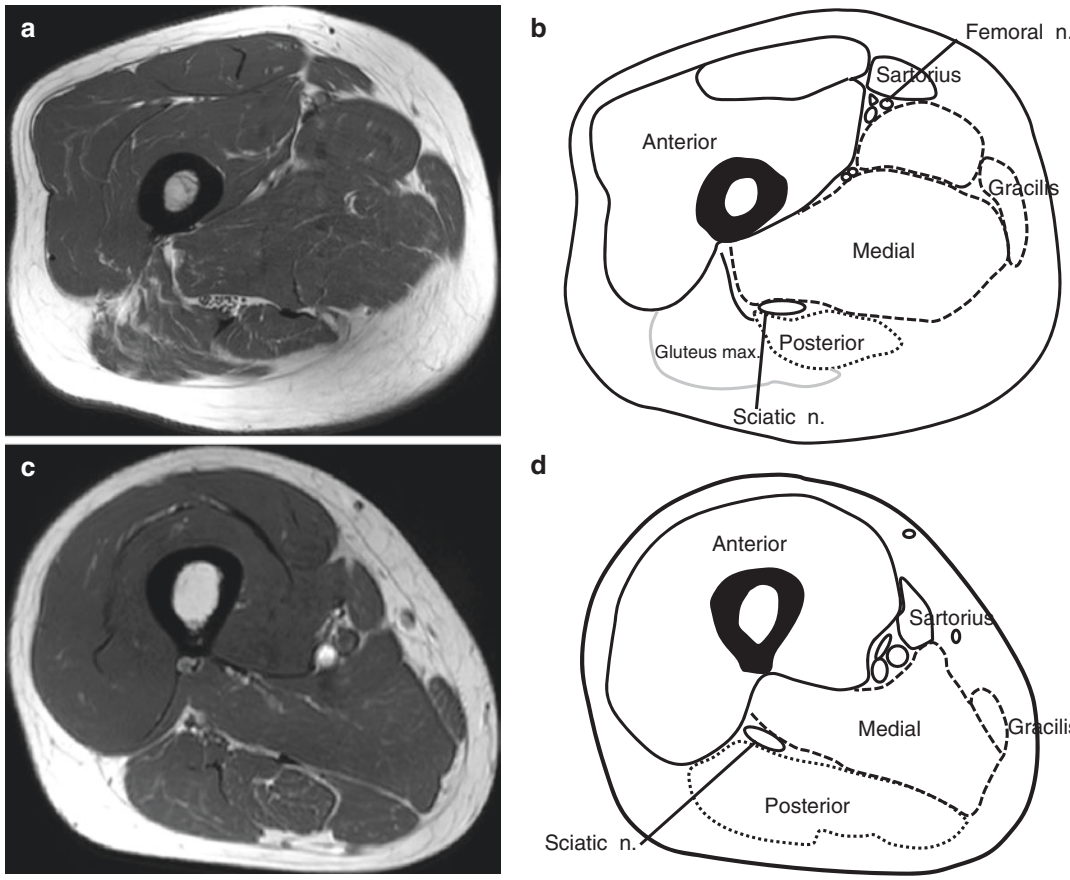

Fig. 2.3 The thigh contains three compartments: anterior (*solid line*), medial (*dashed line*), and posterior (*dotted line*) in axial T1-weighted images (**a**, **c**, **e**) and diagrams (**b**, **d**, **f**). Images were obtained at upper thigh (**a**, **b**), mid-thigh (**c**, **d**) and distal thigh (**e**, **f**) levels

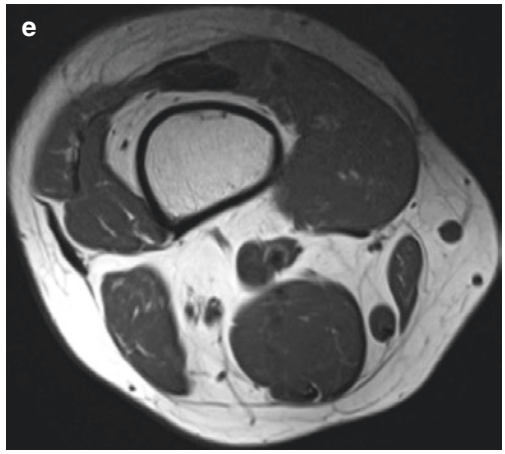

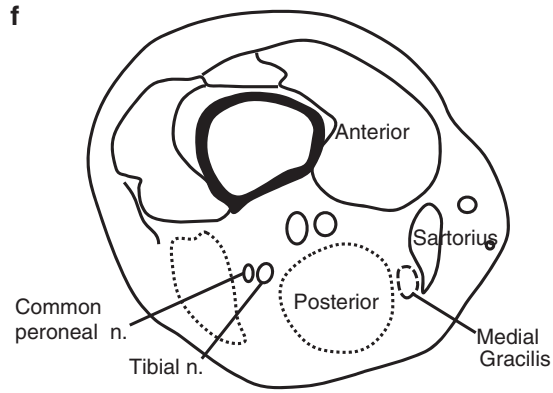

Fig. 2.3 (continued)

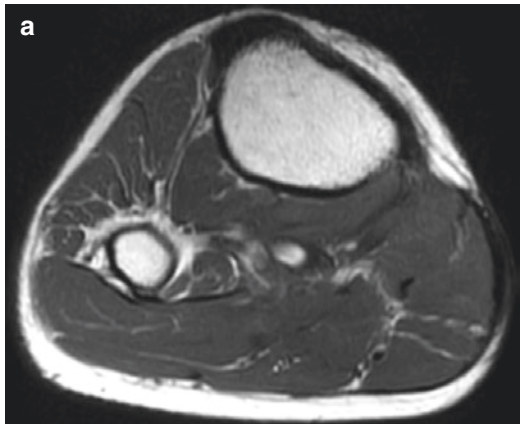

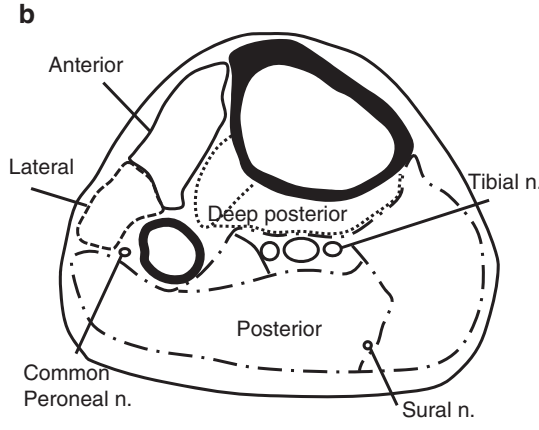

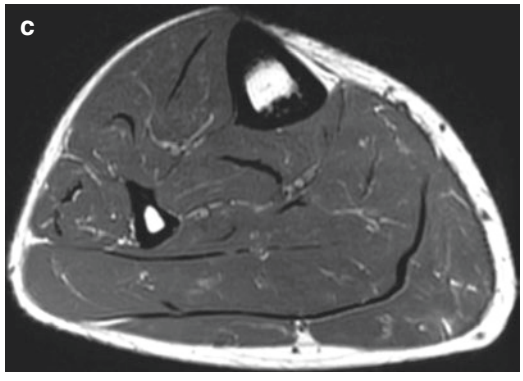

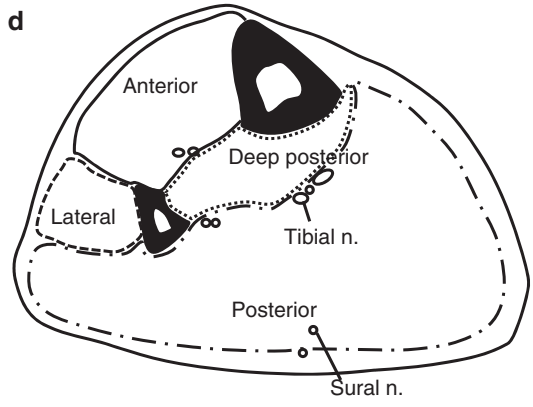

Fig. 2.4 The lower leg contains four compartments: anterior (*solid line*), lateral (*dashed line*), deep posterior (*dotted line*), and posterior (*dash-dot line*) in axial T1-weighted images (**a**, **c**) and diagrams (**b**, **d**). Images were obtained at upper lower leg (**a**, **b**) and mid-lower leg (**c**, **d**) levels

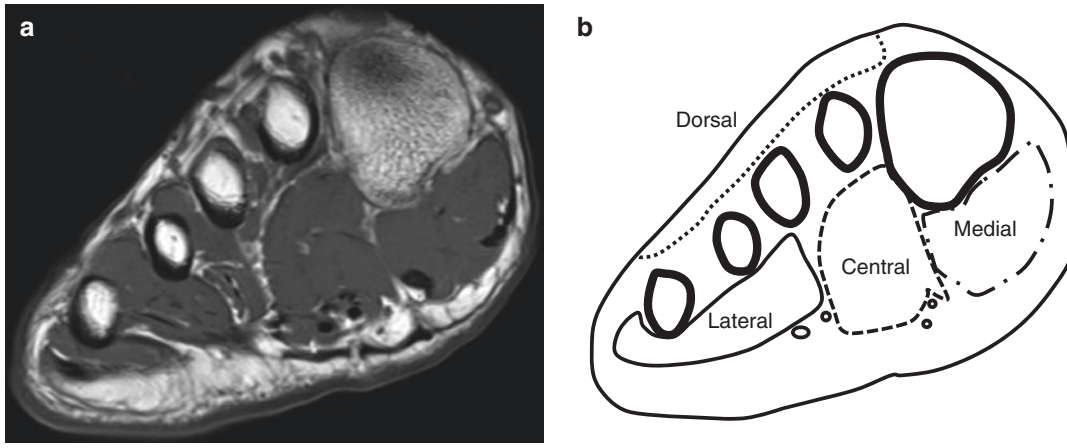

Fig. 2.5 The sole of the foot is divided into three compartments: medial (*dash-dot line*), central (*dashed*), and lateral (*solid*) in an axial T1-weighted image (**a**) and a diagram (**b**). The dorsum of the foot is considered extracompartmental

2.3.2 General Principles of Image-Guided Percutaneous Biopsy

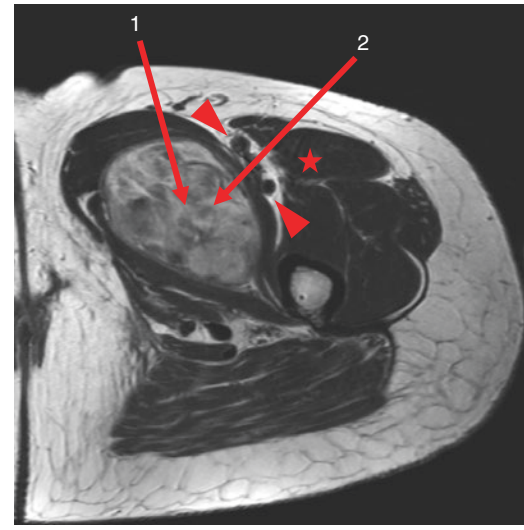

Fig. 2.6 Recommended biopsy needle path to avoid the vital structures. To biopsy the mass in the left adductor muscle, the shortest path between the skin and the lesion (path 1) should be chosen. The needle should not traverse an uninvolved compartment (*star*) or femoral neurovascular bundle (*arrowheads*) (path 2)

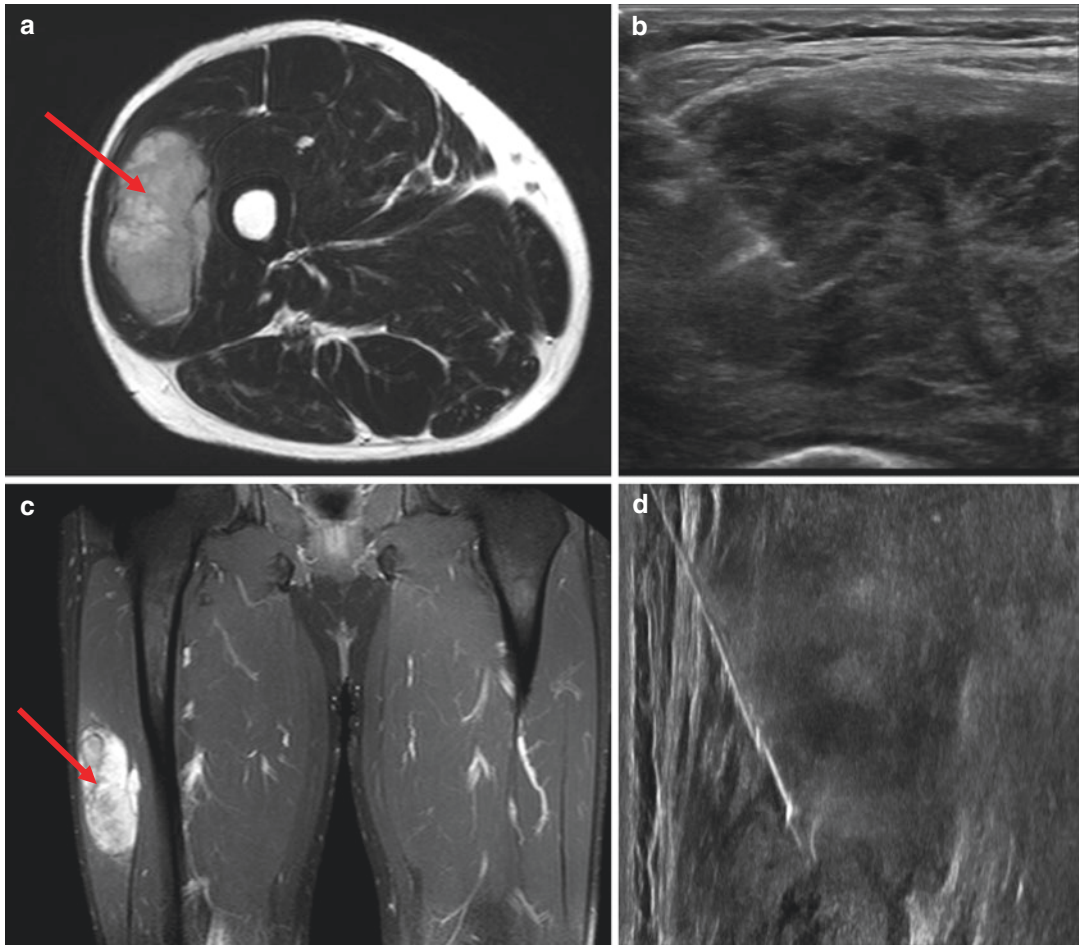

Fig. 2.7 To biopsy the mass in the right vastus lateralis muscle, transverse biopsy path (**a**, **b**) should be avoided because further resection is required upon definitive longitudinal incision (**c**, **d**)

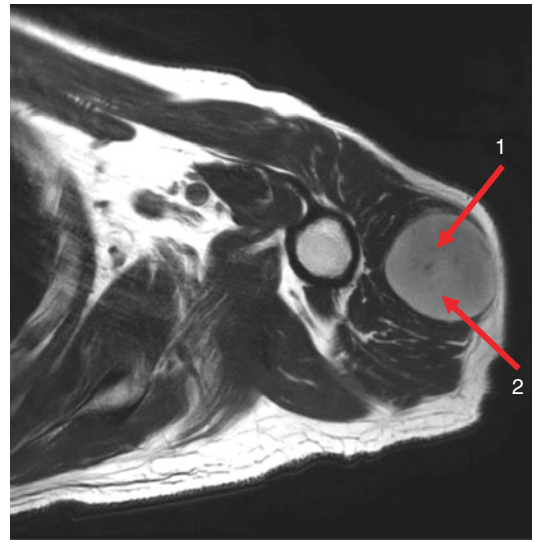

Fig. 2.8 Lesions in the upper arm should be biopsied through the anterior third of the deltoid muscle (path 1) if it is possible because the deltoid muscle is innervated by the axillary nerve from posterior to anterior

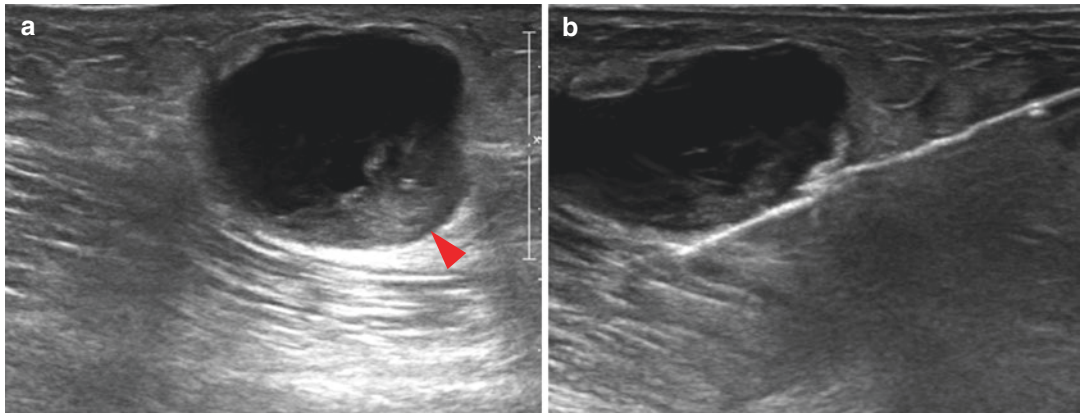

Fig. 2.9 There is a necrotic lymph node in the subcutaneous layer of the thigh (**a**). Biopsy should be performed in the solid portion (*arrowhead*) of the lymph node to obtain the sufficient tissue for histologic examination (**b**)

References

Anderson MW, Temple HT, Dussault RG, Kaplan PA. Compartmental anatomy: relevance to staging and biopsy of musculoskeletal tumors. AJR Am J Roentgenol. 1999;173(6):1663–71. doi:10.2214/ajr.173.6.10584817.

Bancroft LW, Peterson JJ, Kransdorf MJ, Berquist TH, O'Connor MI. Compartmental anatomy relevant to biopsy planning. Semin Musculoskelet Radiol. 2007;11(1):16–27. doi:10.1055/s-2007-984410.

Liu PT, Valadez SD, Chivers FS, Roberts CC, Beauchamp CP. Anatomically based guidelines for core needle biopsy of bone tumors: implications for limb-sparing surgery. Radiographics. 2007;27(1):189–205. doi:10.1148/rg.271065092.

Mankin HJ, Mankin CJ, Simon MA. The hazards of the biopsy, revisited. Members of the musculoskeletal tumor society. J Bone Joint Surg Am. 1996;78(5):656–63.

Toomayan GA, Robertson F, Major NM. Lower extremity compartmental anatomy: clinical relevance to radiologists. Skelet Radiol. 2005;34(6):307–13. doi:10.1007/s00256-005-0910-2.

UyBico SJ, Motamedi K, Omura MC, et al. Relevance of compartmental anatomic guidelines for biopsy of musculoskeletal tumors: retrospective review of 363 biopsies over a 6-year period. J Vasc Interv Radiol. 2012;23(4):511–8. doi:10.1016/j.jvir.2012.01.058.

Staging of Soft Tissue Sarcoma

3

Cancer staging is the process of determining how much cancer is in the body and where it is located. Staging describes the severity of an individual's cancer based on the magnitude of the original (primary) tumor and the extent to which the cancer has spread in the body. The stage of soft tissue sarcoma is the most significant factor in determining each patient's prognosis (the course of the disease and the chances of survival) and in selecting treatment options. Although there are several staging systems for soft tissue sarcomas, staging system of the American Joint Committee on Cancer (AJCC) has generally been considered the standard (Table 3.1) (Gibbs et al. 2016; Fisher et al. 2016; Crago and Lee 2016; Pollock and Maki 2016; Massarweh et al. 2015). Compared to the standard tumor, node, and metastasis (TNM) factors prevalent in all AJCC solid organ-staging systems, a unique characteristic of the soft tissue sarcoma system is the incorporation of histologic grade. It is applicable to all soft tissue sarcoma subtypes, except desmoid tumor/deep fibromatosis and Kaposi sarcoma. In the eighth edition, staging criteria has been specifically separate on the anatomic primary site of the soft tissue sarcoma as follows: (1) extremity and trunk, (2) retroperitoneum, (3) head and neck, and (4) visceral sites.

3.1 Tumor (T-Staging)

The number of AJCC T stages for soft tissue sarcoma of the trunk and extremities in eighth edition (2016) has been increased from two (T1, 5 cm or less in greatest dimension and T2, greater than 5 cm) to four, as follows: T1, 5 cm or less in greatest dimension; T2, more than 5 cm and less than or equal to 10 cm; T3, more than 10 cm and less than or equal to 15 cm; and T4, more than 15 cm. Some tumors, such as pleomorphic sarcoma and myxofibrosarcoma, often have tail-like projections extending for a considerable distance along fascial and neurovascular planes. Surrounding reactive edema, if present, should not be included in the measurement. In comparison to the seventh edition, superficial versus deep location has been removed as part of the T criteria in the eighth edition. For completeness, depth is evaluated relative to the investing fascia, and superficial is defined as the lack of any involvement of superficial investing muscular fascia. For staging, non-superficial head and neck, intrathoracic, intra-abdominal, retroperitoneal, and visceral lesions were considered deep lesions.

H.S. Kang et al., *Oncologic Imaging: Soft Tissue Tumors*, DOI 10.1007/978-981-287-718-5_3

Table 3.1 TNMG staging for soft tissue sarcomas of the trunk and extremities according to the AJCC staging manual[a]

Primary tumor (T)				
TX		Primary tumor cannot be assessed		
	T0	No evidence of primary tumor		
	T1	Tumor ≤5 cm in greatest dimension[a]		
	T2	5 cm < tumor ≤10 cm		
	T3	10 cm < tumor ≤15 cm		
	T4	Tumor >15 cm in greatest dimension[a]		
Regional lymph nodes (N)				
	NX	Regional lymph nodes cannot be assessed		
	N0	No regional lymph node metastasis		
	N1	Regional lymph node metastasis		
Distant metastasis (M)				
	M0	No distant metastasis		
	M1	Distant metastasis		
Histologic grade (G)				
	GX	Grade cannot be assessed		
	G1	Grade 1		
	G2	Grade 2		
	G3	Grade 3		
AJCC prognostic stage groups				
Stage IA	T1	N0	M0	G1, GX
Stage IB	T2	N0	M0	G1, GX
	T3	N0	M0	G1, GX
	T4	N0	M0	G1, GX
Stage II	T1	N0	M0	G2, G3
Stage IIIA	T2	N0	M0	G2, G3
Stage IIIB	T3	N0	M0	G2, G3
	T4	N0	M0	G2, G3
Stage IV	Any T	N1	M0	Any G
	Any T	Any N	M1	Any G

[a]Adapted from AJCC: Soft tissue sarcoma. IN: Yoon SS, Maki RG, Asare EA, et al., eds. AJCC Cancer Manual. 8th ed. New York: Springer; 2016:507–515

3.2 Nodes (N-Stage)

Regional and/or distant metastatic dissemination of soft tissue sarcomas is generally considered to occur through hematogenous and, less commonly, lymphatic spread. Several subtypes with the highest rates of lymph node metastasis are as follows: alveolar/embryonal

rhabdomyosarcoma, clear cell sarcoma, synovial sarcoma, epithelioid sarcoma, and angiosarcoma (Fong et al. 1993; Mazeron and Suit 1987).

3.3 Metastasis (M-Stage)

Metastasis from soft tissue sarcomas may occur to distant organs or present as lesions that are distant from the primary tumor contained within the same anatomic compartment. Metastatic sites for soft tissue sarcoma often depend on the original site of the primary lesion. Pulmonary metastases are the most common manifestations of distant disease for patients with extremity sarcoma, whereas the liver is the most common location for patients with retroperitoneal and gastrointestinal sarcoma (Crago and Lee 2016).

3.4 Histologic Grade (G-Stage)

The histologic grade is the most important component of staging and is itself a predictor of metastatic disease. In line with the FNCLCC (Fédération Nationale des Centres de Lutte Contre la Cancer, French Federation of Cancer Centers) sarcoma grading system, points are assigned using a scoring system ranging from zero to three. Three distinct histologic grades are recognized based on the degree of tumor differentiation, mitotic activity or rate, and degree of necrosis (Massarweh et al. 2015; Coindre 2006; Guillou et al. 1997; Trojani et al. 1984) (Table 3.2). The total score is used to assign a grade of 1 (low grade) through 3 (high grade). Accurate grading requires an adequate sample of well-fixed tissue for evaluation and may not always be possible based on needle biopsies or in tumors that were previously treated with radiation or chemotherapy. Core biopsy with image guidance is thought to be the most accepted method for the initial sampling of suspected sarcomas (Gibbs et al. 2016).

3.5 Proposed Report Format

(1) Primary tumor
   (a) MR imaging signal or CT attenuation characteristics
   (b) Extent and location of necrosis within the tumor
   (c) Location in extremity, including relationship to superficial fascia
   (d) Presence and location of tumor tails
   (e) Size (in three dimensions)
(2) Local extent
   (a) Invasion of muscles, bones, and joints
   (b) Contact with, or encasement of, blood vessels and nerves
   (c) Extension into the lumen of blood vessels
   (d) Presence of nearby satellite nodules
(3) Regional lymph node involvement

3.6 Illustrations: Staging of Soft Tissue Sarcoma

3.6.1 Stage I

Table 3.2 FNCLCC grading system: Parameters for grading

	Score			
Histologic features	0	1	2	3
Tumor differentiation		Sarcomas closely resembling normal adult mesenchymal tissue, e.g., well-differentiated (liposarcoma, fibrosarcoma, MPNST, leiomyosarcoma)	Sarcomas for which histologic typing is certain, e.g., myxoid liposarcoma, fibrosarcoma, myxofibrosarcoma, pleomorphic MFH with storiform pattern, conventional leiomyosarcoma, well-differentiated/conventional angiosarcoma, well-differentiated solitary fibrous tumor	Embryonal and undifferentiated sarcomas, sarcomas of doubtful type, synovial sarcomas, extraskeletal osteosarcomas, Ewing sarcoma/PNET of soft tissue, e.g., round cell/pleomorphic/dedifferentiated liposarcoma, undifferentiated pleomorphic sarcoma, poorly differentiated/epithelioid MPNST, conventional malignant solitary fibrous tumor, poorly differentiated/pleomorphic/epithelioid leiomyosarcoma, pleomorphic rhabdomyosarcoma, extraskeletal myxoid chondrosarcoma, mesenchymal chondrosarcoma, poorly differentiated/epithelioid angiosarcoma, ASPS, epithelioid sarcoma, clear cell sarcoma, malignant rhabdoid tumor, undifferentiated sarcoma, NOS
Mitotic activity		0–9 mitoses per 10 HPF[a]	10–19 mitoses per 10 HPF	≥ 20 mitoses per 10 HPF
Tumor necrosis	No necrosis	<50% tumor necrosis	≥ 50% tumor necrosis	
Histologic grade (G)	Total score			
Grade 1	2–3			
Grade 2	4–5			
Grade 3	6–8			

Adapted from Guillou L, Coindre JM, Bonichon F, et al. (Guillou et al. 1997) Comparative study of the National Cancer Institute and French Federation of Cancer Centers Sarcoma Group grading systems in a population of 410 adult patients with soft tissue sarcoma. J Clin Oncol 1997; 15(1):350–62; and Coindre JM. Grading of soft tissue sarcomas: review and update. Arch Pathol Lab Med 2006; 130(10):1449

[a]HPF measures 0.1734 mm^2

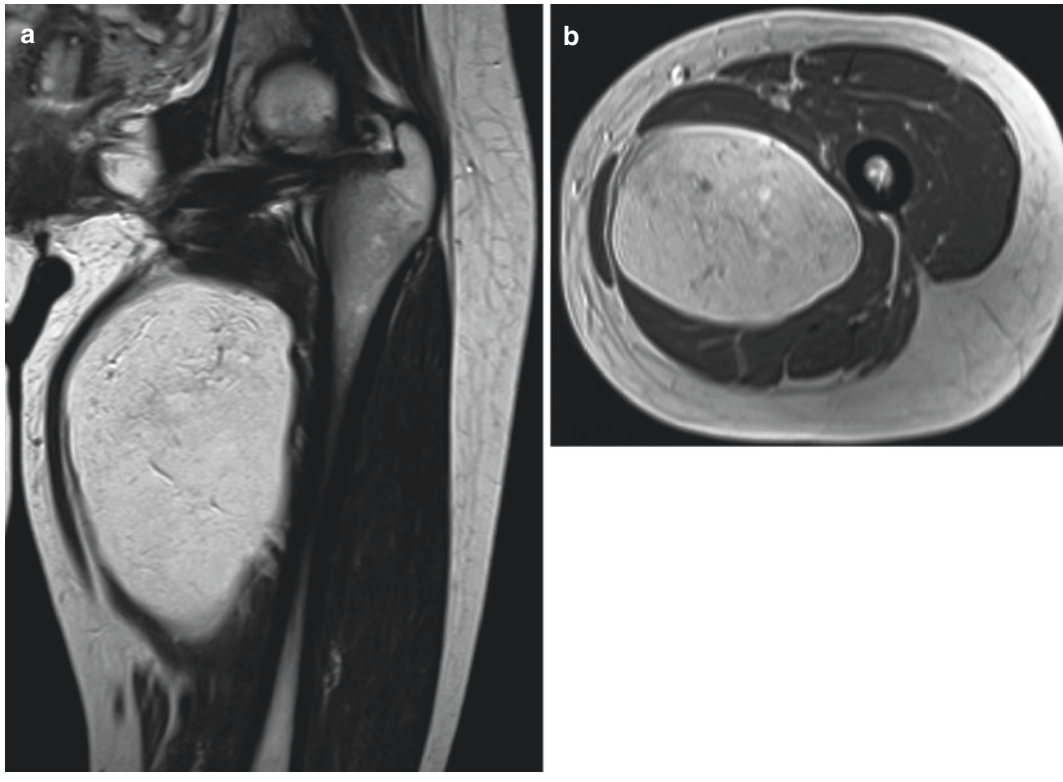

Fig. 3.1 A 35-year-old female with well-differentiated liposarcoma. On coronal T2WI (**a**) and axial T1WI (**b**) of the left thigh, the mass measured 17 cm at its greatest dimension (T4). There is no evidence of regional node metastasis or distant metastasis on other imaging work-up (not shown) (N0, M0). FNCLCC grade is 1: tumor differentiation, well-differentiated (score 1); mitosis count, <1/10 HPF (score 1); and tumor necrosis, 0% (score 0). This patient was ultimately diagnosed with stage IB liposarcoma

3.6.2 Stage II

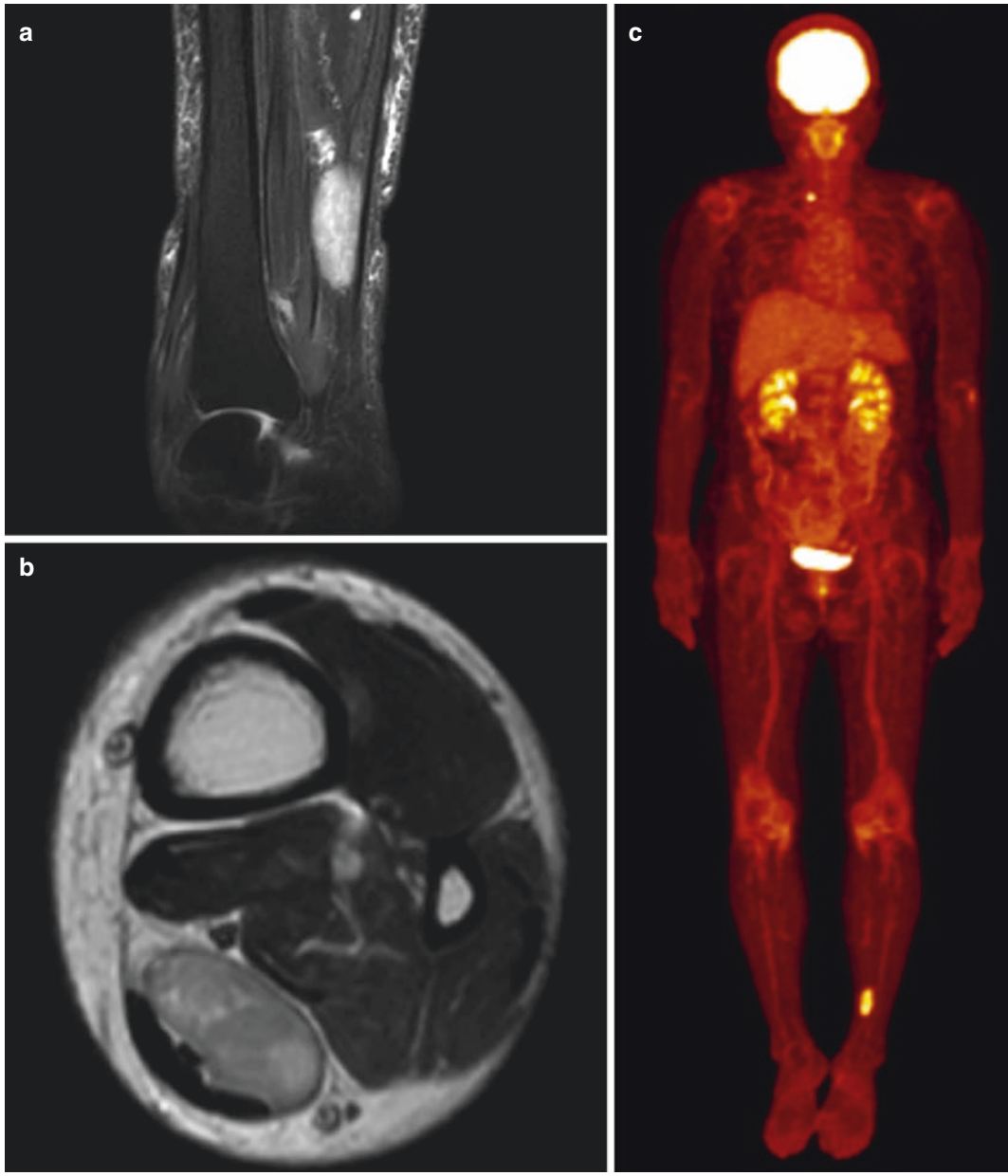

Fig. 3.2 A 62-year-old female with leiomyosarcoma. On sagittal (**a**) FS and axial (**b**) T2WI of the left lower leg, the tumor is smaller than 5.0 cm at its greatest dimension (T1). There is no evidence of regional node metastasis or distant metastasis on PET (**c**) (N0, M0). A very small hypermetabolic lesion in the right lobe of the thyroid gland is confirmed as benign thyroid pathology. FNCLCC grade is 2: tumor differentiation, spindle cell/pleomorphic (score 3); mitosis count, 6/10 HPF (score 1); and tumor necrosis, 0% (score 0). This patient was ultimately diagnosed with stage II leiomyosarcoma

3.6.3 Stage III

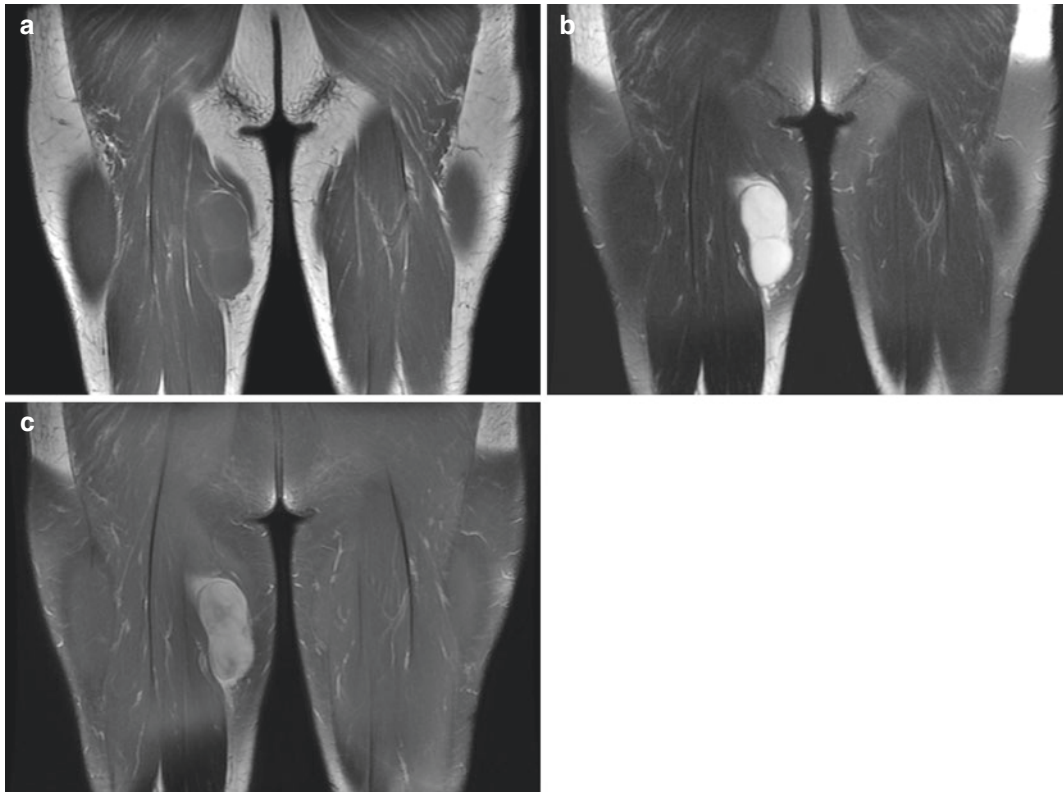

Fig. 3.3 A 57-year-old male with myxofibrosarcoma. Coronal T1WI (**a**) of the thigh reveals a circumscribed, isointense (relative to skeletal muscle) soft tissue mass beneath the superficial fascia. The lesion is bright hyperintense on coronal FS T2WI (**b**) and has inhomogeneous intense contrast enhancement on C+ FS T1WI (**c**). The mass measures 9.3 cm at its greatest dimension (T2). There is no evidence of regional node metastasis or distant metastasis (N0, M0). FNCLCC grade is 2: tumor differentiation, score 2; mitosis count, 3/10 HPF (score 1); and tumor necrosis, 0% (score 0). This patient was ultimately diagnosed with stage IIIA myxofibrosarcoma

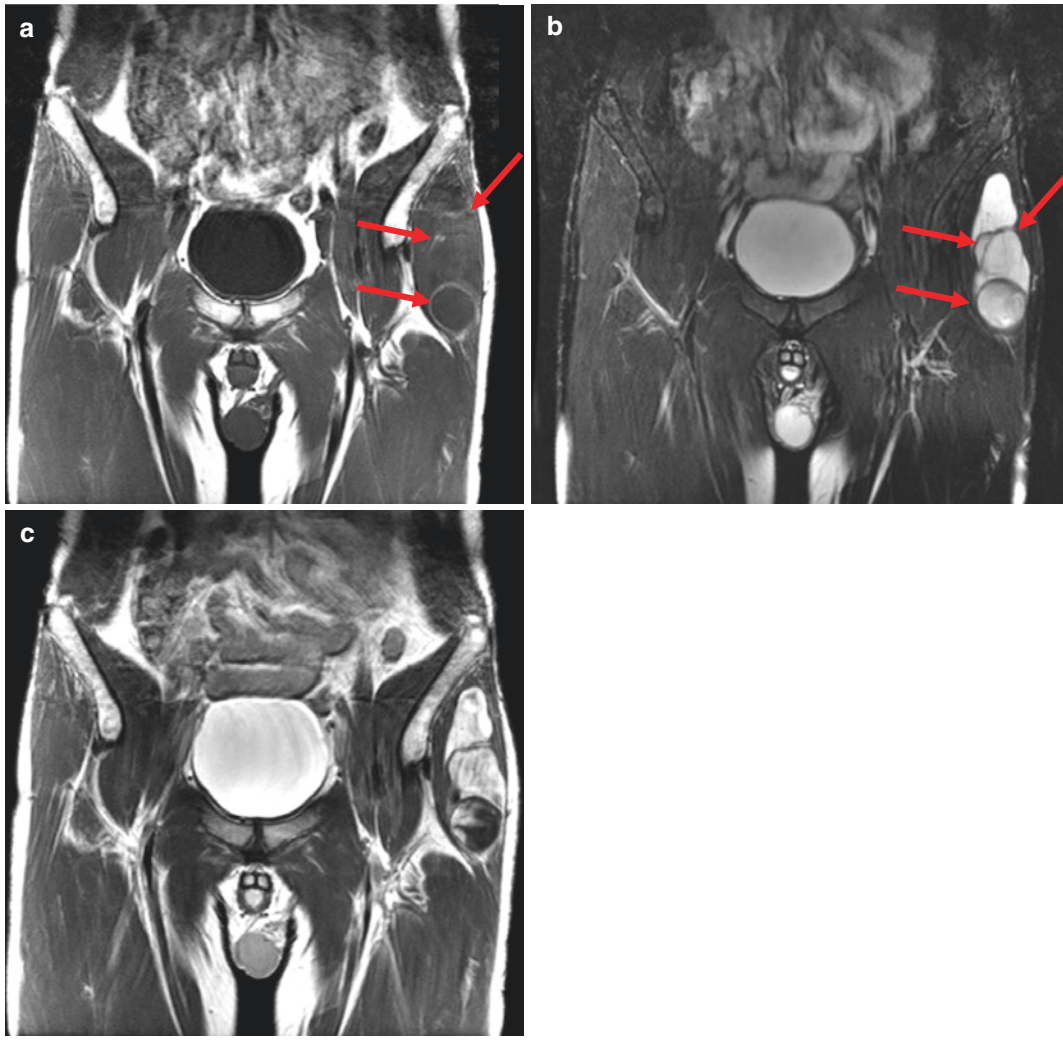

Fig. 3.4 A 32-year-old male with myxoid/round cell liposarcoma. Coronal T1WI (**a**) of the thigh shows an isointense intramuscular soft tissue mass with several thin hyperintense rims or lines (*arrows*). Coronal FS T2WI (**b**) shows the mass to be fluid-equivalent hyperintense, with a signal drop of T1 hyperintense areas. The lesion exhibits heterogeneous contrast enhancement on coronal C+ T1WI (**c**). The mass measures 12 cm at its greatest dimension (T3). There is no evidence of regional node metastasis or distant metastasis on other imaging work-up (not shown) (N0, M0). FNCLCC grade is 3: tumor differentiation, round cell (score 3); mitosis count, 13/10 HPF (score 2); and tumor necrosis, 5% (score 1). Ultimately, this patient was diagnosed with stage IIIB liposarcoma

3.6.4 Stage IV

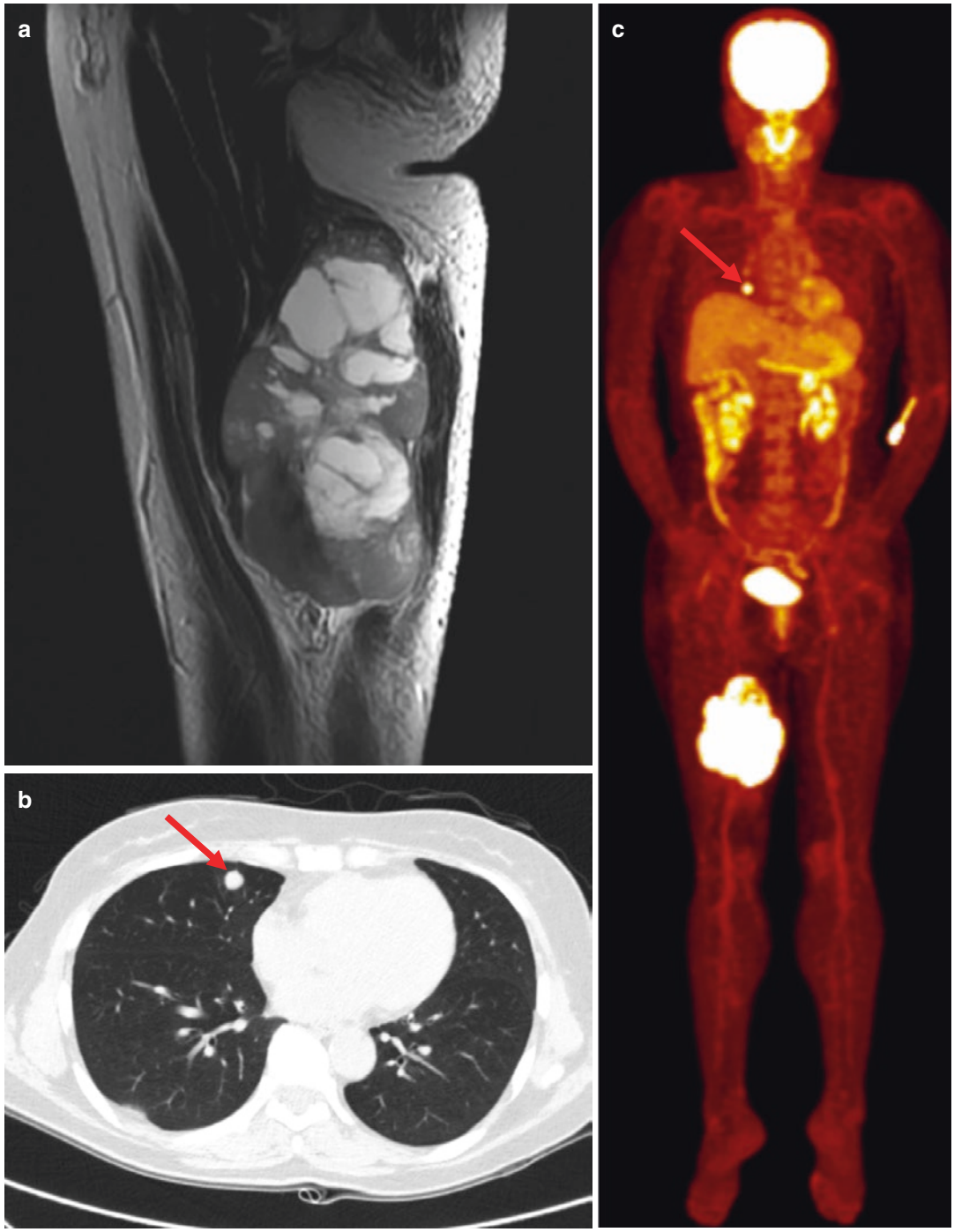

Fig. 3.5 A 62-year-old female with leiomyosarcoma. On sagittal T2WI of the right thigh (**a**), the mass measures 11.0 cm at its greatest dimension and is deeply located beneath the superficial fascia (T3). Note the pulmonary metastasis in the right middle lobe on chest CT (**b**) and PET (**c**). Irrespective of any T-stage, N-stage, and histologic grade, this patient was diagnosed with stage IV leiomyosarcoma

References

Coindre JM. Grading of soft tissue sarcomas: review and update. Arch Pathol Lab Med. 2006;130(10):1448–53. doi:10.1043/1543-2165(2006)130[1448:gostsr]2.0.co;2.

Crago AM, Lee AY. Multimodality management of soft tissue tumors in the extremity. Surg Clin North Am. 2016;96(5):977–92. doi:10.1016/j.suc.2016.05.001.

Fisher SM, Joodi R, Madhuranthakam AJ, Oz OK, Sharma R, Chhabra A. Current utilities of imaging in grading musculoskeletal soft tissue sarcomas. Eur J Radiol. 2016;85(7):1336–44. doi:10.1016/j.ejrad.2016.05.003.

Fong Y, Coit DG, Woodruff JM, Brennan MF. Lymph node metastasis from soft tissue sarcoma in adults. Analysis of data from a prospective database of 1772 sarcoma patients. Ann Surg. 1993;217(1):72–7.

Gibbs J, Henderson-Jackson E, Bui MM. Bone and soft tissue pathology: diagnostic and prognostic implications. Surg Clin North Am. 2016;96(5):915–62. doi:10.1016/j.suc.2016.06.003.

Guillou L, Coindre JM, Bonichon F, Nguyen BB, Terrier P, Collin F, Vilain MO, Mandard AM, Le Doussal V, Leroux A, Jacquemier J, Duplay H, Sastre-Garau X, Costa J. Comparative study of the National Cancer Institute and French Federation of Cancer Centers Sarcoma Group grading systems in a population of 410 adult patients with soft tissue sarcoma. J Clin Oncol. 1997;15(1):350–62. doi:10.1200/jco.1997.15.1.350.

Massarweh NN, Dickson PV, Anaya DA. Soft tissue sarcomas: staging principles and prognostic nomograms. J Surg Oncol. 2015;111(5):532–9. doi:10.1002/jso.23851.

Mazeron JJ, Suit HD. Lymph nodes as sites of metastases from sarcomas of soft tissue. Cancer. 1987;60(8):1800–8.

Pollock RE, Maki RG, Agulnik M, et al. Soft tissue sarcoma. In: Amin MB, editor. AJCC cancer staging manual. 8th ed. New York: Springer; 2016. p. 489–545.

Trojani M, Contesso G, Coindre JM, Rouesse J, Bui NB, de Mascarel A, Goussot JF, David M, Bonichon F, Lagarde C. Soft-tissue sarcomas of adults; study of pathological prognostic variables and definition of a histopathological grading system. Int J Cancer. 1984;33(1):37–42.

Part II

WHO Classification of Soft Tissue Tumors and Radiologic Illustrations

Adipocytic Tumors

4

Benign lipomatous lesions represent a variety of adipose tumors and include lipoma, lipomatosis, lipomatosis of nerve, lipoblastoma/lipoblastomatosis, angiolipoma, myolipoma of soft tissue, chondroid lipoma, spindle cell lipoma/pleomorphic lipoma, and hibernoma. Benign lipomatous lesions often have characteristic imaging features, including diffuse or focal areas that are similar or identical to subcutaneous fat. These imaging characteristics and lesion extent are best appreciated with MR imaging.

Malignant adipocytic tumors account for 10–35% of all soft tissue sarcomas. In fact, liposarcomas represent a heterogeneous group of distinctive lesions that pose several diagnostic difficulties. The World Health Organization (WHO) Committee for the Classification of Soft Tissue Tumors in 2013 categorized liposarcomas into one intermediate and three malignant subtypes, including atypical lipomatous tumor/well-differentiated liposarcoma, dedifferentiated liposarcoma, myxoid liposarcoma, and pleomorphic liposarcoma (Murphey et al. 2005; Dei Tos 2014).

The exact classification of the liposarcoma subtypes is crucial for decision-making in patients given that the aggressiveness of local and systemic treatment modalities may vary substantially (Henze and Bauer 2013). Atypical lipomatous tumor/well-differentiated liposarcoma is a locally aggressive neoplasm that is virtually incapable of systemic spread. Dedifferentiated liposarcoma, despite its high-grade morphology, metastasizes in only 15–20% of cases, mortality being most often related to uncontrolled local recurrences. The clinical behavior of myxoid liposarcoma is determined primarily by histological grade (manifested by the degree of hypercellularity). High-grade (formerly "round cell") myxoid liposarcoma exhibits a remarkable tendency to metastasize to bone and soft tissues. Pleomorphic liposarcoma shares highly aggressive clinical behavior with other pleomorphic sarcomas (Dei Tos 2014).

The MR imaging features of liposarcomas vary according to the wide spectrum of pathologic appearances. Imaging findings contribute to the final histologic diagnosis of these tumors and can be used to orientate the biopsy, which should be performed on both the lipomatous and nonlipomatous components (El Ouni et al. 2010).

4.1 Lipoma

Lipoma is the most common benign soft tissue tumor, is composed of mature fat cells, and is not distinguishable histologically from normal fat. It is either a superficial or deep-seated mass, commonly in subcutaneous fat, muscles, or intermuscular planes. Most lipomas are discrete masses; however, superficial lipomas can blend imperceptibly with the surrounding subcutaneous fat. Intramuscular lipomas can have ill-defined margins due to fat infiltration among muscle fibers in deep-seated lesions (Bancroft et al. 2013).

H.S. Kang et al., *Oncologic Imaging: Soft Tissue Tumors*, DOI 10.1007/978-981-287-718-5_4

At US, lipomas are hyperechoic masses, occasionally with heterogeneity caused by septa or nonadipose tissues. No posterior sonic enhancement is observed. The MR imaging findings of ordinary lipoma are well described, with high signal intensity on both T1- and T2-weighted images and a signal drop on fat-suppressed images. The same pattern is observed for subcutaneous fat. Signal alteration is caused by infarction, hemorrhage, inflammation, and ossification or in cases when lipomas admix with other mesenchymal elements. In these cases, lipomas contain areas with a decreased signal intensity on T1-weighted images and various signal intensities on T2-weighted images (Drevelegas et al. 2004). When a lipoma occurs adjacent to cortical bone, it is commonly associated with reactive changes in the underlying cortex. Lipomas frequently demonstrate intrinsic thin septa (< 2 mm) on CT or MR images. The presence of only thin delicate septa, particularly when few in number, favors the diagnosis of soft tissue lipoma over well-differentiated liposarcoma (Murphey et al. 2004).

4.2 Lipomatosis

Lipomatosis represents a diffuse overgrowth of mature adipose tissue. The multiple types of lipomatosis are typically differentiated by anatomic location, and varying clinical manifestations have been described. These manifestations include multiple symmetric lipomatosis (Madelung's disease), infiltrating congenital lipomatosis of the face, encephalocraniocutaneous lipomatosis, shoulder girdle lipomatosis, adiposis dolorosa, pelvic lipomatosis, and mediastinal lipomatosis. The extensive involvement of both muscle and subcutaneous tissue typically differentiates a large intermuscular or intramuscular lipoma from lipomatosis. Imaging, particularly CT and MR imaging, reveals these infiltrative fatty masses, typically in a subcutaneous distribution but more frequently between the deep muscles (Murphey et al. 2004).

4.3 Lipomatosis of Nerve

Lipomatosis of nerve (LON) is a benign tumor involving peripheral nerve that has been described by various other names, including fibrolipomatous hamartoma, neural fibrolipoma, and fibrofatty proliferation of a nerve. The histologic evaluation demonstrates diffuse nerve enlargement secondary to interfascicular fibrofatty infiltration. LON most commonly occurs in the median nerve and has been reported in multiple other nerve distributions. LON is frequently associated with varying degrees of localized mesenchymal overgrowth in the territory of nerve distribution. This overgrowth ranges from minimal digital enlargement to extensive bone and soft tissue hypertrophy, which is referred to as macrodystrophia lipomatosa (Gupta et al. 2016).

The MR imaging appearance of LON is unique and characteristic, obviating the need for biopsy for diagnosis. Serpentine, low-intensity structures, representing thickened nerve fascicles, are surrounded by or embedded in evenly distributed fat, which appears on MR imaging as high signal intensity on T1-weighted images and low signal intensity on STIR and fat-suppressed T2-weighted images. A coaxial-cable-like appearance in the short-axis plane and a spaghetti-like appearance in the long-axis planes are the most typical findings for this tumor (Van Breuseghem et al. 2003).

4.4 Lipoblastoma/ Lipoblastomatosis

Lipoblastoma is a lipoma variant of the embryonic lipoblast and is categorized into two forms as follows: (1) a localized, superficial, and well-circumscribed or encapsulated form termed lipoblastoma and (2) a diffuse, multicentric, unencapsulated, and infiltrative form termed lipoblastomatosis. Lipoblastomas occur most frequently in male children younger than 3 years of age and have been reported to arise where immature adipose elements persist, namely, the neck,

axilla, and prevertebral soft tissues (Salem et al. 2011).

The imaging of lipoblastomas reflects their histopathology, which typically shows an admixture of mature and immature adipocytes, often with a prominent myxoid matrix. MR imaging usually precisely depicts the well-circumscribed margins of the lipoblastoma, although the margins of lipoblastomatosis may be difficult to identify. CT and MR imaging show a predominantly fatty mass, with the nonlipomatous areas of the mass showing a nonspecific imaging appearance. The imaging appearance of lipoblastomas may simulate that of a liposarcoma; however, such lesions are exceedingly rare in children (Bancroft et al. 2006). The age of the patient is therefore the most useful distinction as there are no known imaging findings which separate these two entities (Moholkar et al. 2006).

4.5 Angiolipoma

Angiolipomas typically present as small (< 2 cm in diameter), painful subcutaneous masses. They most commonly affect young male patients in the second to third decades of life. The most common locations in order of frequency are the forearm, trunk and upper arm. Multiple angiolipomas are reported in approximately 70% of cases.

The MR imaging features of angiolipoma are the presence of fat nodules with or without areas of low signal intensity on T1- and T2-weighted images. The location of the low-signal-intensity areas vary, being either in the peripheral or central portion of the mass. On histopathologic examination, the low-signal-intensity areas on T1- and T2-weighted images correspond to areas of dense capillary proliferation. Only very small portions of the low-signal-intensity areas on T1-weighted images appear as high-signal-intensity areas on T2-weighted images. (Kitagawa et al. 2014). Those vascular components markedly enhance with intravenous contrast material.

4.6 Spindle Cell Lipoma

Spindle cell lipoma is a benign lesion in which mature fat is replaced by a mixture of mature adipocytes and collagen-forming spindle cells. These lesions are usually located in the subcutaneous tissues of the shoulder, neck, and upper back and can exhibit intramuscular extension. A lipoma with a spindle cell subtype can represent a diagnostic challenge to radiologists, pathologists, and surgeons given its frequent presentation as a lesion containing little or no macroscopic or microscopic fat (Khashper et al. 2014).

The imaging features of spindle cell lipoma depend on their adipose and nonadipose contents. The MR examination grading of adipose: nonadipose content of spindle cell lipomas correlates with the histological grading of the excision specimen. The non-adipocytic areas are composed of spindle cells in a fibromyxoid background, which correspond to the low T1 signal and enhance following administration of intravenous contrast material (Kirwadi et al. 2014). Because of the similarity of the imaging features with liposarcoma, preoperative image-guided biopsy is often required.

4.7 Hibernoma

Hibernoma is a rare benign adipose tumor that is composed of brown fat-like multivacuolated cells, univacular cells resembling lipocytes and lipid-free cells with eosinophilic granular cytoplasm. Hibernomas have a variable histological appearance depending on the relative amounts of multivacuolated brown fat cells associated with capillary proliferation and fibrovascular septa.

Compared to the subcutaneous fat, hibernomas are slightly hyperdense, with attenuation values between those of fat and skeletal muscle on CT. On MR imaging, these tumors are slightly hypointense relative to fat on T1-weighted imaging and show incomplete signal suppression on fat-suppressed T2-weighted imaging. Hibernomas often demonstrate prominent internal vascularity with variable tumoral enhancement. Lipoma-like

hibernomas are usually isointense with subcutaneous fat on T1-weighted images. In contrast, non-lipoma-like hibernomas are predominantly slightly hypointense to subcutaneous fat on T1-weighted images, often displaying marked or moderate inhomogeneity, with prominent septa and vessels (Ritchie et al. 2006). Some findings may overlap with other, more common, benign or low-grade lipomatous neoplasms, such as lipoma and atypical lipomatous tumor (ALT), leading to diagnostic difficulty (Liu et al. 2013). Because of their ability to produce heat and exhibit thermoregulation, intense uptake of FDG can be observed on PET.

4.8 Lipoma Arborescens

Lipoma arborescens is a rare intra-articular lipoma-like lesion characterized by fatty infiltration of the subsynovial connective tissue. This frond-like lesion receives its name from its resemblance to a tree in leaf. Lipoma arborescens is generally considered one of the rarest of synovial proliferative lesions (Garner and Bestic 2013). The knee is the most common site of involvement, although the glenohumeral joint, subdeltoid bursa, hip, and elbow can be affected.

Lipoma arborescens has pathognomonic MR imaging findings that include a frond-like synovial mass that is isointense relative to fat with all sequences (including fat-suppression sequences), joint effusion, and a lack of magnetic susceptibility artifact. Three distinct patterns of lipoma arborescens have been identified, the most common of which is a diffuse villous proliferation, although a discrete mass lesion and a mixed pattern can also be observed (Coll et al. 2011). Bone erosions in association with lipoma arborescens may develop in relatively "tight" joints, such as the glenohumeral joint (Chae et al. 2009).

4.9 Atypical Lipomatous Tumor/ Well-Differentiated Liposarcoma

Atypical lipomatous tumor or well-differentiated liposarcoma (ATL/WDLPS) is the most common liposarcoma. ATLs/WDLPS most frequently occurs in the extremities and then in the retroperitoneum. Histologically, this tumor is characterized by the presence of mature adipocytes of irregular size arranged in bands that are separated by thick fibromyxoid septa. These septa characteristically comprise cells with atypical hyperchromatic nuclei that exhibit overexpression of MDM2 and CDK4 (Kind et al. 2009).

At imaging, ATLs/WDLPSs resemble lipomas and have a characteristic appearance as a mass that is predominantly composed of highly differentiated adipose tissue. Nodular or globular nonlipomatous components can be observed, which are usually less than 2 cm in size. ATLs/WDLPS is distinguished from benign lipoma by variation in adipocytic size and the presence of cytologic atypia. Consequently, radiological differentiation of ATLs/WDLPS from lipoma can be challenging. MR imaging of the internal characteristics is useful for the differential diagnosis of these tumors. When a predominantly adipose mass demonstrates multiple thick (> 2 mm) septa with marked enhancement, it is more likely ATLs/WDLPS than lipoma (Ohguri et al. 2003). Other factors favoring the diagnosis of ATLs/WDLPS over lipoma include male sex, age greater than 66 years, lower percentage of fat (less than 75% of the lesion), the presence of calcification, and lesion size greater than 10 cm (Kransdorf et al. 2002).

The sclerosing variant of well-differentiated liposarcoma should be included in the differential diagnosis of any well-circumscribed lipomatous mass containing variable amounts of nonlipomatous elements, particularly when located in the retroperitoneum. The sclerosing variant has a tumor composition ranging from predominantly fatty to entirely devoid of macroscopic fat and may be associated with an increased propensity for dedifferentiation (Bestic et al. 2013).

4.10 Dedifferentiated Liposarcoma

Dedifferentiated liposarcoma (DDLPS) is a subtype of liposarcoma, being a transition from low-grade to high-grade non-lipogenic sarcoma. This

tumor is characterized histologically by two components as follows: one well-differentiated liposarcoma-type component and another component composed of undifferentiated sarcoma-type cells. The cells also exhibit overexpression (immunohistochemistry) and amplification (FISH) of MDM2 and CDK4 (Kind et al. 2009).

The imaging findings of DDLPS are similar with WDLPS and are best appreciated on MR imaging. A nonlipomatous mass (intermediate-to-hypointense T1 signal, intermediate-to-hyperintense T2 signal) arising within or adjacent to a WDLPS is suspicious for dedifferentiation (Gupta et al. 2016). The imaging differential diagnosis for a focal nodular nonlipomatous component within a well-differentiated liposarcoma includes a region of collagenized tissue, metaplastic mineralization, a region of dedifferentiation, and fat necrosis. It is important to recognize these foci, and the biopsy must be directed at both the lipomatous and nonlipomatous components to ensure accurate pathologic diagnosis (Murphey et al. 2005).

4.11 Myxoid Liposarcoma

Myxoid liposarcoma is the second largest group of malignant adipocytic neoplasms, accounting for approximately 30–35% of all liposarcomas. Round cell liposarcoma is defined as a form of myxoid liposarcoma that has an associated round cell component in greater than 5% of the tumor. Previously, myxoid and round cell liposarcomas were considered distinct histologic subtypes. However, the WHO classification of soft tissue tumors has now combined these lesions as myxoid liposarcoma, representing a continuum of these two previous subtypes (Murphey et al. 2005). At histologic analysis, myxoid liposarcomas consist of a myxoid matrix as the predominant component and small amounts of mature fat.

A spectrum of MR imaging abnormalities is observed in myxoid liposarcomas. These findings depend on the amount of fat and myxoid tissue, the cellularity and vascularity, and the presence of necrosis. Because of their high water content, myxoid liposarcomas often pathognomonically present with low signal intensity on T1-weighted MR images and marked high signal intensity on T2-weighted MR images. Most myxoid liposarcomas have lacy or linear, amorphous foci of fat. The fat also typically constitutes only a small volume of the overall mass size (<10% of the lesion) and is often observed in septa (lacy or linear pattern) or as subtle, small nodules in the lesion (Murphey et al. 2005). The use of fat suppression can be helpful to further increase confidence in the detection of adipose content and differentiate fat from hemorrhagic components. Some myxoid liposarcomas appear to be cystic at unenhanced MR imaging, although they enhance similarly to other solid masses on contrast-enhanced MR imaging (Sung et al. 2000). The following three patterns of enhancement are observed: solid, nodular enhancement; peripheral and septal enhancement; and uniform, central enhancement with non-enhancing septations (Wortman et al. 2016a). Myxoid liposarcomas with more prominent round cell components may demonstrate areas of relatively lower water content at MR imaging. These areas may have nonspecific features of solid tissue with intermediate signal intensity on T1- and T2-weighted MR images. Sonographic evaluation can be helpful in cyst-like myxoid liposarcomas on MR imaging by demonstrating that the mass is not truly a cyst.

Extremity myxoid liposarcomas are most frequently intermuscular lesions (70–80% of cases), and an origin in muscle or subcutaneous location is less common. Myxoma is another diagnostic consideration, although myxomas are generally intramuscular lesions with surrounding muscle atrophy and edema, all of which are manifestations not observed in myxoid liposarcoma (Murphey et al. 2005).

Presentation with either primary or recurrent disease, tumor size, and tumor grade are of major importance. Complete tumor resection with negative margins should be the objective of surgery with an evident impact on local control. Myxoid liposarcoma is known to be particularly sensitive to radiotherapy, and MR imaging often shows a decrease in size and enhancement and increase in internal fat following radiotherapy (Wortman et al. 2016b).

4.12 Pleomorphic Liposarcoma

Pleomorphic liposarcoma is a high-grade liposarcoma and the least common subtype of liposarcoma. It occurs in the extremities and, less commonly, in the trunk and retroperitoneum.

Pleomorphic liposarcoma is difficult to differentiate on MR imaging from other soft tissue sarcomas because it has nonspecific signal characteristics (T1 hypointensity and T2 hyperintensity) and because of the paucity of fat. In one study using MR imaging, the tumor demonstrated peritumoral edema (93%), necrosis (86%), intense enhancement (77%), intratumoral hemorrhage (36%), and intratumoral fat (29%). The imaging appearance of pleomorphic liposarcoma overlapped most frequently with high-grade myxoid liposarcoma: distinguishing factors included the presence of thick septations and homogeneity on T2-weighted images in high-grade myxoid liposarcoma, which were very uncommon characteristics in pleomorphic liposarcoma (Wortman et al. 2016a).

4.13 Illustrations: Adipocytic Tumors

4.13.1 Lipoma

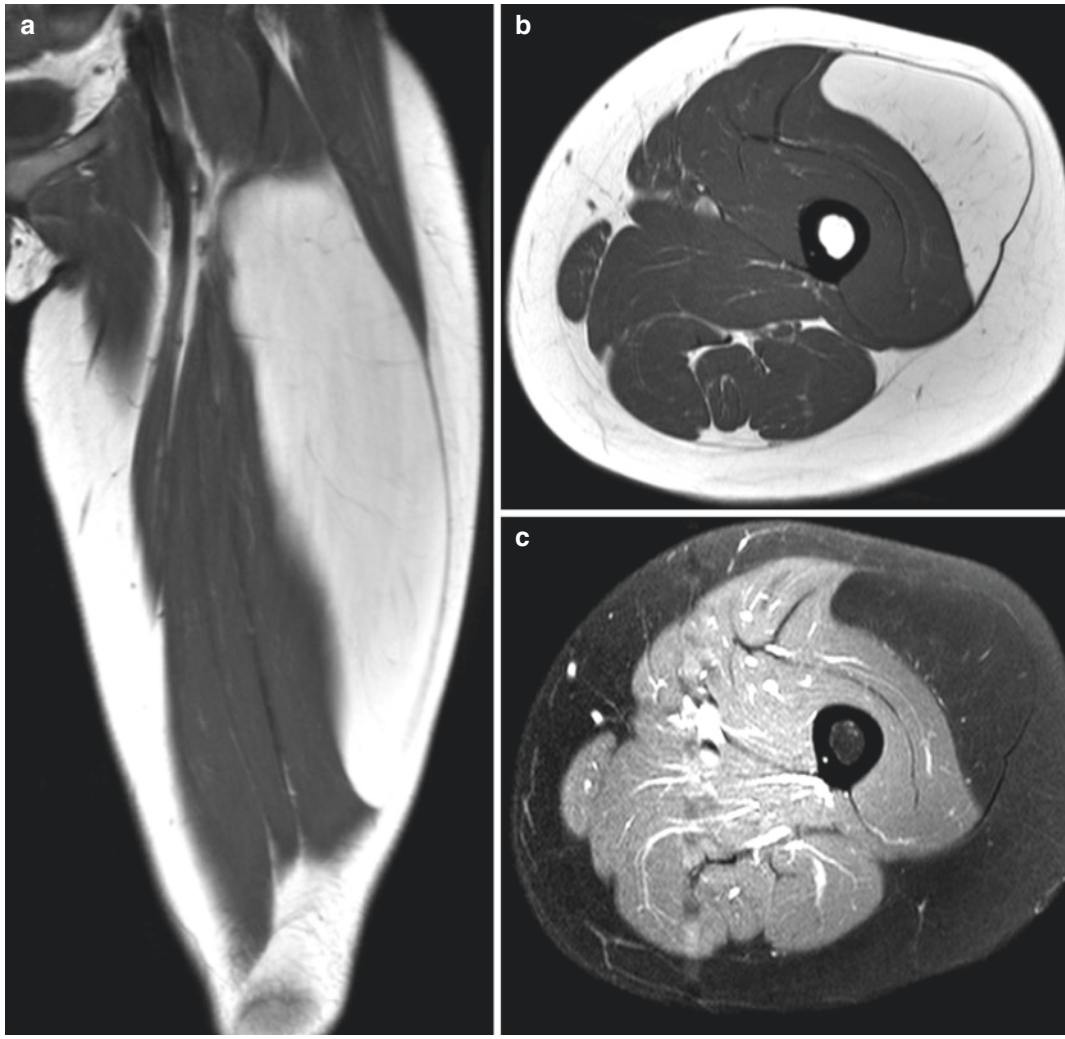

Fig. 4.1 Intramuscular lipoma. Coronal T1WI (**a**) shows a subfascial fatty mass in the left vastus lateralis muscle, with diffuse T1 hyperintensity. Axial T1WI (**b**) shows a predominantly fatty mass and axial postcontrast FS T1WI (**c**) shows a complete loss of signal. There are multiple thin septa with T1 hypointensity and mild enhancement

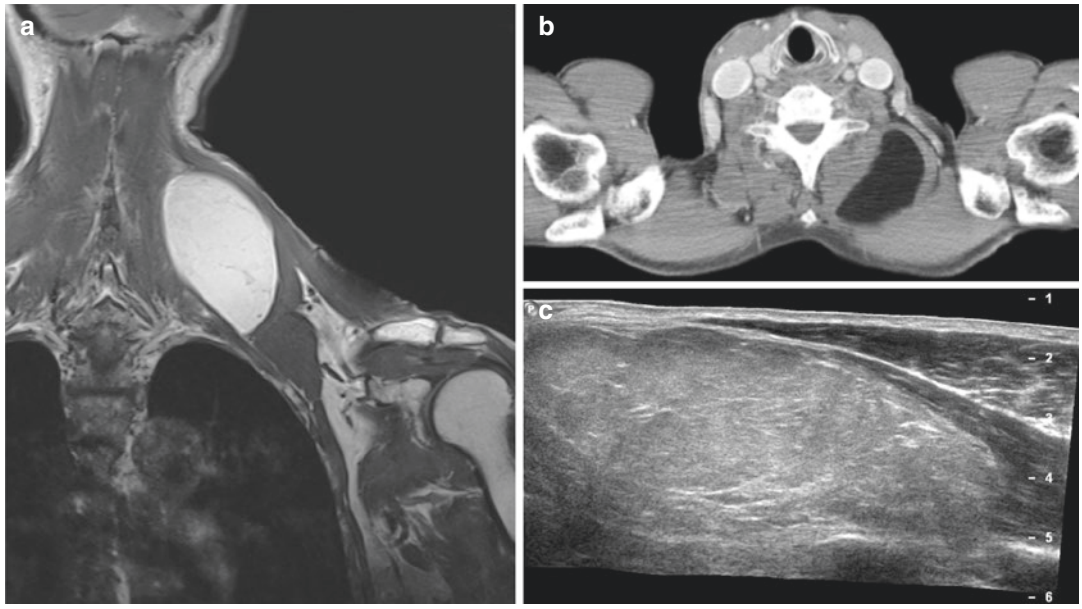

Fig. 4.2 Intermuscular lipoma. Coronal T1WI (**a**) shows a fatty mass between the splenius capitis, levator scapulae, and trapezius muscles. Axial CT scan (**b**) shows a well-demarcated mass with fat attenuation of approximately −100 HU. Longitudinal extended-field-of-view US (**c**) shows a large intermuscular mass that is hyperechoic relative to the adjacent musculature

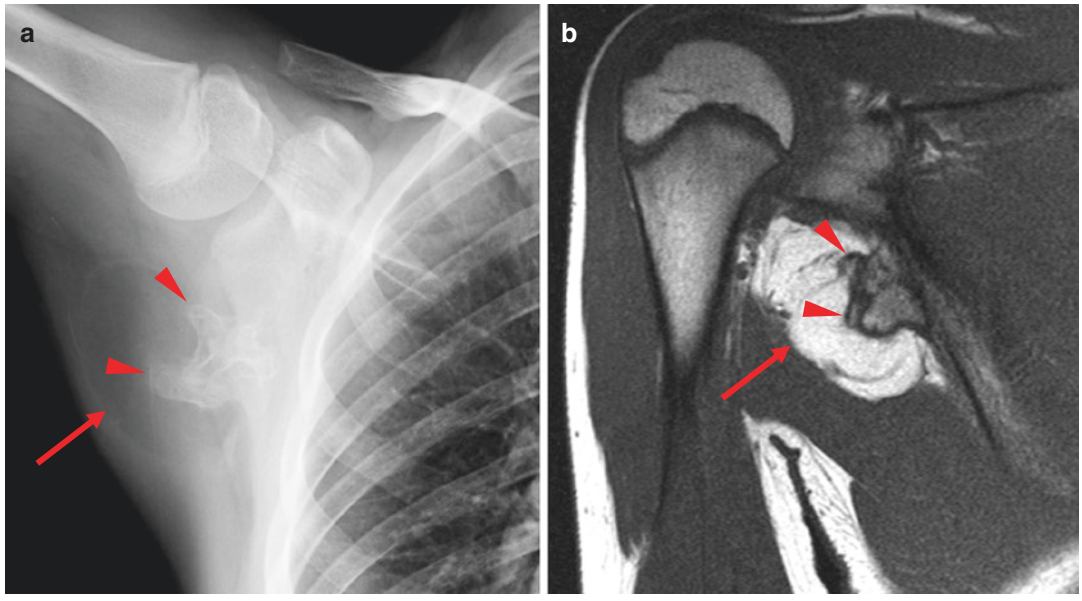

Fig. 4.3 Parosteal lipoma. Right shoulder radiography (**a**) and coronal T1WI (**b**) show a low-density or T1 hyperintense fatty mass (*arrow*) on the lateral aspect of the right scapula. There is a bony excrescence (*arrowheads*) arising from the lateral border of the scapula

4.13.2 Lipomatosis

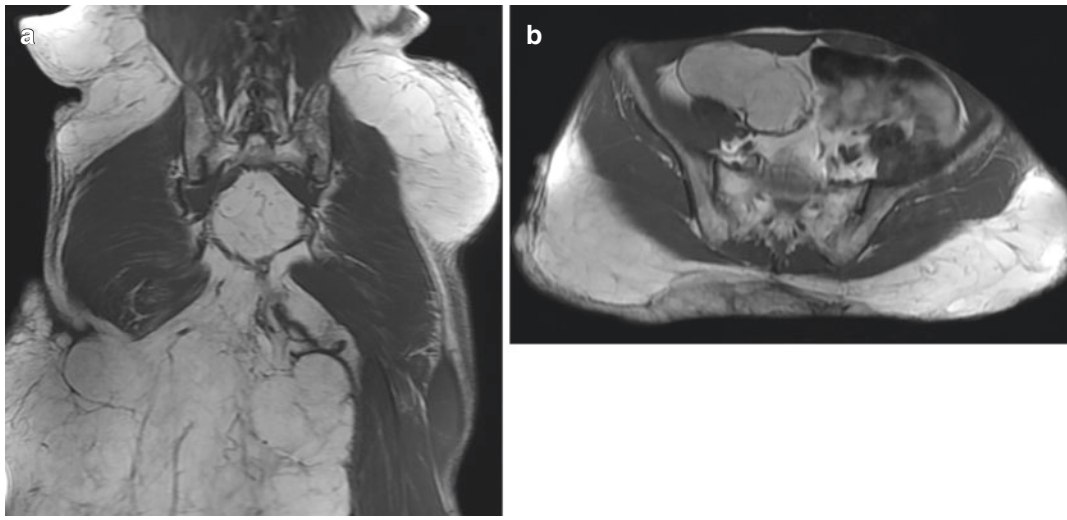

Fig. 4.4 Lipomatosis. Coronal and axial T1WIs (**a**, **b**) show diffuse lipomatous infiltration in the back and right posterior thigh subcutaneous layer

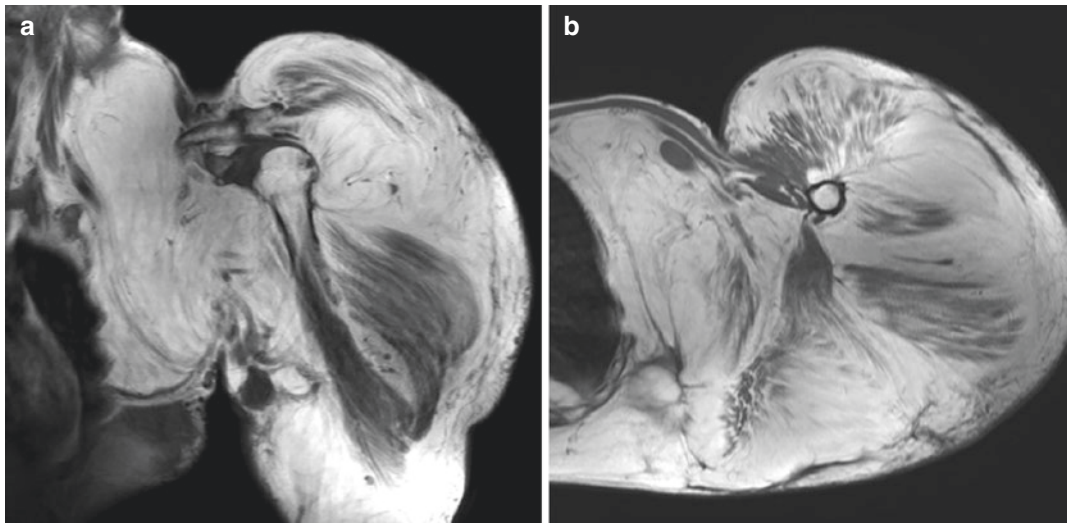

Fig. 4.5 Lipomatosis. Coronal and axial T1WIs (**a**, **b**) show diffuse lipomatous infiltration in the left shoulder and chest wall, affecting both muscles and subcutaneous tissues

4.13.3 Lipomatosis of Nerve

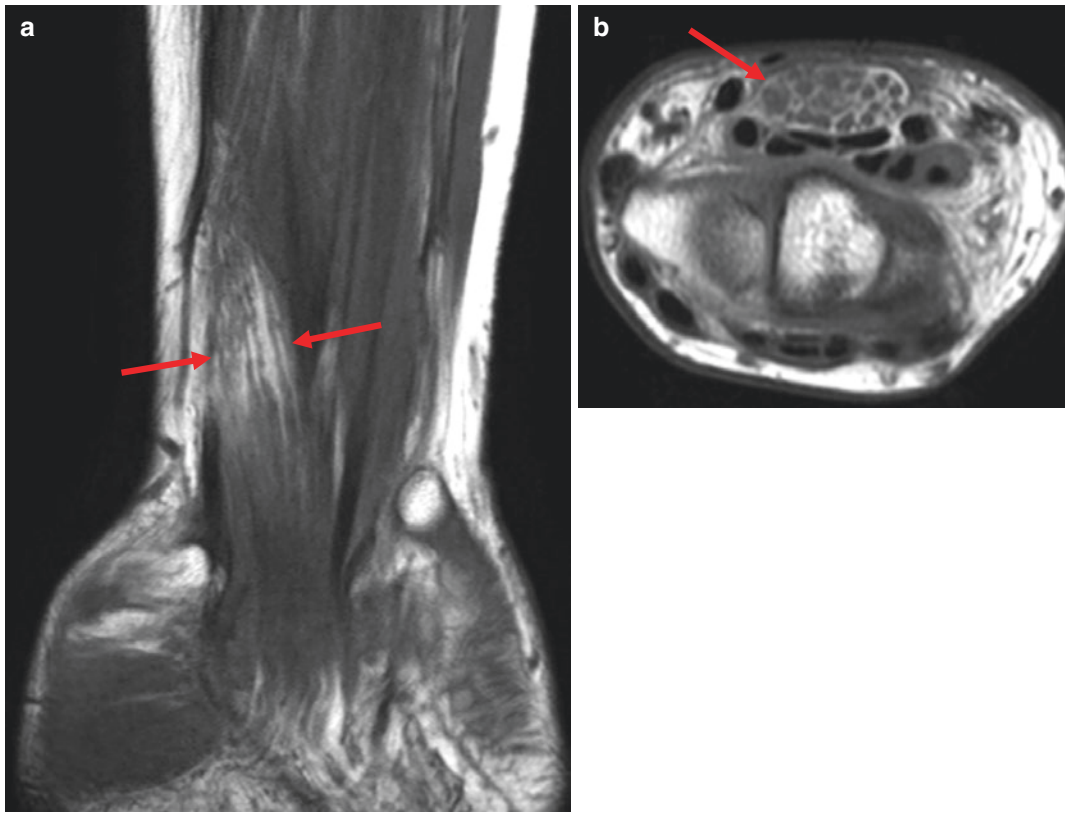

Fig. 4.6 Lipomatosis of nerve. Coronal and axial T1WIs (**a**, **b**) show marked enlargement of the median nerve (*arrow*) with diffuse fat infiltration, resulting in a spaghetti-like (**a**) or coaxial cable-like (**b**) appearance

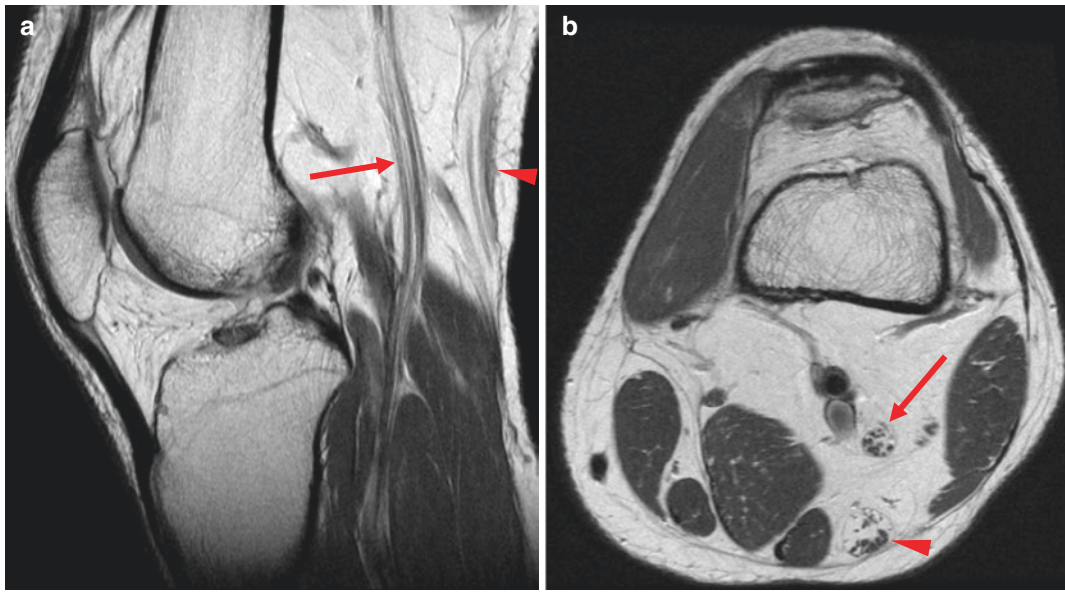

Fig. 4.7 Lipomatosis of nerve. Sagittal and axial T2WIs (**a**, **b**) show diffuse thickening of the tibial (*arrow*) and posterior femoral cutaneous (*arrowhead*) nerves, with interfascicular fat deposition

4.13.4 Lipoblastoma

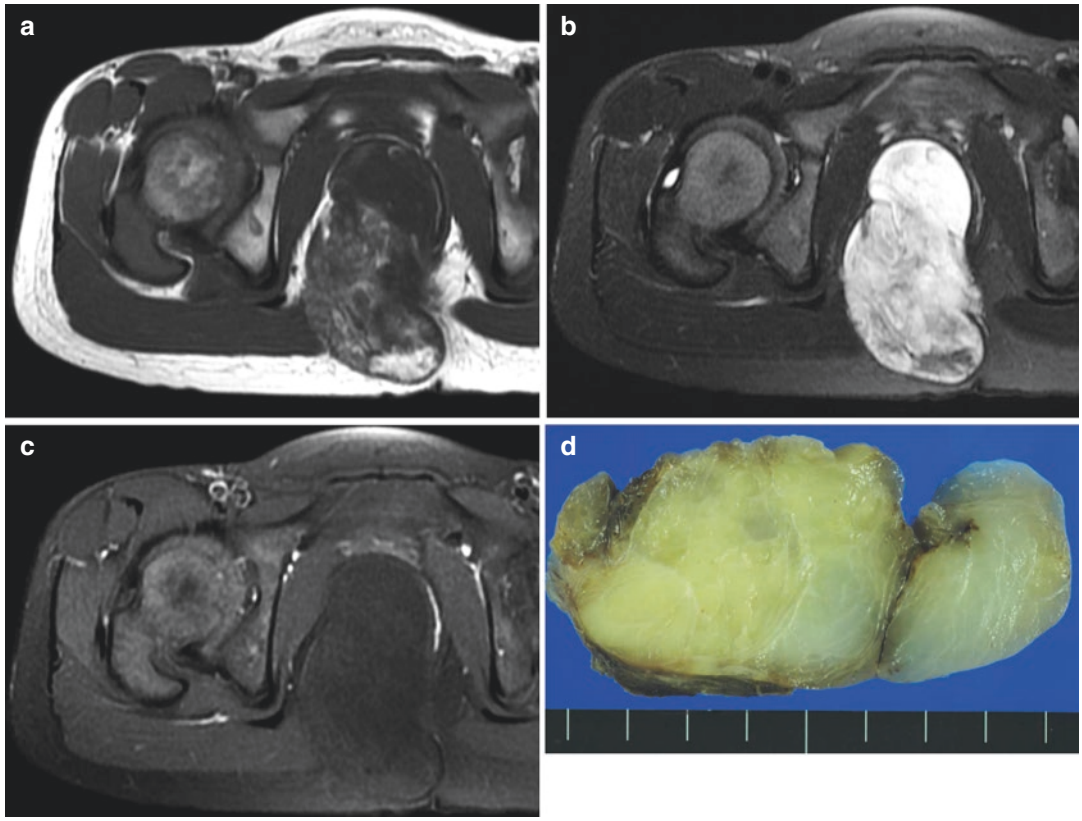

Fig. 4.8 Lipoblastoma. Axial T1WI (**a**) shows a fat-containing mass in the subcutaneous layer of the right paramedian buttock. Axial FS T2WI (**b**) shows a large area of hyperintensity and saturated fat components. Axial postcontrast FS T1WI (**c**) shows a largely non-enhancing mass. (**d**) Gross appearance of lipoblastoma with extensive myxoid change

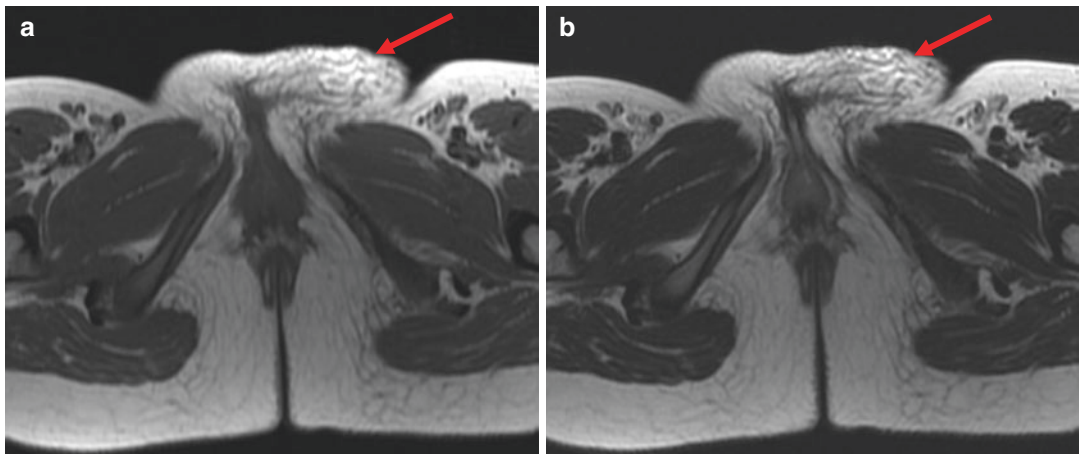

Fig. 4.9 Lipoblastomatosis. Axial T1WI (**a**), T2WI (**b**) and coronal T1WI (**c**) show an infiltrative fatty lesion (*arrow*) with intralesional streaks in the left pubic subcutaneous layer

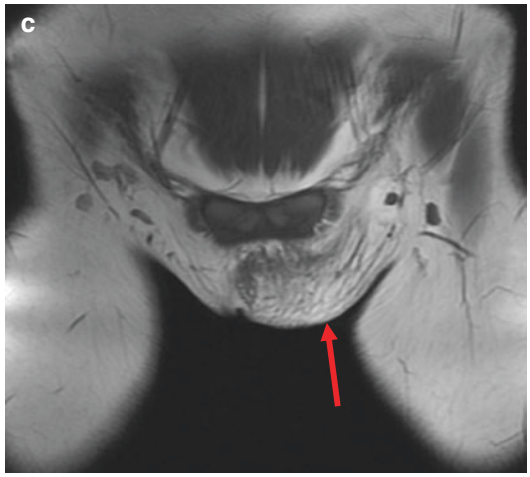

Fig. 4.9 (continued)

4.13.5 Angiolipoma

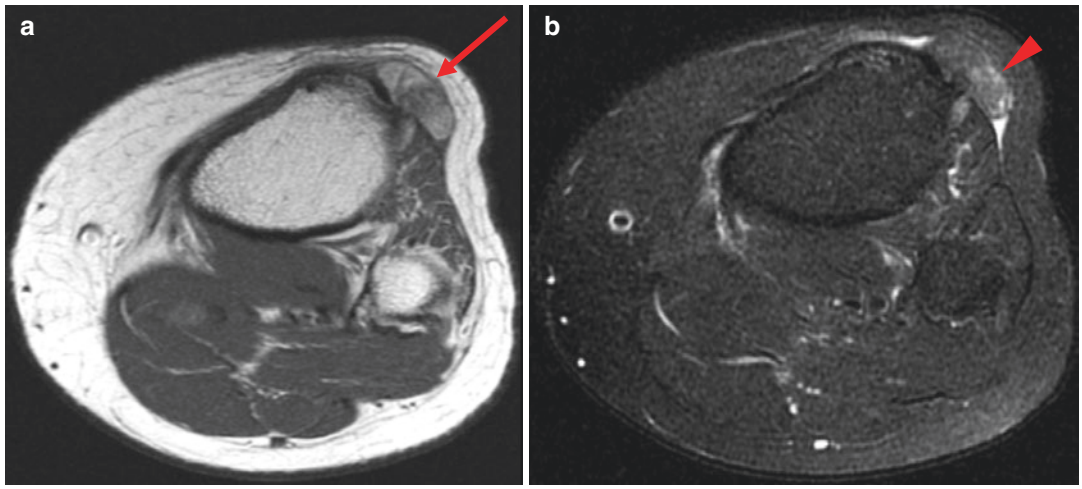

Fig. 4.10 Angiolipoma. Axial T1WI (**a**) shows a perifascial fatty mass (*arrow*) with heterogeneous signal intensity on the anterior proximal lower leg. Axial FS T2WI (**b**) demonstrates suppressed fat components with some hyperintense areas (*arrowhead*). Axial postcontrast FS T1WI (**c**) shows heterogeneous enhancement with a small intramuscular extension (*arrow*) into the tibialis anterior

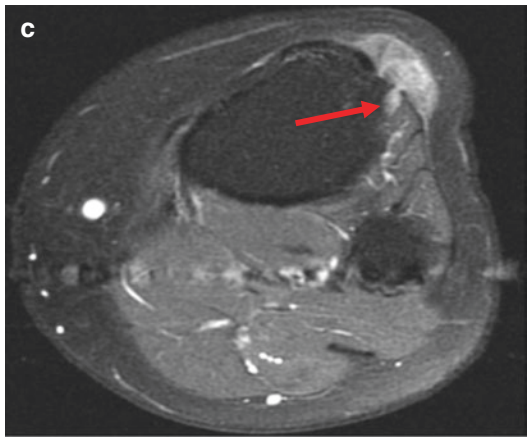

Fig. 4.10 (continued)

4.13.6 Spindle Cell Lipoma

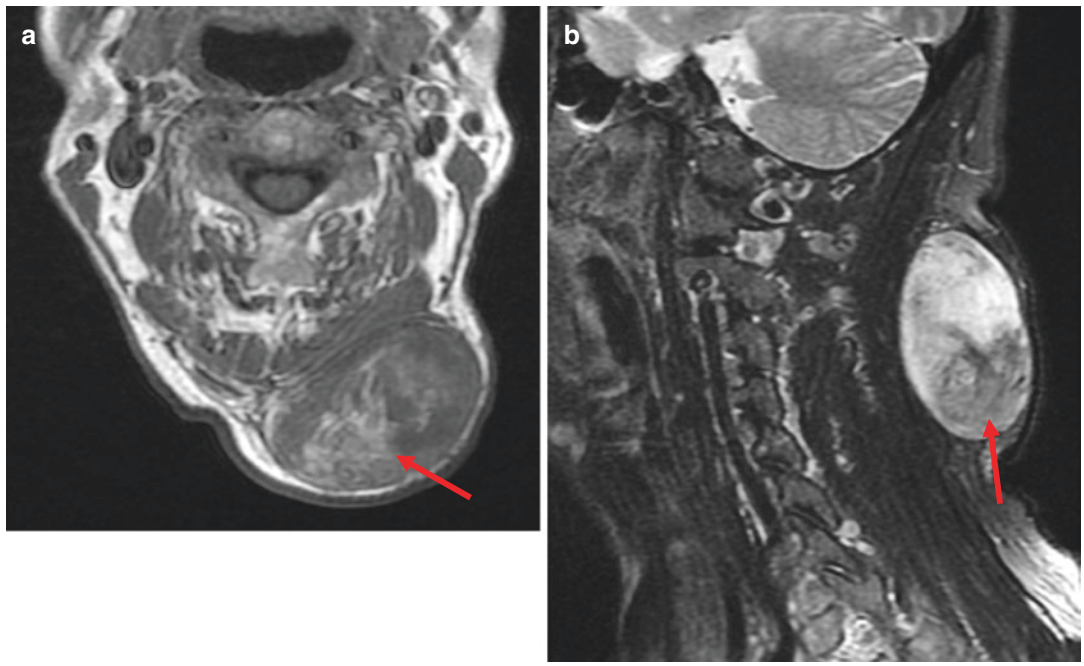

Fig. 4.11 Spindle cell lipoma. Axial T1WI (**a**) shows a well-circumscribed subcutaneous mass in the posterior neck. The mass appears as a mixture of fat (*arrow*) and nonadipose components. Sagittal FS T2WI (**b**) shows a large area of hyperintensity and hypointense fat components (*arrow*). Axial postcontrast FS T1WI (**c**) shows heterogeneous enhancement in the nonadipose elements. (**d**) Gross appearance of spindle cell lipoma showing a predominantly fatty lesion without hemorrhage or necrosis

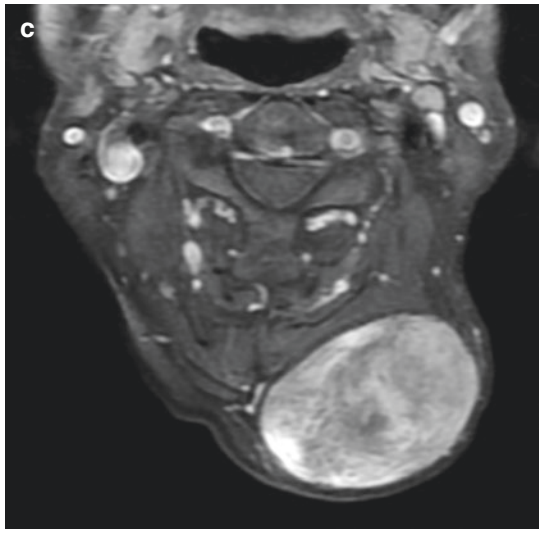

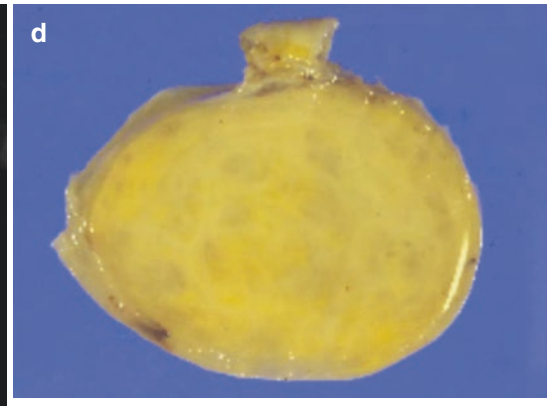

Fig. 4.11 (continued)

4.13.7 Hibernoma

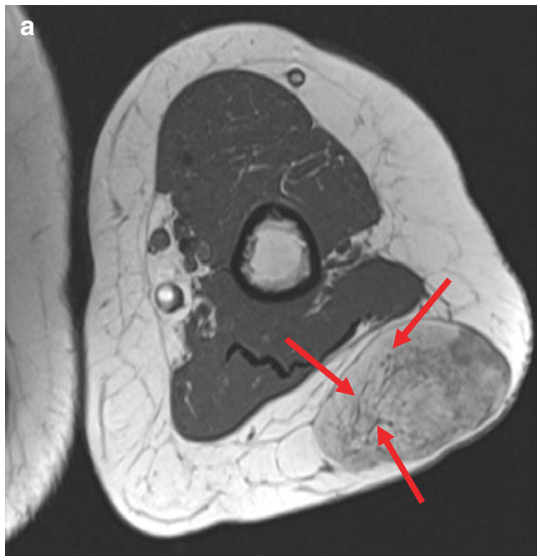

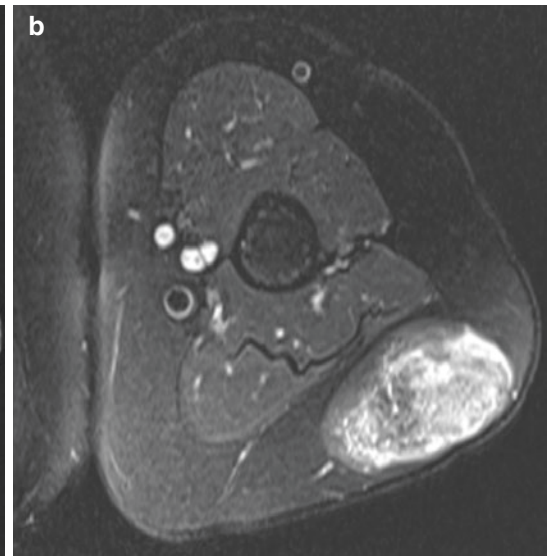

Fig. 4.12 Hibernoma. Axial T1WI (**a**) shows a subcutaneous mass slightly hypointense to the surrounding fat tissues in the left posterior upper arm. There are linear or dot-like structures (*arrows*) in keeping with blood vessels. Axial FS T2WI (**b**) and postcontrast FS T1WI (**c**) show a large area of T2 hyperintensity or prominent contrast enhancement

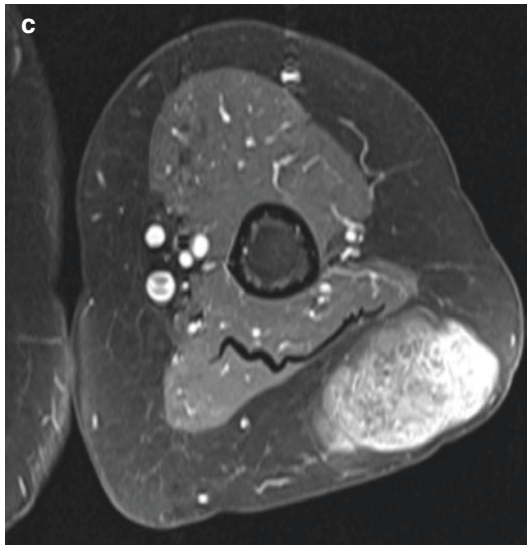

Fig. 4.12 (continued)

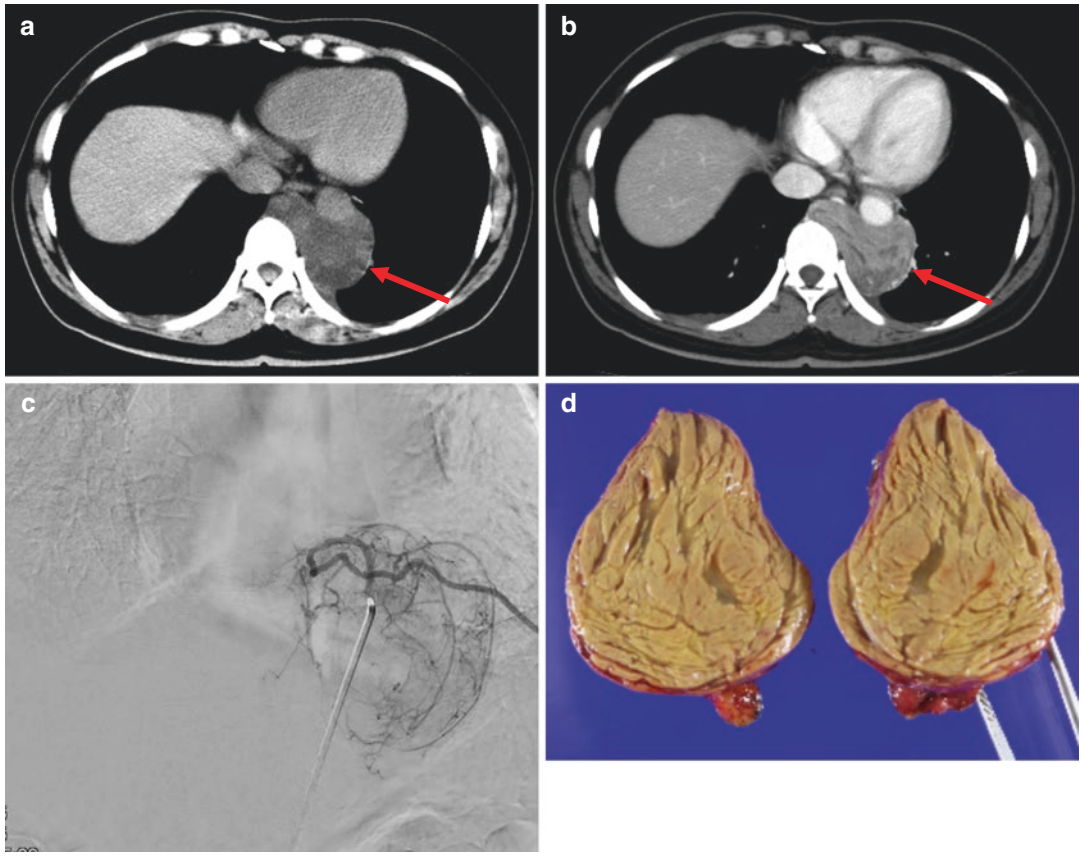

Fig. 4.13 Hibernoma. Precontrast CT scan (**a**) shows a left posterior mediastinal mass (*arrow*) with heterogeneous low attenuation (mean HU 10). Postcontrast CT scan (**b**) shows prominent enhancement of the mass (*arrow*), with hypoattenuating components. (**c**) Left ninth intercostal arteriogram demonstrates marked vascularity of the tumor. (**d**) Cut section of the mass, showing a yellowish solid mass with streaky areas of myxoid changes

4.13.8 Lipoma Arborescens

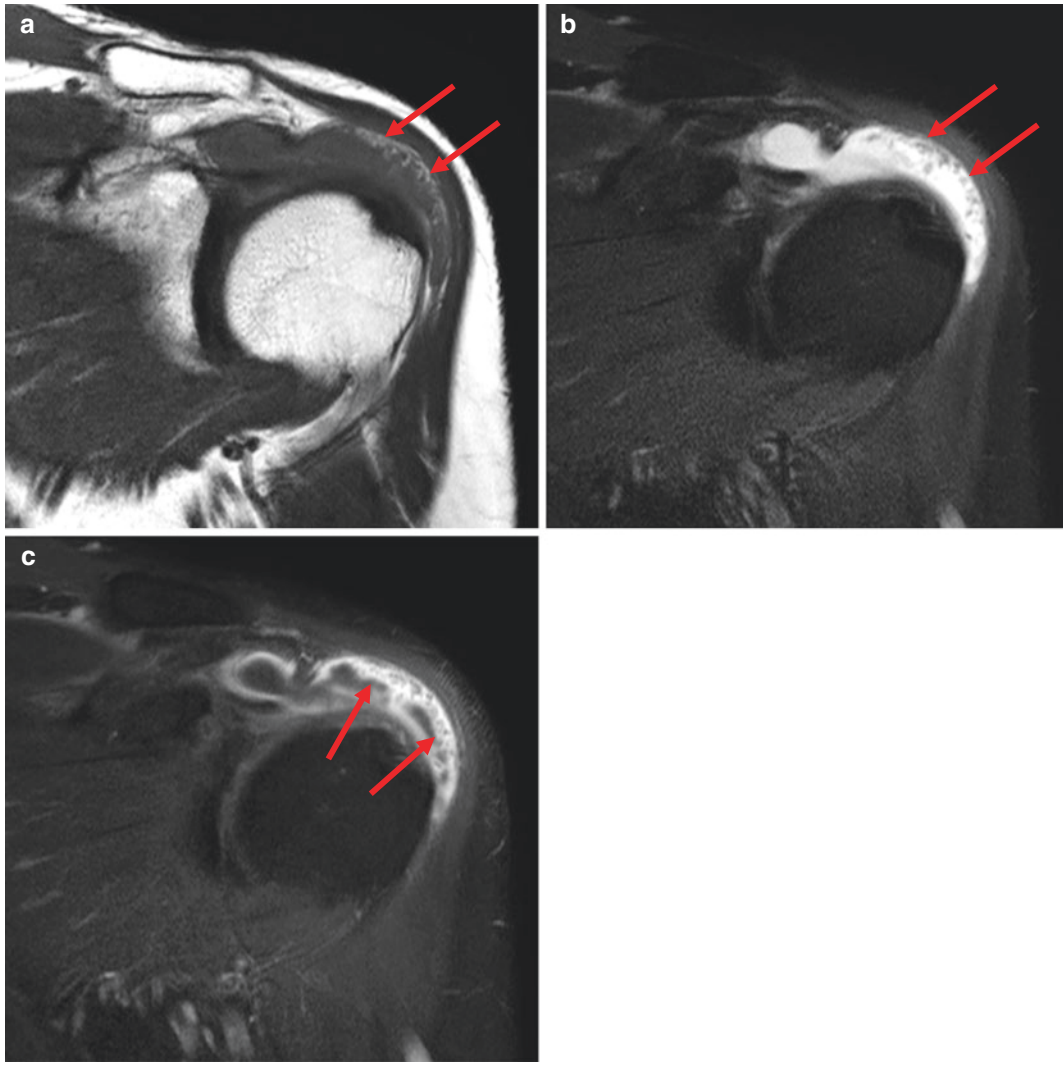

Fig. 4.14 Lipoma arborescens. Oblique coronal T1WI and FS T2WI (**a**, **b**) show lipomatous villous proliferation (*arrows*) within the subacromial subdeltoid bursa. Oblique coronal postcontrast FS T1WI (**c**) shows prominent synovial enhancement (*arrows*) lining over the villous subsynovial fat proliferation

4.13.9 Well-Differentiated Liposarcoma

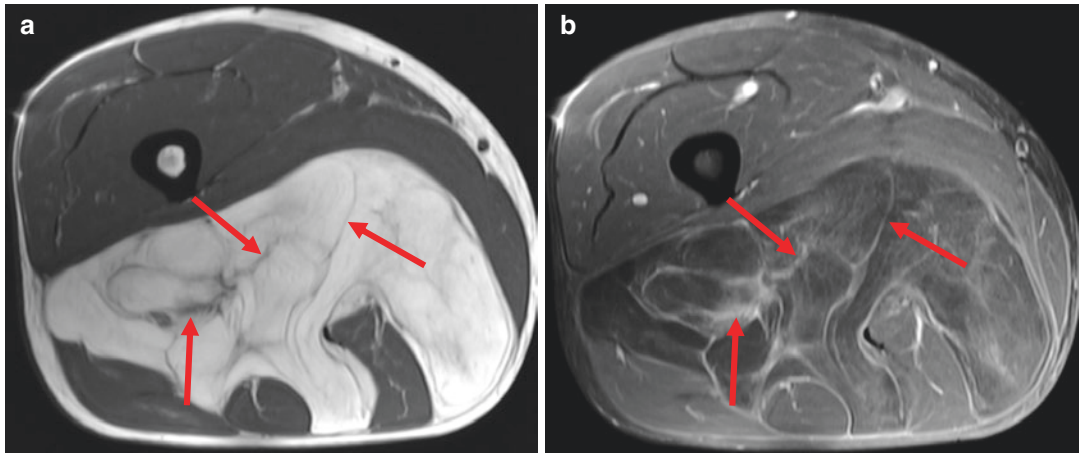

Fig. 4.15 Well-differentiated liposarcoma. Axial T1WI and postcontrast FS T1WI (**a**, **b**) show a very large lipomatous mass in the intermuscular planes of the right posterior thigh. There are multiple septa (*arrows*) with prominent enhancement

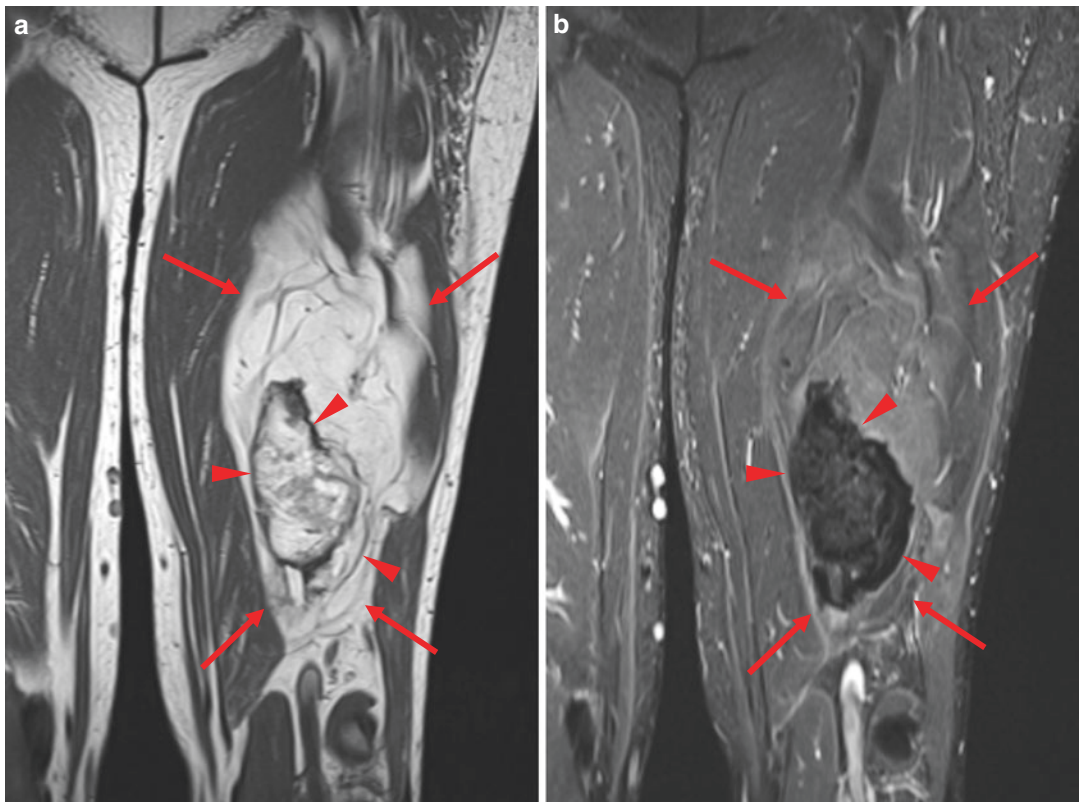

Fig. 4.16 Well-differentiated liposarcoma. Coronal T1WI and STIR (**a**, **b**) show a huge fatty mass (*arrows*) in the left posterior thigh. An intratumoral, non-enhancing geographic area of fat necrosis (*arrowheads*) is seen

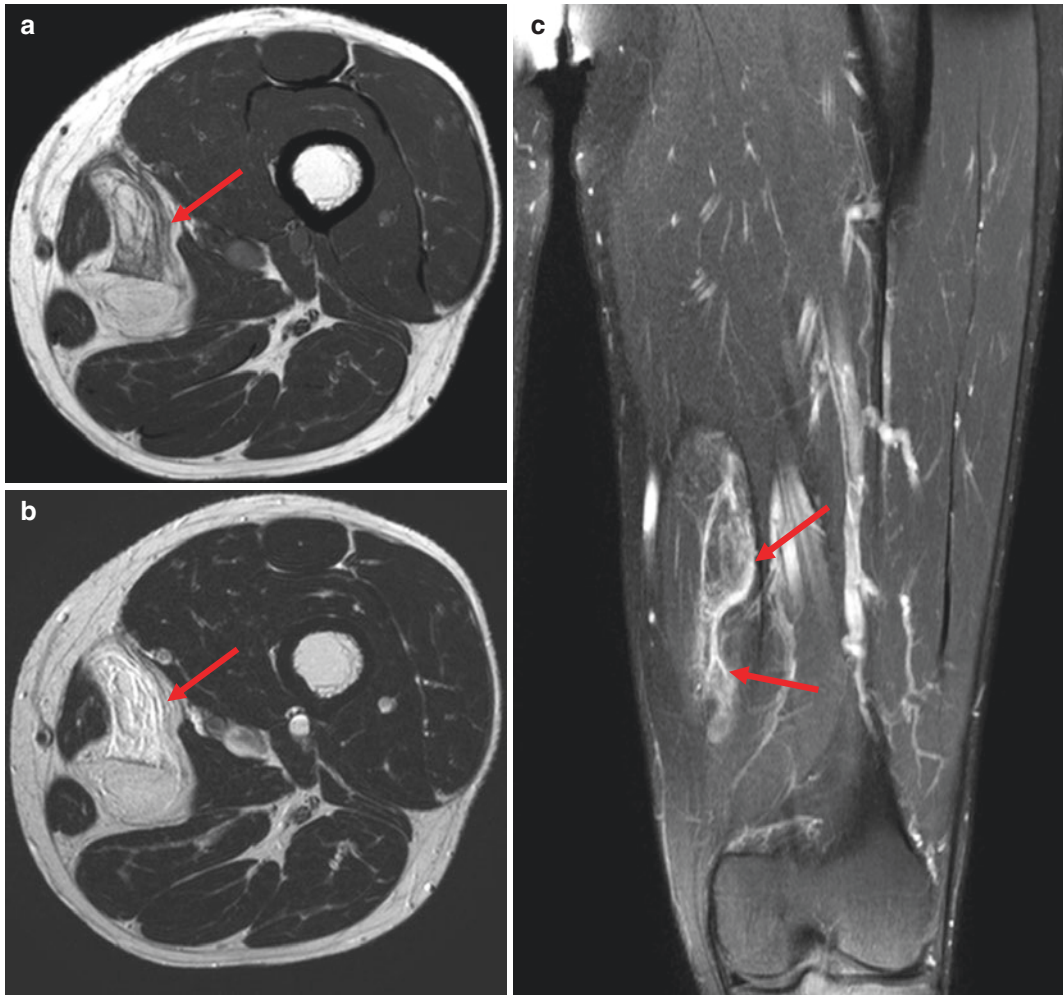

Fig. 4.17 Well-differentiated liposarcoma, sclerosing variant. Axial T1WI and T2WI (**a**, **b**) show an intermuscular fatty mass with hazy and streaky nonadipose components (*arrow*). Coronal postcontrast FS T1WI (**c**) shows prominent enhancement of the nonlipomatous elements (*arrows*)

4.13.10 Dedifferentiated Liposarcoma

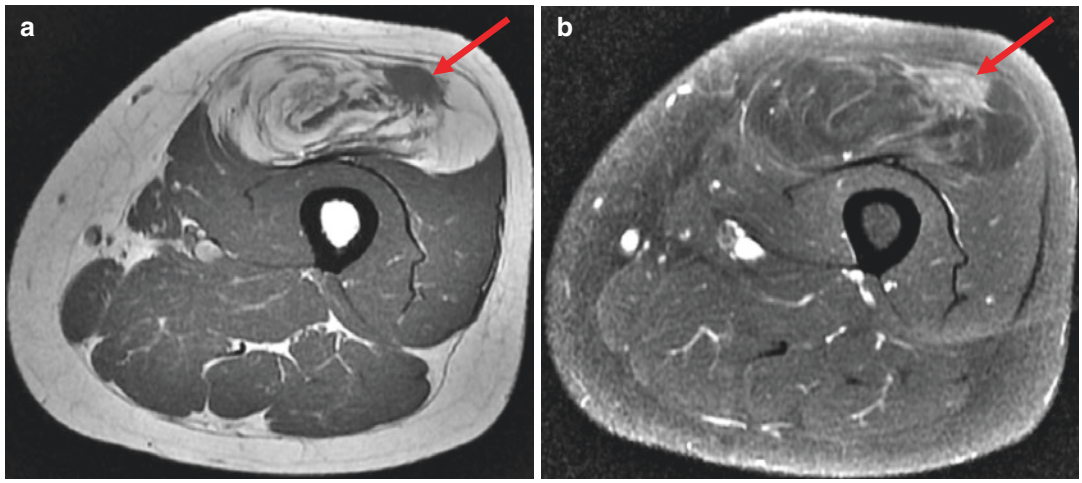

Fig. 4.18 Dedifferentiated liposarcoma. Axial T1WI and postcontrast FS T1WI (**a**, **b**) show an intramuscular fatty tumor with an enhancing nonlipomatous mass (*arrow*) in the left anterior thigh

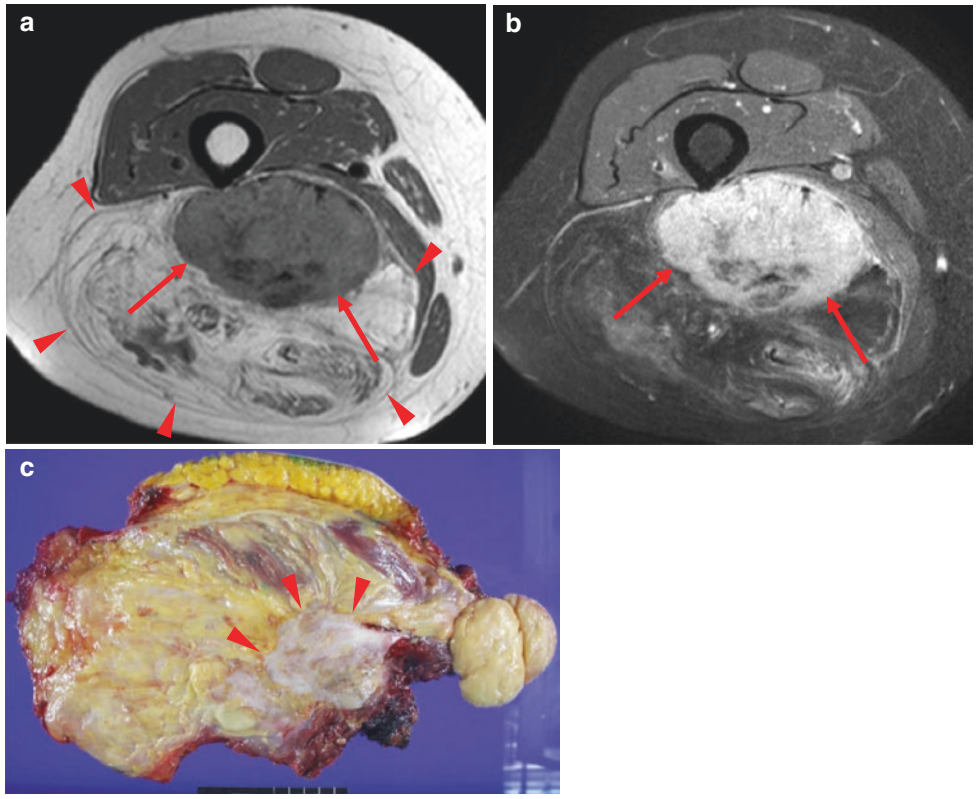

Fig. 4.19 Dedifferentiated liposarcoma. Axial T1WI and postcontrast FS T1WI (**a**, **b**) show diffuse fatty replacement of the posterior compartment (*arrowheads*) of the right thigh. A vividly enhancing mass of high-grade sarcoma is seen with abrupt transition (*arrows*) from well-differentiated liposarcoma. (**c**) Gross appearance of dedifferentiated liposarcoma showing a distinct margin (*arrowheads*) between well-differentiated and dedifferentiated zones

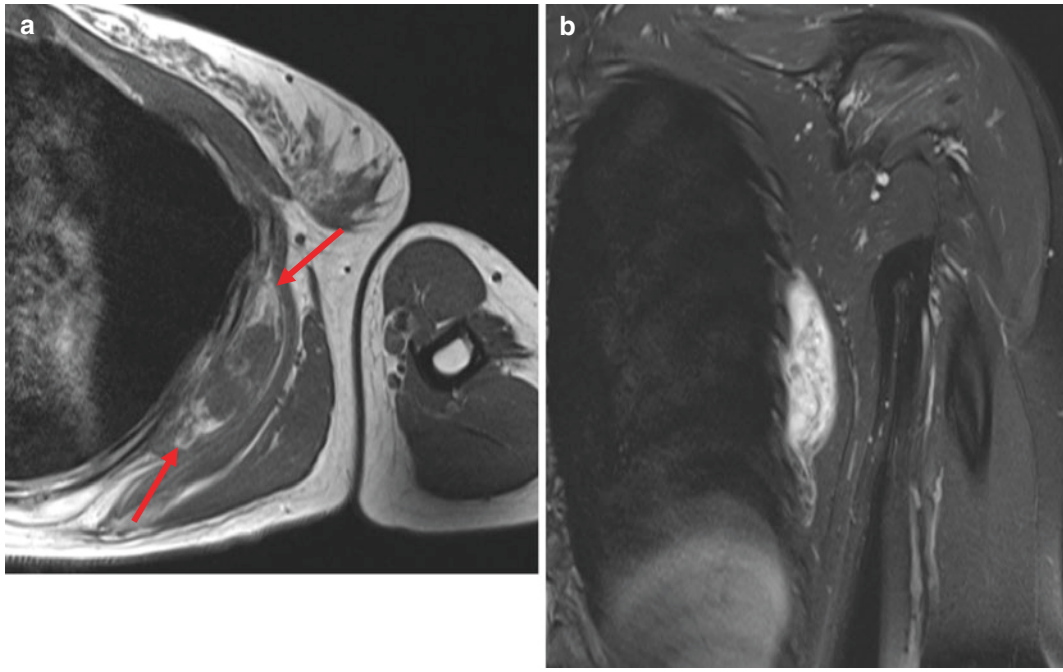

Fig. 4.20 Dedifferentiated liposarcoma. Axial T1WI (**a**) shows a soft tissue mass (*arrows*) between the serratus anterior and the rib cage. The mass consists of fat tissue and nonadipose components. Coronal FS T2WI (**b**) shows a hyperintense nature of the mass with central heterogeneous signal intensity

4.13.11 Myxoid Liposarcoma

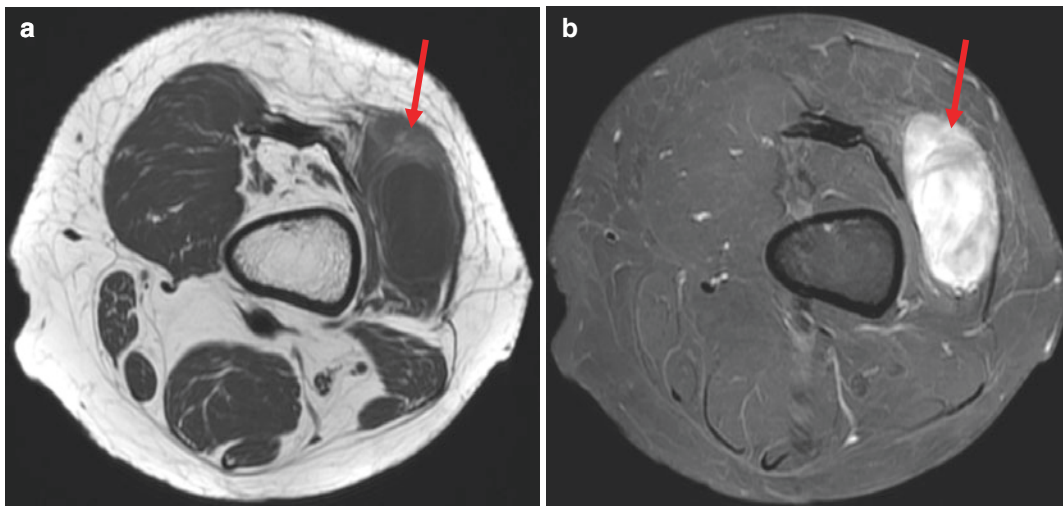

Fig. 4.21 Myxoid liposarcoma. Axial T1WI (**a**) shows a subfascial mass in the vastus lateralis muscle with T1 hypointensity. Small area of fat (*arrow*) is seen on the anterior side of the mass. Axial FS T2WI (**b**) shows a hyperintense myxoid tumor with an area of fat suppression (*arrow*). Axial postcontrast FS T1WI (**c**) shows prominent enhancement

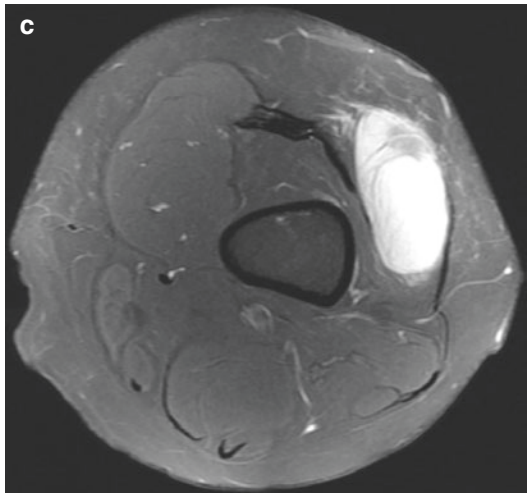

Fig. 4.21 (continued)

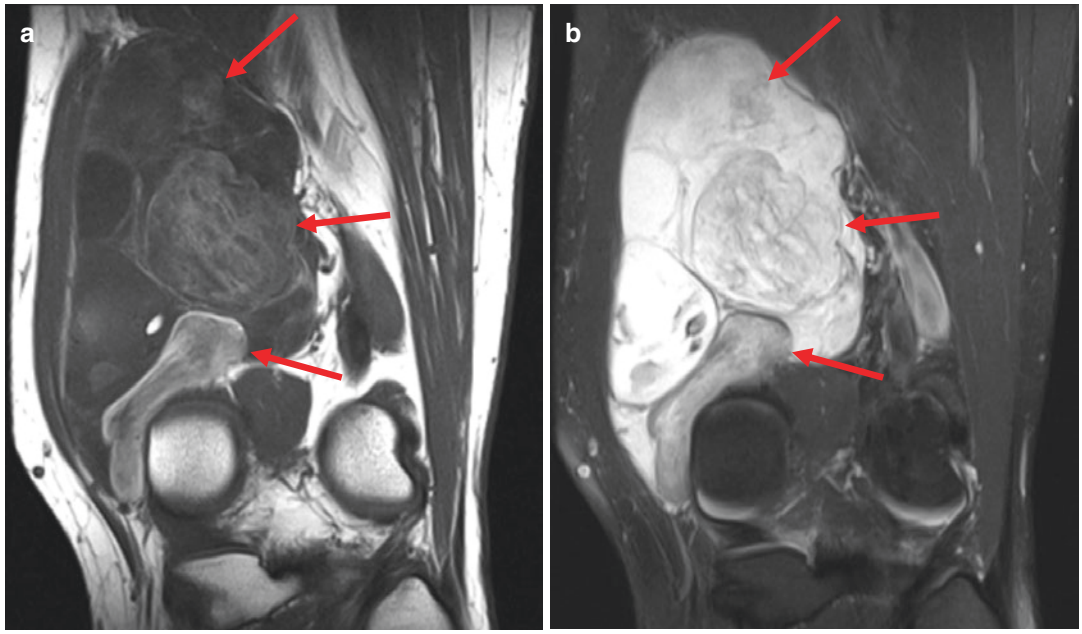

Fig. 4.22 Myxoid liposarcoma. Coronal T1WI (**a**) shows a large lobulated mass in the left distal posterior thigh intermuscular fat plane. There are T1 hypointense (myxoid tissue) and hyperintense (fat components, *arrows*) areas. Coronal FS T2WI (**b**) shows bright high signal in keeping with myxoid tumor. Fatty areas (*arrows*) are of relatively low signal intensity due to fat suppression. Coronal postcontrast FS T1WI (**c**) shows heterogeneous and intense enhancement

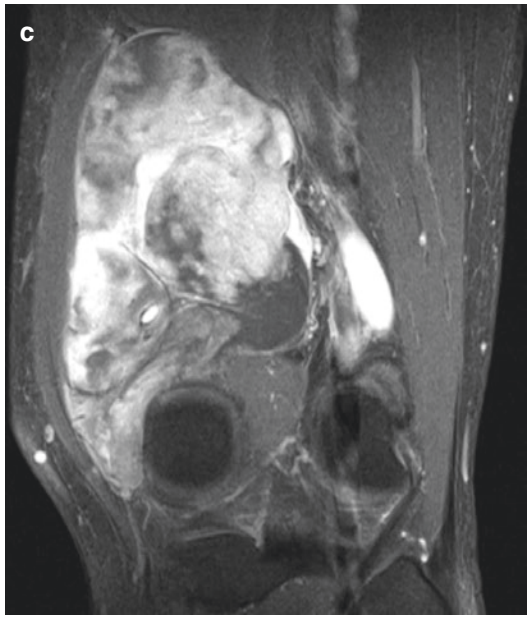

Fig. 4.22 (continued)

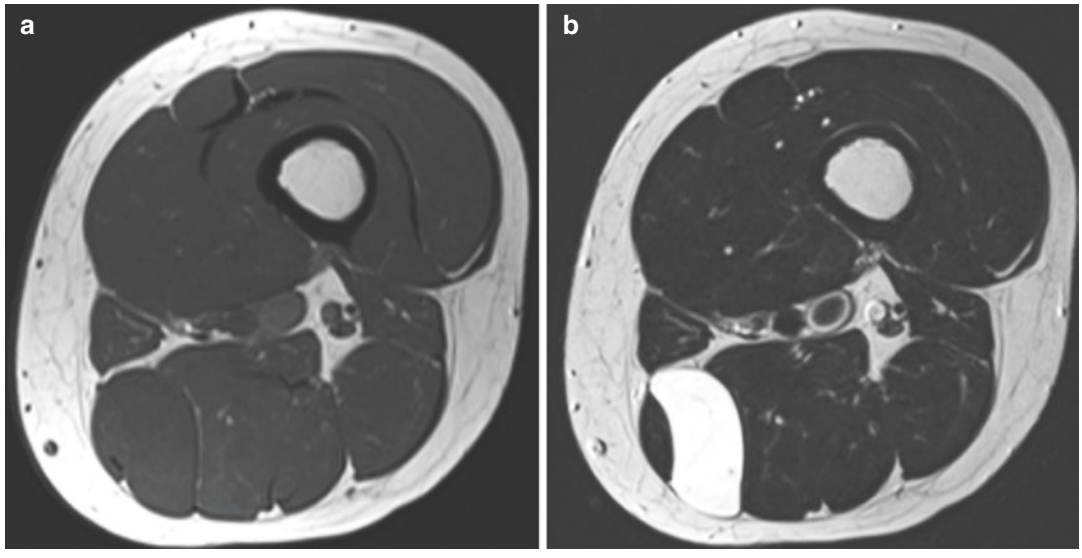

Fig. 4.23 Myxoid liposarcoma. Axial T1WI (**a**) shows a subfascial mass isointense to muscle in the gracilis muscle. There is no discernible intratumoral fat. Axial T2WI (**b**) shows a cyst-like T2 hyperintense mass. Axial post-contrast FS T1WI (**c**) shows homogeneous enhancement suggestive of myxoid tumor rather than cystic mass

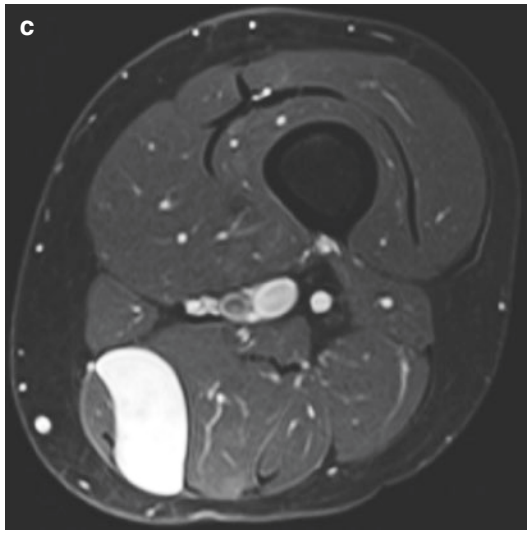

Fig. 4.23 (continued)

4.13.12 Pleomorphic Liposarcoma

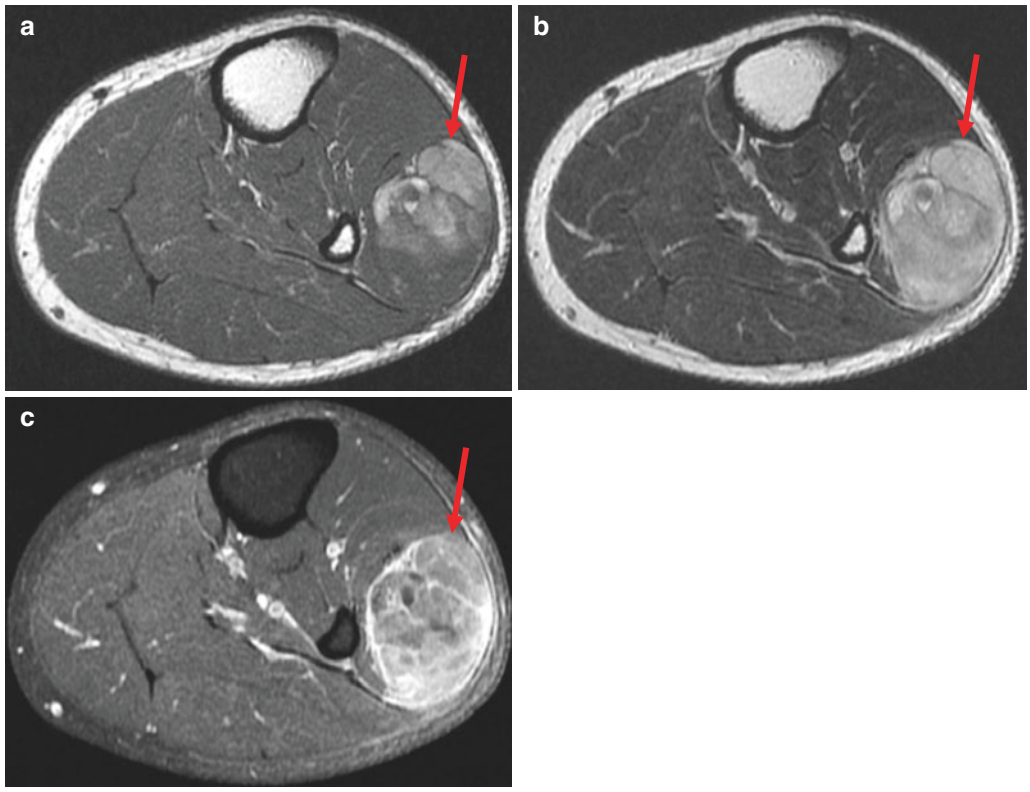

Fig. 4.24 Pleomorphic liposarcoma. Axial T1WI and T2WI (**a**, **b**) show an intramuscular mass of the peroneus longus in the left proximal lower leg. The mass consists of the anterior half of fat-like signal (*arrow*) and the posterior part of nonspecific signal. Axial postcontrast FS T1WI (**c**) shows more prominent enhancement on the posterior portion of the tumor than on the anterior fat-containing area (*arrow*)

References

Bancroft LW, Kransdorf MJ, Peterson JJ, O'Connor MI. Benign fatty tumors: classification, clinical course, imaging appearance, and treatment. Skelet Radiol. 2006;35(10):719–33. doi:10.1007/s00256-006-0189-y.

Bancroft LW, Pettis C, Wasyliw C. Imaging of benign soft tissue tumors. Semin Musculoskelet Radiol. 2013;17(2):156–67. doi:10.1055/s-0033-1343071.

Bestic JM, Kransdorf MJ, White LM, Bridges MD, Murphey MD, Peterson JJ, Garner HW. Sclerosing variant of well-differentiated liposarcoma: relative prevalence and spectrum of CT and MRI features. AJR Am J Roentgenol. 2013;201(1):154–61. doi:10.2214/AJR.12.9462.

Chae EY, Chung HW, Shin MJ, Lee SH. Lipoma arborescens of the glenohumeral joint causing bone erosion: MRI features with gadolinium enhancement. Skelet Radiol. 2009;38(8):815–8. doi:10.1007/s00256-009-0686-x.

Coll JP, Ragsdale BD, Chow B, Daughters TC. Best cases from the AFIP: lipoma arborescens of the knees in a patient with rheumatoid arthritis. Radiographics. 2011;31(2):333–7. doi:10.1148/rg.312095209.

Dei Tos AP. Liposarcomas: diagnostic pitfalls and new insights. Histopathology. 2014;64(1):38–52. doi:10.1111/his.12311.

Drevelegas A, Pilavaki M, Chourmouzi D. Lipomatous tumors of soft tissue: MR appearance with histological correlation. Eur J Radiol. 2004;50(3):257–67. doi:10.1016/j.ejrad.2004.01.022.

El Ouni F, Jemni H, Trabelsi A, Ben Maitig M, Arifa N, Ben Rhouma K, Ben Ayech M, Tlili K. Liposarcoma of the extremities: MR imaging features and their correlation with pathologic data. Orthop Traumatol Surg Res. 2010;96(8):876–83. doi:10.1016/j.otsr.2010.05.010.

Garner HW, Bestic JM. Benign synovial tumors and proliferative processes. Semin Musculoskelet Radiol. 2013;17(2):177–8. doi:10.1055/s-0033-1343095.

Gupta P, Potti TA, Wuertzer SD, Lenchik L, Pacholke DA. Spectrum of fat-containing soft-tissue masses at MR imaging: the common, the uncommon, the characteristic, and the sometimes confusing. Radiographics. 2016;36(3):753–66. doi:10.1148/rg.2016150133.

Henze J, Bauer S. Liposarcomas. Hematol Oncol Clin North Am. 2013;27(5):939–55. doi:10.1016/j.hoc.2013.07.010.

Khashper A, Zheng J, Nahal A, Discepola F. Imaging characteristics of spindle cell lipoma and its variants. Skelet Radiol. 2014;43(5):591–7. doi:10.1007/s00256-014-1834-5.

Kind M, Stock N, Coindre JM. Histology and imaging of soft tissue sarcomas. Eur J Radiol. 2009;72(1):6–15. doi:10.1016/j.ejrad.2009.05.023.

Kirwadi A, Abdul-Halim R, Fernando M, Highland A, Kotnis N. MR imaging features of spindle cell lipoma. Skelet Radiol. 2014;43(2):191–6. doi:10.1007/s00256-013-1765-6.

Kitagawa Y, Miyamoto M, Konno S, Makino A, Maruyama G, Takai S, Higashi N. Subcutaneous angiolipoma: magnetic resonance imaging features with histological correlation. J Nippon Med Sch. 2014;81(5):313–9.

Kransdorf MJ, Bancroft LW, Peterson JJ, Murphey MD, Foster WC, Temple HT. Imaging of fatty tumors: distinction of lipoma and well-differentiated liposarcoma. Radiology. 2002;224(1):99–104. doi:10.1148/radiol.2241011113.

Liu W, Bui MM, Cheong D, Caracciolo JT. Hibernoma: comparing imaging appearance with more commonly encountered benign or low-grade lipomatous neoplasms. Skelet Radiol. 2013;42(8):1073–8. doi:10.1007/s00256-013-1583-x.

Moholkar S, Sebire NJ, Roebuck DJ. Radiological-pathological correlation in lipoblastoma and lipoblastomatosis. Pediatr Radiol. 2006;36(8):851–6. doi:10.1007/s00247-006-0175-5.

Murphey MD, Arcara LK, Fanburg-Smith J. From the archives of the AFIP: imaging of musculoskeletal liposarcoma with radiologic-pathologic correlation. Radiographics. 2005;25(5):1371–95. doi:10.1148/rg.255055106.

Murphey MD, Carroll JF, Flemming DJ, Pope TL, Gannon FH, Kransdorf MJ. From the archives of the AFIP: benign musculoskeletal lipomatous lesions. Radiographics. 2004;24(5):1433–66. doi:10.1148/rg.245045120.

Ohguri T, Aoki T, Hisaoka M, Watanabe H, Nakamura K, Hashimoto H, Nakamura T, Nakata H. Differential diagnosis of benign peripheral lipoma from well-differentiated liposarcoma on MR imaging: is comparison of margins and internal characteristics useful? AJR Am J Roentgenol. 2003;180(6):1689–94. doi:10.2214/ajr.180.6.1801689.

Ritchie DA, Aniq H, Davies AM, Mangham DC, Helliwell TR. Hibernoma—correlation of histopathology and magnetic-resonance-imaging features in 10 cases. Skelet Radiol. 2006;35(8):579–89. doi:10.1007/s00256-006-0114-4.

Salem R, Zohd M, Njim L, Maazoun K, Jellali MA, Zrig A, Mnari W, Harzallah W, Nouri A, Zakhama A, Golli M. Lipoblastoma: a rare lesion in the differential diagnosis of childhood mediastinal tumors. J Pediatr Surg. 2011;46(5):e21–3. doi:10.1016/j.jpedsurg.2011.01.030.

Sung MS, Kang HS, Suh JS, Lee JH, Park JM, Kim JY, Lee HG. Myxoid liposarcoma: appearance at MR imaging with histologic correlation. Radiographics. 2000;20(4):1007–19. doi:10.1148/radiographics.20.4.g00jl021007.

Van Breuseghem I, Sciot R, Pans S, Geusens E, Brys P, De Wever I. Fibrolipomatous hamartoma in the foot: atypical MR imaging findings. Skelet Radiol. 2003;32(11):651–5. doi:10.1007/s00256-003-0684-3.

Wortman JR, Tirumani SH, Jagannathan JP, Tirumani H, Shinagare AB, Hornick JL, Ramaiya NH. Primary extremity liposarcoma: MRI features, histopathology, and clinical outcomes. J Comput Assist Tomogr. 2016a; doi:10.1097/rct.0000000000000431.

Wortman JR, Tirumani SH, Tirumani H, Shinagare AB, Jagannathan JP, Hornick JL, Ramaiya NH. Neoadjuvant radiation in primary extremity liposarcoma: correlation of MRI features with histopathology. Eur Radiol. 2016b;26(5):1226–34. doi:10.1007/s00330-015-3953-3.

Fibroblastic/Myofibroblastic Tumors

5

Fibroblastic and myofibroblastic tumors are a group of mesenchymal tumors that encompass a wide spectrum of benign, intermediate, and malignant lesions. Fibroblasts are the most common cells in fibrous connective tissue and make procollagen, protoelastin, and glycosaminoglycans. Myofibroblasts are a differentiated cell type that are essential for wound healing, participating in tissue remodeling following insults. Myofibroblasts are typically activated fibroblasts, although they can also be derived from other cell types, including epithelial cells, endothelial cells, and mononuclear cells (Watsky et al. 2010). An important step of forward in the 2013 WHO classification of benign fibroblastic/myofibroblastic lesions has been the recognition that nodular fasciitis, and by analogy the variants proliferative fasciitis and proliferative myositis, are in fact neoplastic (Fletcher 2014). Other notable changes in this category include the complete omission of "hemangiopericytoma," the prior synonym of extrapleural solitary fibrous tumor (Jo and Fletcher 2014).

5.1 Nodular Fasciitis

Nodular fasciitis is a self-limiting reactive process of fibroblastic/myofibroblastic differentiation and the most common benign soft tissue tumor of fibrous origin. The lesion often comes to clinical attention due to its rapid growth, rich cellularity, and mitotic activity and can be misdiagnosed as a sarcoma. It usually presents as a rapidly growing mass, and the most common location is the upper extremity, followed by the trunk, head and neck, and lower extremity. This tumor occurs in subcutaneous, fascial, or intramuscular locations. The pathologic diagnosis is made by identifying immature plump fibroblasts that are similar in size, arranged in short irregular bundles and fascicles, a "feathery" appearance, and abundant myxoid changes (Khuu et al. 2014).

Imaging findings of nodular fasciitis are variable and nonspecific as it manifests diverse histologic subtypes composed of myxoid, cellular, and fibrous components. MR imaging shows homogeneous T1 hypointensity, heterogeneous T2 hyperintensity, and heterogeneous enhancement. Some lesions demonstrate an "inverted target sign," with a discrete central T2 hyperintensity, peripheral T2 hypointensity, and a central area that does not enhance following contrast administration (Luo et al. 2014). On US, nodular fasciitis appears as a hypoechoic mass with mixed echogenicity. A "fascial tail" may suggest nodular fasciitis as a potential diagnosis (Khuu et al. 2014).

5.2 Proliferative Fasciitis

Proliferative fasciitis is characterized by a diffuse infiltrative fibroblastic growth that is intimately associated with multifocal proliferation of large basophilic cells, closely resembling ganglion

H.S. Kang et al., *Oncologic Imaging: Soft Tissue Tumors*, DOI 10.1007/978-981-287-718-5_5

cells. The lesion may be confused with sarcoma because of its rapid growth and its bizarre histologic features; however, the lesion is adequately treated by local excision, and there is no indication for radical surgery (Chung and Enzinger 1975).

The imaging appearance of proliferative fasciitis has not been well described. The upper extremity is the most common anatomical location, and most lesions occur in the subcutaneous layer.

5.3 Proliferative Myositis

Proliferative myositis is a rare fibroblastic reactive soft tissue lesion and is the intramuscular counterpart of proliferative fasciitis. Patients with proliferative myositis present with a firm, rapidly growing mass that can double in size within several days. Proliferative myositis diffusely involves the muscular tissue, and there is extensive fibroblast proliferation in the perimysium and epimysium between muscle fascicles.

Transverse US images may show a characteristic checkerboard pattern, which has been described as a thick hypoechoic "scaffolding" that resembles dry, cracked mud (Sarteschi et al. 1997). Longitudinal images reveal the continuity of muscle fibers. On MR imaging, proliferative myositis appears as an expansile mass of the muscle, preserving the muscle fascicles without disruption. The lesion appears hypointense or isointense on T1-weighted images and moderately or markedly hyperintense on T2-weighted images. After intravenous injection of the contrast agent, the lesion demonstrates prominent enhancement. On axial T2-weighted and postcontrast T1-weighted images, geometrical patterns of internal strands of fibroblastic proliferation, which are hyperintense compared to muscle fascicles, are observed within the lesion. This appearance is suggestive of the aforementioned checkerboard-like pattern. Another MR imaging finding of proliferative myositis is perilesional edema and contrast enhancement that extends to the surrounding fascia (Yigit et al. 2009).

5.4 Myositis Ossificans

Historically, the term myositis ossificans (MO) has been used to describe a broad spectrum of conditions, ranging from benign solitary lesions to progressive congenital syndromes (Walczak et al. 2015). Recently, MO has been defined as a benign, solitary, ossifying soft tissue mass that most commonly occurs in the skeletal muscle. MO can also be found in other sites, such as the subcutaneous layer or the fascial planes. MO often has been used interchangeably with heterotopic ossification (HO), which is the formation of bone outside the skeletal system. HO is considered more comprehensive than MO given that the pathologic process of HO can occur in variable sites, such as the skin, subcutaneous tissue, skeletal muscle, fibrous tissue adjacent to joints, blood vessels, ligaments, and mesentery (Mavrogenis et al. 2011).

Three overlapping stages of progression of MO have been defined using the following criteria (Kransdorf et al. 1991). Early lesions primarily consist of a nonossified central core of proliferating benign fibroblasts and myofibroblasts, with a minor component of osteoid and mature lamellar bone at the periphery. Hyaline cartilage can be present as part of the endochondral calcification. Intermediate lesions have either minor or no proliferating fibroblastic core, consisting almost entirely of osteoid rimmed by active osteoblasts and surrounded by a shell of mature lamellar bone. Late lesions consist exclusively of mature lamellar bone.

Radiographs show a soft tissue mass, and the calcification may first appear at 3 or 4 weeks. Over the next few weeks, flocculent calcifications deposit at the periphery of the mass. These calcifications mature during the next several weeks and become coarser and denser. The central zone of the lesion remains lucent or lightly mineralized in late (mature) lesions. CT is the best modality for depicting this zonal phenomenon of calcification in MO.

MR imaging is the most important imaging study for patients with MO. In early lesions, MO appears as a heterogeneous soft tissue mass with increased signal intensity on T2-weighted images

and is accompanied by extensive, diffuse surrounding edema. The margins of early lesions may be difficult to separate from the surrounding edema. When hematoma is present within MO, the area is hyperintense on T1-weighted images and does not enhance after contrast administration. Curvilinear and irregular areas of decreased signal intensity can be observed surrounding intermediate lesions, indicating zonal phenomenon. Adjacent soft tissue edema may persist or disappear at this stage. Late lesions are well-defined masses with a central fat signal surrounded by a low signal rim. The adjacent soft tissue edema is completely resolved around mature lesions.

5.5 Elastofibroma

Elastofibroma dorsi is a benign fibroelastic tumor of unknown etiology. Histologically, it is composed primarily of hyalinized collagen with scattered fibroblasts and entrapped islands of mature adipose tissue. In all cases, variable numbers of characteristically enlarged, hypereosinophilic, refractile, elastic fibrils are present (Kudo 2001). Elastofibroma dorsi is usually found in the infrascapular regions, deep to the serratus anterior and latissimus dorsi muscles. Elastofibroma rarely occurs in other locations, such as the hand, foot, greater trochanter, ischial tuberosity, olecranon, and epidural space.

Imaging findings of elastofibroma dorsi are characteristic in its typical location (i.e., in the infrascapular region). CT and MR imaging show a crescent-shaped soft tissue mass between the rib cage and posterolateral chest wall muscles. CT demonstrates low-attenuation fatty streaks within the mass. On T1-weighted MR images, elastofibroma dorsi appears isointense to the skeletal muscle and may have linear strands of fat. A relatively low signal intensity (slightly higher than muscles) on T2-weighted images can be observed due to dense fibrous connective tissue. The degree of enhancement on CT or MR imaging is variable, from mild to prominent. Elastofibroma has a typical sonographic appearance consisting of arrays of linear strands against an echogenic background. However, in some cases, the sonographic pattern of elastofibroma dorsi may be very similar to that of the surrounding muscular tissue. In these cases, the elastofibroma may be very difficult to distinguish from surrounding tissue (Ozpolat et al. 2008).

5.6 Fibrous Hamartoma of Infancy

Fibrous hamartoma of infancy (FHI) typically presents as a solitary, painless, skin-colored subcutaneous nodule, which is usually freely movable. Most lesions occur within the first year of life, and variable growth rates have been described. This tumor can become quite large, but the size is usually less than 5 cm (Chang et al. 2010). Microscopic evaluation consistently reveals a mixture of three tissue types in varying proportions as follows: well-defined bundles of dense fibrous connective tissue, primitive mesenchyme, and interposed mature adipose tissue (Stensby et al. 2014).

MR images generally reflect the histological characteristics of FHI with the three different tissues. The interspersed fat content of the tumor usually accounts for the high signal intensity on T1-weighted images. Soft tissue strands consisting of mesenchymal and fibrous components appear as T1 hypointense, STIR hyperintense, enhancing tissues. The intervening hypointense septa always reflect the presence of dense fibrous trabeculae.

5.7 Fibromatosis Colli

Fibromatosis colli is an uncommon benign fusiform mass of the sternocleidomastoid, which presents as a slow-growing, palpable neck mass. The affected patients are usually within the first 8 weeks of life, and there is a slight male predominance. Most patients present with unilateral disease. In approximately 20% of cases, there is associated torticollis, causing an ipsilateral tilt of the head and contralateral rotation of the face and chin. In addition, it is thought that 6–20% of affected infants will have associated musculoskeletal abnormalities, such as facial

asymmetry and hip dysplasia (Skelton and Howlett 2014).

US is the imaging modality of choice for diagnosis of fibromatosis colli. It appears as a diffuse or focal enlargement of the sternocleidomastoid and involves the lower two-thirds of the muscle. Fibromatosis colli is typically fusiform in shape and has variable echogenicity as follows: hyperechoic, isoechoic or hypoechoic. CT imaging of fibromatosis colli demonstrates focal or diffuse isodense enlargement of the sternocleidomastoid muscle. On MR imaging, there may be a decrease in signal intensity on T2-weighted images due to the presence of fibrous tissue; however, the signal characteristics may vary, similar to its echogenicity on US (Ablin et al. 1998; Skelton and Howlett 2014).

5.8 Fibroma of Tendon Sheath

The designation "fibroma of tendon sheath" has been used to describe a group of clinically and pathologically similar lesions occurring in the distal aspects of the extremities (Pulitzer et al. 1989). This tumor has a predilection for the flexor aspect of the digits and palm and is frequently attached to the tendon sheath. The tumor has circumscribed margins with spindle/stellate cells in a collagenous stroma and slit-like vessels. Many tumors show areas of hypercellularity adjacent to areas of hypocellularity (Al-Qattan 2014).

The diagnosis of fibroma of the tendon sheath is favored when the mass is located in an upper extremity adjacent to a tendon and MR imaging shows a focal nodular mass with decreased signal on all pulse sequences and little or no enhancement. Fibroma of the tendon sheath, however, can have different imaging features if areas of increased cellularity or myxoid change are present (Fox et al. 2003). This histologic heterogeneity makes the tumor have various signal intensities and variable enhancement.

5.9 Desmoplastic Fibroblastoma

Desmoplastic fibroblastoma, also referred to as collagenous fibroma, is a slow-growing benign fibroblastic/myofibroblastic tumor that involves the subcutaneous or deep soft tissue. This tumor is composed of spindle- and stellate-shaped fibroblasts and abundant interstitial collagen. Desmoplastic fibroblastoma should be differentiated from fibromatosis, which has a high risk of local recurrence if simple local excision is performed. Fibromatosis is more cellular and shows short fascicular arrangements of tumor cells and greater infiltration at the periphery than desmoplastic fibroblastoma (Fukunaga and Ushigome 1999).

MR imaging shows a well-defined mass with a predominantly low signal intensity on T2-weighted images. Those areas of marked T2 hypointensity do not enhance on gadolinium-enhanced images and correspond to a hypocellular component with dense collagen fibers. The interspersed areas showing intermediate signal intensity on T2-weighted images correspond to hypercellular areas within the lesion that reflect its loose collagen fibers (Shuto et al. 2002). Unlike fibromatosis, desmoplastic fibroblastomas are clearly circumscribed and do not have areas showing very high signal intensity on T2-weighted images.

5.10 Calcifying Aponeurotic Fibroma

Calcifying aponeurotic fibroma, also known as juvenile aponeurotic fibroma, is a rare benign soft tissue tumor with intermediately aggressive biologic behavior. It is found most commonly during the first and second decade of life, and the commonly involved sites are the hand, finger and foot. This type of fibroma occasionally arises in other sites, including the elbow, ankle, knee, and thigh. Most of these tumors are predominantly subcutaneous, but some involve the intermuscular layers. Calcifying aponeurotic fibroma has irregular, ill-defined contours and typically contains the following two components: (1) fibromatosis-like spindle-shaped cell elements; and (2) distinctive, round or oval, fibrocartilaginous, often calcified foci that are composed of epithelioid cells (Murphey et al. 2009).

Radiography may show stippled calcifications and cortical erosion of the adjacent bone. On MR

imaging, most of these tumors are ill-defined, lobulated soft tissue masses with adherence to surrounding structures. T2-weighted images show homogeneous or heterogeneous high signal intensity. Areas demonstrating low signal intensity on T2-weighted image have marked hypocellularity and abundant collagen (Kwak et al. 2004). Gadolinium-enhanced images show heterogeneous, relatively strong enhancement. Speckled foci of calcification can also be observed on MR images.

5.11 Palmar/Plantar Fibromatosis

Fibromatosis can be divided into superficial and deep subtypes. Superficial fibromatoses are usually small (< 5 cm) slow-growing lesions that rarely involve deep structures. Superficial fibromatosis include palmar and plantar fibromatosis (Lee et al. 2006). Patients with palmar fibromatosis present clinically with painless, subcutaneous nodules. These nodules may progress slowly to fibrous cords or bands that attach to and cause traction on the underlying flexor tendons, resulting in flexion contractures of the digits (Dupuytren's contractures). Ulnar-sided rays, particularly the fourth and fifth digits, are those that are most commonly involved in palmar fibromatosis (Murphey et al. 2009). In patients with palmar fibromatosis, predominantly low signal intensity on T2-weighted images corresponds to relative hypocellularity caused by a mass that predominantly consists of dense collagen. Those lesions that demonstrate intermediate signal intensity on T2-weighted images are more cellular and thus more likely to locally recur (Robbin et al. 2001). Plantar fibromatosis occurs most commonly in the medial aspect of the plantar aponeurosis. They may appear as single or multiple subcutaneous nodules on US and MR imaging. Most plantar fibromatoses demonstrate iso- to high signal intensity on T2-weighted images, while mature lesions have low signal intensity.

5.12 Desmoid-Type Fibromatosis

Desmoid-type fibromatosis (DF), also known as aggressive fibromatosis, is a locally aggressive fibroblastic neoplasm with no potential for metastasis. DF is defined as a benign soft tissue neoplasm composed of a clonal proliferation of fibroblasts and myofibroblasts. In addition, DF grows with infiltrative margins and is composed of a proliferation of uniform spindle cells with collagen production (Fletcher et al. 2013). This tumor can arise anywhere in the body. Its high tendency to recur after surgical resection makes DF an important cause of morbidity and, occasionally, mortality (Braschi-Amirfarzan et al. 2016).

The principal role of imaging in the management of DF is preoperative planning and the detection of recurrence or disease progression in nonsurgically managed patients (Lee et al. 2006). MR imaging is the modality of choice for evaluating abdominal wall and extra-abdominal DF. The lesions may be well defined or infiltrative, and the signal intensity is variable depending on the relative amount of collagen, spindle cells, and extracellular matrix. The MR signal characteristics of DF are a mixed pattern, low to high signal on T2-weighted images and low to iso-signal on T1-weighted images. In most cases of DF, there are very low T2 signal components corresponding to areas of collagen deposition. These regions do not enhance after administration of gadolinium-based contrast material. The other, more cellular, portions exhibit moderate-to-marked enhancement. The observation of T2 hypointense, non-enhancing band-like components increases diagnostic confidence.

5.13 Dermatofibrosarcoma Protuberans

Dermatofibrosarcoma protuberans (DFSP) is a low-grade sarcoma that originates in the reticular dermis of the skin. It most commonly affects young to middle-aged adults, with the tumor predominantly occurring on the trunk, followed by the extremities and head and neck region. DFSP typically presents as a firm, skin-colored, indurated plaque, 1–5 cm in diameter, with one or more reddish-purple exophytic nodules. Although it superficially tends to spare the epidermis, the deep edge classically shows infiltration along fibrous septa into underlying subcutaneous fat,

encircling adipocytes and giving rise to a distinctive "honeycomb pattern" (Kuzel et al. 2015).

DFSPs are nodular soft tissue mass involving the skin and subcutaneous tissue on MR imaging with nonspecific signal intensity and enhancement pattern. Although most cases of the tumor are superficial and well-defined, some may be found in a deep location, and rare cases are poorly defined in appearance (Torreggiani et al. 2002). MR imaging is superior to clinical palpation in detecting the depth of infiltration of DFSP. For DFSPs in which the tumor has been excised with positive margins, however, MR imaging is not useful for determining the persistence of the tumor. MR imaging does not appear to be useful for determining the lateral limits of DFSP (Serra-Guillen et al. 2011).

5.14 Solitary Fibrous Tumor

Solitary fibrous tumor (SFT) shows a wide spectrum of histological features, ranging from heterogeneous, multinodular, partially sclerotic lesions to monotonous, highly cellular lesions. There are two main subtypes of SFT, one being fibrous (SFT of the pleura). The other is a cellular form, which characteristically contains numerous thin-walled vessels with little intervening fibrosis; these tumors are virtually indistinguishable from conventional hemangiopericytoma (Gengler and Guillou 2006). Solitary fibrous tumor shows no gender predilection, and most patients are in the fifth to seventh decades. The pleura is the most common site of occurrence and the orbits, and the extremities (muscles and subcutaneous layer) are the most common extrapleural sites.

On US, SFT is a well-demarcated mass with homogeneous or heterogeneous hypoechoic pattern. The power Doppler intratumoral signal shows either a peripheral or a diffuse pattern, and a vascular pedicle is commonly observed. On MR imaging, the extrapleural SFT is observed as a multilobulating mass in the muscle or subcutaneous layer, with nonspecific signal intensities and strong enhancement. T2-weighted imaging characteristics are helpful in identifying fibrous content of tumors because dense mature fibrous tissue has low T2 signal intensity. Occasionally, tumors can have focal or diffuse myxoid stroma, which is apparent as a hyperintense T2 signal. Malignant areas within tumors also tend to show intermediate-to-high signal intensity on T2-weighted images, corresponding to edema and increased vascularity. Histopathological correlation studies have demonstrated that hemorrhage, cystic degeneration, and necrosis are rare, occurring in fewer than 5% of cases. However, these findings can be observed in larger and malignant tumors (Musyoki et al. 2012). The radiological features that correlate better with malignant criteria are tumor size, heterogeneous signal intensity, and heterogeneous uptake of contrast on MR imaging (Garcia-Bennett et al. 2012). SFTs tend to displace adjacent structures but occasionally invade them.

5.15 Inflammatory Myofibroblastic Tumor

Myofibroblasts are one of the main cell types in connective tissue that share ultrastructural features of both fibroblasts and smooth muscle cells. Myofibroblastic neoplasms encompass a range of benign to malignant disease. Among malignant tumors, only low-grade forms are currently accepted as a diagnostic category. Inflammatory myofibroblastic tumor (IMT) and low-grade myofibroblastic sarcoma are important intermediate- or low-grade malignant neoplasms in this spectrum (Qiu et al. 2008). IMT is defined as a disease that primarily consists of myofibroblastic spindle cells, with variable infiltration of plasma cells and/or lymphocytes (Tan et al. 2016). IMT is more common in children and young adults and occurs at a median age of 9 years. IMT can be found anywhere in the body, and the common sites include the lung, soft tissue, and viscera.

The imaging features of IMT are variable and nonspecific. Contrast-enhanced CT may show a homogeneous or heterogeneous enhancement of the lesion. These tumors typically manifest as lobulated heterogeneous masses, which may have calcifications. Large lesions can have non-enhancing central necrotic areas and calcifica-

tions (Sargar et al. 2016). On MR imaging, IMTs are isointense to muscle on T1-weighted images and hypo- to hyperintense on T2-weighted images, depending on the relative quantity of fibrous tissue, cellular material, and necrosis. A dark signal on T2-weighted images is more likely dense fibrosis. Heterogeneous and variably strong contrast enhancement is observed on post-contrast MR images.

5.16 Myxofibrosarcoma

Myxofibrosarcoma (MFS) is a soft tissue sarcoma that typically presents on the extremities of elderly patients. It has formerly been referred to as myxoid malignant fibrous histiocytoma. The histology of the tumors reveals haphazardly arranged fascicles of atypical spindle-shaped cells, with a varying amount of myxoid matrix. Nuclear atypia is variable. A curvilinear vascular network is well developed (Kaya et al. 2008).

Whereas most soft tissue sarcomas grow as discrete round or oval masses, MFS often exhibit an infiltrative margin that extends into surrounding tissues for substantial distances along normal anatomical planes, particularly fascial planes, resulting in distant microscopic tumor deposits that predispose to local recurrence after resection. On MR imaging, this infiltrative spread may manifest as curvilinear projections that extend from the primary mass-like portion of the MFS (Lefkowitz et al. 2013). Gadolinium-enhanced MR images depict this infiltrative tumor extension more accurately than T2-weighted images. These MR imaging appearances and the tail sign may indicate tumor infiltration along the fascial plane and may also be associated with worse local recurrence-free survival (Yoo et al. 2014).

5.17 Low-Grade Fibromyxoid Sarcoma

Low-grade fibromyxoid sarcoma (LGFMS) is a rare spindle cell tumor exhibiting bland histological features but aggressive clinical behavior. LGFMS typically presents during young or middle adult life, but there have been an increasing number of reports of this tumor in the pediatric age group. LGFMS are observed most frequently on the deep soft tissue of the lower extremity or thoracic wall, followed by the shoulder and inguinal area. Most lesions arise in the deep soft tissue, but subcutaneous masses can be found in children. On histology, LGFMS shows two distinct zones (myxoid and fibrous), bland regular spindle cells, and a swirling or whorled pattern, with absent or sparse mitotic activity.

On MR imaging, LGFMS appears heterogeneous due to the presence of two distinct internal zones (myxoid and fibrous). LGFMS shows areas of low signal intensity on both T1- and T2-weighted images due to the fibrous component (Sargar et al. 2015). On fluid-sensitive sequences, a distinct gyriform pattern with multiple folded layers of predominantly low to iso-signal intensity areas that mimic brain gyri has been reported (Hwang et al. 2012).

5.18 Low-Grade Myofibroblastic Sarcoma

Low-grade myofibroblastic sarcoma occurs primarily in adult patients but has been described in patients between 7 and 85 years of age. Local recurrences are common, but distant metastases are infrequent (San Miguel et al. 2004). These tumors have been found in the oral cavity, limbs, abdominal/pelvic cavity, and chest wall. Imaging findings of low-grade myofibroblastic sarcoma are not well described. The tumors in the somatic soft tissue are located in the muscle, perifascial tissue, or subcutaneous layer.

5.19 Sclerosing Epithelioid Fibrosarcoma

Sclerosing epithelioid fibrosarcoma (SEF) is a rare malignant fibroblastic tumor and a unique variant of fibrosarcoma. SEF is characterized by epithelioid cells that are arranged in nests and strands in a densely hyalinized collagenous

matrix. SEF often occurs in deep soft tissue of the lower extremities, limb girdles, trunk, upper extremities, and the head and neck area (Yoon et al. 2012). Most of the lesion is heterogeneously isointense to muscle on T1-weighted images and hyperintense on T2-weighted images. A central stellate core of very low signal intensity on both T1- and T2-weighted images has been reported as a distinctive feature (Christensen et al. 1997).

5.20 Illustrations: Fibroblastic/Myofibroblastic Tumors

5.20.1 Nodular Fasciitis

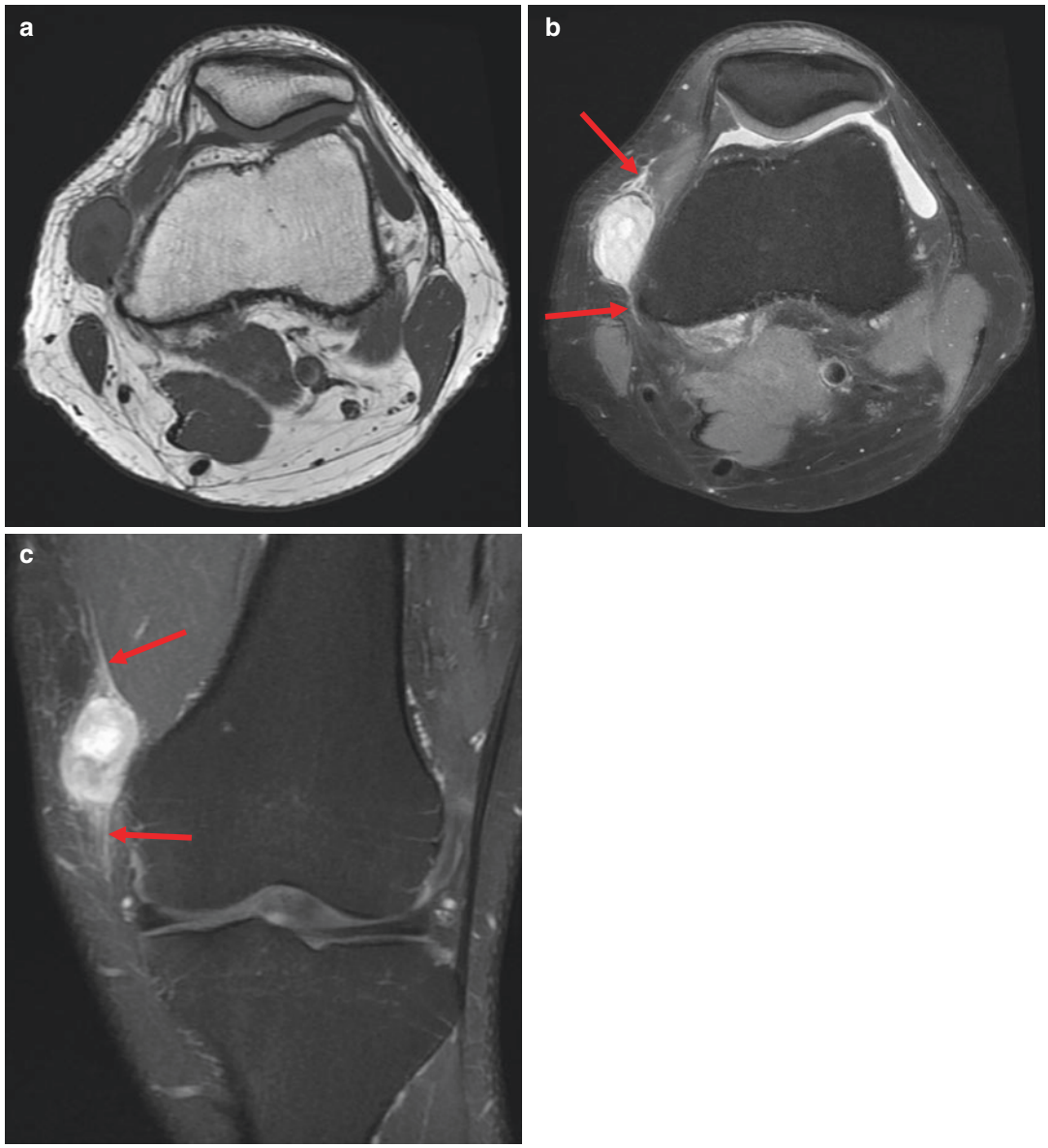

Fig. 5.1 Nodular fasciitis. Axial T1WI (**a**) shows a perifascial mass on the left medial knee. Axial PDWI (**b**) and coronal postcontrast FS T1WI (**c**) show a hyperintense or enhancing mass with mild heterogeneity. Tail-like T2 hyperintensity or enhancement (*arrows*) extends along the fascia

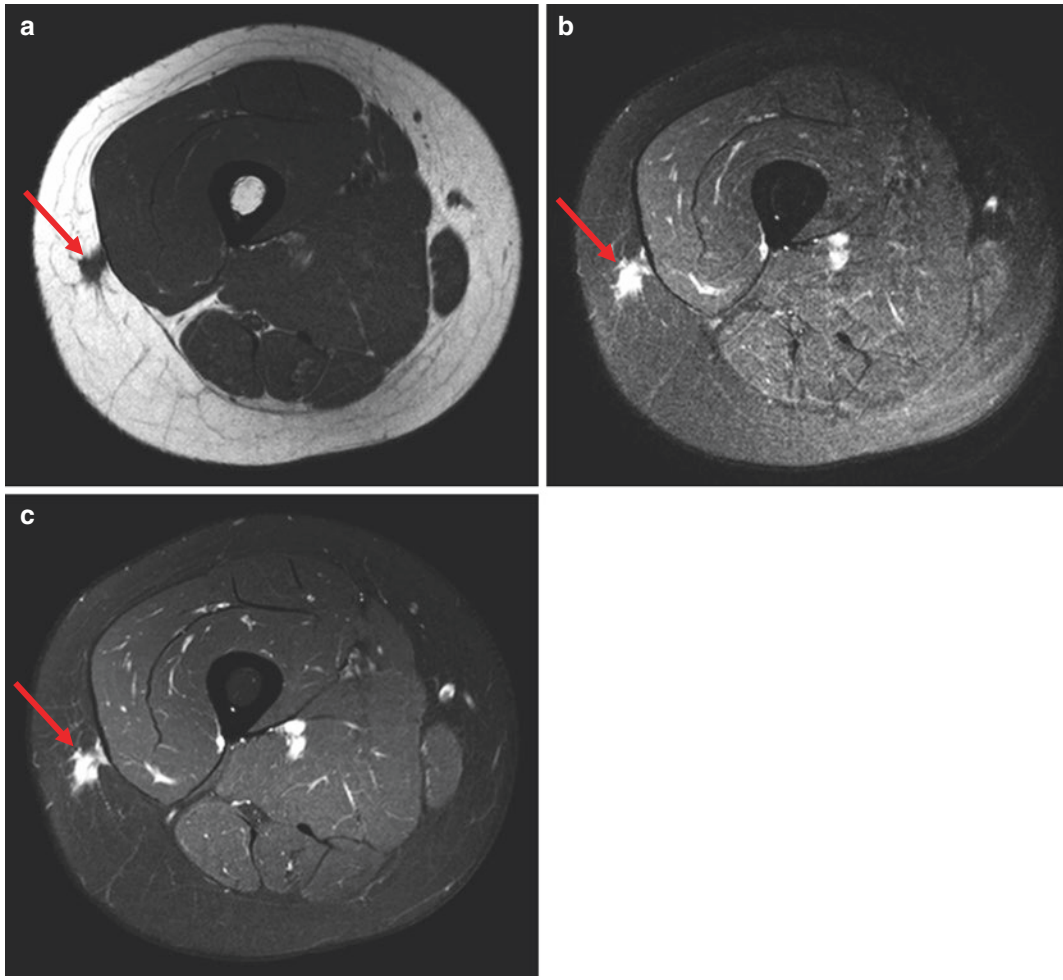

Fig. 5.2 Nodular fasciitis. Axial T1WI (**a**) shows a nodular subcutaneous mass (*arrow*) with an infiltrative margin in the right proximal thigh. Axial FS T2WI (**b**) shows the hyperintense nature of the mass, and axial postcontrast FS T1WI (**c**) show intense enhancement. The mass abuts the deep fascia over the vastus lateralis

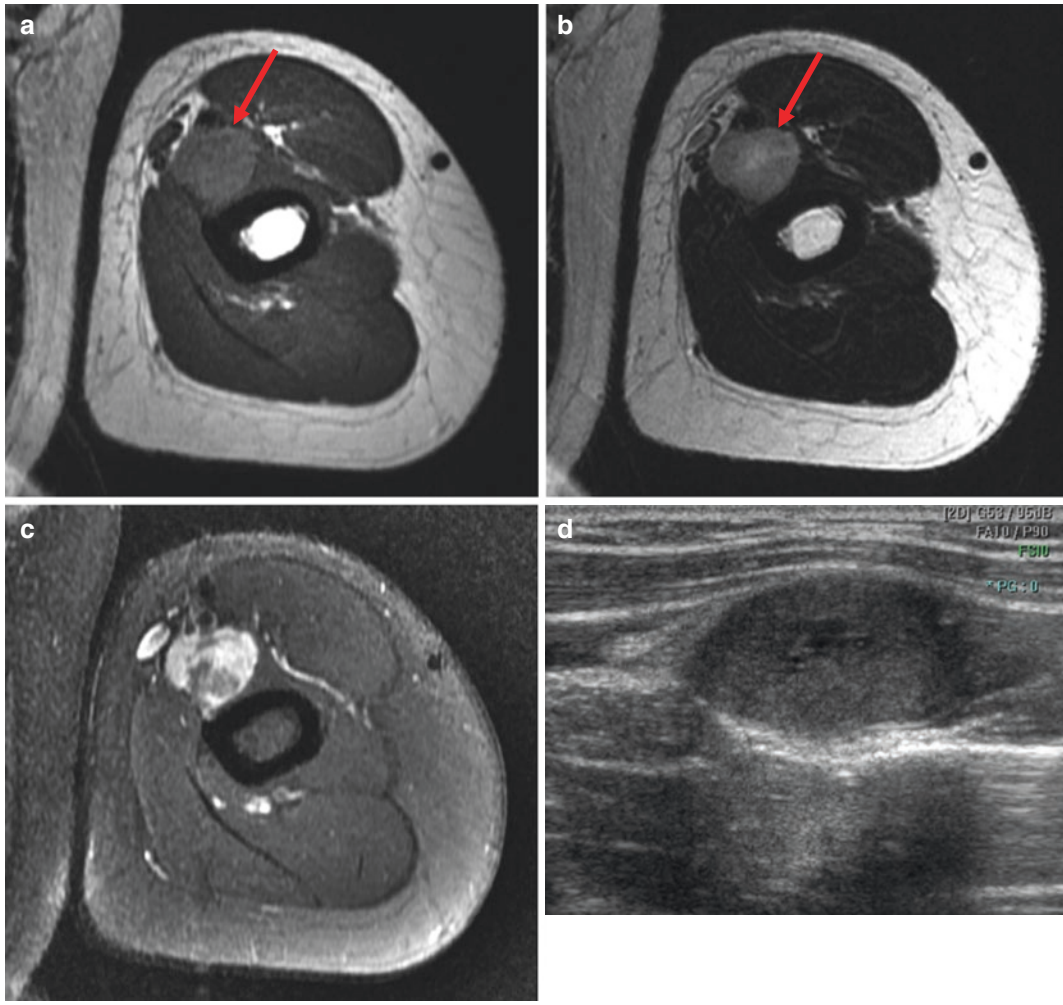

Fig. 5.3 Nodular fasciitis. Axial T1WI (**a**) shows a slightly hyperintense mass (*arrow*) between the left brachial artery and brachialis muscle. Axial T2WI (**b**) shows heterogeneous signal intensity of the mass (*arrow*) with central hyperintensity. Axial postcontrast FS T1WI (**c**) shows heterogeneous enhancement. On longitudinal US (**d**), the mass has medium-level echogenicity with central hypoechoic area

5.20.2 Proliferative Fasciitis

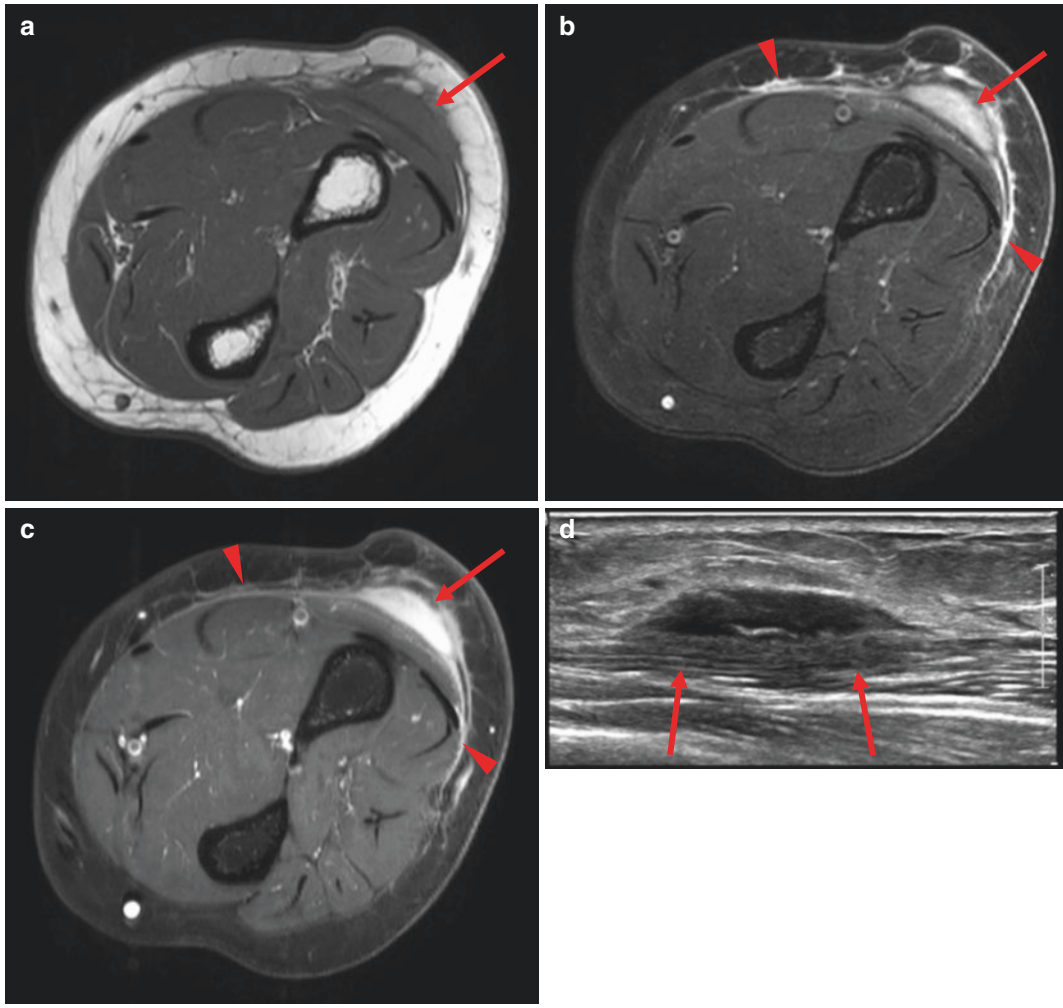

Fig. 5.4 Proliferative fasciitis. Axial T1WI (**a**), FS T2WI (**b**), and postcontrast FS T1WI (**c**) show a perifascial mass (*arrow*) on the radial side of the left proximal forearm. The mass appears with T2 hyperintensity and prominent enhancement. There are edema-like signals and enhancement along the fascia (*arrowheads*). Longitudinal US (**d**) shows a hypoechoic mass involving the deep fascia (*arrow*) and subcutaneous layer

5.20.3 Proliferative Myositis

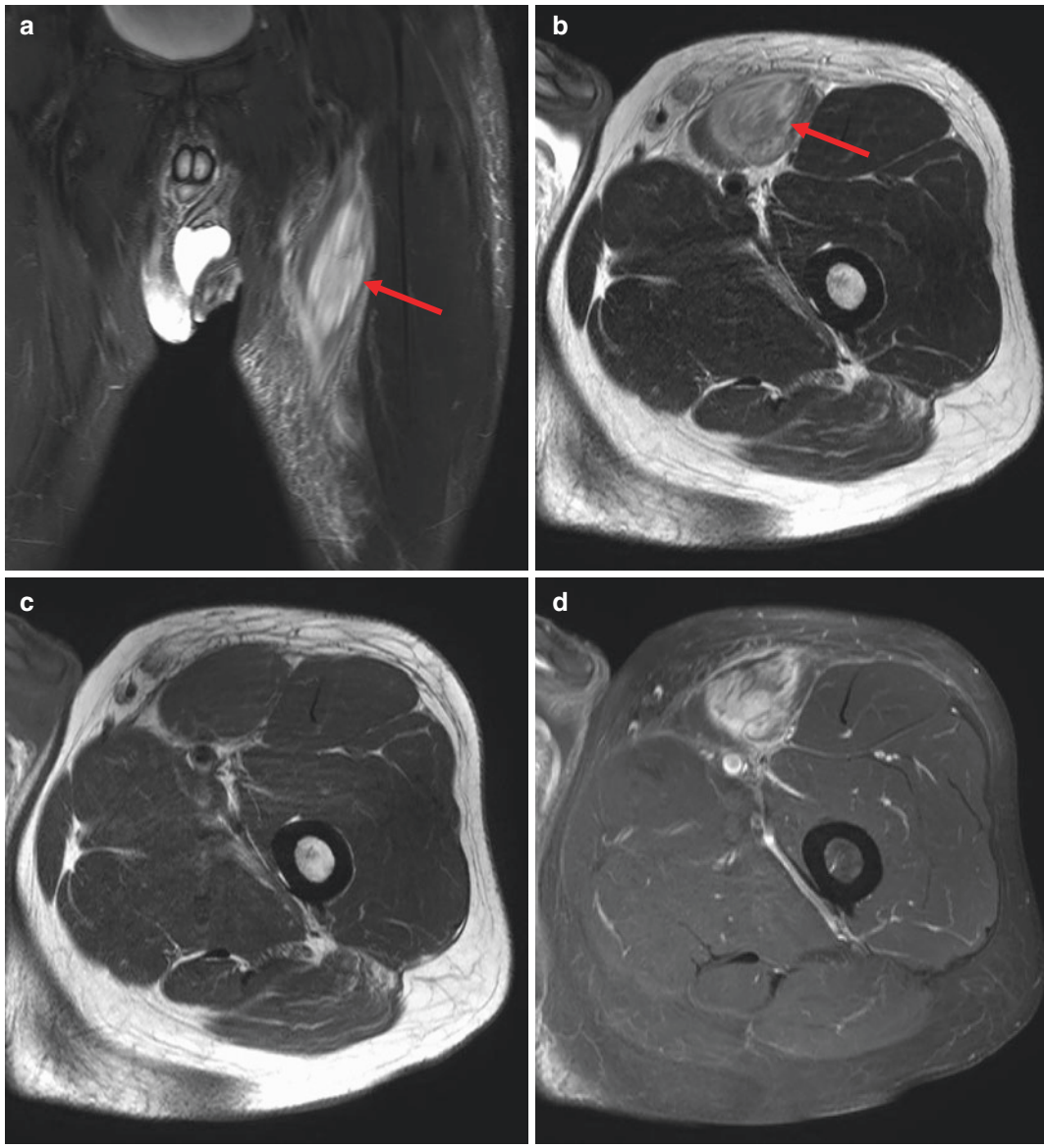

Fig. 5.5 Proliferative myositis. Coronal FS (**a**) and axial (**b**) T2WIs show fusiform hypertrophy of the left sartorius muscle, with a poorly demarcated mass (*arrow*). The intralesional muscle fascicles are preserved and separated by hyperintense perimysia. There is prominent edema-like signal in the surrounding muscle and adjacent subcutaneous layer. Axial T1WI (**c**) shows isointensity and axial postcontrast FS T1WI (**d**) shows heterogeneous enhancement

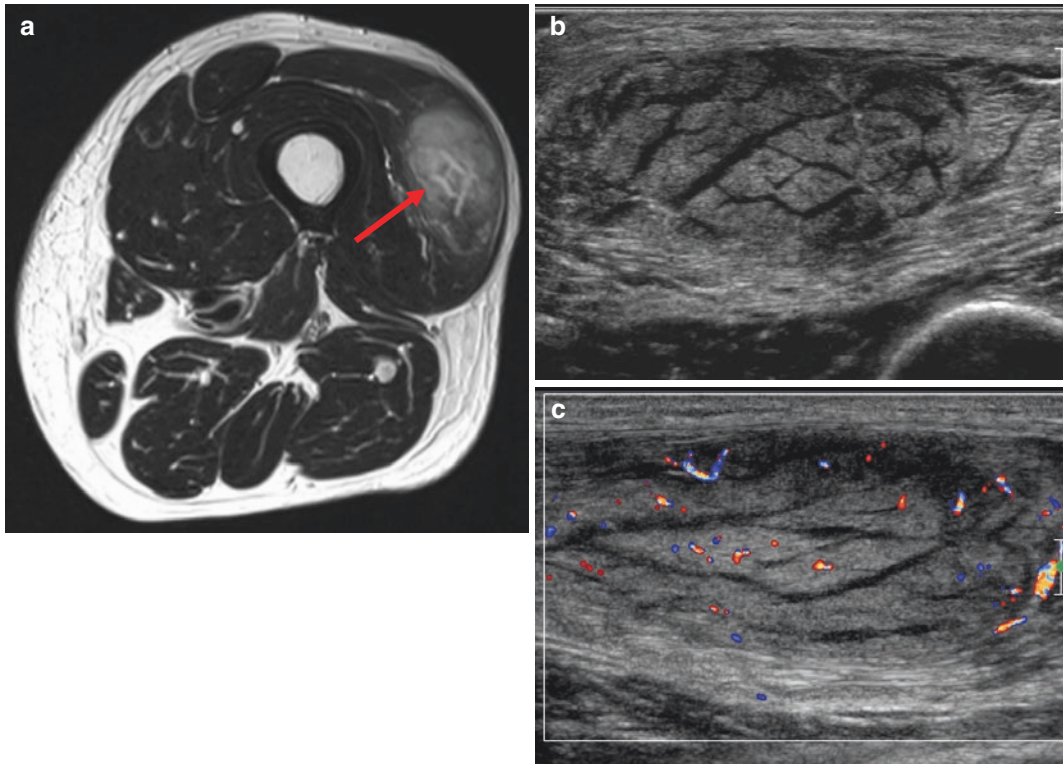

Fig. 5.6 Proliferative myositis. Axial T2WI (**a**) shows a hyperintense mass (*arrow*) in the left vastus lateralis muscle. There are band-like hyperintensities in keeping with fibroblastic proliferation in the perimysium. Transverse US (**b**) shows "checkerboard appearance consisting of hypertrophied muscle fascicles and thickened hypoechoic perimysia. Longitudinal Doppler US (**c**) shows increased vascularity

5.20.4 Myositis Ossificans

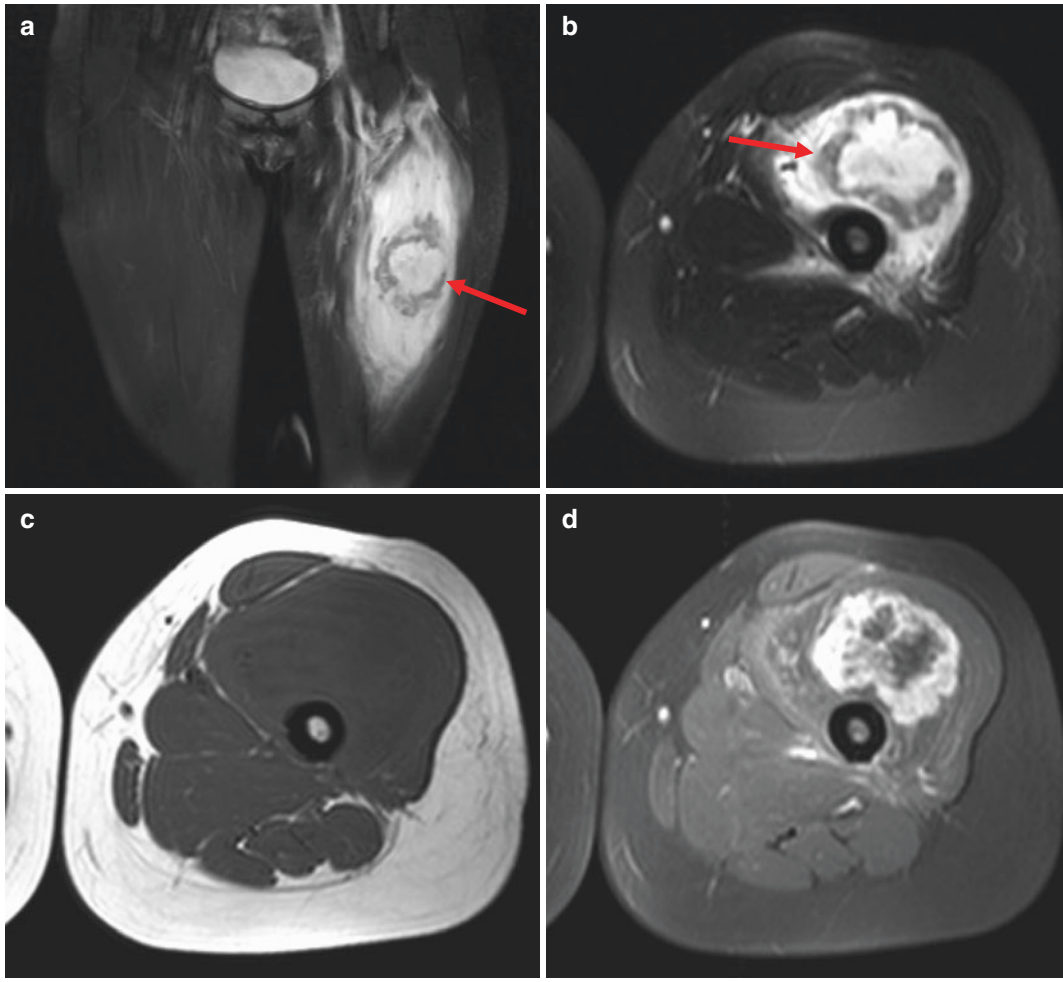

Fig. 5.7 Myositis ossificans. Coronal and axial FS T2WI (**a**, **b**) show a hyperintense intramuscular mass surrounded by intermediate signal rind (*arrow*). There is an extensive muscle edema in the left vastus intermedius. The mass is iso- to slightly hypointense to muscle on T1WI (**c**). Axial postcontrast FS T1WI (**d**) reveals a lobulated mass with prominent peripheral enhancement. After 6 months, axial T1WI (**e**) shows a well-demarcated mature lesion with a central fat signal (*arrows*). Axial T2WI (**f**) shows complete resolution of the surrounding soft tissue edema around the mature lesion. Lateral radiograph (**g**) of the left thigh, which was taken at the same time as the images in **e** and **f**, shows mature bone formation

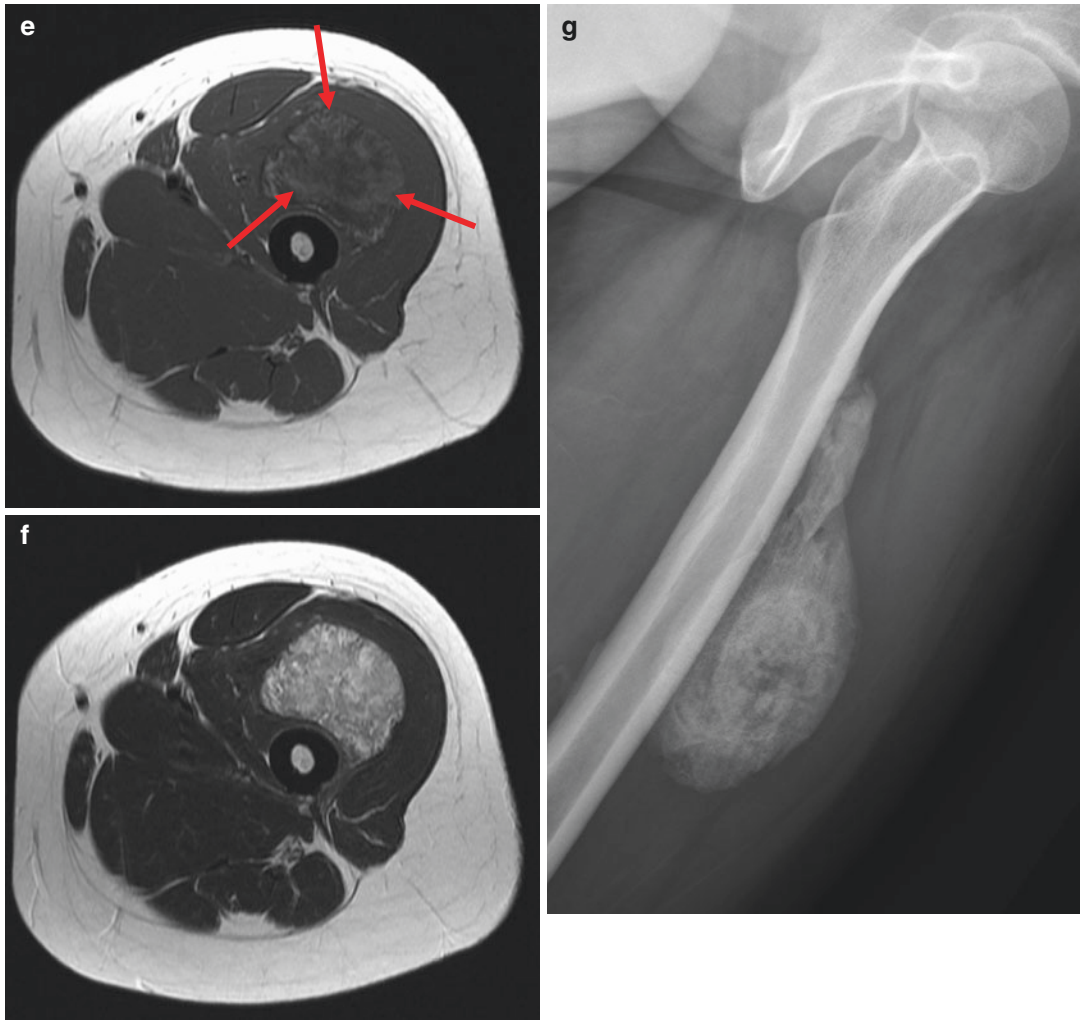

Fig. 5.7 (continued)

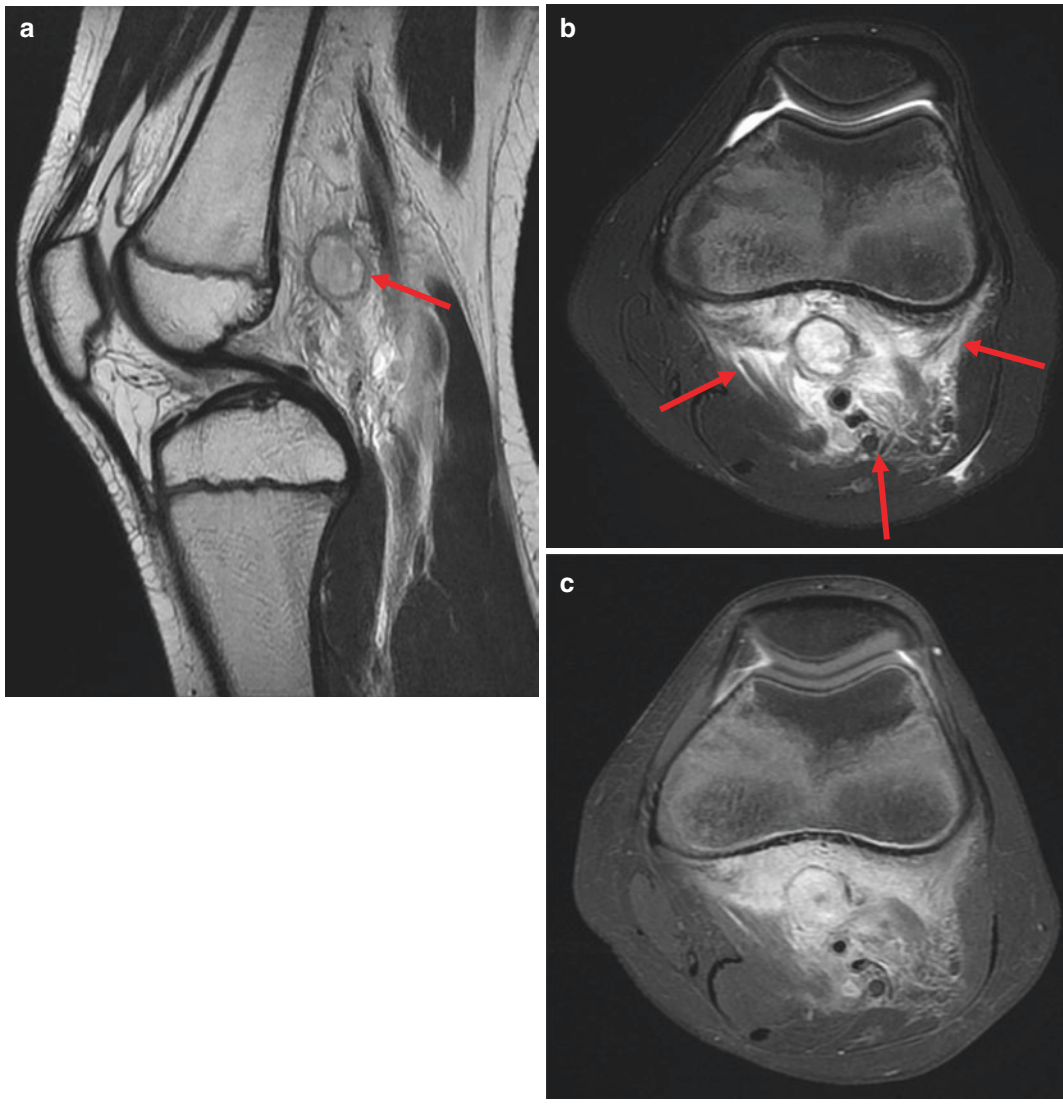

Fig. 5.8 Myositis ossificans. Sagittal T2WI (**a**) shows a hyperintense mass (*arrow*) surrounded by a low signal rim in the left popliteal fossa. Axial FS T2WI (**b**) shows extensive soft tissue edema (*arrows*) around the mass. Axial postcontrast FS T1WI (**c**) shows the contrast-avid mass, with prominent enhancement in the surrounding soft tissue

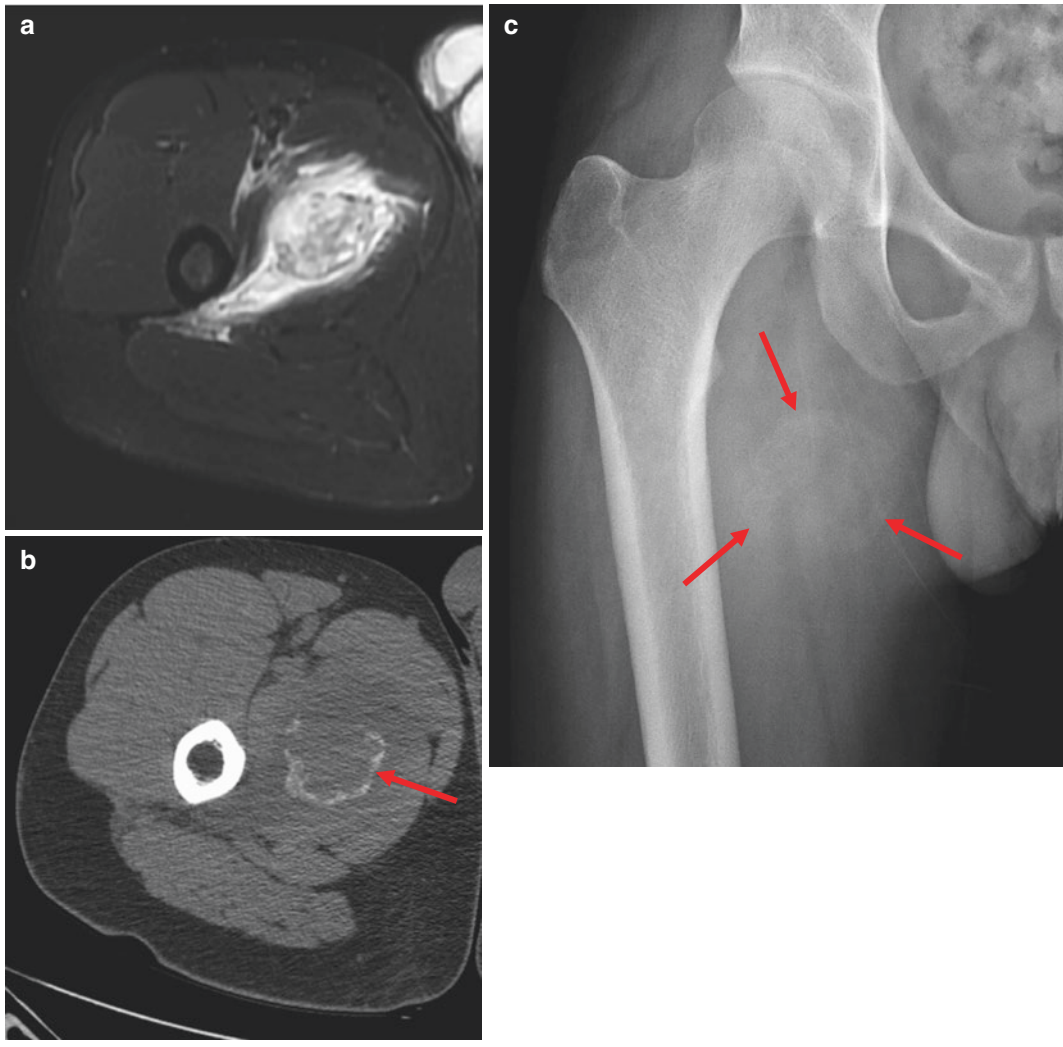

Fig. 5.9 Myositis ossificans. (**a**) One week after onset, axial STIR shows an intramuscular mass in the right adductor magnus, with surrounding edema. (**b**) Two weeks after onset, axial CT demonstrates the typical mineralization pattern (*arrow*) at the periphery of the mass. (**c**) Four weeks after onset, AP radiograph of the right hip shows a medial thigh mass with faint mineralization (*arrows*)

5.20.5 Elastofibroma Dorsi

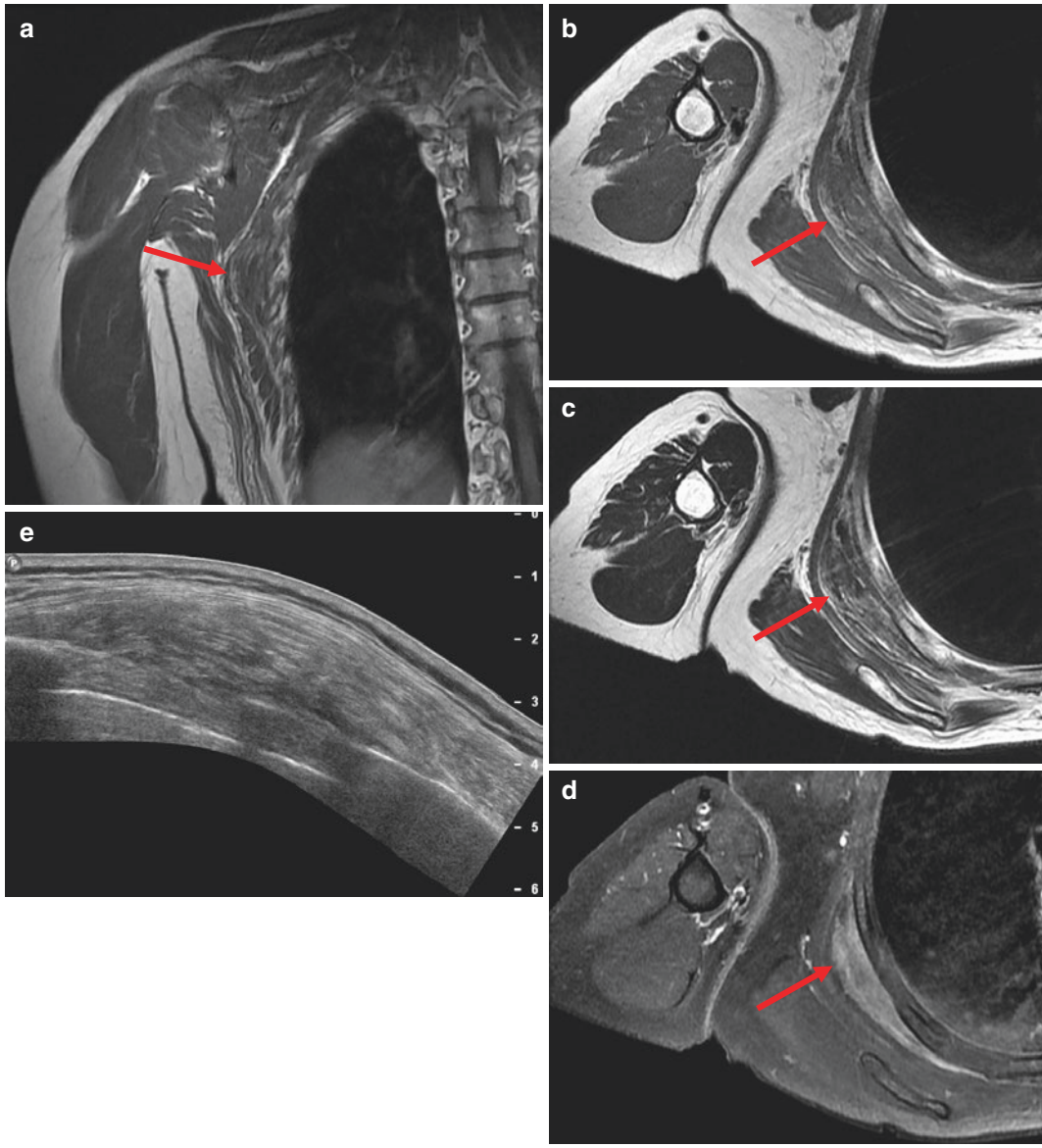

Fig. 5.10 Elastofibroma dorsi. Coronal and axial T1WIs (**a**, **b**) show a soft tissue mass (*arrow*) with interspersed lines of high signal between the right rib cage and serratus anterior. Axial T2WI (**c**) shows the mass (*arrow*) with a mixed intermediate and high signal. Axial postcontrast FS T1WI (**d**) shows heterogeneous enhancement of the mass (*arrow*). Longitudinal extended field of view US (**e**) shows an intratumoral, multilayered pattern of hypoechoic linear areas of fat deposition intermixed with echogenic fibroelastic tissue

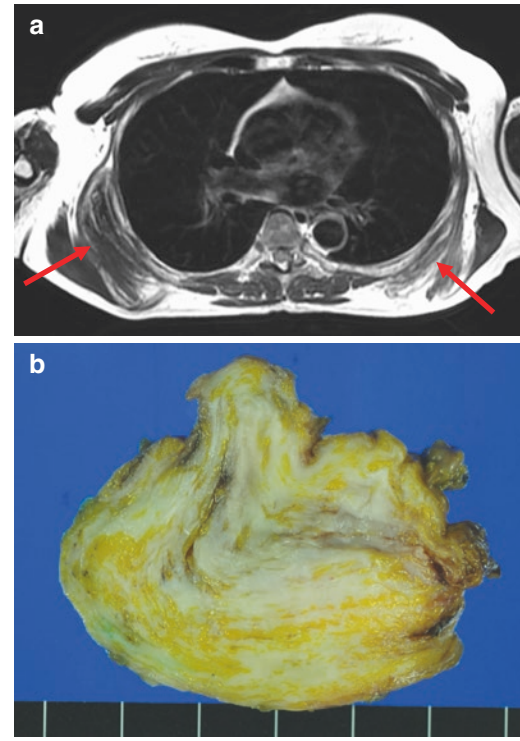

Fig. 5.11 Elastofibroma dorsi. Axial T1WI (**a**) show bilateral soft tissue masses (*arrows*) in the infrascapular regions. (**b**) Gross specimen demonstrating patterns of alternating bands of dense fibrous and fat tissue

5.20.6 Fibrous Hamartoma of Infancy

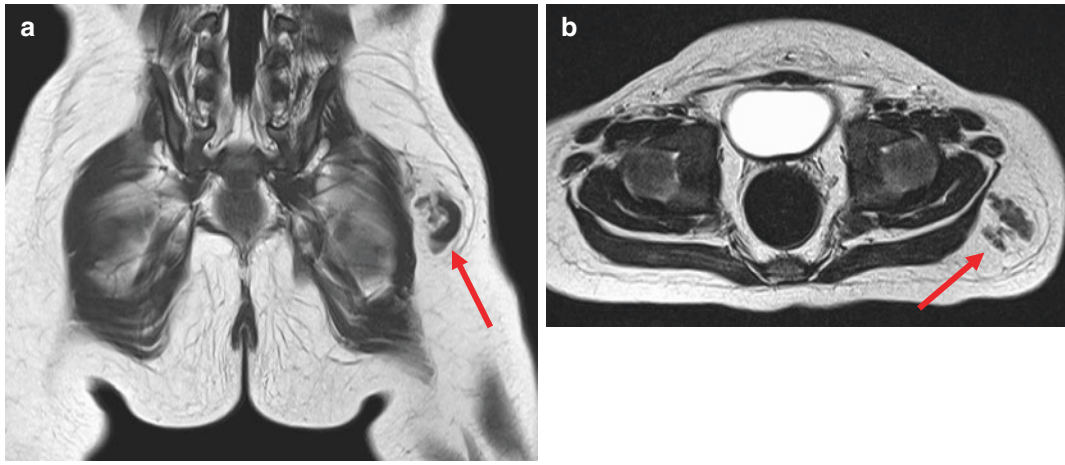

Fig. 5.12 Fibrous hamartoma of infancy. Coronal T1WI (**a**) and axial T2WI (**b**) show a subcutaneous mass (*arrow*) in the left buttock. The mass has high signal fat component and low signal mesenchymal and fibrous components. Axial postcontrast FS T1WI (**c**) shows enhancement of the nonadipose components. Longitudinal US (**d**) shows a poorly demarcated hyperechoic mass (*arrows*) with intervening hypoechoic portions. (**e**) Cut section showing a gray-white tumor with fibrous tissue

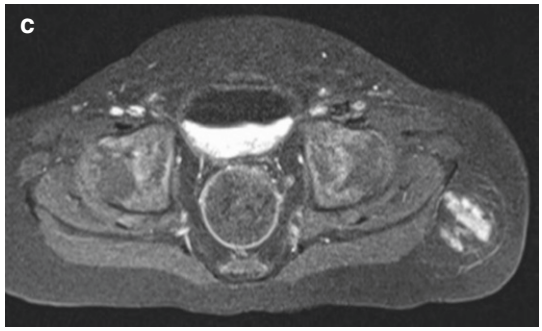

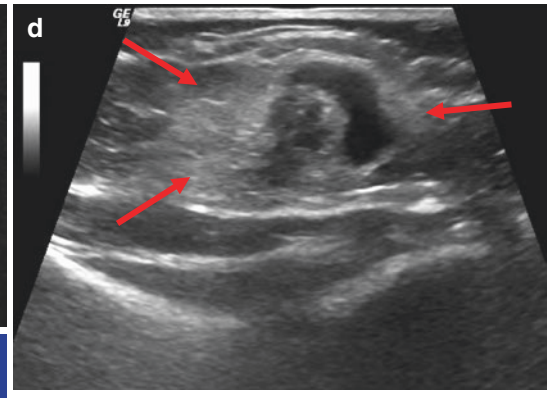

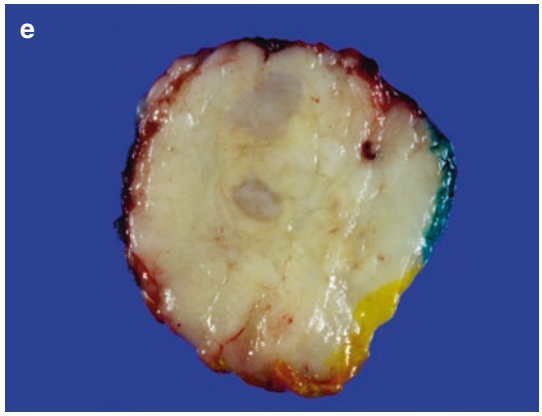

Fig. 5.12 (continued)

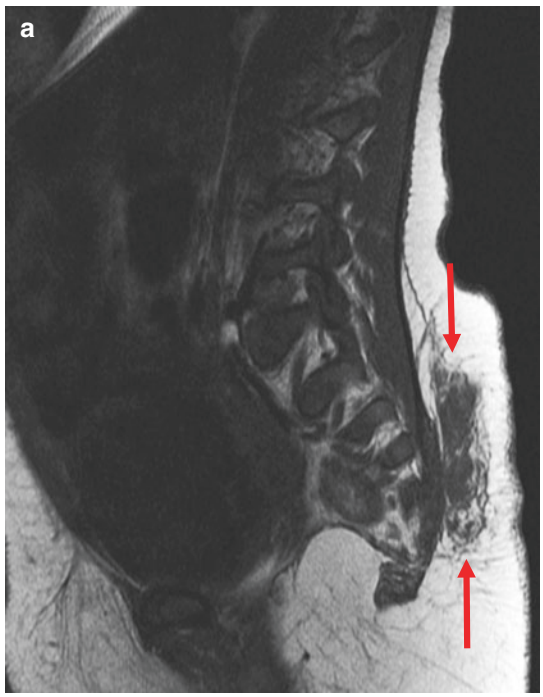

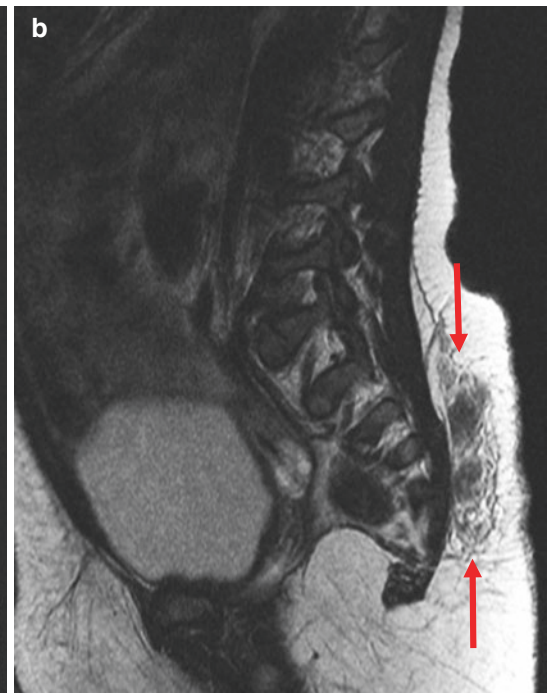

Fig. 5.13 Fibrous hamartoma of infancy. Sagittal T1WI and T2WI (**a**, **b**) show a poorly circumscribed subcutaneous mass (*arrows*) with interspersed fat and soft tissue strands at the sacral level

5.20.7 Fibromatosis Colli

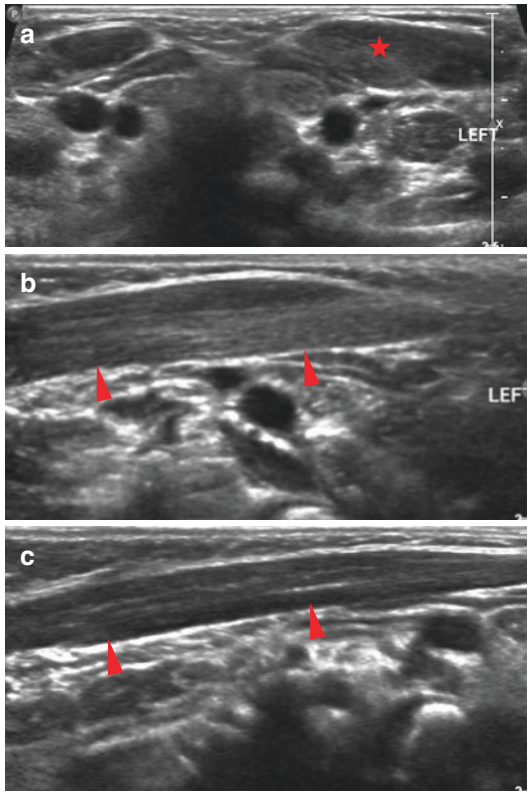

Fig. 5.14 Fibromatosis colli. Transverse US (**a**) of the anterior neck shows asymmetrical thickening of the left sternocleidomastoid muscle (*star*). Longitudinal scan (**b**) shows fusiform enlargement of the left sternocleidomastoid (*arrowheads*) Longitudinal scan (**c**) shows a normal appearance of the right sternocleidomastoid (*arrowheads*)

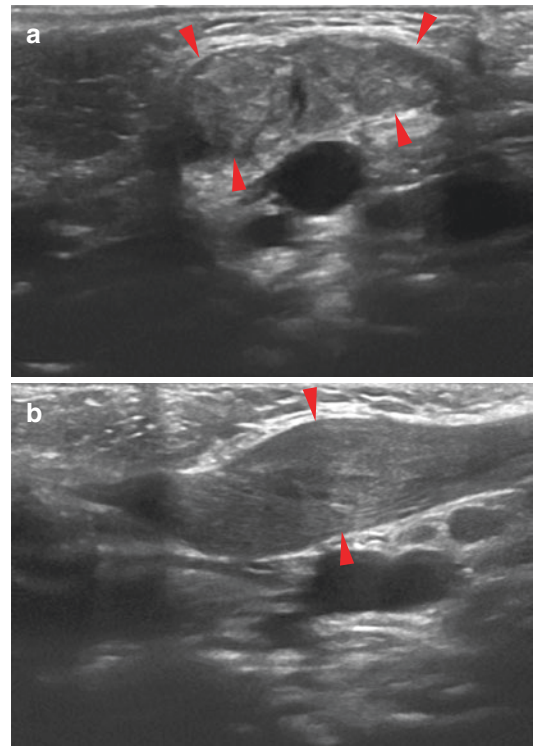

Fig. 5.15 Fibromatosis colli. Transverse US (**a**) shows a hyperechoic mass (*arrowheads*) of the left sternocleidomastoid muscle. Longitudinal US (**b**) shows a mass-forming lesion (*arrowheads*) of the left sternocleidomastoid without extramuscular involvement

5.20.8 Fibroma of Tendon Sheath

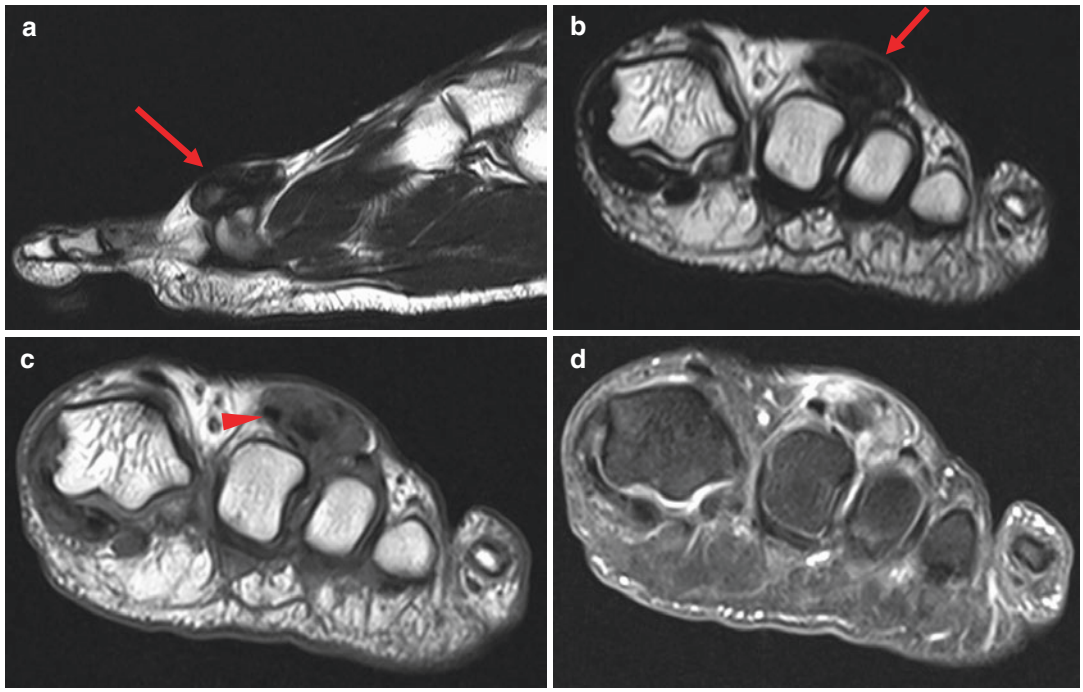

Fig. 5.16 Fibroma of tendon sheath. Sagittal and axial T2WIs (**a**, **b**) show a nodular subcutaneous mass (*arrow*) over the left second MTP. A heterogeneous, but predominantly hypointense signal is observed on T2WIs. Axial T1WI (**c**) shows the mass encasing the second extensor digitorum longus tendon (*arrowhead*). Axial postcontrast FS T1WI (**d**) shows heterogeneous enhancement of the tumor

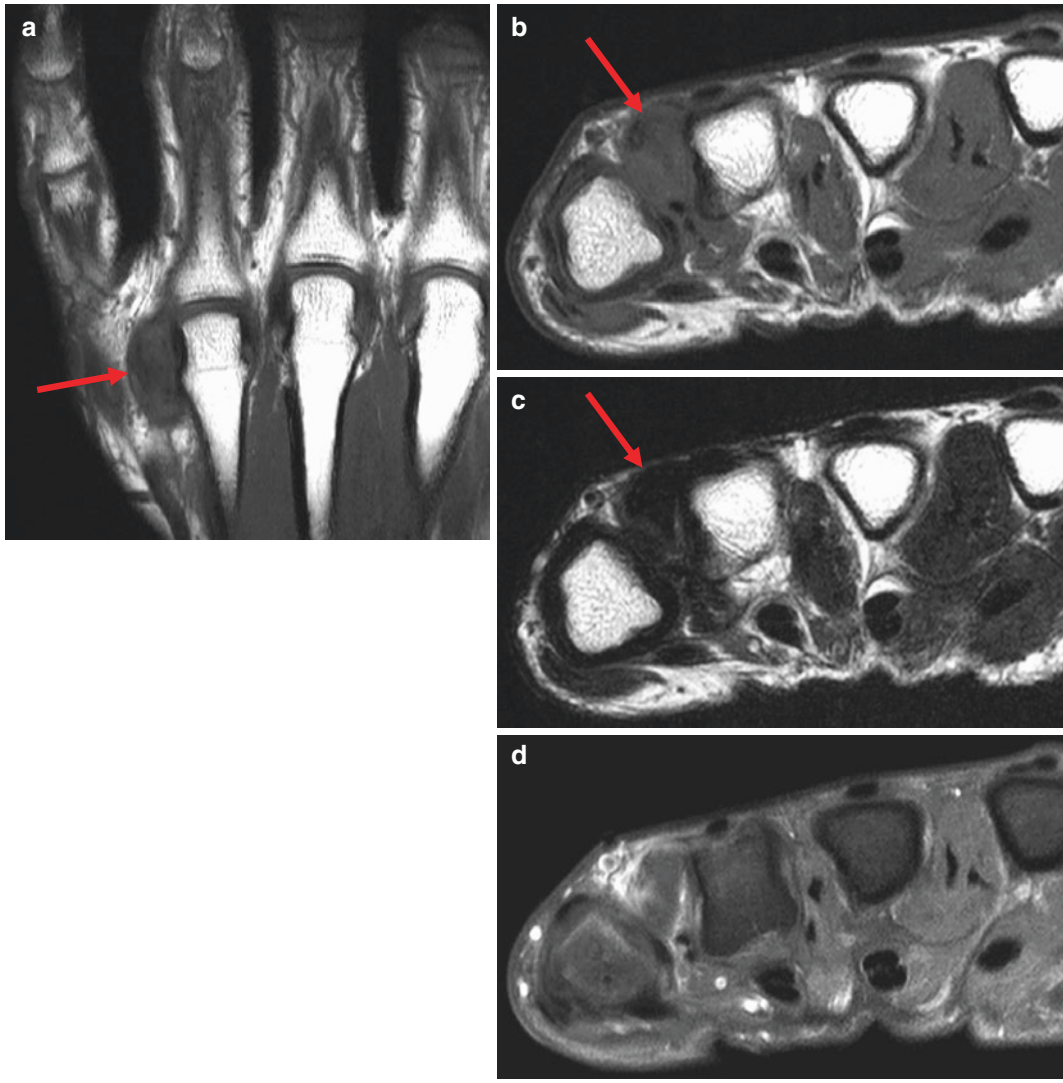

Fig. 5.17 Fibroma of tendon sheath. Coronal and axial T1WIs (**a**, **b**) show a nodular mass (*arrows*) in the right fourth intermetacarpal space. Axial T2WI (**c**) reveals marked hypointensity of the mass (*arrow*). Axial postcontrast FS T1WI (**d**) shows a large area of non-enhancement at the center of the mass

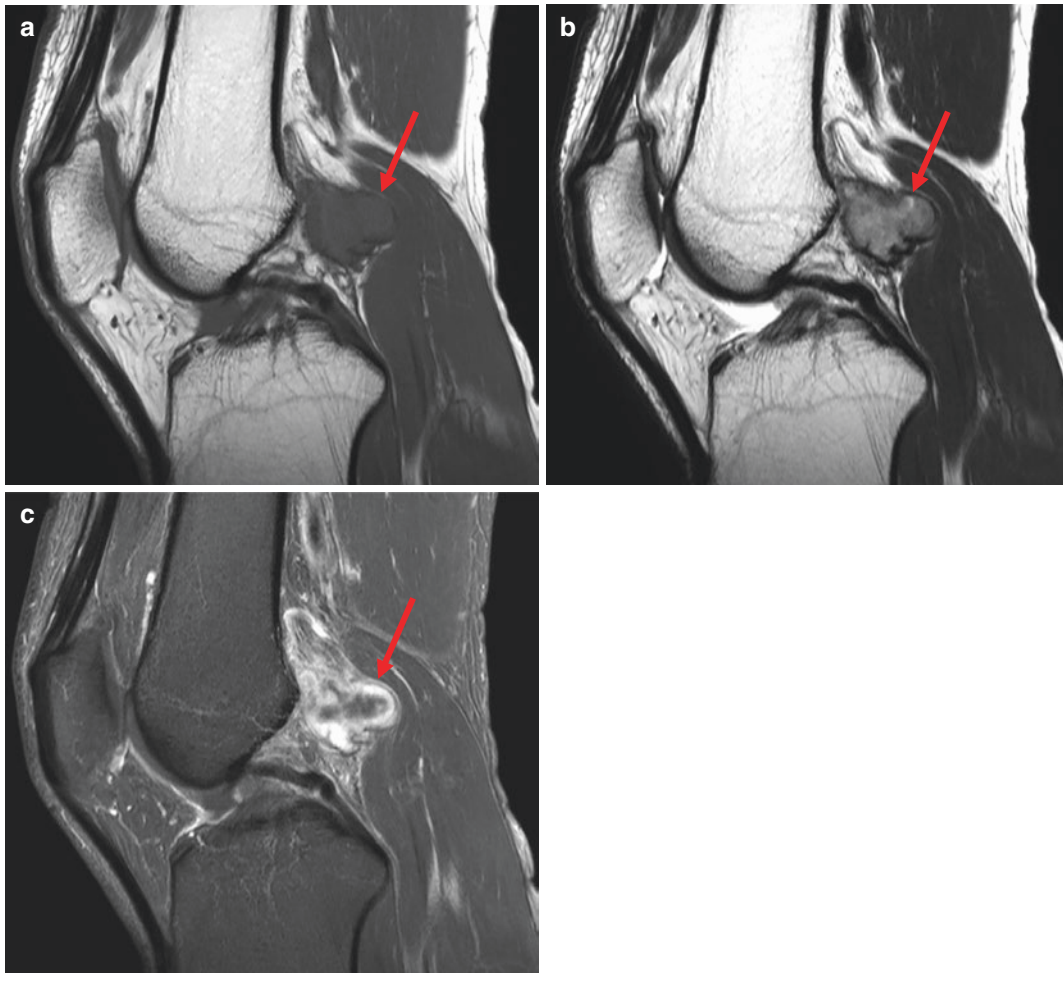

Fig. 5.18 Fibroma of tendon sheath. Sagittal T1WI (**a**) shows a lobulated mass (*arrow*) attached to the posterior knee joint capsule. Sagittal T2WI (**b**) shows the mass (*arrow*) with intermediate signal intensity and hypointense rind. Sagittal postcontrast FS T1WI (**c**) shows heterogeneous enhancement of the mass (*arrow*), an effect that is more prominent at the periphery

5.20.9 Desmoplastic Fibroblastoma

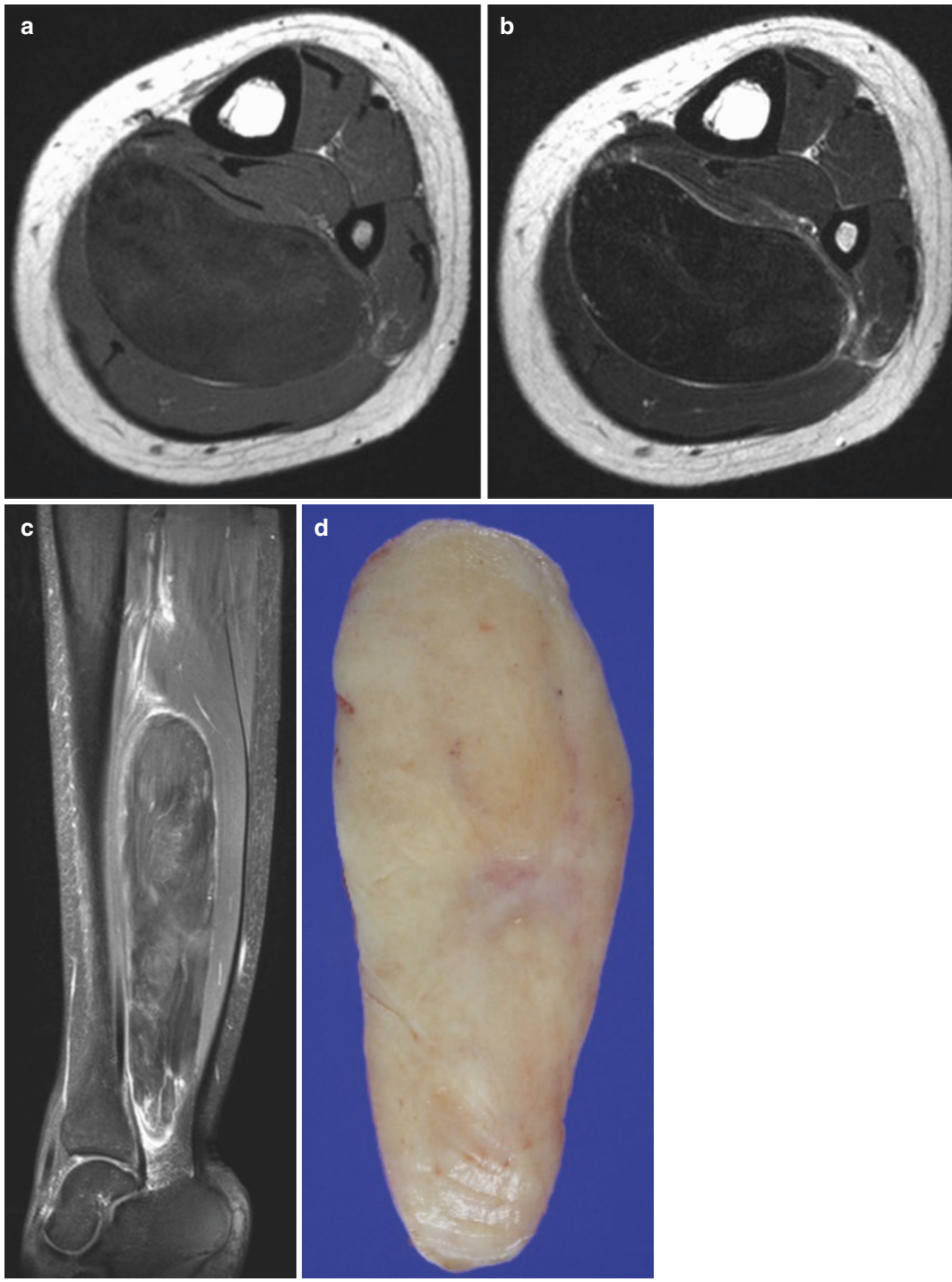

Fig. 5.19 Desmoplastic fibroblastoma. Axial T1WI and T2WI (**a**, **b**) show a large intermuscular mass in the right lower leg. The mass is observed with marked low signal intensity. Sagittal postcontrast FS T1WI (**c**) shows mild, heterogeneous enhancement. (**d**) Gross specimen demonstrating fibrous tumor with some myxoid changes

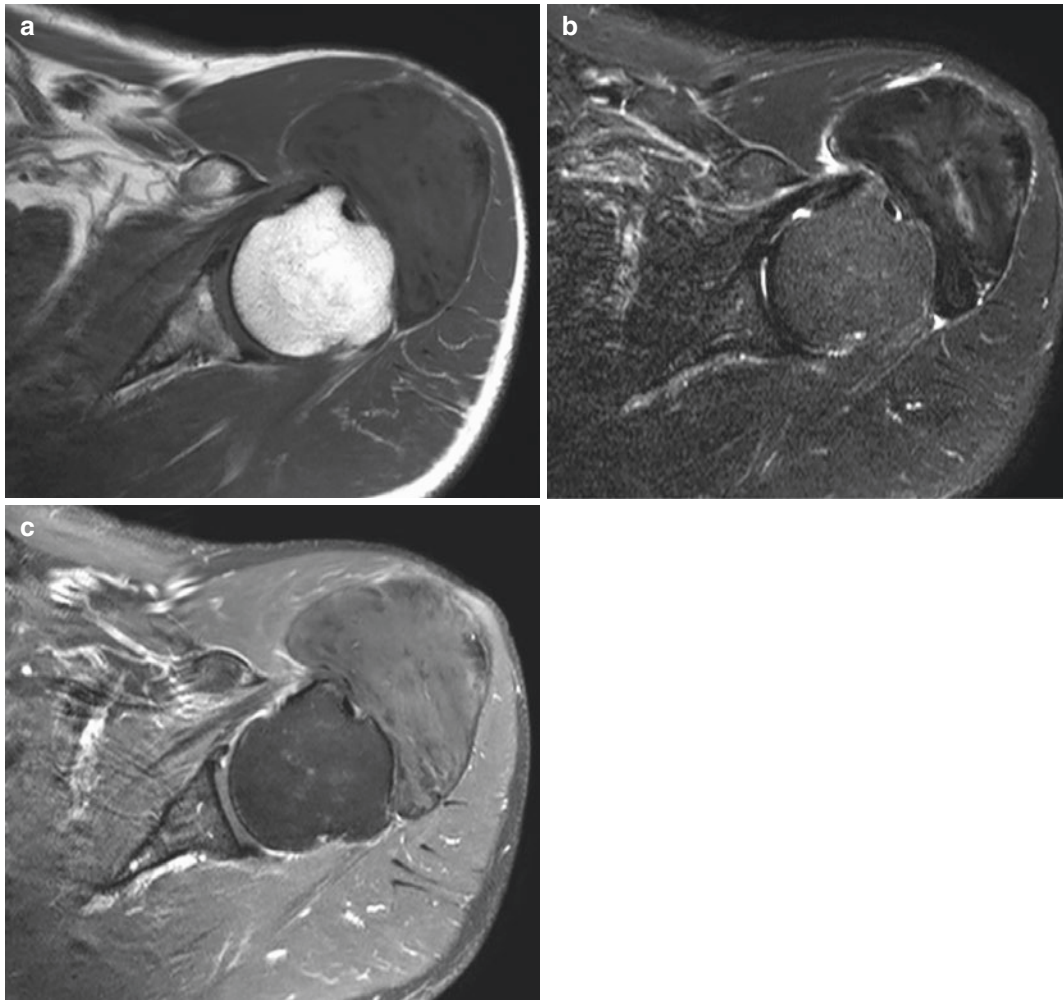

Fig. 5.20 Desmoplastic fibroblastoma. Axial T1WI (**a**) shows a well-demarcated soft tissue mass with low to iso-signal intensity in the left lateral shoulder. Axial FS T2WI (**b**) shows the mass with a heterogeneous signal intensity but predominantly hypointense to muscle. Axial postcontrast FS T1WI (**c**) shows minimal enhancement throughout the mass

5.20.10 Calcifying Aponeurotic Fibroma

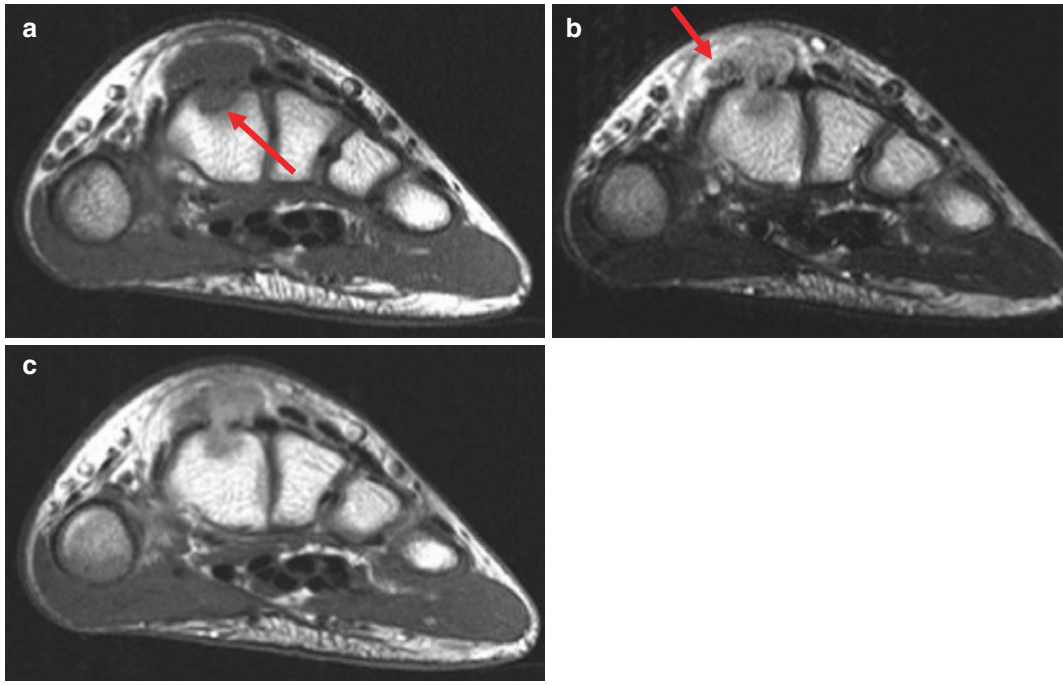

Fig. 5.21 Calcifying aponeurotic fibroma. Axial T1WI (**a**) shows a soft tissue mass over the second metacarpal base. There is a bone erosion (*arrow*) at the dorsal side of second metacarpal base. Axial FS T2WI (**b**) shows speckled foci of calcification (*arrow*) of low signal intensity. Axial postcontrast FS T1WI (**c**) shows heterogeneous enhancement of the mass

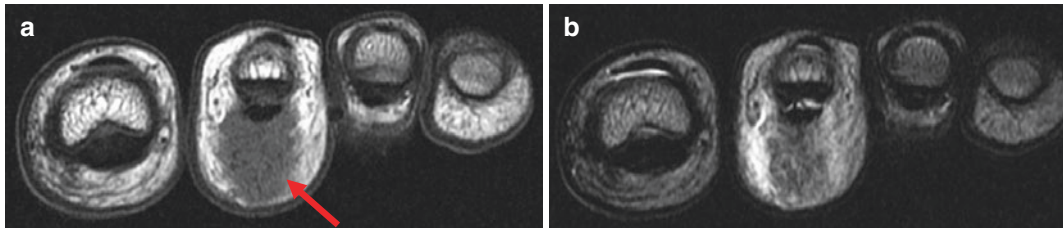

Fig. 5.22 Calcifying aponeurotic fibroma. Axial T1WI (**a**) shows a soft tissue mass (*arrow*) at the plantar side of the left second toe proximal phalanx. The second flexor digitorum longus tendon is partially encased by the mass. Axial T2WI (**b**) shows central low and peripheral high signal intensity of the mass. The mass has a fascicular appearance in the central hypointense area. Sagittal postcontrast FS T1WI (**c**) shows prominent enhancement of the mass (*arrow*). Transverse US (**d**) shows a lobulated hypoechoic mass (*arrowheads*) with punctate hyperechoic foci

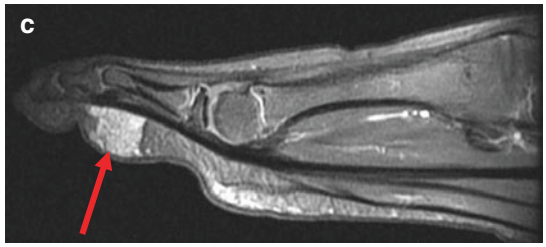

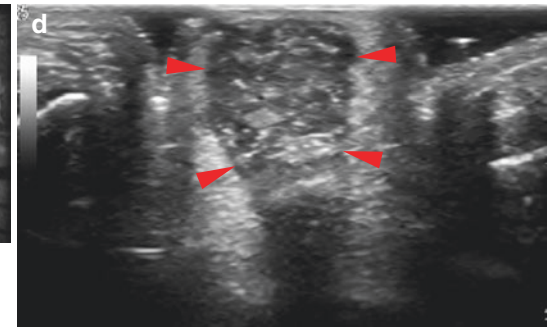

Fig. 5.22 (continued)

5.20.11 Palmar/Plantar Fibromatosis

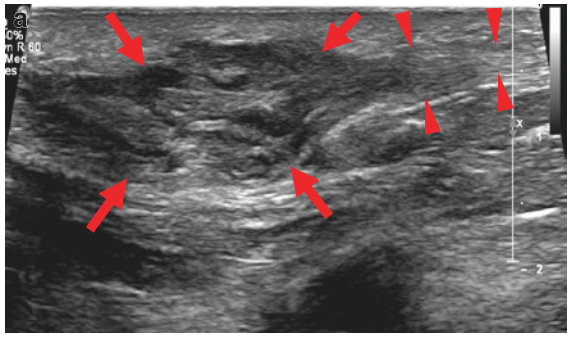

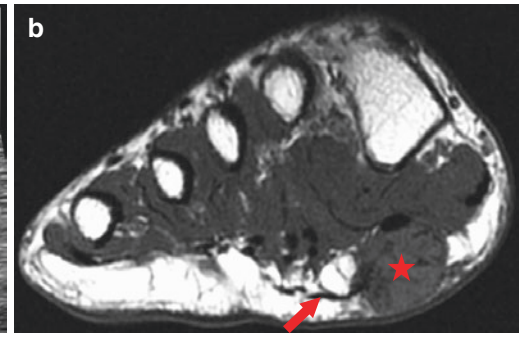

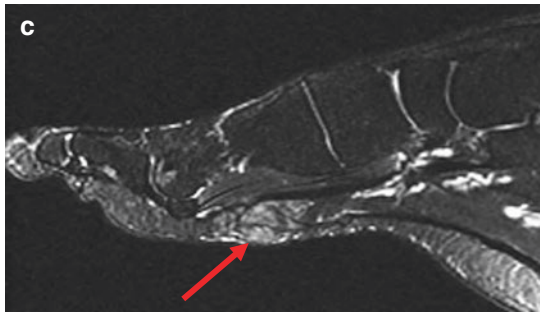

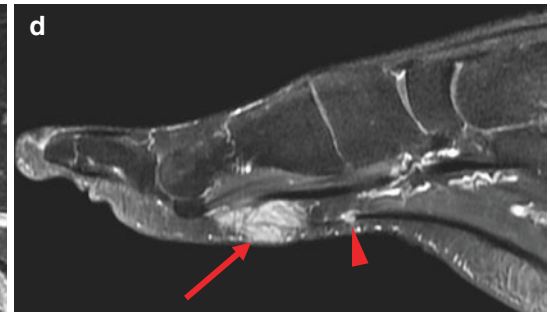

Fig. 5.23 Plantar fibromatosis. Longitudinal US (**a**) of the sole reveals a soft tissue mass (*arrows*) arising within the plantar fascia (*arrowheads*) on the plantar side of the right first metatarsal. The mass has an irregular margin and heterogeneous echotexture. Axial T1WI (**b**) shows an iso-signal intensity mass (*star*) with low signal foci attached to the plantar fascia (*arrow*). Sagittal FS T2WI (**c**) shows the hyperintense mass (*arrow*) with scattered low signal components. Sagittal postcontrast FS T1WI (**d**) shows prominent enhancement of the mass (*arrow*). Another small enhancing lesion (*arrowhead*) is observed in the plantar fascia proximal to the main mass

5.20.12 Desmoid-Type Fibromatosis

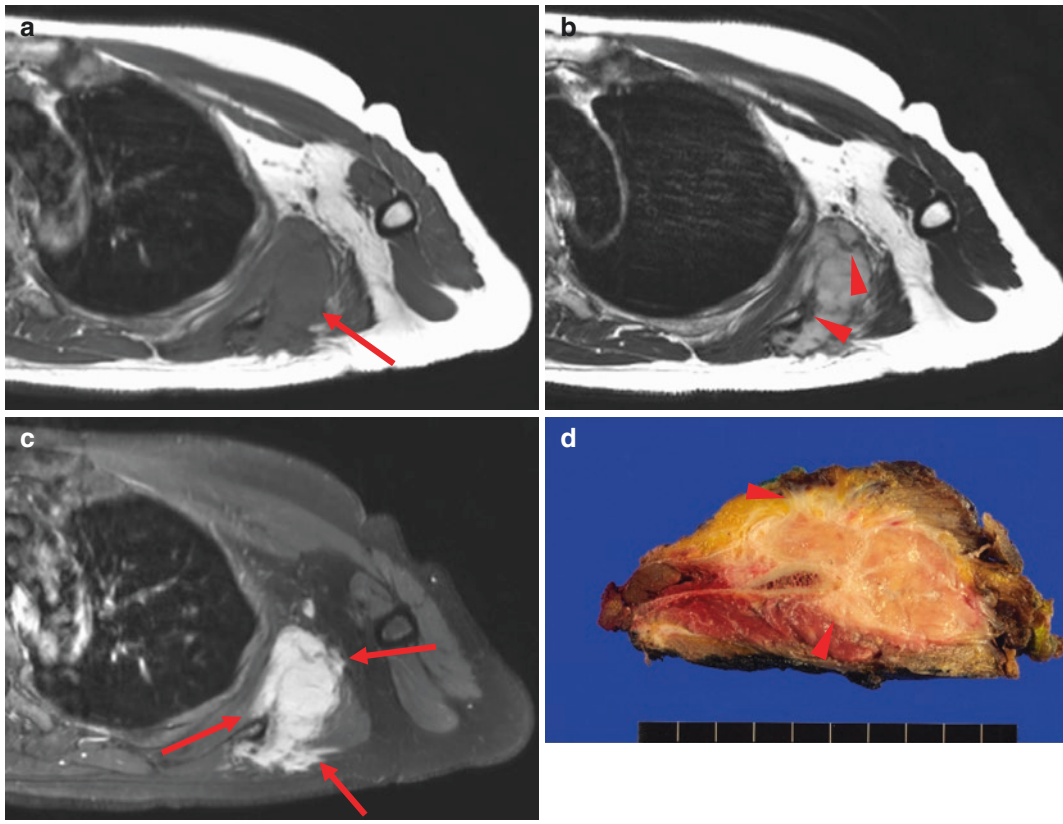

Fig. 5.24 Desmoid-type fibrosis. Axial T1WI (**a**) shows a deep soft tissue mass (*arrow*) that is isointense to muscle around the left scapula inferior angle. On axial T2WI (**b**), the mass is hyperintense and has some band-like low signal components (*arrowheads*). Axial postcontrast FS T1WI (**c**) shows prominent enhancement of the mass, which has an infiltrative margin (*arrows*) with the adjacent muscle and subcutaneous fat. (**d**) Cut section showing infiltrative margins (*arrowheads*) of the tumor with the subcutaneous fat and muscle

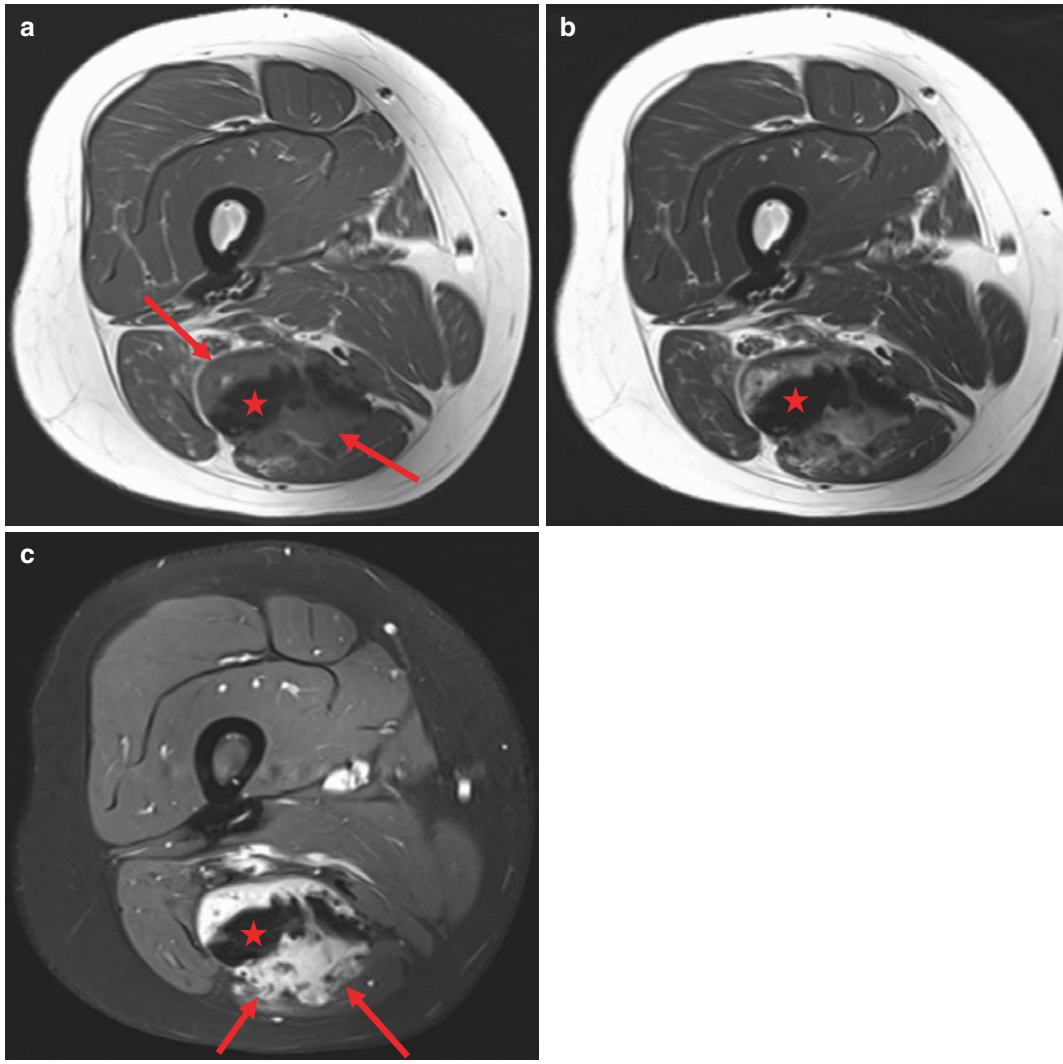

Fig. 5.25 Desmoid-type fibrosis. Axial T1WI (**a**) shows an intermuscular mass (*arrows*) in the posterior compartment of the right thigh. The mass is isointense to muscle and markedly hypointense at the center (*star*). Axial T2WI (**b**) shows a mass with a high signal intensity and a portion with a very low signal intensity (*star*). Axial post-contrast FS T1WI (**c**) shows prominent enhancement of the mass, except the densely fibrotic area (*star*). The posterior margin of the tumor is infiltrative and extends into the semitendinosus muscle (*arrows*)

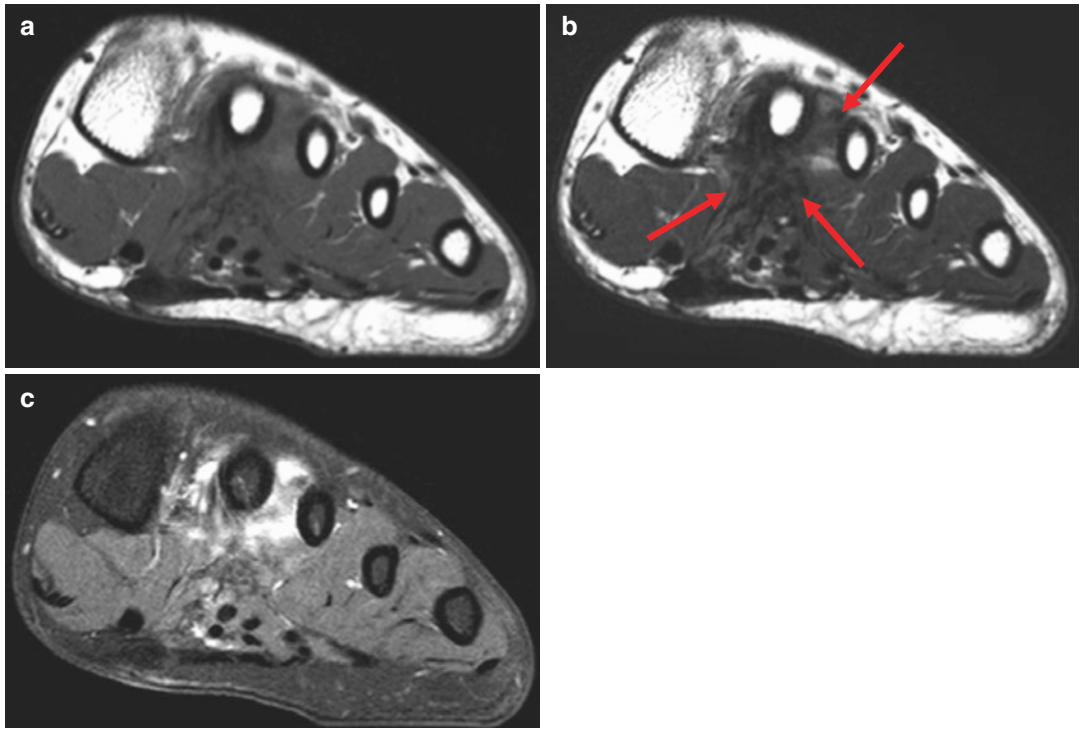

Fig. 5.26 Desmoid-type fibrosis. Axial T1WI (**a**) shows a poorly defined soft tissue mass around the left second metatarsal. Axial T2WI (**b**) shows the infiltrative mass with predominantly low signal intensity (*arrows*). Axial postcontrast FS T1WI (**c**) shows interspersed enhancing and non-enhancing parts of the mass

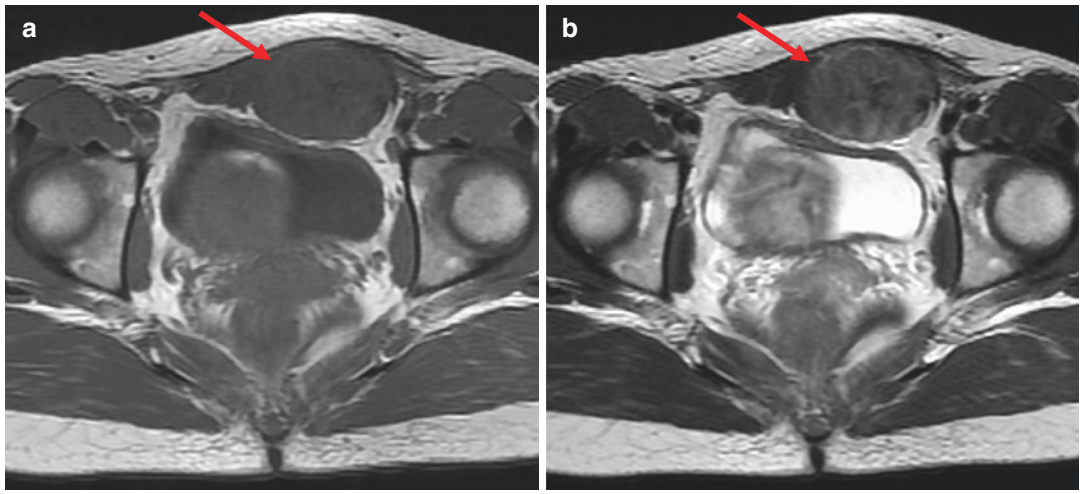

Fig. 5.27 Desmoid tumor of the abdominal wall. Axial T1WI (**a**) shows a soft tissue mass (*arrow*) in the left rectus abdominis; the mass is largely isointense to muscle. Axial T2WI (**b**) shows the relatively well-demarcated mass (*arrow*) to be slightly hyperintense to muscle, with several small areas of low signal intensity. Coronal postcontrast FS T1WI (**c**) shows prominent enhancement of the tumor, with an irregular non-enhancing segment in the distal portion (*arrow*)

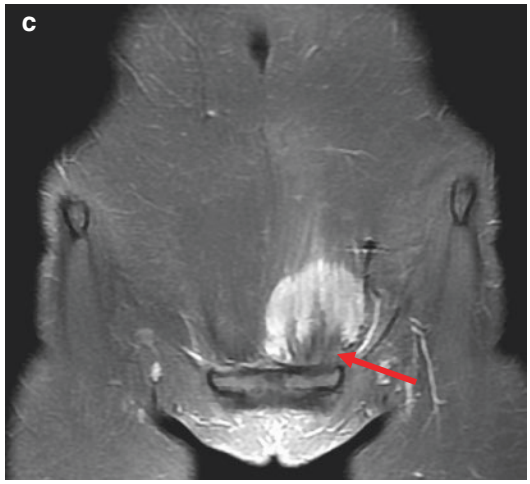

Fig. 5.27 (continued)

5.20.13 Dermatofibrosarcoma Protuberans

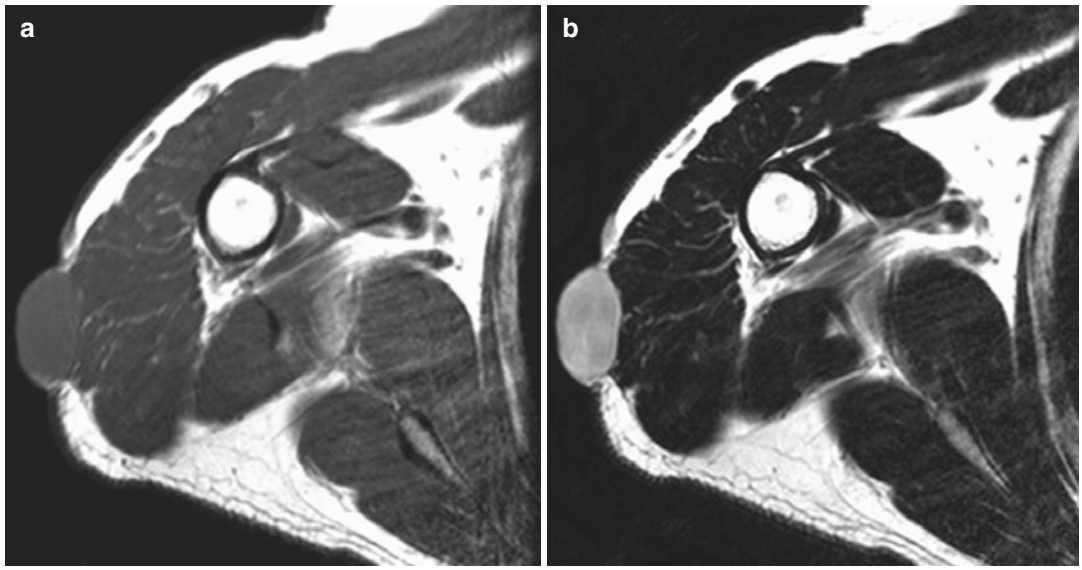

Fig. 5.28 Dermatofibrosarcoma protuberans. Axial T1WI (**a**) shows an exophytic mass with slight hyperintensity in the right lateral proximal upper arm. Axial T2WI (**b**) shows the hyperintense subcutaneous mass, which slightly compresses the subjacent deltoid muscle. The mass is slightly hyperintense to muscle, with several small areas of lower signal intensity. Coronal postcontrast FS T1WI (**c**) clearly reveals a small satellite lesion (*arrow*) on the anterior side of the main tumor

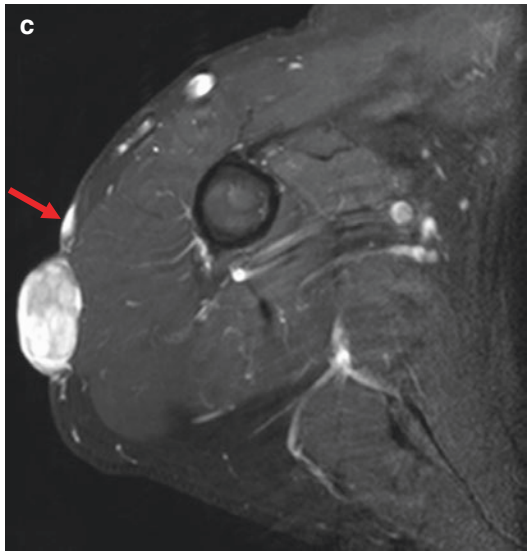

Fig. 5.28 (continued)

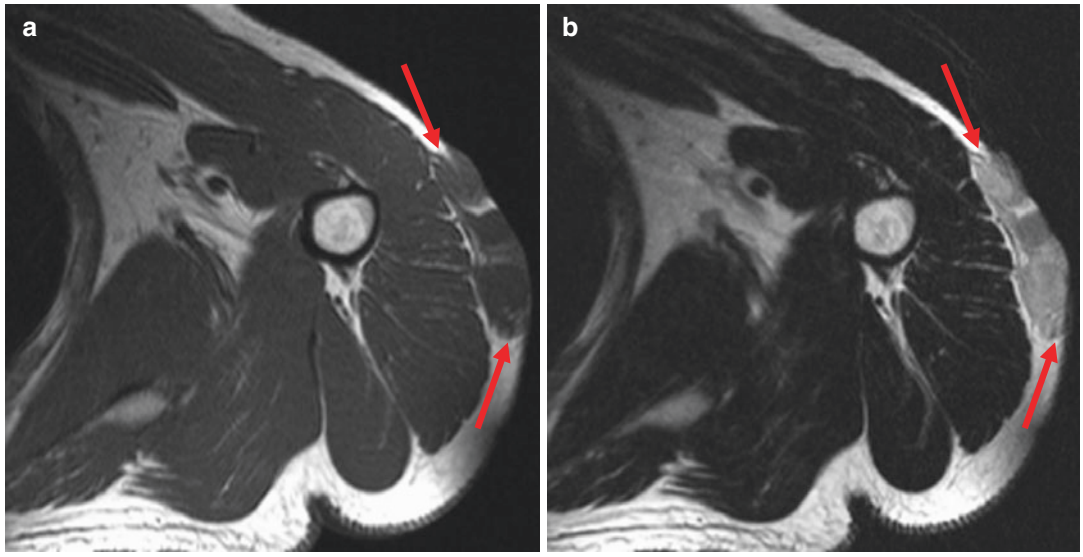

Fig. 5.29 Dermatofibrosarcoma protuberans. Axial T1WI (**a**) shows a subcutaneous mass (*arrows*) that abuts the skin in the left lateral proximal upper arm. Axial T2WI (**b**) shows the mass (*arrows*) with heterogeneous hyperintensity. Coronal postcontrast FS T1WI (**c**) shows strong enhancement of the lesion, with a central non-enhancing portion

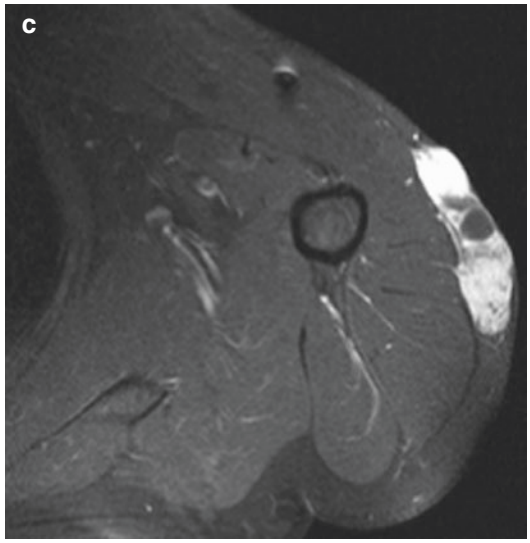

Fig. 5.29 (continued)

5.20.14 Solitary Fibrous Tumor

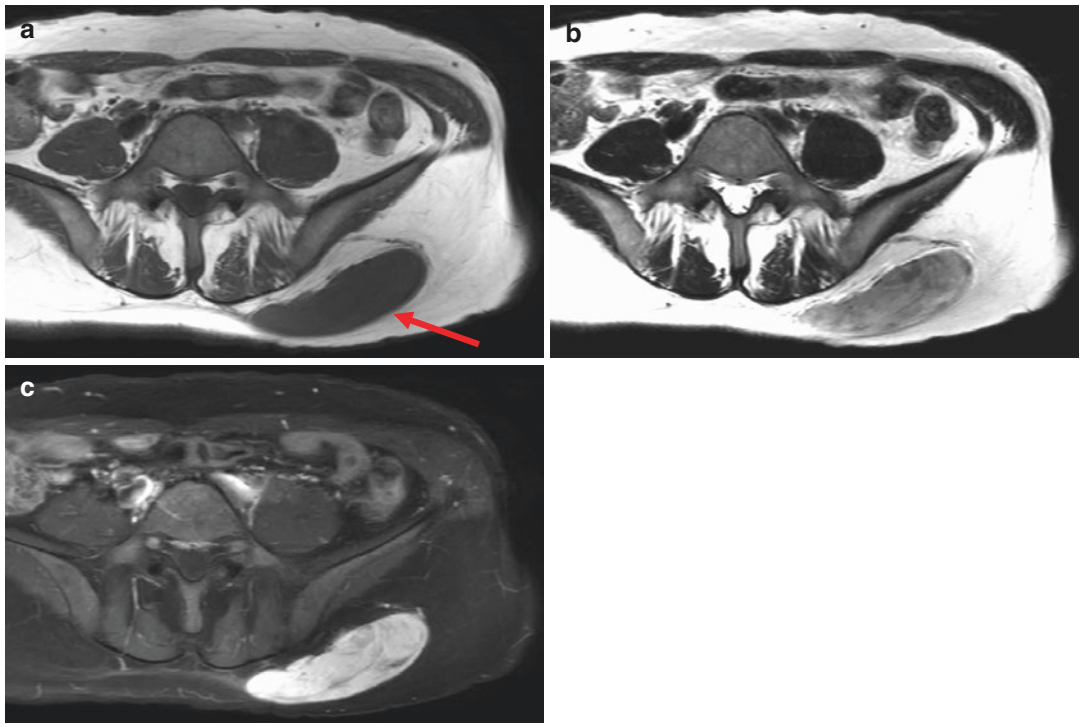

Fig. 5.30 Solitary fibrous tumor. Axial T1WI (**a**) shows an isointense subcutaneous mass (*arrow*) in the left buttock. Axial T2WI (**b**) shows a hyperintense mass with scattered low signal foci, suggestive of dense fibrous tissue. Axial postcontrast FS T1WI (**c**) shows marked enhancement of the lesion and several non-enhancing fibrotic components

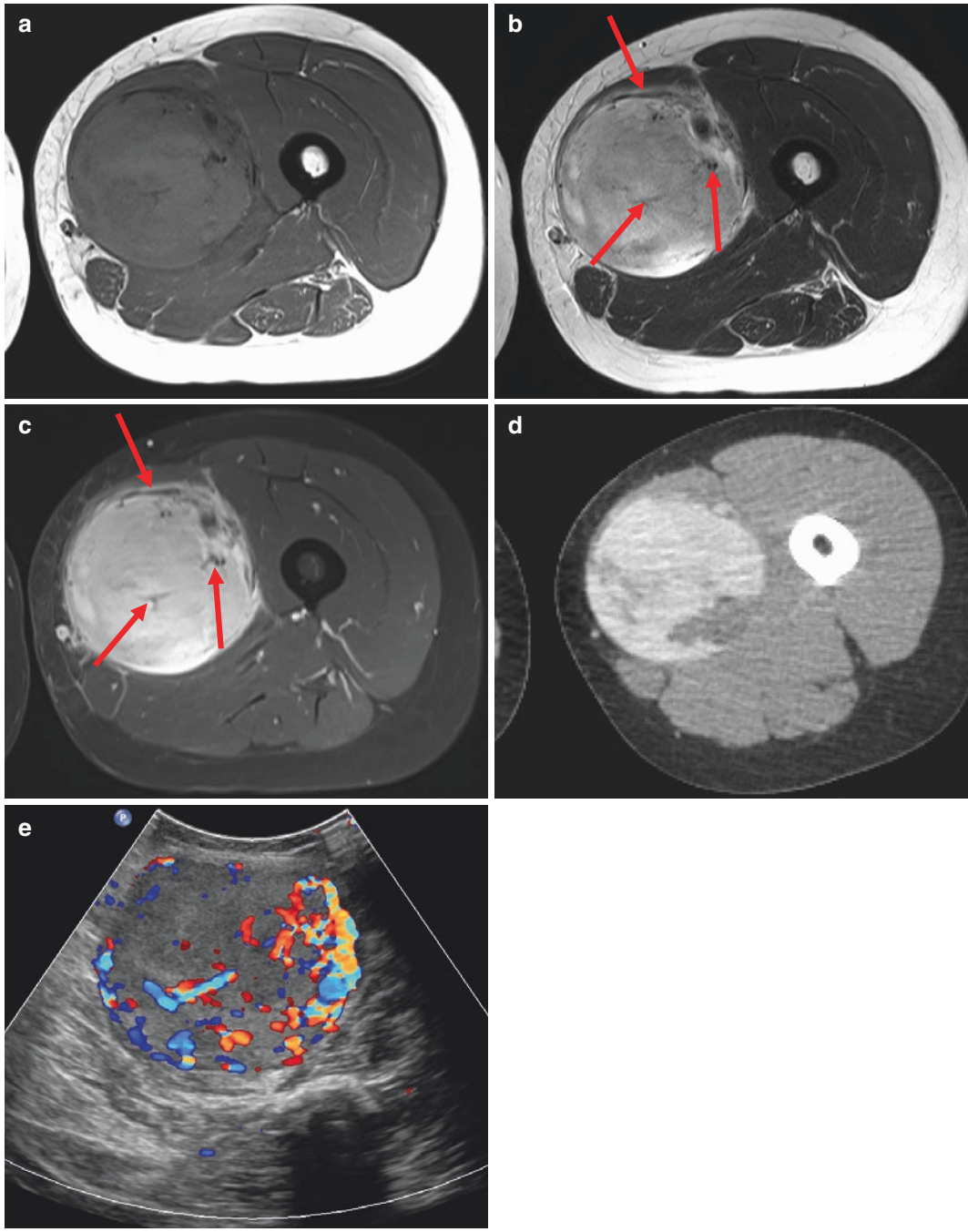

Fig. 5.31 Solitary fibrous tumor. Axial T1WI (**a**) shows an intermuscular mass between the sartorius and the adductor longus in the left thigh. The mass appears rather heterogeneous, iso- to hyperintense to muscle. Axial T2WI (**b**) shows the mass with heterogeneous hyperintensity. Axial postcontrast FS T1WI (**c**) shows a homogeneous enhancement of the lesion. There are multiple intratumoral serpentine vessels with signal voids (*arrows* in **b**, **c**). Contrast-enhanced CT scan (**d**) shows the intensely enhancing mass with some non-enhancing areas. Color Doppler US (**e**) demonstrates prominent vascularity within the tumor

5.20.15 Inflammatory Myofibroblastic Tumor

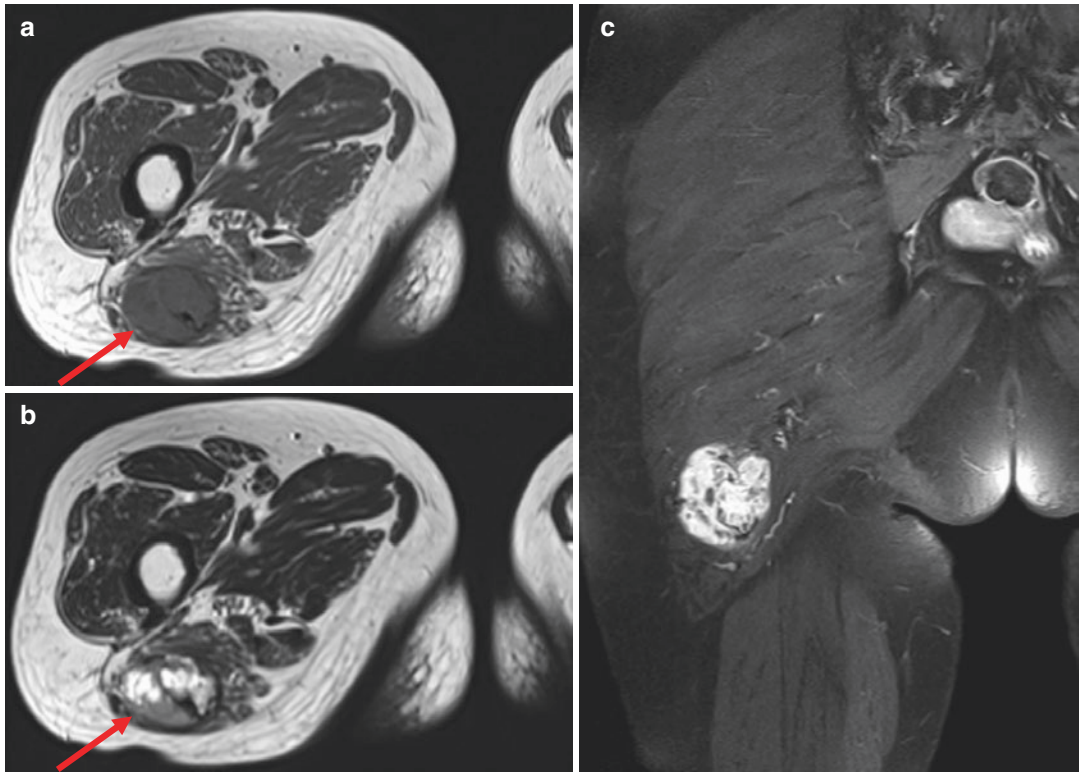

Fig. 5.32 Inflammatory myofibroblastic tumor. Axial T1WI (**a**) shows an intramuscular mass (*arrow*) in the right gluteus maximus. Axial T2WI (**b**) shows a mixed hyper- and hypointense mass (*arrow*) with dark components. Coronal postcontrast FS T1WI (**c**) shows a lobulated mass with prominent enhancement

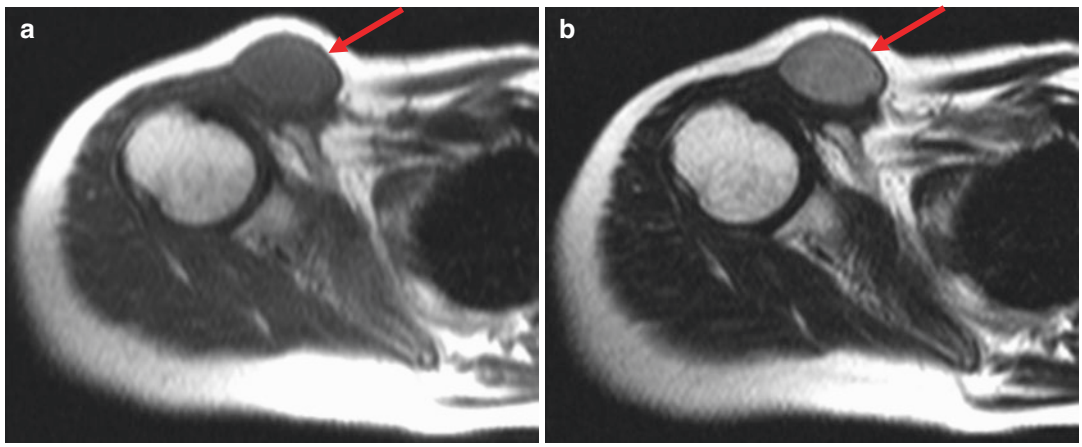

Fig. 5.33 Inflammatory myofibroblastic tumor. Axial T1WI (**a**) and T2WI (**b**) show a subfascial mass (*arrows*) in the right anterior deltoid muscle. The mass is moderately hyperintense relative to the muscle. Transverse US (**c**) shows a well-demarcated hypoechoic mass with fine internal echogenicity

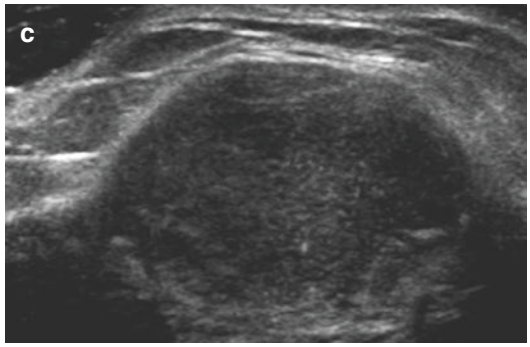

Fig. 5.33 (continued)

5.20.16 Myxofibrosarcoma

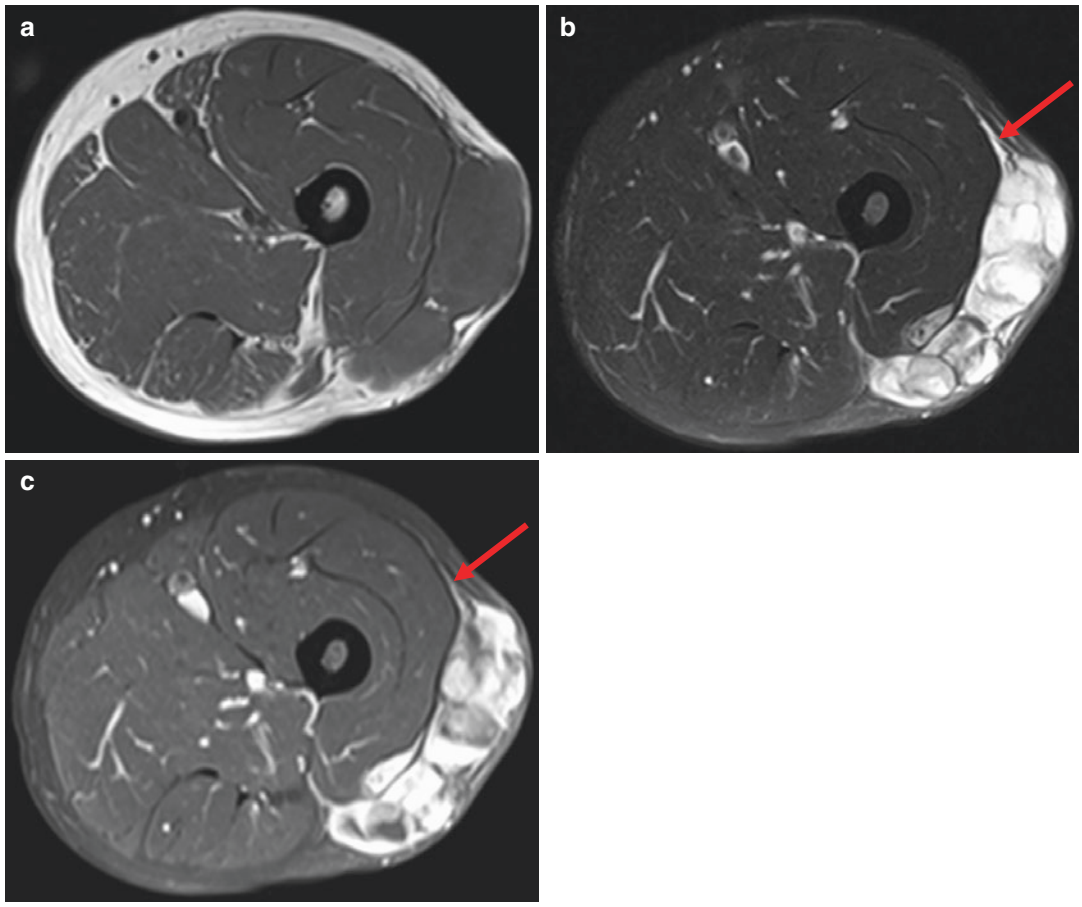

Fig. 5.34 Myxofibrosarcoma. Axial T1WI (**a**) shows a subcutaneous mass in the left lateral thigh. Axial FS T2WI (**b**) shows a mass with predominantly myxoid tissue and multiple hypointense linear fibrous septa. Axial postcontrast FS T1WI (**c**) shows prominent and heterogeneous enhancement of the mass. The tumor has a tail-like extension (*arrows* in **b**, **c**) along the fascial plane

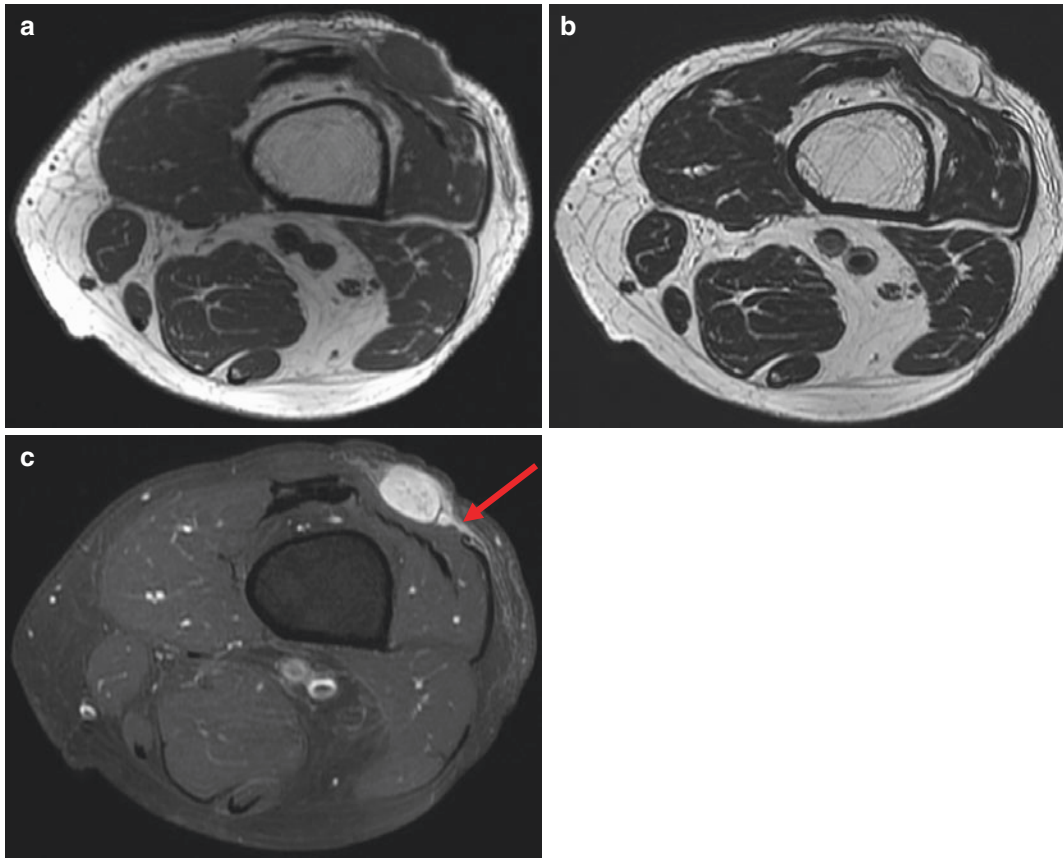

Fig. 5.35 Myxofibrosarcoma. Axial T1WI (**a**) shows a subcutaneous mass in the left distal anterior thigh. Axial T2WI (**b**) shows a hyperintense mass with some hypointense components. Axial postcontrast FS T1WI (**c**) shows strong enhancement of the mass and clearly demonstrates an enhancing tail-like structure (*arrow*)

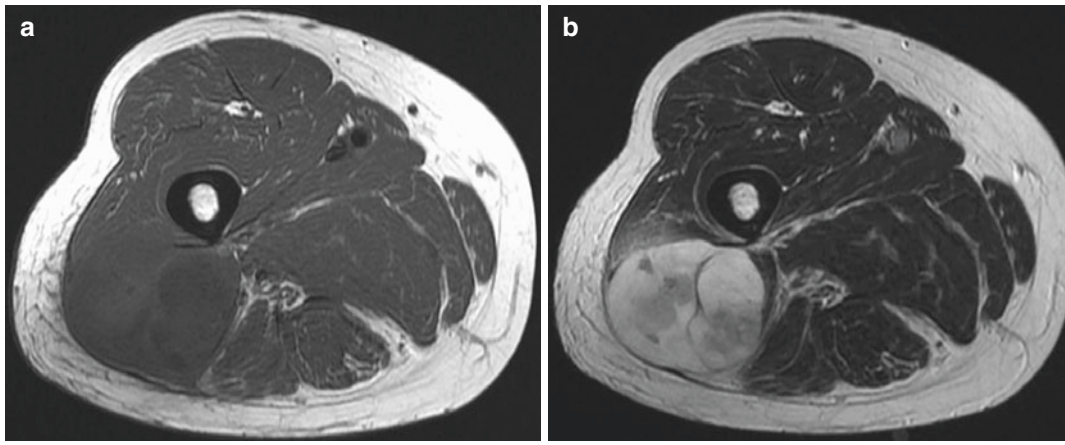

Fig. 5.36 Myxofibrosarcoma. Axial T1WI (**a**) shows an intermuscular mass with iso- and low signal intensity in the right lateral thigh. Axial T2WI (**b**) shows a heterogeneously hyperintense mass. Axial postcontrast FS T1WI (**c**) shows heterogeneous enhancement of the mass. There are tail-like enhancing lesions along the fascia (*arrows*) and fuzzy enhancement in the adjacent vastus lateralis muscle (*thick arrow*). (**d**) Gross specimen showing myxoid stroma with areas of hemorrhage and necrosis

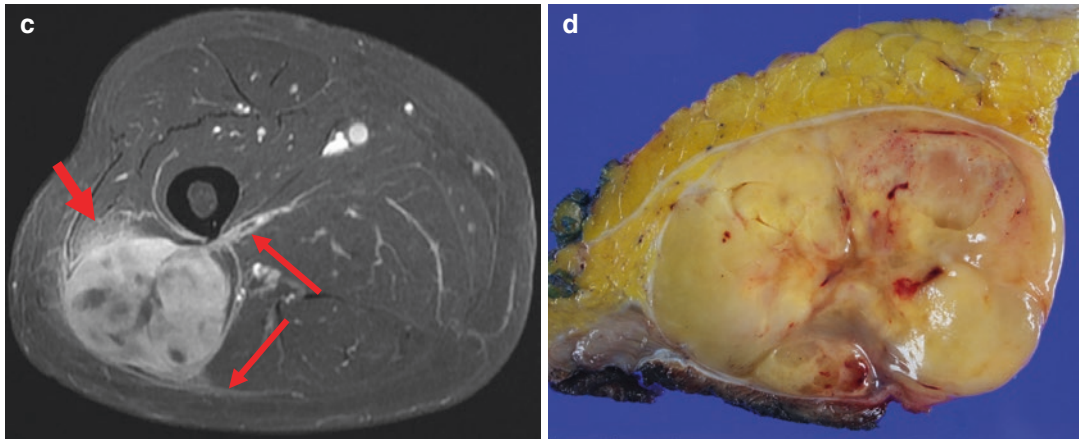

Fig. 5.36 (continued)

5.20.17 Low-Grade Fibromyxoid Sarcoma

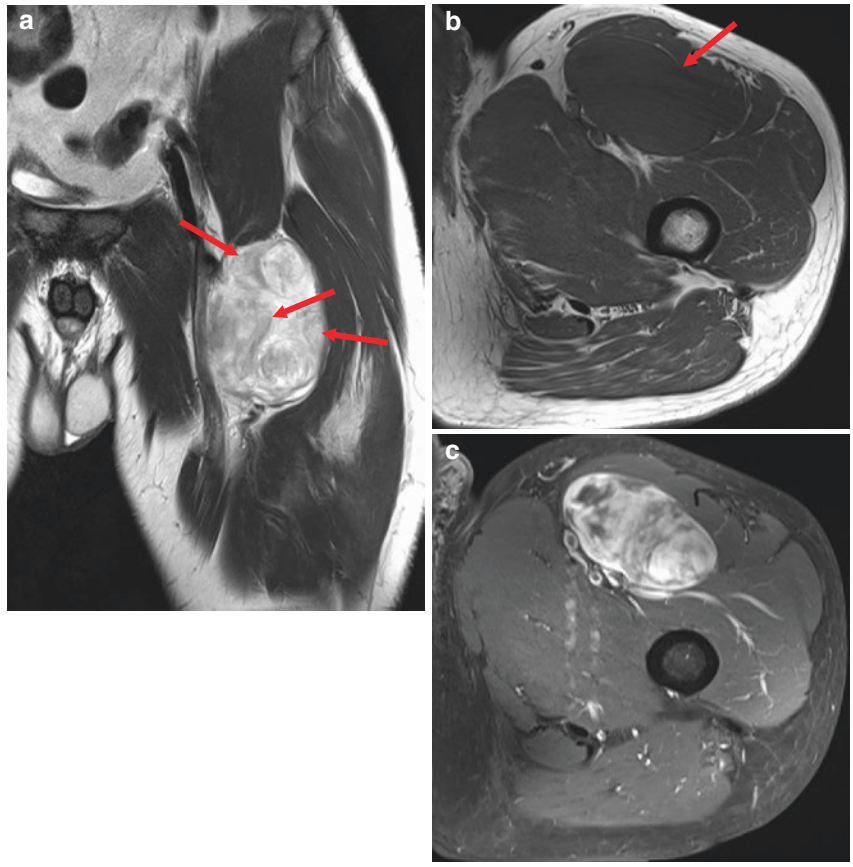

Fig. 5.37 Low-grade fibromyxoid sarcoma. Coronal T2WI (**a**) shows an intermuscular mass in the left proximal thigh. There is a gyriform pattern (*arrows*) that consists of multiple folds with relatively low signal intensity. Axial T1WI (**b**) shows an isointense mass (*arrow*). Axial postcontrast FS T1WI (**c**) shows heterogeneous enhancement of the mass, which exhibits a myxoid pattern

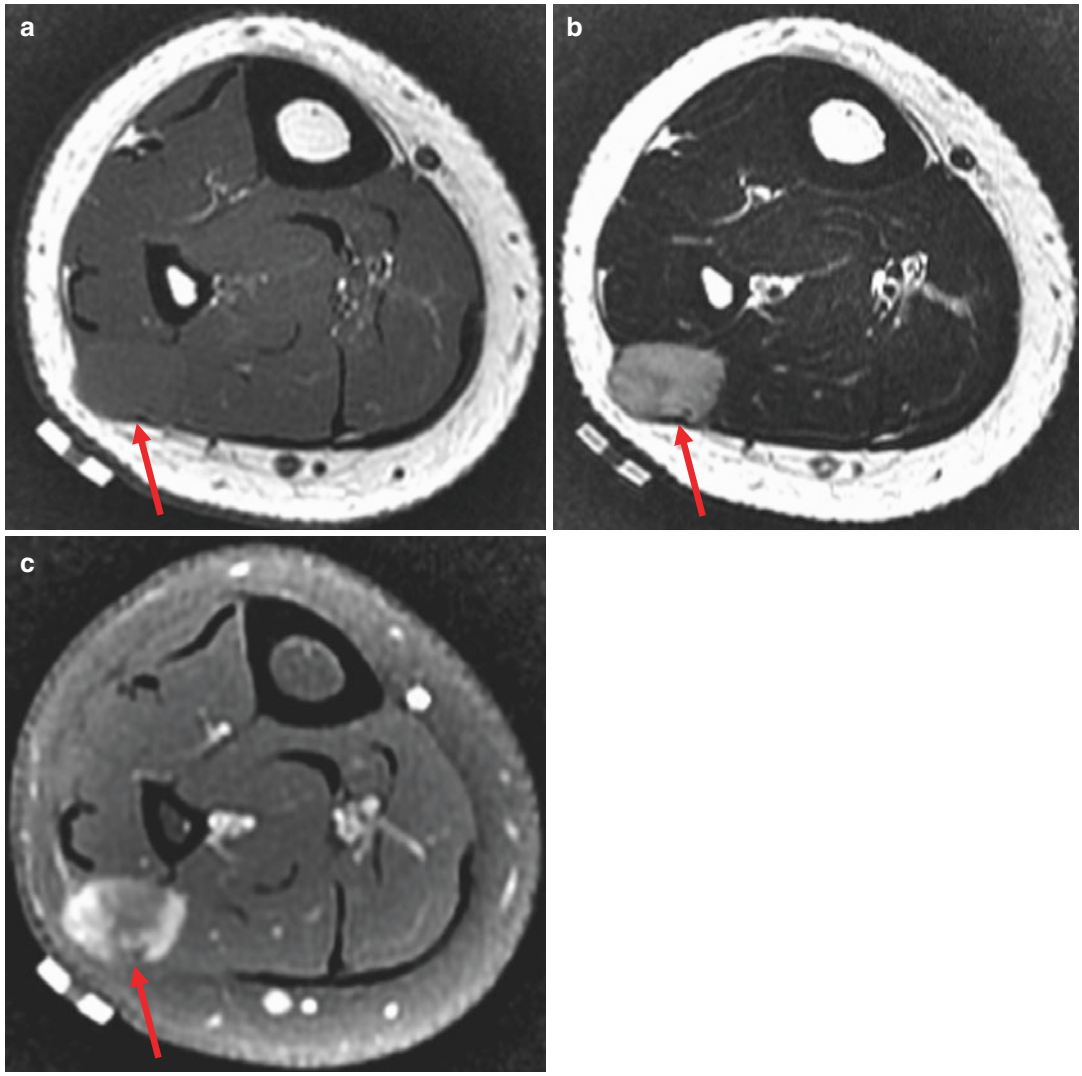

Fig. 5.38 Low-grade fibromyxoid sarcoma. Axial T1-, T2-, and postcontrast FS T1WI (**a**–**c**) show a subfascial mass (*arrow*) in the right posterolateral lower leg. The mass involves the deep fascia and extends to the subcutaneous layer

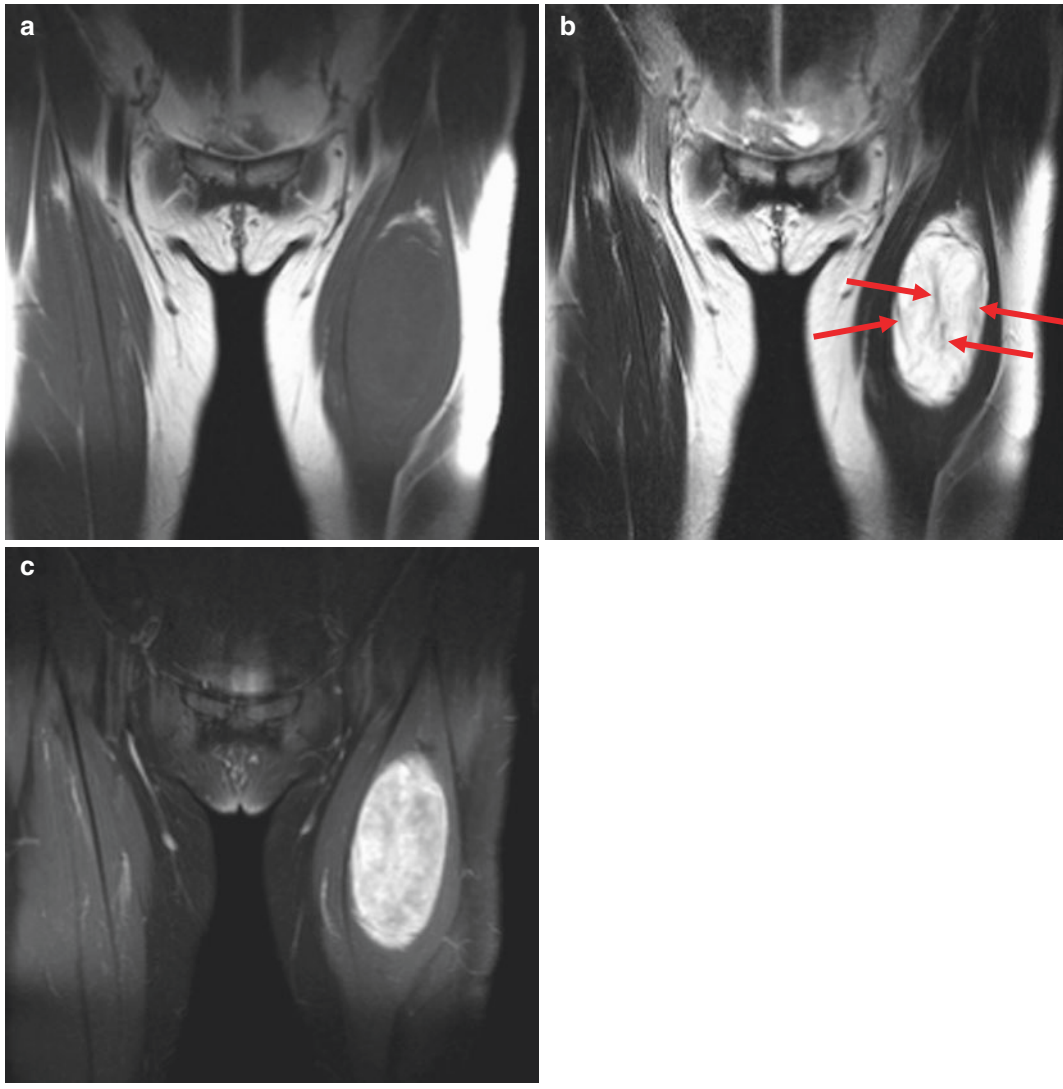

Fig. 5.39 Low-grade fibromyxoid sarcoma. Coronal T1WI (**a**) shows an intramuscular mass in the left rectus femoris. Coronal T2WI (**b**) reveals a T2 hyperintense mass with a predominantly myxoid appearance. Multiple band-like low signal components (*arrows*) correspond to fibrous tissue. Coronal postcontrast FS T1WI (**c**) shows prominent enhancement of the largely myxoid tumor

5.20.18 Low-Grade Myofibroblastic Sarcoma

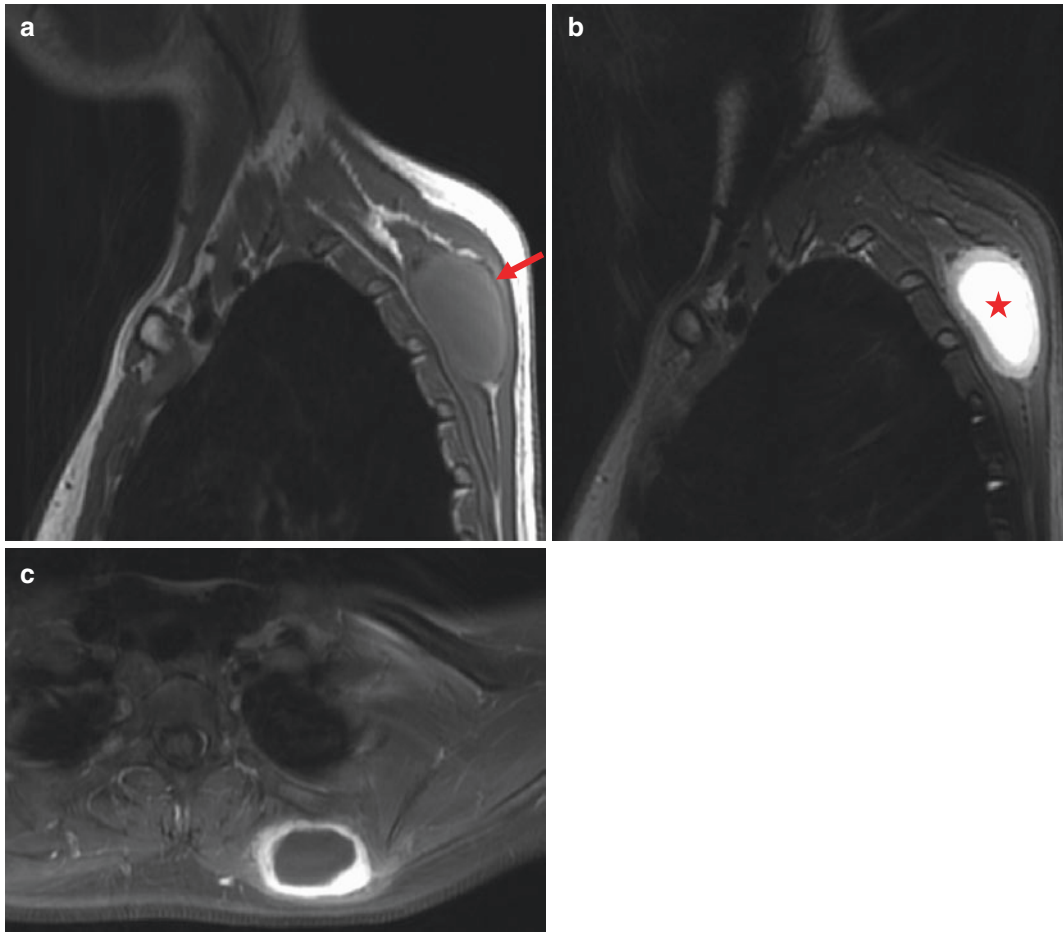

Fig. 5.40 Low-grade myofibroblastic sarcoma. Sagittal T1WI (**a**) shows an intermuscular mass (*arrow*) between the rhomboid major and trapezius. Sagittal FS T2WI (**b**) shows a hyperintense mass with a large central area (*star*) exhibiting a fluid-like signal. Axial postcontrast FS T1WI (**c**) shows prominent enhancement at the peripheral portion of the tumor

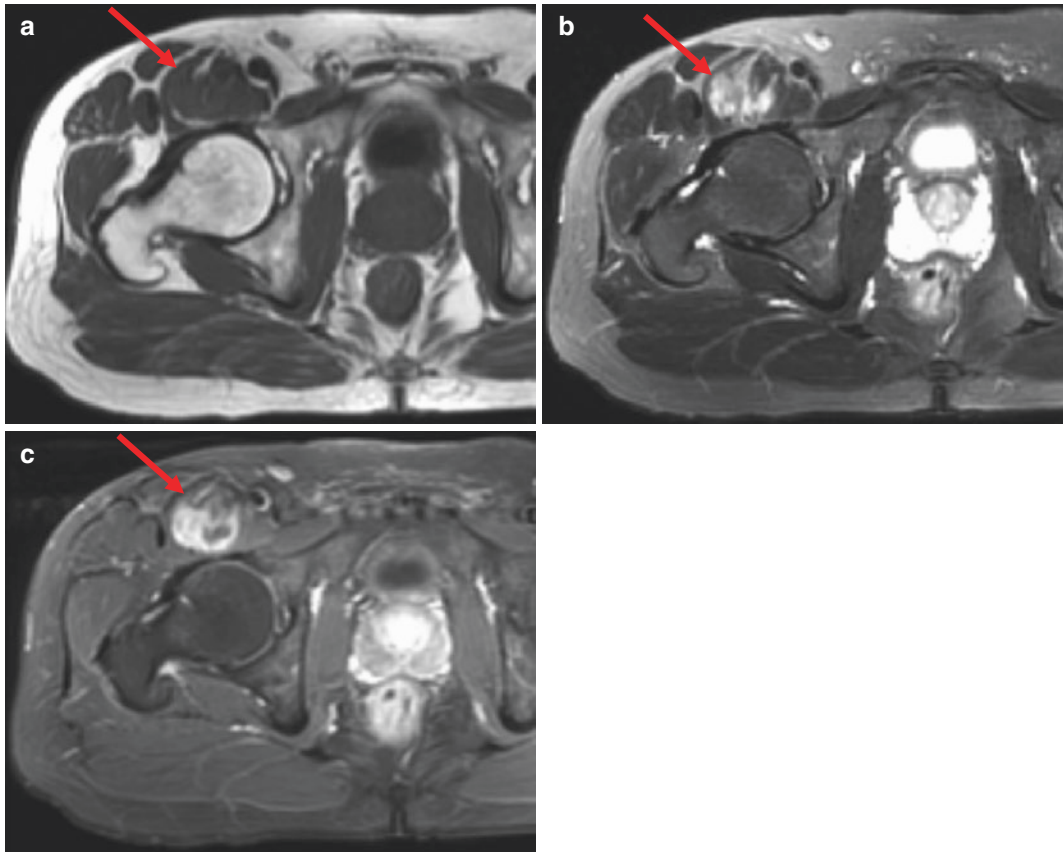

Fig. 5.41 Low-grade myofibroblastic sarcoma. Axial T1WI (**a**) shows an isointense mass (*arrow*) in the right iliopsoas muscle. Axial FS T2WI (**b**) shows a heterogeneously hyperintense mass (*arrow*) intermingled with muscle fascicles. Axial postcontrast FS T1WI (**c**) shows heterogeneous enhancement of the mass (*arrow*)

5.20.19 Sclerosing Epithelioid Fibrosarcoma

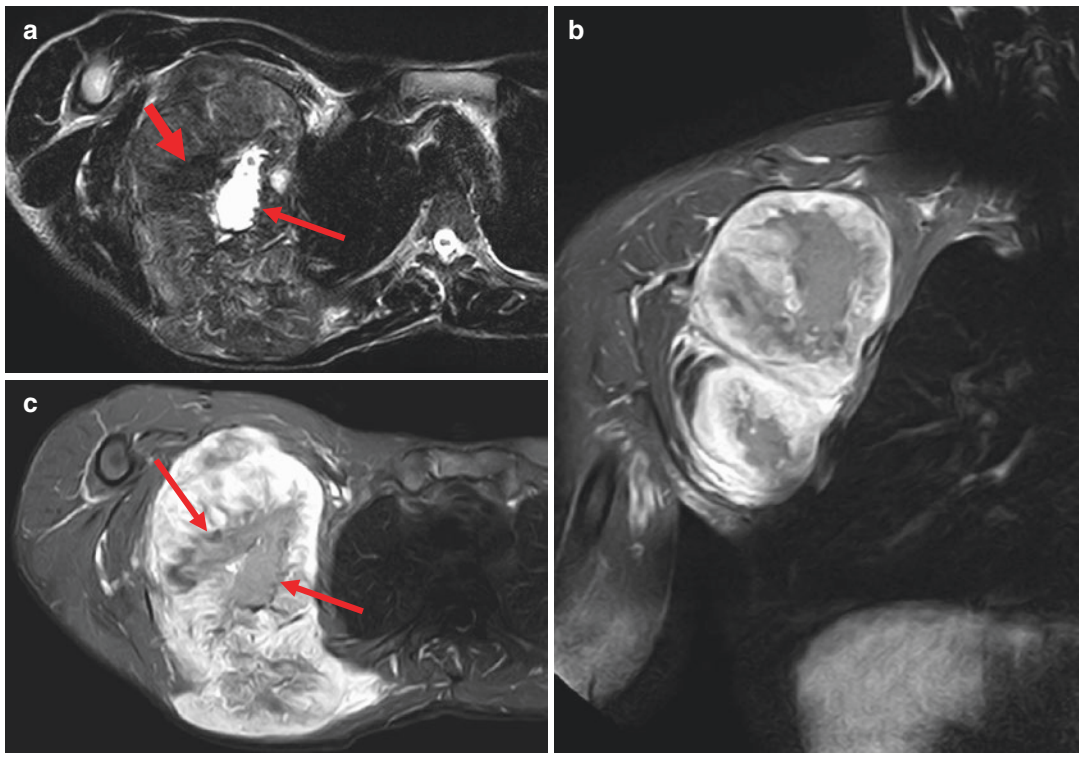

Fig. 5.42 Sclerosing epithelioid fibrosarcoma. Axial T2WI (**a**) reveals a large axillary mass with a relative T2 hypointensity. There are areas of central fluid-like signal (*arrow*) and marked T2 hypointensity (*thick arrow*), in keeping with dense fibrosis. Axial and coronal postcontrast FS T1WI (**b**, **c**) shows heterogeneous enhancement of the mass, which exhibits central non-enhancing areas (*arrows*)

References

Ablin DS, Jain K, Howell L, West DC. Ultrasound and MR imaging of fibromatosis colli (sternomastoid tumor of infancy). Pediatr Radiol. 1998;28(4):230–3. doi:10.1007/s002470050337.

Al-Qattan MM. Fibroma of tendon sheath of the hand: a series of 20 patients with 23 tumours. J Hand Surg Eur. 2014;39(3):300–5. doi:10.1177/1753193412469146.

Braschi-Amirfarzan M, Keraliya AR, Krajewski KM, Tirumani SH, Shinagare AB, Hornick JL, Baldini EH, George S, Ramaiya NH, Jagannathan JP. Role of imaging in management of desmoid-type fibromatosis: a primer for radiologists. Radiographics. 2016;36(3):767–82. doi:10.1148/rg.2016150153.

Chang WC, Huang GS, Lee HS, Lee CH. Fibrous hamartoma of infancy at the wrist. Pediatr Int. 2010;52(2):317–8. doi:10.1111/j.1442-200X.2010.03028.x.

Christensen DR, Ramsamooj R, Gilbert TJ. Sclerosing epithelioid fibrosarcoma: short T2 on MR imaging. Skelet Radiol. 1997;26(10):619–21.

Chung EB, Enzinger FM. Proliferative fasciitis. Cancer. 1975;36(4):1450–8.

Fletcher CD. The evolving classification of soft tissue tumours—an update based on the new 2013 WHO classification. Histopathology. 2014;64(1):2–11. doi:10.1111/his.12267.

Fletcher CDM, Bridge JA, Hogendoorn P, Martens F. WHO classification of tumours of soft tissue and bone. 4th ed. Lyon: IARC Pess; 2013.

Fox MG, Kransdorf MJ, Bancroft LW, Peterson JJ, Flemming DJ. MR imaging of fibroma of the tendon sheath. AJR Am J Roentgenol. 2003;180(5):1449–53. doi:10.2214/ajr.180.5.1801449.

Fukunaga M, Ushigome S. Collagenous fibroma (desmoplastic fibroblastoma): a distinctive fibroblastic soft tissue tumor. Adv Anat Pathol. 1999;6(5):275–80.

Garcia-Bennett J, Olive CS, Rivas A, Dominguez-Oronoz R, Huguet P. Soft tissue solitary fibrous tumor. Imaging findings in a series of nine cases. Skelet Radiol.2012;41(11):1427–33.doi:10.1007/s00256-012-1364-y.

Gengler C, Guillou L. Solitary fibrous tumour and haemangiopericytoma: evolution of a concept. Histopathology.2006;48(1):63–74.doi:10.1111/j.1365-2559.2005.02290.x.

Hwang S, Kelliher E, Hameed M. Imaging features of low-grade fibromyxoid sarcoma (Evans tumor). Skelet Radiol.2012;41(10):1263–72.doi:10.1007/s00256-012-1417-2.

Jo VY, Fletcher CD. WHO classification of soft tissue tumours: an update based on the 2013 (4th) edition. Pathology. 2014;46(2):95–104. doi:10.1097/PAT.0000000000000050.

Kaya M, Wada T, Nagoya S, Sasaki M, Matsumura T, Yamaguchi T, Hasegawa T, Yamashita T. MRI and histological evaluation of the infiltrative growth pattern of myxofibrosarcoma. Skelet Radiol. 2008;37(12):1085–90. doi:10.1007/s00256-008-0542-4.

Khuu A, Yablon CM, Jacobson JA, Inyang A, Lucas DR, Biermann JS. Nodular fasciitis: characteristic imaging features on sonography and magnetic resonance imaging. J Ultrasound Med. 2014;33(4):565–73. doi:10.7863/ultra.33.4.565.

Kransdorf MJ, Meis JM, Jelinek JS. Myositis ossificans: MR appearance with radiologic-pathologic correlation. AJR Am J Roentgenol. 1991;157(6):1243–8. doi:10.2214/ajr.157.6.1950874.

Kudo S. Elastofibroma dorsi: CT and MR imaging findings. Semin Musculoskelet Radiol. 2001;5(2):103–5. doi:10.1055/s-2001-15661.

Kuzel P, Mahmood MN, Metelitsa AI, Salopek TG. A clinicopathologic review of a case series of dermatofibrosarcoma protuberans with fibrosarcomatous differentiation. J Cutan Med Surg. 2015;19(1):28–34. doi:10.2310/7750.2014.13192.

Kwak HS, Lee SY, Kim JR, Lee KB. MR imaging of calcifying aponeurotic fibroma of the thigh. Pediatr Radiol. 2004;34(5):438–40. doi:10.1007/s00247-003-1110-7.

Lee JC, Thomas JM, Phillips S, Fisher C, Moskovic E. Aggressive fibromatosis: MRI features with pathologic correlation. AJR Am J Roentgenol. 2006;186(1):247–54. doi:10.2214/AJR.04.1674.

Lefkowitz RA, Landa J, Hwang S, Zabor EC, Moskowitz CS, Agaram NP, Panicek DM. Myxofibrosarcoma: prevalence and diagnostic value of the "tail sign" on magnetic resonance imaging. Skelet Radiol. 2013;42(6):809–18. doi:10.1007/s00256-012-1563-6.

Luo Y, Hu W, Wu H, Xue H, Huo L, Li F, Zhao Y, Dai M. (1)(8)F-fluorodeoxyglucose PET/CT features and correlations with histopathologic characteristics in sclerosing epithelioid fibrosarcoma. Int J Clin Exp Pathol. 2014;7(10):7278–85.

Mavrogenis AF, Soucacos PN, Papagelopoulos PJ. Heterotopic ossification revisited. Orthopedics. 2011;34(3):177. doi:10.3928/01477447-20110124-08.

Murphey MD, Ruble CM, Tyszko SM, Zbojniewicz AM, Potter BK, Miettinen M. From the archives of the AFIP: musculoskeletal fibromatoses: radiologic-pathologic correlation. Radiographics. 2009;29(7):2143–73. doi:10.1148/rg.297095138.

Musyoki FN, Nahal A, Powell TI. Solitary fibrous tumor: an update on the spectrum of extrapleural manifestations. Skelet Radiol. 2012;41(1):5–13. doi:10.1007/s00256-010-1032-z.

Ozpolat B, Yazkan R, Yilmazer D, Kocak N, Yucel E. Elastofibroma dorsi: report of a case with diagnostic features. J Ultrasound Med. 2008;27(2):287–91.

Pulitzer DR, Martin PC, Reed RJ. Fibroma of tendon sheath. A clinicopathologic study of 32 cases. Am J Surg Pathol. 1989;13(6):472–9.

Qiu X, Montgomery E, Sun B. Inflammatory myofibroblastic tumor and low-grade myofibroblastic sarcoma: a comparative study of clinicopathologic features and further observations on the immunohistochemical profile of myofibroblasts. Hum Pathol. 2008;39(6):846–56. doi:10.1016/j.humpath.2007.10.010.

Robbin MR, Murphey MD, Temple HT, Kransdorf MJ, Choi JJ. Imaging of musculoskeletal fibromatosis. Radiographics. 2001;21(3):585–600. doi:10.1148/radiographics.21.3.g01ma21585.

San Miguel P, Fernandez G, Ortiz-Rey JA, Larrauri P. Low-grade myofibroblastic sarcoma of the distal phalanx. J Hand Surg Am. 2004;29(6):1160–3. doi:10.1016/j.jhsa.2004.05.003.

Sargar K, Kao SC, Spunt SL, Hawkins DS, Parham DM, Coffin C, McCarville MB. MRI and CT of low-grade fibromyxoid sarcoma in children: a report from children's oncology group study ARST0332. AJR Am J Roentgenol. 2015;205(2):414–20. doi:10.2214/AJR.14.13972.

Sargar KM, Sheybani EF, Shenoy A, Aranake-Chrisinger J, Khanna G. Pediatric fibroblastic and myofibroblastic tumors: a pictorial review. Radiographics. 2016;36(4):1195–214. doi:10.1148/rg.2016150191.

Sarteschi M, Ciatti S, Sabo C, Massei P, Paoli R. Proliferative myositis: rare pseudotumorous lesion. J Ultrasound Med. 1997;16(11):771–3.

Serra-Guillen C, Sanmartin O, Llombart B, Nagore E, Deltoro C, Martin I, Borella-Estrada R, Requena C, Martorell-Calatayud A, Cervera J, Guillen C. Correlation between preoperative magnetic resonance imaging and surgical margins with modified Mohs for dermatofibrosarcoma protuberans. Dermatol Surg. 2011;37(11):1638–45. doi:10.1111/j.1524-4725.2011.02077.x.

Shuto R, Kiyosue H, Hori Y, Miyake H, Kawano K, Mori H. CT and MR imaging of desmoplastic fibroblastoma. Eur Radiol. 2002;12(10):2474–6. doi:10.1007/s00330-001-1217-x.

Skelton E, Howlett D. Fibromatosis colli: the sternocleidomastoid pseudotumour of infancy. J Paediatr Child Health. 2014;50(10):833–5. doi:10.1111/jpc.12506.

Stensby JD, Conces MR, Nacey NC. Benign fibrous hamartoma of infancy: a case of MR imaging paralleling histologic findings. Skelet Radiol. 2014;43(11):1639–43. doi:10.1007/s00256-014-1940-4.

Tan H, Wang B, Xiao H, Lian Y, Gao J Radiologic and clinicopathologic findings of inflammatory myofibroblastic tumor. J Comput Assist Tomogr. 2016. doi:10.1097/RCT.0000000000000444.

Torreggiani WC, Al-Ismail K, Munk PL, Nicolaou S, O'Connell JX, Knowling MA. Dermatofibrosarcoma protuberans: MR imaging features. AJR Am J Roentgenol. 2002;178(4):989–93. doi:10.2214/ajr.178.4.1780989.

Walczak BE, Johnson CN, Howe BM. Myositis ossificans. J Am Acad Orthop Surg. 2015;23(10):612–22. doi:10.5435/JAAOS-D-14-00269.

Watsky MA, Weber KT, Sun Y, Postlethwaite A. New insights into the mechanism of fibroblast to myofibroblast transformation and associated pathologies. Int Rev Cell Mol Biol. 2010;282:165–92. doi:10.1016/S1937-6448(10)82004-0.

Yigit H, Turgut AT, Kosar P, Astarci HM, Kosar U. Proliferative myositis presenting with a checkerboard-like pattern on CT. Diagn Interv Radiol. 2009;15(2):139–42.

Yoo HJ, Hong SH, Kang Y, Choi JY, Moon KC, Kim HS, Han I, Yi M, Kang HS. MR imaging of myxofibrosarcoma and undifferentiated sarcoma with emphasis on tail sign; diagnostic and prognostic value. Eur Radiol. 2014;24(8):1749–57. doi:10.1007/s00330-014-3181-2.

Yoon N, Kwon JW, Seo SW, Ahn G, Choi YL. Sclerosing epithelioid fibrosarcoma: cytogenetic analysis of FUS rearrangement. Pathol Int. 2012;62(1):65–8. doi:10.1111/j.1440-1827.2011.02752.x.

So-Called Fibrohistiocytic Tumors

6

Using electron microscopy, immunohistochemistry, and cytogenetics, it has come to be understood that most tumors that were initially considered to be various types of fibrohistiocytic tumors are actually not histiocytic in origin. Rather, these tumors are a diverse group of neoplasms that only appear histologically similar to fibrohistiocytic tumors. In the revised 2013 WHO classification of soft tissue sarcomas, the term "malignant fibrous histiocytoma" was removed from the "so-called fibrohistiocytic tumor" category. The so-called fibrohistiocytic tumors are composed of the following four tumors: tenosynovial giant cell tumor, deep benign fibrous histiocytoma, plexiform fibrohistiocytic tumor, and giant cell tumor of soft tissue.

6.1 Tenosynovial Giant Cell Tumor

Tenosynovial giant cell tumors (TSGCT) encompass a family of lesions that arise from the synovium of joints, bursae, or tendon sheath, which show synoviocytic differentiation (Boland et al. 2009). These tumors are divided into intra- or extra-articular types according to their location and into localized or diffuse types according to their growth pattern. The localized type of TSGCT is also known as giant cell tumor of tendon sheath or nodular tenosynovitis. This is a benign neoplasm composed of synovial-like mononuclear cells, accompanied by a variable number of multinucleate osteoclast-like cells, foamy histiocytes (xanthoma cells with cholesterol clefts), siderophages (hemosiderin deposit), and inflammatory cells. The diffuse type of TSGCT is referred to as diffuse-type giant cell tumor, pigmented villonodular synovitis, or pigmented villonodular tenosynovitis. This tumor is a locally aggressive neoplasm but is composed of similar cells as in the localized type (de Saint Aubain Somerhausen and van de Rijn 2013).

The localized type of TSGCT is the most common type of giant cell tumors. These tumors usually occur in patients between 30 and 50 years of age and exhibit a 2:1 female predominance. This lesion occurs predominantly in the hand and is the second most common benign tumor of the hand after ganglion cysts. The diffuse type of TSGCT tends to affect younger patients (aged < 40 years) than the localized type. Diffuse type TSGCTs affect large joints, predominantly the knee, followed by the hip, ankle, elbow, and shoulder. The localized type of TSGCT often presents with a firm, slow-growing, non-tender mass. Patients with the diffuse type complain of pain, tenderness, swelling, or limitation of motion (de Saint Aubain Somerhausen and van de Rijn 2013; Ushijima et al. 1986).

Radiographic appearances vary by the type and size of the lesions. Localized extra-articular lesions appear as soft tissue masses, with occasional pressure erosion of the adjacent bone.

H.S. Kang et al., *Oncologic Imaging: Soft Tissue Tumors*, DOI 10.1007/978-981-287-718-5_6

The diffuse intra-articular lesions commonly manifest as joint effusion, soft tissue swelling, absence of mineralization, extrinsic erosions of bone, preservation of joint space, and normal bone mineralization (Murphey et al. 2008). On US, TSGCTs of the localized type may appear as a well-circumscribed, solid, homogeneous, or heterogeneous hypoechoic soft tissue mass close to the tendon or joint, with detectable internal vascularity on color or power Doppler US (Middleton et al. 2004). MR imaging is the modality of choice for diagnosis of TSGCT. TSGCT typically displays a low-to-intermediate signal on T1-weighted images. Intralesional hypointense foci on T2-weighted images due to the paramagnetic effect of hemosiderin are characteristic of TSGCT. On gradient-echo images, the paramagnetic effect of hemosiderin (blooming effect) is further exaggerated, creating areas of very low signal intensity. MR imaging effects of hemosiderin vary more in the localized type of TSGCT. In cases with more limited hemosiderin deposits, signal intensity may be hyperintense on T2-weighted images than expected. Diffuse contrast enhancement of varying degree is observed in most cases (Al-Nakshabandi et al. 2004; Murphey et al. 2008). Additional MR imaging features of diffuse intra-articular TSGCT include heterogeneous, diffuse, plaque-like, or nodular synovial thickening, bone erosion or subchondral cysts, septation, edema in the adjacent bone or soft tissue, and articular cartilage defects (Hughes et al. 1995).

The recurrence rate for the localized type is generally lower than for the diffuse type. The recurrence following surgical resection of the localized type of TSGCT ranges from 0% to 44%; however, these recurrences are usually non-destructive and controllable by surgical re-excision. Factors that have been suggested to increase the recurrence rate include lesion location, history of previous operations, and positive surgical margins (Murphey et al. 2008; Schwartz et al. 1989; Flandry and Hughston 1987). Therefore, diffuse type of TSGCT is regarded as a locally aggressive but non-metastasizing neoplasm, and wide excision is the treatment of choice (de Saint Aubain Somerhausen and van de Rijn 2013).

6.2 Deep Benign Fibrous Histiocytoma

Benign fibrous histiocytoma (BFH) is among the most common soft tissue skin tumor and is composed of bland fibroblasts arranged in a storiform pattern with variable giant cells and foamy histiocytes (Gleason and Fletcher 2008; Fletcher 1990). BFH is classified into cutaneous and deep types. Deep BFH is very rare, comprising fewer than 5% of all BFHs, and arises in subcutaneous or deep soft tissue. This type is commonly found in the lower extremities, followed by the head and neck region. It develops at any age and show a slight predominance in males (Fletcher 1990).

The radiologic findings for this type are not specific. It is reported that US reveals a well-defined hyperechoic soft tissue mass with occasional hypervascularity on Doppler images. CT and MR imaging demonstrate a well-circumscribed, smoothly marginated soft tissue mass in the subcutaneous fat or deep soft tissue, with variable contrast enhancement depending on the vascularity, intralesional hemorrhage, and necrosis (Thomas et al. 2015; Jo et al. 2015; Chung et al. 2011; Machiels et al. 1998). When the lesion is large or necrotic, one must differentiate deep BFH from superficial soft tissue sarcomas, such as undifferentiated pleomorphic sarcoma, cutaneous leiomyosarcoma, and dermatofibrosarcoma protuberans (Thomas et al. 2015).

The optimal treatment for BFH includes a wide excision and continuous follow-up given that local recurrence or metastasis can occur in deep fibrous histiocytomas (Gleason and Fletcher 2008).

6.3 Giant Cell Tumor of Soft Tissue

Giant cell tumor of soft tissue (GCT-ST) is a rare primary soft tissue neoplasm that clinically and morphologically resembles a giant cell tumor of bone. GCT-ST displays a multinodular architecture, with nodules composed of a mixture of round to oval mononuclear cells and osteoclast-like giant cells immersed in a richly vascularized stroma (Oliveira 2013). Additional histologic features include blood-filled cystic

spaces similar to those within aneurysmal bone cysts, metaplastic bone formation in the lesion periphery, stromal hemorrhage, marked stromal fibrosis, and clusters of foamy macrophages (Oliveira 2013; O'Connell et al. 2000). GCT-ST is associated with a local recurrence rate of 12% and very rare cases of metastases or death. GCT-ST is regarded as an intermediate malignancy (rarely metastasizing) according to the 2013 WHO classification of soft tissue tumors. Therefore, complete removal of GCT-ST with negative surgical margin is advised.

GCT-ST usually presents as a well-circumscribed, slow-growing mass, which usually occurs in middle-aged to older individuals, although age at presentation varies. There is no sex predilection. This lesion occurs most commonly in the lower limbs, followed by the trunk and upper limbs. It usually involves the superficial soft tissue but can occur in deep soft tissue (Oliveira et al. 2000; O'Connell et al. 2000).

As GCT-ST is rare, there have been only a small number of reports regarding imaging findings for this lesion. US of GCT-ST reveals a well-demarcated, heterogeneous hypoechoic solid mass with intralesional vascularity on color Doppler images. On MR imaging, this tumor shows hyperintense signal relative to muscle on T2-weighted images and intermediate to hypointense signal on T1-weighted images, with intense contrast enhancement. Hemorrhagic cystic changes with fluid-fluid levels have been occasionally reported, similar to aneurysmal bone cysts (Meana Moris et al. 2010; An et al. 2008).

6.4 Illustrations: So-Called Fibrohistiocytic Tumors

6.4.1 Tenosynovial Giant Cell Tumor, Localized Type

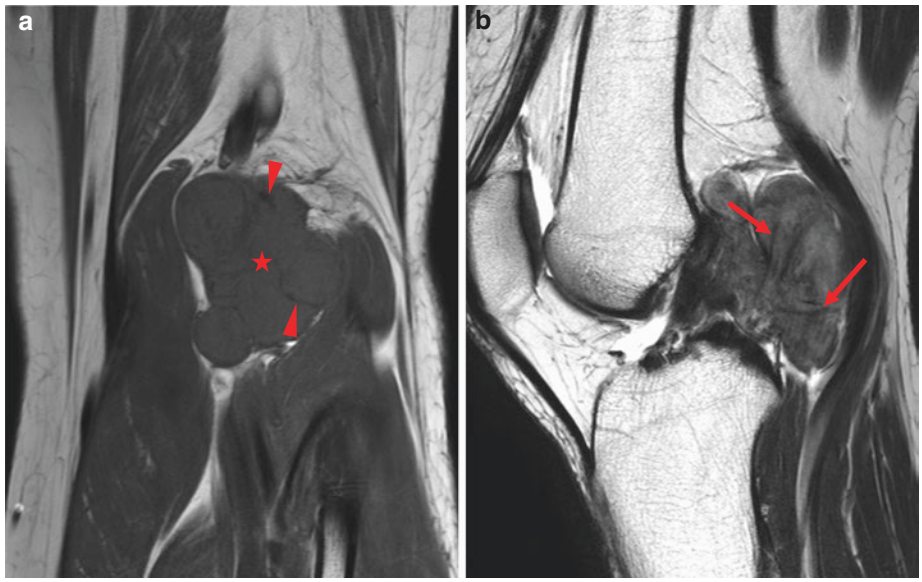

Fig. 6.1 Tenosynovial giant cell tumor, localized type. Coronal T1WI (**a**) shows a multilobulated mass (*star*) that is located within the intermuscular space of the popliteal fossa of the knee. This mass is slightly hyperintense relative to skeletal muscle. Note multifocal nodular or curvilinear dark foci (*arrowheads*), in keeping with hemosiderin deposits. On sagittal T2WI (**b**), the mass is intimately associated with the anterior cruciate ligament and posterior joint capsule of the knee. The mass has an inhomogeneous low to intermediate hyperintensity relative to skeletal muscle. Small dark foci (hemosiderin deposits) throughout the lesion are seen. In addition, some thick hypointense lines (*arrows*) represent fibrous septae with hemosiderin deposits. Sagittal postcontrast FS T1WI (**c**) shows the mass to have heterogeneous intense enhancement. There is no synovial hypertrophy or abnormal enhancement of the knee. US (**d**) reveals a well-marginated solid mass in the deep popliteal fossa (*star*) with a heterogeneous echo pattern, ranging from small hypoechoic foci to regions that are isoechoic to hyperechoic relative to subcutaneous fat. A photograph of the specimen (**e**) shows a well-circumscribed, multilobulated, yellowish mass with multifocal brown areas (*arrowheads*)

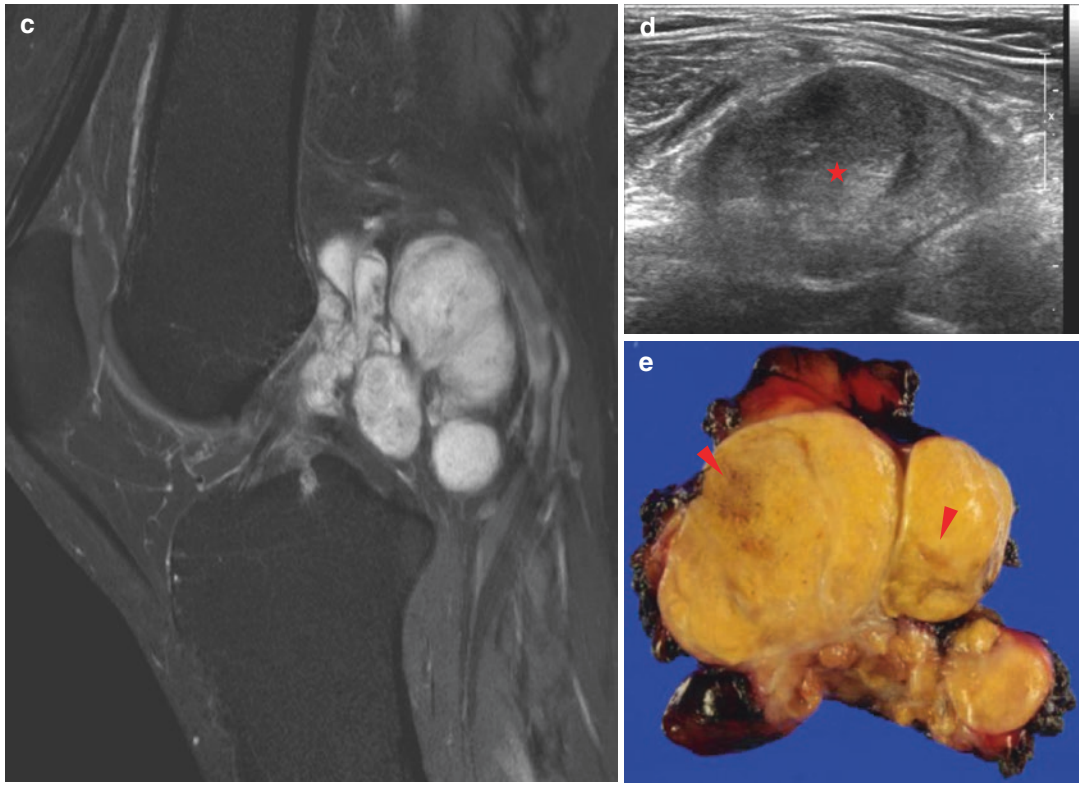

Fig. 6.1 (continued)

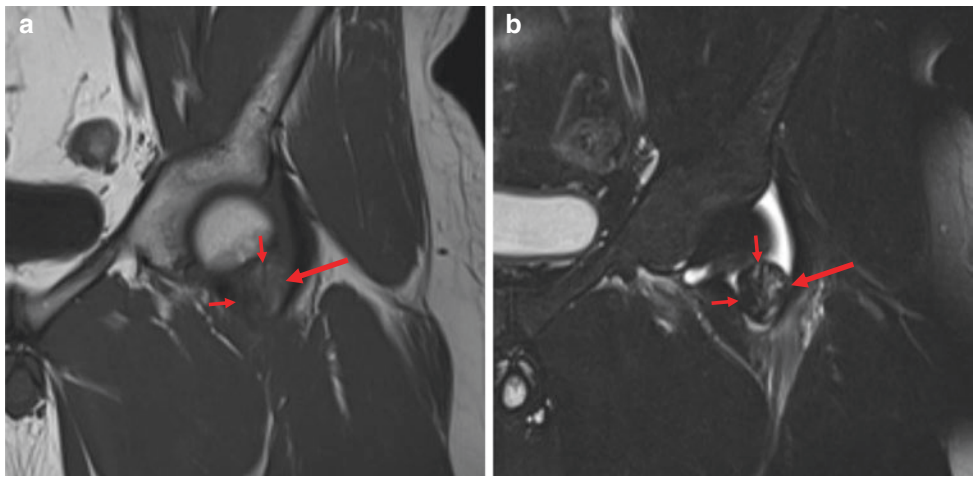

Fig. 6.2 Tenosynovial giant cell tumor, localized type. Coronal T1WI (**a**) reveals a circumscribed intra-articular hyperintense (relative to muscle) soft tissue mass (*arrow*) in the left hip joint. Coronal FS T2WI (**b**) shows the lesion to have a mixed dark intensity to hyperintensity. The lesion is hyperintense on axial T1WI (**c**) and heterogeneously enhanced on postcontrast FS T1WI (**d**). Hypointense foci (*small arrows*) on all sequences represent hemosiderin deposits. There is a moderate amount of effusion in the left hip joint, with mild pericapsular soft tissue edema and enhancement around the anteroinferior recess

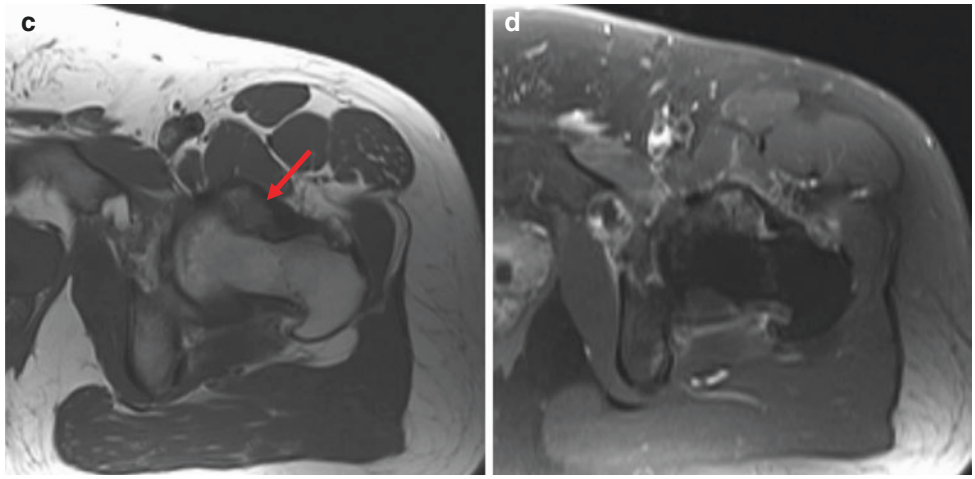

Fig. 6.2 (continued)

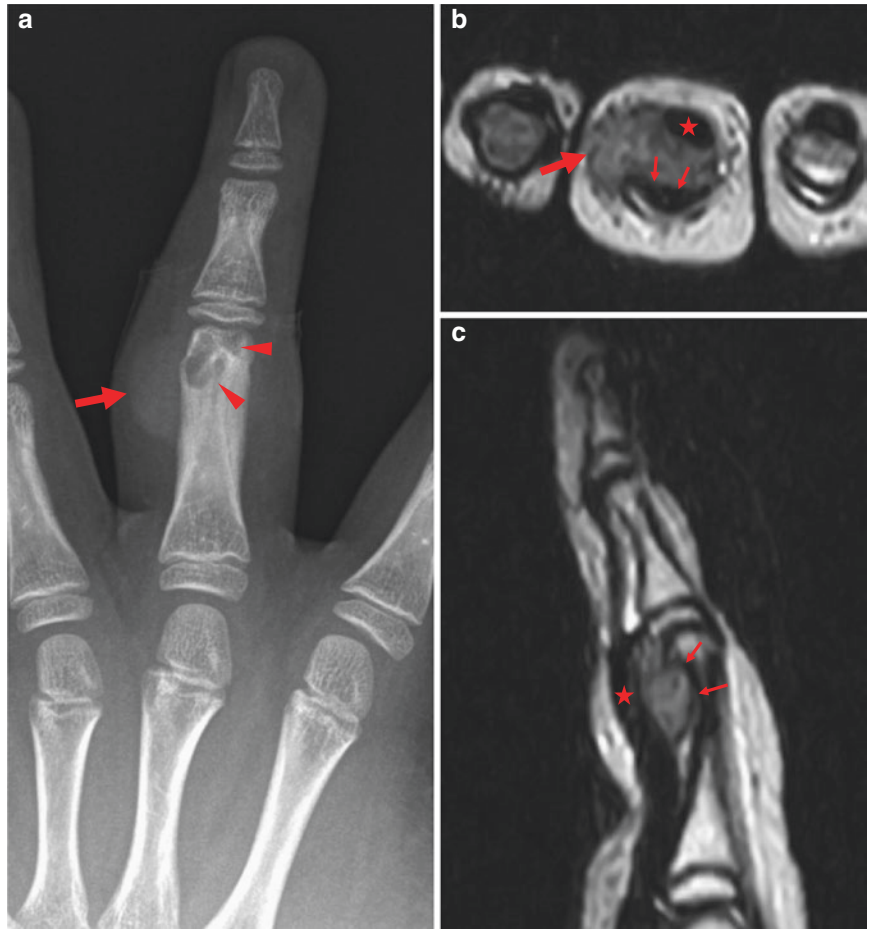

Fig. 6.3 Tenosynovial giant cell tumor, localized type. Radiograph (**a**) reveals a nonspecific periarticular soft tissue mass (*arrow*) along the ulnar aspect of the proximal phalanx of the long finger. Note the mildly expansile osteolytic change (*arrowheads*) at the adjacent phalangeal head. Axial (**b**) and sagittal (**c**) T2WIs show the lobulated mass (*arrows*) to exhibit a heterogeneous (intermediate to hyperintense) signal, with typical dark signal foci that correspond to hemosiderin deposition. This mass arises between the flexor tendon (*star*) and bone with adjacent bone erosion (*thin arrows*)

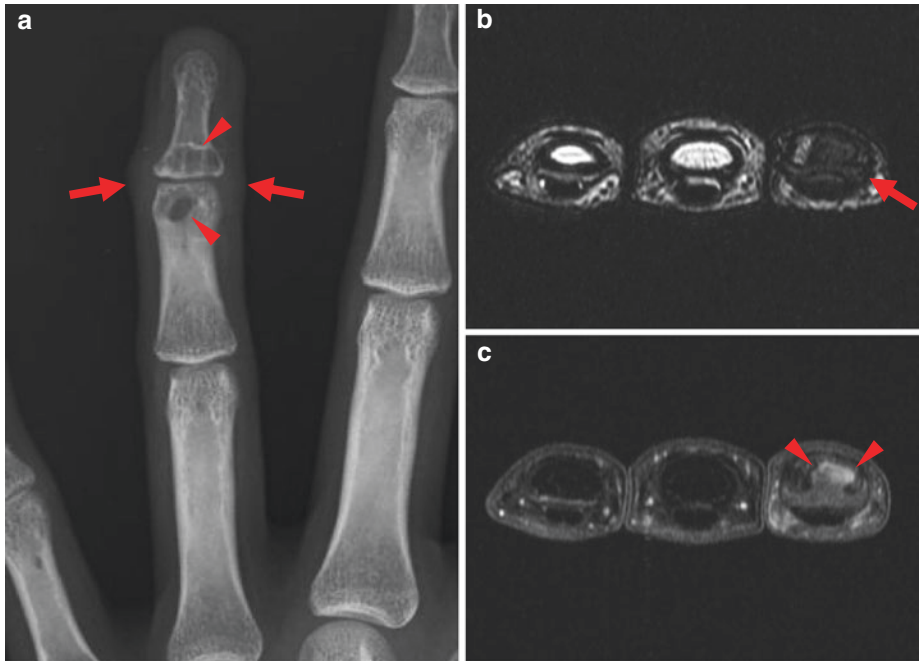

Fig. 6.4 Tenosynovial giant cell tumor, localized type. Radiograph (**a**) reveals a nonspecific periarticular soft tissue swelling (*arrow*) around the distal interphalangeal joint with well-demarcated multifocal osteolytic changes (*arrowheads*) in the neighboring bones. Axial T2WI (**b**) shows the mass to have marked hypointensity with inhomogeneous contrast enhancement on postcontrast FS T1WI (**c**). This lesion is located between bone and flexor tendon with large bone erosion (*arrowheads*)

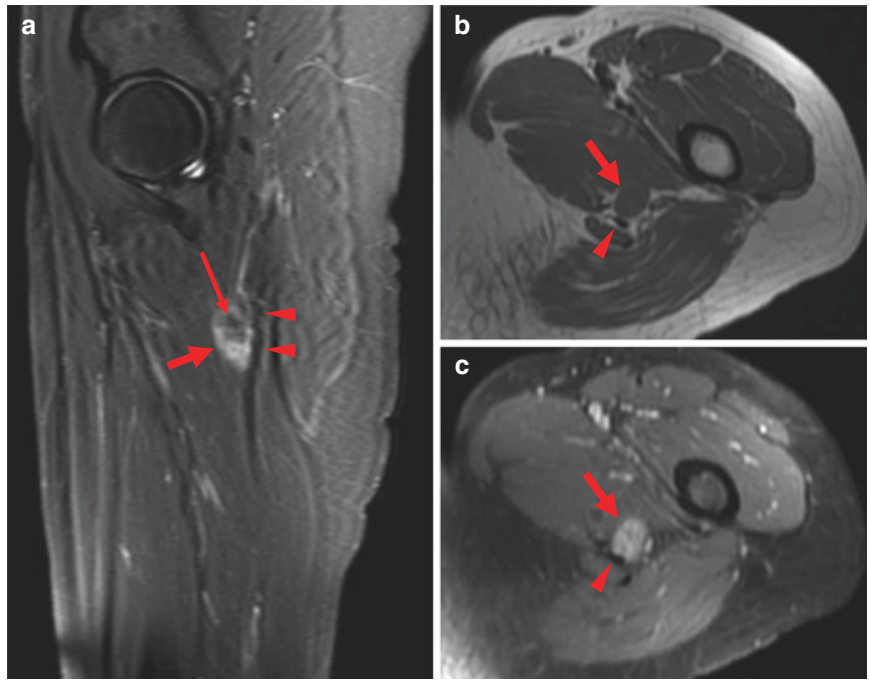

Fig. 6.5 Tenosynovial giant cell tumor, localized type. Sagittal FS T2WI of the thigh (**a**) shows an extra-articular ovoid soft tissue mass (*arrows*). This mass is located along the ventral surface of the semimembranosus tendon (*arrowheads*). It is hyperintense relative to skeletal muscle, with some hypointense to dark areas (*thin arrow*). These regions correspond to hemosiderin deposition. Axial T1WI (**b**) shows the mass to be isointense relative to skeletal muscle, with inhomogeneous enhancement on postcontrast FS T1WI (**c**)

6.4.2 Tenosynovial Giant Cell Tumor, Diffuse Type

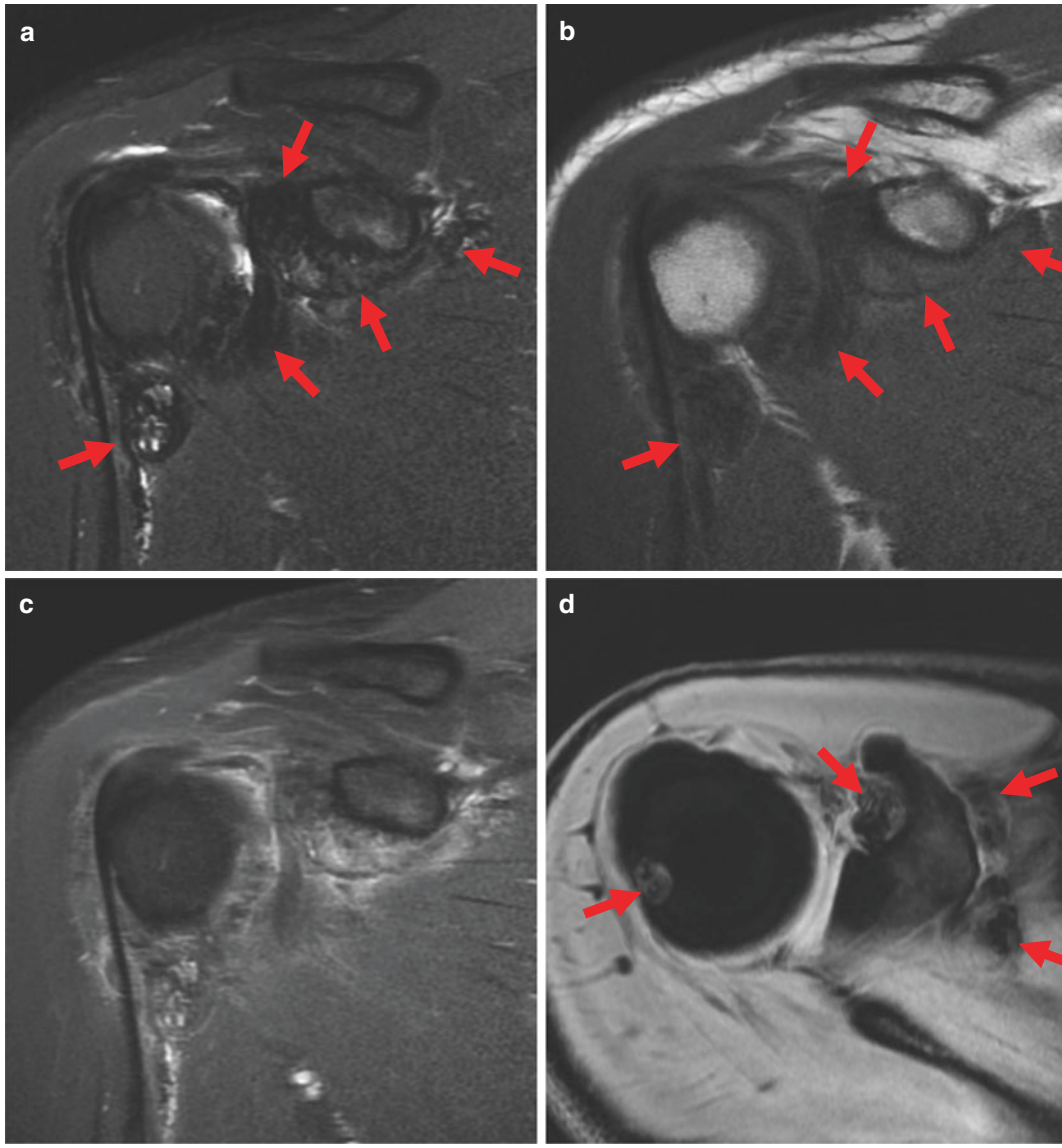

Fig. 6.6 Tenosynovial giant cell tumor, diffuse type. Coronal FS T2WI of the shoulder (**a**) shows numerous, diffuse, variably sized low signal nodules (*arrows*) within the glenohumeral joint, in addition to synovial thickening. The lesions have heterogeneous hypointense or slightly hyperintense signal on coronal T1WI (**b**) with inhomogeneous contrast enhancement on postcontrast FS T1WI (**c**). Axial GRE image (**d**) demonstrates a "blooming" effect of the low signal nodules (*arrows*). The nodules appear larger and darker than they do on T2WI. Radiograph (**e**) shows periarticular increased opacity with neighboring normal bone density. Arthroscopic photograph (**f**) reveals marked villous, frond-like, thick, yellowish-red synovial proliferation

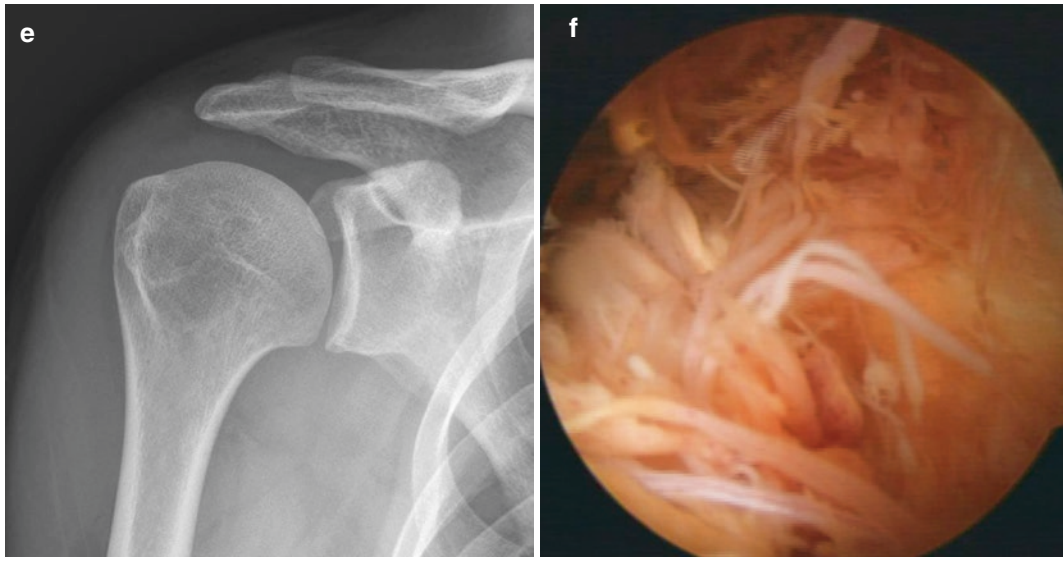

Fig. 6.6 (continued)

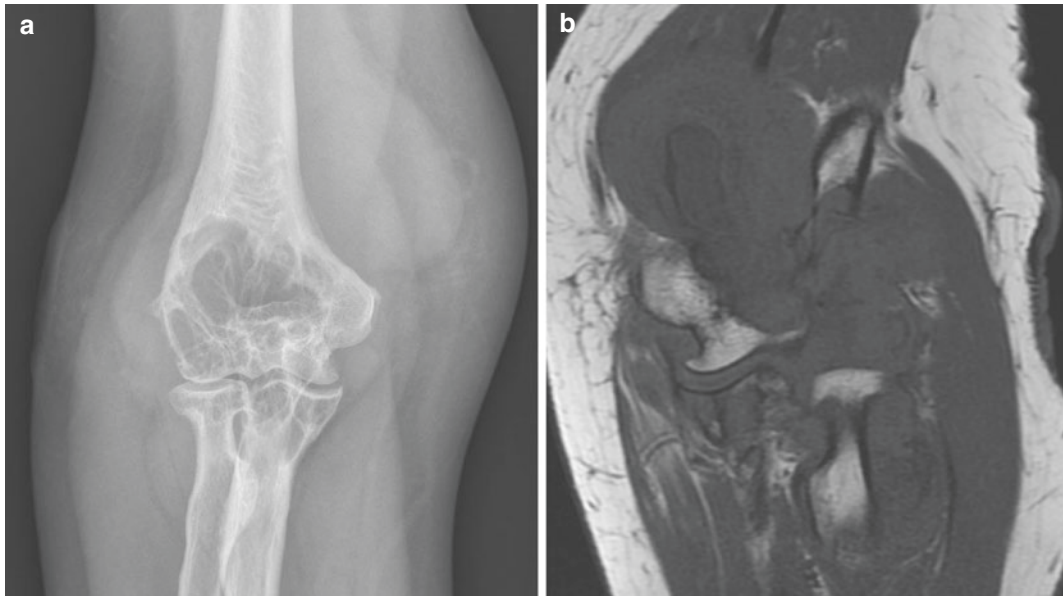

Fig. 6.7 Tenosynovial giant cell tumor, diffuse type. Radiograph (**a**) shows multilobulated soft tissue mass around the elbow. Extensive bone erosion is seen, but the joint spaces are preserved and perilesional bone density is normal. The lesions are isointense on coronal T1WI (**b**), with small dark signal foci. A heterogeneous signal is observed on T2WI (**c**), ranging from a dark signal to one that is hyperintense to the muscle. Heterogeneous but intense contrast enhancement is observed on postcontrast T1WI (**d**). Sagittal GRE image (**e**) demonstrates a "blooming" effect of the low signal foci or regions (*thin arrows*)

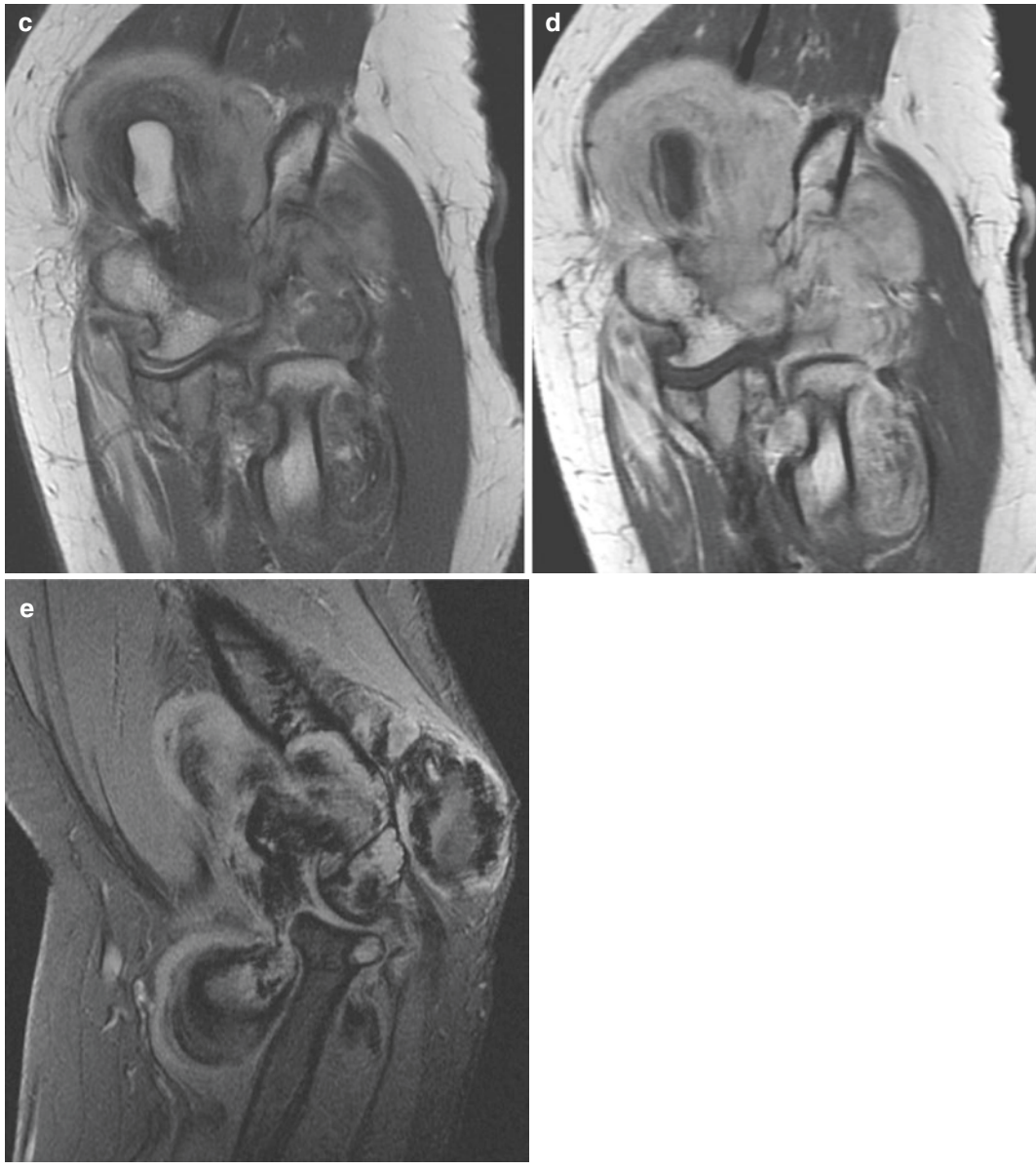

Fig. 6.7 (continued)

6.4.3 Giant Cell Tumor of Soft Tissue

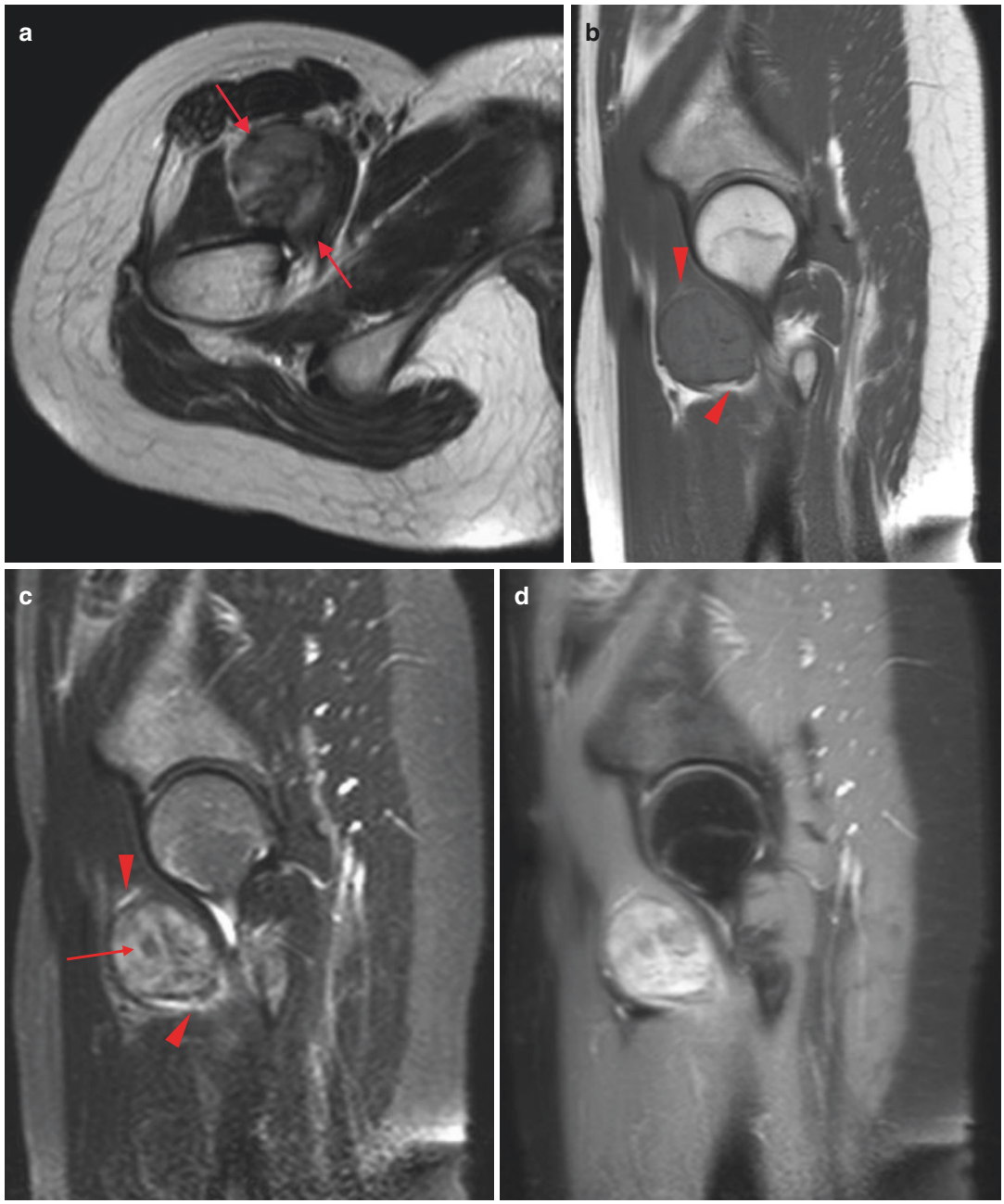

Fig. 6.8 Giant cell tumor of soft tissue. Axial T2WI of the thigh (**a**) shows a circumscribed, extra-articular oval soft tissue mass within the right iliopsoas muscle, with a subfascial location. This lesion has mild hyperintensity to the muscle on sagittal T1WI (**b**) and heterogeneous hyperintensity with dark areas (*thin arrow*) corresponding to hemosiderin deposition on T2WI (**a**, **c**). Postcontrast FS T1WI (**d**) shows inhomogeneous contrast enhancement of the mass. A fatty rim (*arrowheads*) around the mass is noted. US (**e**) reveals a slightly heterogeneous hypoechoic mass. A photograph of the specimen (**f**) reveals a well-encapsulated, pale yellowish mass with multifocal, irregularly shaped, intense sun-yellow areas. In addition, multiple hemorrhagic foci are shown on the cut surface

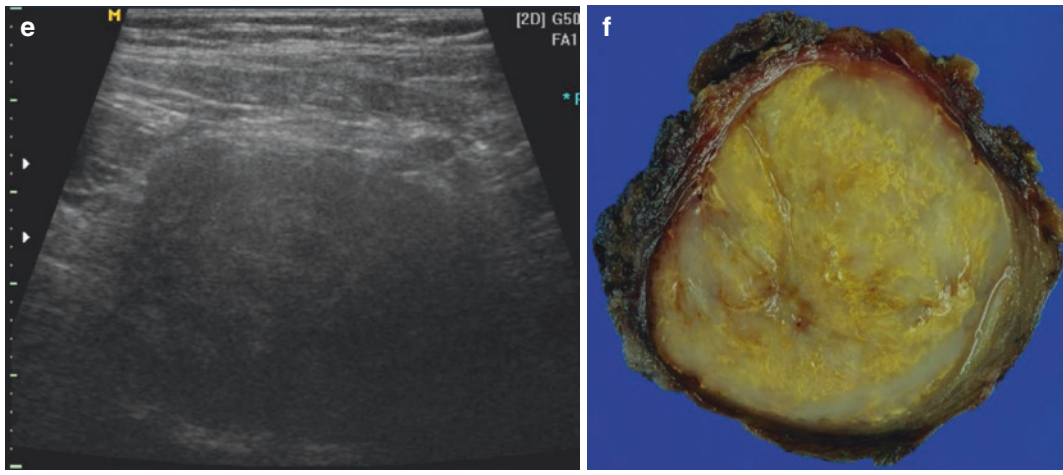

Fig. 6.8 (continued)

6.4.4 Deep Benign Fibrous Histiocytoma

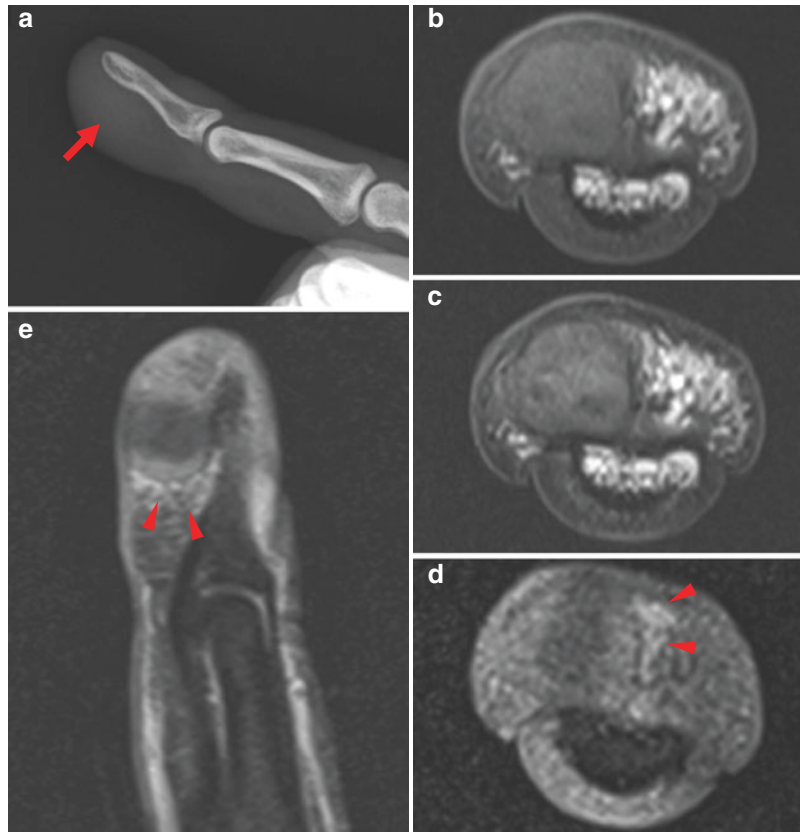

Fig. 6.9 Deep benign fibrous histiocytoma. Lateral radiograph (**a**) reveals a nonspecific soft tissue mass (*arrow*) along the palmar aspect of the distal phalanx. There is no osseous involvement. This well-circumscribed subcutaneous mass is isointense to slightly hyperintense on T1WI (**b**) and hyperintense on T2WI (**c**). Axial (**d**) and sagittal (**e**) postcontrast FS T1WIs show the mass to have mild peripheral thick enhancement, with a central, large non-enhancing area. Perilesional soft tissue edema and enhancement (*arrowheads*) are also seen

References

Al-Nakshabandi NA, Ryan AG, Choudur H, Torreggiani W, Nicoloau S, Munk PL, Al-Ismail K. Pigmented villonodular synovitis. Clin Radiol. 2004;59(5):414–20. doi:10.1016/j.crad.2003.11.013.

An SB, Choi JA, Chung JH, Oh JH, Kang HS. Giant cell tumor of soft tissue: a case with atypical US and MRI findings. Korean J Radiol. 2008;9(5):462–5. doi:10.3348/kjr.2008.9.5.462.

Boland JM, Folpe AL, Hornick JL, Grogg KL. Clusterin is expressed in normal synoviocytes and in tenosynovial giant cell tumors of localized and diffuse types: diagnostic and histogenetic implications. Am J Surg Pathol. 2009;33(8):1225–9. doi:10.1097/PAS.0b013e3181a6d86f.

Chung J, Namkoong S, Sim JH, Lee JS, Hong SP, Kim MH, Park BC. Deep penetrating benign fibrous histiocytoma of the foot associated with throbbing pain. Ann Dermatol. 2011;23(Suppl 2):S239–42. doi:10.5021/ad.2011.23.S2.S239.

de Saint Aubain Somerhausen N, van de Rijn M. Tenosynovial giant cell tumour. In: WHO classiciation of tumours of soft tissue and bone. 4th ed. Lyon: International Agency for Research on Cancer; 2013. p. 100–3.

Flandry F, Hughston JC. Pigmented villonodular synovitis. J Bone Joint Surg Am. 1987;69(6):942–9.

Fletcher CD. Benign fibrous histiocytoma of subcutaneous and deep soft tissue: a clinicopathologic analysis of 21 cases. Am J Surg Pathol. 1990;14(9):801–9.

Gleason BC, Fletcher CD. Deep "benign" fibrous histiocytoma: clinicopathologic analysis of 69 cases of a rare tumor indicating occasional metastatic potential. Am J Surg Pathol. 2008;32(3):354–62. doi:10.1097/PAS.0b013e31813c6b85.

Hughes TH, Sartoris DJ, Schweitzer ME, Resnick DL. Pigmented villonodular synovitis: MRI characteristics. Skelet Radiol. 1995;24(1):7–12.

Jo E, Cho ES, Kim HS, Nam W. Deep benign fibrous histiocytoma in the oral cavity: a case report. J Korean Assoc Oral Maxillofac Surg. 2015;41(5):270–2. doi:10.5125/jkaoms.2015.41.5.270.

Machiels F, De Maeseneer M, Chaskis C, Bourgain C, Osteaux M. Deep benign fibrous histiocytoma of the knee: CT and MR features with pathologic correlation. Eur Radiol. 1998;8(6):989–91. doi:10.1007/s003300050502.

Meana Moris AR, Garcia Gonzalez P, Fuente Martin E, Gonzalez Suarez C, Moro Barrero L. Primary giant cell tumor of soft tissue: fluid-fluid levels at MRI (2010:3b). Eur Radiol. 2010;20(6):1539–43. doi:10.1007/s00330-009-1528-x.

Middleton WD, Patel V, Teefey SA, Boyer MI. Giant cell tumors of the tendon sheath: analysis of sonographic findings. AJR Am J Roentgenol. 2004;183(2):337–9. doi:10.2214/ajr.183.2.1830337.

Murphey MD, Rhee JH, Lewis RB, Fanburg-Smith JC, Flemming DJ, Walker EA. Pigmented villonodular synovitis: radiologic-pathologic correlation. Radiographics. 2008;28(5):1493–518. doi:10.1148/rg.285085134.

O'Connell JX, Wehrli BM, Nielsen GP, Rosenberg AE. Giant cell tumors of soft tissue: a clinicopathologic study of 18 benign and malignant tumors. Am J Surg Pathol. 2000;24(3):386–95.

Oliveira AM. Giant cell tumours of soft tissue. In: Fletcher CDM, Bridge JA, Hogendoorn PCW, Mertens F, editors. WHO classiciation of tumours of soft tissue and bone. 4th ed. Lyon: International Agency for Research on Cancer; 2013. p. 100–3.

Oliveira AM, Dei Tos AP, Fletcher CD, Nascimento AG. Primary giant cell tumor of soft tissues: a study of 22 cases. Am J Surg Pathol. 2000;24(2):248–56.

Schwartz HS, Unni KK, Pritchard DJ. Pigmented villonodular synovitis. A retrospective review of affected large joints. Clin Orthop Relat Res. 1989;247:243–55.

Thomas KL, Henderson-Jackson E, Caracciolo JT. Test yourself: answer—deep benign fibrous histiocytoma. Skelet Radiol. 2015;44(8):1151–2. doi:10.1007/s00256-015-2113-9.

Ushijima M, Hashimoto H, Tsuneyoshi M, Enjoji M. Giant cell tumor of the tendon sheath (nodular tenosynovitis). A study of 207 cases to compare the large joint group with the common digit group. Cancer. 1986;57(4):875–84.

Smooth Muscle Tumors

7

7.1 Leiomyoma of Deep Soft Tissue

Leiomyoma of deep soft tissue is a rare benign neoplasm that occurs in deep soft tissue in the retroperitoneum or abdominal cavity. This tumor is composed of orderly intersecting fascicles of spindled to slightly epithelioid cells, similar to normal smooth muscle cells. Most lesions are paucicellular, and degenerative or regressive changes, including fibrosis, calcification, hyalinization, and myxoid changes, are common in large lesions. It is known that calcification, hyalinization, and myxoid changes are common for this lesion (Miettinen and Quade 2013).

Leiomyomas of deep soft tissue present as a large mass and/or pain. Leiomyomas of deep soft tissue of the retroperitoneum or abdominal cavity occur almost exclusively in women, primarily in young adulthood or middle age. The very rare leiomyomas in the deep peripheral soft tissue occur at almost any age and exhibit no sex predilection. Leiomyomas rarely occur in the extremities and are more common in the lower limb than in the upper extremities (Robinson and Kalish 1990). The treatment of choice is complete surgical excision of the tumor along with the surrounding muscle. The rate of recurrence is very rare, and this tumor rarely undergoes malignant transformation (Miettinen and Quade 2013).

Imaging findings of leiomyoma of deep soft tissue are nonspecific. Radiograph may demonstrate soft tissue swelling with intralesional scattered calcifications. Sonographic findings include a well-defined, noncompressible, heterogeneous, relatively hypoechoic mass with or without intralesional vascularity on color or power Doppler images (Paluck et al. 2015). On MR imaging, this lesion is isointense or slightly hyperintense on T1-weighted images and hyperintense or somewhat hypointense on T2-weighted images, with prominent contrast enhancement (Bommireddy and Gurram 2016; Chalidis and Dimitriou 2007; Jalgaonkar et al. 2012; Ramachandran et al. 2014).

7.2 Leiomyosarcoma

Leiomyosarcoma is a rare malignant mesenchymal neoplasm showing pure smooth muscle differentiation, comprising approximately 10% of all soft tissue sarcomas and being the second or third most common soft tissue sarcoma (Salas et al. 2009; Kransdorf 1995). Soft tissue smooth muscle tumors with both nuclear atypia and mitotic activity are generally diagnosed as leiomyosarcoma, acknowledging the potential for metastasis (Miettinen 2014). Leiomyosarcomas are subclassified into uterine; soft tissue, which includes cutaneous, major vessel, and deep soft tissue; and bone leiomyosarcomas (Weiss 2002).

Leiomyosarcoma of the soft tissue presents with a mass lesion. Leiomyosarcomas usually occur in the fifth and sixth decade of life (Svarvar et al. 2007; Massi et al. 2004; Kransdorf 1995).

H.S. Kang et al., *Oncologic Imaging: Soft Tissue Tumors*, DOI 10.1007/978-981-287-718-5_7

Uterine and retroperitoneal leiomyosarcomas show a marked female predominance, but no sex predilection at other sites. These tumors most commonly occur in the uterus and retroperitoneum, and less commonly in the viscera, bone, soft tissue, and skin (Weiss 2002). According to the largest recent series from the Scandinavian Sarcoma Group (Svarvar et al. 2007), nonvisceral leiomyosarcomas occur most commonly in the extremities, followed by the trunk wall and head/neck. Regarding tumor depth, subcutaneous involvement (45%) is more common, followed by deep-seated (39%) and cutaneous (16%). Patients with superficial leiomyosarcoma have longer survival, which is likely related to the small size and earlier diagnosis of these tumors (Gordon et al. 2014; Svarvar et al. 2007). Deep soft tissue leiomyosarcoma of the extremities, in contrast to leiomyosarcomas arising at other sites, has a greater propensity for local recurrence, with a rate of approximately 27% (Lamyman et al. 2011). The metastasis rate is 20% for subcutaneous and 60% for deep intramuscular leiomyosarcomas (Svarvar et al. 2007).

Radiologic findings of leiomyosarcoma are usually not specific. Radiographs demonstrate a soft tissue mass. Mineralization may be uncommonly observed and is caused by either nonneoplastic ossification or dystrophic mineralization in the tumor (Bush et al. 2003). Sonography, CT, and MR imaging demonstrate a well-circumscribed soft tissue mass with a variable degree of necrotic or cystic change, hemorrhage, and contrast enhancement (Beaman et al. 2007; Gordon et al. 2014; Kransdorf 2006). Deep soft tissue leiomyosarcomas tend to be larger than superficial leiomyosarcoma and heterogeneous in enhancement because of internal hemorrhage and necrosis. Due to their smaller size at presentation, the superficial (i.e., subcutaneous) tumors are homogeneous in enhancement (Gordon et al. 2014).

7.3 Illustrations: Smooth Muscle Tumors

7.3.1 Leiomyoma of Deep Soft Tissue

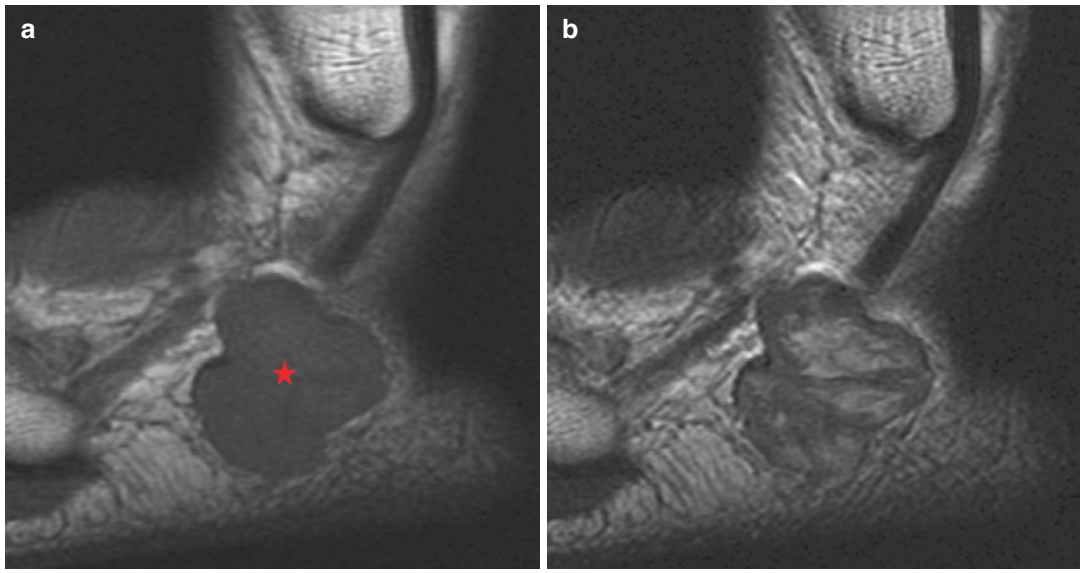

Fig. 7.1 Leiomyoma of deep soft tissue. Sagittal T1WI (**a**) shows a well-demarcated, multilobulated soft tissue mass (*star*) that is located in the subcutis of the lateral aspect of the right midfoot. This lesion is slightly hypointense to isointense relative to skeletal muscle on T1WI (**a**) and heterogeneously isointense to hyperintense on T2WI (**b**). Inhomogeneous intense contrast enhancement is observed on postcontrast FS T1WI (**c**, **d**). US shows a smoothly marginated solid mass with mixed hypo- and hyperechogenicity and prominent intralesional blood flow on the color Doppler image (**e**). A photograph of the specimen (**f**) shows a circumscribed, multilobulated, yellowish mass with multifocal peripheral mucoid change (*star*) and brown areas (*arrowheads*)

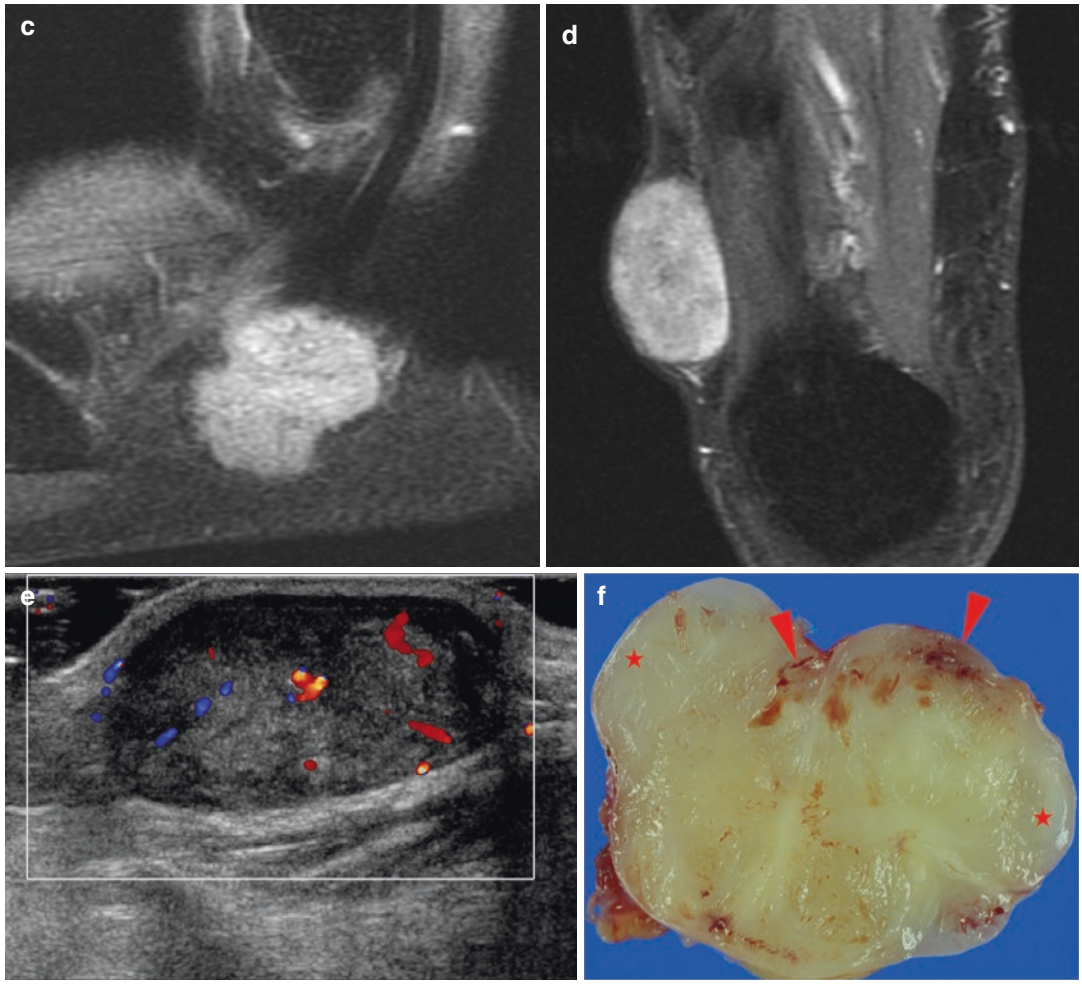

Fig. 7.1 (continued)

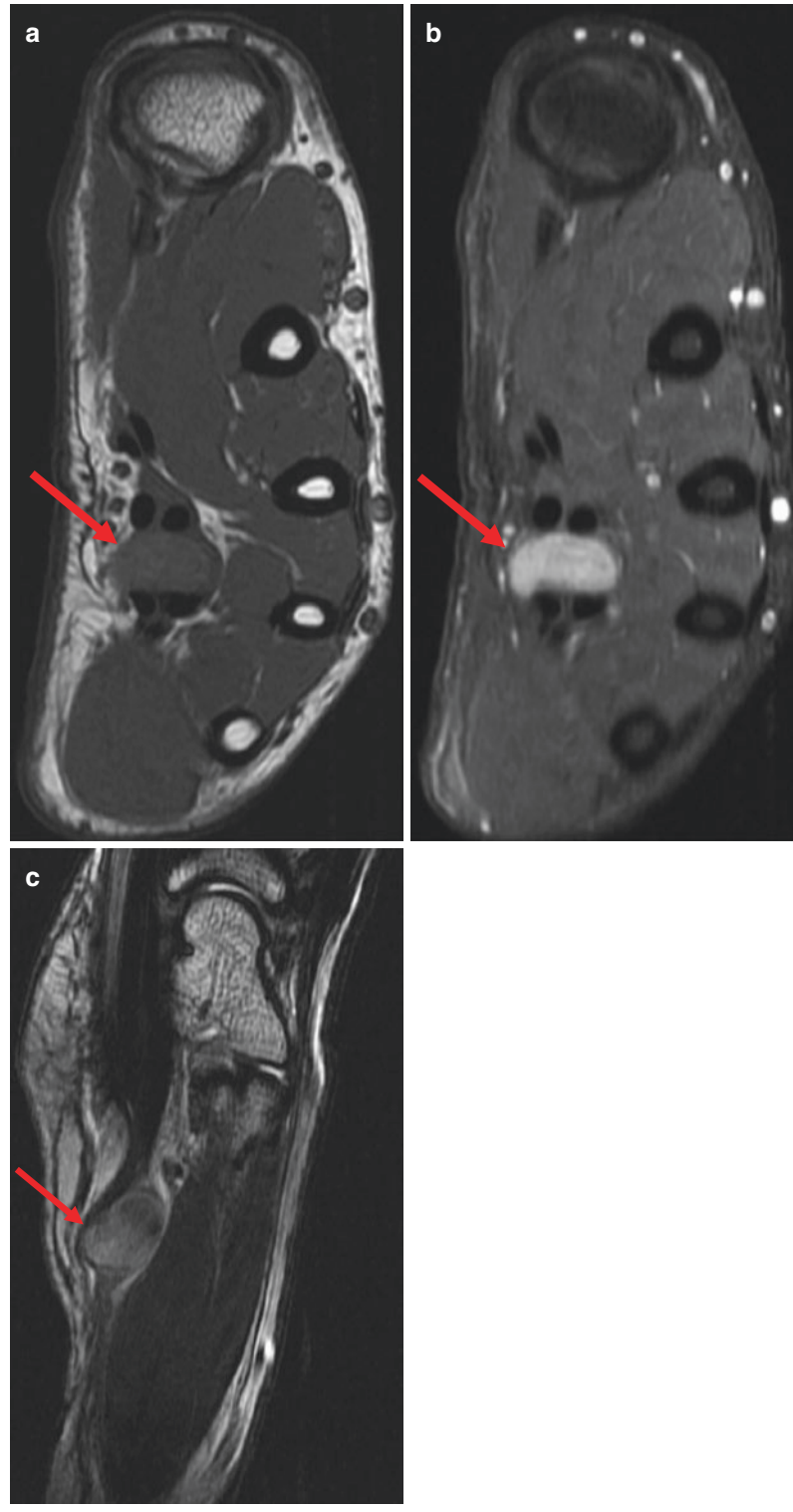

Fig. 7.2 Leiomyoma of deep soft tissue. Axial T1WI (**a**) shows a circumscribed intramuscular soft tissue mass (*arrow*) arising from the lumbrical muscle of the hand. This lesion is hyperintense relative to skeletal muscle on T1WI with homogeneous intense contrast enhancement (**b**). Sagittal T2WI (**c**) shows a smoothly marginated oval mass to have heterogeneous, mildly hyperintense signal relative to skeletal muscle, with small hypointense foci

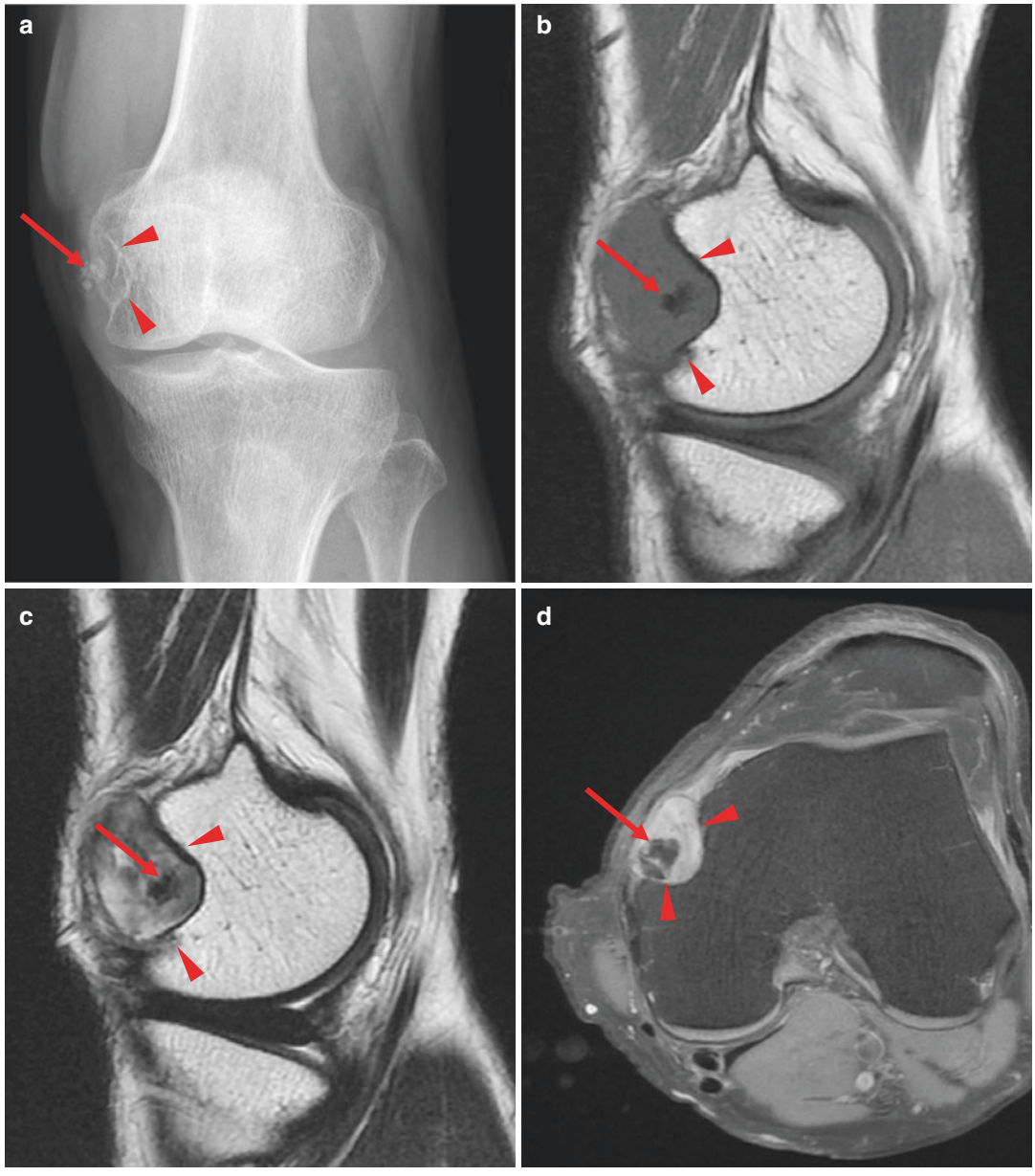

Fig. 7.3 Leiomyoma of deep soft tissue. Radiograph (**a**) shows an intra-articular soft tissue mass medial to the medial femoral condyle. The tumor is isointense to muscle on sagittal T1WI (**b**) and has mixed signal intensity on T2WI (**c**), ranging from hypointensity to hyperintensity. Strong enhancement is observed on axial postcontrast FS T1WI (**d**). Note the multiple nodular dark-signal calcifications (*arrow*) and adjacent bone erosion, with a thin sclerotic rim (*arrowheads*)

7.3.2 Leiomyosarcoma

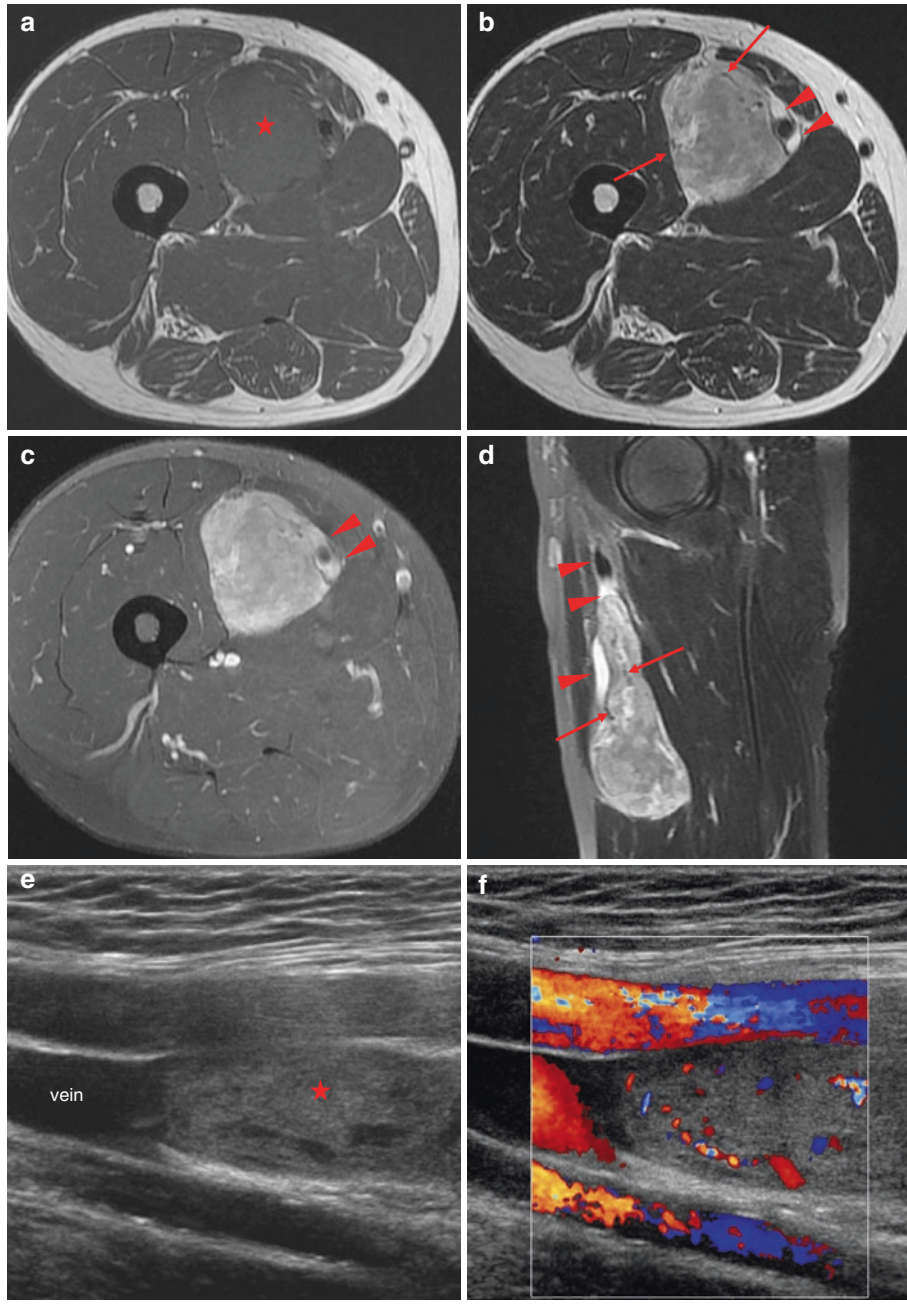

Fig. 7.4 Leiomyosarcoma. Axial T1WI (**a**) shows a well-demarcated soft tissue mass (*star*) that is located in the intermuscular fat plane among the muscles of the thigh. This mass is intimately associated with the superficial femoral vessels (*arrowheads*), with craniocaudal extension along the vessels on axial (**b**) and sagittal (**d**) T2WIs. It is isointense to slightly hyperintense to skeletal muscle on T1WI (**a**), with inhomogeneous low to intermediate hyperintense signal intensity relative to skeletal muscle on T2WI (**b**, **d**). There are central and peripheral tubular signal void structures (*thin arrows*) corresponding to intratumoral vascularities. Axial postcontrast FS T1W (**c**) shows the mass to have inhomogeneous intense contrast enhancement. US (**e**) reveals a circumscribed hyperechoic solid mass (*star*) with intratumoral anechoic tubular structures and internal blood flow on the color Doppler image (**f**), in keeping with intratumoral vessels. Note the intraluminal tumor extension into the adjacent superficial femoral vein. A photograph of the specimen (**g**) shows a well-circumscribed mass with a whitish cut surface and multifocal blood-filled vessels. Direct tumor extension into the adjacent vein is shown

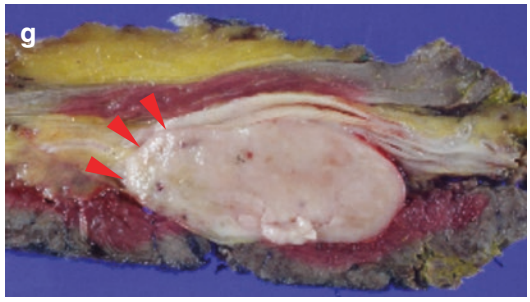

Fig. 7.4 (continued)

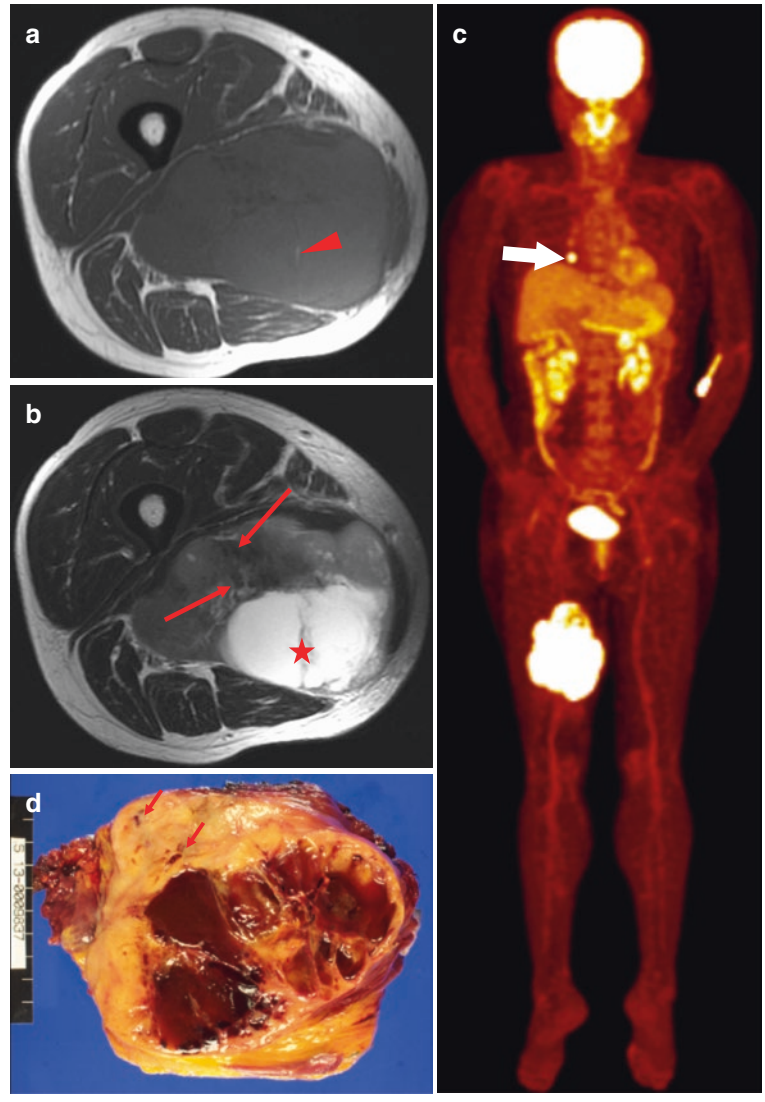

Fig. 7.5 Leiomyosarcoma. Axial T1WI (**a**) shows a well-demarcated soft tissue mass located within the adductor magnus muscle of the thigh. This lesion is mildly hyperintense relative to skeletal muscle, with focal hyperintense foci (*arrowhead*) that correspond to hemorrhaging. Axial T2WI (**b**) reveals the mass to have heterogeneous hypo- to hyperintense signal intensity relative to skeletal muscle. Small dark foci (*thin arrows*) that suggest vessels are seen, as is a large, fluid-equivalent hyperintense cystic or necrotic change (*star*). In addition to a hypermetabolic primary mass in right thigh, PET (**c**) reveals a hypermetabolic lung metastasis (*white arrow*). Gross specimen photograph (**d**) shows a well-circumscribed flesh-colored and yellowish mass with a large hemorrhagic, necrotic or cystic change and intratumoral vascularities (*thin arrows*)

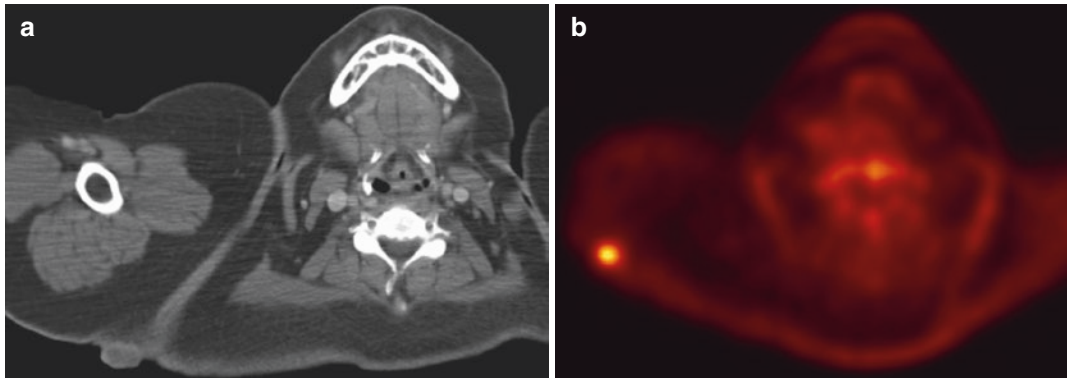

Fig. 7.6 Cutaneous leiomyosarcoma. Postcontrast CT scan (**a**) shows a small exophytic skin nodule from the posterior shoulder, with peripheral rim enhancement. PET (**b**) shows the lesion to be hypermetabolic

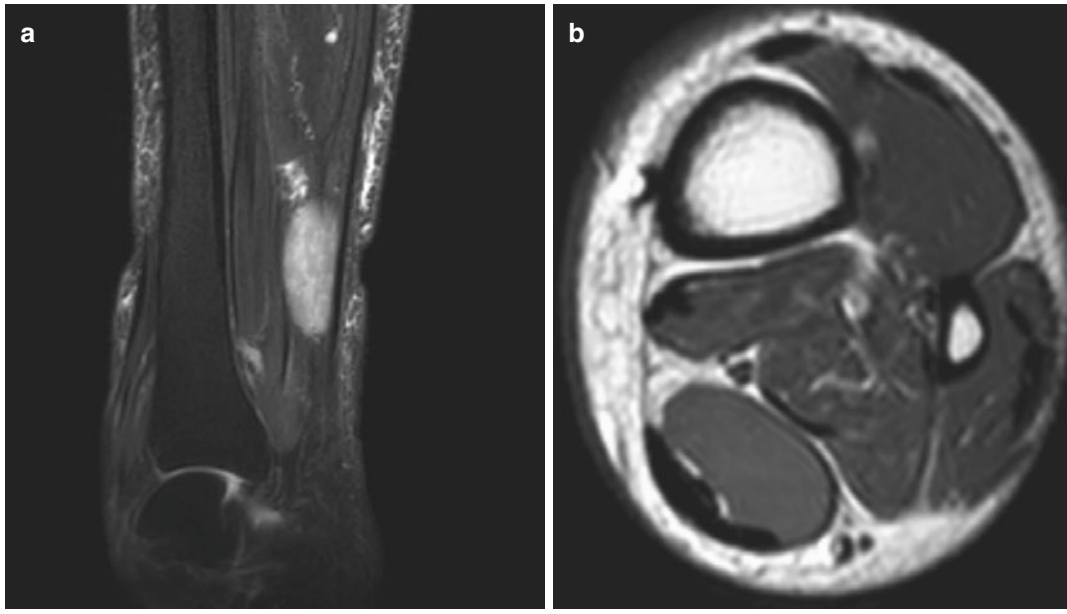

Fig. 7.7 Leiomyosarcoma. Sagittal FS T2WI (**a**) shows a well-demarcated inhomogeneous hyperintense soft tissue mass (relative to skeletal muscle) closely abutting the proximal Achilles tendon. The mass has mild hyperintensity to muscle on axial T1WI (**b**) and a heterogeneous signal on T2WI, ranging from intermediate to hyperintense. (**c**) Inhomogeneous enhancement is observed on postcontrast FS T1WI (**d**). US (**e**) shows the mass to be heterogeneously hypoechoic, with posterior sonic enhancement. The appearance of the mass is nonspecific. However, PET reveals the mass to be fairly hypermetabolic (SUV 8.0)

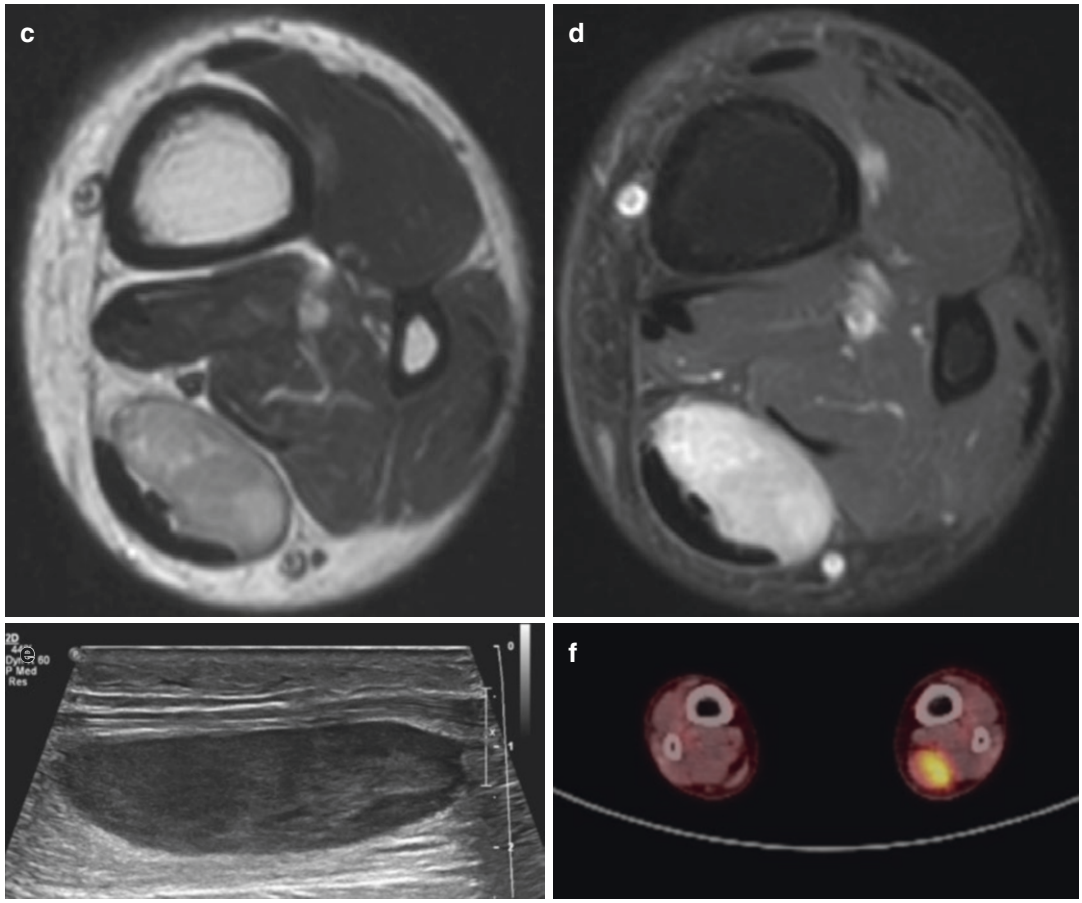

Fig. 7.7 (continued)

References

Beaman FD, Kransdorf MJ, Andrews TR, Murphey MD, Arcara LK, Keeling JH. Superficial soft-tissue masses: analysis, diagnosis, and differential considerations. Radiographics. 2007;27(2):509–23. doi:10.1148/rg.272065082.

Bommireddy B, Gurram V. Deep soft tissue leiomyoma of forearm: a case report and review of literature. J Clin Diagn Res. 2016;10(6):RD03–5. doi:10.7860/JCDR/2016/19059.8055.

Bush CH, Reith JD, Spanier SS. Mineralization in musculoskeletal leiomyosarcoma: radiologic-pathologic correlation. AJR Am J Roentgenol. 2003;180(1):109–13. doi:10.2214/ajr.180.1.1800109.

Chalidis BE, Dimitriou CG. Carpal tunnel syndrome due to an atypical deep soft tissue leiomyoma: the risk of misdiagnosis and mismanagement. World J Surg Oncol. 2007;5:92. doi:10.1186/1477-7819-5-92.

Gordon RW, Tirumani SH, Kurra V, Shinagare AB, Jagannathan JP, Hornick JL, Ramaiya NH. MRI, MDCT features, and clinical outcome of extremity leiomyosarcomas: experience in 47 patients. Skelet Radiol. 2014;43(5):615–22. doi:10.1007/s00256-014-1823-8.

Jalgaonkar A, Mohan A, Dawson-Bowling S, Skinner J, Briggs TW. Deep soft tissue leiomyoma mimicking fibromatosis in a 5-year-old male. J Foot Ankle Surg. 2012;51(1):110–3. doi:10.1053/j.jfas.2011.10.013.

Kransdorf MJ. Malignant soft-tissue tumors in a large referral population: distribution of diagnoses by age, sex, and location. AJR Am J Roentgenol. 1995;164(1):129–34. doi:10.2214/ajr.164.1.7998525.

Kransdorf MJ. Muscle tumors. In: Kransdorf MJ, editor. Imaging of soft tissue tumors, vol. 2nd. Philadelphia: Lippincott Williams & Wilkins; 2006. p. 306–12.

Lamyman MJ, Giele HP, Critchley P, Whitwell D, Gibbons M, Athanasou NA. Local recurrence and assessment of sentinel lymph node biopsy in deep soft tissue leiomyosarcoma of the extremities. Clin Sarcoma Res. 2011;1(1):7. doi:10.1186/2045-3329-1-7.

Massi D, Beltrami G, Mela MM, Pertici M, Capanna R, Franchi A. Prognostic factors in soft tissue leiomyosarcoma of the extremities: a retrospective analysis of 42 cases. Eur J Surg Oncol. 2004;30(5):565–72. doi:10.1016/j.ejso.2004.03.002.

Miettinen M. Smooth muscle tumors of soft tissue and non-uterine viscera: biology and prognosis. Mod Pathol. 2014;27(Suppl 1):S17–29. doi:10.1038/modpathol.2013.178.

Miettinen MM, Quade B. Leiomyoma of deep soft tissue. In: Fletcher CDM, Bridge JA, Hogendoorn PCW, Mertens F, editors. WHO classification of tumours of soft tissue and bone. 4th ed. Lyon: International Agency for Research on Cancer; 2013. p. 100–3.

Paluck M, Hager N, Gellhorn AC. Sonographic evaluation of trigger finger at the wrist and carpal tunnel syndrome resulting from a deep soft tissue leiomyoma. J Ultrasound Med. 2015;34(3):545–7. doi:10.7863/ultra.34.3.545.

Ramachandran R, Rangaswami R, Raja DK, Shanmugasundaram G. Deep soft-tissue leiomyoma of the forearm mimicking a primary bone tumor of the ulna. Radiol Case Rep. 2014;9(3):960. doi:10.2484/rcr.v9i3.960.

Robinson SC, Kalish RJ. Leiomyoma in the hand. A case report. Clin Orthop Relat Res. 1990;255:121–3.

Salas S, Stoeckle E, Collin F, Bui B, Terrier P, Guillou L, Trassard M, Ranchere-Vince D, Gregoire F, Coindre JM. Superficial soft tissue sarcomas (S-STS): a study of 367 patients from the French Sarcoma Group (FSG) database. Eur J Cancer. 2009;45(12):2091–102. doi:10.1016/j.ejca.2009.03.006.

Svarvar C, Bohling T, Berlin O, Gustafson P, Folleras G, Bjerkehagen B, Domanski HA, Sundby Hall K, Tukiainen E, Blomqvist C, Scandinavian Sarcoma Group Leiomyosarcoma Working Group. Clinical course of nonvisceral soft tissue leiomyosarcoma in 225 patients from the Scandinavian Sarcoma Group. Cancer. 2007;109(2):282–91. doi:10.1002/cncr.22395.

Weiss SW. Smooth muscle tumors of soft tissue. Adv Anat Pathol. 2002;9(6):351–9.

Pericytic (Perivascular) Tumors

8

Pericytes are contractile cells that wrap around the endothelial cells of capillaries and venules throughout the body. These supportive perivascular cells are essential to angiogenesis, tissue homeostasis, vessel permeability, and blood pressure control (Scott et al. 2015). Pericytic/perivascular soft tissue tumors are generally composed of modified vascular smooth muscle cells and tend to grow in a circumferential fashion around blood vessels (Scott et al. 2015; Flope et al. 2013).

8.1 Glomus Tumor

Glomus tumors are benign tumors arising from a contractile neuromyoarterial glomus body, a specialized arteriovenous anastomosis involved in thermoregulation. These tumors account for approximately 2% of the soft tissue tumors, and most are diagnosed between the age of 30 and 50 years. The prevalence of glomus tumors is nearly equal in men and women, except for a female predilection in subungual lesions. Most of these tumors occur in the distal extremities, especially the subungual region, hand, wrist, and foot, but rare tumors have been reported in almost every location. Clinically, glomus tumors are small (less than 1 cm), red-bluish subungual nodules with a classic clinical triad of pain, pinpoint tenderness with blunt palpation, and cold sensitivity (Flope et al. 2013). The gold standard of the treatment for glomus tumors is complete excision, and clinical outcomes are generally good.

Radiographs detect a small soft tissue mass located along the dorsal surface of the finger, either medially or laterally, related to the nail bed and occasionally with extrinsic bone erosion. The common sonographic findings of subungual glomus tumors are solid, hypoechoic or isoechoic nodules beneath the nail plate; hypervascularity on color or power Doppler imaging; and occasionally neighboring bony erosion. MR imaging reveals small soft tissue nodules with intermediate or low signal intensity on T1-weighted images, marked hyperintensity on T2-weighted images, and strong enhancement after intravenous contrast (Baek et al. 2010).

Solid glomus tumors comprise approximately 75% of all glomus tumors, consisting of nests of glomus cells that surround capillary-sized vessels. One variant, known as glomangioma or glomuvenous malformation, is composed of typical glomus cells but has a similar structure to a cavernous hemangioma. Another variant, glomangiomyoma, shows partial or focal smooth muscle differentiation. Glomangiomatosis (diffuse glomus tumor) is extremely rare and defined as (1) diffuse growth resembling angiomatosis, with a prominent glomus component investing vessel walls, and (2) a lack of the criteria for a malignant glomus tumor or glomus tumor of uncertain malignant potential. The conversion of the glomus tumor to a malignant tumor is reported to be

H.S. Kang et al., *Oncologic Imaging: Soft Tissue Tumors*, DOI 10.1007/978-981-287-718-5_8

very rare, less than approximately 1%. The criteria for malignant glomus tumor are as follows: (1) tumors with a deep location, (2) a size more than 2 cm, (3) atypical mitotic figures or obvious nuclear atypia, and (4, 5) more mitotic figures/50 high-power fields (Scott et al. 2015; Folpe et al. 2001, 2013).

8.2 Myopericytoma, Including Myofibroma

Myopericytomas are tumors characterized by a hemangiopericytoma-like vascular architectural pattern, with features of perivascular myoid (myopericytic) differentiation, and show a spectrum of growth patterns that overlap with myofibroma. These tumors can be histopathologically categorized as myopericytoma or myofibroma depending on the predominant growth pattern, namely, the presence of a concentric perivascular arrangement of plump, spindle shaped cells in myopericytoma and a zonal/biphasic appearance in myofibroma (Dray et al. 2006).

Myopericytoma presents with a painless, slowly growing, superficially located nodule. They are most often dermal or subcutaneous solitary tumors typically found in the lower extremities and more commonly in men (Scott et al. 2015). Myofibromas may present as painless, purple to pink, solitary or multicentric lesions (infantile myofibromatosis). Infantile myofibromatosis occurs primarily at birth and in children less than 2 years of age. These tumors primarily arise in dermal and subcutaneous tissues, and the extremities, head and neck region, and trunk are the usual sites. Superficial myopericytomas or myofibromas tend to follow a benign course, with few recurring after complete excision, whereas deeper-seated tumors, multinodular tumors in childhood, and multiple visceral lesions may pursue a more aggressive course (Weiss and Goldblum 2001).

Radiologic findings of myopericytoma and myofibroma/myofibromatosis are fairly nonspecific. US demonstrates a well-circumscribed hypoechoic or heterogeneous echoic mass in dermal and subcutaneous tissue, with hypervascularity on Doppler images. MR imaging shows heterogeneous, but predominantly hyperintense, pattern on T2-weighted images and an isointense signal on T1-weighted images, with strong contrast enhancement (Choi et al. 2014; Harish et al. 2007; Kayes et al. 2002). Intralesional hemorrhage may be present due to prominent vascularity (Harish et al. 2007).

8.3 Angioleiomyoma

Angioleiomyoma, also referred to as angiomyoma or vascular leiomyoma, is a benign smooth muscle tumor that arises from the arterial smooth muscle cells or the tunica media of the veins and is composed of well-differentiated smooth muscle cells with intervening vascular channels (Hachisuga et al. 1984).

Angioleiomyoma is a common tumor, accounting for approximately 4–5% of benign soft tissue tumors. It can occur anywhere in the body but is most often observed in the extremities, particularly the lower leg, followed by the head and neck. Tumors in the lower extremities occur in females twice as frequently as in males, whereas those in the upper extremities or head are more frequent in males. These tumors can be located in the dermis, the subcutaneous fat, or the superficial fasciae of the extremities. Lesions occur at all ages but are more common in the fourth to sixth decades. They present as a small, slowly growing firm, and mobile nodule. Pain, and/or tenderness, is manifested in approximately 60% of patients (Hachisuga et al. 1984). Pain is thought to be caused by the active contraction of smooth muscle, resulting in local ischemia. Treatment usually consists of simple excision.

Sonographic findings of angioleiomyoma include a well-circumscribed subcutaneous or superficial located mass with a parallel orientation to the skin; homogeneous hypoechogenicity;

straight and linear vessels in the tumor, with convergence to one point on color Doppler; and the absence of calcifications (Park et al. 2012; Zhang et al. 2016). MR imaging demonstrates a well-demarcated subcutaneous mass of isointense signal on T1-weighted images and a heterogeneous high signal intensity on T2-weighted images, with homogeneous strong enhancement and an adjacent tortuous vascular structure (Yoo et al. 2009).

8.4 Illustrations: Pericytic (Perivascular) Tumors

8.4.1 Glomus Tumor

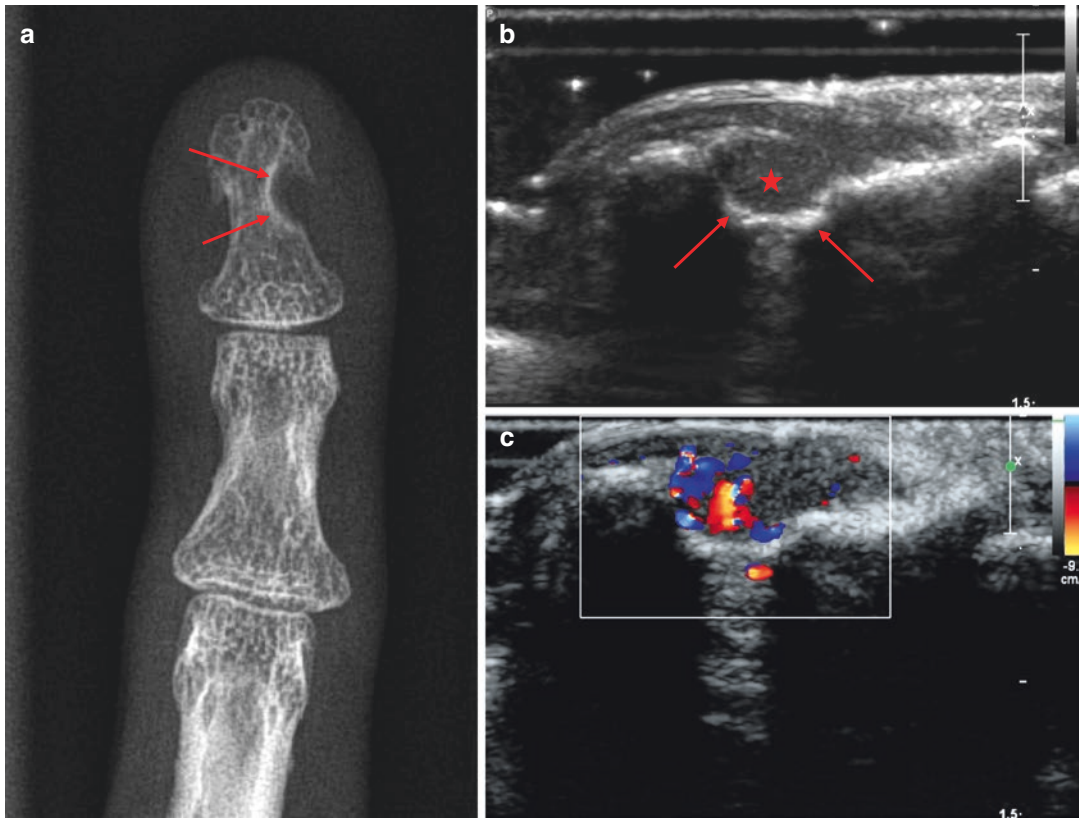

Fig. 8.1 Glomus tumor. Radiograph (**a**) shows extrinsic scalloping (*thin arrows*) of the distal phalanx and a sclerotic rim. Longitudinal US (**b**) reveals a circumscribed homogenous hypoechoic nodule (*star*) in the subungual region, with focal bone erosion (*thin arrows*) in the dorsal cortex of the distal phalanx. Prominent blood flow is observed on the color Doppler image (**c**)

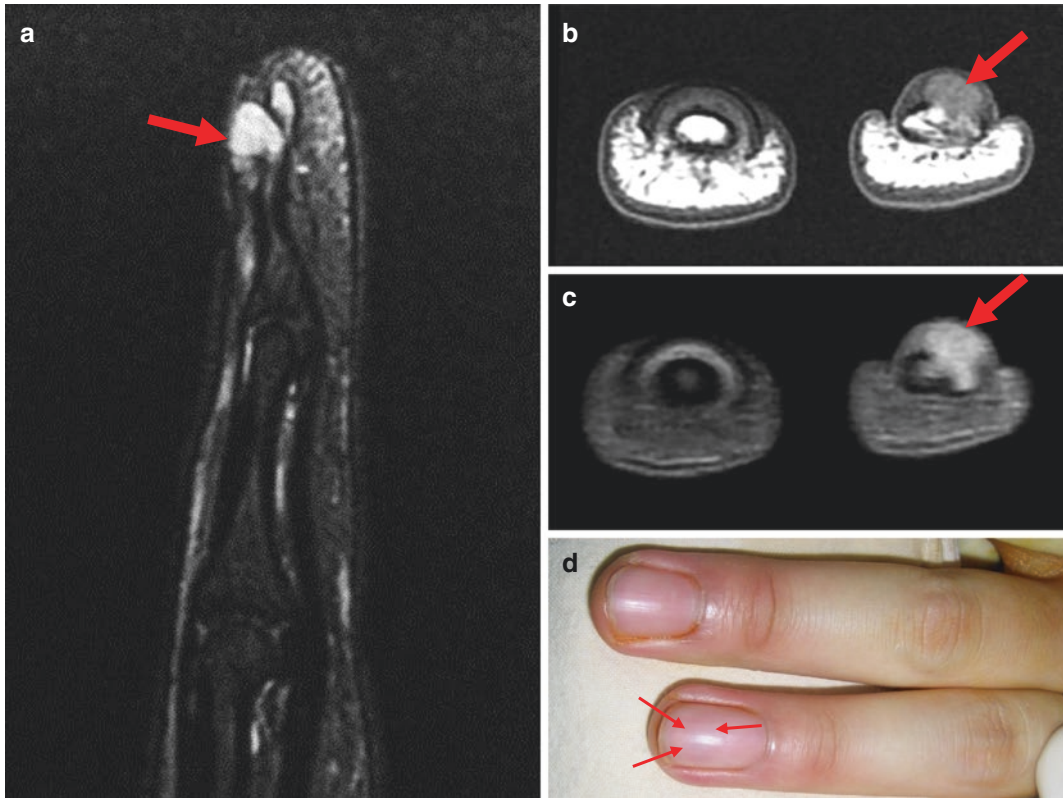

Fig. 8.2 Glomus tumor. Sagittal FS T2WI (**a**) shows a circumscribed, lobulated hyperintense nodule (*arrow*) in the subungual region, with marked bony erosion of neighboring distal phalanx. This lesion exhibits hyperintense signal intensity on axial T1WI (**b**) and homogenous intense enhancement on postcontrast FS T1WI (**c**). Intraoperative photograph (**d**) shows a faint blue colored spot (*thin arrows*) beneath the nail

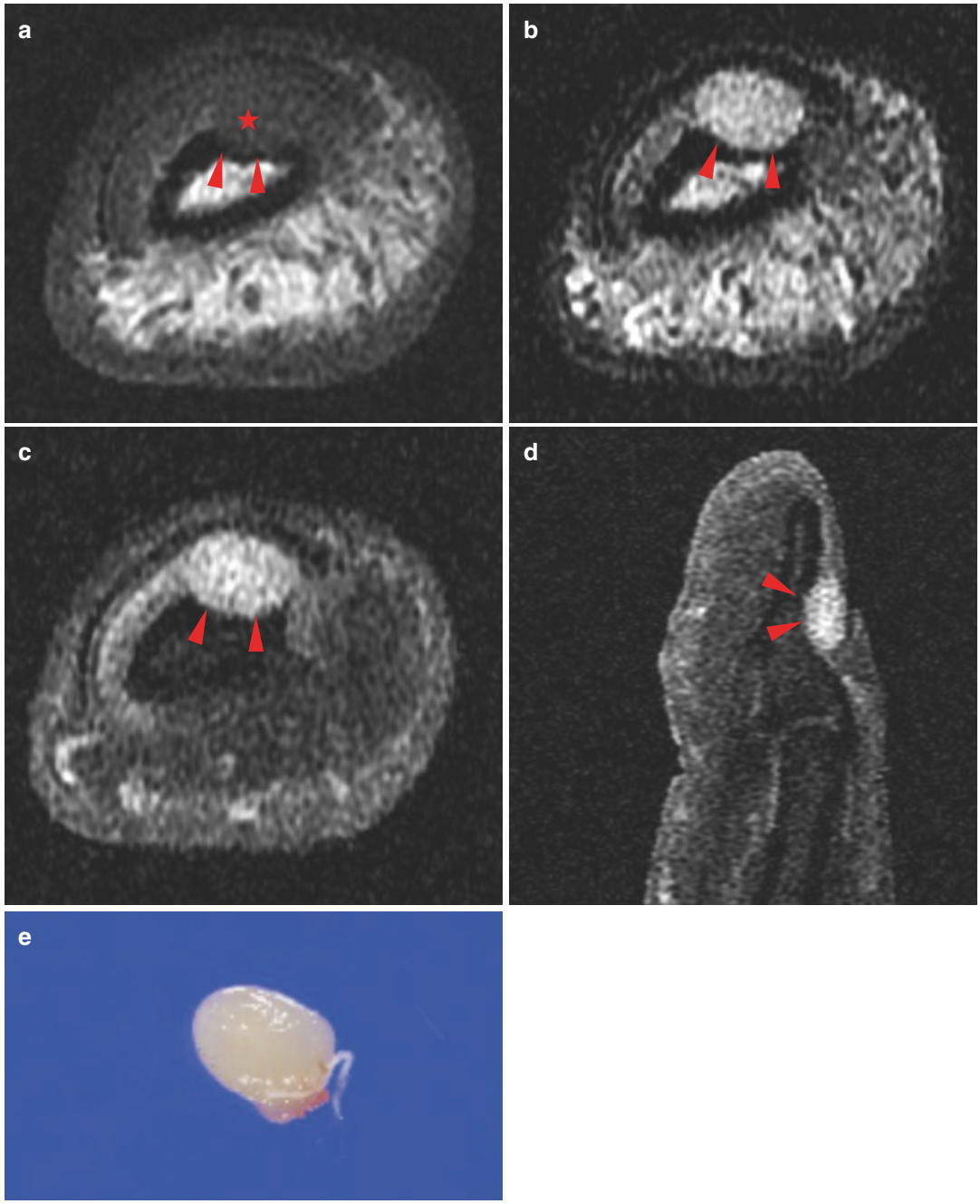

Fig. 8.3 Glomus tumor. Axial T1WI (**a**) shows a small isointense soft tissue nodule (*star*) in the subungual region. This circumscribed oval lesion is hyperintense on T2WI (**b**) and has homogeneous strong enhancement on axial (**c**) and sagittal (**d**) postcontrast FS T1WI. Note the dorsal bone erosion of the neighboring distal phalanx (*arrowheads*). The specimen photograph (**e**) shows an oval grayish-white nodule with a smooth and glossy cut surface

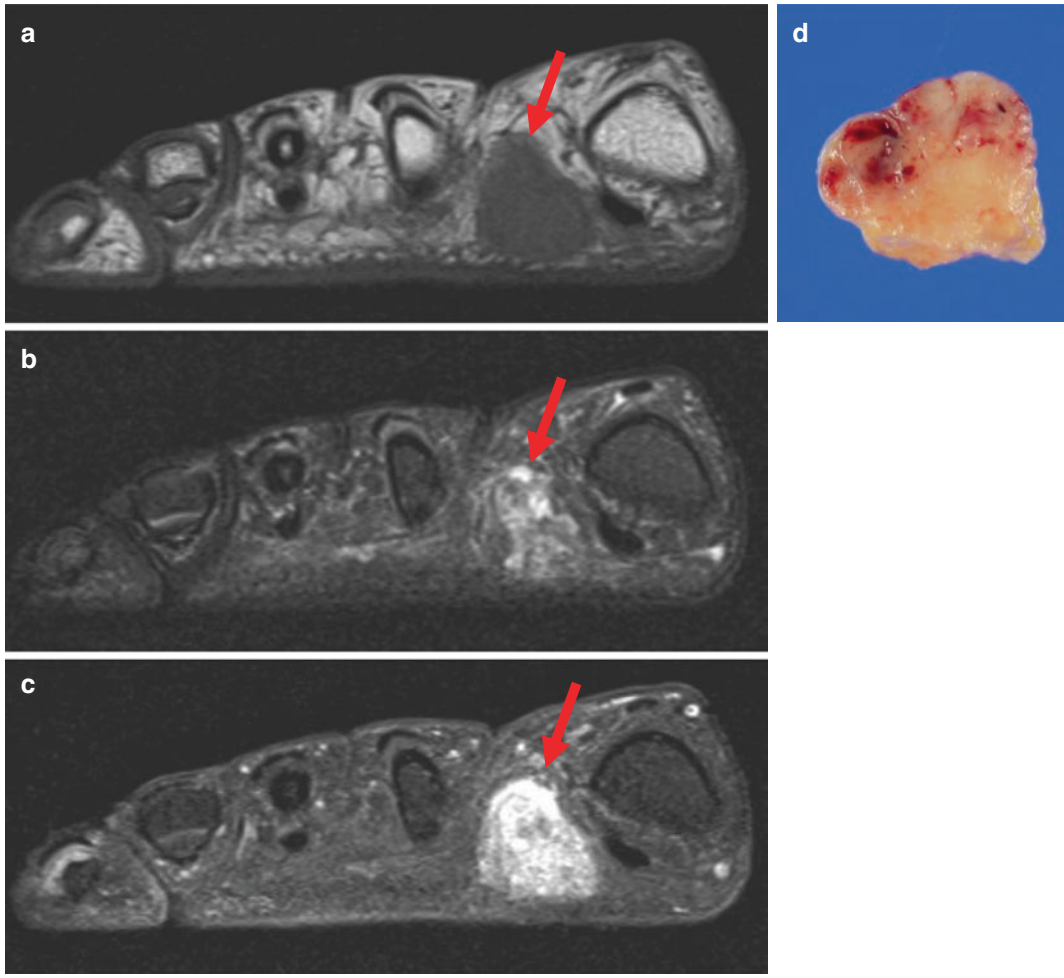

Fig. 8.4 Glomus tumor. Axial T1WI (**a**) shows a small subcutaneous soft tissue mass (*arrow*) in the plantar subcutaneous fat layer between the big toe and the second toe, separate from the neighboring bones. The mass is isointense relative to skeletal muscle. This lesion is heterogeneously hypointense to hyperintense on FS T2WI (**b**). Prominent heterogeneous contrast enhancement of the mass is observed on postcontrast FS T1WI (**c**). A specimen photograph (**d**) reveals a yellowish cut surface of the circumscribed lobulated tumor and multifocal intratumoral hemorrhage

8.4.2 Glomangioma

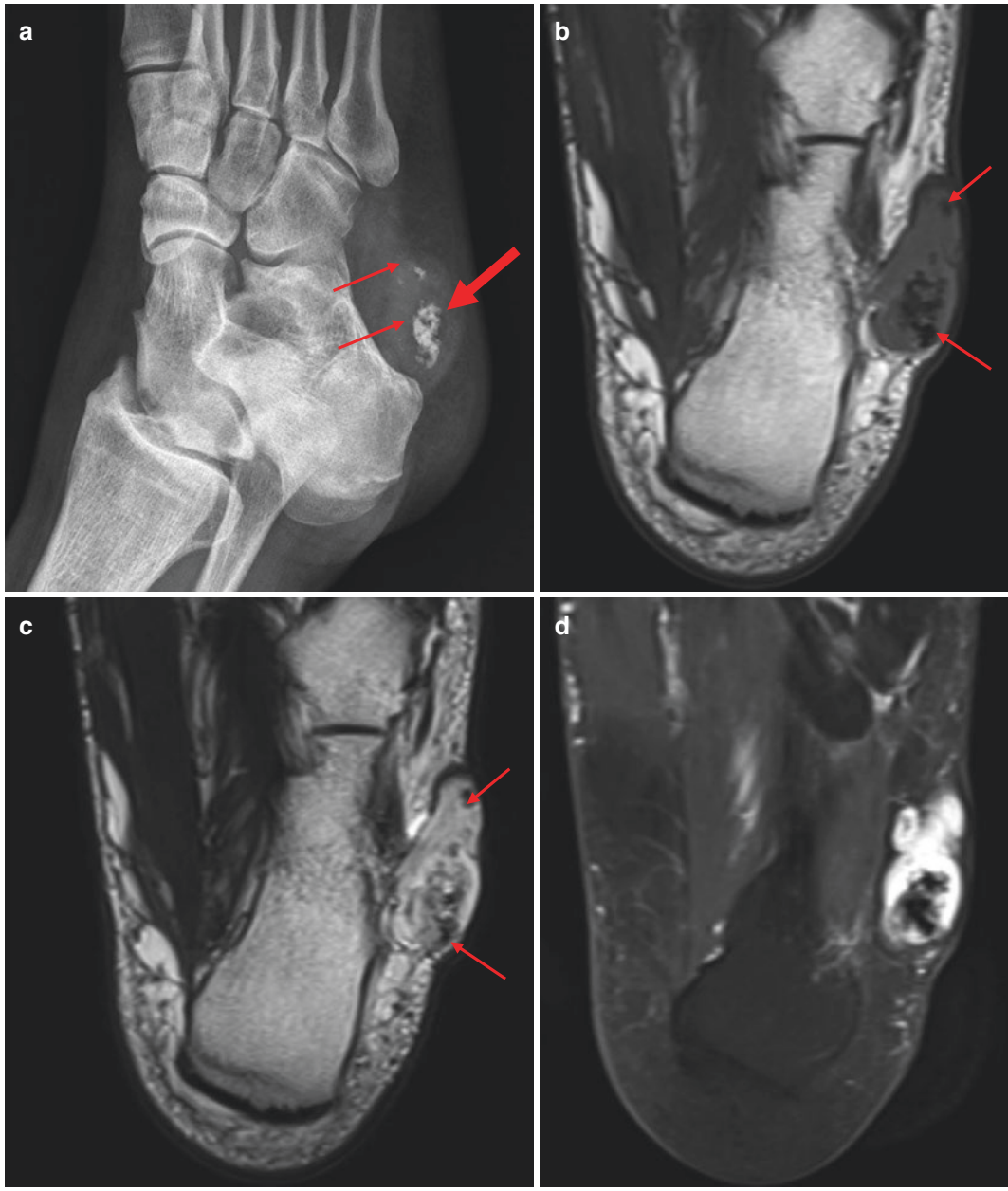

Fig. 8.5 Glomangioma. Oblique radiograph (**a**) reveals a nonspecific soft tissue mass (*arrow*) along the plantar aspect of the calcaneus. Highly irregular mineralization (*thin arrows*) is observed within the mass. This well-circumscribed subcutaneous mass is slightly hyperintense on T1WI (**b**) and heterogeneous hyperintense on T2WI (**c**). Heterogeneous intense enhancement is observed on postcontrast FS T1WI (**d**). Multifocal dark signal voids (*thin arrows*) are seen, corresponding to mineralization. US (**e**) shows a solid heterogeneous hypoechoic mass with prominent blood flow on color Doppler image. Multifocal bright hyperechogenic foci (*thin arrows*) with posterior shadowing reflect mineralization

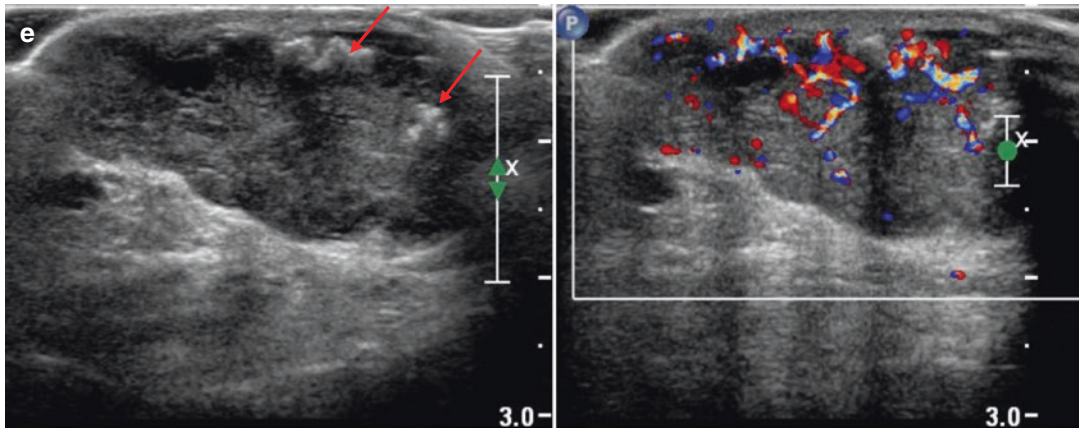

Fig. 8.5 (continued)

8.4.3 Glomangiomatosis

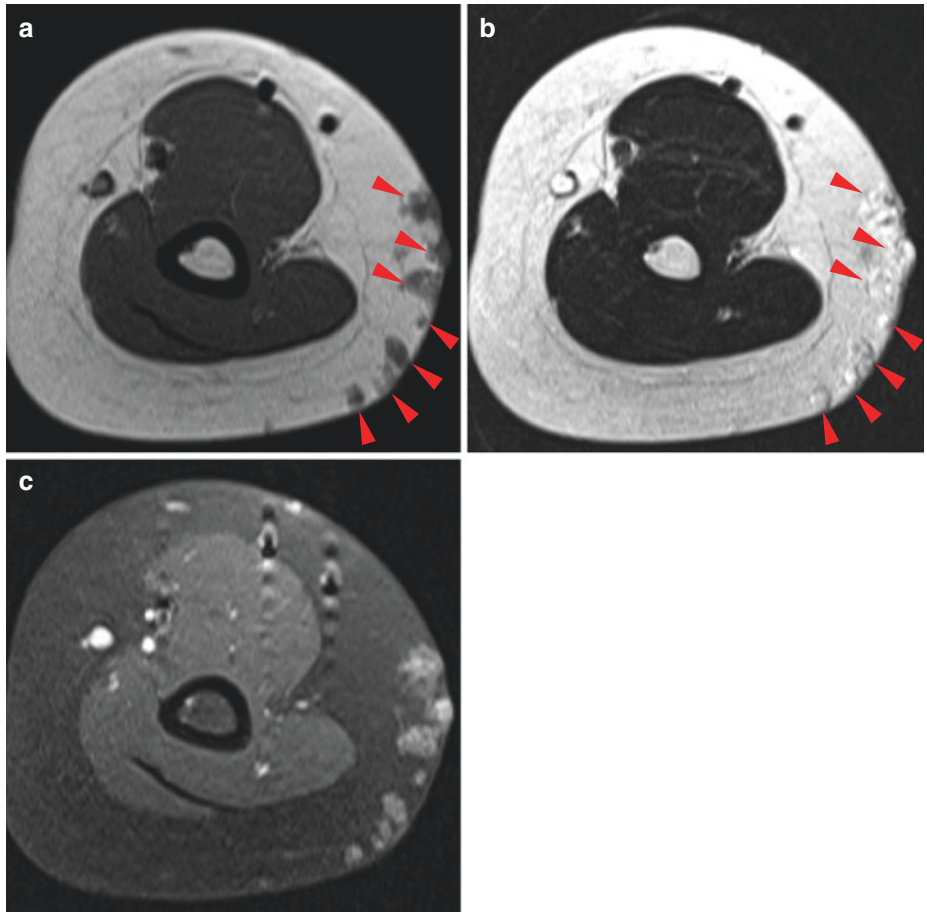

Fig. 8.6 Glomangiomatosis. Axial T1WI (**a**) shows variably sized, multifocal nodular lesions (*arrowheads*) involving the skin and superficial subcutaneous fat layer of the dorsolateral aspect of the upper arm. The lesions show inhomogeneous, mild hyperintensity on T1WI (**a**) and inhomogeneous hyperintensity on T2WI (**b**). Postcontrast FS T1WI (**c**) shows inhomogeneous intense contrast enhancement

8.4.4 Myofibroma

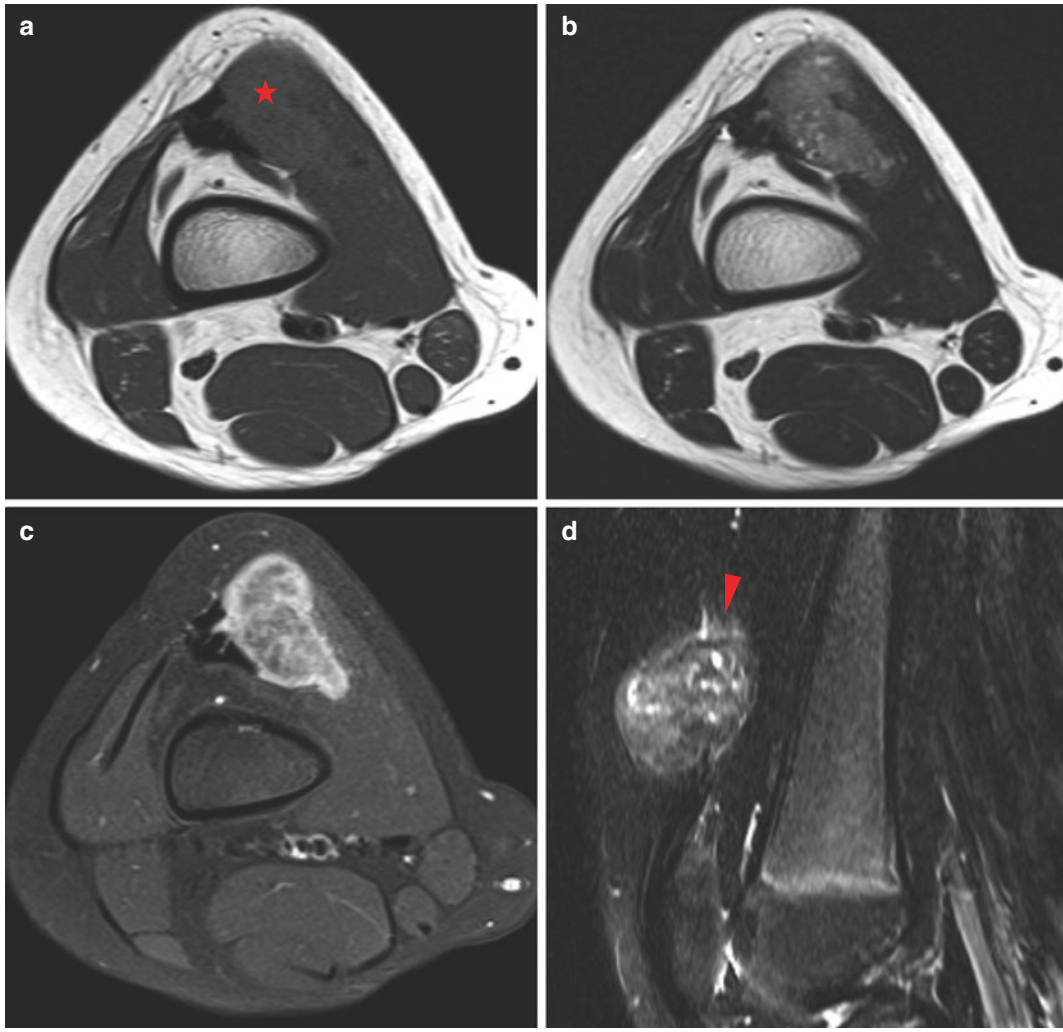

Fig. 8.7 Myofibroma. Axial T1WI (**a**) shows a lobulated intramuscular soft tissue mass (*star*) in the vastus medialis muscle, with inhomogeneous, mild hyperintensity. On T2WI (**b**), the circumscribed mass has a heterogeneous hyperintense signal and small fluid-equivalent hyperintense foci (*thin arrows*). Postcontrast FS T1WI (**c**) reveals heterogeneous enhancement, i.e., more intense peripheral rim enhancement and less enhancement centrally. Multifocal non-enhancing foci (*thin arrows*) are fluid-equivalent hyperintense on T2WI, corresponding to cystic changes. Sagittal FS T2WI (**d**) shows a heterogeneous mixed signal (ranging from dark to fluid-equivalent), brightly hyperintense, with a peritumoral, mildly hyperintense area (*arrowhead*), in keeping with soft tissue edema. Longitudinal US (**e**) shows a heterogeneous hypoechoic solid soft tissue mass (*star*) with infiltrating margins (*thin arrows*) and posterior sonic enhancement (*arrowheads*). Some peripheral blood flow is observed on the power Doppler image (**f**). A photograph of the specimen (**g**) shows a circumscribed lobulated mass with a yellowish-white cut surface and small, empty cystic change

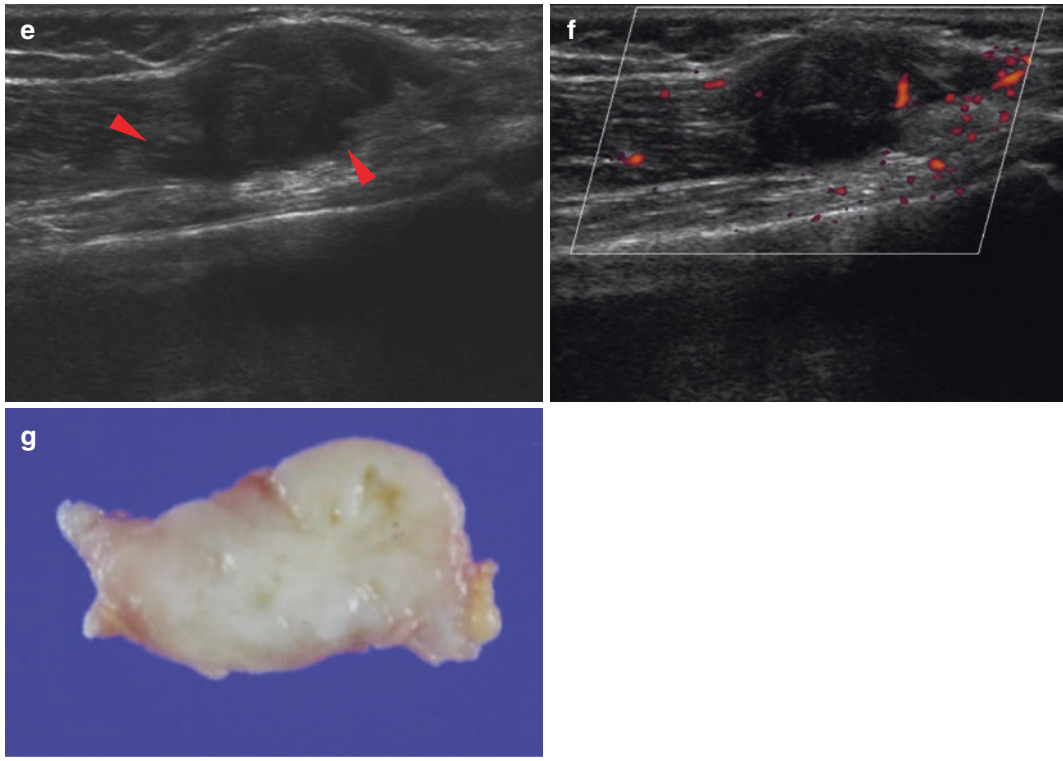

Fig. 8.7 (continued)

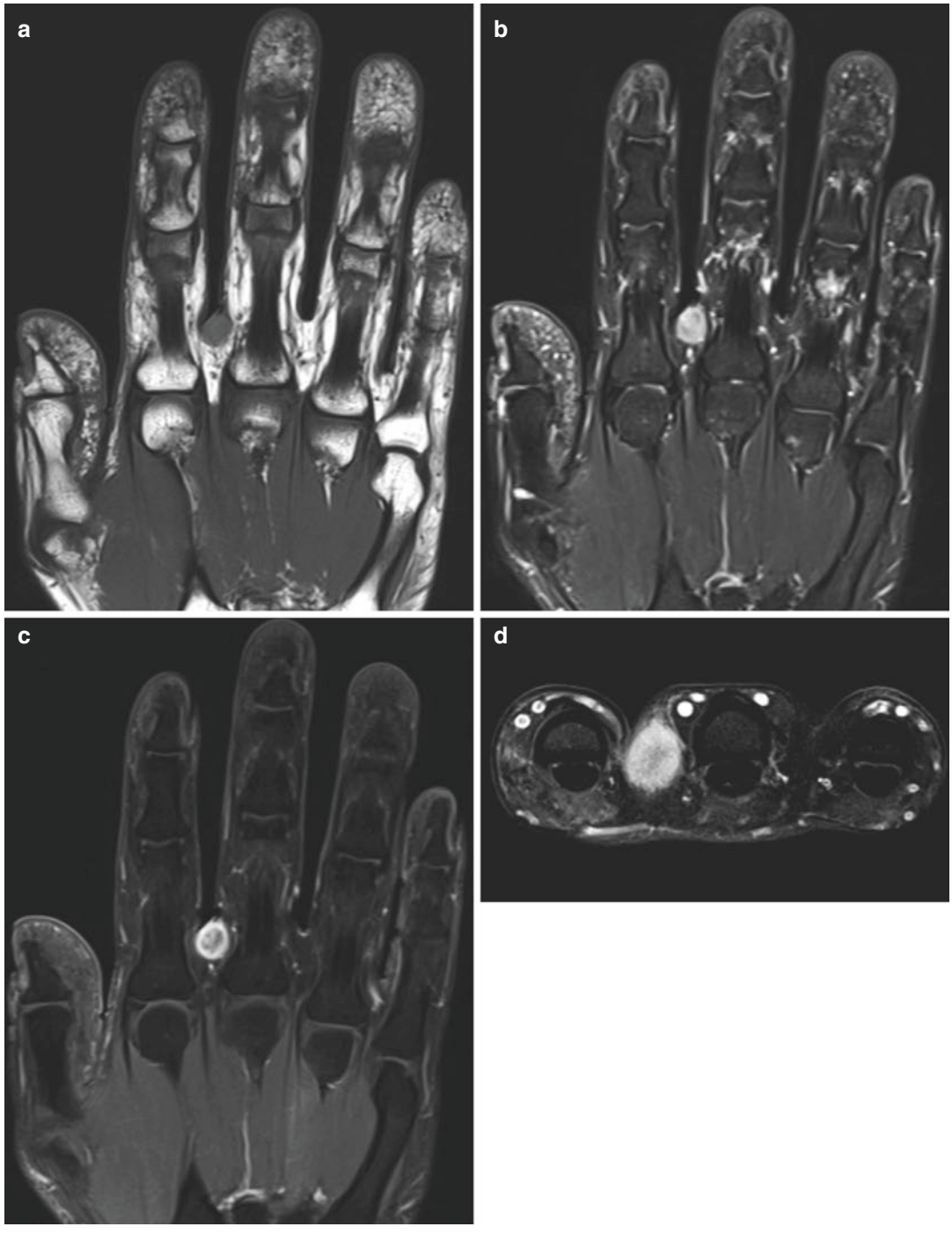

Fig. 8.8 Myofibroma. Coronal T1WI of the hand (**a**) reveals a small, well-described, slightly hyperintense (to muscle) nodule affecting the skin and the hypodermal fat tissue of the digital web space. The lesion shows inhomogeneous hyperintensity on FS T2WI (**b**). Coronal (**c**) and axial (**d**) postcontrast FS T1WIs demonstrate early peripheral thick rim enhancement and delayed, gradual central fill-in enhancement

8.4.5 Myopericytoma

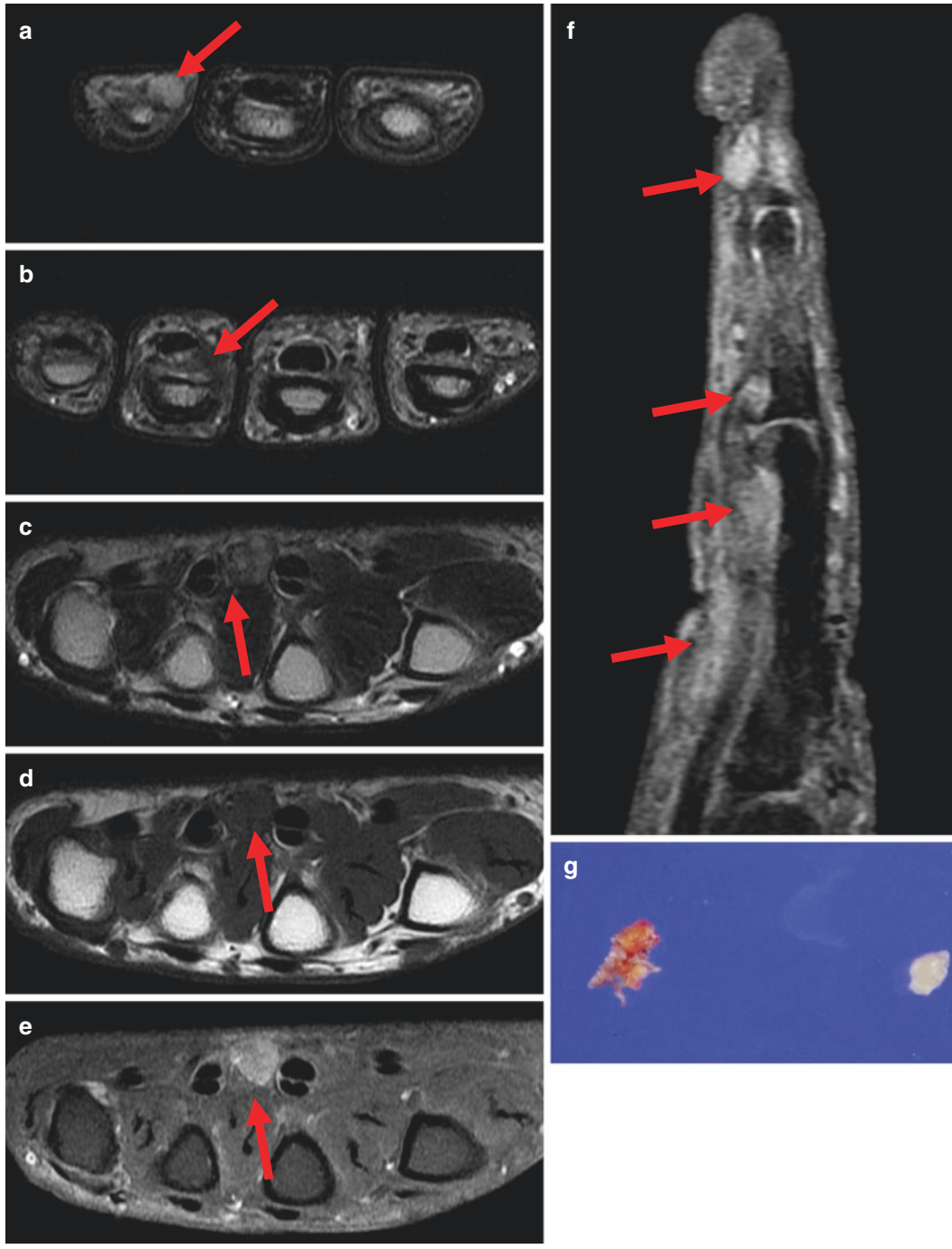

Fig. 8.9 Myopericytoma. Axial T2WIs (**a**, **b**, **c**) of fourth finger show multifocal soft tissue lesions (*arrows*) in the palmar subcutaneous tissue. The lesions shows heterogeneous signal, ranging from isointense to hyperintense to muscle on T2WI and isointense on T1WI (**d**). Axial (**e**) and sagittal (**f**) postcontrast FS T1WIs demonstrate multifocal inhomogeneous enhancing lesions along the long axis of the affected finger. Specimen photograph (**g**) shows white or reddish-white colored soft tissue lesions with mildly glossy cut surfaces

8.4.6 Angioleiomyoma

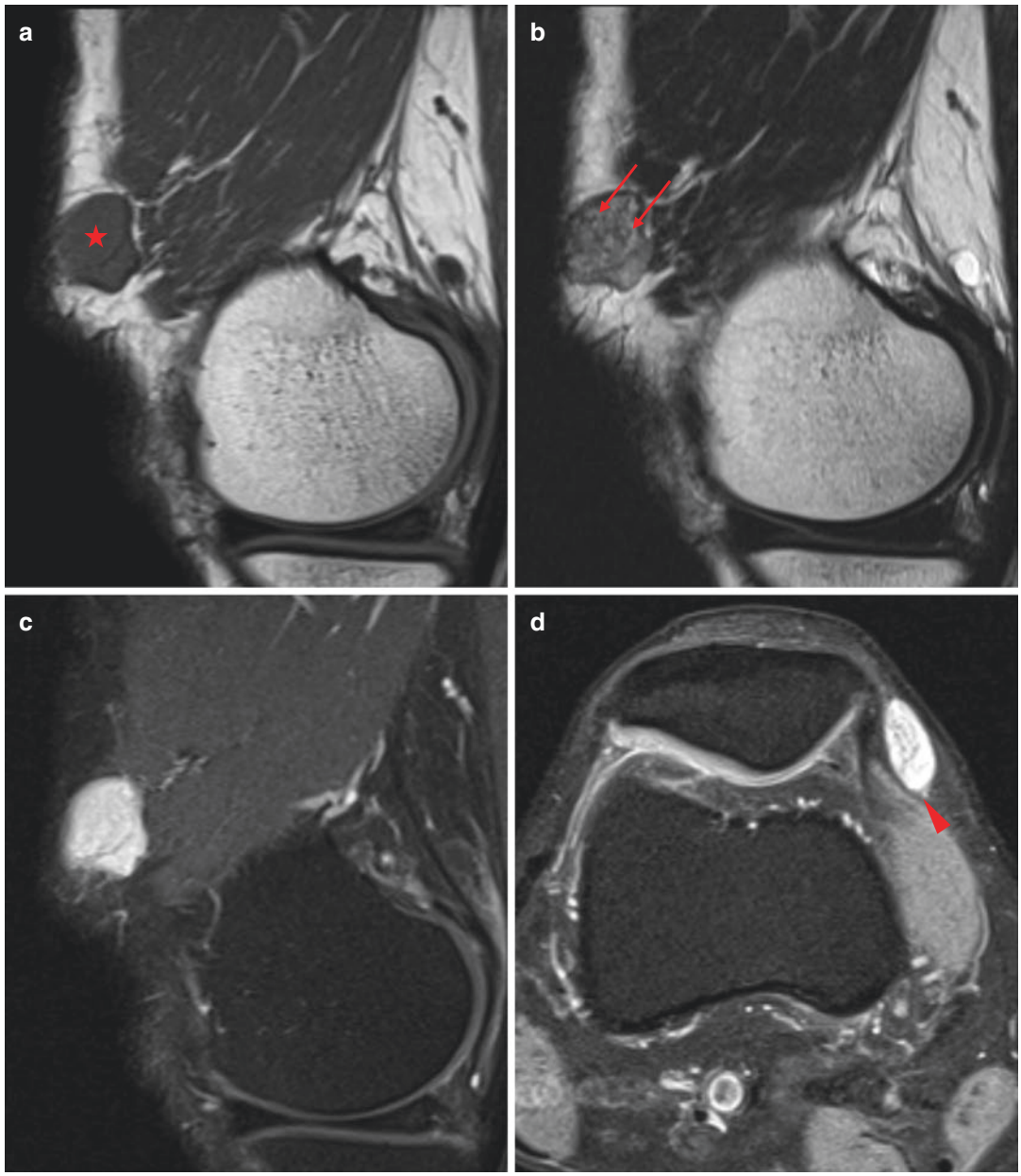

Fig. 8.10 Angioleiomyoma. Sagittal T1WI (**a**) reveals a circumscribed, lobulated subcutaneous mass (*star*), which is heterogeneously hyperintense on T2WI (**b**) and exhibits tubular signal voids (*thin arrows*). Postcontrast FS T1WIs (**c**, **d**) show strong contrast enhancement. Note that the lesion is closely abutting the surrounding subcutaneous vascular structure (*arrowheads*)

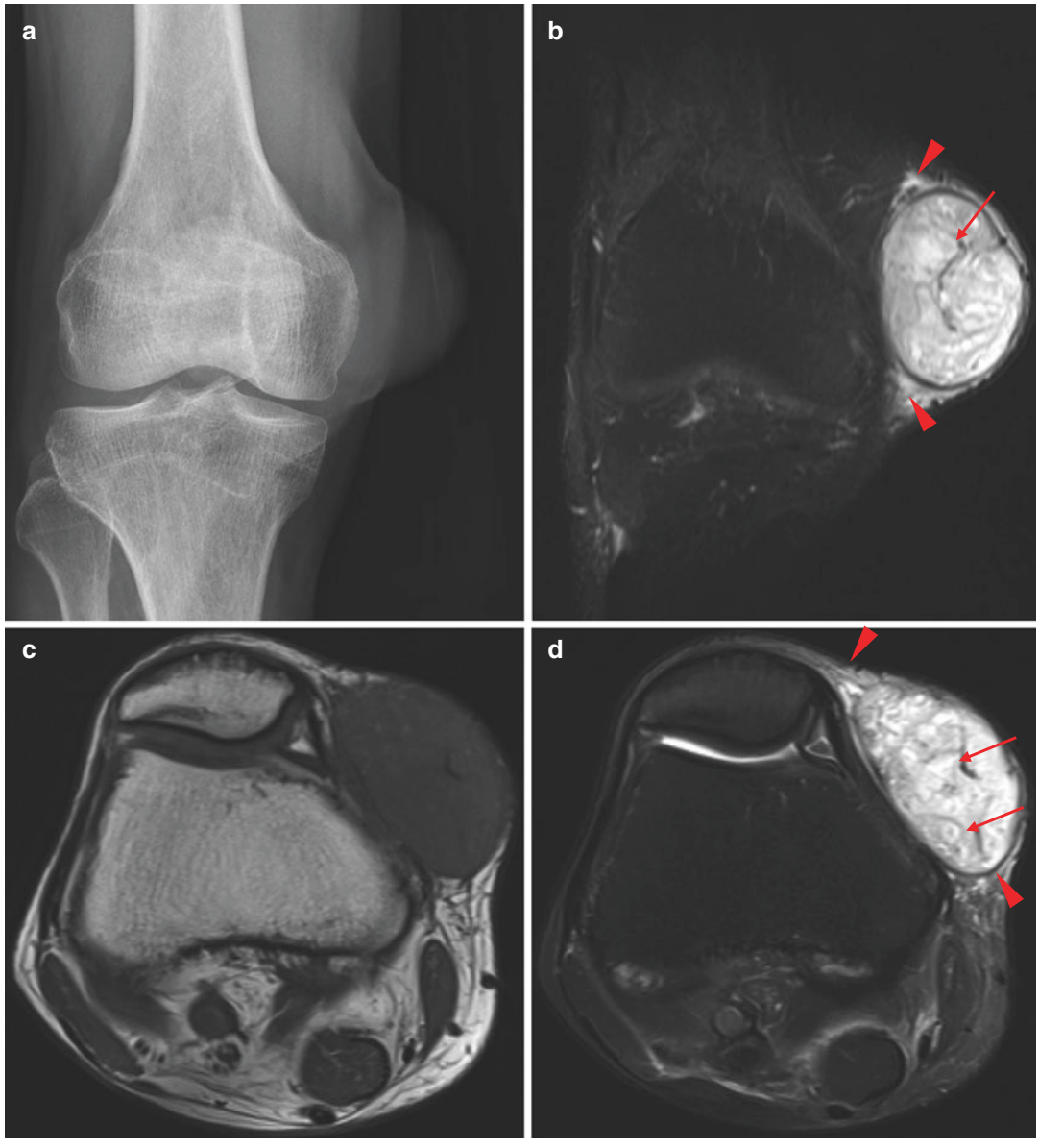

Fig. 8.11 Angioleiomyoma. AP radiograph (**a**) reveals a bulging, contoured soft tissue mass in the medial aspect of the knee. There is no mineralization within the lesion. Compared to skeletal muscle, the lesion shows a heterogeneous hyperintense signal on FS T2WI (**b**, **d**) and mild hyperintensity on T1WI (**c**). Tubular signal voids (*thin arrows*) are observed within the mass. Perilesional subcutaneous signal changes (*arrowheads*) are noted. US (**e**) reveals marked heterogeneous hyperechogenicity with multifocal anechoic tubular structures, which are observed as blood flow on the color Doppler image (**f**). Specimen photo (**g**) shows a sharply circumscribed, whitish-yellow mass with multiple blood-filled channels (*arrowheads*) and hemorrhages

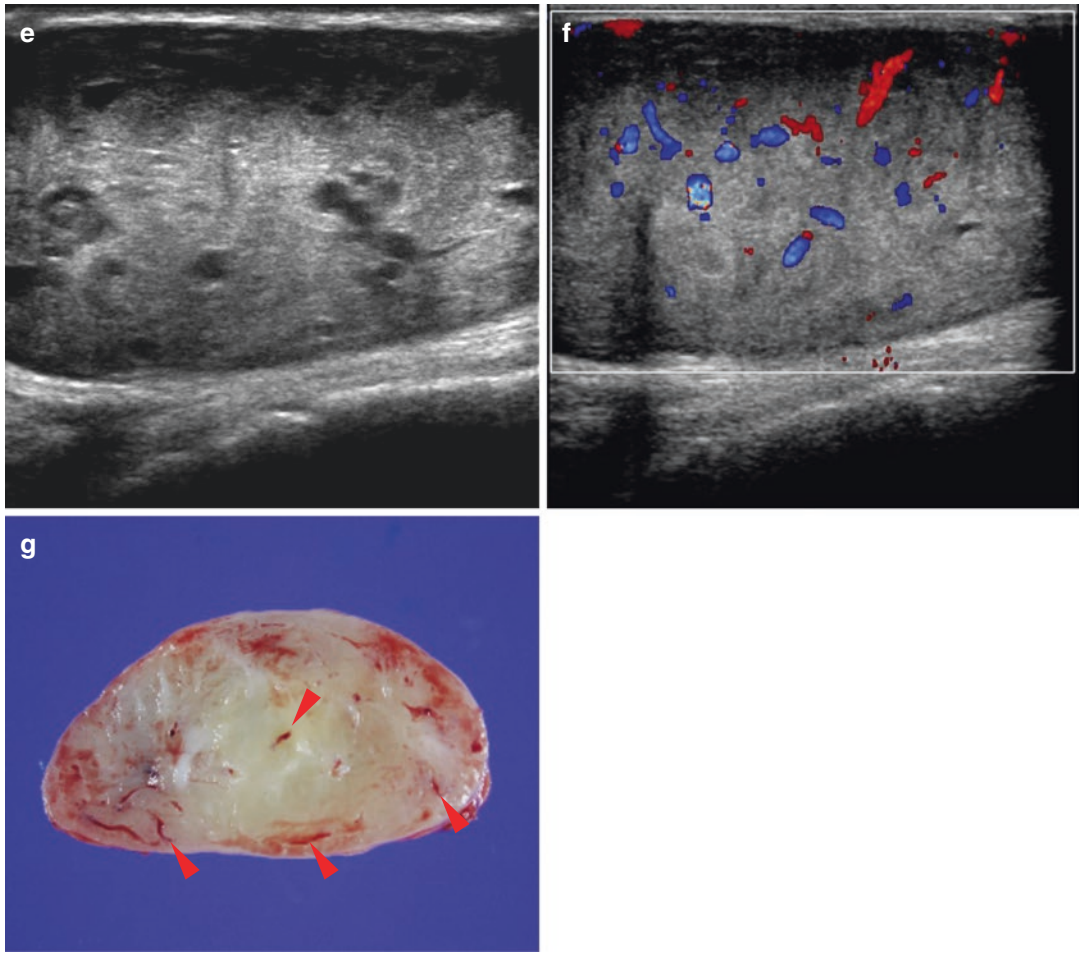

Fig. 8.11 (continued)

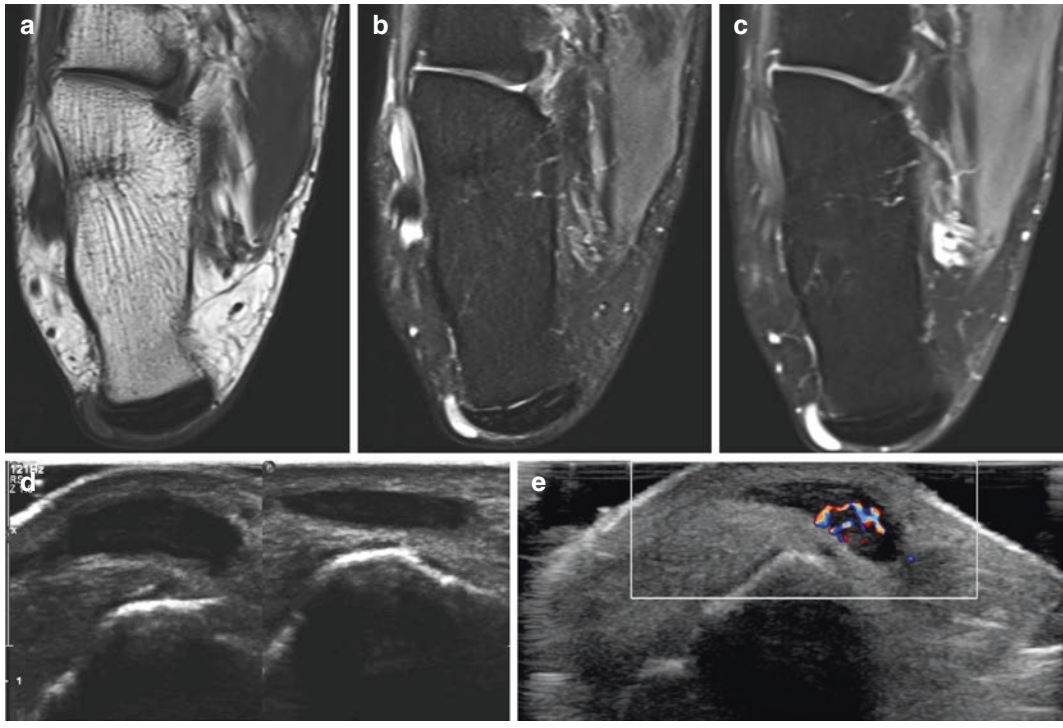

Fig. 8.12 Angioleiomyoma. Axial T1WI (**a**) of the ankle shows a circumscribed, isointense subcutaneous lesion near the Achilles tendon. The lesion is hyperintense on FS T2WI (**b**), and strong enhancement is observed on postcontrast FS T1WI (**c**). US (**d**) reveals a homogenous hypoechoic lesion with compression due to mild pressure. Color Doppler image (**e**) reveals intratumoral hypervascularity

References

Baek HJ, Lee SJ, Cho KH, Choo HJ, Lee SM, Lee YH, Suh KJ, Moon TY, Cha JG, Yi JH, Kim MH, Jung SJ, Choi JH. Subungual tumors: clinicopathologic correlation with US and MR imaging findings. Radiographics. 2010;30(6):1621–36. doi:10.1148/rg.306105514.

Choi GW, Yang JH, Seo HS, Kim WT, Lee MJ, Yoon JR. Myopericytoma around the knee: mimicking a neurogenic tumour. Knee Surg Sports Traumatol Arthrosc. 2014; doi:10.1007/s00167-014-3390-x.

Dray MS, McCarthy SW, Palmer AA, Bonar SF, Stalley PD, Marjoniemi V, Millar E, Scolyer RA. Myopericytoma: a unifying term for a spectrum of tumours that show overlapping features with myofibroma. A review of 14 cases. J Clin Pathol. 2006;59(1):67–73. doi:10.1136/jcp.2005.028704.

Flope AL, Brems H, Legius E. Glomus tumours. In: WHO classification of tumours of soft tissue and bone. 4th ed. Lyon: International Agency for Research on Cancer; 2013. p. 116–7.

Folpe AL, Fanburg-Smith JC, Miettinen M, Weiss SW. Atypical and malignant glomus tumors: analysis of 52 cases, with a proposal for the reclassification of glomus tumors. Am J Surg Pathol. 2001;25(1):1–12.

Hachisuga T, Hashimoto H, Enjoji M. Angioleiomyoma. A clinicopathologic reappraisal of 562 cases. Cancer. 1984;54(1):126–30.

Harish S, O'Donnell P, Briggs TW, Saifuddin A, Flanagan AM. Myopericytoma in Kager's fat pad. Skelet Radiol. 2007;36(2):165–9. doi:10.1007/s00256-006-0108-2.

Kayes AV, Bancroft LW, Tennyson GS, O'Connor MI. Myofibroma of the upper arm in a 52-year-old woman. Skelet Radiol. 2002;31(4):240–5. doi:10.1007/s00256-002-0478-z.

Park HJ, Kim SS, Lee SY, Choi YJ, Chung EC, Rho MH. Sonographic appearances of soft tissue angioleiomyomas: differences from other circumscribed soft tissue hypervascular tumors. J Ultrasound Med. 2012;31(10):1589–95.

Scott MA, Shen J, Lam K, Yen Y-H, Mravic M, Lugassy C, James AW. Review of pericytes in tumor biology. International Journal of Orthopaedics. 2015;2(3):300–6. doi:10.17554/j.issn.2311-5106.2015.02.64.

Weiss SW, Goldblum JR. Myofibroma and myofibromatosis. In: Enzinger and Weiss's soft tissue tumors. St Louis, MO: Mosby; 2001. p. 357–63.

Yoo HJ, Choi JA, Chung JH, Oh JH, Lee GK, Choi JY, Hong SH, Kang HS. Angioleiomyoma in soft tissue of extremities: MRI findings. AJR Am J Roentgenol. 2009;192(6):W291–4. doi:10.2214/AJR.07.3952.

Zhang JZ, Zhou J, Zhang ZC. Subcutaneous angioleiomyoma: clinical and sonographic features with histopathologic correlation. J Ultrasound Med. 2016;35(8):1669–73. doi:10.7863/ultra.15.06056.

Skeletal Muscle Tumors

9

9.1 Rhabdomyosarcoma

Rhabdomyosarcomas are malignant soft tissue tumors showing skeletal muscle or rhabdomyoblastic differentiation. The WHO classifies rhabdomyosarcoma into four types as follows: embryonal, alveolar, pleomorphic, and spindle cell/sclerosing.

Embryonal rhabdomyosarcoma has phenotypical and biological features of embryonic skeletal muscle cells, being composed of rounded-short spindle cells, often with loose myxoid foci, and containing variable numbers of eosinophilic rhabdomyoblasts. It is the most common type of all rhabdomyosarcomas, primarily occurring in the first decade of life. Embryonal rhabdomyosarcoma is more common in males, with a male-to-female ratio of 1.4:1. It most frequently occurs within the head and neck, followed by the genitourinary system. In general, the embryonal type shows the most favorable prognosis, and children have a better outcome than adults (Parham et al. 2013; Ognjanovic et al. 2009; Van Rijn et al. 2008).

Alveolar rhabdomyosarcoma consists of uniform population of primitive cells with round nuclei in an alveolar pattern or in diffuse sheets with wreath-like multinucleated giant cells (Parham and Barr 2013; Allen et al. 2007; Hawkins et al. 2001). This type is a high-grade sarcoma with a high rate of early regional and distant metastasis. Alveolar rhabdomyosarcoma is the second most common type and primarily occurs in adolescents and young adults. It more commonly affects the extremities (Harms 1995).

Pleomorphic rhabdomyosarcoma is a high-grade sarcoma composed of sheets of large, atypical, bizarre, and frequently multinucleated polygonal eosinophilic cells or of undifferentiated round to spindle cells that display skeletal muscle differentiation without embryonal or alveolar components (Montgomery and Barr 2013). This type usually occurs in adults, with a high prevalence of patients in the sixth to seventh decades of life. Pleomorphic rhabdomyosarcoma is most frequently encountered in the deep soft tissue, most often in the lower extremities (Allen et al. 2007; Hawkins et al. 2001).

Spindle cell/sclerosing rhabdomyosarcoma is an uncommon type, being predominantly composed of spindled neoplastic cells with infiltrative edges, with a fascicular or storiform growth pattern. Occasionally, this lesion may show focal, subtotal, or total stromal hyalinization, with tumor cells arranged in nests, microalveoli, or trabeculae, imparting a pseudovascular appearance (Nascimento and Barr 2013). This type affects both children and adults, with a strong male predilection. Spindle cell/sclerosing rhabdomyosarcoma most frequently involves the paratesticular regions in children, while it usually affects in the head and neck region in adults. It has a favorable outcome in children, whereas it does not in adults due to the high rate of recurrence and metastasis.

There are no specific radiologic imaging findings for rhabdomyosarcoma. On CT and MR imaging, it usually manifests as a nonspecific soft

H.S. Kang et al., *Oncologic Imaging: Soft Tissue Tumors*, DOI 10.1007/978-981-287-718-5_9

tissue mass, with occasional intralesional necrosis and heterogeneous contrast enhancement. Areas of hyperintense signal on T1-weighted images may show a degree of hemorrhaging, protein, or hyaline collagenous stroma (Saboo et al. 2012; Van Rijn et al. 2008).

9.2 Illustrations: Skeletal Muscle Tumors

9.2.1 Embryonal Rhabdomyosarcoma

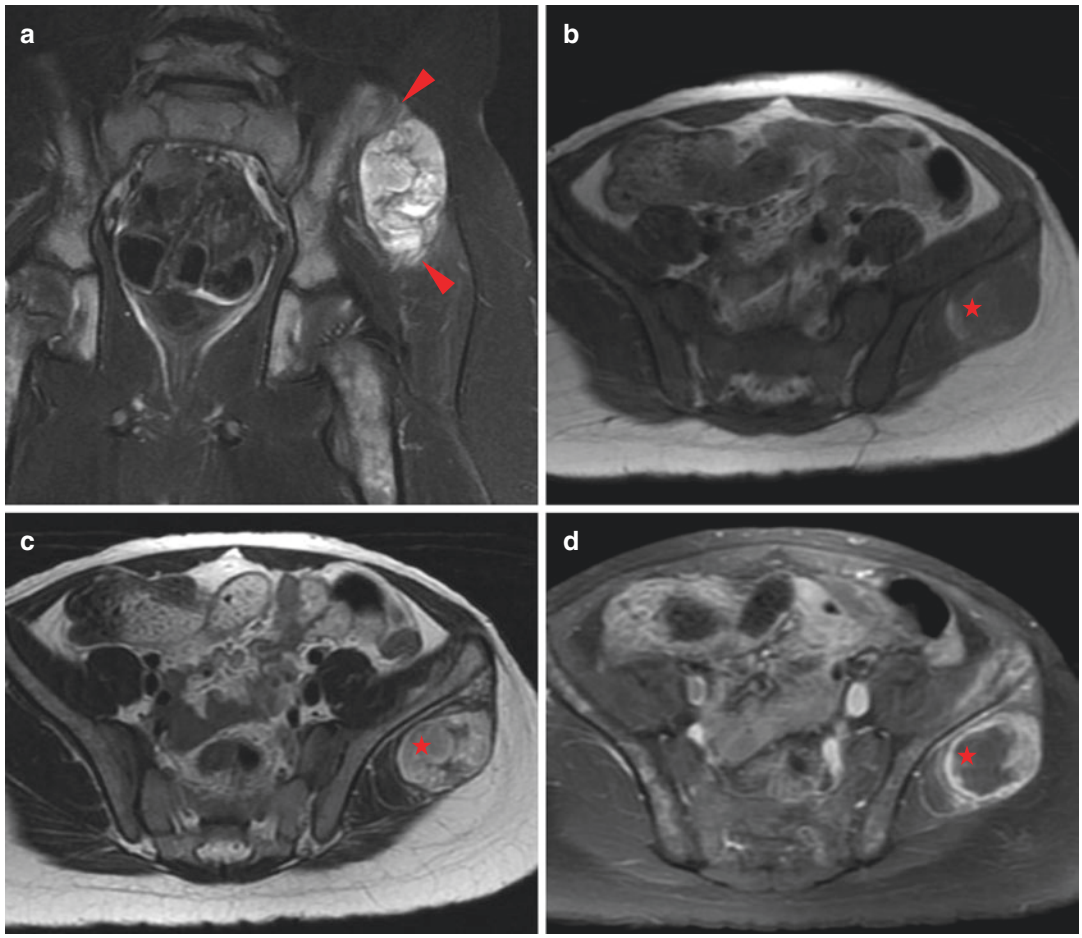

Fig. 9.1 Embryonal rhabdomyosarcoma. Coronal FS T2WI (**a**) of the pelvis shows a circumscribed mass within the gluteus maximus muscle. The lesion exhibits mixed iso- and hyperintensity to muscle on T1WI (**b**), heterogeneous hyperintensity on T2WI (**c**), and a peripheral rim and some solid mural enhancement on postcontrast FS T1WI (**d**). Peritumoral FS T2 shows associated hyperintense soft tissue edema (*arrowheads*). A mildly T1 hyperintense region with an intermediate T2 signal and no enhancement (*star*) represents a hemorrhage

9.2.2 Alveolar Rhabdomyosarcoma

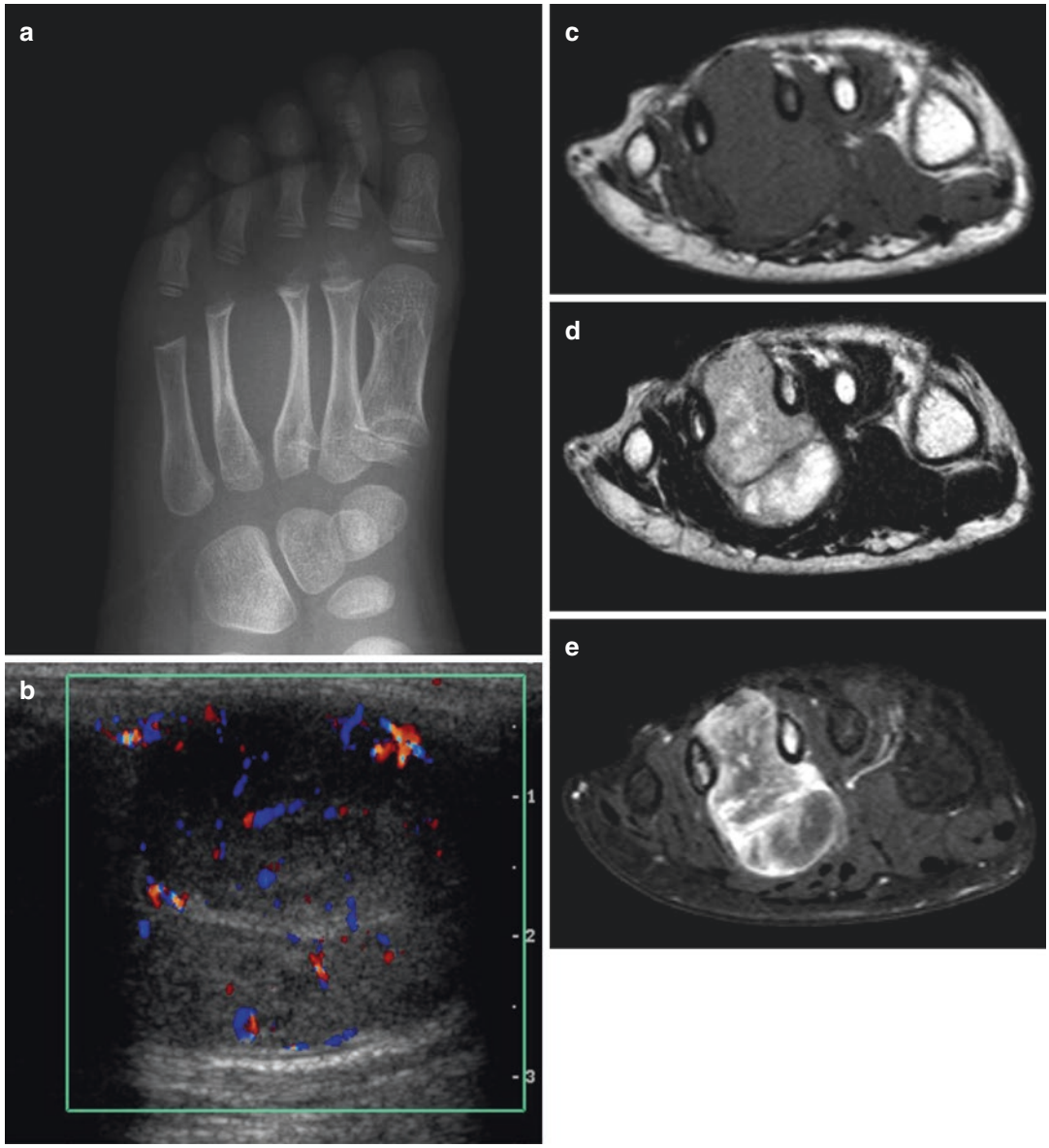

Fig. 9.2 Alveolar rhabdomyosarcoma. Radiograph (**a**) shows extrinsic scalloping of adjacent metatarsal bones by the soft tissue mass. Color Doppler image (**b**) reveals a circumscribed, inhomogeneous hypoechoic mass with intralesional hypervascularity and posterior sonic enhancement. The mass located between the metatarsal bones shows slight hyperintensity to muscle on T1WI (**c**), heterogeneous intermediate to hyperintensity on T2WI (**d**), and inhomogeneous enhancement on postcontrast FS T1WI (**e**). It is accompanied by bone marrow signal alteration in the neighboring metatarsal bones, without cortical destruction

9.2.3 Pleomorphic Rhabdomyosarcoma

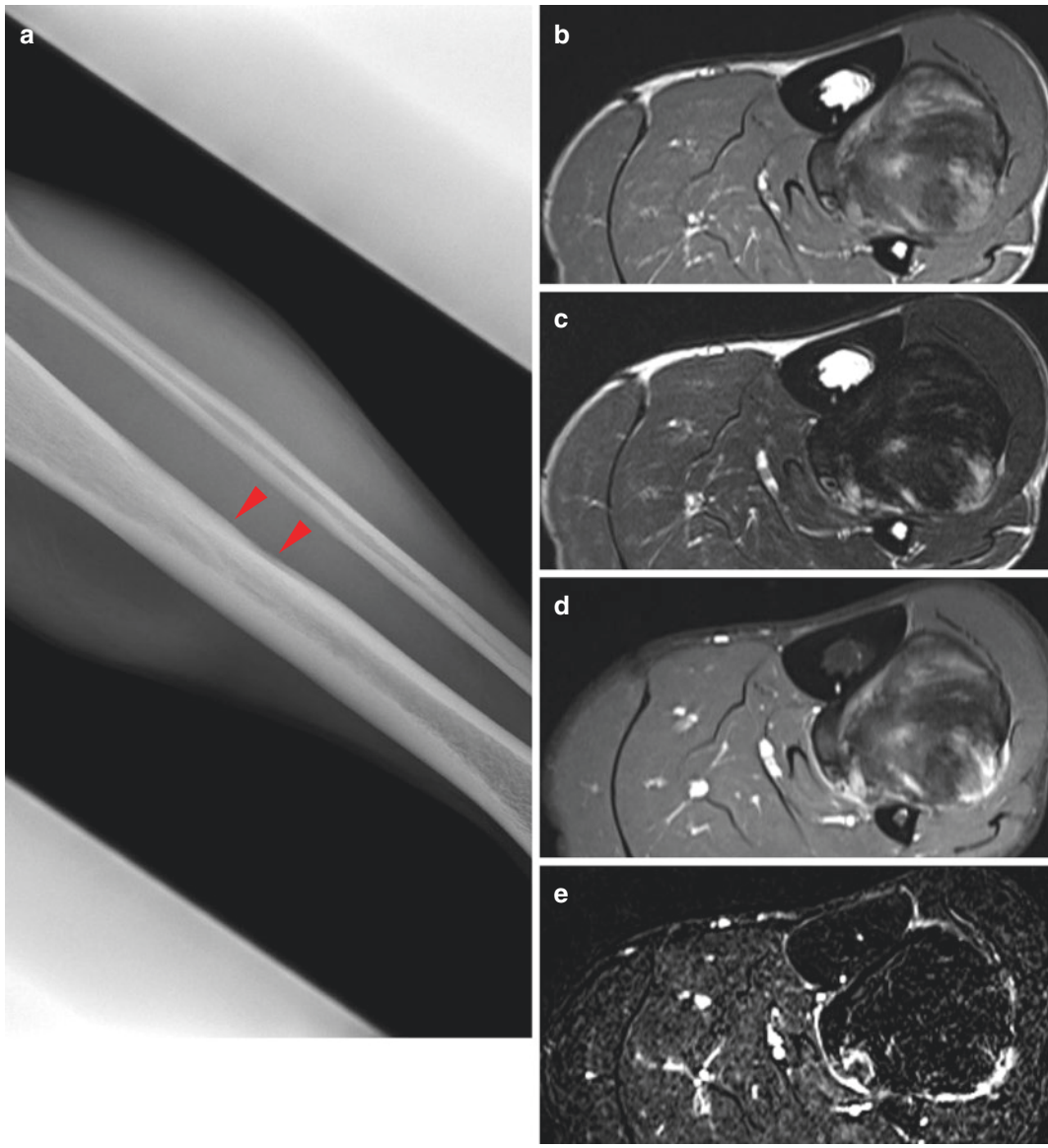

Fig. 9.3 Pleomorphic rhabdomyosarcoma. Radiograph (**a**) shows shallow cortical scalloping (*arrowheads*) of the tibial shaft. Axial T1WI (**b**) reveals a circumscribed mass between the tibia and fibula, with a mixed signal that ranges from dark to hyperintense. The lesion has dark signal on T2WI (**c**) and has hyperintense foci. Postcontrast FS T1WI (**d**) shows the mass to have internal heterogeneous hyperintensity, but a subtracted image (**e**) reveals peripheral rim enhancement. The cut surface of the gross specimen reveals a large hemorrhagic necrotic area (more than 50%) in the mass (not shown)

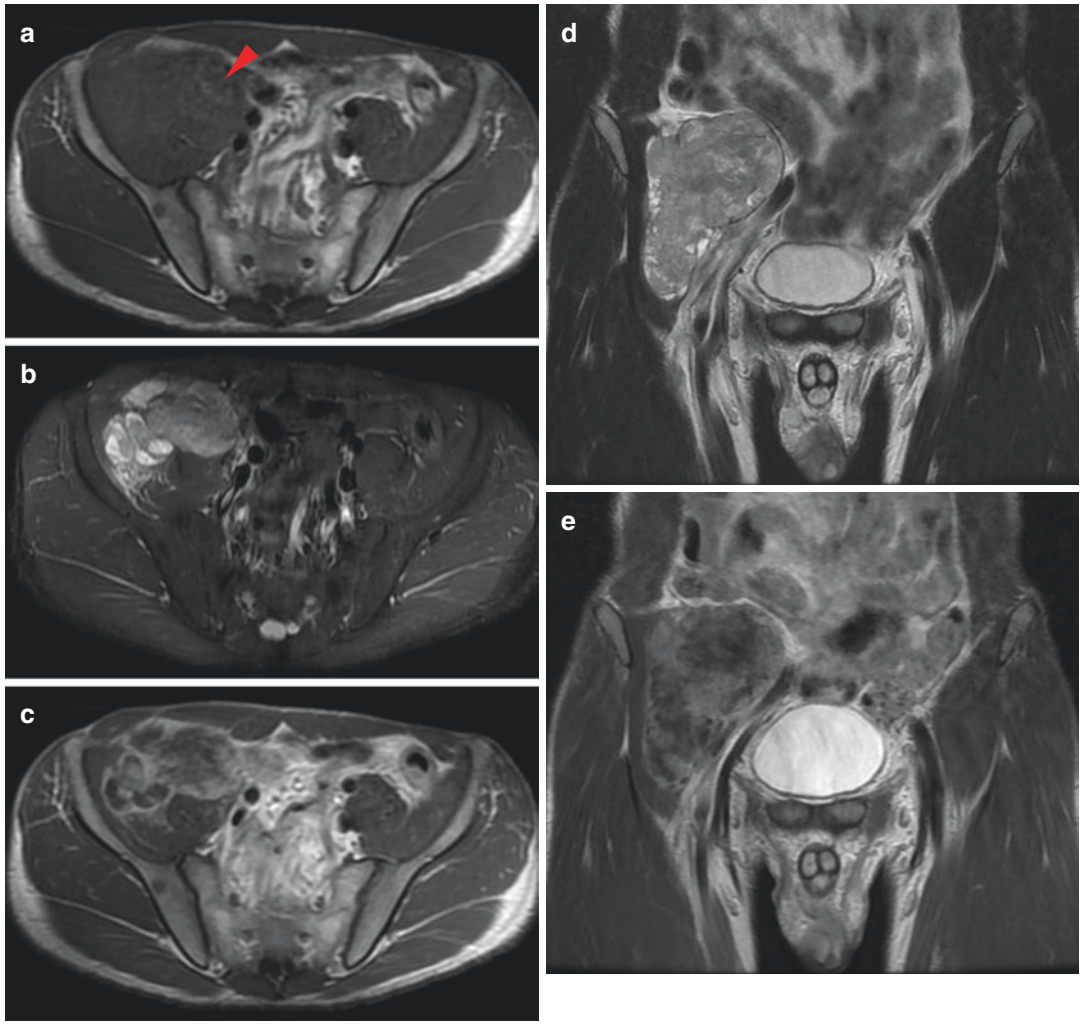

Fig. 9.4 Pleomorphic rhabdomyosarcoma. Axial T1WI (**a**) of the pelvis reveals an inhomogeneously isointense soft tissue mass in the right iliac fossa, with intralesional foci that are slightly hyperintense (*arrowhead*). Axial (**b**) and coronal (**d**) FS T2WIs show the mass to be heterogeneously hyperintense and involve the neighboring iliacus and psoas muscles. Axial (**c**) and coronal (**e**) postcontrast T1WIs reveal heterogeneous and irregular peripheral and septal enhancement. PET (**f**) shows the mass to be strikingly hypermetabolic (SUV 10.7). A photograph of the specimen (**g**) shows the dark brown-red-yellowish soft tissue mass with a large intratumoral hemorrhage

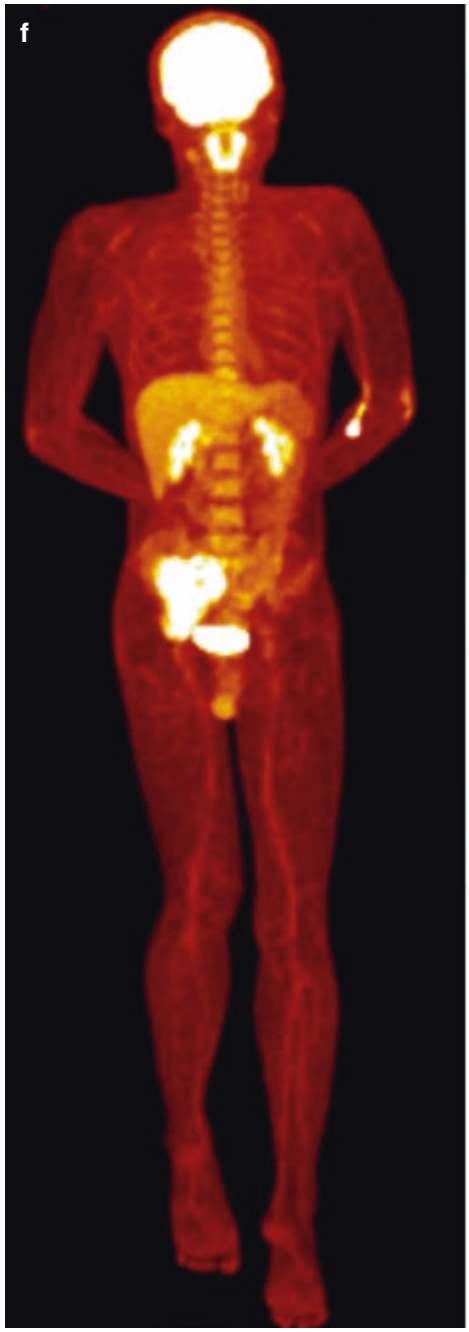

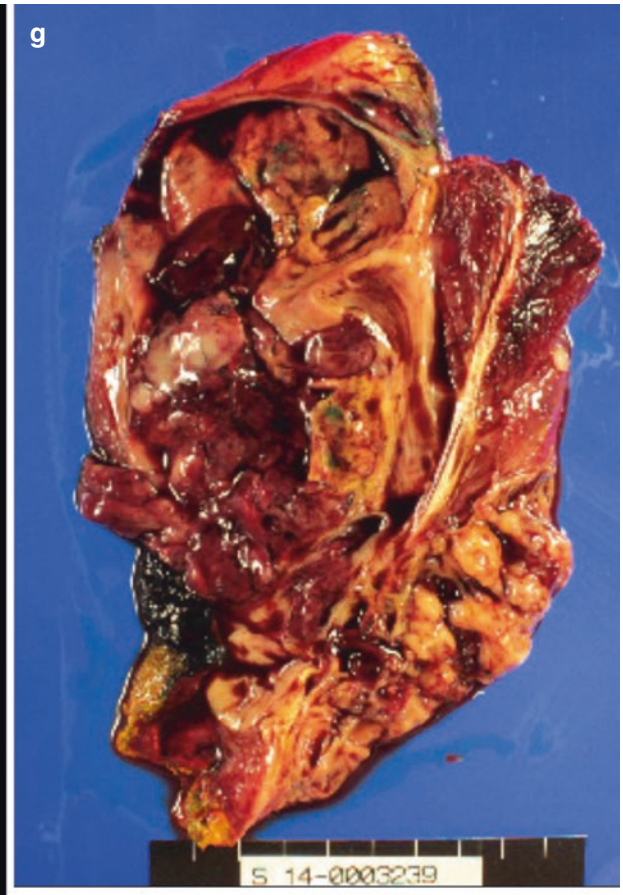

Fig. 9.4 (continued)

9.2.4 Spindle Cell Rhabdomyosarcoma

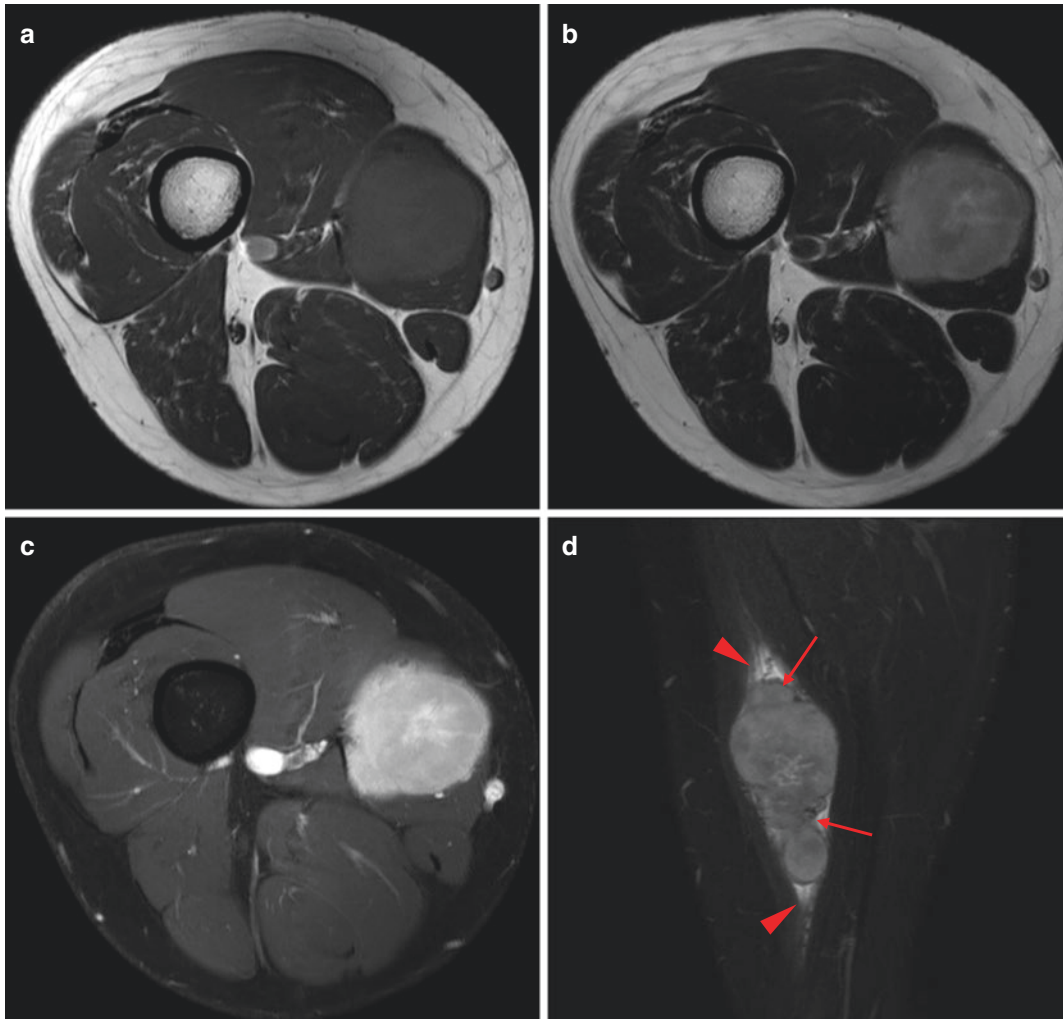

Fig. 9.5 Spindle cell rhabdomyosarcoma. Axial T1WI (**a**) of the thigh shows a slightly hyperintense (relative to skeletal muscle) intramuscular mass in the sartorius muscle. The mass has heterogeneous hyperintensity on T2WI (**b**) and strong enhancement on postcontrast FS T1WI (**c**), with a partially infiltrative border. Sagittal FS T2WI (**d**) reveals the multilobulated contour of the lesion, prominent peripheral signal flow voids (*thin arrows*), and craniocaudally oriented, peritumoral edema (*arrowheads*)

References

Allen SD, Moskovic EC, Fisher C, Thomas JM. Adult rhabdomyosarcoma: cross-sectional imaging findings including histopathologic correlation. AJR Am J Roentgenol. 2007;189(2):371–7. doi:10.2214/AJR.07.2065.

Harms D. Alveolar rhabdomyosarcoma: a prognostically unfavorable rhabdomyosarcoma type and its necessary distinction from embryonal rhabdomyosarcoma. Curr Top Pathol. 1995;89:273–96.

Hawkins WG, Hoos A, Antonescu CR, Urist MJ, Leung DH, Gold JS, Woodruff JM, Lewis JJ, Brennan MF. Clinicopathologic analysis of patients with adult rhabdomyosarcoma. Cancer. 2001;91(4):794–803.

Montgomery EA, Barr FG. Pleomorphic rhabdomyosarcoma. In: Fletcher CDM, Bridge JA, Hogendoorn PCW, Mertens F, editors. WHO classification of tumours of soft tissue and bone. 4th ed. Lyon: International Agency for Research on Cancer; 2013. p. 100–3.

Nascimento AF, Barr FG. Spindle cell/sclerosing rhabdomyosarcoma. In: Fletcher CDM, Bridge JA, Hogendoorn PCW, Mertens F, editors. WHO classification of tumours of soft tissue and bone. 4th ed. Lyon: International Agency for Research on Cancer; 2013. p. 100–3.

Ognjanovic S, Linabery AM, Charbonneau B, Ross JA. Trends in childhood rhabdomyosarcoma incidence and survival in the United States, 1975–2005. Cancer. 2009;115(18):4218–26. doi:10.1002/cncr.24465.

Parham DM, Barr FG. Alveolar rhabdomyosarcoma. In: Fletcher CDM, Bridge JA, Hogendoorn PCW, Mertens F, editors. WHO classification of tumours of soft tissue and bone. 4th ed. Lyon: International Agency for Research on Cancer; 2013. p. 100–3.

Saboo SS, Krajewski KM, Zukotynski K, Howard S, Jagannathan JP, Hornick JL, Ramaiya N. Imaging features of primary and secondary adult rhabdomyosarcoma. AJR Am J Roentgenol. 2012;199(6):W694–703. doi:10.2214/AJR.11.8213.

Van Rijn RR, Wilde JC, Bras J, Oldenburger F, McHugh KM, Merks JH. Imaging findings in noncraniofacial childhood rhabdomyosarcoma. Pediatr Radiol. 2008;38(6):617–34. doi:10.1007/s00247-008-0751-y.

Vascular Tumors

10

Pathologists, clinicians, and radiologists have traditionally confused the diagnosis of vascular anomalies. The International Society for the Study of Vascular Anomalies (ISSVA) advocated a classification that divided vascular anomalies into the following two major categories: tumors and malformations. This classification system is now widely accepted for properly diagnosing and treating vascular anomalies (Sepulveda and Buchanan 2014; Lowe et al. 2012). According to this classification system, vascular tumors (except congenital hemangiomas) are endothelial neoplasms that grow via endothelial hyperplasia, are not clinically present at birth, have a period of rapid growth, and spontaneously involute (except noninvoluting congenital hemangiomas). Vascular malformations are composed of capillaries, veins, lymphatics, and/or arteries with normal endothelial cell turnover, are present at birth, and grow proportionally with the child. However, vascular tumors will be the focus of this chapter, based on 2013 WHO classification of soft tissue tumors.

10.1 Hemangiomas

Based on 2013 WHO classification, hemangiomas are classified into the following four groups: synovial hemangioma, intramuscular angioma, venous hemangioma, and arteriovenous malformation/hemangioma (AVM/H). Synovial hemangioma is a benign proliferation of blood vessels that arises in a synovium-lined surface; the most common site is the knee. Intramuscular angioma is referred to as intramuscular hemangioma or intramuscular infiltrating angiolipoma and is a benign proliferation of blood vessels within skeletal muscles. This type of hemangioma is primarily associated with variable amounts of mature adipose tissue. It is one of the most common deep-seated soft tissue tumors, and occurs most frequently in the lower limbs. Venous hemangioma is rare and composed of variable-sized veins with thick muscular walls. It presents in the subcutaneous or deep-seated soft tissue and is relatively common in the limbs. Arteriovenous malformation/hemangioma is a benign vascular lesion characterized by the presence of arteriovenous shunting. It predominantly affects the head and neck, followed by the limbs. All types of hemangiomas primarily affect children and young adults. Most hemangiomas present as slowly growing lesions, and synovial hemangioma is often associated with swelling and joint effusion/hemarthrosis. Intramuscular angioma is occasionally painful after exercise. The symptoms of AVM/H are associated with the degree of arteriovenous shunting, which can lead to limb hypertrophy, venous distension, increased overlying skin temperature, heart failure, and even consumption coagulopathy (Kasabach-Merritt syndrome). Histopathologically, hemangiomas basically consist of various-sized vessels, such as the capillary (small), cavernous (large), and mixed vessels (Kransdorf and Murphey 2014; Calonge 2013).

H.S. Kang et al., *Oncologic Imaging: Soft Tissue Tumors*, DOI 10.1007/978-981-287-718-5_10

Radiographs are occasionally normal or demonstrate a nonspecific soft tissue mass. Calcifications, such as phleboliths, metaplastic ossification, or localized cortical/periosteal hypertrophy, can be noted. A Swiss cheese appearance, with multiple rings and arc-like ossifications with a coarse trabecular pattern, may be observed in ossifying hemangiomas. On CT, hemangioma is observed as a soft tissue mass, occasionally with strong enhancing serpentine vascular components, fat overgrowth, and phleboliths. US may reveal a well-defined soft tissue mass with variable echogenicity. Hemangiomas may be hypoechoic or hyperechoic relative to surrounding tissue and may have a homogeneous or complex appearance. If phleboliths are associated, they appear as hyperechoic spots with posterior shadowing. Color Doppler imaging also reveals various flow signal patterns. Hemangiomas with slow blood flow may show only sparse monophasic (venous) blood flow or no blood flow signal, but a dynamic maneuver, such as a repeated compression-decompression technique, can help visualize internal blood flow. That is, one can watch for collapse or non-visualization of the flow signal on compression and reappearance of the signal with gradual decompression. Lesions with high blood flow reveal high blood flow signals or networks on color Doppler imaging and high systolic arterial flow pattern on spectral Doppler imaging. In addition, adjacent dilated draining veins are frequently noted. MR imaging shows a low-to-intermediate signal intensity, occasionally with areas of hyperintensity, representing slow blood flow, hemorrhage, or thrombosis on T1-weighted images. A homogenous or heterogeneous, intermediate to very high signal intensity is observed on T2-weighted images. Frequently, intratumoral fat deposition is observed within and around the lesion. The vascular channels and spaces of hemangioma have round/oval, linear, or serpentine appearance, with either high or low signal intensity. Hemorrhagic areas have high signal intensity on T1- and T2-weighted images or fluid-fluid levels. Phleboliths are observed as circular dark or hypointense nodules. Occasionally, an intratumoral thrombus can be observed as areas of mild hyperintensity on T1-weighted images and hypointensity on T2-weighted images. Hemangioma shows diffuse contrast enhancement of varying degree, from strong solid enhancement to gradual centripetal enhancement. *Synovial hemangioma* is characterized by an intra-articular location, often with a juxta-articular location. This lesion is frequently associated with hemorrhagic synovitis characterized by effusion or hemarthrosis and synovial hypertrophy observed with occasional hemosiderin deposits on MRI. *Intramuscular angioma* is diagnosed when the hemangioma is located in the muscle. *Venous hemangiomas* show slow-flow serpentine vessels and a tendency to be oriented along the long axis of the extremities and neurovascular bundle. These hemangiomas also have multifocal involvement and are characterized by muscle atrophy, with increased subcutaneous fat. AVM/H tends to have clusters of serpentine signal voids on MR imaging. The lack of enhancing soft tissue masses distinguishes AVM/H from other hypervascular soft tissue sarcomas (Lowe et al. 2012; Murphey et al. 1995).

10.2 Angiomatosis

When arteriovenous malformation/hemangiomas involve a large segment of the body in a contiguous fashion, either (1) by longitudinal extension to affect multiple different tissue planes or (2) by crossing muscle compartments to affect similar tissue types, these lesions are termed "angiomatosis." This lesion occurs commonly in the first two decades of life and in the lower extremities. It presents as diffuse, persistent swelling of the affected location, which may wax and wane in size and is affected by strenuous activity. If the prominent arteriovenous shunting is associated, increased skin temperature, thrill, pulsation, or hypertrophy of the affected part can be detected. The imaging appearance of angiomatosis is similar to those for previously described hemangiomas. However, angiomatoses are infiltrative and affect multiple tissue planes. In addition, abundant adipose tissue is frequently involved (Aviv et al. 2001; Rao and Weiss 1992).

10.3 Lymphangioma

Lymphangiomas consist of dilated lymphatic channels and exist in two forms as follows: microcystic (capillary, smaller than 2 mm) and macrocystic (cavernous, larger cysts of variable sizes), commonly referred to as cystic hygroma and lymphatic malformation. This lesion presents in the first 2 years of life as a palpable soft fluctuant soft tissue mass and commonly affects the head and neck or axilla (Dubois and Garel 1999).

Radiographs of lymphangioma reveal a nonspecific soft tissue mass with rare calcifications. At US, this lesion appears as a unilocular or multilocular anechoic or hypoechoic mass, with septa of variable thicknesses. In addition, if it is bloody, chylous, or infected, the lesion may show internal echogenicity of variable amounts and degree (Sheth et al. 1987). CT demonstrates a unilocular or multilocular mass of low attenuation similar to water, with peripheral and septal enhancement. On MR imaging, lymphangiomas are observed as lobulated, septated masses with T1-weighted iso- to hypointensity and T2-weighted bright hyperintensity relative to skeletal muscle. Peripheral and septal contrast enhancement is also observed. Internal fluid-fluid levels or other debris may be shown due to intralesional bleeding or inflammation/infection (Moukaddam et al. 2009).

10.4 Kaposiform Hemangioendothelioma

Kaposiform hemangioendothelioma (KHE) is a locally aggressive vascular tumor frequently associated with Kasabach-Merritt phenomenon (severe thrombocytopenia). This lesion occurs commonly in the first decade of life with male predominance and most often involves the extremities. It presents with a blue-red mass located superficially or in the deep soft tissue. KHE shows no tendency to regress spontaneously. Histologically, the tumor consists of irregular vascular lobules growing in an infiltrative fashion and evokes a dense hyaline stromal response. Surgical resection is the most effective treatment. Mortality from this tumor is approximately 10% due to extensive local disease or thrombocytopenia (Lyons et al. 2004).

On MR imaging, KHE has similar features to hemangioma but is characterized by an ill-defined margin, sunburst-shaped stranding, and no fat deposition. Prominent flow voids representing vascular channels in the mass are usually observed (Tamai et al. 2010).

10.5 Retiform Hemangioendothelioma

Retiform hemangioendothelioma (RH) is a locally aggressive, rarely metastasizing vascular tumor characterized by distinctive arborizing blood vessels lined by typical hobnail endothelial cells. RH is uncommon and primarily found in young to middle-aged adults, with no sex predilection. They present as red/bluish slow-growing plaques or nodular tumors that affect the skin and subcutaneous tissue of the distal extremities, especially the lower limb. Local recurrences are common in more than 50% of patients because of the infiltrative growth pattern of RH, but distant metastases are extremely rare. Treatment consists of surgical excision with adequate surgical tumor margins and monitoring for local reoccurrence (Zheng et al. 2014; Calonge 2013). The imaging appearance of RH has not been well documented. It may show a soft tissue mass that affects the skin and subcutaneous tissue, with nodular skin thickening on US, CT, or MR imaging.

10.6 Kaposi Sarcoma

Kaposi sarcoma (KS) is a locally aggressive, endothelial tumor or a tumor-like lesion that manifests as one of four forms as follows: (1) classic indolent KS, which occurs primarily in elderly men of Mediterranean/East European and Ashkenazi Jews, with male predominance; (2) endemic African KS, which affects middle-aged men in equatorial Africa who are not infected with HIV; (3) iatrogenic (organ transplant-related)

KS, which is related to chronic drug-induced immunosuppression for various diseases; and (4) AIDS-associated KS, the most aggressive form of the disease, frequently found in homosexual male AIDS patients (Tappero et al. 1993). KS usually presents with purplish, reddish blue or dark brown multifocal cutaneous patches, plaques, or nodules occurring frequently in distal extremities. However, KS may also involve different mucosal sites, lymph nodes, and visceral organs. Musculoskeletal involvement by KS is infrequent and occurs secondary to local extension from the cutaneous lesions. Thus, KS of the soft tissue is almost always accompanied by concomitant noticeable cutaneous changes. Chronic lymphedema has been reported to promote KS development due to a combination of collateral vessels, lymphangiogenesis, and immune impairment (Lee et al. 2014).

The imaging appearance of primary KS of the soft tissue has only been minimally documented. US reveals solid, vascular, heterogeneous skin or subcutaneous soft tissue lesions. In our experience, KS appears as solitary or multifocal plaques or nodules that affect the skin and areas below the subcutis on MR imaging. They are isointense to muscle on T1-weighted images and hyperintense on T2-weighted images with solid vascular contrast enhancement and spiculated margins (Pantanowitz et al. 2008). KS may be accompanied by lymphedema, appearing as a diffuse, honeycomb, or reticular pattern of subcutaneous tissue on MR imaging.

10.7 Epithelioid Hemangioendothelioma

Epithelioid hemangioendothelioma (EHE) is a rare malignant angiocentric vascular tumor composed of cords of epithelioid endothelial cells in a distinctive myxohyaline stroma and arise from medium to large blood vessels. This lesion commonly occurs in the fourth and fifth decades, with a slight female predominance. EHE manifests as a slightly painful mass, frequently on the extremities. Radical surgical excision is the mainstay of treatment. Most EHEs are indolent, but 20–30% of tumors metastasize (Deyrup et al. 2008).

The imaging appearance of EHE is nonspecific. On ultrasonography, EHE appears as hypoechoic or hyperechoic, with prominent cystic areas due to hemorrhaging. Doppler imaging may reveal AV shunting. On MR imaging, EHE may demonstrate imaging features of nonspecific hypervascular tumors, with frequent flow voids and no fat deposition (Nuthakki et al. 2007).

10.8 Angiosarcoma of Soft Tissue

Angiosarcoma is an aggressive vascular malignancy of endothelial cell origin. It is rapidly proliferating, with extensively infiltrating anaplastic cells derived from blood vessels, and lines irregular blood-filled spaces. It can be caused by therapeutic radiation or chronic lymphedema (Sepulveda and Buchanan 2014). AS of soft tissue has a peak incidence in the seventh decade of life and a male predominance. It most commonly involves the skin, followed by soft tissues, such as deep muscle of the lower extremities. The lesion manifests with a painful rapidly enlarging mass. More than half of the patients with AS die within the first year. Local recurrence is observed in 20% of cases and distant metastases in approximately 50%. These metastases are frequently to the lungs, followed by the lymph nodes, soft tissues, and bone (Meis-Kindblom and Kindblom 1998).

The imaging characteristics of AS of soft tissue overlap with those of other hypervascular soft tissue sarcomas. On MR imaging, the tumor may show more aggressive features of soft tissue masses that involve the skin, subcutaneous tissue, or muscle. Other features include infiltration into the surrounding tissue, no fat deposition, intense contrast enhancement with prominent serpentine flow voids, and hemorrhagic areas of T1-hyperintense foci or fluid-fluid levels. Secondary cystic degeneration and necrosis are often observed (Moukaddam et al. 2009). AS of soft tissue may be frequently accom-

panied by lymphedema, appearing as a diffuse, honeycomb, or reticular pattern of subcutaneous tissue on MR imaging.

10.9 Illustrations: Vascular Tumors

10.9.1 Hemangioma

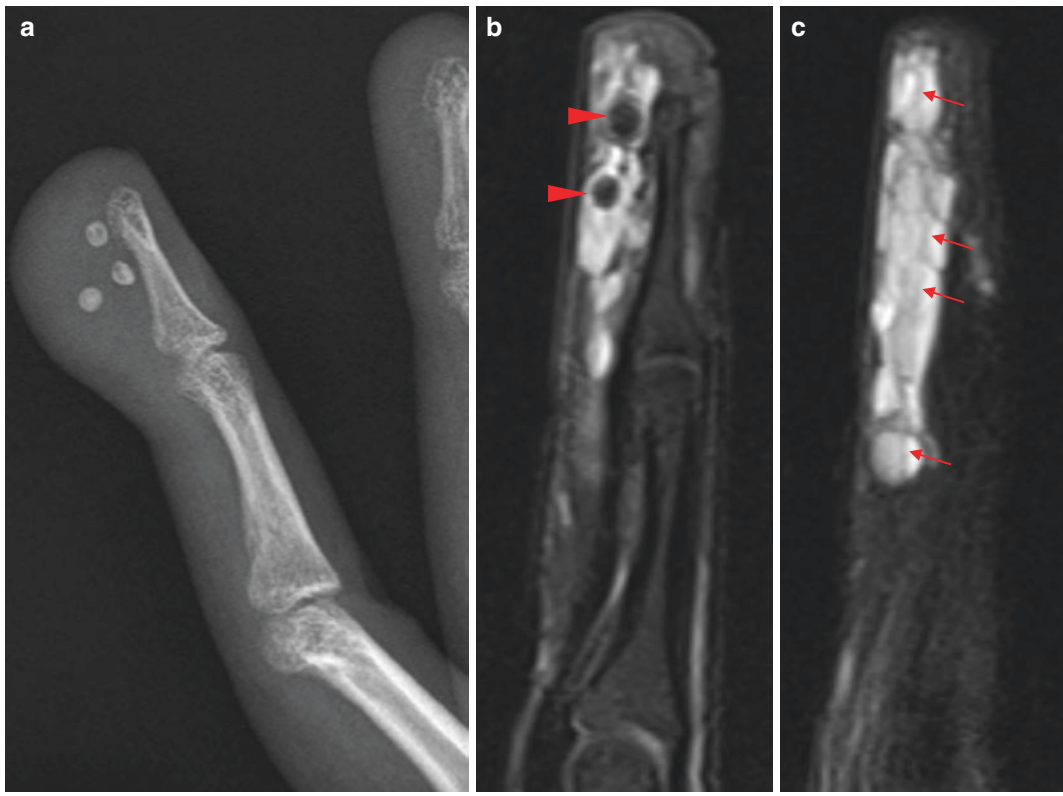

Fig. 10.1 Hemangioma. Radiograph of finger (**a**) shows several calcifications with the classic appearance of phleboliths and dystrophic mineralization in an organizing thrombus. Sagittal FS T2WIs (**b**, **c**) show round or oval dark signal foci (*arrowheads*) within the bright hyperintense, multiloculated subcutaneous mass with fluid-fluid levels (*small arrows*)

10.9.2 Synovial Hemangioma

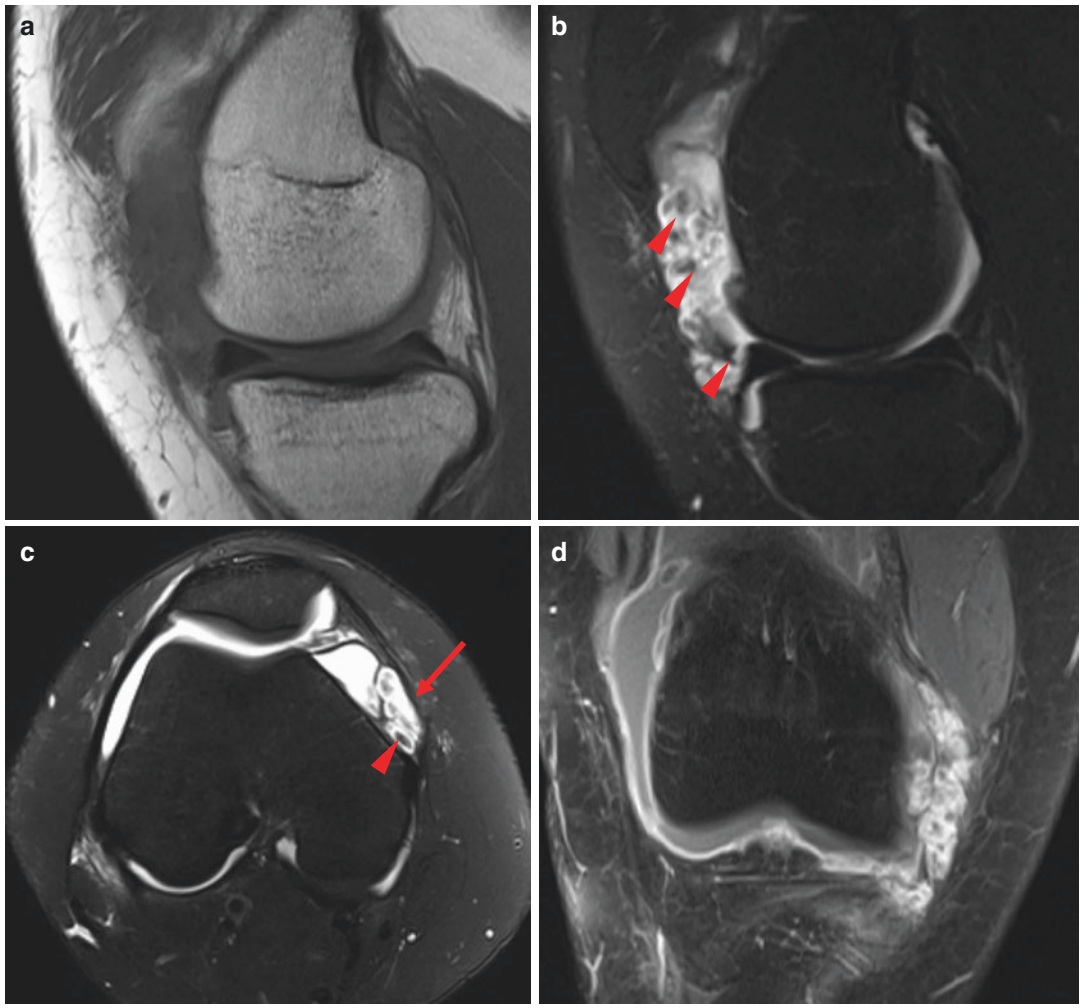

Fig. 10.2 Synovial hemangioma. MR image of the knee shows a multilobulated, multiloculated intra-articular soft tissue mass (*arrows*) with inhomogeneous hyperintensity relative to muscle on T1WI (**a**) and heterogeneous hyperintensity on FS T2WI (**b**, **c**). The lesion is located along the synovial surface of the medial suprapatellar bursa. Multifocal, oval, mildly T1 hyperintense and dark T2 foci (*arrowheads*) are noted within some locules. These findings are suggestive of thrombi because there were no phleboliths on the radiograph (not shown). Coronal post-contrast FS T1WI (**d**) shows the mass to have heterogeneous enhancement in the subsynovial space

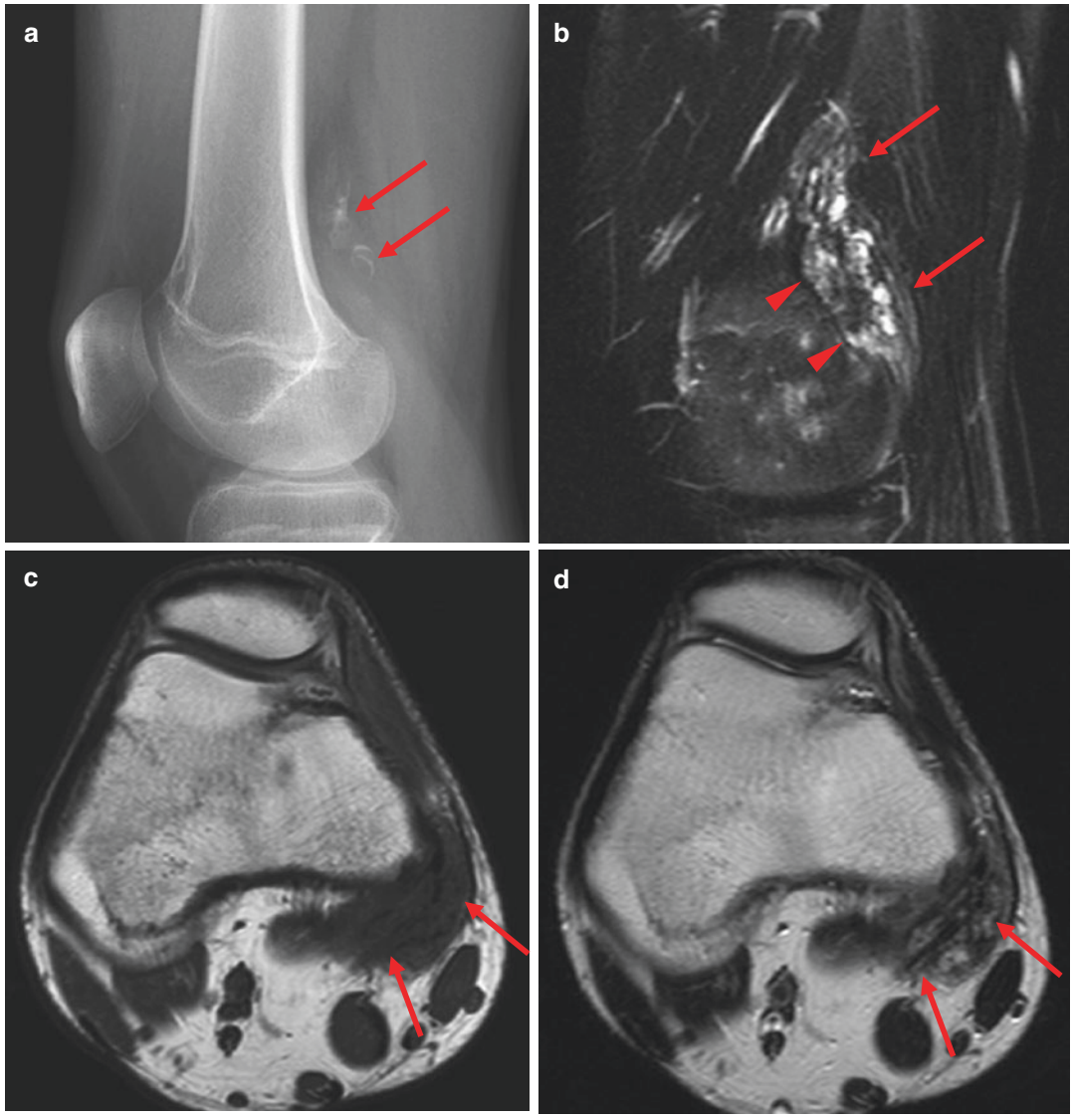

Fig. 10.3 Synovial hemangioma. Radiograph (**a**) shows irregular ossifications (*arrows*) near the subgastrocnemius recess of the posterior supracondylar area of the knee. Sagittal FS T2WI (**b**) reveals an ill-defined, multilobular, multiseptated soft tissue mass (*arrows*) with mixed signal intensity and mild pressure bone erosion (*arrowheads*). The lesion is isointense to muscle on axial T1WI (**c**) and heterogeneously hyperintense on T2WI (**d**), with intense contrast enhancement (**e**). The lesion affects intra- and juxta-articular spaces. Hypointense lines within the tumor reflect mineralization on all sequences. Specimen photo (**f**) shows the irregularly bordered soft tissue mass containing multifocal mineralization, such as calcifications and some ossifications (*arrowheads*)

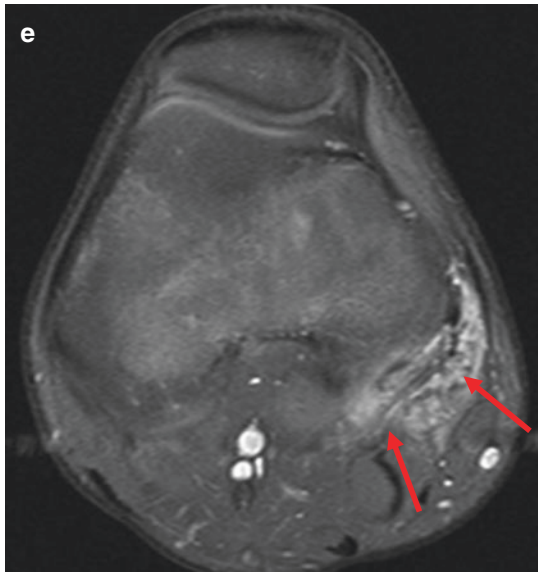

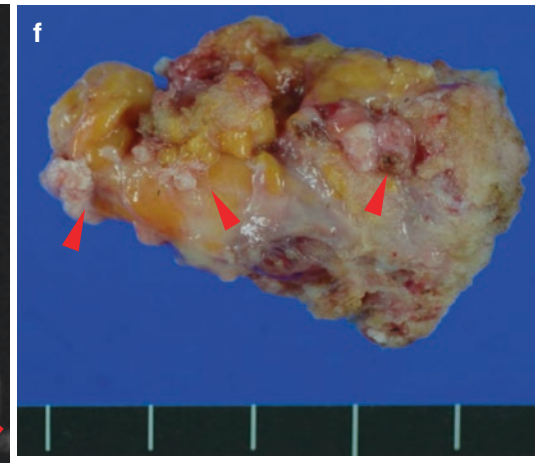

Fig. 10.3 (continued)

10.9.3 Intramuscular Angioma

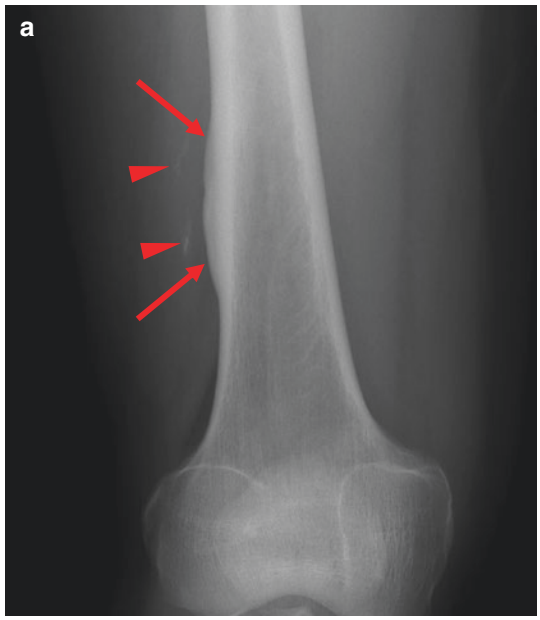

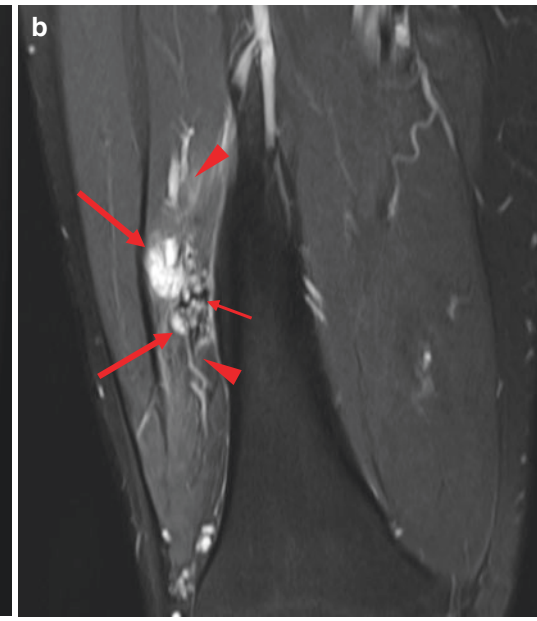

Fig. 10.4 Intramuscular angioma. Radiograph (**a**) shows localized cortical hypertrophy (*arrow*) of the right distal femur, with subtle mineralization (*arrowheads*). Coronal FS T2WI (**b**) reveals an ill-defined hyperintense soft tissue mass (*arrows*) within the vastus lateralis muscle. Note the surrounding engorged veins (*arrowheads*) and small signal void spots, representing intratumoral mineralization (*thin arrow*). The tumor is mildly hyperintense to muscle on T1WI (**c**) and inhomogeneously hyperintense on T2WI (**d**), with mild inhomogeneous contrast enhancement on postcontrast FS T1WI (**e**). Peripheral fat overgrowth (*arrowheads*) is noted. Specimen photo (**f**) reveals the intramuscular, irregularly marginated hemorrhagic soft tissue mass with multifocal mineralization, including ossification (*thin arrows*)

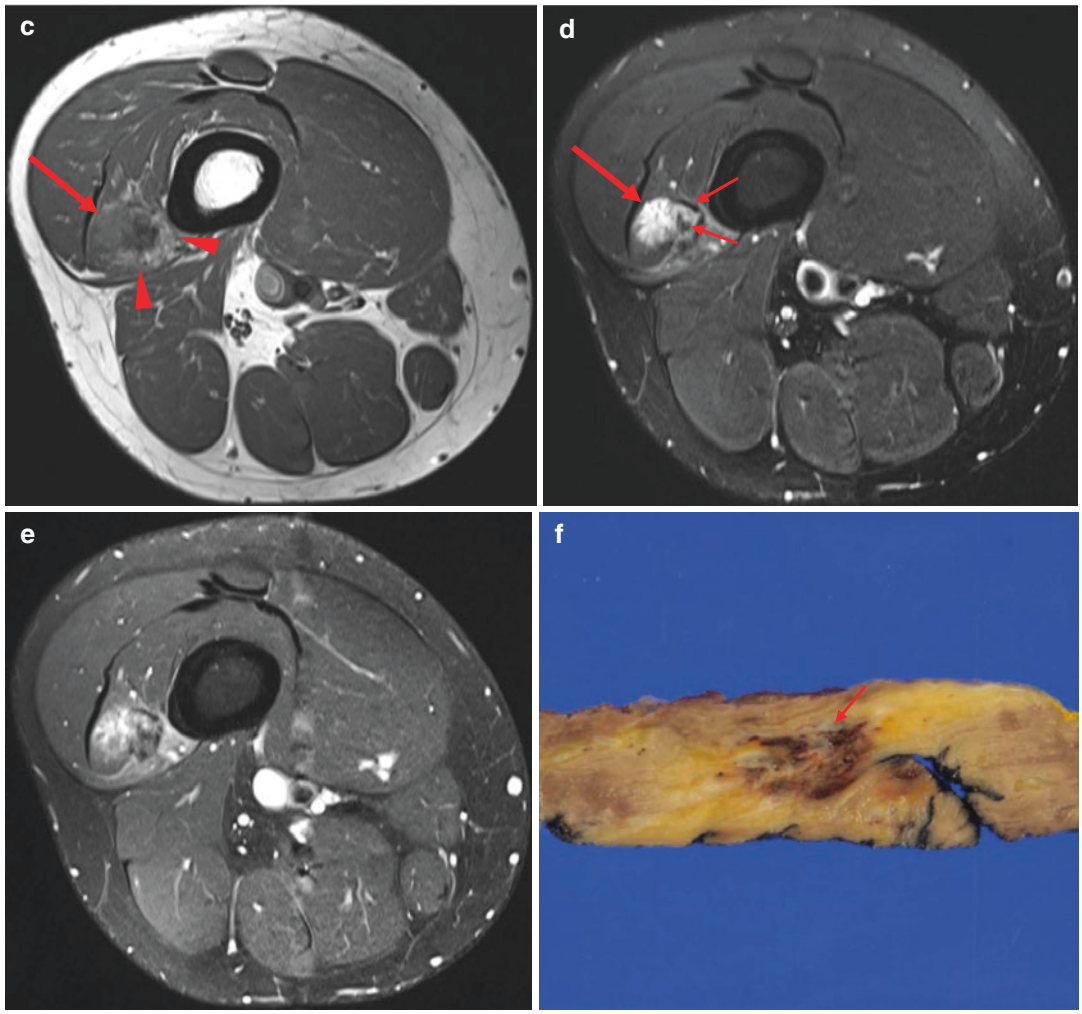

Fig. 10.4 (continued)

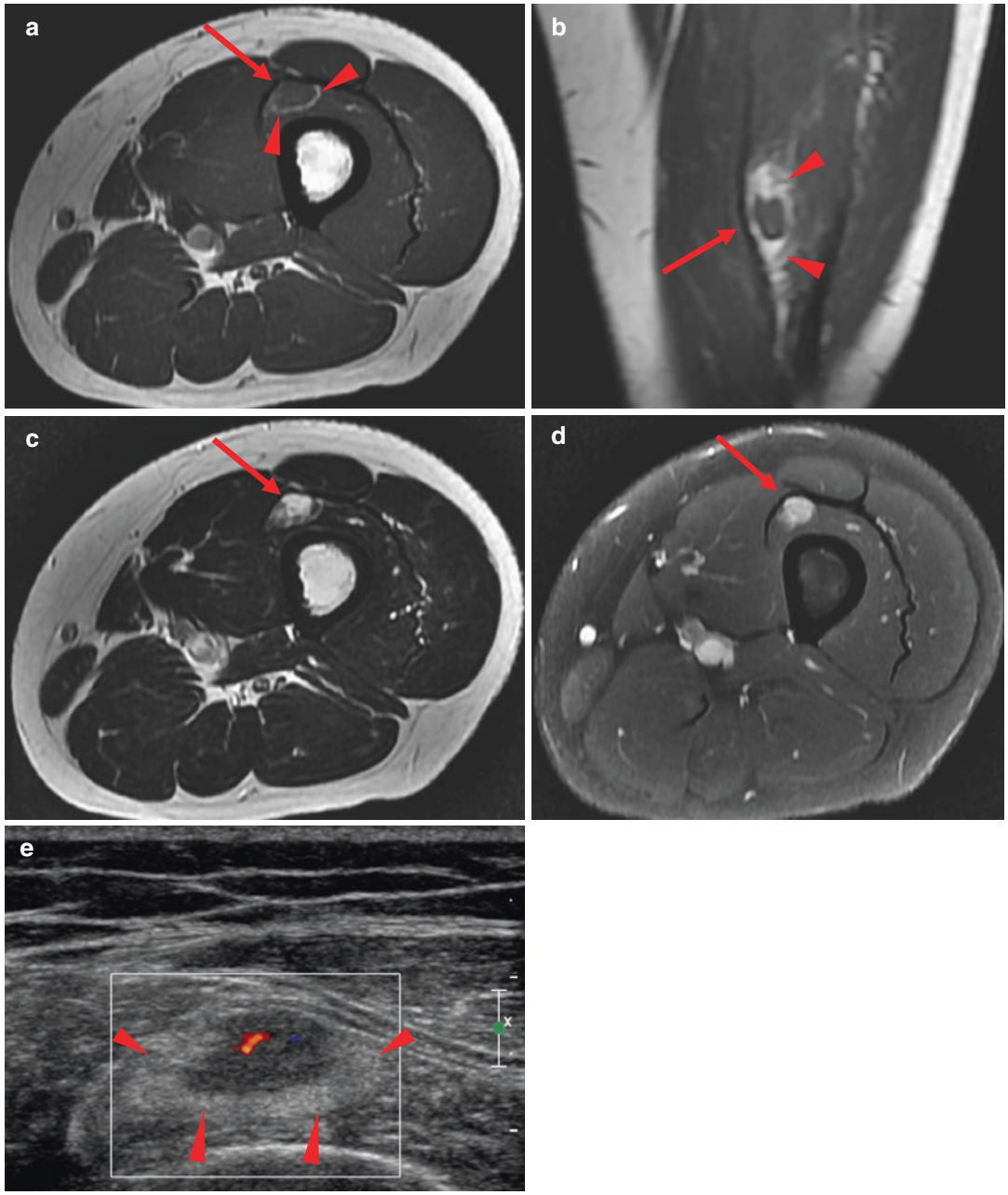

Fig. 10.5 Intramuscular angioma. Axial (**a**) and coronal (**b**) T1WIs show an isointense or slightly hyperintense mass (*arrow*) within the vastus intermedius muscle, with surrounding fat overgrowth (*arrowheads*). The lesion has inhomogeneous hyperintensity on T2WI (**c**) and intense enhancement on postcontrast FS T1WI (**d**). US (**e**) reveals a central isoechoic mass relative to the muscle echo, with a focal ill-defined margin and surrounding hyperechoic fat tissue (*arrowheads*). Color Doppler imaging shows intralesional focal blood

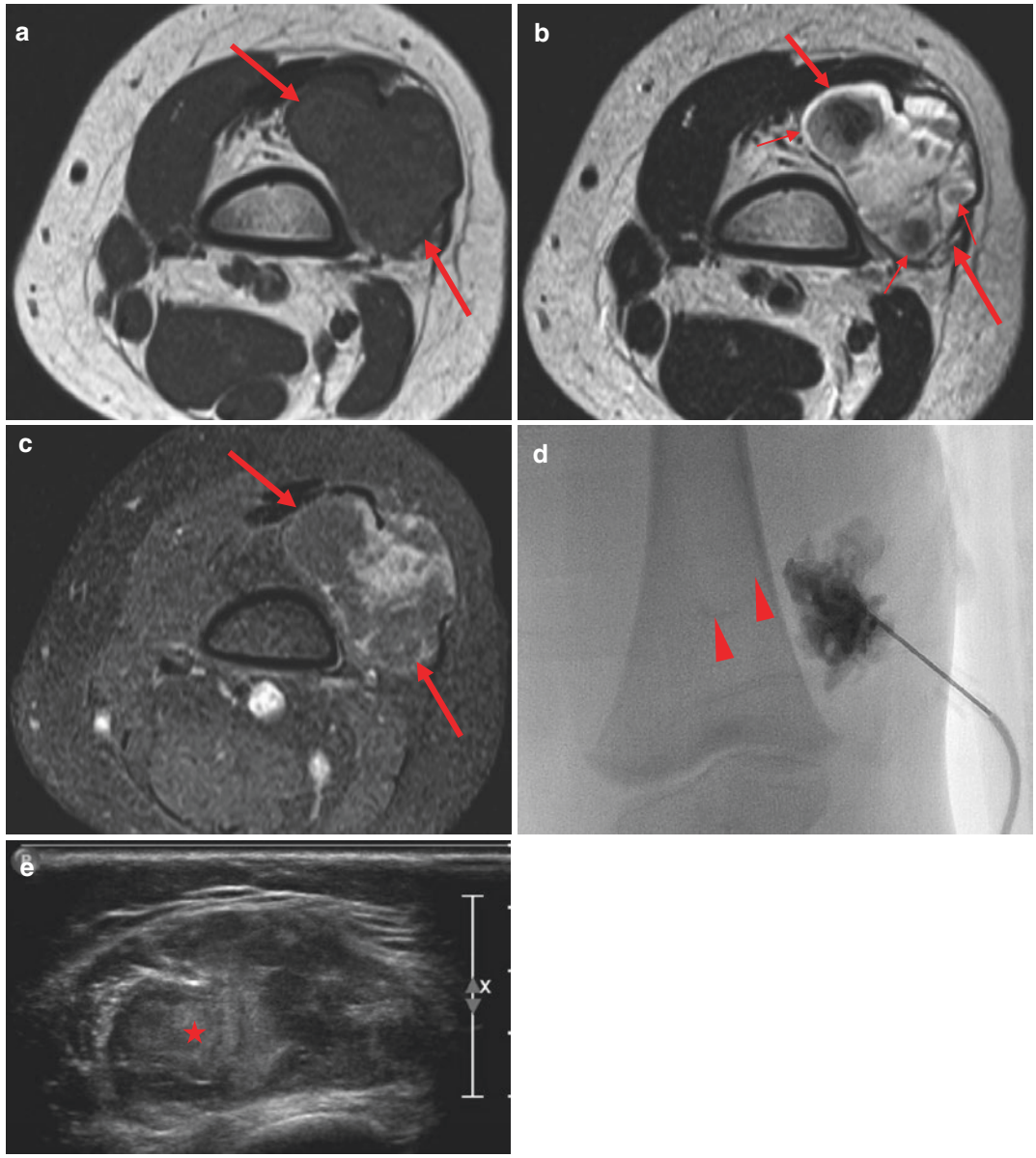

Fig. 10.6 Intramuscular angioma, cavernous type. MR images reveal a circumscribed, multilobulated, multiloculated soft tissue mass (*arrows*) in the vastus lateralis muscle. The mass exhibits inhomogeneous iso- and mildly hyperintensity on T1WI (**a**), heterogeneous hyperintensity on T2WI (**b**), and irregular peripheral and some solid enhancement on postcontrast FS T1WI (**c**). Variably sized T2 hypointense foci (*thin arrows*) represent thrombi. Direct puncture angiography (**d**) reveals prolonged contrast stagnation in variably sized blood-filled spaces, with the exception of opacification of a small, early draining vein (*arrowheads*). On US (**e**), the lesion has a multiloculated appearance with a mixed appearance, including a central hyperechoic thrombosis or clots (*star*) and anechoic/hypoechoic fluid

10.9.4 Ossifying Intramuscular Angioma

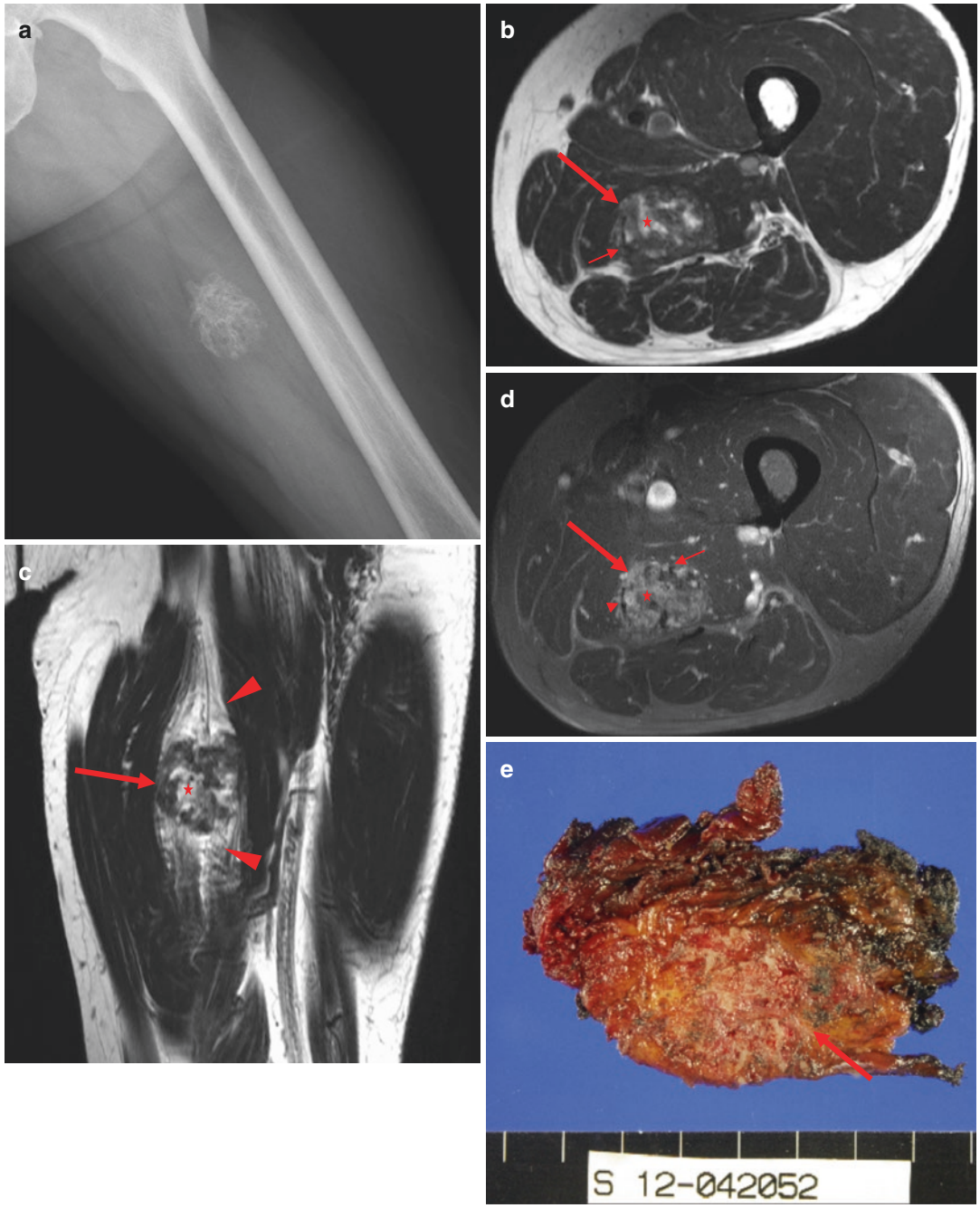

Fig. 10.7 Ossifying intramuscular angioma. Radiograph (**a**) of the distal thigh shows an ossified mass with Swiss cheese appearance. Axial T1WI (**b**) reveals a heterogeneously hyperintense soft tissue mass (*arrow*) relative to muscle in the adductor magnus muscle. Prominent craniocaudal perilesional fat overgrowth (*arrowheads*) is noted on coronal T2WI (**c**). Axial postcontrast FS T1WI (**d**) reveals inhomogeneous mild contrast enhancement. Intratumoral hyperintense foci (*stars*) on T1- and T2-weighted images with fat suppression reflect intratumoral fat or fatty marrow (ossification). Prominent tubular flow voids (*thin arrows*) are observed in the mass. A photograph of the specimen (**e**) shows a reddish-yellow mass with large internal ossification (*arrow*), intervening hemorrhage and vascular channels

10.9.5 Venous Hemangioma

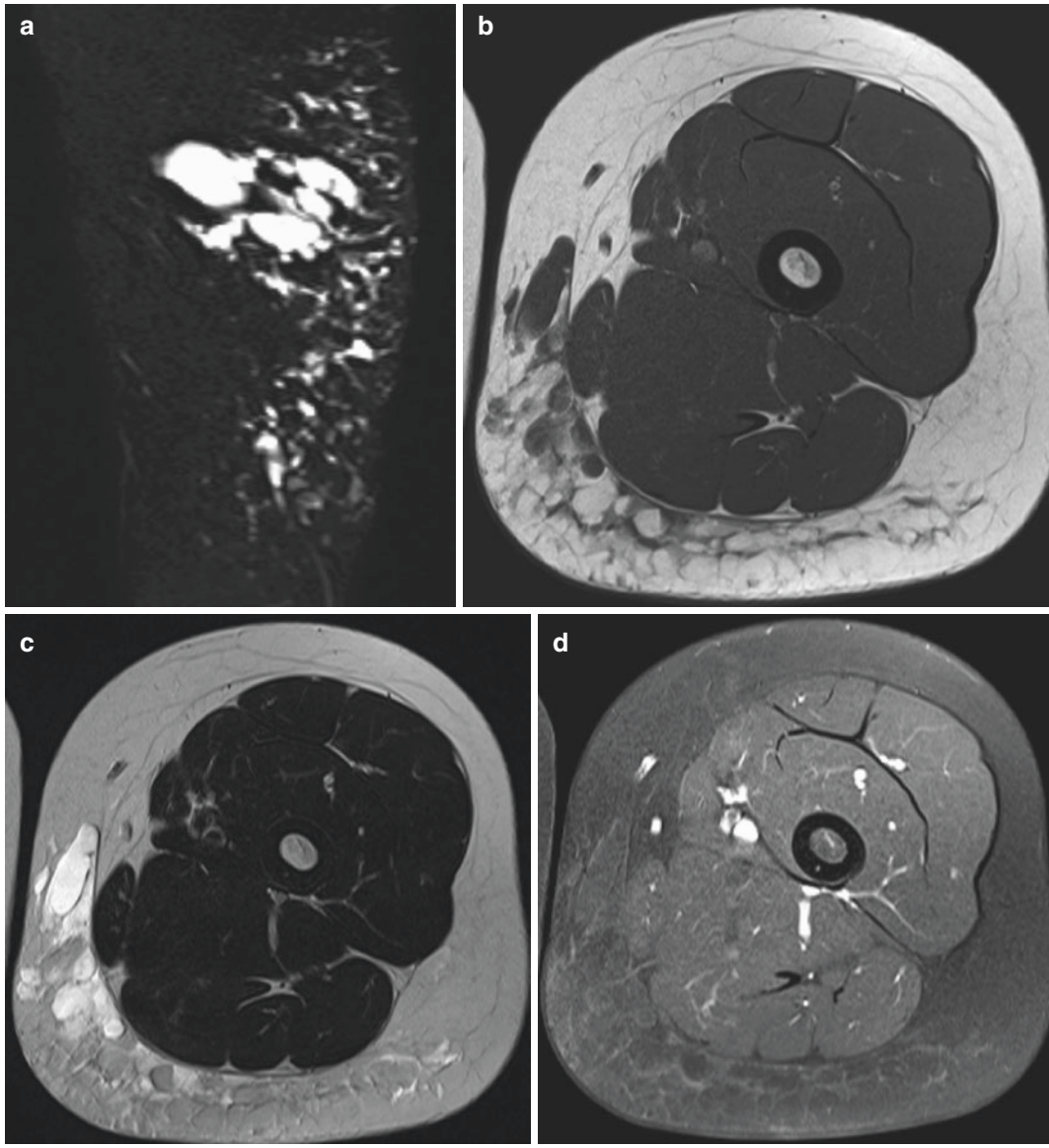

Fig. 10.8 Venous hemangioma. Sagittal FS T2WI of the thigh (**a**) shows variably sized vascular channels that primarily affect subcutaneous tissue, with beaded and a somewhat reticular appearance. This lesion is isointense to muscle on T1WI (**b**), hyperintense on T2WI (**c**), and has a faint peripheral rim or reticular enhancement on postcontrast FS T1WI (**d**). Intraoperative photograph (**e**) reveals reddish-purple plaque in the skin overlying the mass. A photograph of the specimen (**f**) shows dilated vascular channels with congestion within a background reactive fat overgrowth. According to the surgical record, a large amount of blood gushed out immediately after the skin incision

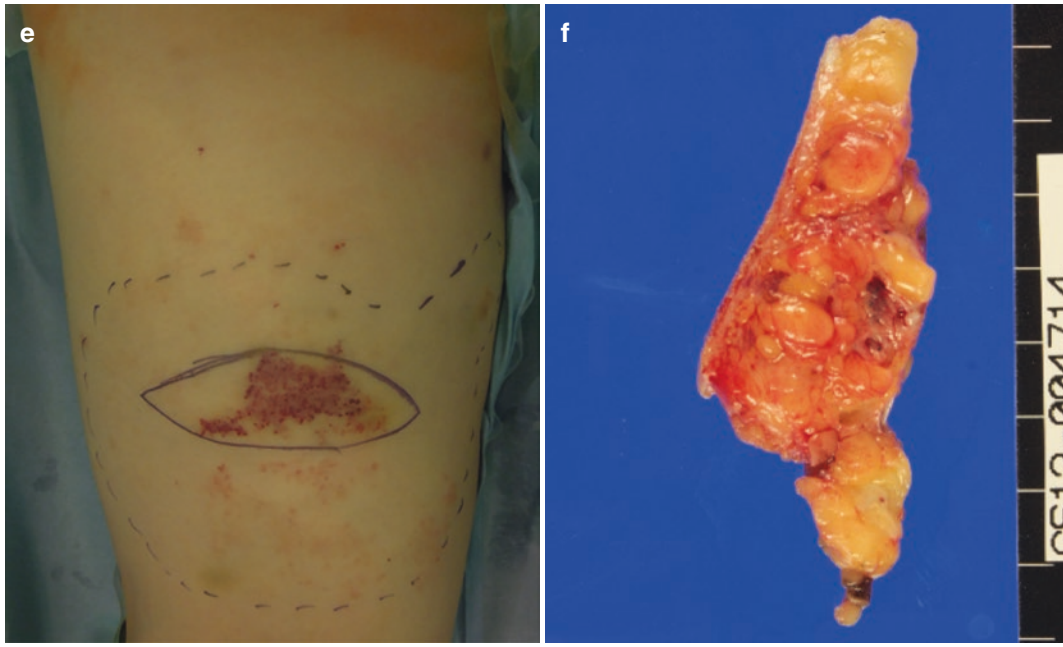

Fig. 10.8 (continued)

10.9.6 Arteriovenous Malformation/Hemangioma

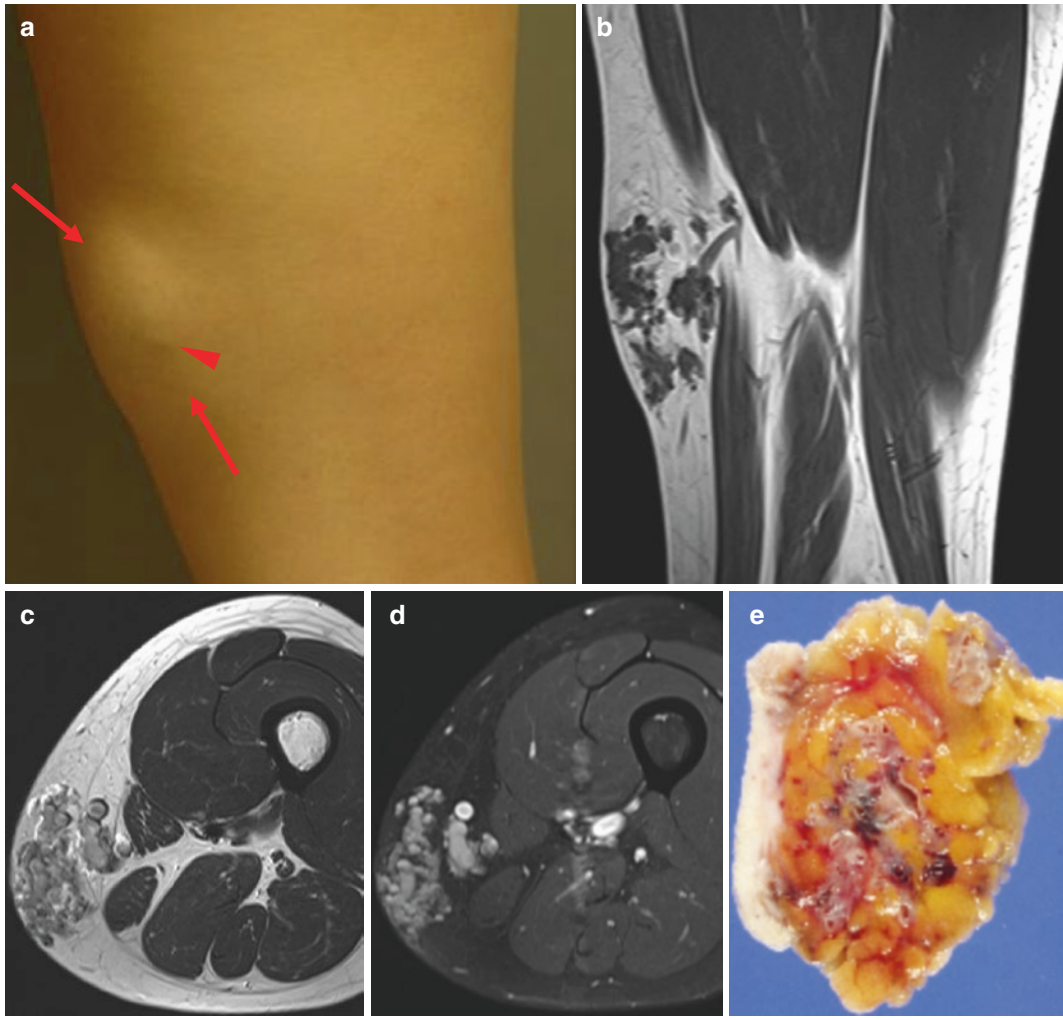

Fig. 10.9 Arteriovenous malformation/hemangioma. Clinical photograph (**a**) of the medial thigh shows a localized soft tissue bulging (*arrow*), with visualization of bluish engorged vascular structures (*arrowhead*). Coronal T1WI (**b**) reveals subcutaneous tortuous, dilated vascular channels, with some flow voids and surrounding fat overgrowth. This lesion has mixed signals ranging from flow voids to bright hyperintensity on T2WI (**c**). Variable enhancement is observed on postcontrast FS T1WI (**d**). In the specimen photograph (**e**), variable numbers of small and large blood vessels are seen, many of which are dilated with hypertrophied fat tissue

10.9.7 Angiomatosis

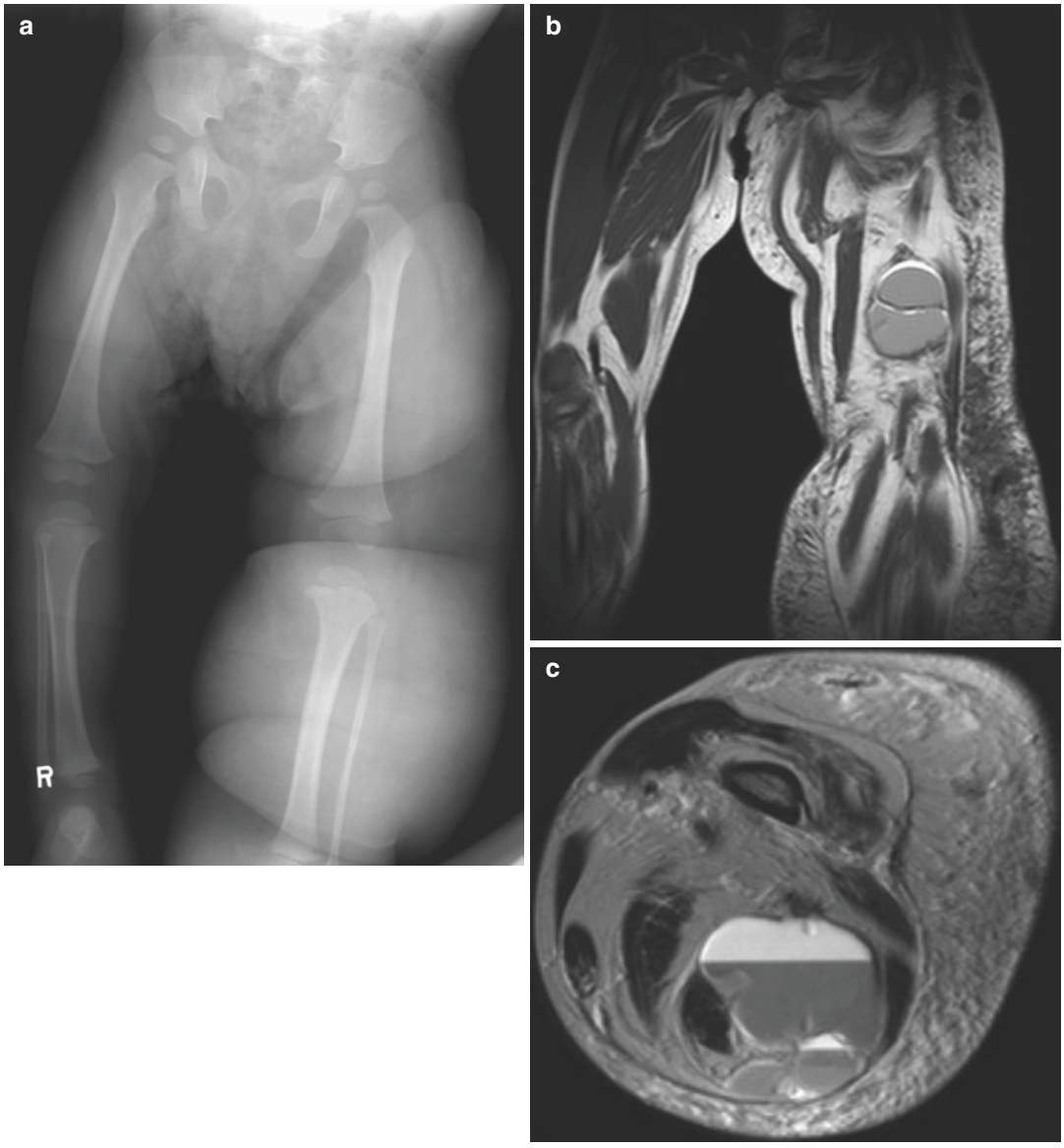

Fig. 10.10 Angiomatosis. Teleradiograph of the lower extremity (**a**) shows extensive soft tissue enlargement. Coronal T1WI (**b**) and axial T2WI (**c**) show extensive multi-tissue plane involvement of hemangiomas of various types

10.9.8 Lymphangioma

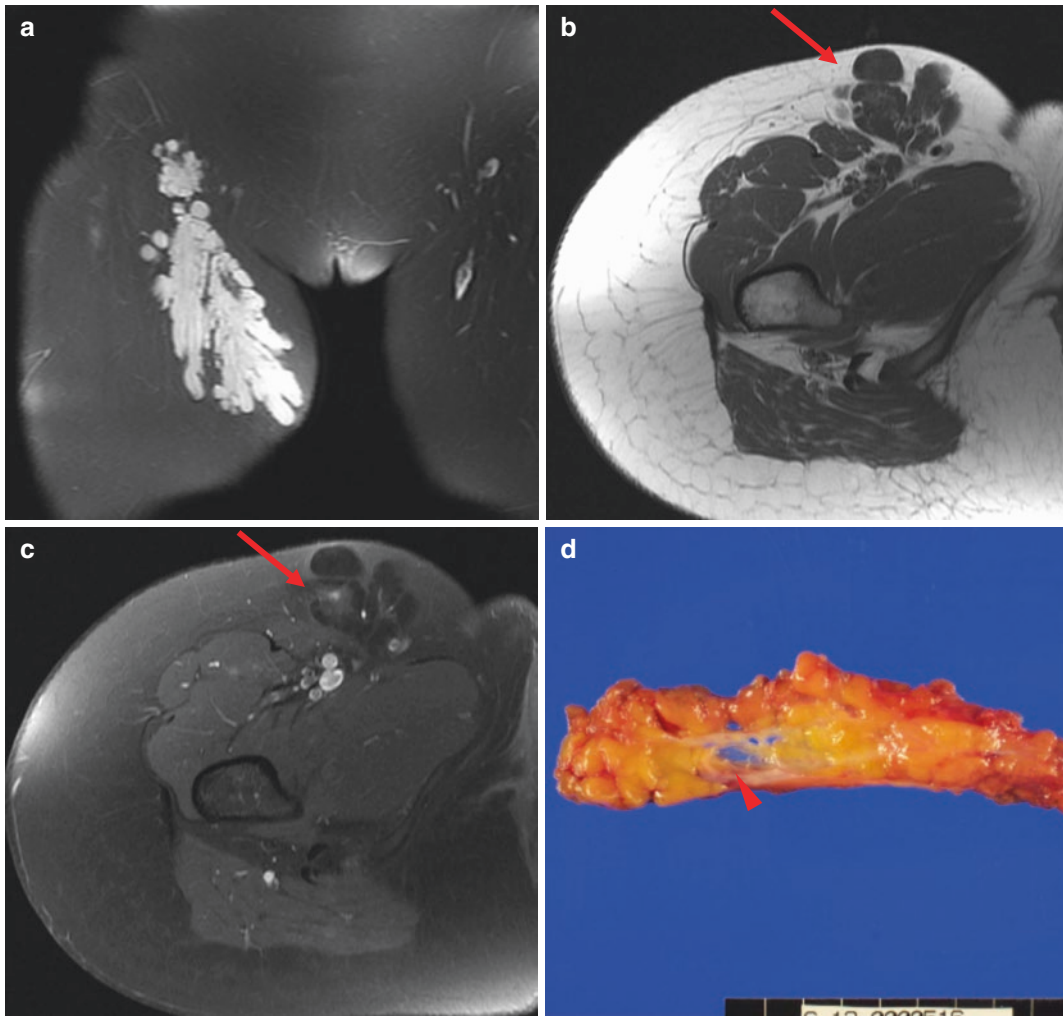

Fig. 10.11 Lymphangioma. Coronal FS T2WI of the thigh (**a**) shows an elongated, branched, multilobulated, bright hyperintense, subcutaneous soft tissue mass in the right inguinal region. This lesion (*arrows*) has isointensity relative to muscle on T1WI (**b**) and little peripheral rim enhancement on postcontrast FS T1WI (**c**), with preserved intervening normal vessels. Photograph of the specimen (**d**) shows that the tumor has a multicystic or sponge- or bubble-like appearance (*arrowheads*)

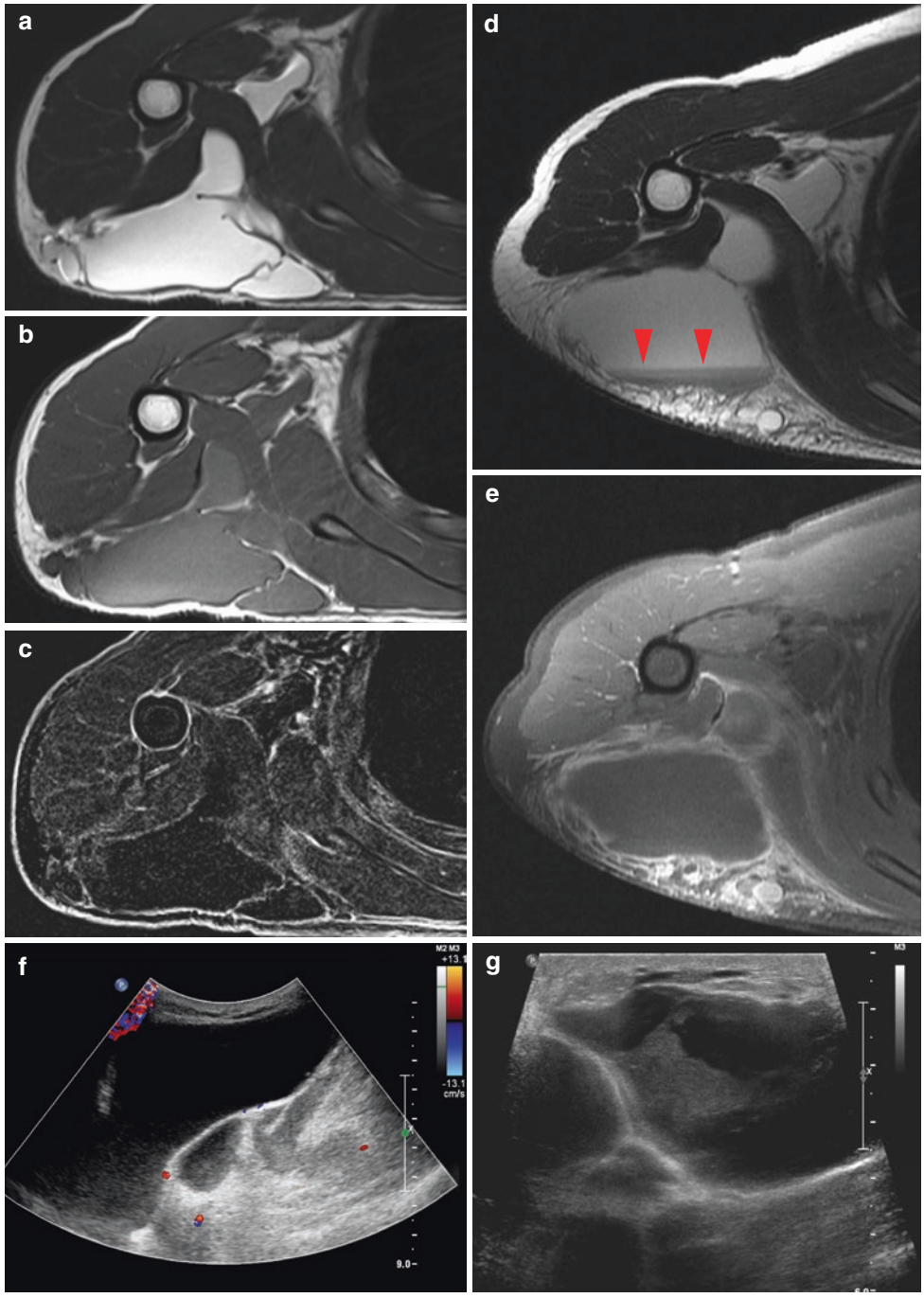

Fig. 10.12 Lymphangioma, complicated. On MR image of the shoulder, a large multilobulated, multiseptated cystic mass is observed affecting the subcutaneous and deep axillary tissue. This lesion shows bright hyperintensity on T2WI (**a**), hyperintensity relative to muscle on T1WI (**b**), and mild thin peripheral and septal contrast enhancement on the subtracted image (**c**). Two years later, the patient complained of sudden pain, fever, and increased mass size. Follow-up T2WI (**d**) reveals further increase in the size of the pre-existing cystic mass, with a fluid-fluid level (*arrowheads*), representing hemorrhage, and surrounding subcutaneous reticular edematous change. Postcontrast FS T1WI (**e**) shows thick peripheral wall enhancement of the mass and infiltrative subcutaneous and perifascial enhancement. On US (**f**), the mass initially has anechoic, multiloculated appearance, with relatively thin and sparse septa. However, follow-up US (**g**) shows thickening of the wall and septa of the lymphangioma, with abnormal intralocular debris and surrounding subcutaneous edematous change. Hemorrhagic pus was confirmed by US-guided aspiration

10.9.9 Kaposiform Hemangioendothelioma

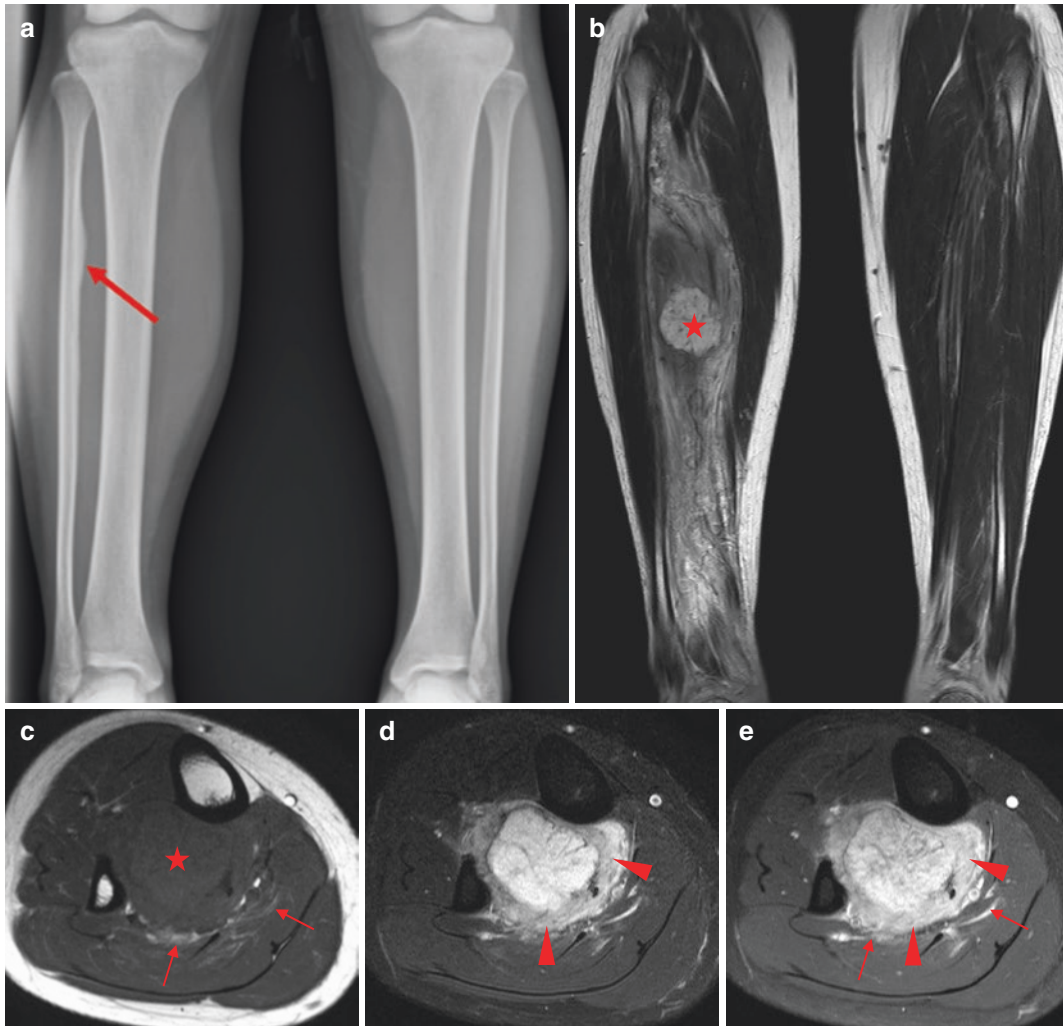

Fig. 10.13 Kaposiform hemangioendothelioma. Radiograph (**a**) shows diffuse soft tissue swelling of the right lower leg. Note the localized cortical hypertrophy (*arrow*) on the medial aspect of the proximal fibula. Coronal T2WI (**b**) reveals a central multilobulated, hyperintense soft tissue mass (*star*) with tubular signal voids within the tibialis posterior muscle, which is craniocaudally swollen and exhibits tortuous, dilated flow voids. The tumor is isointense to muscle on T1WI (**c**), bright hyperintense on T2WI (**d**), and strongly enhancing on postcontrast FS T1WI (**e**). The affected muscle (*arrowheads*) has an intermediate signal on T2WI, with less prominent enhancement than the tumor. Mild peritumoral hyperintense curvilinear structures (*small arrows*) without fat suppression reflect slow-flow vascular structures in the adjacent deep intermuscular fat plane and soleus muscle. On US (**f**), the lesion shows heterogeneous hyperechogenicity (*star*) with posterior sonic enhancement (*arrowheads*) compared with hypoechogenicity of the affected muscle. Prominent intra- and peritumoral blood flows are observed on color Doppler image (**g**). A photograph of the specimen (**h**) shows irregularly shaped central fibrosis (*star*) with surrounding areas of multifocal brownish-gray hemorrhaging

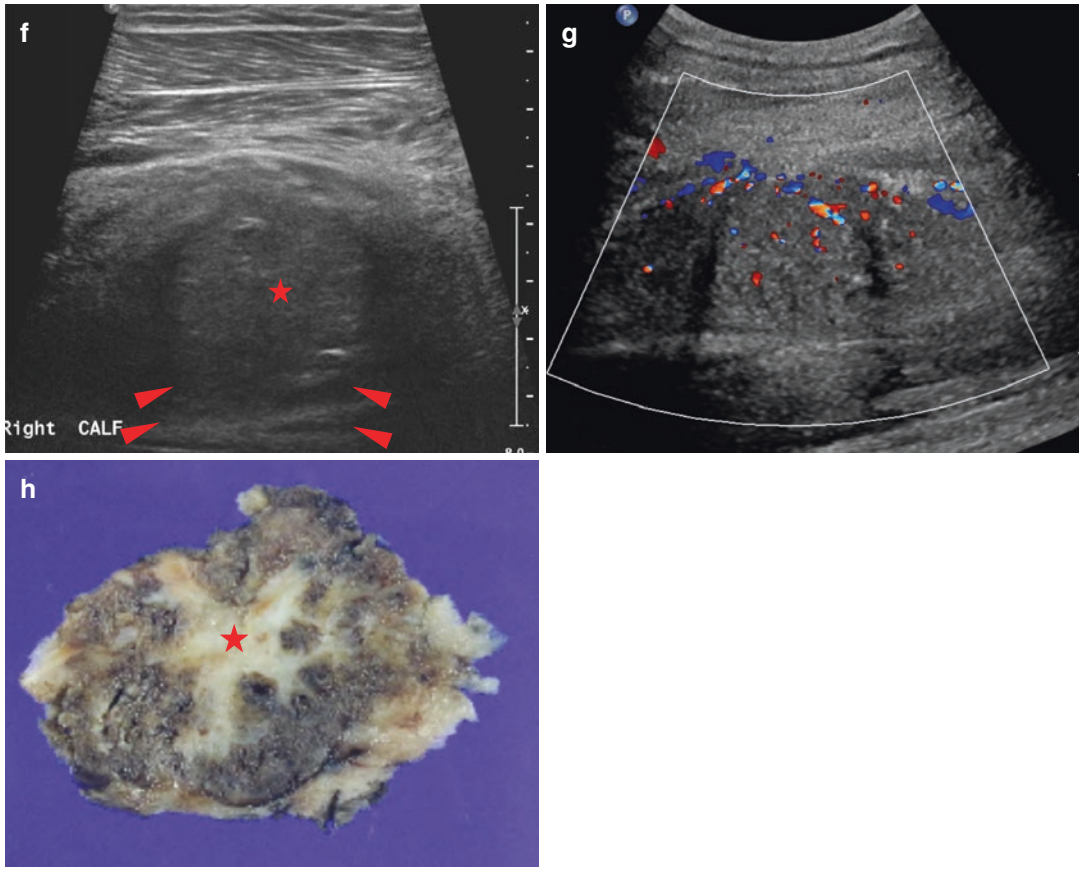

Fig. 10.13 (continued)

10.9.10 Retiform Hemangioendothelioma

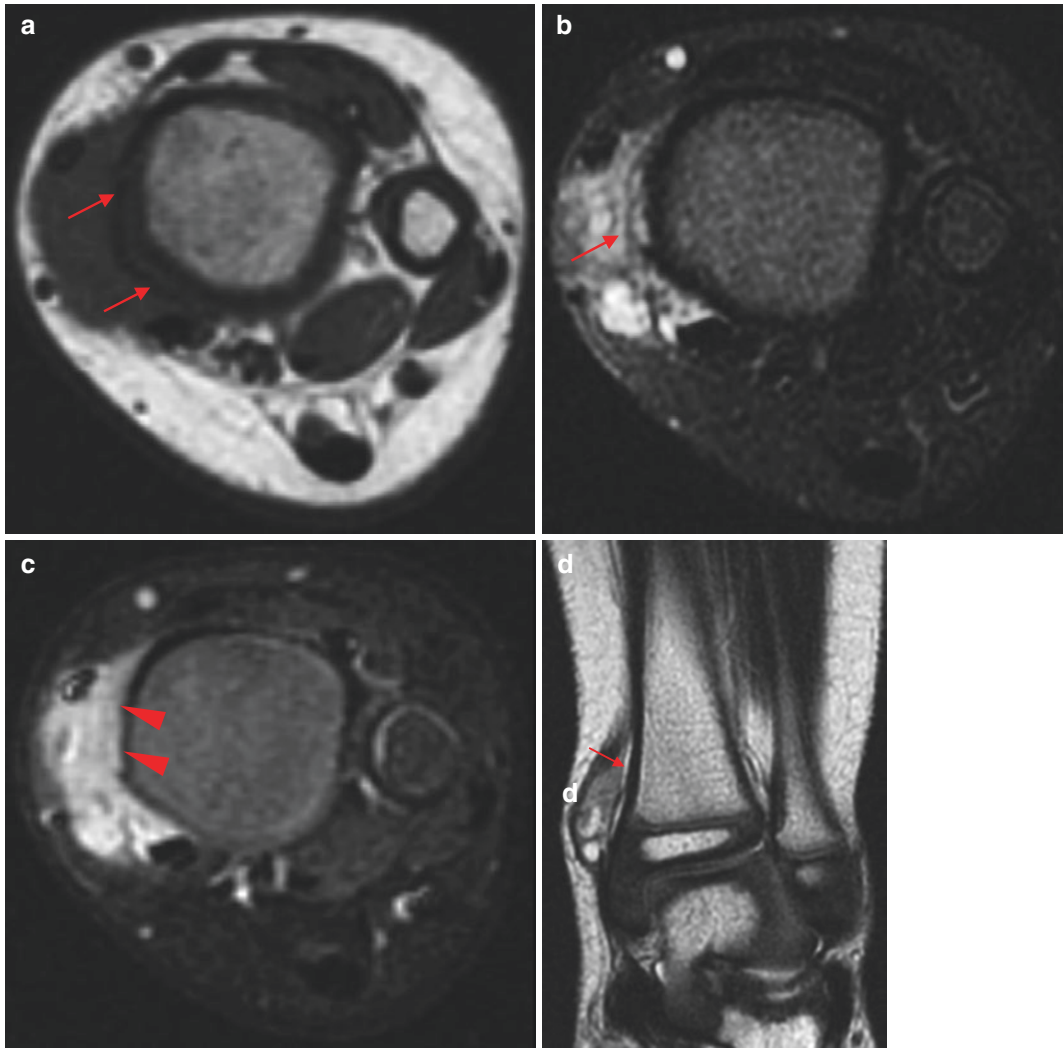

Fig. 10.14 Retiform hemangioendothelioma. MR image of the ankle shows an irregularly bordered subcutaneous soft tissue mass that closely abuts the distal tibia. The lesion shows isointensity on T1WI (**a**), heterogeneous hyperintensity on FS T2WI (**b**), and intense contrast enhancement on postcontrast FS T1WI (**c**). The mass directly extends beneath the adjacent tibial periosteum (*small arrows*), with mild cortical pressure saucerization (*arrowheads*). The tumor also encompasses, but does not compromise, the subcutaneous superficial vascular structure (**a**, **c**). The mass shows heterogeneous signals, ranging from intermediate to bright hyperintensity on coronal T2WI (**d**). Multifocal intratumoral thin flow void structures are noted on all sequences

10.9.11 Kaposi Sarcoma

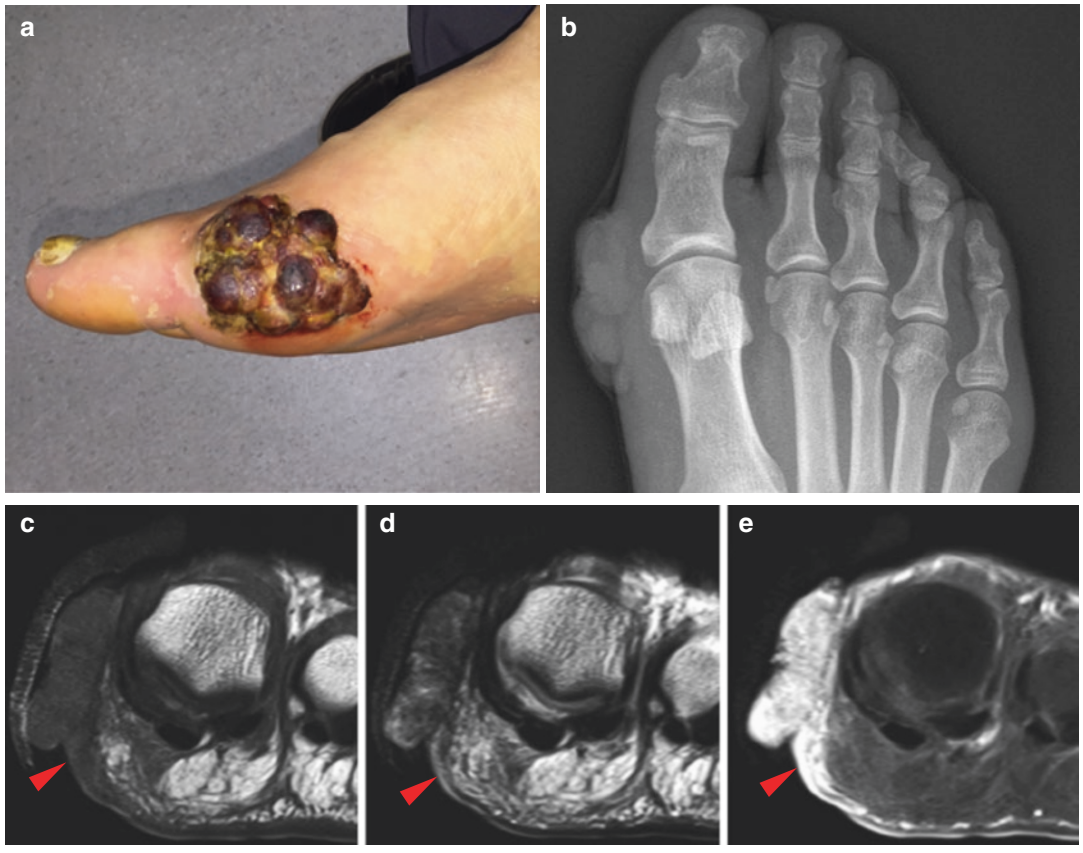

Fig. 10.15 Kaposi sarcoma. Clinical photograph (**a**) of the medial foot shows a dark bluish-purple multinodular mass. Radiograph (**b**) demonstrates exophytic, multinodular skin and subcutaneous mass, without neighboring bone erosion or intratumoral mineralization. The lesion primarily affects the skin with secondary hypodermal tissue and is isointense to muscle on T1WI. (**c**) A heterogeneous signal with central irregular hypointensity and peripheral hyperintensity is observed on T2WI (**d**), and inhomogeneous avid enhancement is observed on post-contrast FS T1WI (**e**). Surrounding skin thickening with signal alteration (*arrowheads*) is noted

10.9.12 Epithelioid Hemangioendothelioma

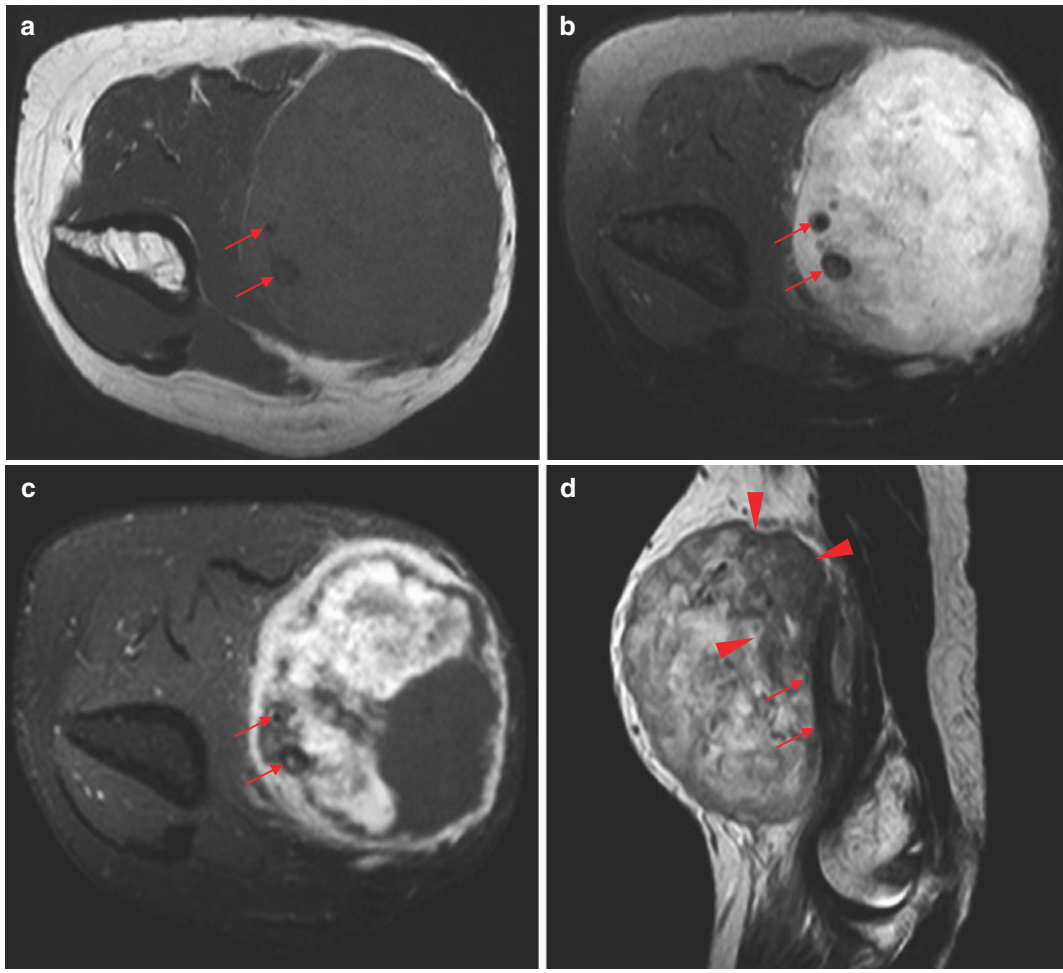

Fig. 10.16 Epithelioid hemangioendothelioma. MR image of the elbow reveals a circumscribed intermuscular soft tissue mass in the subfascial location of the distal upper arm. The lesion shows mild hyperintensity to muscle on T1WI (**a**), hyperintensity on FS T2WI (**b**), and heterogeneous contrast enhancement with large non-enhancing area on postcontrast FS T1WI (**c**), suggesting hemorrhage or necrosis. The mass encases, but does not compromise, the segmental brachial neurovascular bundles (*small arrows*). Tubular signal voids are observed on sagittal T2WI (**d**). Irregularly shaped hypointense areas (*arrowheads*) are histologically confirmed as ossifications. US (**e**) shows the well-marginated, mixed echogenic mass with a "snowstorm" appearance, ranging from hypoechoic areas to hyperechoic foci with posterior shadowing, suggesting intratumoral mineralization. Photograph of the specimen (**f**) shows it as a whitish-yellow mass with considerable ossification (*arrowheads*) and multifocal hemorrhagic areas

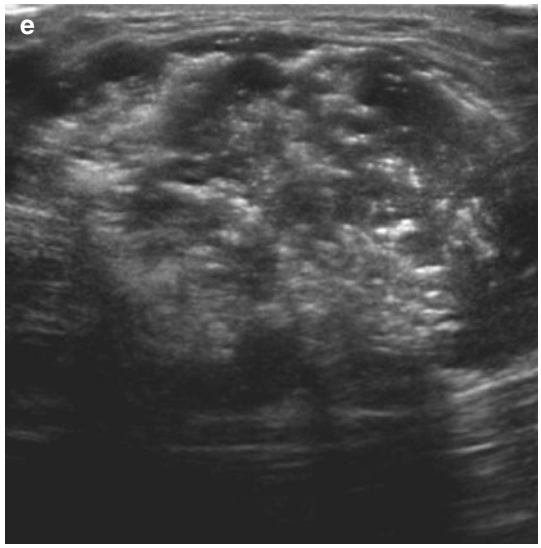

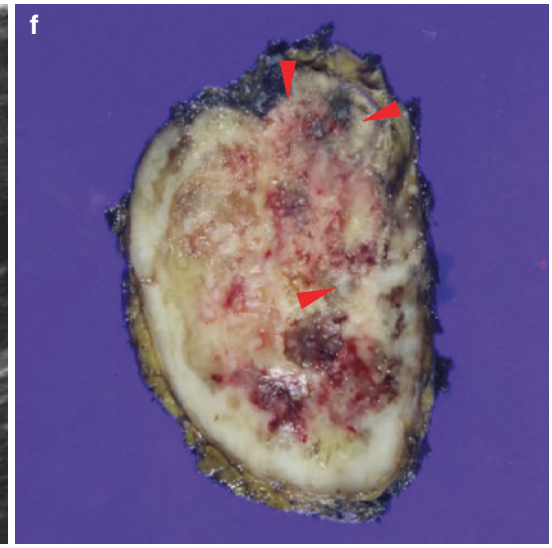

Fig. 10.16 (continued)

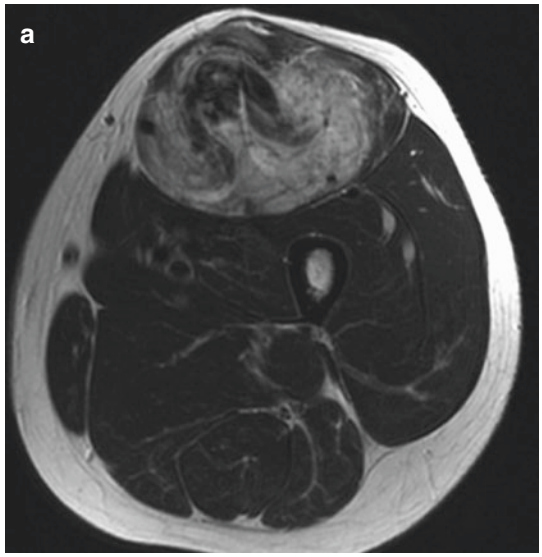

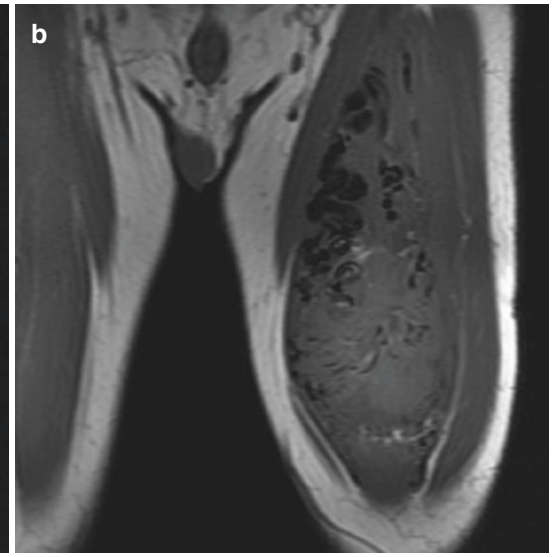

Fig. 10.17 Epithelioid hemangioendothelioma. Axial T2WI (**a**) of the thigh shows an irregularly bordered soft tissue mass confined to the rectus femoris muscle, which is markedly enlarged. The mass is slightly hyperintense to muscle on T1WI (**b**) and hyperintense on T2WI (**c**), with avid contrast enhancement on postcontrast T1WI (**d**). Prominent intratumoral flow voids are seen. Note the large serpentine, dilated signal void of vascular structures outside the tumor, representing AV shunting. US (**e**) reveals heterogeneous hypoechoic mass with numerous, variably sized, anechoic cystic spaces that are fully filled with flow signals on the color Doppler image (**f**), suggesting vascular channels. PET (**g**) shows the mass (*arrow*) to be mildly hypermetabolic with SUV 2.2. The arteriogram (**h**) reveals marked vascularity with enlarged feeding arteries, staining, and early draining veins. Photograph of gross specimen (**i**) shows a reddish-white mass without infiltration outside the investing fascia, with variably sized vessels and some myxoid change

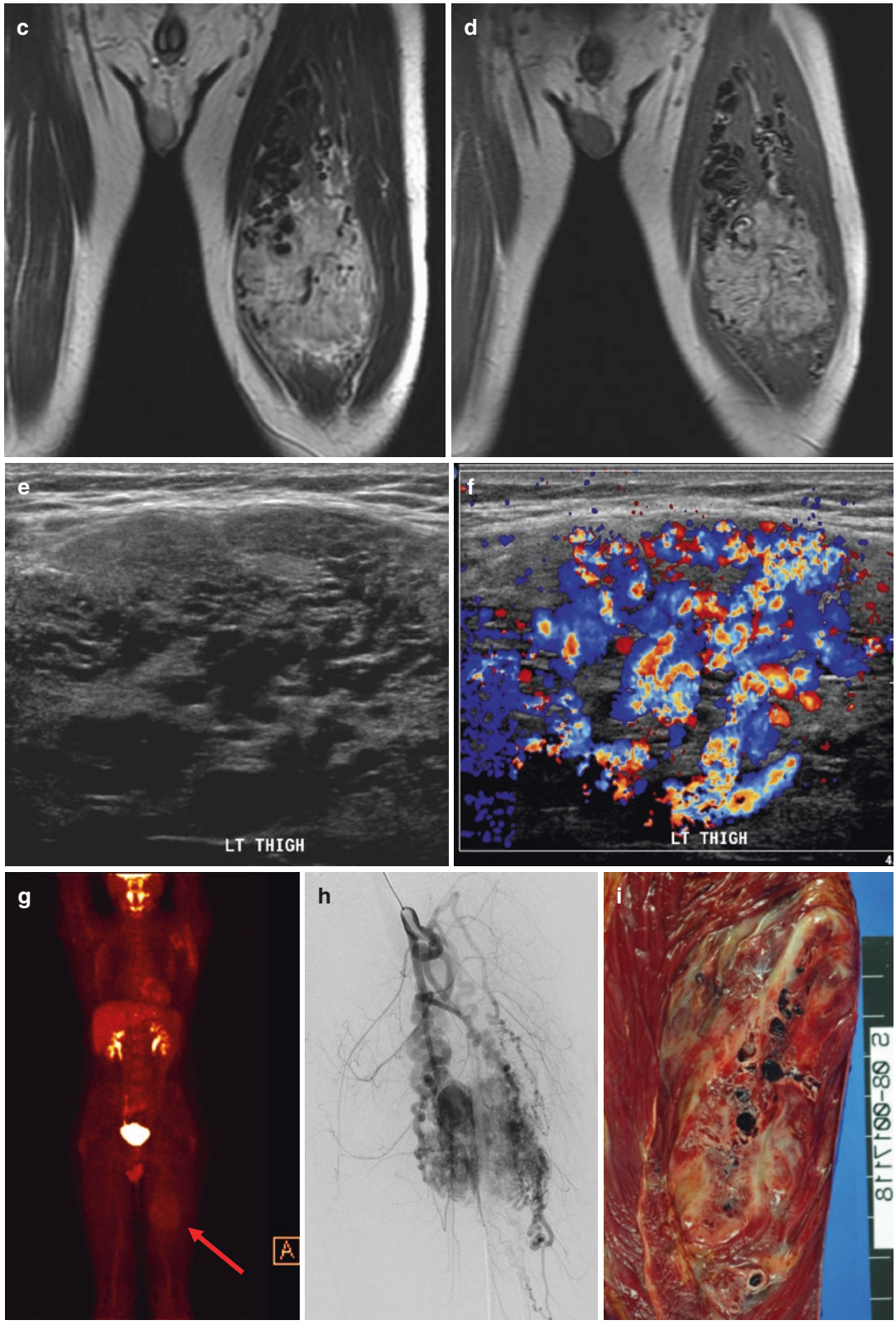

Fig. 10.17 (continued)

10.9.13 Angiosarcoma of Soft Tissue

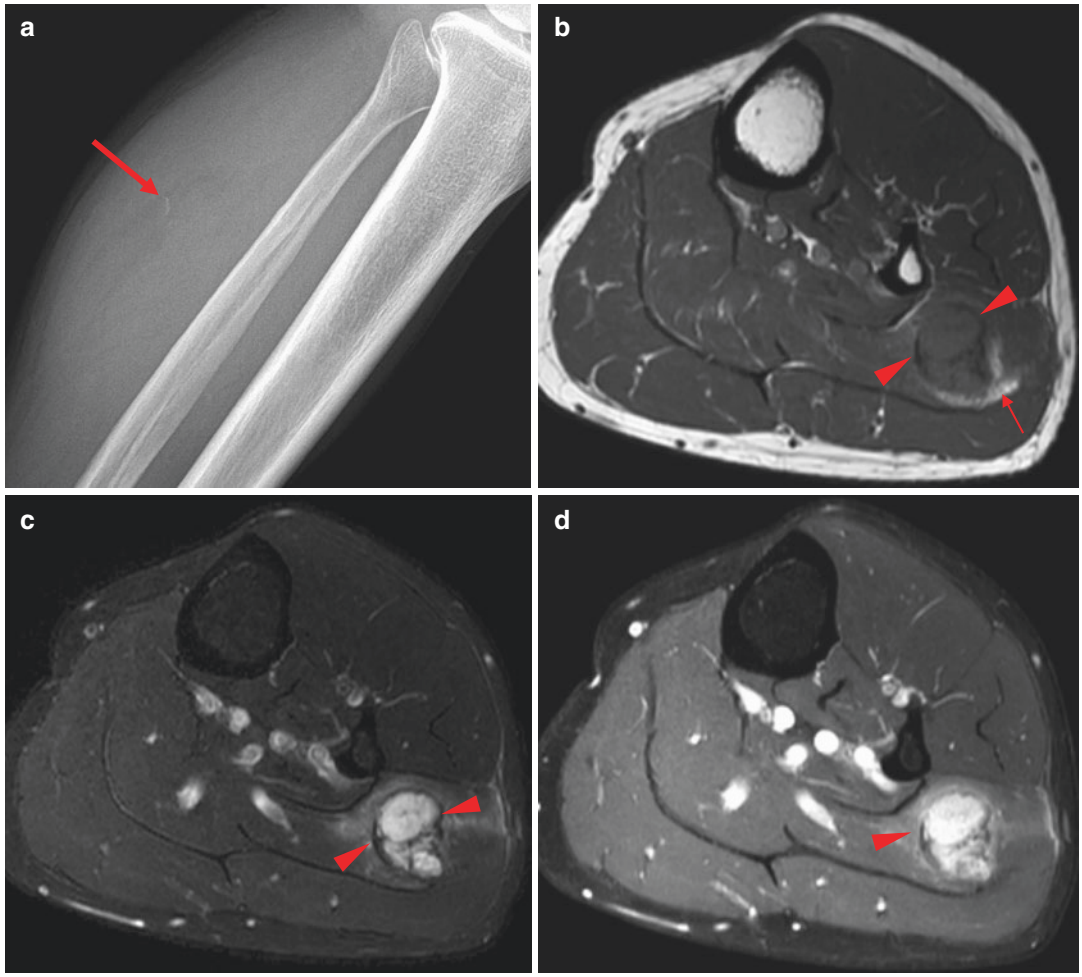

Fig. 10.18 Angiosarcoma of soft tissue. Radiograph (**a**) of the lower leg shows small curvilinear soft tissue mineralization (*arrow*). The tumor is observed as an irregularly bordered, multilobulated mass in the soleus muscle. The mass exhibits iso- to mild hyperintensity to muscle on T1WI (**b**), hyperintensity on T2WI (**c**), and inhomogeneous, but intense contrast enhancement on postcontrast FS T1WI (**d**). Multifocal thin tubular flow voids are seen. Note the curvilinear dark signal rim (*arrowheads*) along the tumor margin on all sequences, suggesting a hemosiderin rim. In addition, uneven fat overgrowth (*small arrows*) is depicted around the mass (**b**). On US (**e**), the mass has heterogeneous hypoechogenicity and an irregular and speculated margin. Surrounding hyperechoic fat overgrowth (*small arrows*) is also noted. Color Doppler image (**f**) shows intratumoral hypervascularity

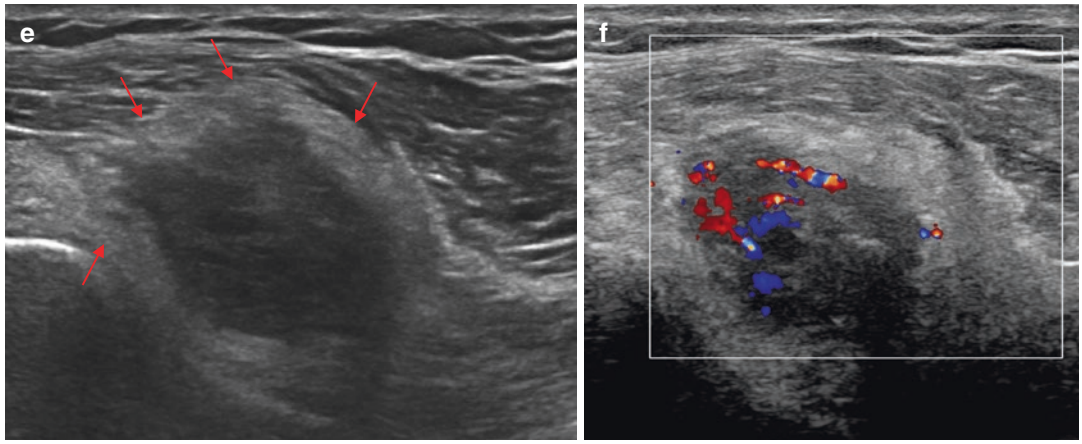

Fig. 10.18 (continued)

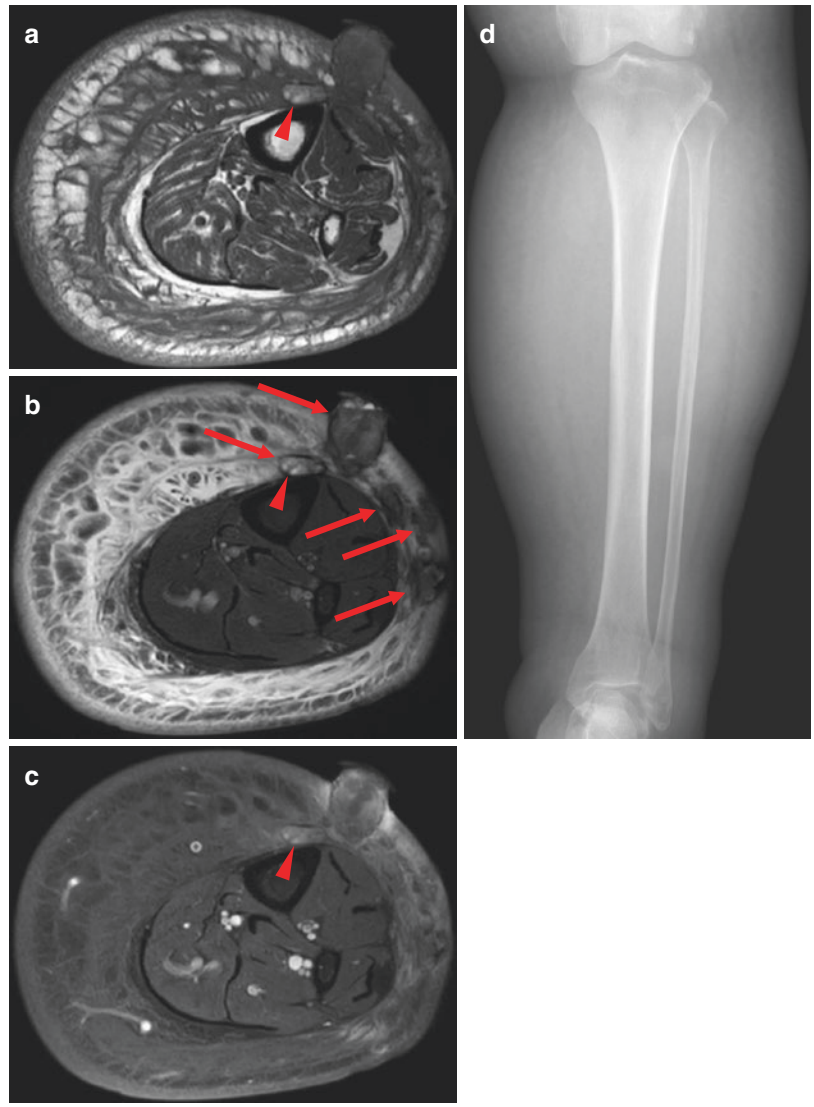

Fig. 10.19 Angiosarcoma of soft tissue. MR images (**a**, **b**, **c**) and radiograph (**d**) show diffuse enlargement of the lower leg with subcutaneous edema due to chronic lymphedema. This condition developed after cervical cancer surgery and radiation therapy 9 years ago. Multifocal lobular subcutaneous masses (*arrows*) are noted, the largest of which shows exophytic growth. The mass is heterogeneous iso- to mildly hyperintense to muscle on T1WI (**a**) and inhomogeneous, intermediate to hyperintense on T2WI (**b**) with heterogeneous contrast enhancement on postcontrast FS T1WI (**c**). A thin dark-signal rim around the lesions represents hemosiderin deposition, which can be observed on all sequences. T1- and T2-hyperintense areas (*arrowheads*) within the lesions, not suppressed on FS sequences, correspond to hemorrhagic changes

References

Aviv RI, McHugh K, Hunt J. Angiomatosis of bone and soft tissue: a spectrum of disease from diffuse lymphangiomatosis to vanishing bone disease in young patients. Clin Radiol. 2001;56(3):184–90. doi:10.1053/crad.2000.0606.

Calonge JE. Retiform haemangioendothelioma. In: Fletcher CDM, Bridge JA, Hogendoorn PCW, Mertens F, editors. WHO classification of tumours of soft tissue and bone. 4th ed. Lyon: International Agency for Research on Cancer; 2013. p. 147–8.

Deyrup AT, Tighiouart M, Montag AG, Weiss SW. Epithelioid hemangioendothelioma of soft tissue: a proposal for risk stratification based on 49 cases. Am J Surg Pathol. 2008;32(6):924–7.

Dubois J, Garel L. Imaging and therapeutic approach of hemangiomas and vascular malformations in the pediatric age group. Pediatr Radiol. 1999;29(12):879–93. doi:10.1007/s002470050718.

Kransdorf MJ, Murphey MD. Vascular and lymphatic tumors. In: Kransdorf MJ, editor. Imaging of soft tissue tumors, vol. 3rd. Philadelphia: Lippincott Williams & Wilkins; 2014. p. 179–230.

Lee R, Saardi KM, Schwartz RA. Lymphedema-related angiogenic tumors and other malignancies. Clin Dermatol. 2014;32(5):616–20. doi:10.1016/j.clindermatol.2014.04.008.

Lowe LH, Marchant TC, Rivard DC, Scherbel AJ. Vascular malformations: classification and terminology the radiologist needs to know. Semin Roentgenol. 2012;47(2):106–17. doi:10.1053/j.ro.2011.11.002.

Lyons LL, North PE, Mac-Moune Lai F, Stoler MH, Folpe AL, Weiss SW. Kaposiform hemangioendothelioma: a study of 33 cases emphasizing its pathologic, immunophenotypic, and biologic uniqueness from juvenile hemangioma. Am J Surg Pathol. 2004;28(5):559–68.

Meis-Kindblom JM, Kindblom LG. Angiosarcoma of soft tissue: a study of 80 cases. Am J Surg Pathol. 1998;22(6):683–97.

Moukaddam H, Pollak J, Haims AH. MRI characteristics and classification of peripheral vascular malformations and tumors. Skelet Radiol. 2009;38(6):535–47. doi:10.1007/s00256-008-0609-2.

Murphey MD, Fairbairn KJ, Parman LM, Baxter KG, Parsa MB, Smith WS. From the archives of the AFIP. Musculoskeletal angiomatous lesions: radiologic-pathologic correlation. Radiographics. 1995;15(4):893–917. doi:10.1148/radiographics.15.4.7569134.

Nuthakki S, Fessell D, Lal N, Shirkhoda A, Irwin T, Irwin R. Epithelioid hemangioendothelioma mimicking a nerve sheath tumor clinically and on MR imaging. Skelet Radiol. 2007;36(Suppl 1):S58–62. doi:10.1007/s00256-006-0197-y.

Pantanowitz L, Mullen J, Dezube BJ. Primary Kaposi sarcoma of the subcutaneous tissue. World J Surg Oncol. 2008;6:94. doi:10.1186/1477-7819-6-94.

Rao VK, Weiss SW. Angiomatosis of soft tissue. An analysis of the histologic features and clinical outcome in 51 cases. Am J Surg Pathol. 1992;16(8):764–71.

Sepulveda A, Buchanan EP. Vascular tumors. Semin Plast Surg. 2014;28(2):49–57. doi:10.1055/s-0034-1376260.

Sheth S, Nussbaum AR, Hutchins GM, Sanders RC. Cystic hygromas in children: sonographic-pathologic correlation. Radiology. 1987;162(3):821–4. doi:10.1148/radiology.162.3.3544038.

Tamai N, Hashii Y, Osuga K, Chihara T, Morii E, Aozasa K, Yoshikawa H. Kaposiform hemangioendothelioma arising in the deltoid muscle without the Kasabach-Merritt phenomenon. Skelet Radiol. 2010;39(10):1043–6. doi:10.1007/s00256-010-0917-1.

Tappero JW, Conant MA, Wolfe SF, Berger TG. Kaposi's sarcoma. Epidemiology, pathogenesis, histology, clinical spectrum, staging criteria and therapy. J Am Acad Dermatol. 1993;28(3):371–95.

Zheng LQ, Han XC, Huang Y, Fan JY. Cutaneous retiform hemangioendothelioma on the right foot with an unusual clinicopathological feature. Am J Dermatopathol. 2014;36(9):757–9. doi:10.1097/DAD.0b013e31829ae357.

Chondro-Osseous Tumors 11

Chondro-osseous tumors comprise various types of soft tissue lesions and may contain bone or cartilage matrix. Imaging correlation is essential for soft tissue tumors containing bone or cartilage. First and foremost, imaging confirms that the lesion originates from the soft tissue. This chapter focuses on chondro-osseous tumors, which are defined by the presence of a skeletal matrix in the 2013 WHO classification of soft tissue tumors.

11.1 Soft Tissue Chondroma

Soft tissue chondroma (STC) is a benign neoplasm consisting of chondrocytes in a hyaline cartilage matrix, arising in extraosseous and extrasynovial tissues. Synonyms include extraskeletal chondroma and chondroma of soft parts. These tumors usually occur in middle age with a slight male predominance. They affect most frequently the digits, particularly the fingers, followed by the hands and feet. STCs present as slowly growing soft tissue masses, with occasional pain or tenderness. The proper treatment is surgical excision, and the prognosis is excellent (Cho and Horvai 2015; Kransdorf and Meis 1993).

Radiography shows a well-demarcated soft tissue lesion with occasional erosion or periosteal reaction of the neighboring bone. Focal chondroid calcifications with ringlike, stippled, punctate, or curvilinear appearances can be seen. MR imaging shows a soft tissue mass with hypo- to isointensity relative to muscle on T1-weighted images and hyperintensity on T2-weighted images, representing the high water content of the mucopolysaccharide component or myxoid change (Hondar Wu et al. 2006; Kransdorf and Meis 1993). Areas with decreased signal intensity on T1- and T2-weighted images correspond to calcifications. Postcontrast T1-weighted images reveal various patterns of enhancement, ranging from non-enhancement, peripheral and septal enhancement, to homogeneous enhancement (Vaseenon et al. 2014; Suganuma et al. 2011; Adaletli et al. 2011; Le Corroller et al. 2008; Hondar Wu et al. 2006).

11.2 Extraskeletal Osteosarcoma

Extraskeletal osteosarcomas or soft tissue osteosarcomas are malignant neoplasms composed of malignant cells that produce osteoid or bone and are located in the soft tissue, without attachment to bone or periosteum. This tumor usually presents later (mid- to late adulthood) compared with conventional intraosseous osteosarcoma and has a slight male predominance. The deep soft tissue of the lower limbs is most commonly involved, usually the thigh and buttock regions. The mass presents as an enlarging soft tissue mass. Most cases develop de novo, but 4–13% are associated with previous exposure to radiation (Lee et al. 1995; Kransdorf and Meis 1993; Chung and

H.S. Kang et al., *Oncologic Imaging: Soft Tissue Tumors*, DOI 10.1007/978-981-287-718-5_11

Enzinger 1987). Local recurrence and distant metastasis are common and usually occur by 3 years after excision (Lee et al. 1995).

Radiography reveals a soft tissue mass with variable amounts of intratumoral osteoid matrix mineralization, which appears as an ill-defined, fluffy, cloud-like, or amorphous region of increased opacity. MR imaging findings are nonspecific. MR imaging shows a well-demarcated large (5–15 cm) soft tissue mass with mixed hypointensity on T1-weighted images and mixed, but predominant hyperintensity, on T2-weighted images. Cystic, hemorrhagic non-enhancing, or solid enhancing components can occasionally be observed on postcontrast T1-weighted images (Cho and Horvai 2015; Varma et al. 1993; Kransdorf and Meis 1993). The hypointense, non-enhancing osteoid component is usually observed centrally within the mass or is arbitrarily located. The central location of the osteoid in the tumor is referred to as a "reverse zoning phenomenon," in contradistinction to the peripheral deposition ("zonal phenomenon") observed in cases of myositis ossificans (Lidang Jensen et al. 1998).

11.3 Illustrations: Chondro-Osseous Tumors

11.3.1 Soft Tissue Chondroma

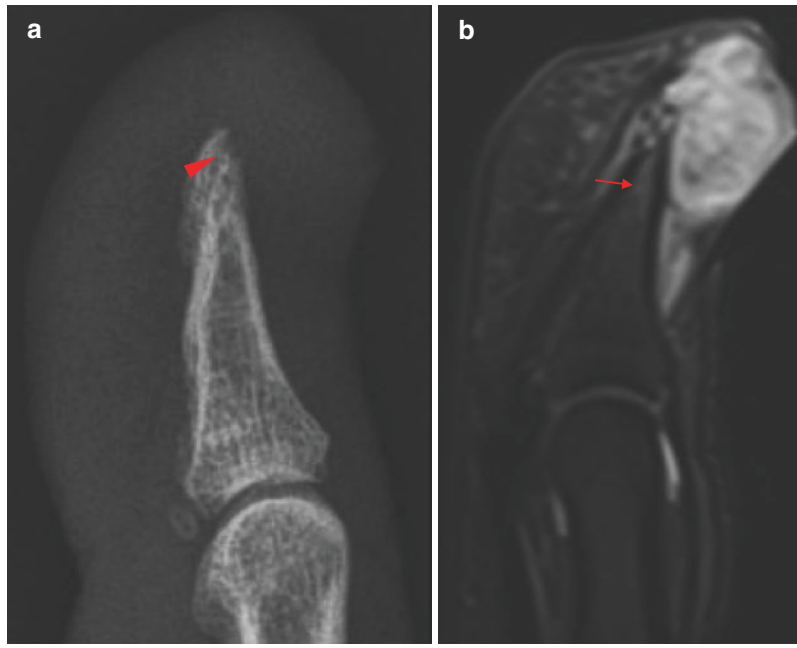

Fig. 11.1 Soft tissue chondroma. Lateral radiograph (**a**) shows soft tissue lesion in the dorsum of the distal phalanx of the thumb, with shallow bone erosion (*arrowhead*). There is no mineralization. Sagittal FS T2WI (**b**) reveals a circumscribed hyperintense soft tissue mass closely abutting the phalanx, with subtle bone marrow hyperintensity (*small arrow*). The tumor has slight hyperintensity to muscle on T1WI (**c**), heterogeneous hyperintensity on T2WI (**d**), and inhomogeneous enhancement on postcontrast FS T1WI (**e**). US (**f**) shows a hypoechoic mass and shallow neighboring bone erosion (*arrowheads*). Some intralesional vascularity is depicted on color Doppler image (not shown)

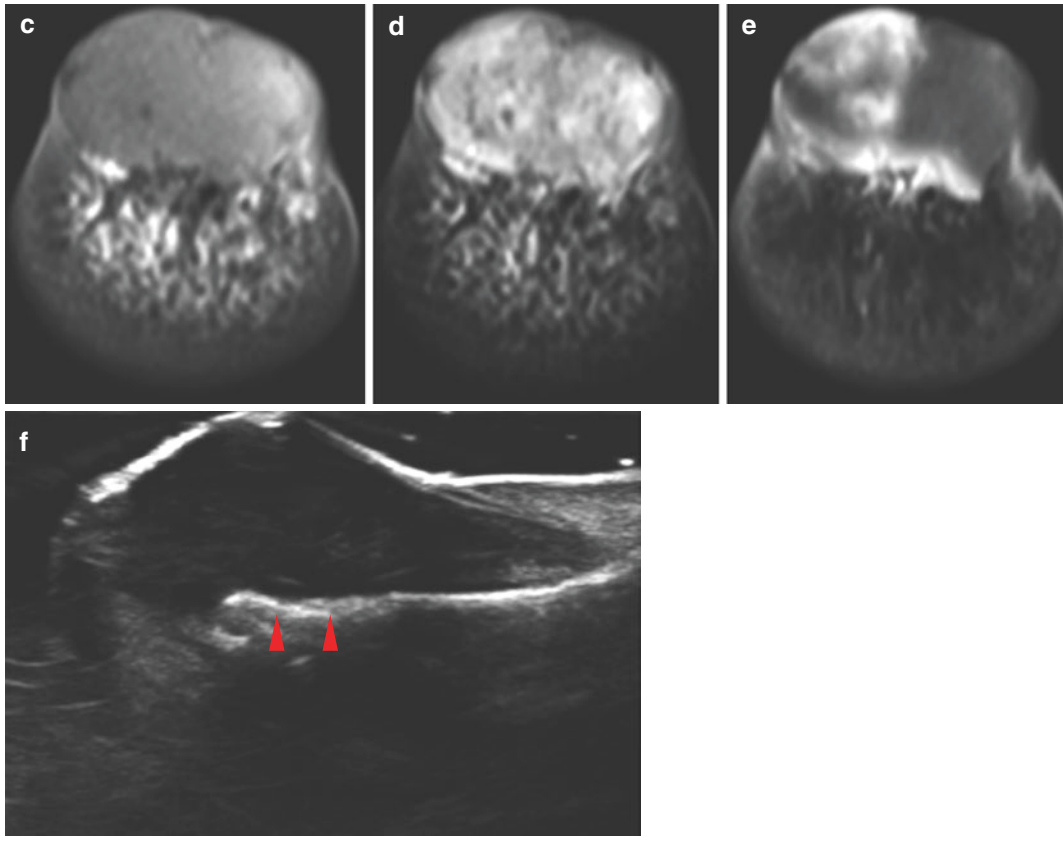

Fig. 11.1 (continued)

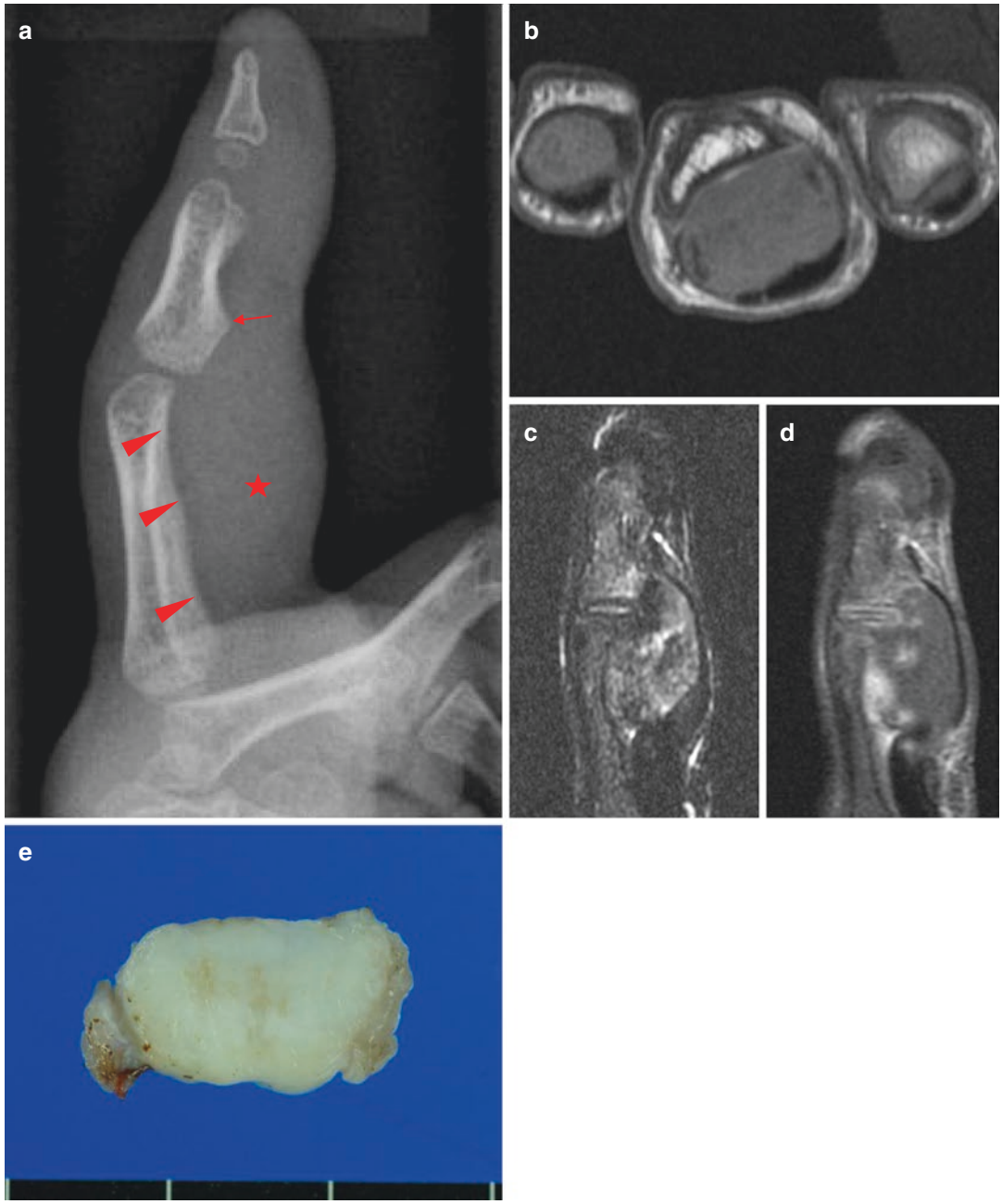

Fig. 11.2 Soft tissue chondroma. Lateral radiograph of the finger (**a**) shows soft tissue lesion (*star*) in the palmar aspect of the proximal phalanx of the middle finger, with scalloping (*arrowheads*), periosteal reaction, and bone remodeling (*small arrows*). No intratumoral calcification is seen. Axial T1WI (**b**) reveals a well-demarcated isointense mass between the bone and flexor tendon. Scalloping and remodeling of the neighboring bone are noted. The tumor has mixed signal, ranging from dark to hyperintense on T2WI (**c**), with some peripheral and tiny central nodular enhancement on postcontrast FS T1WI (**d**). The specimen photograph (**e**) reveals a circumscribed, whitish firm mass

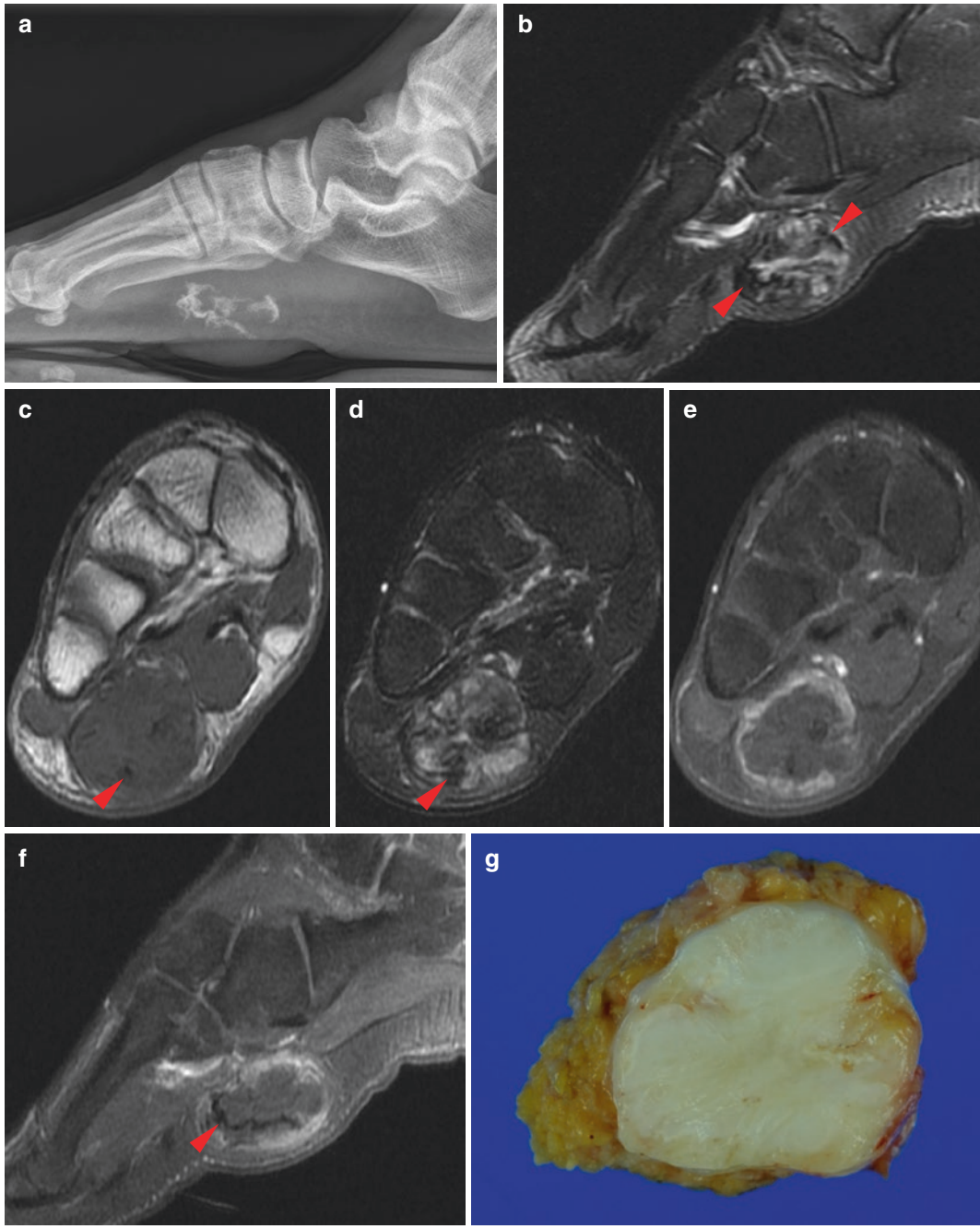

Fig. 11.3 Soft tissue chondroma. Lateral radiograph of the foot (**a**) shows a soft tissue lesion in the plantar aspect of the midfoot, with bulging soft tissue contours. Multifocal rings and arcs as well as curvilinear and popcorn-like calcifications are noted. Sagittal (**b**) and axial (**d**) FS T2WIs reveal a circumscribed subcutaneous mass with a mixed signal, ranging from dark to hyperintensity. The lesion is isointense to muscle on T1WI (**c**) with irregular thick rim enhancement along the periphery on postcontrast FS T1WIs (**e**, **f**). Multifocal hypointense foci (*arrowheads*) on all sequences correspond to calcification. A photograph of the specimen (**g**) shows multilobulated yellowish-white firm mass with internal whitish calcific foci

11.3.2 Extraskeletal Osteosarcoma

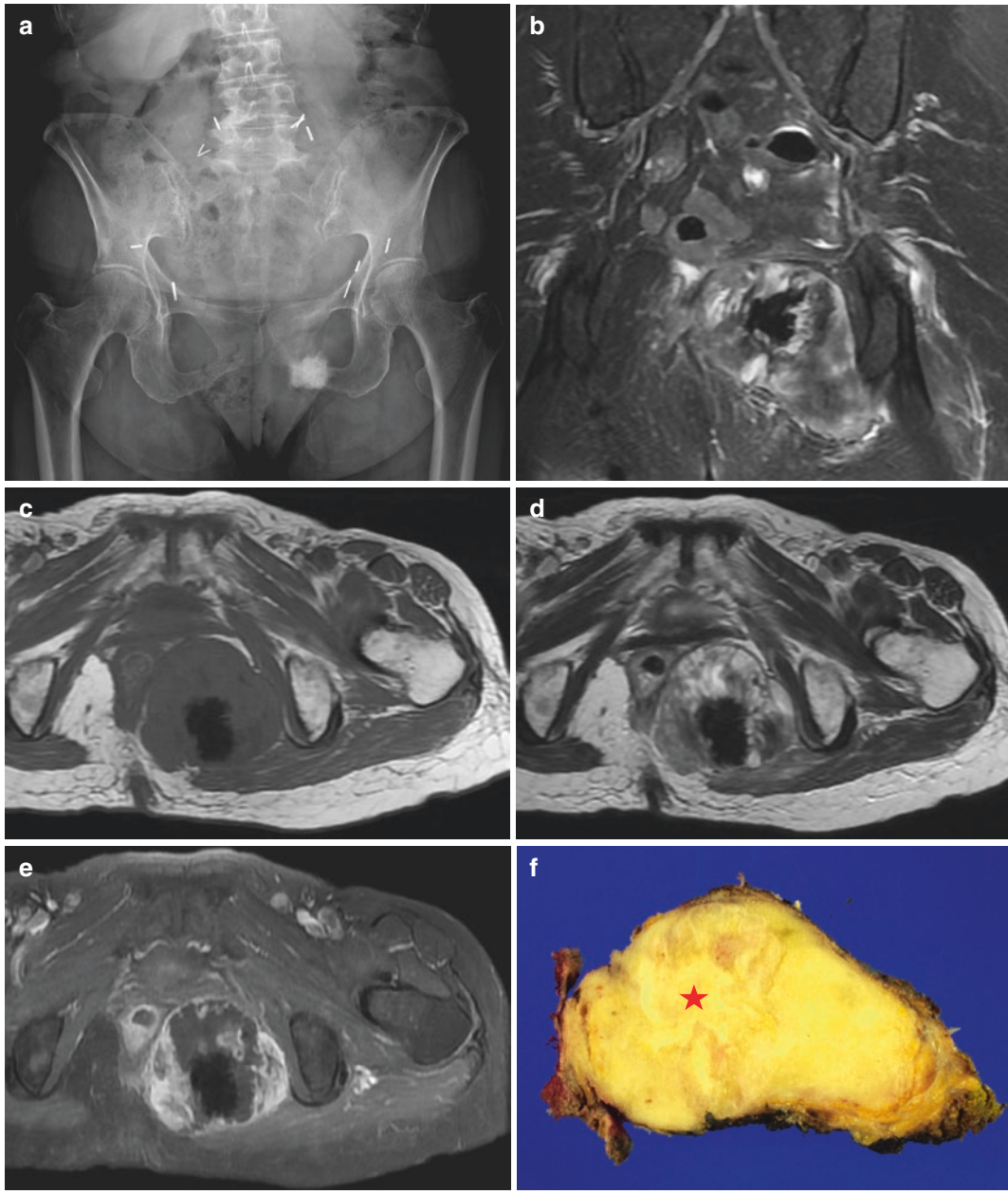

Fig. 11.4 Extraskeletal osteosarcoma. A patient underwent a total abdominal hysterectomy of a cervical cancer, followed by a course of radiation therapy 27 years ago. She presented with left pelvic pain 3 weeks ago. Pelvis radiograph (**a**) shows a multilobulated, multinodular dense calcification with some speculated margin adjacent to left ischium. Coronal FS T2WI (**b**) shows a large soft tissue mass in left ischiorectal fossa, medial to left ischium. The well-demarcated mass is isointense to muscle on T1WI (**c**) and heterogeneously hyperintense on T2WI (**b**, **d**). Postcontrast FS T1WI (**e**) shows heterogeneous enhancement with large non-enhancing areas. Irregular-shaped dark signal area on all sequences represents the osteoid matrix mineralization. A photograph of the specimen (**f**) shows a yellowish mass with central large mineralization (*star*) and some hemorrhagic foci

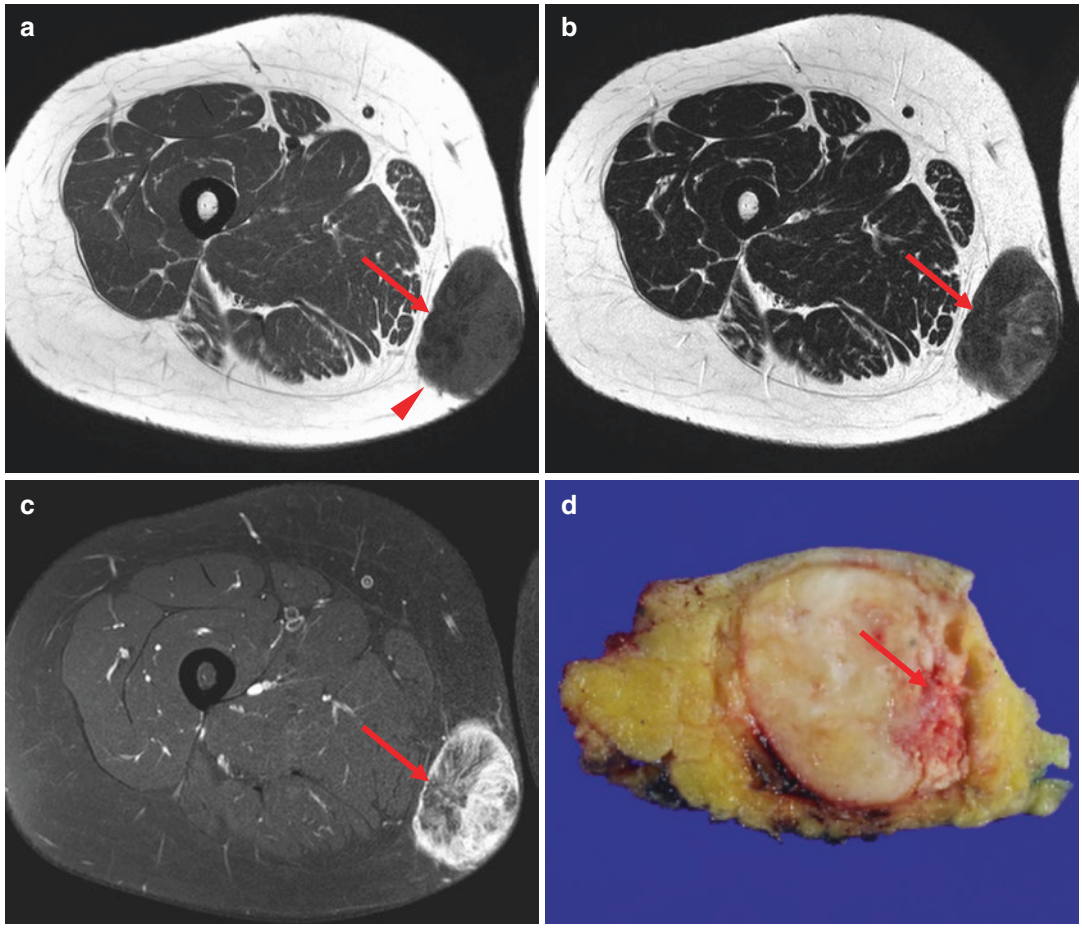

Fig. 11.5 Extraskeletal osteosarcoma. MR image of the thigh reveals a circumscribed, large subcutaneous soft tissue with some infiltrative border (*arrowhead*). The tumor has heterogeneous hypo- to mild hyperintensity to muscle on T1WI (**a**) and a mixed signal, ranging from dark to hyperintense on T2WI (**b**), with heterogeneous contrast enhancement on postcontrast FS T1WI (**c**). A large irregularly shaped non-enhancing hypointense component (*arrows*) suggests osteoid mineralization. A photograph of the specimen (**d**) demonstrates whitish-yellow mass with eccentric mineralization (*arrow*) and focal hemorrhagic foci

References

Adaletli I, Laor T, Yin H, Podberesky DJ. Extraskeletal chondroma: another diagnostic possibility for a soft tissue axillary mass in an adolescent. Case Rep Orthop.2011;2011:309328.doi:10.1155/2011/309328.

Cho SJ, Horvai A. Chondro-osseous lesions of soft tissue. Surg Pathol Clin. 2015;8(3):419–44. doi:10.1016/j.path.2015.05.004.

Chung EB, Enzinger FM. Extraskeletal osteosarcoma. Cancer. 1987;60(5):1132–42.

Hondar Wu HT, Chen W, Lee O, Chang CY. Imaging and pathological correlation of soft-tissue chondroma: a serial five-case study and literature review. Clin Imaging. 2006;30(1):32–6. doi:10.1016/j.clinimag.2005.01.027.

Kransdorf MJ, Meis JM. From the archives of the AFIP. Extraskeletal osseous and cartilaginous tumors of the extremities. Radiographics. 1993;13(4):853–84. doi:10.1148/radiographics.13.4.8356273.

Le Corroller T, Bouvier-Labit C, Champsaur P. Diffuse mineralization of forearm extraskeletal chondroma. Joint Bone Spine. 2008;75(4):479–81. doi:10.1016/j.jbspin.2007.06.019.

Lee JS, Fetsch JF, Wasdhal DA, Lee BP, Pritchard DJ, Nascimento AG. A review of 40 patients with extraskeletal osteosarcoma. Cancer. 1995;76(11):2253–9.

Lidang Jensen M, Schumacher B, Myhre Jensen O, Steen Nielsen O, Keller J. Extraskeletal osteosarcomas: a clinicopathologic study of 25 cases. Am J Surg Pathol. 1998;22(5):588–94.

Suganuma S, Tada K, Tsuchiya H. Giant extraskeletal chondroma of the index finger: a case report. J Plast Reconstr Aesthet Surg. 2011;64(10):1377–9. doi:10.1016/j.bjps.2011.02.024.

Varma DG, Ayala AG, Guo SQ, Moulopoulos LA, Kim EE, Charnsangavej C. MRI of extraskeletal osteosarcoma. J Comput Assist Tomogr. 1993;17(3):414–7.

Vaseenon T, Cheewawattanachai C, Pattamapaspong N, Settakorn J, Leerapun T. Extraskeletal chondroma on the sole of the foot. Foot Ankle Spec. 2014;7(3):232–6. doi:10.1177/1938640013516790.

Nerve Sheath Tumors

12

Neurogenic neoplasms comprise 12% of all benign and 7–8% of all malignant soft tissue tumors. According to the 2013 WHO classification of tumors of soft tissue, the tumors discussed in this chapter include schwannoma (including variants), neurofibroma (including variants), perineurioma, granular cell tumor, malignant peripheral nerve sheath tumor, and malignant granular cell tumor. Other neuromas, such as traumatic or Morton's neuroma, are reactive hyperplastic lesions and not true tumors; a complete discussion of these subtypes is therefore beyond the scope of this chapter.

12.1 Schwannoma (Including Variants)

Schwannoma, also known as neurilemmoma or neurinoma, is a common, benign, usually encapsulated peripheral nerve sheath tumor (PNST) composed of well-differentiated Schwann cells. This tumor has characteristic biphasic components, with varying amounts of each. The first of these, Antoni A tissues, are compact areas of spindle cells that show occasional palisading (Verocay bodies). Antoni B tissues are hypocellular, less organized, more myxoid, and loosely arranged areas with lipid-laden histiocytes and thick-walled, hyalinized blood vessels. Cellular schwannoma consists exclusively of Antoni A tissue. Plexiform schwannoma is defined as a schwannoma affecting multiple nerve fascicles or a nerve plexus, growing into thinly encapsulated plexiform or multinodular tumors. Large schwannomas with degenerative change, including cyst formation, hemorrhage, calcification, hyalinization, or fibrosis, are often referred to as "ancient" schwannomas. These tumors affect all ages, with a peak incidence in the 4–6th decade of life; there is no sex predilection. These schwannomas commonly arise in the peripheral nerves of the skin and subcutaneous tissue of the head and neck or along the flexor surfaces of the extremities. Ancient schwannomas usually present as asymptomatic masses or incidental findings on imaging studies. Multiple schwannomas may be associated with neurofibromatosis type 2 (accompanied by bilateral vestibular schwannoma, meningioma, or glioma) or schwannomatosis (without vestibular schwannoma or meningioma). The treatment of schwannoma is surgical resection. The affected nerve is frequently separable from the tumor during the operation, permitting postsurgical functionality of the native nerve. The lesion does not usually recur if treated by gross total resection. Malignant transformation is exceptionally rare (Antonescu et al. 2013b).

Radiographs are frequently normal and occasionally reveal a nonspecific soft tissue mass. Adjacent bone erosion or mineralizations are infrequently seen. On US and MR imaging, the entering and exiting nerve is occasionally

H.S. Kang et al., *Oncologic Imaging: Soft Tissue Tumors*, DOI 10.1007/978-981-287-718-5_12

detected in schwannomas that affect large, deep nerves ("string sign"); however, the nerve is difficult to identify in superficial or small lesions. The tumors may appear fusiform, oriented along the long axis of the affected nerve. The lesions may be located eccentrically to the affected nerve with increasing tumor size. US examination demonstrates a well-defined homogeneous or heterogeneous hypoechoic soft tissue mass with posterior acoustic enhancement. A target sign can be seen, characterized by a hypoechoic peripheral zone and a hyperechoic central zone. Hyperechoic calcifications and cystic formation or necrosis are occasionally observed in larger lesions. Doppler imaging reveals peripheral blood flow signals that occasionally enter from the proximal and distal poles. On MR imaging, schwannomas show a target sign consisting of a central hypo- to isointensity and a peripheral hyperintensity on T2-weighted images. These characteristics represent histologically the central fibrocollagenous tissue and peripheral myxoid stroma. The lesions showing a target sign typically enhance more prominently at the center, with a surrounding area of non-enhancing myxoid tissue, effectively reversing the target sign. A fascicular sign is another characteristic imaging finding, defined as multiple small round intermediate signal structures with a higher signal intensity at the periphery on T2-weighted images. The split-fat sign is frequently observed as a rim of fat around the tumor, especially on T1-weighted images, representing the tumor's location in the intermuscular space around the neurovascular bundle. The enhancement pattern ranges from little enhancement, due to the abundant avascular myxoid tissue, to diffuse gradual enhancement. The tumor may occasionally be accompanied by denervation changes, such as striated, increased intramuscular fat content or decreased muscle volume under the territory of the affected nerve. In larger lesions or ancient schwannomas, calcification, hemorrhage, degenerative cyst formation, or necrosis may be noted on MR imaging (Abreu et al. 2013; Gruber et al. 2007; Banks 2005).

12.2 Neurofibroma (Including Variants)

Neurofibroma is the most common benign PNST, being composed of differentiated Schwann cells, perineurial-like cells, fibroblasts, mast cells, and residual interspersed myelinated and unmyelinated axons embedded in the extracellular matrix. This lesion manifests as one of the following five types: (1) localized cutaneous, nodular or polypoid lesions; (2) diffuse cutaneous, plaque-like lesions that extend into the subcutaneous tissue, with overlying hyperpigmentation; (3) localized intraneural, solitary, segmental fusiform enlargements of sizeable nerves; (4) plexiform, intraneural, lumpy masses or worm-like growths that involve a nerve plexus or multiple fascicles of a single nerve; and (5) massive diffuse soft tissue plexiforms, ranging from a uniform regional soft tissue enlargement to pendulous, bag-like, or cape-like masses with widespread overlying skin hyperpigmentation. Most lesions occur sporadically as solitary lesions. Multiple or numerous neurofibromas are observed in individuals with neurofibromatosis (NF) type 1. All ages and both sexes are affected. The lesions most commonly affect the small nerves of the skin, followed by deeply located nerves of medium-size, nerve plexi or major nerve trunks. The treatment is often surgical resection. In contrast to schwannomas, neurofibroma tumor cells diffusely infiltrate the affected nerve. Complete excision of the tumor may therefore require sacrifice of the affected nerve, leading to neurological deficits. Plexiform neurofibromas and localized intraneural neurofibromas are precursor lesions of malignant PNST. The prevalence of malignant transformation varies from 2% to 29% in patients with NF type 1 (Abreu et al. 2013; Antonescu et al. 2013a).

The imaging findings of neurofibromas are similar to those observed with schwannomas, as previously described, and in many cases, these two entities cannot be distinguished. No

single imaging feature or combination of features allows for definitive differentiation between neurofibromas and schwannomas. When the parent nerve is identified, a centrally located mass relative to the parent nerve, with an occasionally poorly defined or infiltrative nerve-tumor transition, suggests a neurofibroma. In contrast, as previously described, eccentrically located masses suggest a schwannoma (Ryu et al. 2015; Abreu et al. 2013; Tsai et al. 2008). A target sign is reported more commonly in neurofibromas than in schwannomas, whereas, in our experience, the reverse has been the case. The fascicular sign is reported to be more common in schwannomas than in neurofibromas (Jee et al. 2004). Schwannomas are more commonly associated with cyst formation, necrosis, and calcification than neurofibromas (Abreu et al. 2013). In terms of enhancement pattern, different reports show inconsistent and contradictory results, although the following signs have been proposed: Most neurofibromas are less vascular than schwannomas (Ryu et al. 2015); neurofibromas are frequently associated with central enhancement, whereas schwannomas exhibit diffuse enhancement (Jee et al. 2004); both tumors are entirely hypervascular, with no significant difference between them (Tsai et al. 2008). Diffuse neurofibroma is frequently observed as a plaque-like or infiltrative lesion that involves the skin and subcutaneous tissues. In addition, this lesion commonly has prominent internal vascularity and tends to spread along connective tissue septa, surrounding rather than destroying adjacent normal structures (Hassell et al. 2008). Plexiform neurofibroma has typical imaging findings, such as multiple nodules with a target sign along a long nerve segment, nerve plexus, or its branches. This pattern results in a characteristic serpentine "bag of worms" appearance. In addition, diffuse neurofibromas may exhibit ill-defined margins due to their subcutaneous spread along connective tissue septa (Murphey et al. 1999).

12.3 Perineurioma

Perineurioma is a rare benign peripheral nerve sheath tumor composed entirely of perineurial cells. Two main types exist as follows: (1) the rare intraneural type (also known as localized hypertrophic neuropathy), which is restricted to the peripheral nerve boundary, and (2) the more common extraneural type, which commonly manifests in soft tissues and skin without connecting to the peripheral nerves. Intraneural perineurioma primarily affects young adults and children with accompanied motor deficiency and occasional sensory loss. Extraneural perineurioma commonly arises in the subcutaneous tissue of the limb and trunk, with a peak incidence in middle-aged adults and usually presenting as a painless mass (Macarenco et al. 2007). Intraneural perineurioma is static or slowly progressive, remaining confined to its original distribution and having a low morbidity; it should therefore not be resected routinely (Mauermann et al. 2009). Regarding extraneural perineurioma, the surgical resection is the treatment of choice.

Intraneural perineurioma may demonstrate characteristic MR imaging findings, including a fusiform enlargement of the affected major nerve of considerable length. A hypo- or isointense signal is observed on T1-weighted images, a hyperintense signal on T2-weighted images, and intense homogeneous enhancement. Extraneural perineurioma exhibits a circumscribed subcutaneous or deep soft tissue lesion with hypointensity on T1-weighted images, hyperintensity on T2-weighted images, and inhomogeneous enhancement, with a gradually enhancing nature after contrast injection.

12.4 Granular Cell Tumor

Granular cell tumor (GrCT) is a rare benign tumor that exhibits neuroectodermal differentiation and is composed of large, oval to round cells with copious eosinophilic granular cytoplasm. GrCT

commonly affects adults in the 4–6th decade of life, with a male predominance. This lesion occurs frequently in the head and neck, including the tongue, followed by chest wall, breast, back, and extremities. This tumor commonly affects the skin/subcutis, submucosa, and uncommonly deep soft tissue, such as the muscle. GrCT presents as a painless mass or is asymptomatic (Lazar 2013; Billeret Lebranchu 1999; Lack et al. 1980).

Radiography shows a nonspecific soft tissue swelling. US may demonstrate a circumscribed or irregularly bordered, heterogeneous hypoechoic soft tissue mass in the subcutaneous tissue or muscle. This mass may be accompanied by a thin echogenic rim with poorly defined fuzzy margins, occasional posterior sonic enhancement, tiny internal calcifications, and focal vascularity on color Doppler imaging (Kim et al. 2016; Kim et al. 2011; Gruber et al. 2007). On MR imaging, GrCT is observed as a well-defined or ill-defined round or oval soft tissue mass in the subcutaneous tissue or muscle. Isointensity or mild hyperintensity relative to the muscle is observed on T1-weighted images, and peripheral hyperintensity and central hypo- to isointensity relative to the muscle are observed on T2-weighted images. The contrast enhancement pattern is variable. Intratumoral hypointense areas on T1- and T2-weighted images may be attributable to a fibrous/collagenous component or possibly a ribbonlike or trabecular arrangement of tumor cells (Blacksin et al. 2005). One author reported a "stripe" sign of GrCT on US and MR imaging, observed as hypointense intratumoral lines that are continuous with the adjacent muscle fibers at the craniocaudal portion of the mass, representing preservation of the adjacent muscle fibers (Kim et al. 2016).

12.5 Malignant Peripheral Nerve Sheath Tumor

Malignant peripheral nerve sheath tumor (MPNST) is a rare, highly aggressive tumor arising either from a peripheral nerve, from a preexisting benign PNST (usually neurofibroma), or from neurofibromatosis type 1 (NF-1) (Nielsen et al. 2013). MPNSTs account for 3–10% of soft tissue sarcomas and are diagnosed most commonly in patients aged between 20 and 50 years. Patients with NF-1 present with MPNST less than 10 years earlier than those patients with non-NF-1 MPNST (Grobmyer et al. 2008). MPNST presents as an enlarging mass or unexplained change in size or the development of new symptoms in NF-1 patients. Malignant PNST can also be a secondary neoplasm related to previous radiation therapy. Such tumors develop after a long latent period (10–20 years) following irradiation (Wanebo et al. 1993). The treatment of MPNST is complete surgical excision with wide resection margins. Despite this aggressive treatment, local recurrence and distant metastases are common (Grobmyer et al. 2008).

No imaging criteria can reliably differentiate malignant from benign PNSTs, but some imaging features could be useful for the differential diagnosis of MPNST, as follows: peripheral enhancement with non-cystic appearance or remarkable heterogeneous enhancement, large tumor (>5 cm), ill-defined margins, invasion of fat planes, perilesional edema, intratumoral lobulation, absence of a target sign, and bone destruction (Yu et al. 2016; Abreu et al. 2013; Pilavaki et al. 2004; Murphey et al. 1999).

12.6 Illustrations: Nerve Sheath Tumors

12.6.1 Schwannoma

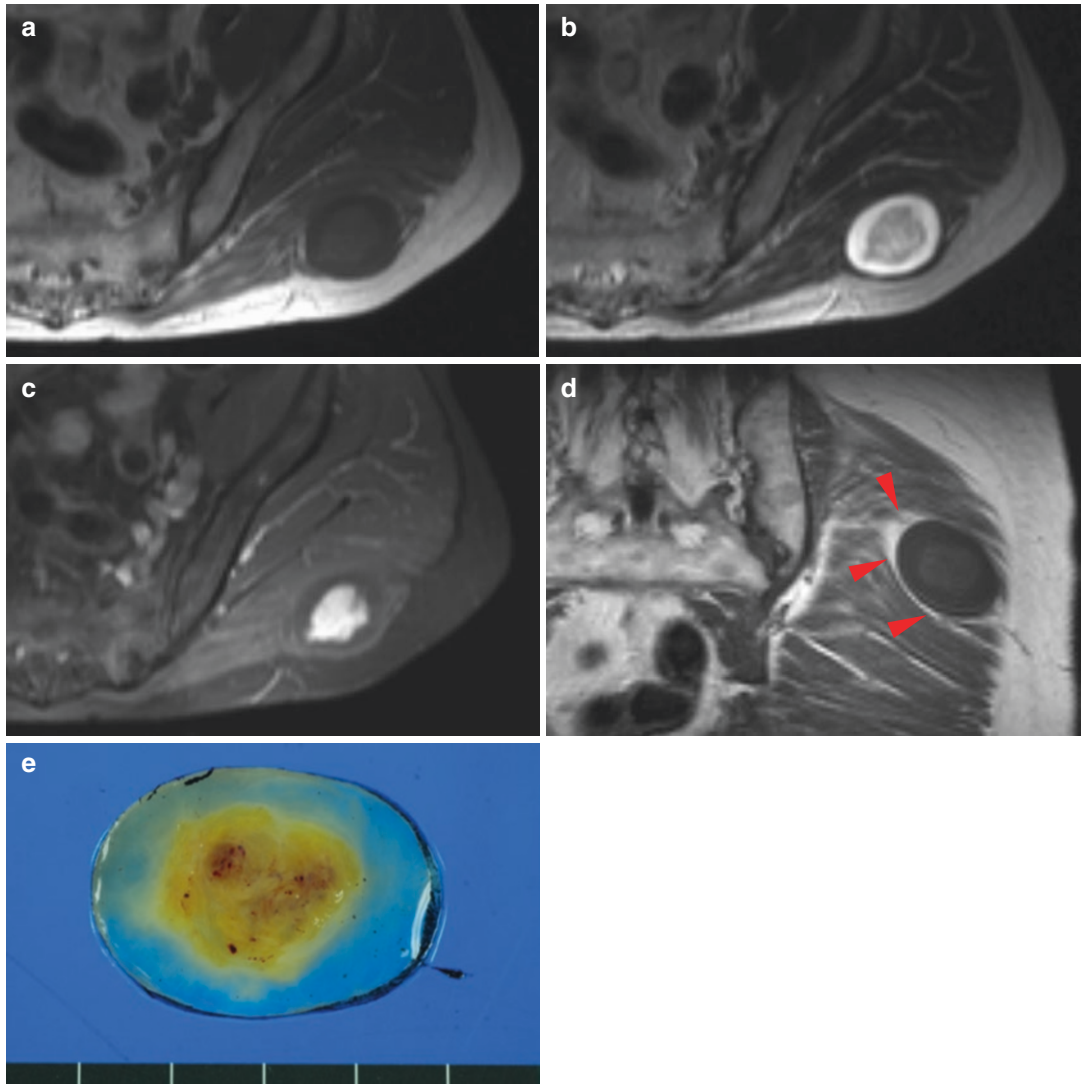

Fig. 12.1 Schwannoma. Axial T1WI of the pelvis (**a**) shows a circumscribed oval soft tissue mass within the gluteus maximus muscle, with a mild central hyperintensity and peripheral hypointensity to muscle. T2WI (**b**) reveals a target sign consisting of central hypo/isointensity and peripheral bright hyperintensity, whereas post-contrast FS T1WI (**c**) reveals a reverse target sign composed of central intense enhancement and peripheral non-enhancing myxoid tissue. A split-fat sign (*arrowheads*) observed as a rim of fat around the tumor is noted on coronal T1WI (**d**). A photograph of the specimen (**e**) shows encapsulated soft tissue mass consisting of central white/yellowish cellular or fibrocollagenous areas or patches of hemorrhage and peripheral, translucent, glistening myxoid tissue

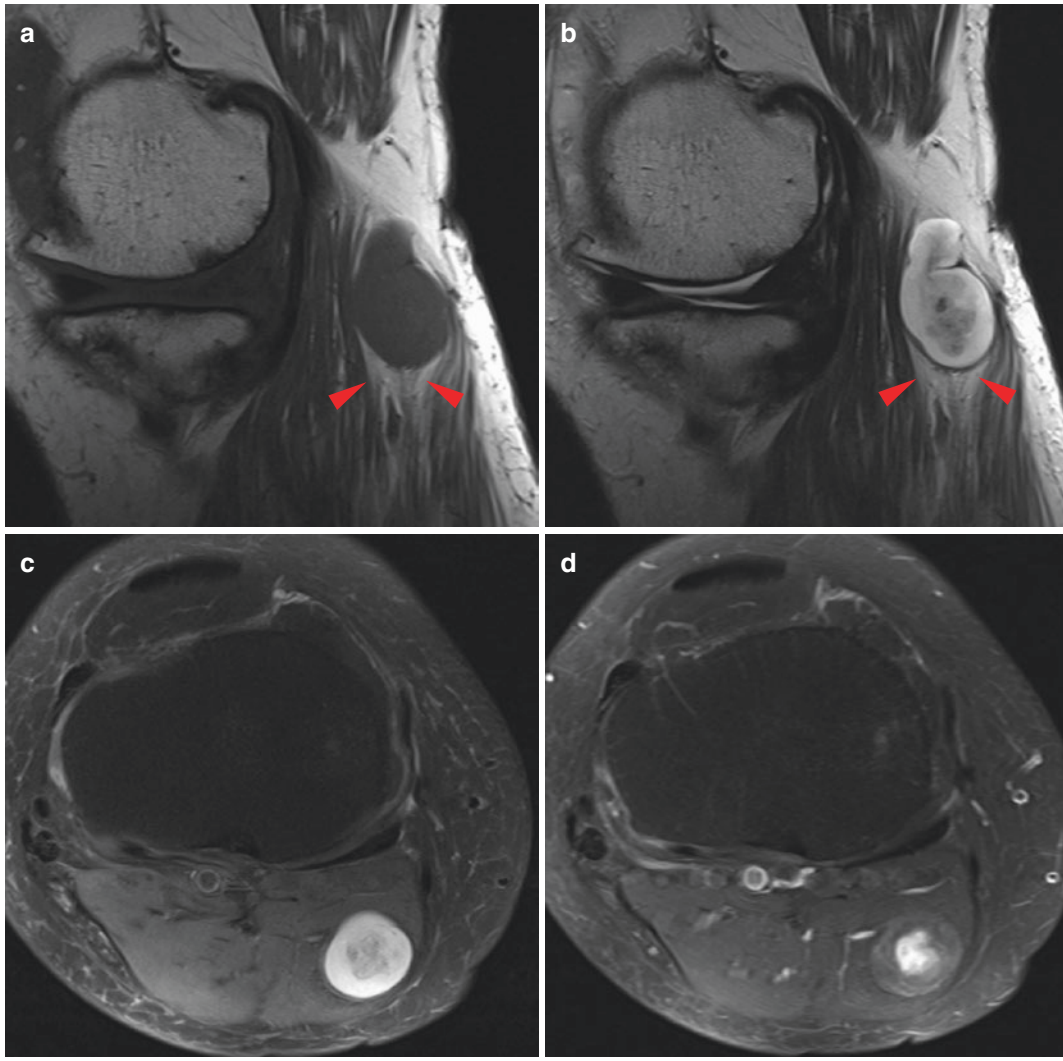

Fig. 12.2 Schwannoma. Sagittal T1WI (**a**) and T2WI (**b**) of the knee show a circumscribed, multilobulated, fusiform soft tissue mass within the lateral head of the gastrocnemius muscle. The lesion is isointense to muscle on T1WI. On T2WI (**b**, **c**), the mass shows central multilobulated hypointensity and peripheral fluid-equivalent bright hyperintensity, generating the target sign. A split-fat sign (*arrowheads*) is observed as fat around the tumor. Axial postcontrast FS T1WI (**d**) reveals central intense enhancement and peripheral sparse enhancement, reversing the target sign. US (**e**) demonstrates well-bordered intramuscular mass with a target sign composed of a heterogeneous hyperechoic central area and a homogeneous anechoic to hypoechoic periphery. The lesion has posterior sonic enhancement and some peripheral vascularity on color Doppler image (**f**). The entering/exiting nerve is not depicted on US. A photograph of the specimen (**g**) shows a well-circumscribed mass consisting of central white/yellowish cellular or fibrocollagenous areas with some internal hemorrhaging and peripheral, translucent, glistening yellow myxoid tissue

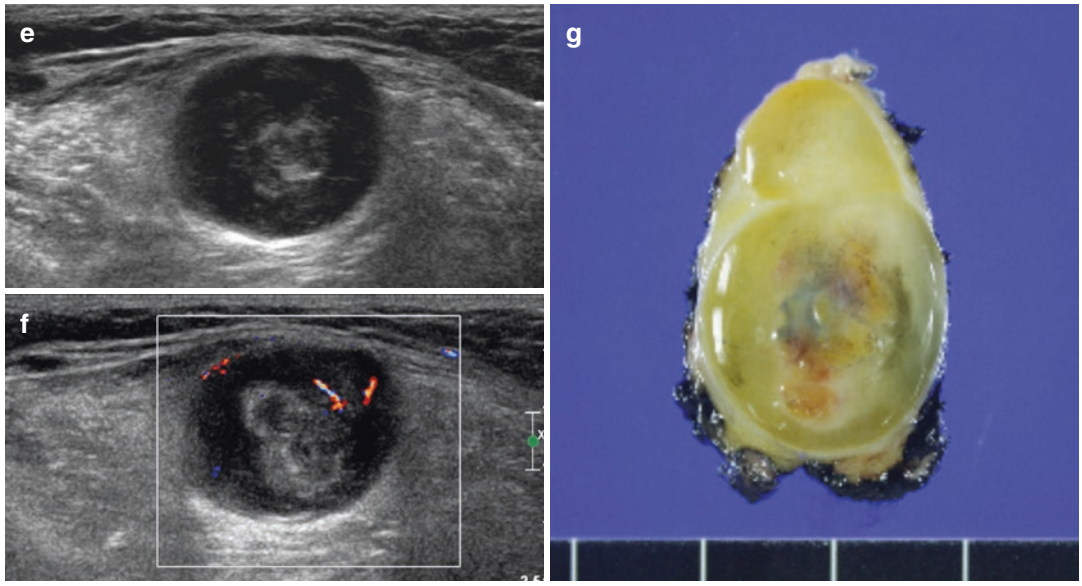

Fig. 12.2 (continued)

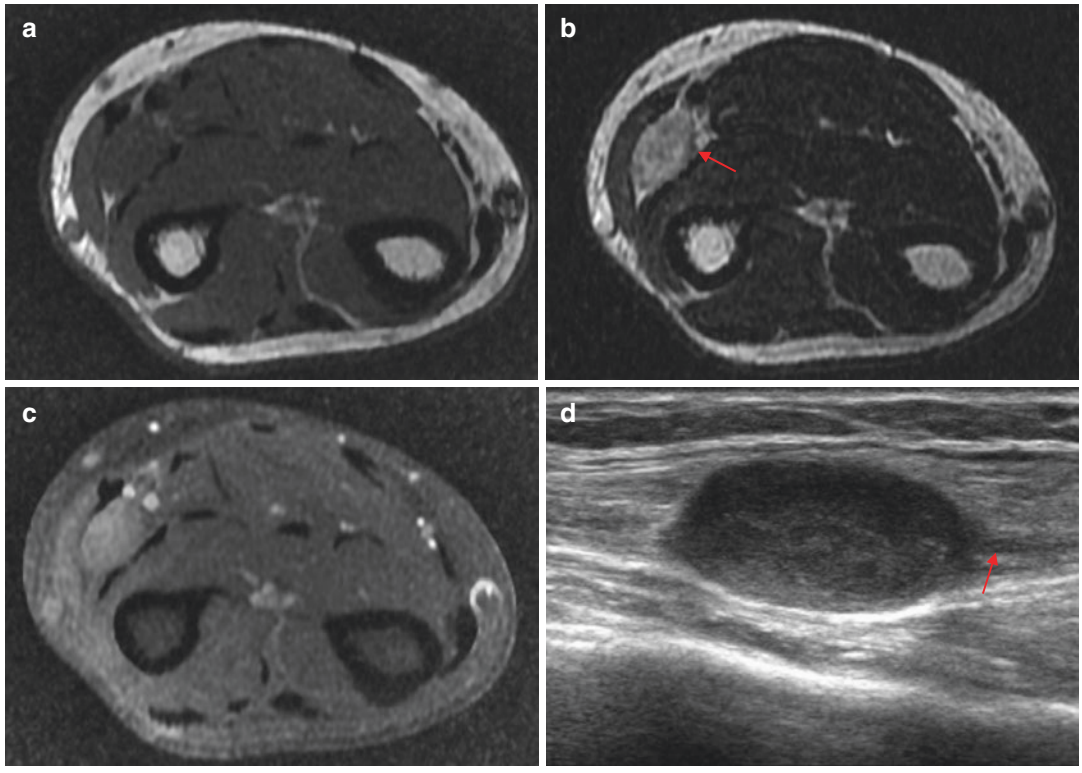

Fig. 12.3 Schwannoma. Axial T1WI (**a**) and T2WI (**b**) of the forearm show a circumscribed, oval, intermuscular soft tissue mass along the ulnar nerve. The lesion is isointense to muscle on T1WI and heterogeneous hyperintensity on T2WI, with inhomogeneous mild enhancement on postcontrast FS T1WI (**c**). The ulnar nerve (*small arrow*) is located eccentrically to the mass. Longitudinal US (**d**) reveals a well-demarcated, fusiform, heterogeneous hypoechoic mass with posterior sonic enhancement. The ulnar nerve (*small arrow*) is located eccentrically to the mass. Intralesional vascularity is absent on color Doppler image (not shown)

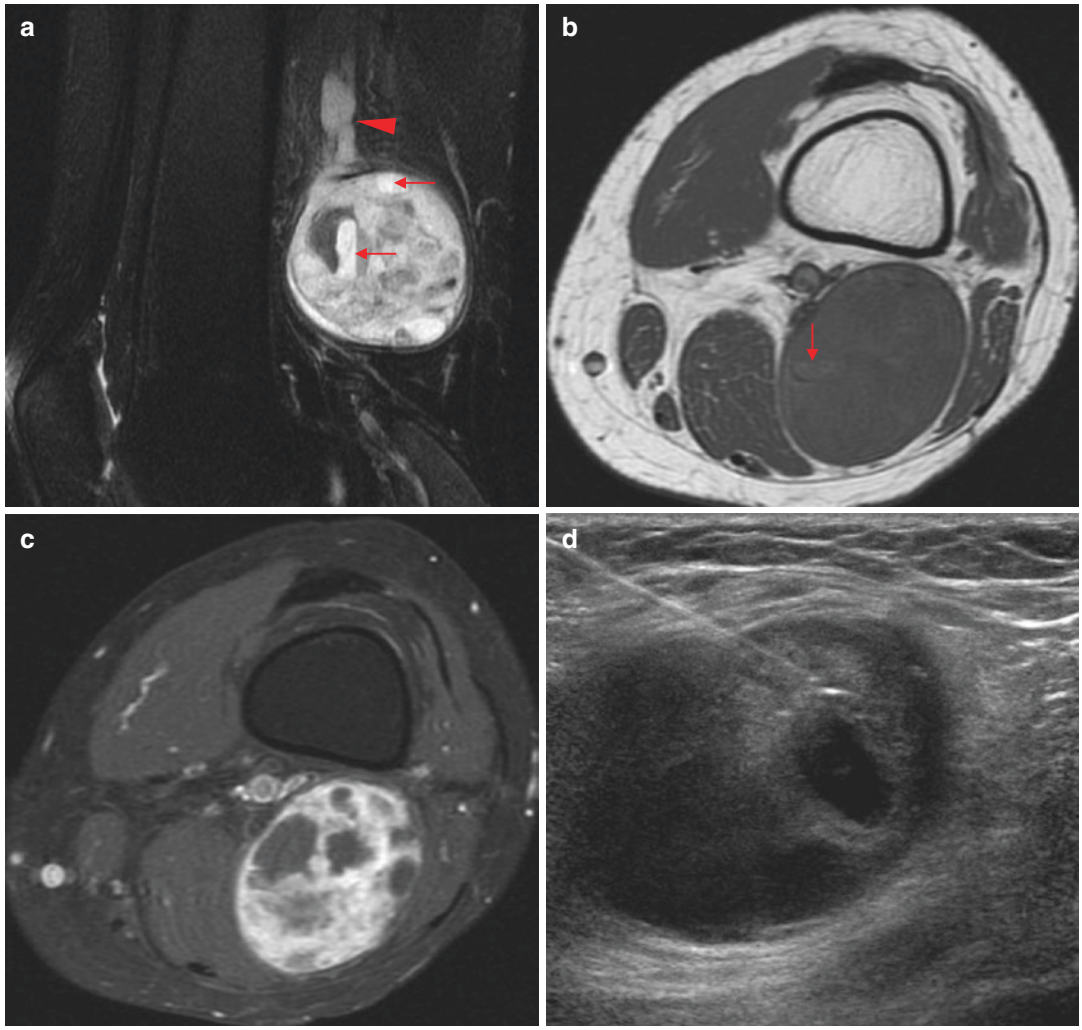

Fig. 12.4 Schwannoma with cystic degeneration. Sagittal FS T2WI (**a**) of the distal thigh shows a circumscribed soft tissue mass arising from the distal sciatic nerve (*arrowhead*). The mass has a heterogeneous signal on T2WI, ranging from a fluid-fluid level (representing hemorrhage) to bright hyperintensity. On axial T1WI (**b**), the mass has an inhomogeneous isointense to mildly hyperintense signal (to muscle). Axial postcontrast FS T1WI (**c**) shows heterogeneous peripheral and septal enhancement, with multifocal non-enhancing cystic or hemorrhagic necrotic areas. US (**d**) reveals the heterogeneous echogenic soft tissue mass, with a signal ranging from anechoic to hyperechoic, with posterior sonic enhancement. A biopsy was performed to target the solid component of the mass

12.6.2 Cellular Schwannoma

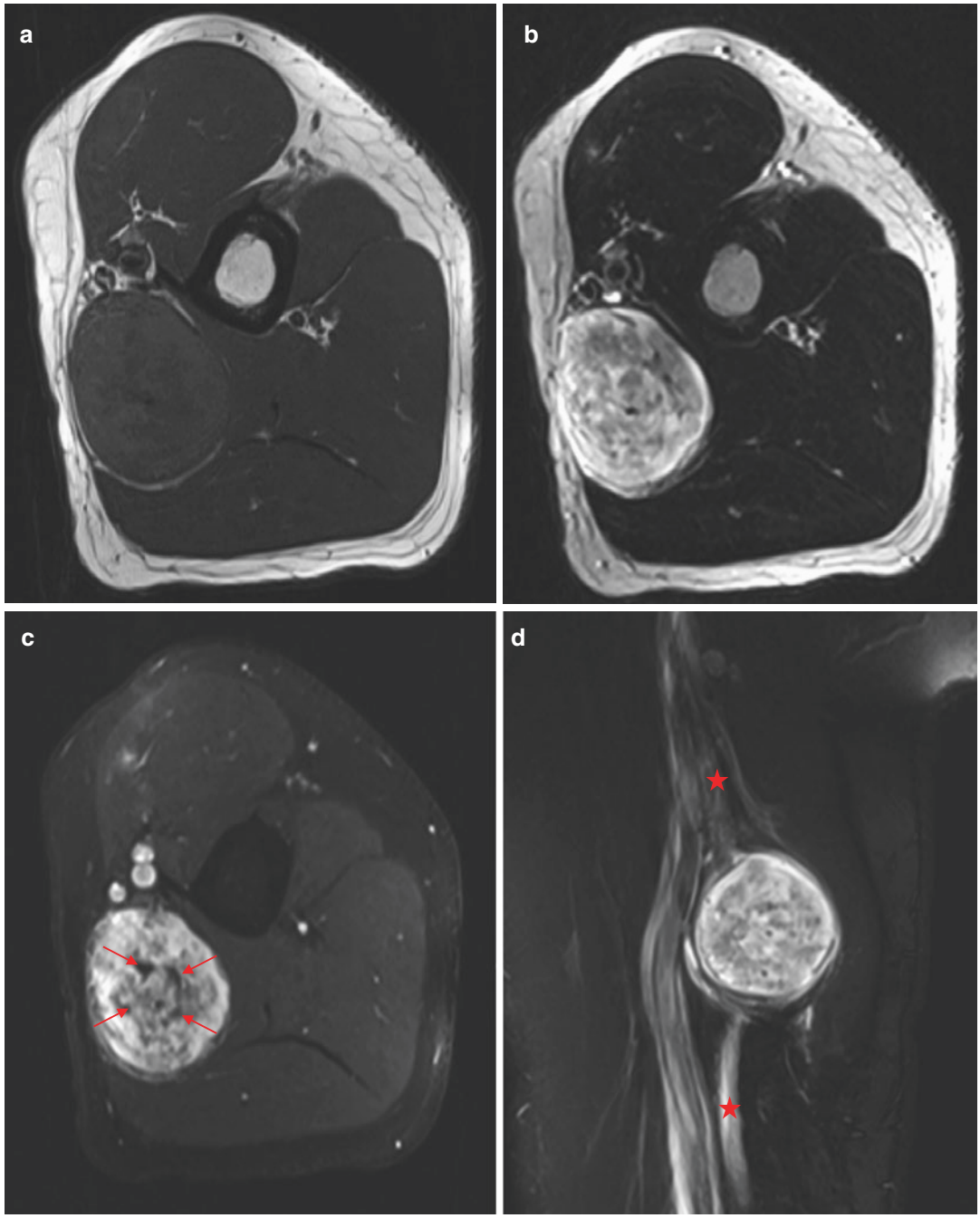

Fig. 12.5 Cellular schwannoma. Axial T1WI of the upper arm (**a**) reveals an oval mass, slightly hyperintense to muscle, located along the path of the ulnar nerve. T2WI (**b**) reveals a fascicular sign, observed as multiple small round intermediate signal structures with peripheral higher signal intensity. The tumor has heterogeneous enhancement on postcontrast FS T1WI (**c**), with multifocal non-enhancing foci (*small arrows*), and is slightly hyperintense on T1WI (**a**), representing hemorrhagic areas. A string sign is noted on sagittal FS T2WI (**d**) in which the entering and exiting nerve (*stars*) is visualized at both ends of a vertically oriented mass. Sectioned surface of the specimen (**e**) reveals a firm, yellowish mass with spotty hemorrhagic foci

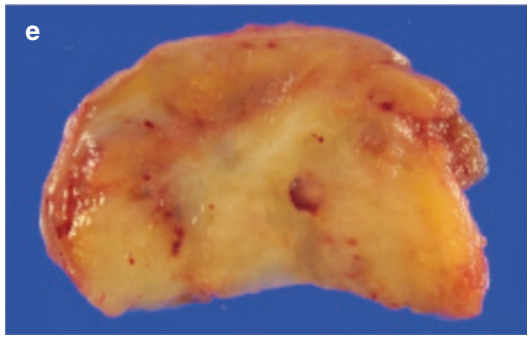

Fig. 12.5 (continued)

12.6.3 Plexiform Schwannoma

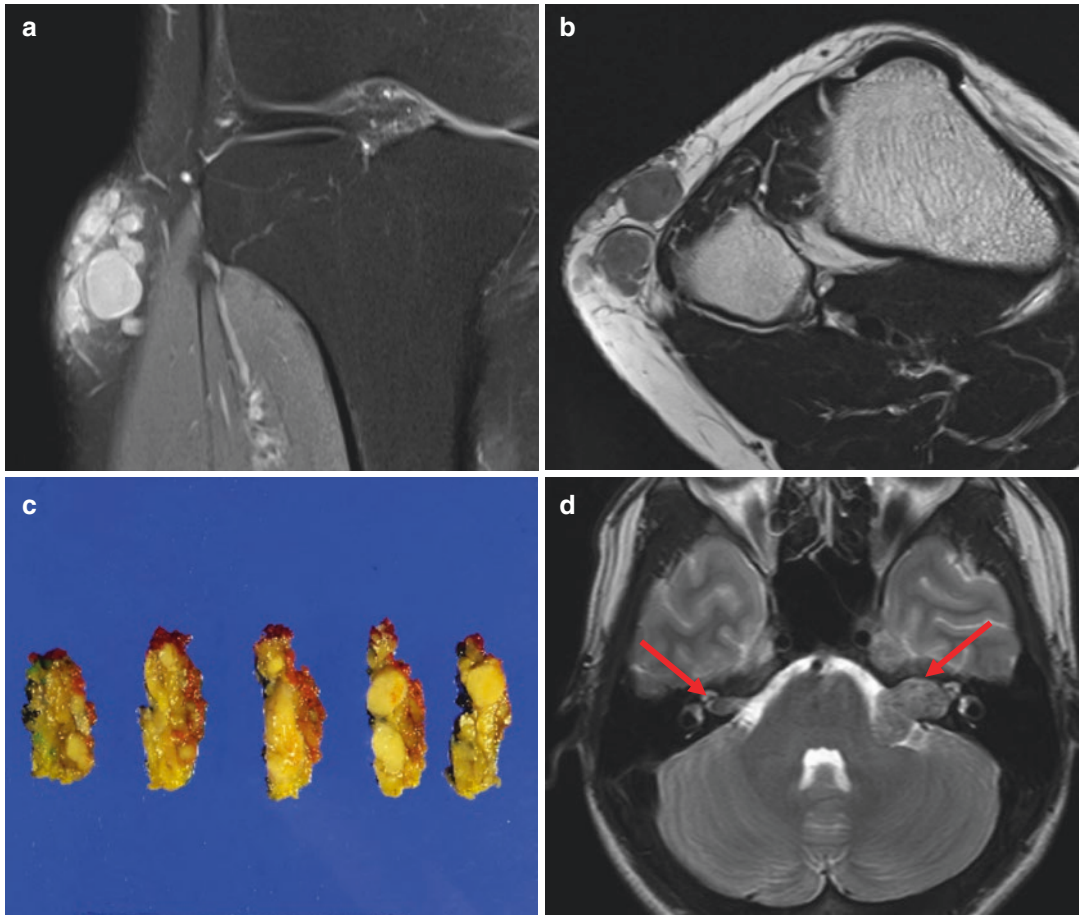

Fig. 12.6 Plexiform schwannoma. Coronal FS (**a**) and axial (**b**) T2WIs of the knee show aggregation of variably sized, circumscribed soft tissue lesions affecting the skin and subcutaneous tissue, which are represented by a central intermediate signal area and a thin peripheral hyperintense rim, respectively. Sequentially cut surfaces of the specimen (**c**) reveal multiple, well-encapsulated masses and a firm yellowish surface. Brain MR image (**d**) of the same patient shows bilateral vestibular schwannomas (*arrows*), representing neurofibromatosis type 2

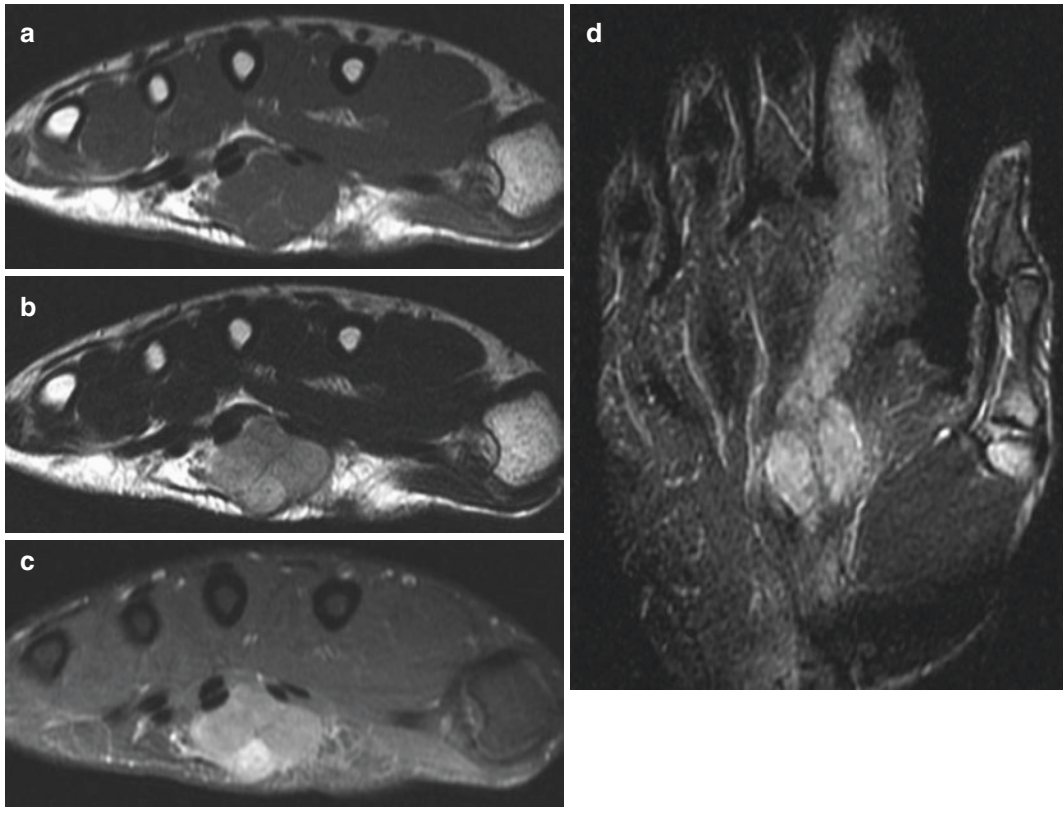

Fig. 12.7 Plexiform schwannoma. Axial T1WI of the hand (**a**) shows a deep subcutaneous multinodular iso- to mildly hyperintense mass in the palm. The tumor is hyperintense on T2WI (**b**) and exhibits gradual diffuse enhancement on postcontrast FS T1WI (**c**). Marked, cord-like, diffuse enlargement of the affected palmar digital nerve of the index finger is observed on coronal FS T2WI (**d**)

12.6.4 Ancient Schwannoma

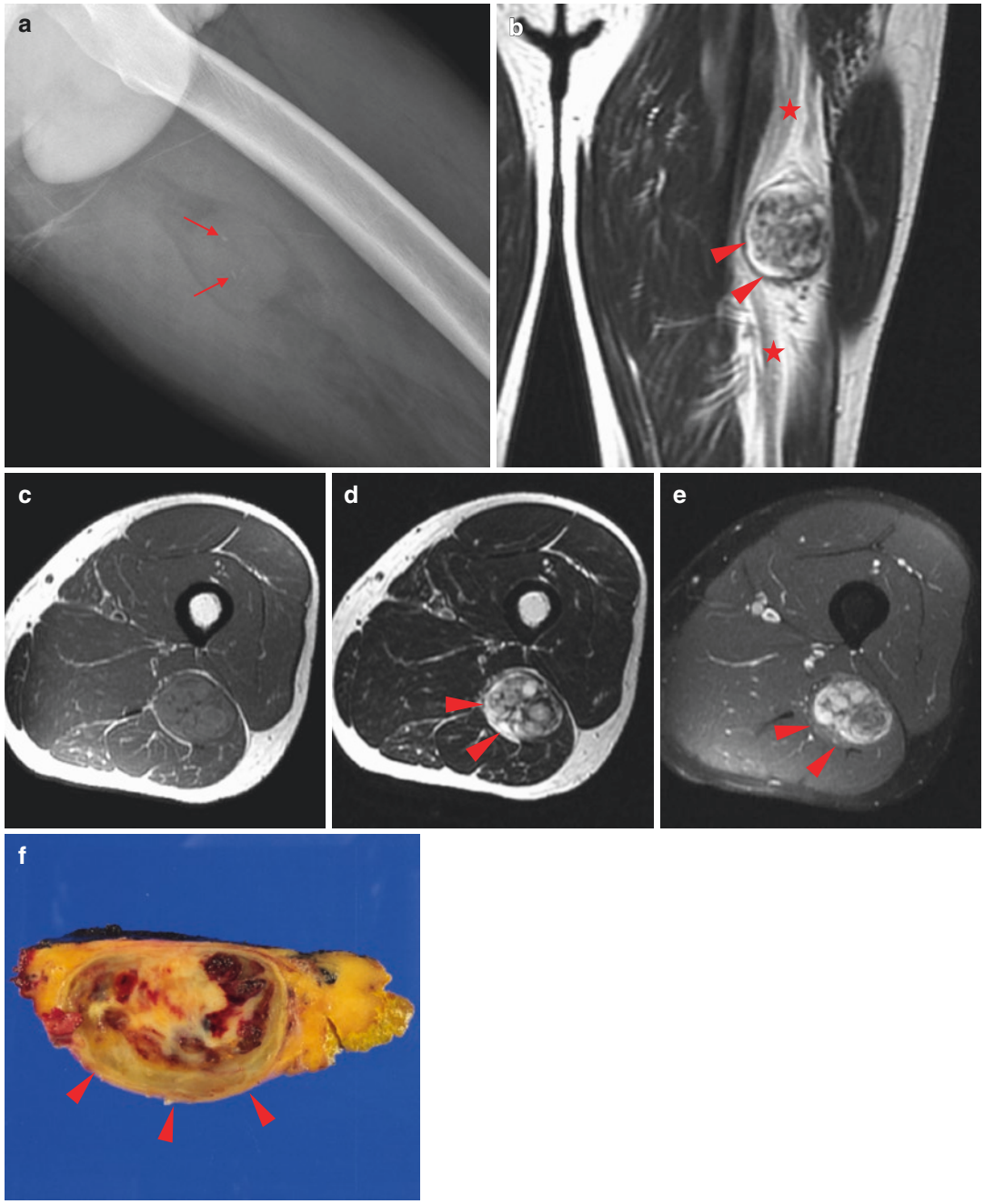

Fig. 12.8 Ancient schwannoma. Radiograph of the thigh (**a**) shows a circumscribed soft tissue mass with internal spotty calcifications (*small arrows*). The tumor is eccentrically located along the sciatic nerve (*stars*), with prominent peritumoral fat overgrowth on coronal T2WI (**b**). The lesion is inhomogeneously hyperintense to muscle on T1WI (**c**) and mixed signal on T2WI (**d**). Heterogeneous enhancement and some non-enhancing areas are observed on postcontrast FS T1WI (**e**). A photograph of the specimen (**f**) reveals many hemorrhagic areas and central hyalinization. The non-enhancing peripheral hyperintense rim (*arrowheads*) on T2WI (**b**, **d**) corresponds to myxoid tissue

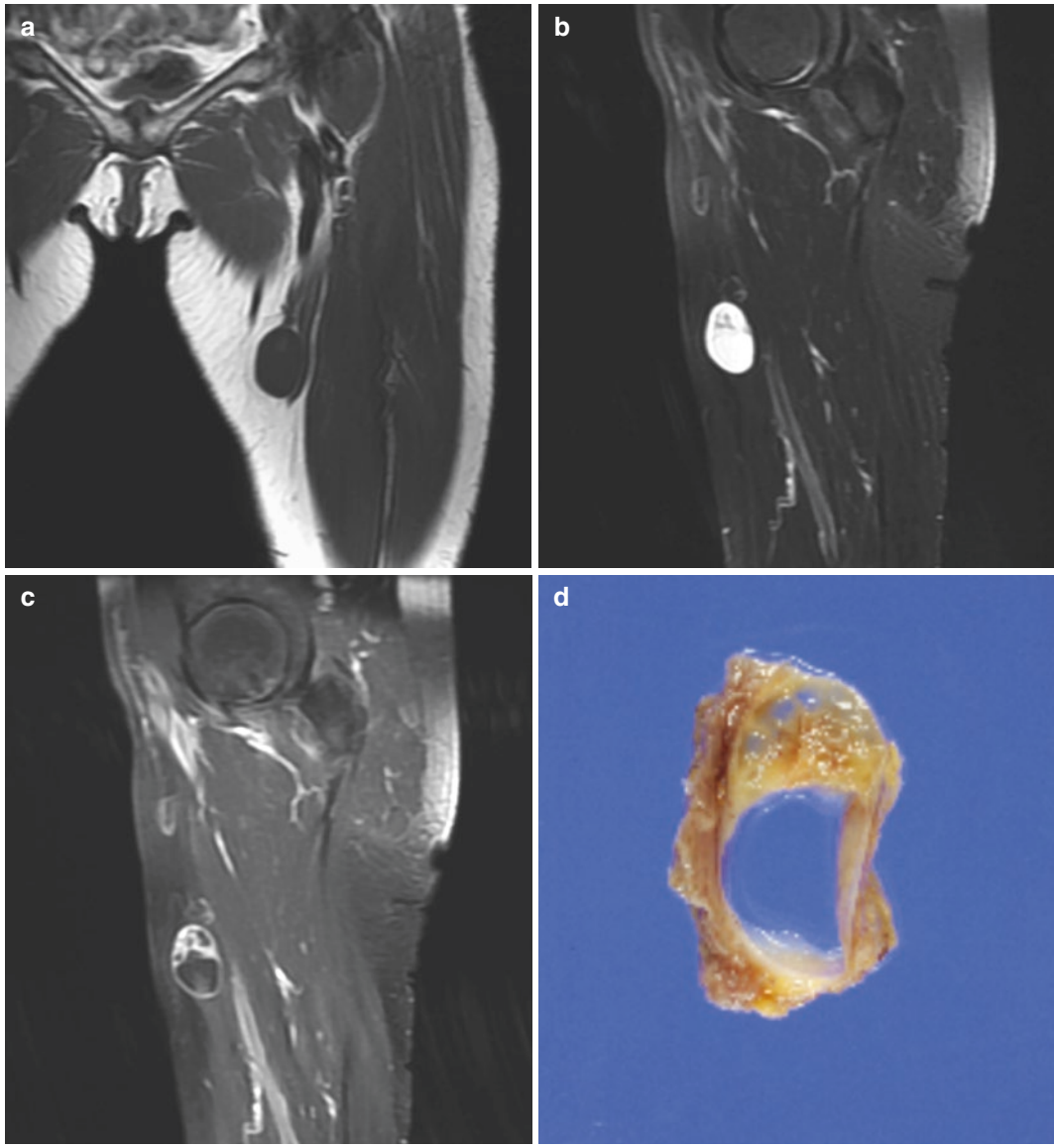

Fig. 12.9 Ancient schwannoma. Coronal T1WI (**a**) of the thigh shows a well-defined, deep subcutaneous hypointense oval mass. The tumor has fluid-equivalent hyperintensity on T2WI (**b**), with a peripheral rim and some septal/solid enhancement on postcontrast FS T1WI (**c**). A photograph of the specimen (**d**) reveals a large cyst with upper, mixed smaller cystic, and myxoid solid areas

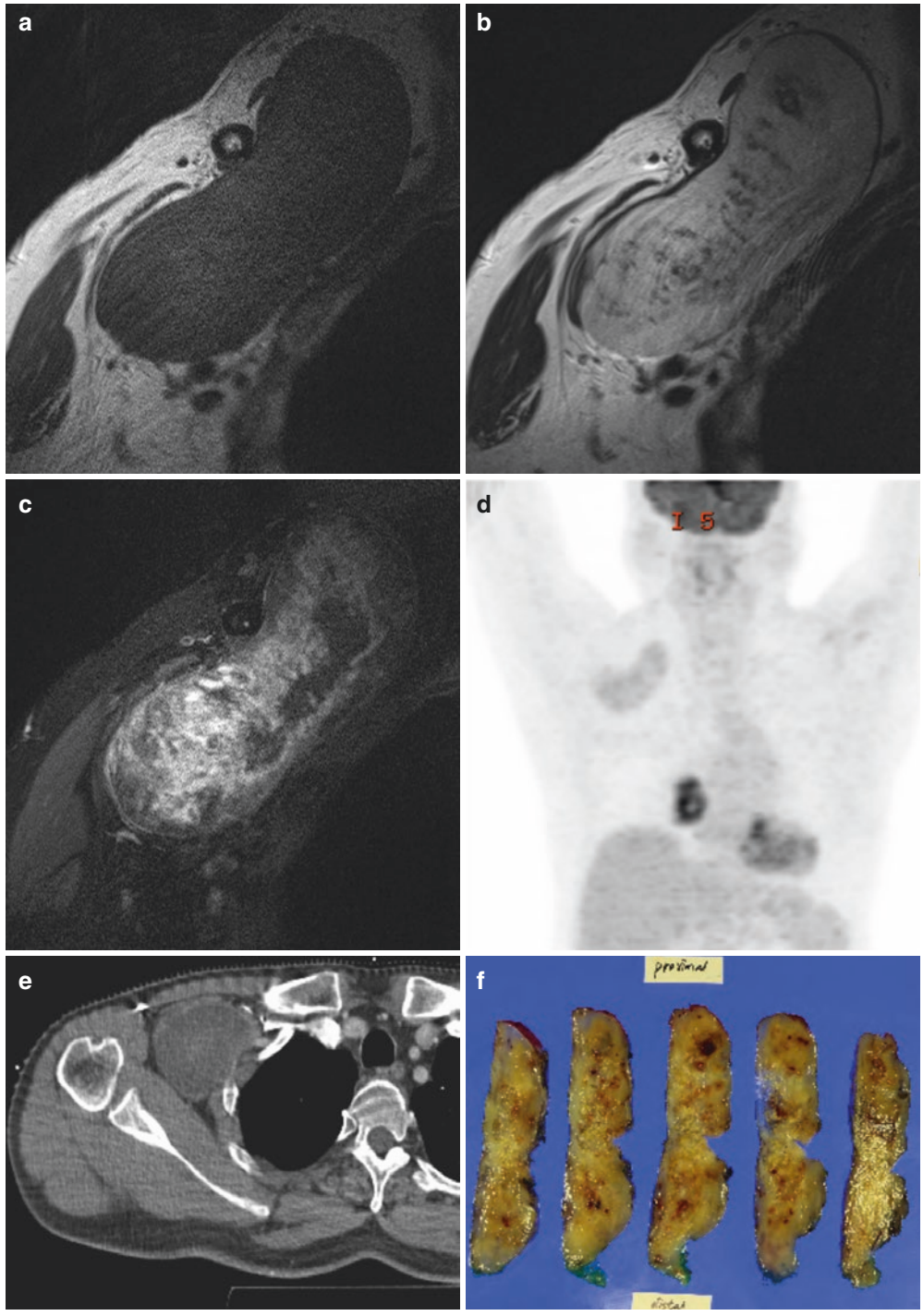

Fig. 12.10 Ancient schwannoma. Coronal T1WI (**a**) of the shoulder shows a circumscribed large hypointense mass adjacent to the brachial plexus. The mass has heterogeneous hyperintensity with multifocal hypointense foci on T2WI (**b**) and heterogeneous enhancement with a large central non-enhancing area on postcontrast FS T1WI (**c**). PET (**d**) shows the mass to be mildly hypermetabolic. Contrast CT (**e**) reveals a well-defined heterogeneous low-attenuation mass with an internal fuzzy enhancing area and thin peripheral rim enhancement. Intratumoral calcification is not depicted on CT. Photograph of a sequentially cut surface (**f**) reveals a large myxoid mass with an internal hemorrhagic area and calcific foci

12.6.5 Neurofibroma

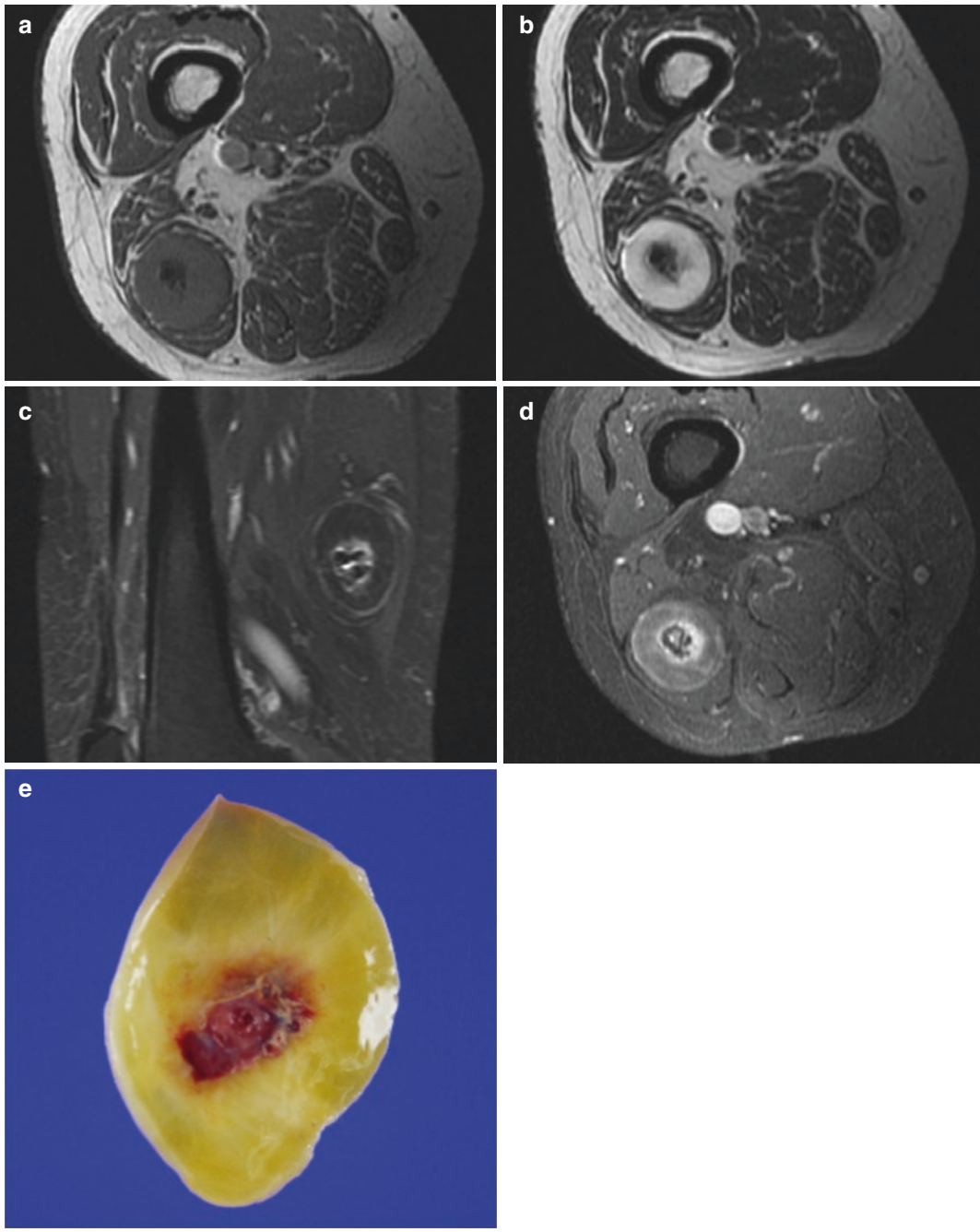

Fig. 12.11 Neurofibroma. Axial T1WI (**a**) of the thigh reveals a circumscribed mass with central mild hyperintensity to dark signal within the biceps femoris muscle. The tumor shows central hypointensity and peripheral hyperintensity, so-called, target sign on T2WI (**b**). Sagittal postcontrast FS T1WI (**c**) reveals central enhancing area and surrounding non-enhancing tissue, which shows delayed gradual mild enhancement on axial postcontrast FS T1WI (**d**). Focal central signal voids on all sequences suggest hemosiderin deposit. A photograph of the specimen (**e**) shows central whitish-yellow solid area with internal large hemorrhagic component, and surrounding semitranslucent glistening myxoid tissue

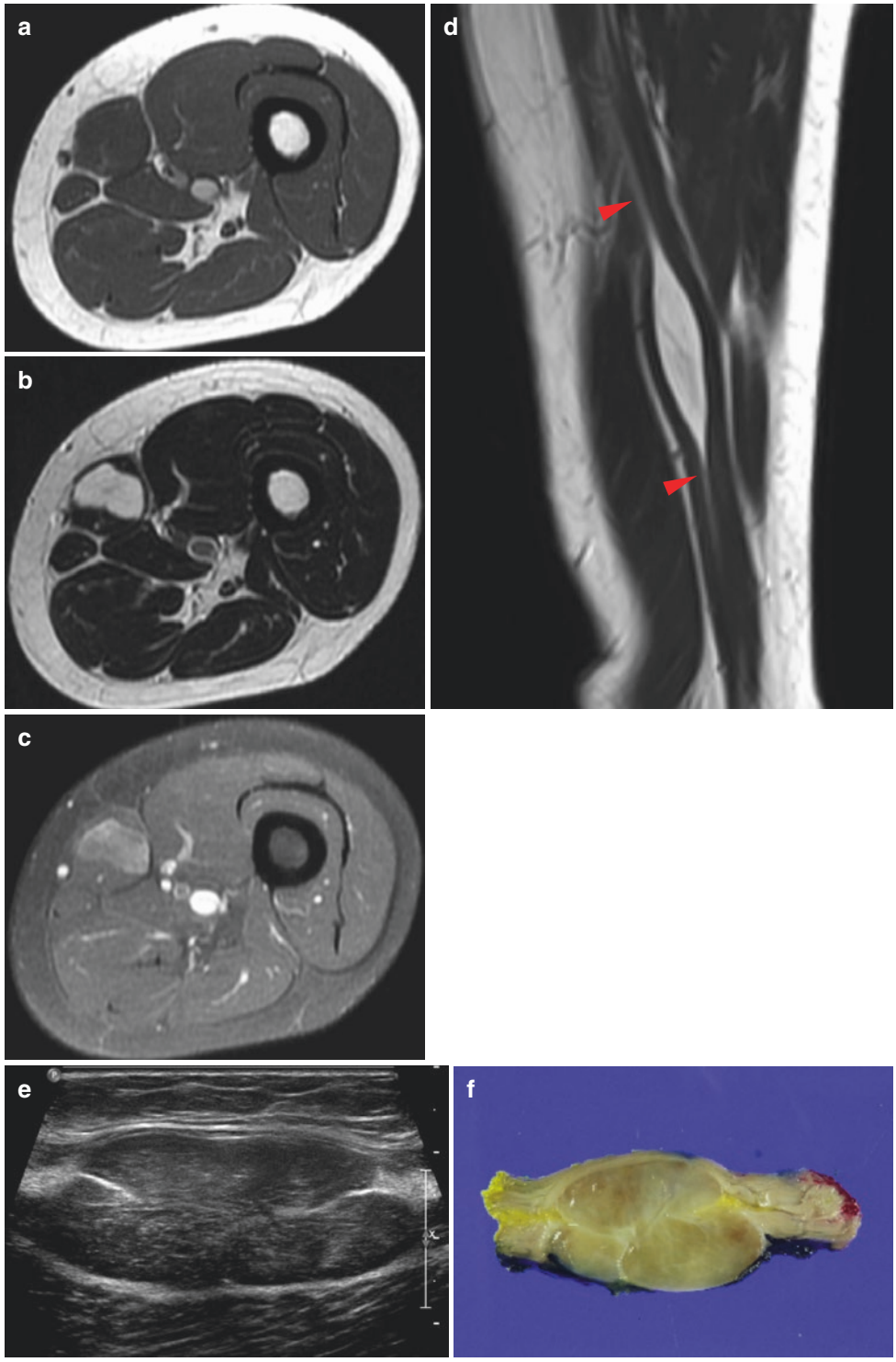

Fig. 12.12 Neurofibroma. MR images of the thigh reveal a circumscribed fusiform mass within the sartorius muscle. The tumor is isointense to muscle on T1WI (**a**) and hyperintense on T2WI (**b**), with fuzzy inhomogeneous enhancement on postcontrast FS T1WI (**c**). Sagittal T2WI (**d**) reveals a string sign with a central location to the nerve (*arrowheads*). On US (**e**), the tumor has a smooth surface and lobulation, with heterogeneous isoechogenicity to muscle. The sectioned surface (**f**) is smooth, glistening, semitranslucent, and firm

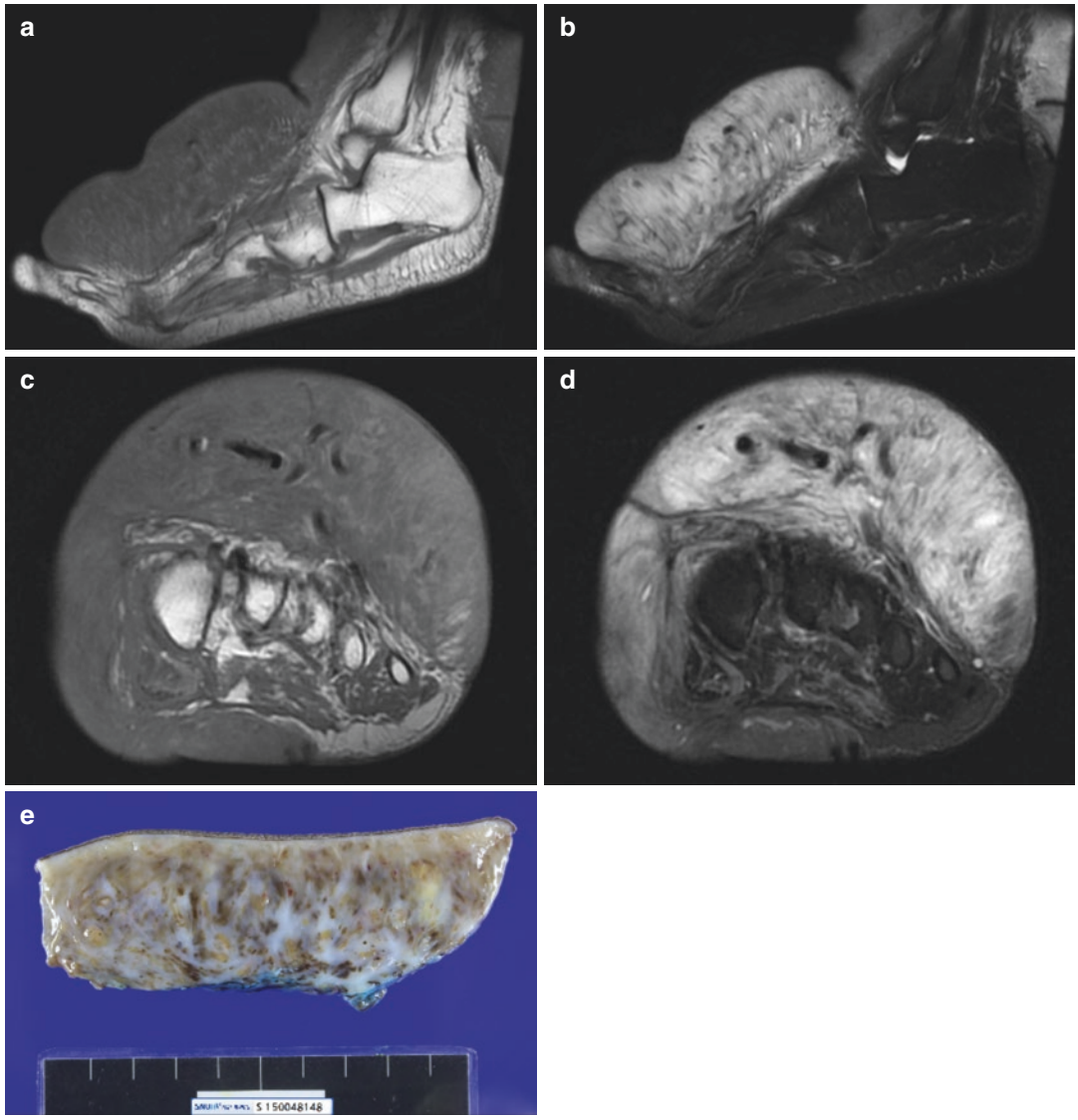

Fig. 12.13 Neurofibroma, diffuse type. Sagittal (**a**) and axial (**c**) T1WIs show a very large plaque-like, infiltrating, inhomogeneous isointense mass in the subcutaneous fat of the foot dorsum, extending from the skin to the fascia. Sagittal FS T2WI (**b**) shows the mass to be generally hyperintense with intralesional tortuous flow voids and multiple thin, linear hypointensities. Axial postcontrast FS T1WI (**d**) shows heterogeneous enhancement. The cut surface (**e**) is variably whitish-ivory in color, with scattered dark brown or brown hemorrhagic foci

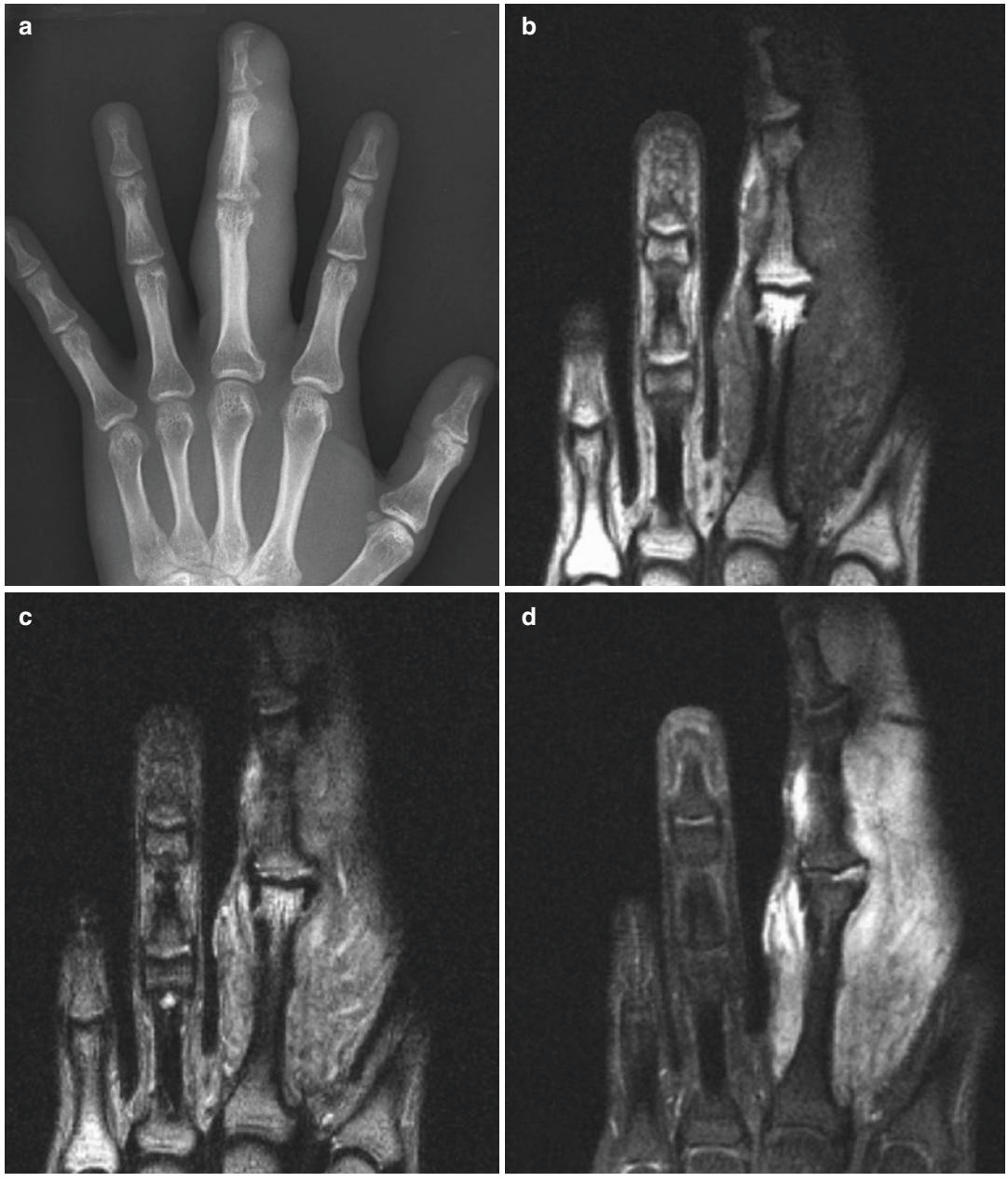

Fig. 12.14 Neurofibroma, diffuse type. Radiograph (**a**) shows increased soft tissue around the middle finger in addition to abnormal elongation, bone pressure erosions, and some proliferation. The infiltrating skin and subcutaneous mass show heterogeneous isointensity on coronal T1WI (**b**) and heterogeneous hyperintensity on T2WI (**c**). Inhomogeneous intense enhancement is observed on post-contrast FS T1WI (**d**)

12.6.6 Extraneural Perineurioma

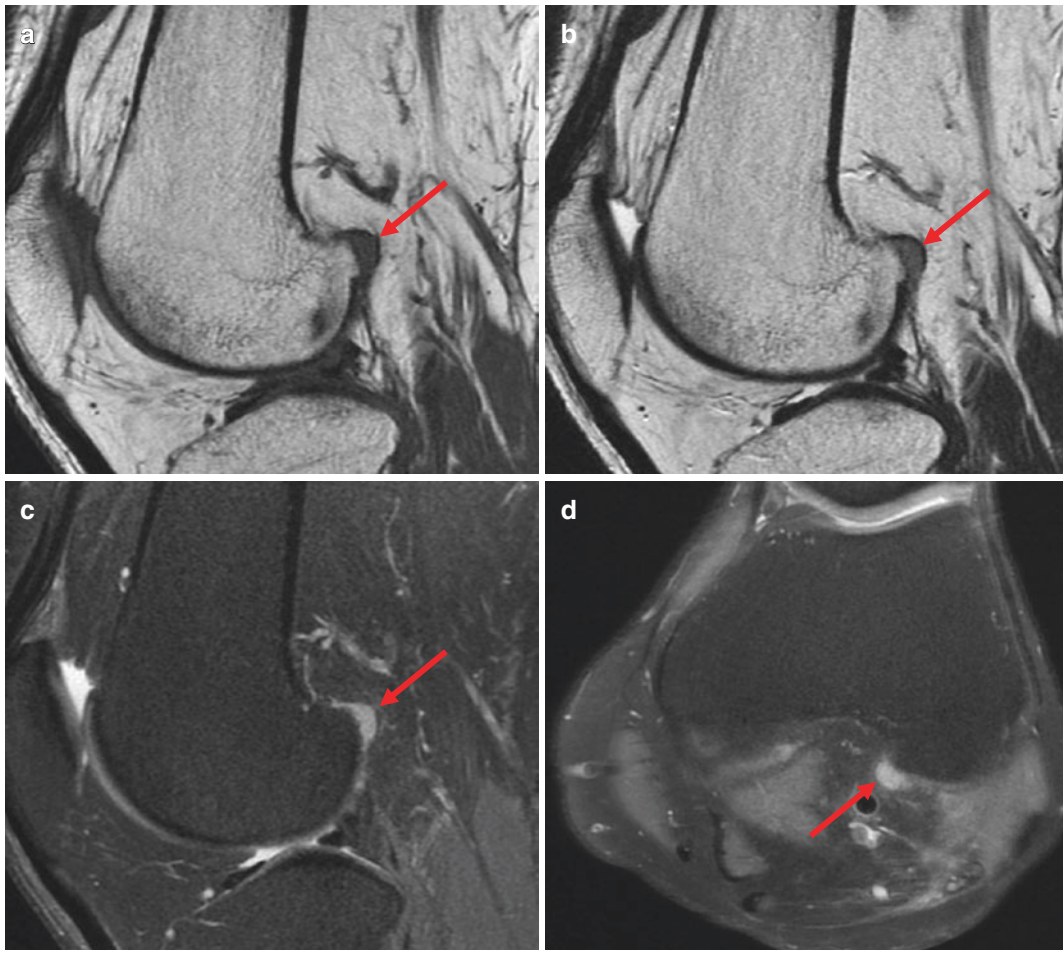

Fig. 12.15 Extraneural perineurioma. Sagittal T1WI (**a**) of the knee reveals a small, circumscribed, periarticular soft tissue nodule that is isointense to muscle. The mass is located posterior to the posterior lateral femoral condyle. The lesion has intermediate signal on T2WI (**b**) and homogeneous contrast enhancement on postcontrast FS T1WI (**c**). Axial FS PDWI (**d**) shows the juxta-articular location of the small hyperintense nodule

12.6.7 Intraneural Perineurioma

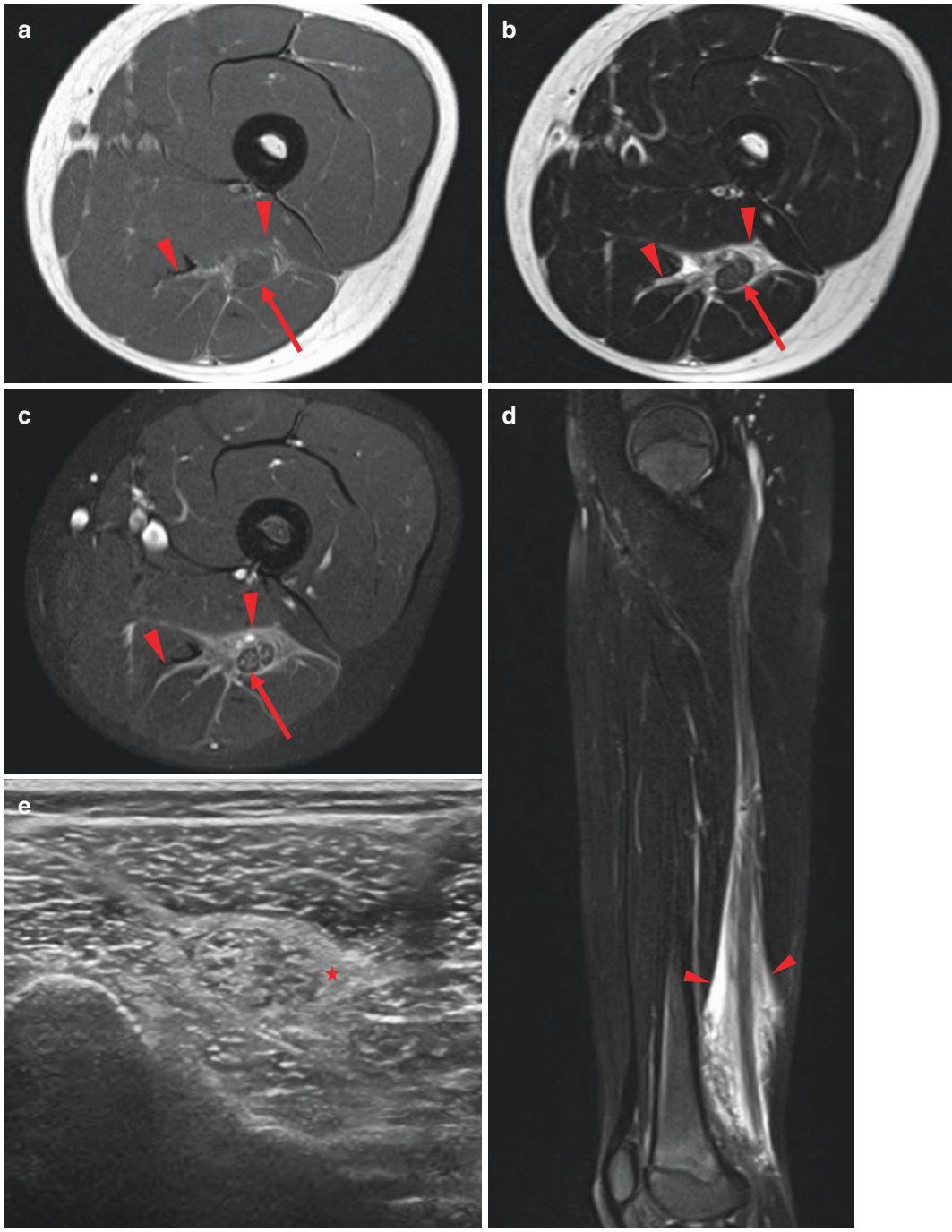

Fig. 12.16 Intraneural perineurioma. Axial T1WI of the thigh (**a**) shows a mild isointense swelling of the sciatic nerve (*arrow*). The affected sciatic nerve has an intermediate signal on T2WI (**b**) and heterogeneous enhancement on postcontrast FS T1WI (**c**), with preservation of the internal fascicular appearance. Sagittal FS T2WI (**d**) demonstrates diffuse involvement of the sciatic nerve, with particularly severe involvement of the distal half. Note the extensive and infiltrative soft tissue change in the intermuscular fat plane around the nerve (*arrowheads*). An enlarged sciatic nerve is observed on US (**e**), with relative preservation of nerve fascicular structures and hyperechoic perineural soft tissue hypertrophy (*star*)

12.6.8 Granular Cell Tumor

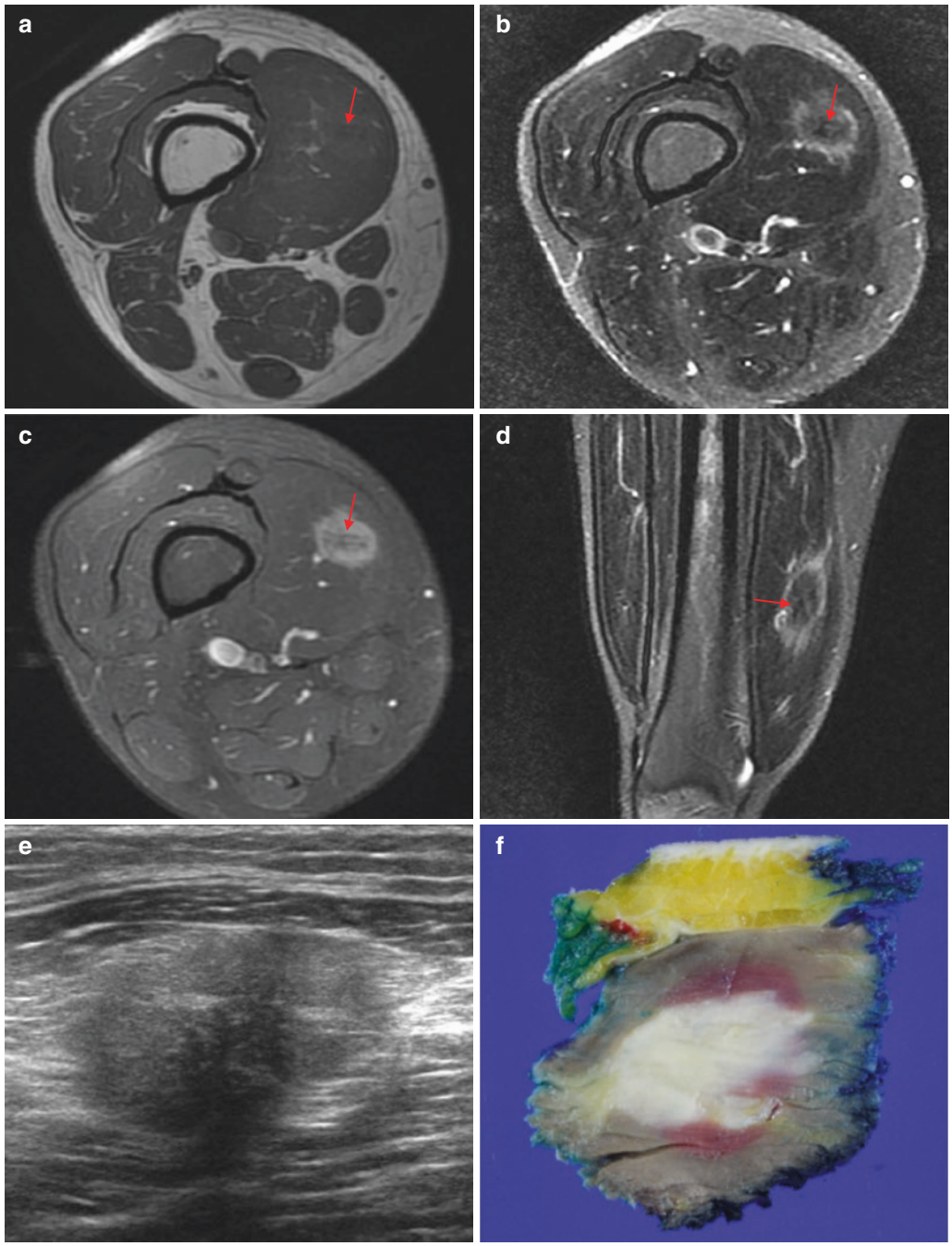

Fig. 12.17 Granular cell tumor. MR images of the thigh show an irregular, speculated bordered soft tissue mass within the vastus medialis muscle. The lesion is isointense to muscle on T1WI (**a**), central heterogeneous hypo/isointensity and peripheral hyperintensity on T2WI (**b**), and inhomogeneous enhancement on postcontrast FS T1WI (**c**). Coronal FS T2WI (**d**) reveals an intermediate signal ovoid mass with irregularly marginated, peripheral T2 hyperintensity. Intratumoral dark signal foci (*small arrows*) on all sequences represent a fibrocollagenous component. US (**e**) on the transverse plane reveals an ill-defined heterogeneous hypoechoic mass with a surrounding, irregular hyperechoic rim. A photograph of the specimen (**f**) shows an irregularly bordered whitish firm mass without hemorrhage or cyst/necrosis

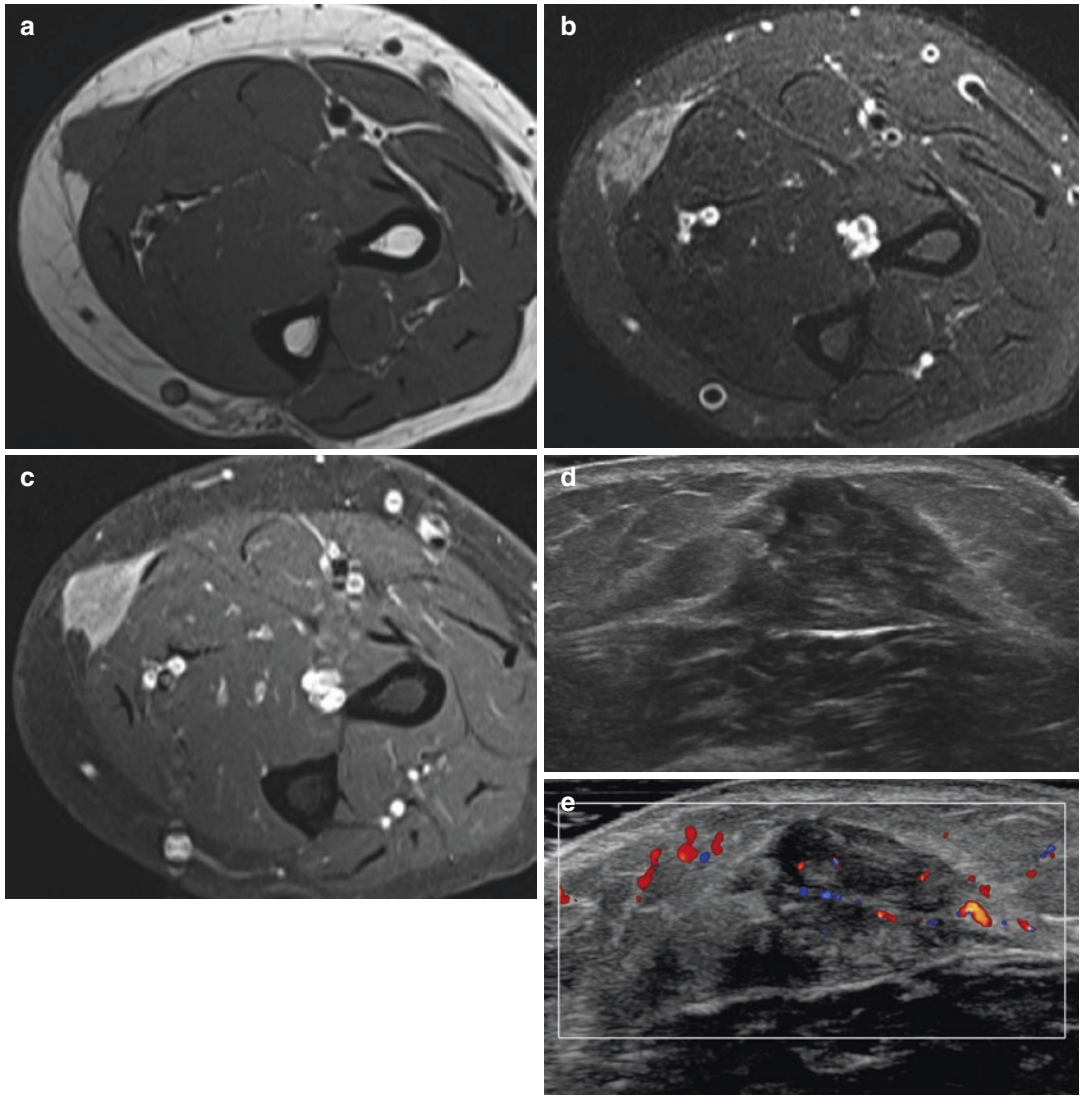

Fig. 12.18 Granular cell tumor. Axial T1WI of the forearm (**a**) reveals an irregularly bordered iso- to slightly hyperintense (relative to muscle) subcutaneous mass, based on the deep fascia. The tumor shows inhomogeneous hyperintensity on FS T2WI (**b**) and intense enhancement on postcontrast FS T1WI (**c**). The tumor has mild mass effect on adjacent muscle without direct tumor extension. US reveals heterogeneous hypoechoic subcutaneous mass with perilesional thin hyperechoic rim and mild intratumoral hypervascularity on color Doppler image (**e**)

12.6.9 Malignant Granular Cell Tumor

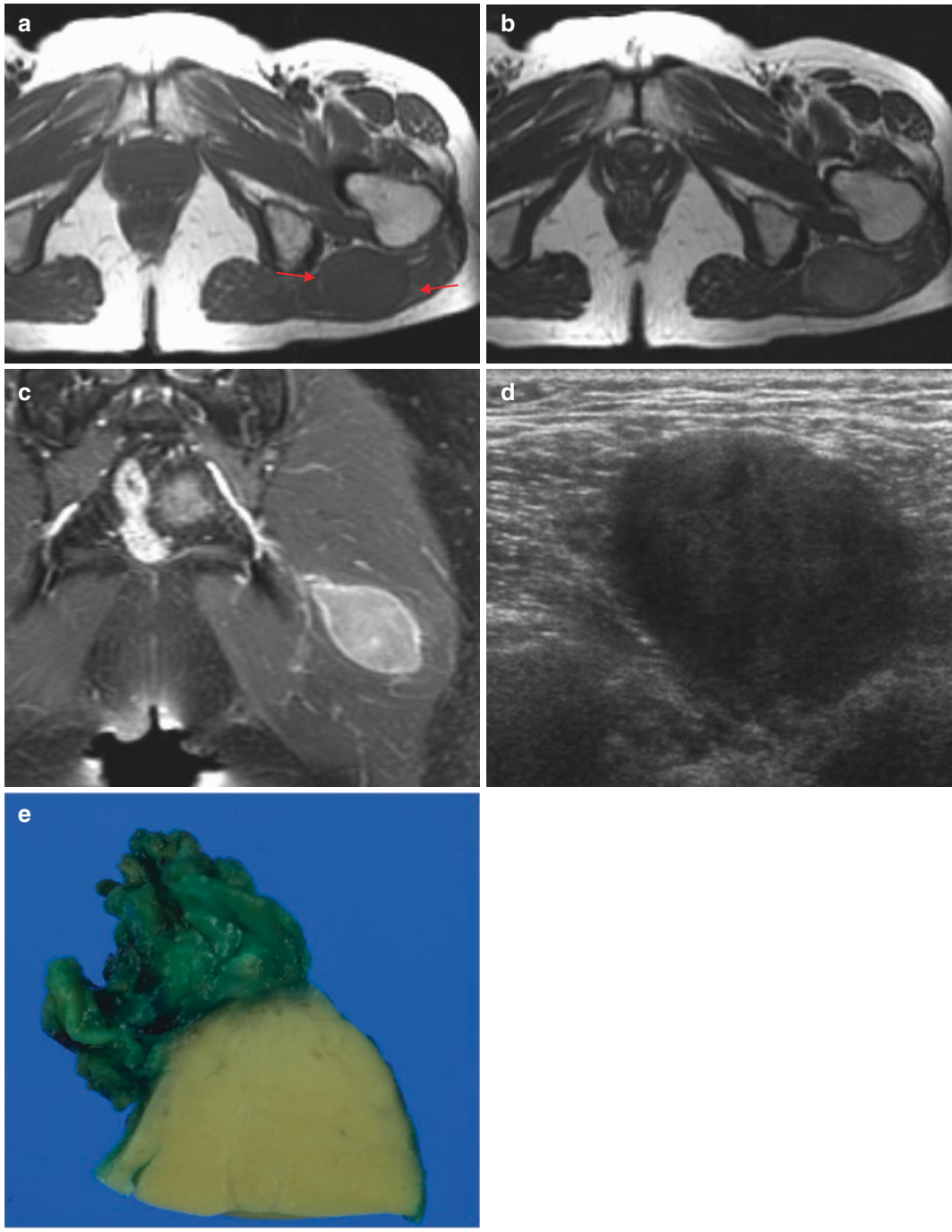

Fig. 12.19 Malignant granular cell tumor. Axial T1WI of the pelvis (**a**) shows a circumscribed, ovoid, isointense (to muscle) mass within the gluteus maximus muscle, with a split-fat sign (*small arrow*). The mass shows inhomogeneous intermediate signal on T2WI (**b**) and heterogeneous enhancement on coronal postcontrast FS T1WI (**c**), with more intense peripheral rim enhancement. US (**d**) reveals a circumscribed, homogeneously hypoechoic intramuscular mass. A photograph of the specimen (**e**) shows a thinly encapsulated, yellowish mass with some myxoid change and no hemorrhaging or necrosis

12.6.10 Malignant Peripheral Nerve Sheath Tumor

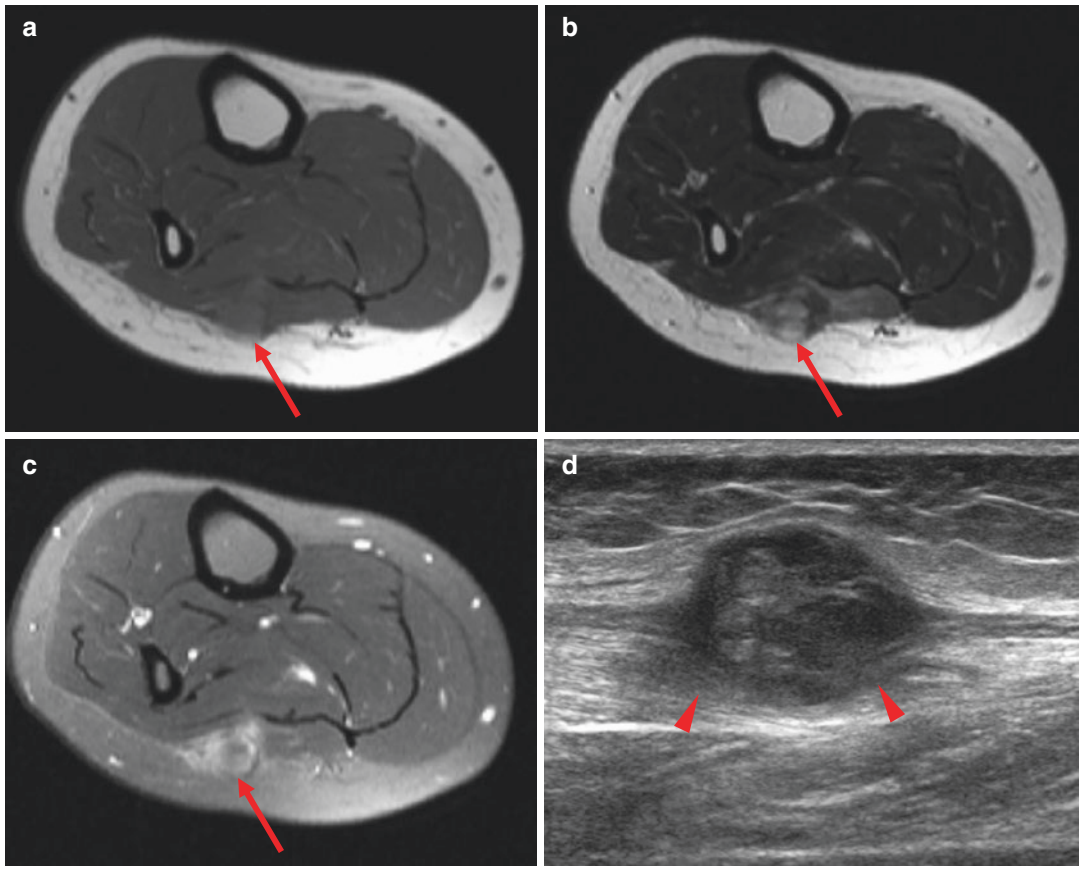

Fig. 12.20 Malignant peripheral nerve sheath tumor. Axial T1WI of the lower leg (**a**) shows an ill-defined, deep-seated, mildly hyperintense soft tissue mass (*arrow*) beneath the crural fascia. The lesion has heterogeneous hyperintensity on T2WI (**b**). Heterogeneous contrast enhancement with an infiltrative border and a focal, internal non-enhancing area are observed on postcontrast FS T1WI (**c**). Longitudinal US (**d**) reveals a heterogeneous hypoechoic mass with some infiltrative borders (*arrowheads*), mild posterior sonic enhancement, and an entering/exiting nerve. Mild perilesional vascularity is observed on the color Doppler images (not shown)

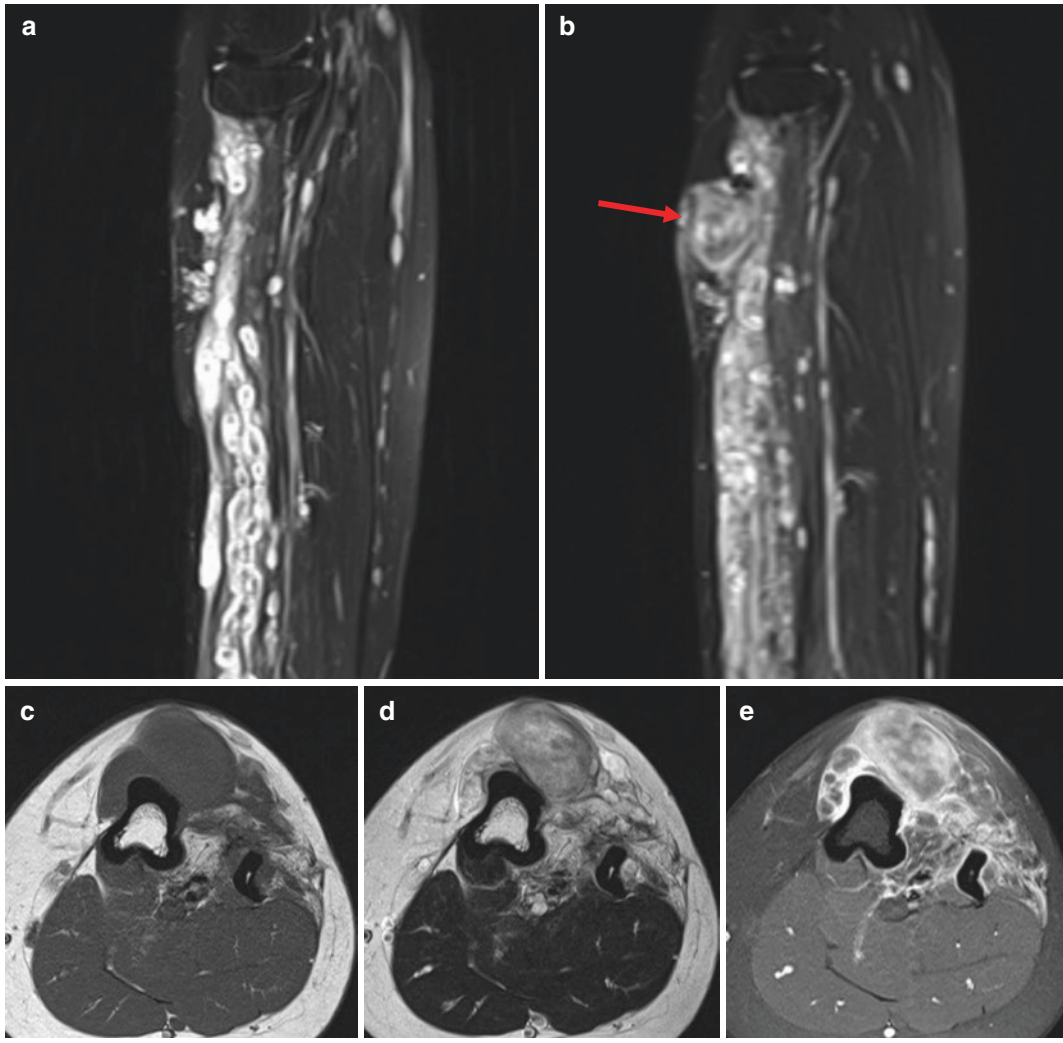

Fig. 12.21 Malignant peripheral nerve sheath tumor. Sagittal FS T2WI (**a**) of the lower leg in a patient with NF-1 shows a typical appearance: a diffuse thickened nerve with nodular plexiform neurofibroma affecting the common peroneal nerve and its branches. The target sign with low signal centrally and high signal intensity peripherally is observed in numerous lesions. Two years later, the patient complained of local pain and swelling at the proximal tibial level. Follow-up sagittal T2WI (**b**) shows internal development of a large subcutaneous mass (*arrow*). The mass is isointense to muscle on T1WI (**c**) and is heterogeneously hyperintense on T2WI (**d**), with inhomogeneous enhancement on postcontrast FS T1WI (**e**). PET (**f**) shows the mass to have higher metabolism (SUV 3.3) (*arrow*) compared with other neurofibromas. On US (**g**), the mass has heterogeneous hypoechogenicity with prominent internal vascularity on the color Doppler image (**h**). Photograph of the sequentially cut surface (**i**) reveals a large firm yellowish mass with an internal curvilinear hemorrhagic area

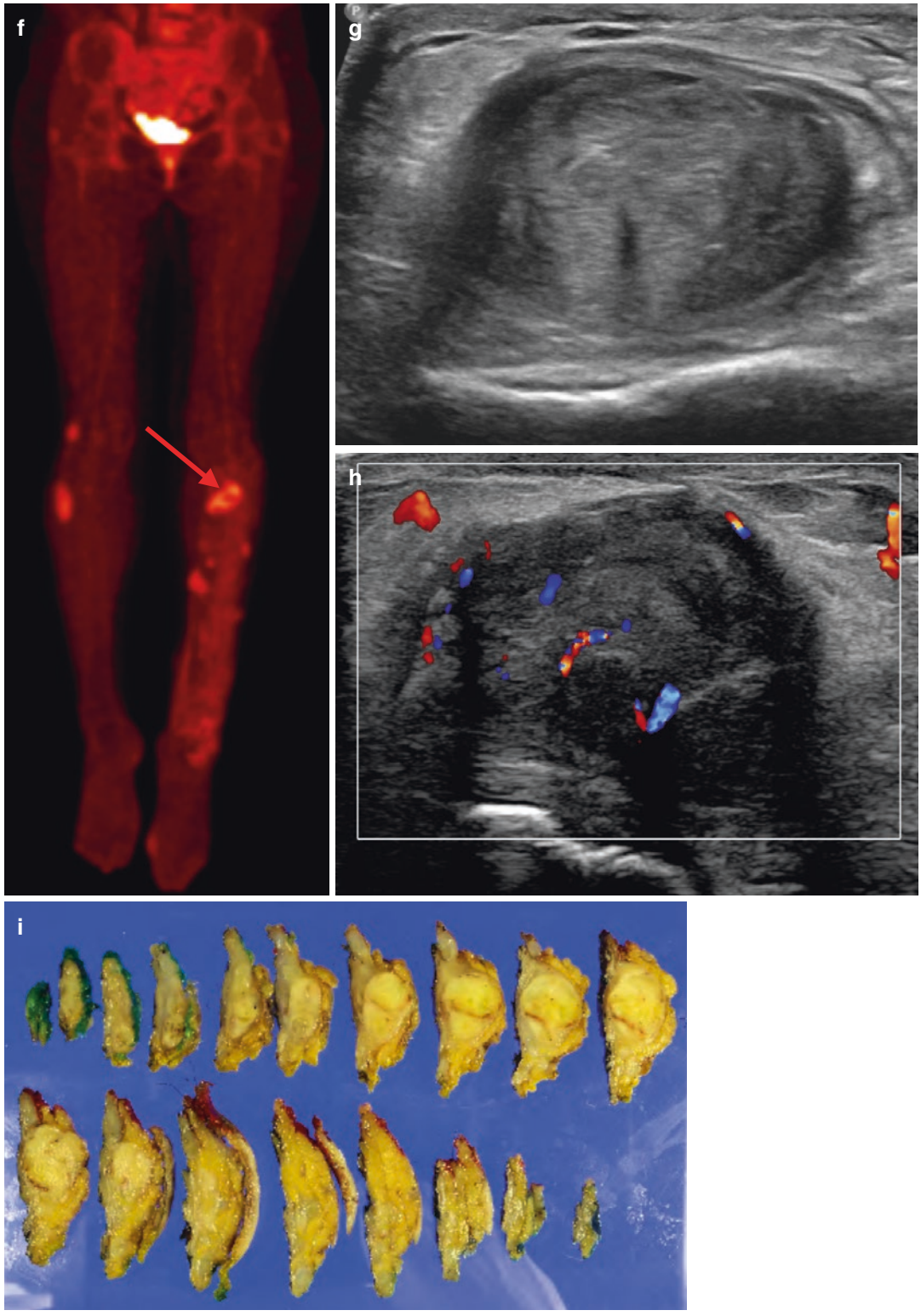

Fig. 12.21 (continued)

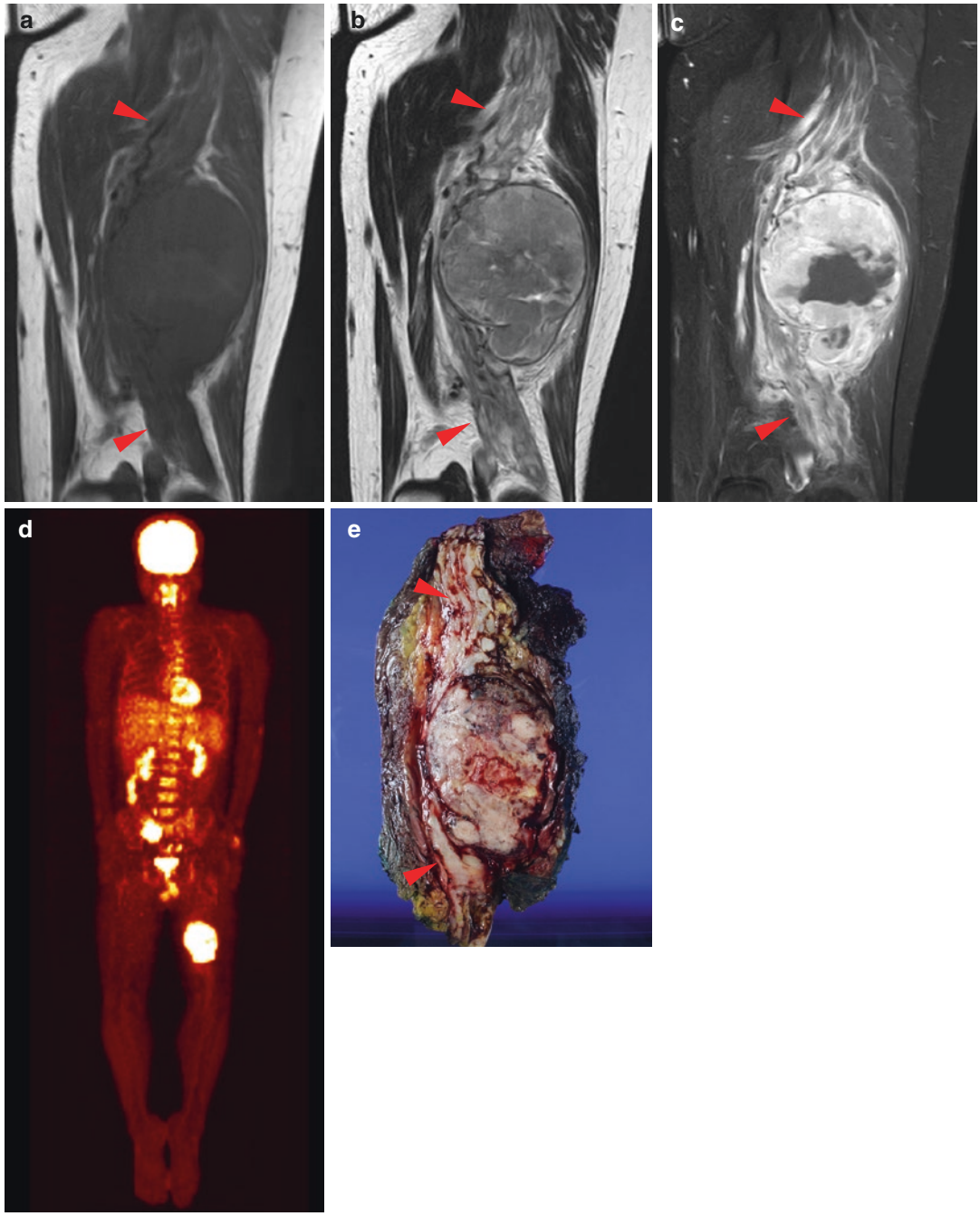

Fig. 12.22 Malignant peripheral nerve sheath tumor. Coronal MR images of the thigh in a patient with NF-1 show a diffuse thickened and nodular sciatic nerve with a "bag of worms" appearance (*arrowheads*), representing plexiform neurofibroma. The large mass eccentric to the sciatic nerve is depicted with inhomogeneous isointense signal (to muscle) on T1WI (**a**), heterogeneous signal (ranging from hypo- to hyperintensity) on T2WI (**b**), and heterogeneous intense enhancement on postcontrast FS T1WI (**c**). A central, mildly T1 hyperintense, T2 intermediate, non-enhancing area is suggestive of hemorrhage. PET (**d**) shows the mass to be markedly hypermetabolic (SUV 18.5) compared with other neurofibromas. A photograph of the specimen (**e**) reveals a large, multinodular, firm whitish mass with an internal hemorrhagic area arising from the underlying plexiform neurofibroma (*arrowheads*)

References

Abreu E, Aubert S, Wavreille G, Gheno R, Canella C, Cotten A. Peripheral tumor and tumor-like neurogenic lesions. Eur J Radiol. 2013;82(1):38–50. doi:10.1016/j.ejrad.2011.04.036.

Antonescu CR, Brems H, Legius E, Woodruff JM. Neurofibroma (including variants). In: Fletcher CDM, Bridge JA, Hogendoorn PCW, Mertens F, editors. WHO classification of tumours of soft tissue and bone. 4th ed. Lyon: International Agency for Research on Cancer; 2013a. p. 174–6.

Antonescu CR, Perry A, Woodruff JM. Schwannoma (including variants). In: Fletcher CDM, Bridge JA, Hogendoorn PCW, Mertens F, editors. WHO classification of tumours of soft tissue and bone. 4th ed. Lyon: International Agency for Research on Cancer; 2013b. p. 170–2.

Banks KP. The target sign: extremity. Radiology. 2005;234(3):899–900. doi:10.1148/radiol.2343030946.

Billeret Lebranchu V. Granular cell tumor. Epidemiology of 263 cases. Arch Anat Cytol Pathol. 1999;47(1):26–30.

Blacksin MF, White LM, Hameed M, Kandel R, Patterson FR, Benevenia J. Granular cell tumor of the extremity: magnetic resonance imaging characteristics with pathologic correlation. Skelet Radiol. 2005;34(10):625–31. doi:10.1007/s00256-005-0925-8.

Grobmyer SR, Reith JD, Shahlaee A, Bush CH, Hochwald SN. Malignant peripheral nerve sheath tumor: molecular pathogenesis and current management considerations. J Surg Oncol. 2008;97(4):340–9. doi:10.1002/jso.20971.

Gruber H, Glodny B, Bendix N, Tzankov A, Peer S. High-resolution ultrasound of peripheral neurogenic tumors. Eur Radiol. 2007;17(11):2880–8. doi:10.1007/s00330-007-0645-7.

Hassell DS, Bancroft LW, Kransdorf MJ, Peterson JJ, Berquist TH, Murphey MD, Fanburg-Smith JC. Imaging appearance of diffuse neurofibroma. AJR Am J Roentgenol. 2008;190(3):582–8. doi:10.2214/AJR.07.2589.

Jee WH, Oh SN, McCauley T, Ryu KN, Suh JS, Lee JH, Park JM, Chun KA, Sung MS, Kim K, Lee YS, Kang YK, Ok IY, Kim JM. Extraaxial neurofibromas versus neurilemmomas: discrimination with MRI. AJR Am J Roentgenol. 2004;183(3):629–33. doi:10.2214/ajr.183.3.1830629.

Kim EY, Kang DK, Kim TH, Jung YS, Kim KS, Yim H. Granular cell tumor of the male breast: two case descriptions and brief review of the literature. J Ultrasound Med. 2011;30(9):1295–301.

Kim ES, Lee SA, Kim BH, Kim CH. Intramuscular granular cell tumor: emphasizing the stripe sign. Skelet Radiol. 2016;45(1):147–52. doi:10.1007/s00256-015-2247-9.

Lack EE, Worsham GF, Callihan MD, Crawford BE, Klappenbach S, Rowden G, Chun B. Granular cell tumor: a clinicopathologic study of 110 patients. J Surg Oncol. 1980;13(4):301–16.

Lazar A. Granular cell tumor. In: Fletcher CDM, Bridge JA, Hogendoorn PCW, Mertens F, editors. WHO classification of tumours of soft tissue and bone. 4th ed. Lyon: International Agency for Research on Cancer; 2013. p. 178–9.

Macarenco RS, Ellinger F, Oliveira AM. Perineurioma: a distinctive and underrecognized peripheral nerve sheath neoplasm. Arch Pathol Lab Med. 2007;131(4):625–36. doi:10.1043/1543-2165(2007)131[625:PADAUP]2.0.CO;2.

Mauermann ML, Amrami KK, Kuntz NL, Spinner RJ, Dyck PJ, Bosch EP, Engelstad J, Felmlee JP, Dyck PJ. Longitudinal study of intraneural perineurioma—a benign, focal hypertrophic neuropathy of youth. Brain. 2009;132(Pt 8):2265–76. doi:10.1093/brain/awp169.

Murphey MD, Smith WS, Smith SE, Kransdorf MJ, Temple HT. From the archives of the AFIP. Imaging of musculoskeletal neurogenic tumors: radiologic-pathologic correlation. Radiographics. 1999;19(5):1253–80. doi:10.1148/radiographics.19.5.g99se101253.

Nielsen GP, Antonescu CR, Lothe RA. Malignant peripheral nerve sheath tumor. In: Fletcher CDM, Bridge JA, Hogendoorn PCW, Mertens F, editors. WHO classification of tumours of soft tissue and bone. 4th ed. Lyon: International Agency for Research on Cancer; 2013. p. 187–9.

Pilavaki M, Chourmouzi D, Kiziridou A, Skordalaki A, Zarampoukas T, Drevelengas A. Imaging of peripheral nerve sheath tumors with pathologic correlation: pictorial review. Eur J Radiol. 2004;52(3):229–39. doi:10.1016/j.ejrad.2003.12.001.

Ryu JA, Lee SH, Cha EY, Kim TY, Kim SM, Shin MJ. Sonographic differentiation between schwannomas and neurofibromas in the musculoskeletal system. J Ultrasound Med. 2015;34(12):2253–60. doi:10.7863/ultra.15.01067.

Tsai WC, Chiou HJ, Chou YH, Wang HK, Chiou SY, Chang CY. Differentiation between schwannomas and neurofibromas in the extremities and superficial body: the role of high-resolution and color Doppler ultrasonography. J Ultrasound Med. 2008;27(2):161–6. quiz 168–169

Wanebo JE, Malik JM, VandenBerg SR, Wanebo HJ, Driesen N, Persing JA. Malignant peripheral nerve sheath tumors. A clinicopathologic study of 28 cases. Cancer. 1993;71(4):1247–53.

Yu YH, Wu JT, Ye J, Chen MX. Radiological findings of malignant peripheral nerve sheath tumor: reports of six cases and review of literature. World J Surg Oncol. 2016;14:142. doi:10.1186/s12957-016-0899-0.

Tumors of Uncertain Differentiation

13

Tumors of uncertain differentiation include many soft tissue tumors that have an unclear line of cellular differentiation. In some tumors (e.g., mixed tumors, synovial and clear cell sarcomas), a line of differentiation can be identified, but a cellular counterpart of the tumor cannot be defined in normal mesenchymal tissues (Kransdorf 2014).

There were some minor changes in the latest version of the WHO classification (Fletcher et al. 2013); specifically, two tumors were added to this category. The first of these is 'hemosiderotic fibrolipomatous tumor (HFLT)', which is a locally aggressive neoplasm that commonly arises around the ankle or wrist. The second addition to this category is 'phosphaturic mesenchymal tumor (PMT)'. In addition, in the 2013 WHO classification, the term 'primitive neuroectodermal tumor (PNET)' has been removed as a synonym for Ewing sarcoma with a variable degree of neuronal differentiation. This change was made to minimize confusion with PNET of the central nervous system and female genital tract, which is histologically and genetically different from PNET in the extremities (Fletcher et al. 2013).

13.1 Intramuscular Myxoma

Intramuscular myxoma is a benign mesenchymal lesion composed of spindle- to stellate-shaped fibroblasts, paucicellular myxoid matrix, and sparse blood vessels (Luna et al. 2005). Patients usually present with a slowly growing palpable mass without pain or tenderness. The age of presentation is 40–70 years of age, with a female predilection (Zou et al. 2013). The most frequent sites of these tumors are the intramuscular compartments of the thigh (51%), upper arm (9%), calf (7%), or buttock (7%) (Murphey et al. 2002). The coexistence of multiple myxomas and fibrous dysplasia of the bone, generally in the same anatomic region, is referred to as Mazabraud syndrome (Kabukcuoglu et al. 2004; Delabrousse et al. 2001; Perez Sanchez and Gonzalez Llorente 2014).

Imaging findings of myxoma are similar to those of a cyst on CT and MR imaging, showing a lesion composed of a large amount of mucin and a low collagen content, as observed histologically (Murphey et al. 2002). Myxoma is a well-circumscribed, homogeneous intramuscular mass with very high signal intensity on T2-weighted MR images, quite similar to the signal characteristic of fluid (Murphey et al. 2002; Yao et al. 2007; Bancroft et al. 2002). This lesion shows a variable degree of contrast enhancement proportional to the amount of solid myxoid tissue and fibrous septa within the tumor, allowing it to be differentiated from cystic lesions. US shows a well-defined, heterogeneous hypoechoic mass surrounded by normal muscle, occasionally accompanied by small, fluid-filled clefts and cystic areas. The detection of internal echoes of the mass is useful in the differentiation of a solid mass from a cystic lesion. A sonographic bright rim sign of echogenicity around the mass may

H.S. Kang et al., *Oncologic Imaging: Soft Tissue Tumors*, DOI 10.1007/978-981-287-718-5_13

reflect increased fat deposition around intramuscular myxoma (Girish et al. 2006; Kim 2014). On color Doppler study, these lesions often show little or no vascularity due to a paucity of vascular structures within the tumor. Mucoid material may leak into the immediately adjacent muscle, which could lead to muscle atrophy with surrounding fat deposition and/or muscle edema. These histologic findings correspond to presence of a small rim of fat and/or surrounding edema on MR imaging and a bright rim sign of echogenicity around the mass on ultrasonography (Bancroft et al. 2002; Girish et al. 2006; Murphey et al. 2002).

13.2 Synovial Sarcoma

Synovial sarcoma is a relatively common soft tissue sarcoma in adults, accounting for approximately 5–10% of soft tissue sarcomas (Kransdorf 1995; Kempson et al. 2001). Synovial sarcoma typically occurs in adolescents and young adults between 15 and 35 years of age. Patients with synovial sarcoma usually present with a palpable, slowly growing soft tissue mass that may give a false impression of a benign process, and there is often a delay in diagnosis.

Synovial sarcoma is a misnomer because it does not arise from or differentiate toward the synovium. Synovial sarcoma is thought to originate from primitive (uncommitted) mesenchymal cells with variable degrees of epithelial differentiation. Histologically, synovial sarcoma is composed of two morphologically different cell types (epithelial and spindle cells) and can be classified into three subtypes depending on cell type composition and differentiation. The biphasic type consists of spindle cells and epithelial cells (usually forming glands). The monophasic type is predominantly made up of mesenchymal spindle cells and is relatively common. The poorly differentiated type consists of cells that are generally epithelioid in morphology and have high mitotic activity; the clinical behavior of this type is more aggressive (Murphey et al. 2006; Vliet et al. 2009; Bakri et al. 2012). A specific chromosomal translocation t(X;18)(p11;q11) has been reported in association with synovial sarcoma (Murphey et al. 2006).

Unlike other soft tissue sarcomas, eccentric or peripheral mineralization is identified within the mass in approximately 20–30% of cases on radiography (Murphey et al. 1999). CT is useful for detecting calcification and bone involvement in synovial sarcoma (Murphey et al. 2006; Vliet et al. 2009). On T2-weighted MR images, synovial sarcoma has a markedly heterogeneous signal intensity pattern that is referred to as a 'triple sign', being characterized by intermixed areas of low (dystrophic calcifications and fibrotic bands), intermediate (soft tissue components), and high signal intensity (necrosis and hemorrhage) (Murphey et al. 2006; Vliet et al. 2009). There may be areas of hemorrhage with fluid-fluid levels in up to 10–25% of the tumors, a sign that is known as a 'bowl of grapes' (Jones et al. 1993; Murphey et al. 2006; Vliet et al. 2009). Lesions smaller than 5 cm are often superficial and frequently well-defined, mimicking benign processes in terms of homogeneous signal characteristics and a lack of invasion into adjacent structures (Jones et al. 1993; Murphey et al. 2006; Vliet et al. 2009). Contrast enhancement is usually prominent and can be heterogeneous or homogeneous. Dynamic contrast-enhanced MR images (DCE-MRI) show a rapid progressive linear increase in signal intensity followed by a washout or plateau in 60% of cases (Van Rijswijk et al. 2001). Several MR features have been reported as prognostic parameters associated with high tumor grade and a less favorable prognosis. Imaging findings favoring a diagnosis of high-grade tumor included proximal distribution, large tumor size, the absence of calcifications, the presence of cysts, the presence of hemorrhage, and the presence of a triple signal pattern (Tateishi et al. 2004).

13.3 Phosphaturic Mesenchymal Tumor

Phosphaturic mesenchymal tumor (PMT) is a rare soft tissue or bone tumor that is often associated with a paraneoplastic syndrome known as tumor-induced (oncogenic) osteomalacia (TIO). The tumor appears to overexpress fibroblast growth factor 23 (FGF-23), which inhibits renal tubular

epithelial phosphate transport, resulting in osteomalacia (Folpe et al. 2004). Previously, these tumors were considered a heterogeneous group of bone and soft tissue tumors, including hemangiopericytoma, hemangioma, giant cell tumor, or osteoblastoma. However, it has been recognized by certain investigators that many of these tumors are, in fact, quite distinctive when carefully evaluated (Folpe et al. 2004). In 1987, Weidner and Santa Cruz used the term 'phosphaturic mesenchymal tumor, mixed connective tissue type (PMTMCT)' to describe these unique lesions, which are characterized by a distinctive admixture of spindled cells, osteoclast-like giant cells, microcysts, prominent blood vessels, cartilage-like matrix, and bone (Weidner and Santa Cruz 1987). The authors divided PMTs into the following four subtypes based on histology: (1) mixed connective tissue tumors (PMTMCT); (2) osteoblastoma-like tumors; (3) non-ossifying fibroma-like tumors; and (4) ossifying fibroma-like tumors. PMTMCT is the most common type, accounting for over 90% of TIO-associated mesenchymal tumors (Weidner and Santa Cruz 1987; Folpe et al. 2004).

PMT often occurs in middle-aged adults in the soft tissue and bone. In many cases, the patients presented with a long-standing history of osteomalacia, generalized fatigue, and pain with multiple pathologic fractures. Those nonspecific symptoms and a vague clinical presentation often result in a long delay in the diagnosis and treatment of patients with PMT. Once the diagnosis of PMT is considered, tumor localization is the next challenging issue due to their variable location and small size. Compartmental venous sampling of FGF-23 has been useful in localization of the body region in which the tumor is located. Then, MR imaging of the body region can be performed to identify the lesion. Octreotide scanning is another helpful imaging technique for localizing these small tumors because they may express somatostatin receptors.

Although most PMTs are histologically and clinically benign, surgical resection of the causative tumor is the treatment of choice to completely resolve the symptoms. The prognosis of PMT is generally good, but rare metastatic cases have been described (Ogose et al. 2001).

13.4 Epithelioid Sarcoma

Epithelioid sarcoma typically affects adolescents and young adults between 10 and 35 years of age (Hanna et al. 2002). There are two principal types of epithelioid sarcoma as follows: the conventional (classical or distal) type and the proximal type (Guillou et al. 1997; Chbani et al. 2009). Conventional-type epithelioid sarcoma most commonly arises on the flexor surfaces of the fingers, hands, and forearm, followed by the knee/lower leg and the buttocks/thigh (Chase and Enzinger 1985). The proximal-type epithelioid sarcoma has a predilection for arising in axial locations (e.g., perineum, pelvis, vulva, and buttocks) and more aggressive behavior (Tateishi et al. 2002). The tumor occurs in both the superficial and deep soft tissues. When located superficially, it usually presents as a firm nodule that may be solitary or multiple. Superficial lesions are often elevated above the skin surface and become ulcerated in 10% of cases. Deep-seated lesions are usually firmly attached to tendons, tendon sheaths, or fascial structures, being infiltrative and heterogeneous in appearance (Hanna et al. 2002).

Radiograph or CT can reveal calcification or, rarely, ossification in 8–28% of cases (Lo et al. 1977; Tateishi et al. 2002). The MR features are generally nonspecific. The tumor may present as infiltrative intramuscular masses or as cutaneous nodules. Large lesions can exhibit an inhomogeneous signal pattern on T2-weighted images due to the presence of hemorrhage or necrosis. The tumor is usually isointense to the muscle on T1-weighted images but occasionally demonstrates high signal intensity, which corresponds to areas of hemorrhagic necrosis. A peritumoral edema-like signal that affects the surrounding muscles is observed in nearly 70% of cases and histologically corresponds to intense inflammation (Hanna et al. 2002). The tumor may demonstrate multiple intrinsic hypointense foci on both T1- and T2-weighted images, corresponding to abundant soft tissue calcifications. Other common findings include tumor encasement of the adjacent neurovascular bundle and enlarged regional lymph nodes (Hanna et al. 2002). Although the tumor has nonspecific

imaging findings, suspicion for epithelioid sarcoma should arise in patients presenting with multiple soft tissue nodules or persistent punched-out ulcers involving the skin and subcutaneous tissues, particularly of the extremities (Hanna et al. 2002). Epithelioid sarcoma is notorious for multiple recurrences and high propensity to metastasize to regional lymph nodes and the lung (Chase and Enzinger 1985; Hanna et al. 2002).

13.5 Alveolar Soft Part Sarcoma

Alveolar soft part sarcoma is a relatively rare malignant soft tissue tumor, constituting fewer than 1% of all soft tissue sarcomas. This tumor was named by Christopherson et al., who observed the cells to have a characteristic 'pseudoalveolar or organoid arrangement' formed by aggregates of large granular cells surrounded by vascular channels that mimic the pattern of respiratory alveoli (Christopherson et al. 1952).

Alveolar soft part sarcoma occurs principally in adolescents and young adults and is most frequently observed in the thigh or buttock (Lieberman et al. 1966; Lieberman et al. 1989; Portera et al. 2001; Anderson et al. 2005; Pennacchioli et al. 2010). When the tumor affects infants and children, it is often located in the region of the head and neck, especially the orbit and tongue (Casanova et al. 2000; Orbach et al. 2013). It usually presents as a slowly growing, painless mass. The mass may be pulsatile with an associated bruit. Although the tumor is slow growing, it has a high rate of metastasis, which is thought to be due to the extreme vascularity of the tumor and its early microvascular invasion (Anderson et al. 2005). The common sites of metastases are the lung, followed by the brain and bone.

Radiographs may demonstrate a nonspecific soft tissue mass, but punctate calcification may be observed (Lorigan et al. 1989). Alveolar soft part sarcoma is so hypervascular that angiography reveals hypervascularity with prominent draining veins and prolonged capillary staining (Suh et al. 2000; McCarville et al. 2014; Tian et al. 2016). Ultrasonography may be useful to identify the hypervascular nature of the tumor. CT demonstrates a soft tissue mass with isoattenuation to that of the adjacent muscle. After contrast administration, the mass enhances markedly with prominent feeding arteries and draining veins (Tian et al. 2016). On MR imaging, this tumor typically shows an equal or hyperintense signal intensity on T1-weighted images and a heterogeneous high signal intensity on T2-weighted images, with multiple flow voids. Serpentine flow voids can be observed at the margin of the lesion and within the mass. After contrast medium administration, intense enhancement and tortuous and dilated vessels can be observed in and around the mass. Although arteriovenous malformation (AVM) could be considered a differential diagnosis, AVM differs from alveolar soft part sarcoma based on a rapid washout of contrast on dynamic contrast-enhanced MR images and a lack of a soft tissue component (Suh et al. 2000; McCarville et al. 2014; Tian et al. 2016).

13.6 Clear Cell Sarcoma

Clear cell sarcoma predominantly affects young adults between the ages of 20 and 40 years (Goldblum et al. 2014). The patient presents with a slowly growing mass, which causes pain or tenderness in nearly half of cases. In the past, this tumor has been referred to as 'malignant melanoma of soft parts' due to its histologic similarities to malignant melanoma (Chung and Enzinger 1983; Lucas et al. 1992; Graadt van Roggen et al. 1998). Intracellular melanin can be identified in 72% of cases (Chung and Enzinger 1983, 163). However, clear cell sarcoma is clinically and biologically distinct from cutaneous melanoma. This tumor primarily arises in the deep soft tissues of the lower extremities (foot, ankle, knee and thigh), adjacent to tendons, aponeuroses, and fascial structures (Lucas et al. 1992). Most of the tumor has a consistent balanced translocation t(2;22)(q13;q12) that can help distinguish it from cutaneous malignant melanoma (Reeves et al. 1992; Rodriguez et al. 1992; Langezaal et al. 2001; Segal et al. 2003).

Radiographs do not contribute to the diagnosis and may only show the nonspecific soft tissue mass. On MR imaging, clear cell sarcomas usually

present as well-circumscribed lesions with variable signal intensity on T1-weighted and T2-weighted images. Approximately 50% of tumors have slightly increased signal intensity on T1-weighted images compared with the muscle and display melanocytic differentiation (De Beuckeleer et al. 2000; Hourani et al. 2005). The paramagnetic effect of intratumoral melanin causes a shortening of T1 relaxation time, leading to increased signal intensity on T1-weighted images. As T1 hyperintensity is rarely observed in soft tissue tumors, this characteristic MR image helps to narrow the list of differential diagnoses (De Beuckeleer et al. 2000; Hourani et al. 2005). After intravenous contrast administration, strong enhancement is observed in most cases. As clear cell sarcoma has a benign-looking appearance on MR imaging, the diagnosis should be suspected when the lesion is a well-defined, homogeneous, strongly enhancing mass with a slightly higher signal intensity compared with the muscle on T1-weighted images.

13.7 Extraskeletal Myxoid Chondrosarcoma

Extraskeletal myxoid chondrosarcomas typically occur in the extremities, with a predilection for the thigh. It commonly affects patients aged 50–60 years but is also known to occur in younger people (Enzinger and Shiraki 1972; Kapoor et al. 2014). The tumor is more common in males, with a male:female ratio of 2:1 (Kransdorf and Meis 1993; Kapoor et al. 2014). Histologically, the tumor composed of chondroblast-like cells in an abundant myxoid matrix resembling embryonic cartilage. However, despite its name, the WHO has classified it as a tumor of uncertain differentiation due to its lack of cartilaginous differentiation. Additionally, cytogenetic studies have shown that the tumor has a reciprocal translocation, t(9;22)(q22;q12), not observed in conventional skeletal chondrosarcoma (Kapoor et al. 2014; Drilon et al. 2008).

Radiography or CT shows a soft tissue mass that does not contain calcifications or bone formation. The tumor appears on CT and MR imaging as a well-defined, large, and multilobular soft tissue mass. Highly myxoid lesions exhibit low attenuation on CT and very high signal intensity on T2-weighted MR images, indicating its extremely high water content. Lobules of very high signal intensity may be defined by thin fibrous septa of low signal intensity on T2-weighted image. On T1-weighted images, the tumor is heterogeneously isointense to the muscle and frequently shows hyperintense foci that correspond to hemorrhagic changes within the tumor. After intravenous contrast administration, the tumor also shows peripheral/septal enhancement, as observed in a chondroid tumor (Gebhardt et al. 1999; Tateishi et al. 2006; Kapoor et al. 2014).

13.8 Extraskeletal Ewing Sarcoma

Extraskeletal Ewing sarcoma usually manifests in young patients between 10 and 30 years of age. Males are affected slightly more commonly than females. Clinically, patients often have a large, rapidly growing, solitary, superficial, or deep soft tissue mass (Murphey et al. 2013). The most commonly reported locations of extraskeletal Ewing sarcoma include the paravertebral region (32%), lower extremities (26%), chest wall (18%), retroperitoneum (11%), pelvis and hip (11%), and upper extremities (3%) (Murphey et al. 2013). Histologically, the tumor has monotonous proliferation of solidly packed small blue round cells with no differentiating features. Necrosis, cystic changes, and hemorrhage are commonly found. Extraskeletal Ewing sarcoma shares the same cytogenetic marker [translocation of chromosomes t(11;22)(q24;q12)] with other Ewing sarcoma tumors (i.e., osseous Ewing sarcoma, soft tissue primitive neuroectodermal tumor, and Askin tumor).

Extraskeletal Ewing sarcoma commonly demonstrates a nonspecific radiologic appearance of a large soft tissue mass affecting the paraspinal region or lower extremity. CT commonly exhibits isoattenuation to the muscle but may demonstrate low attenuation, likely corresponding to areas of hemorrhage or necrosis. Calcification is atypical, occurring in approximately 10% of tumors at presentation (Javery et al. 2011). MR imaging demonstrates heterogeneous signal intensity similar to that of the muscle on T1-weighted images and intermediate to high signal intensity on

T2-weighted images. The high cellularity of the tumor likely accounts for the intermediate signal intensity on T2-weighted image. Areas of hemorrhage appear as high signal intensity, and focal areas of necrosis are observed as low signal intensity on T1-weighted images and high signal intensity on T2-weighted images. The presence of high-flow vascular channels is an additional image feature of extraskeletal Ewing sarcoma. These channels have low signal intensity for all pulse sequences. This finding can be observed in hypervascular lesions, but the possibility of extraskeletal Ewing sarcoma should be considered if flow voids are observed in young adults with a large intramuscular mass (Murphey et al. 2013).

13.9 Extrarenal Malignant Rhabdoid Tumor

Extrarenal malignant rhabdoid tumors are extremely rare. Most tumors occur in children less than 1 year of age and have a very poor prognosis (Oda and Tsuneyoshi 2006; Abdullah et al. 2010). The tumors may arise at a variety of locations, including the liver, heart, and gastrointestinal system. Soft tissue lesions seem to arise most frequently in deep, axial locations, including the trunk, extremities, neck, and paraspinal regions (Kodet et al. 1991; Garces-Inigo et al. 2009). Cutaneous lesions are also described. Clinically, the tumor presents as a rapidly growing soft tissue mass.

CT images reveal a well-defined, large, and low-attenuated mass, and T2-weighted MR images show heterogeneous high signal intensity (Garces-Inigo et al. 2009). The tumor is heterogeneously enhanced after intravenous contrast administration. The imaging characteristics of soft tissue rhabdoid tumors have yet to be determined, largely because of their rarity.

13.10 Myoepithelioma/ Parachordoma

Tumors in this category are extremely rare tumors composed of epithelial and myoepithelial elements in varying proportions; these tumors exist within a hyalinized to chondromyxoid stroma. The tumor resembles pleomorphic adenoma, and a lack of obvious ductal differentiation leads to a designation of myoepithelioma. Parachordoma closely resembles myoepithelioma and is best considered within this spectrum (Fisher and Miettinen 1997). This tumor is histologically similar to chordoma but is observed in non-axial soft tissues, usually occurring in the deep soft tissues of the extremities and occasionally in the retroperitoneum. Previous reports have revealed a male predilection, occurring in the fourth to sixth decade of life. These tumors have a nonspecific imaging appearance on CT and MR imaging (Abbes et al. 2008; Clabeaux et al. 2008; Ali et al. 2013).

13.11 Pleomorphic Hyalinizing Angiectatic Tumor

The pleomorphic hyalinizing angiectatic tumor (PHAT) is a rare tumor of uncertain lineage described by Smith et al. in 1996 (Smith et al. 1996). The tumor is histologically composed of clusters of ectatic, fibrin-lined, thin-walled vessels surrounded by sheets and fascicles of spindled and pleomorphic cells. A variable inflammatory component is also observed (Smith et al. 1996). The tumor occurs most commonly in the subcutaneous tissues of the lower extremities in adults. The tumor may be associated with hemorrhage, giving the clinical impression of a hematoma or Kaposi's sarcoma. While the tumor may be locally aggressive with a high rate of local recurrence (33–50%), no case of metastatic disease has been reported (Folpe and Weiss 2004; Subhawong et al. 2012).

The imaging findings of PHAT have not been reported in detail in the radiology literature. A relatively small number of studies have described nonspecific MR characteristics for this tumor, namely, that it is isointense to the muscle on T1-weighted images and heterogeneously hyperintense on T2-weighted images, with enhancement on contrast-enhanced T1-weighted images (Subhawong et al. 2012; Suzuki et al. 2014).

13.12 Illustrations: Tumors of Uncertain Differentiation

13.12.1 Intramuscular Myxoma

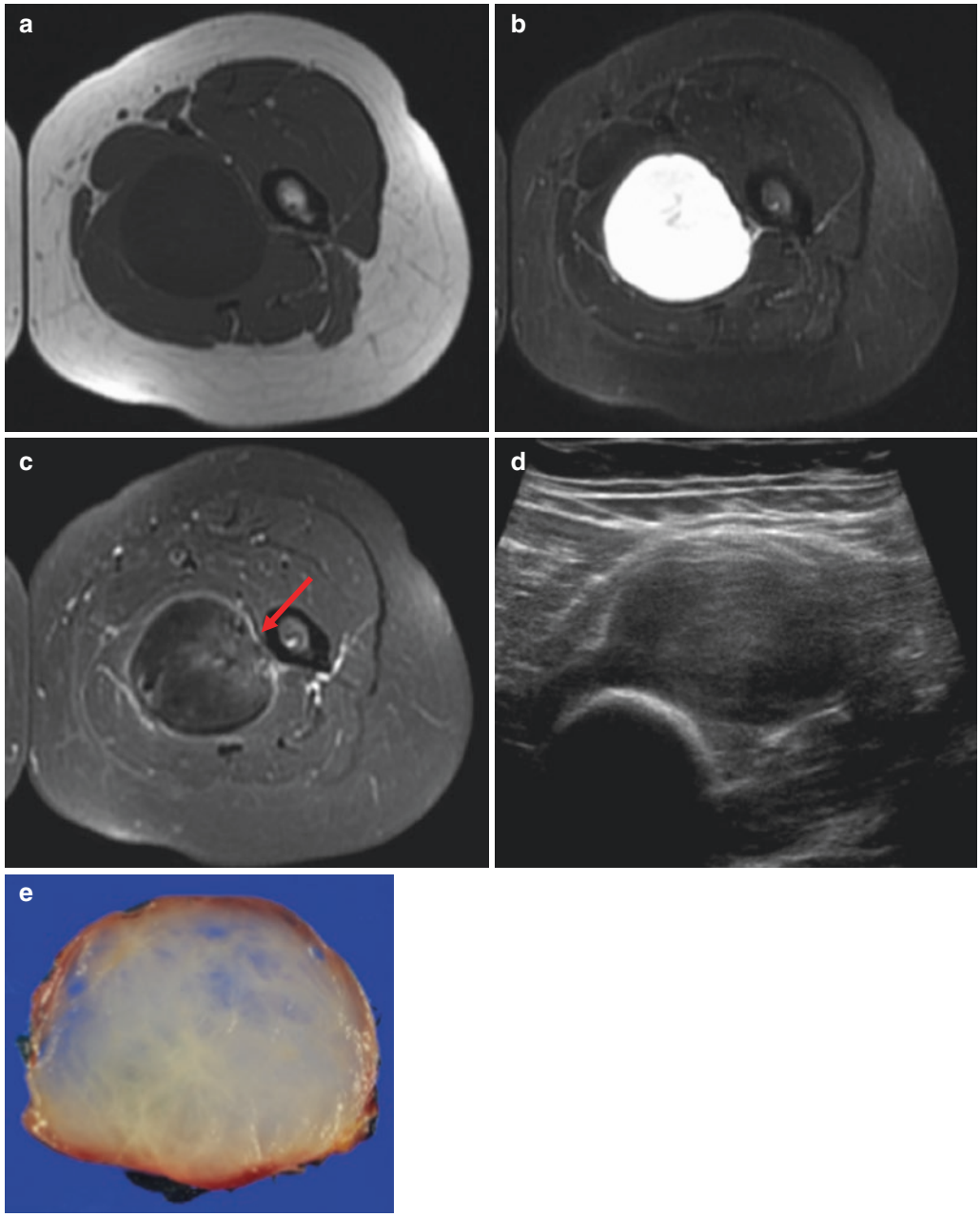

Fig. 13.1 Intramuscular myxoma. Axial T1WI (**a**) reveals the intramuscular mass to be homogeneously hypointense relative to the adjacent muscle. Axial FS T2WI (**b**) shows a well-defined bright hyperintense soft tissue mass located within the adductor magnus muscle. Axial postcontrast FS T1WI (**c**) demonstrates typical minimal patchy enhancement (*arrow*) of the mass. US (**d**) shows a low echoic mass with detectable internal echoes, a finding that is useful in differentiating it from the cystic mass. Surgical specimen (**e**) shows a well-circumscribed, gelatinous mass with internal septa

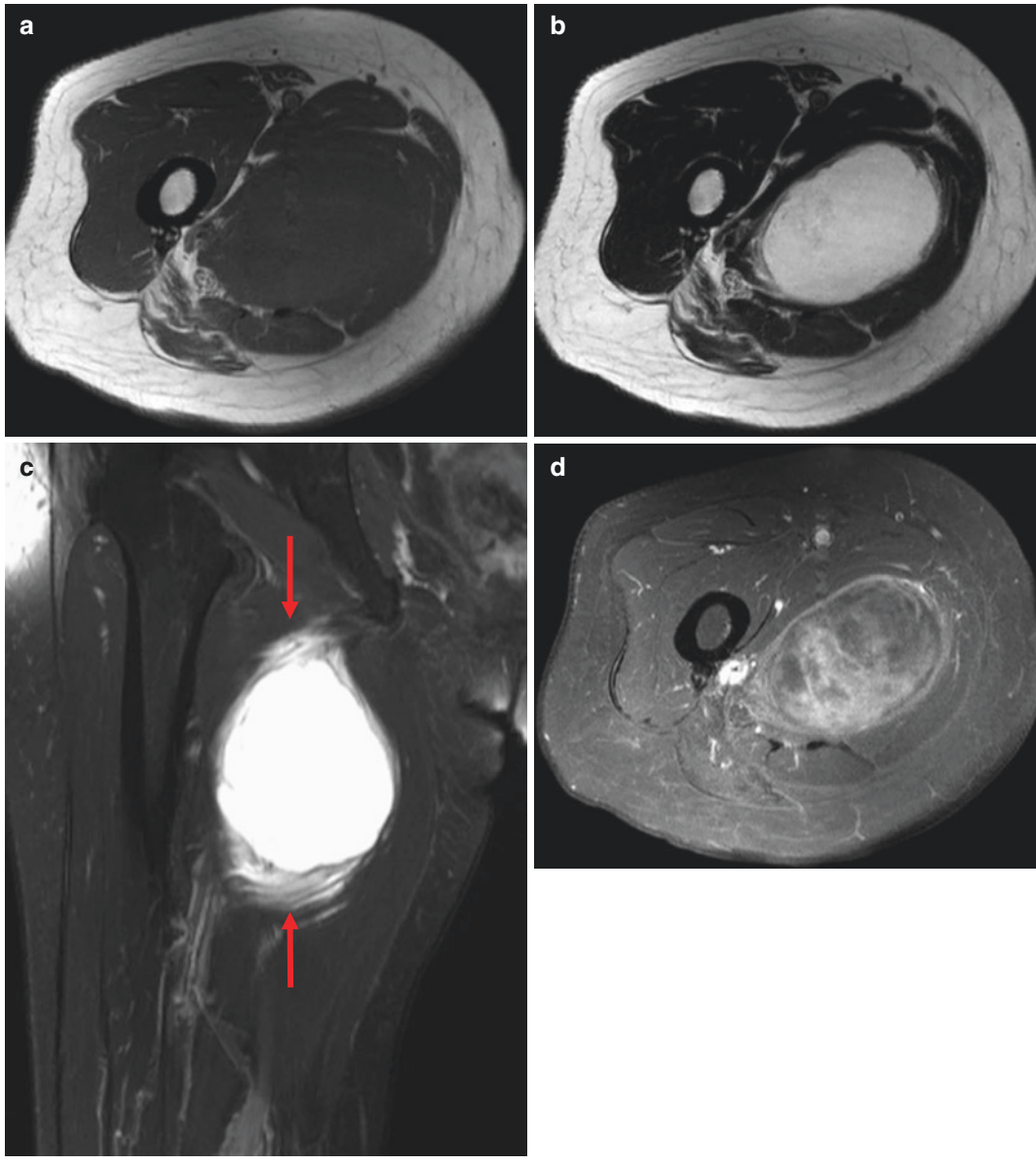

Fig. 13.2 Intramuscular myxoma. Axial T1WI (**a**) reveals the intramuscular mass to be homogeneously hypointense relative to adjacent muscle. Axial and coronal T2WIs (**b**, **c**) show a well-defined fairly homogeneous fluidlike hyperintense mass located within the adductor magnus muscle. Coronal FS T2WI (**c**) reveals a brushlike hyperintensity around the proximal and distal poles of the lesion (*arrows*). This pattern is due to leakage of myxoid tissue content. Axial postcontrast FS T1WI (**d**) shows typical, moderate patchy enhancement of the mass

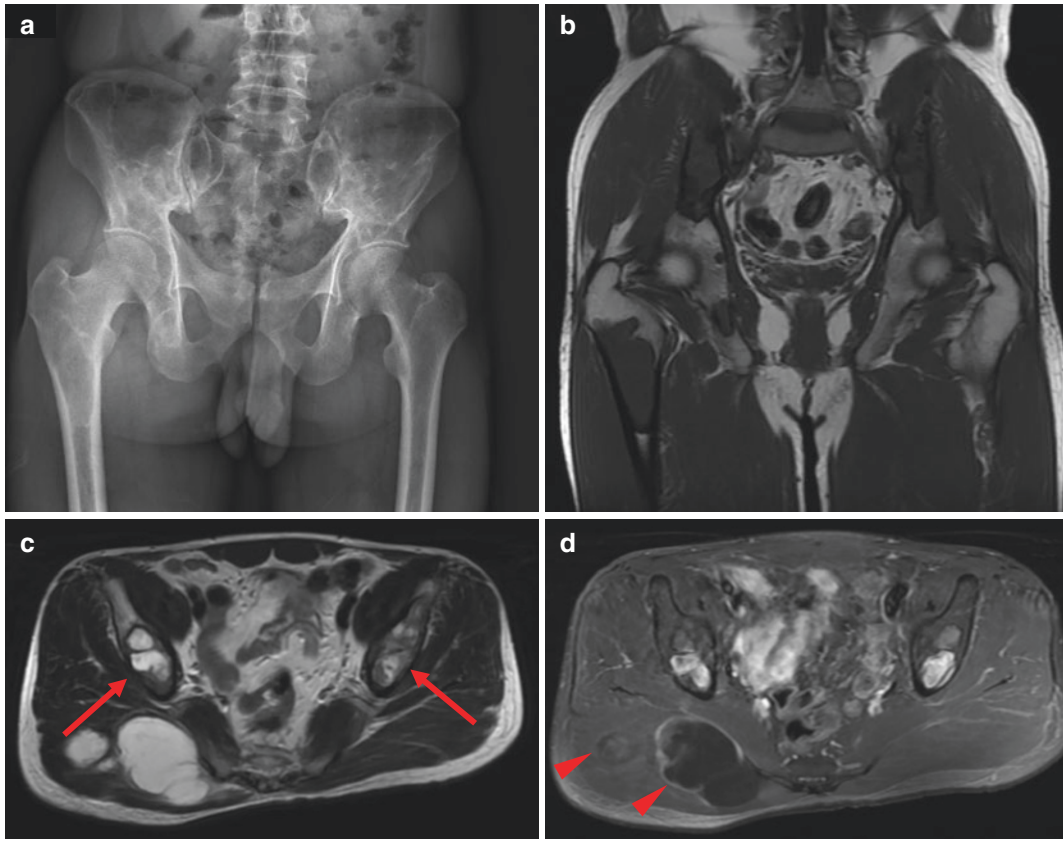

Fig. 13.3 Mazabraud syndrome. AP radiograph of the pelvis (**a**) reveals multifocal osteolytic lesions with thin sclerotic margins involving the ilium and the right femur, in keeping with polyostotic fibrous dysplasia. On coronal T1WI (**b**), the corresponding bone lesions appear to be hypointense. Axial T2WI (**c**) shows multiple intramuscular myxomas within the gluteus maximus and fibrous dysplasia in the acetabulum (*arrows*). Axial postcontrast FS T1WI (**d**) demonstrates variable enhancement of the tumors (*arrowheads*)

13.12.2 Synovial Sarcoma

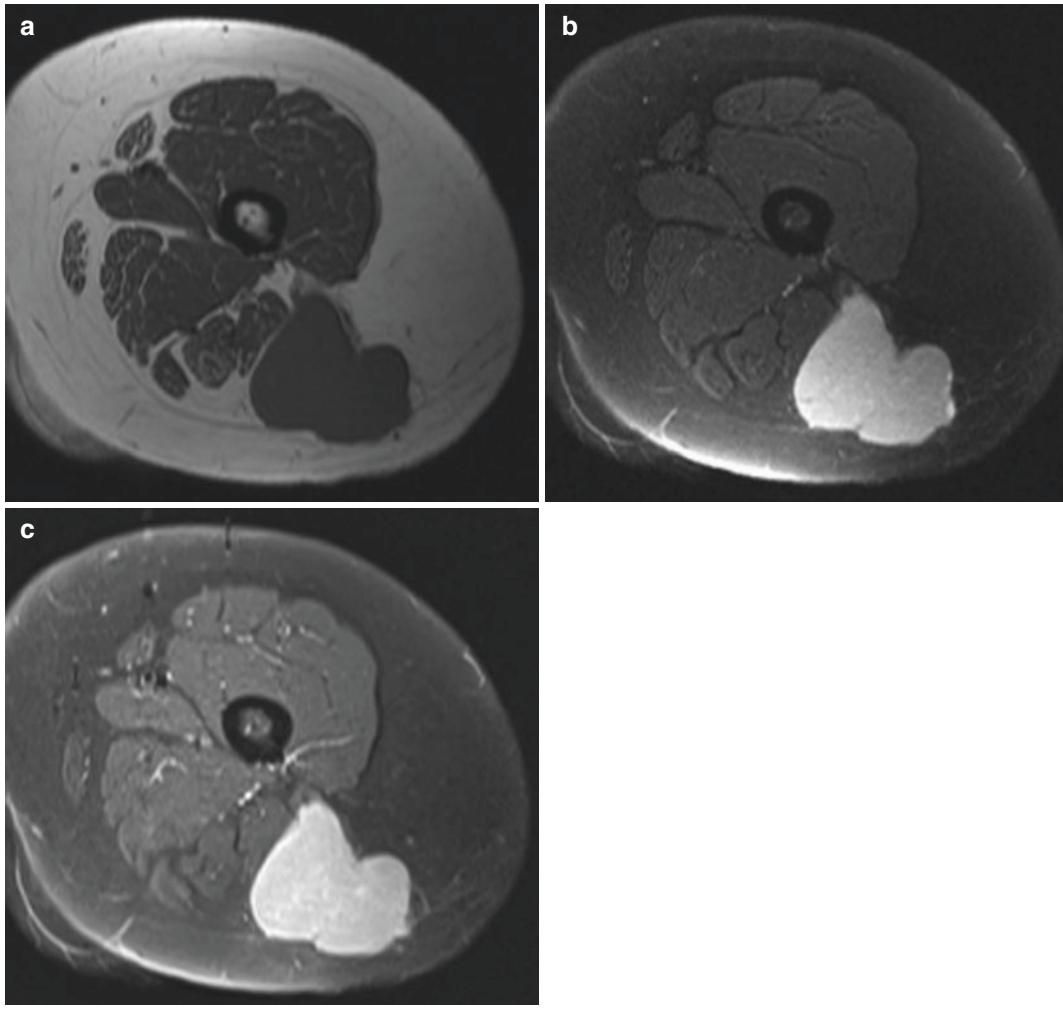

Fig. 13.4 Synovial sarcoma. Axial T2WI (**a**) reveals a well-defined lobular soft tissue mass located in the subfascial region that is iso- to hypointense to adjacent skeletal muscle. Axial FS T2WI (**b**) shows the mass that exhibits a homogeneous, high signal intensity. Axial postcontrast FS T1WI (**c**) shows homogeneously intense enhancement

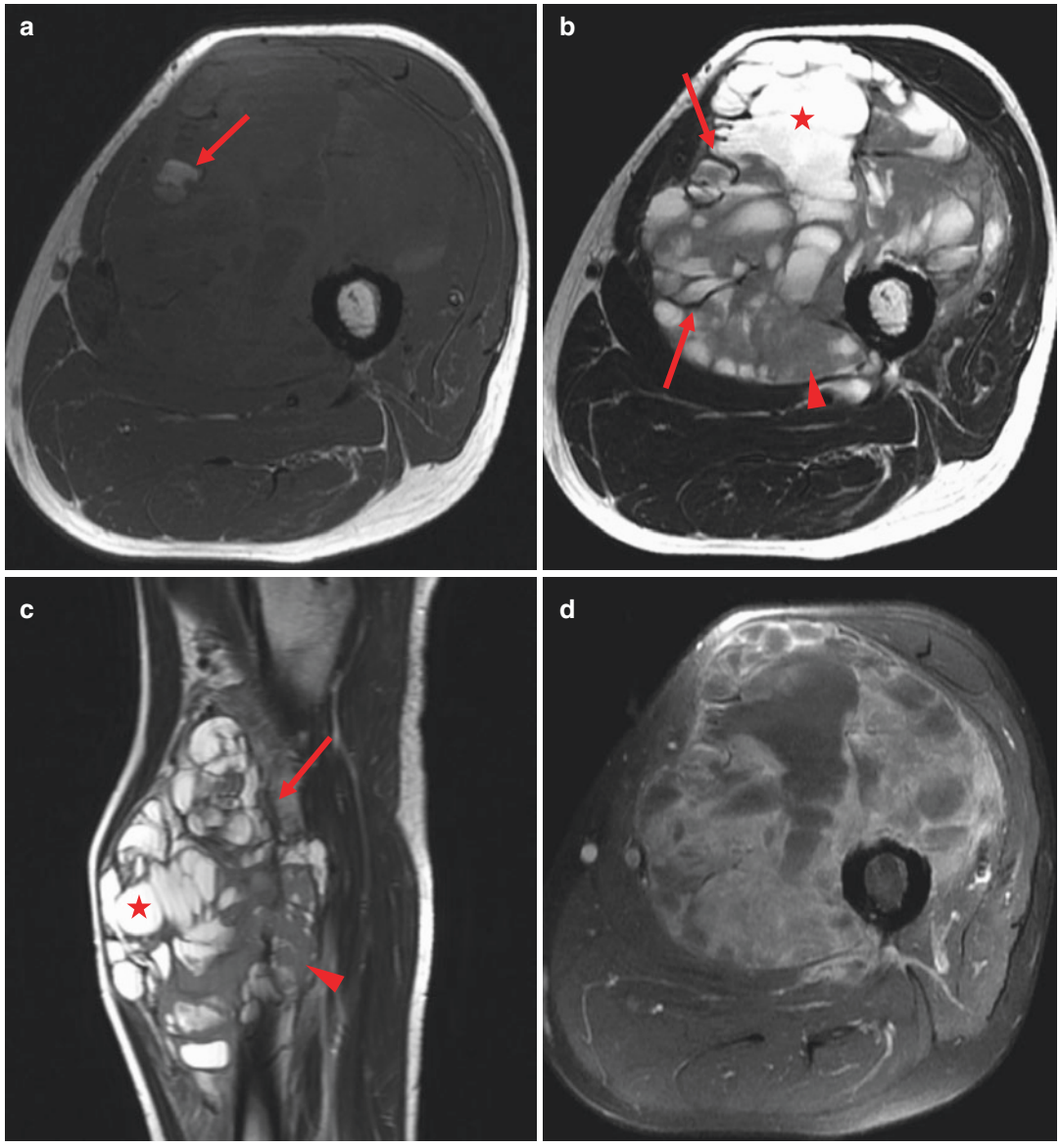

Fig. 13.5 Synovial sarcoma. Axial T1WI (**a**) shows a large intramuscular mass in the thigh, with a focal area of high signal intensity (*arrow*), suggestive of intratumoral hemorrhage. Axial and sagittal T2WIs (**b**, **c**) show a large heterogeneous mass containing three different signal intensities. This triple sign is due to the combination of areas of solid cellular elements (intermediate signal intensity, *arrowhead*), hemorrhage or necrosis (high signal intensity, *star*), and calcified or fibrotic collagenized regions (low signal intensity, *arrows*), which is often observed in synovial sarcoma. Axial postcontrast FS T1WI (**d**) demonstrates prominent heterogeneous enhancement of the mass

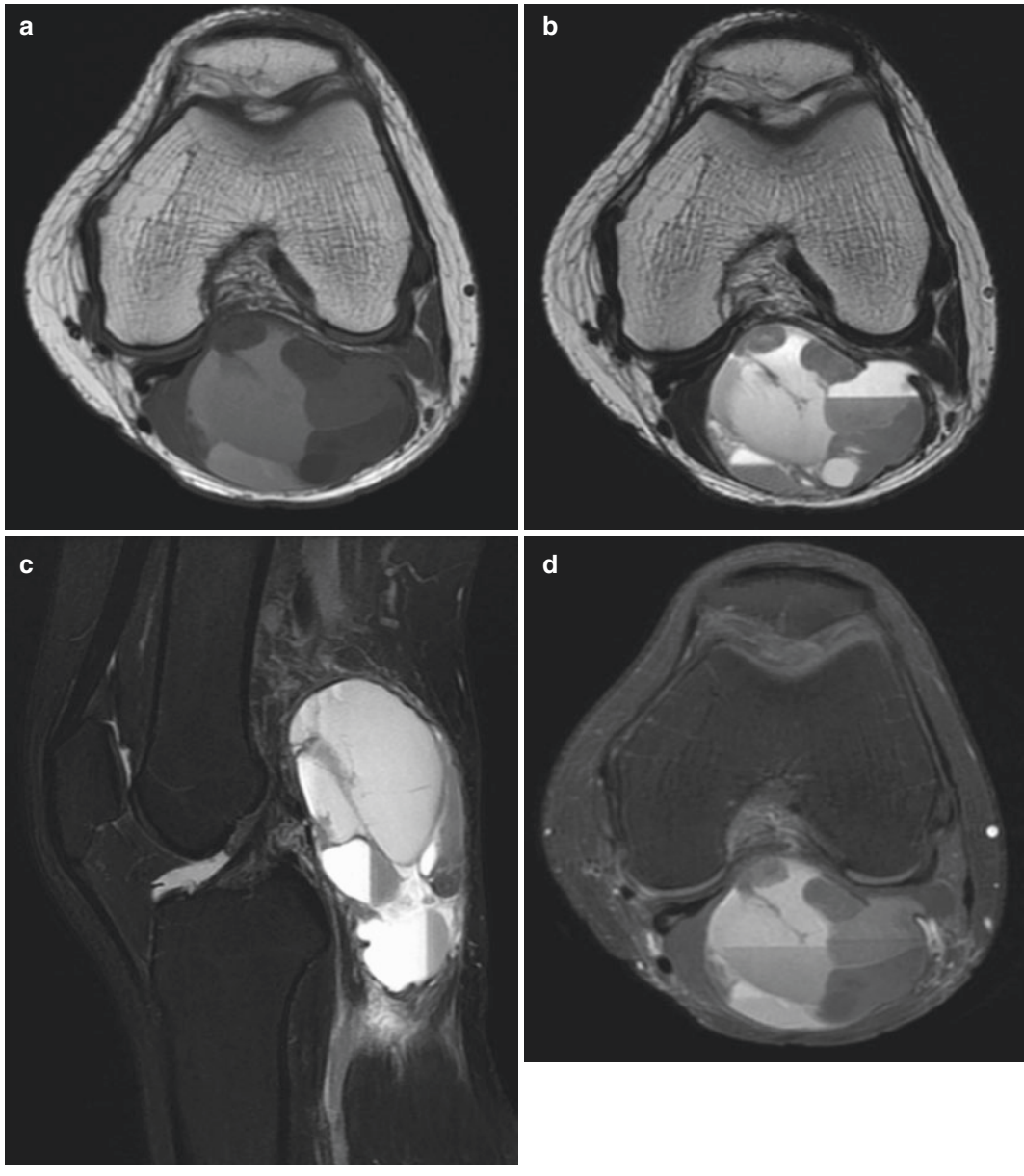

Fig. 13.6 Synovial sarcoma. Axial T1WI (**a**) shows largely cystic areas with high signal intensity, suggestive of hemorrhagic components. Axial and sagittal T2WIs (**b**, **c**) show a multiseptated mass with marked signal heterogeneity and a fluid-fluid level, creating a 'bowl of grapes' appearance. Axial postcontrast FS T1WI (**d**) reveals large non-enhancing hemorrhagic regions with fluid-fluid levels

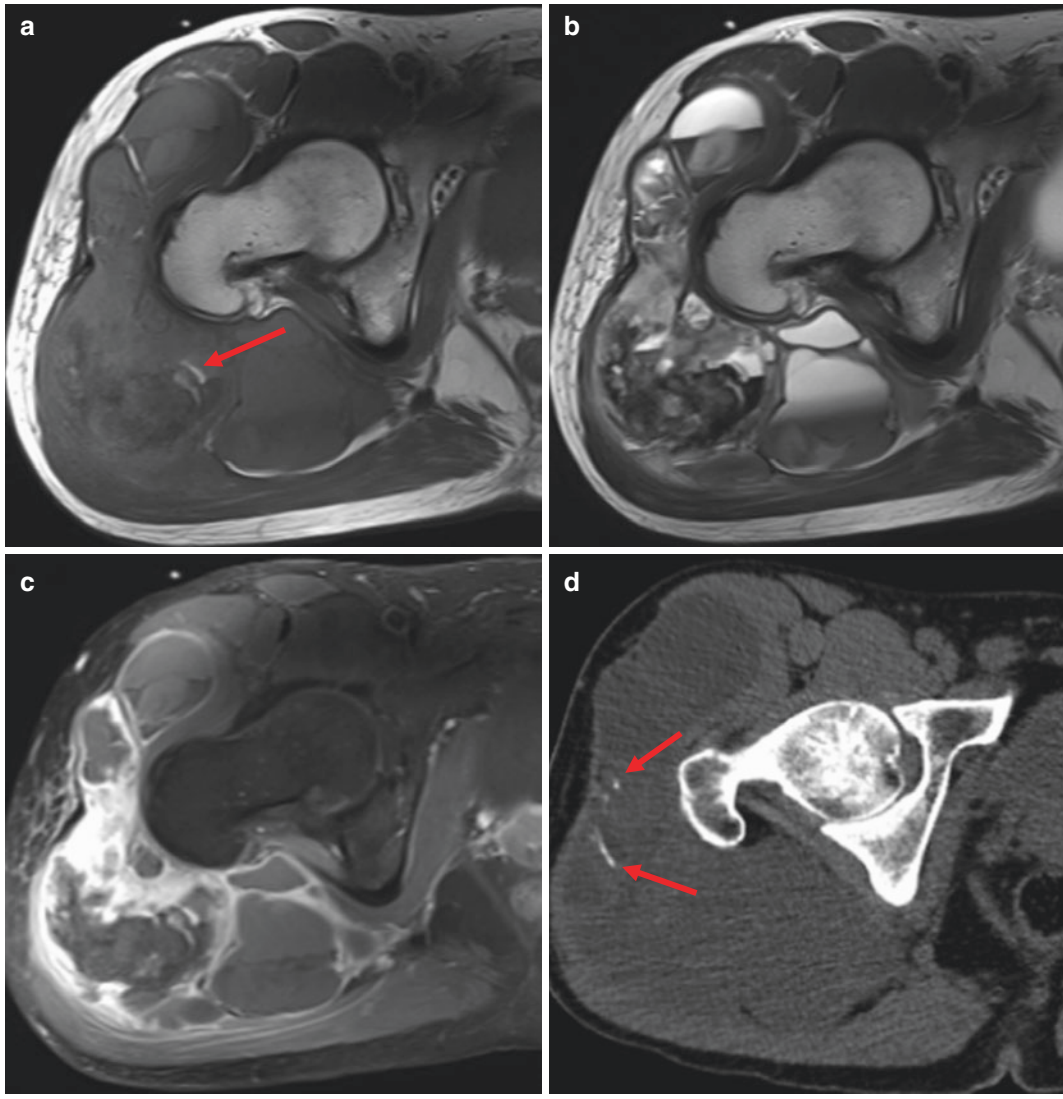

Fig. 13.7 Synovial sarcoma. Axial T1WI (**a**) shows a large mass in the right buttock, with a focal area of high signal intensity, suggestive of intratumoral hemorrhage (*arrow*). Axial T2WI (**b**) shows heterogeneous signal intensities known as a triple sign. A combination of solid cellular elements (intermediate signal intensity), hemorrhage or necrosis (high signal intensity), and calcified or fibrotic collagenized regions (low signal intensity) is seen. Axial postcontrast FS T1WI (**c**) demonstrates both enhancing solid elements and non-enhancing hemorrhagic or necrotic elements. Axial CT (**d**) shows a low-attenuated mass with internal focal calcifications (*arrows*)

13.12.3 Phosphaturic Mesenchymal Tumor

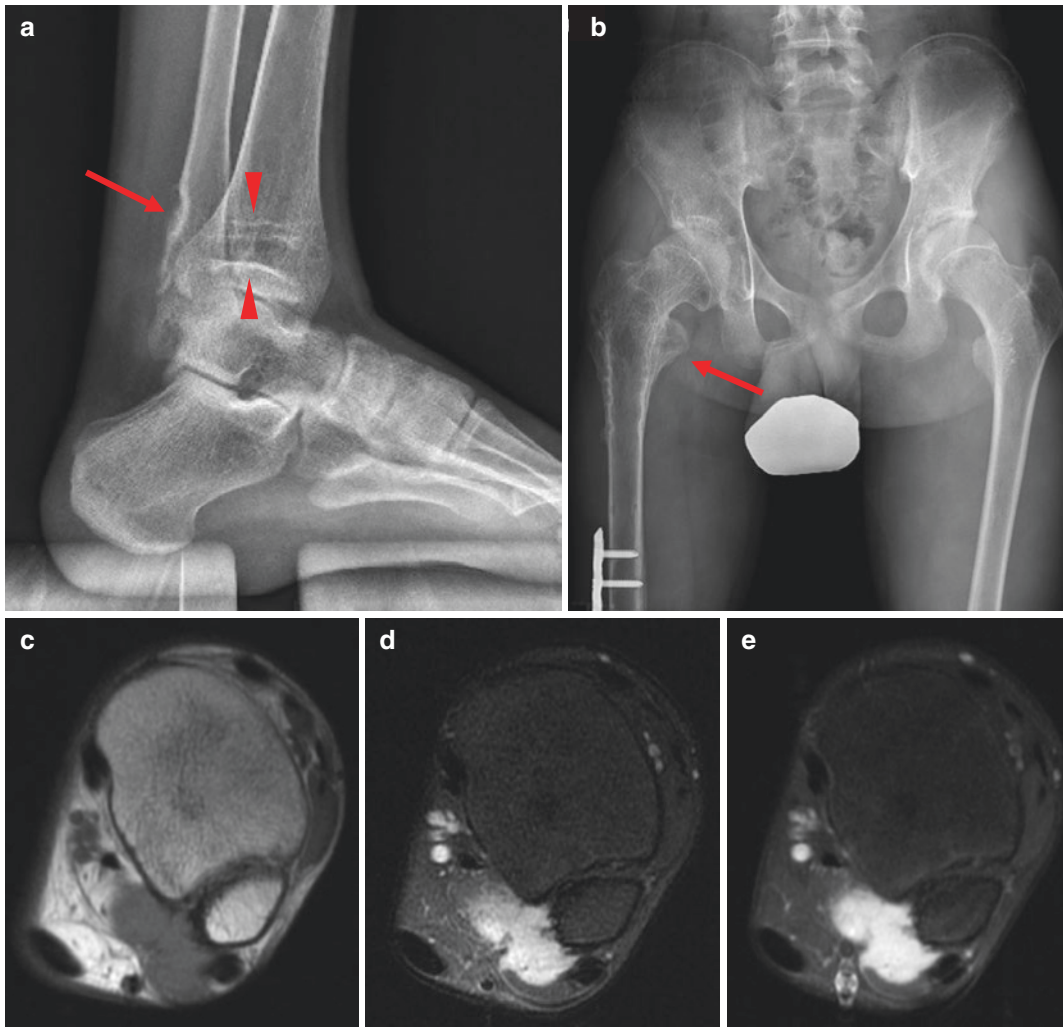

Fig. 13.8 Phosphaturic mesenchymal tumor/mixed connective tissue tumor (PMTMCT). Lateral radiograph of the ankle (**a**) shows a subtle soft tissue density in the posterior ankle, with cortical saucerization (*arrow*) in the adjacent posterior cortex of the distal fibula. There are several transverse sclerotic lines in the distal tibia (*arrowheads*), indicating insufficiency fracture due to uncontrollable osteomalacia. (**b**) AP radiograph of the pelvis shows diffuse osteopenia with remote fracture in the right proximal femur (*arrow*). Axial T1WI (**c**) shows a lobulated mass on the posterior aspect of distal fibula, with isointensity to the adjacent muscle. Axial FS T2WI (**d**) shows a homogeneous hyperintense mass abutting the posterior cortex of the distal fibula. Axial postcontrast FS T1WI (**e**) demonstrates homogeneous strong enhancement of the mas

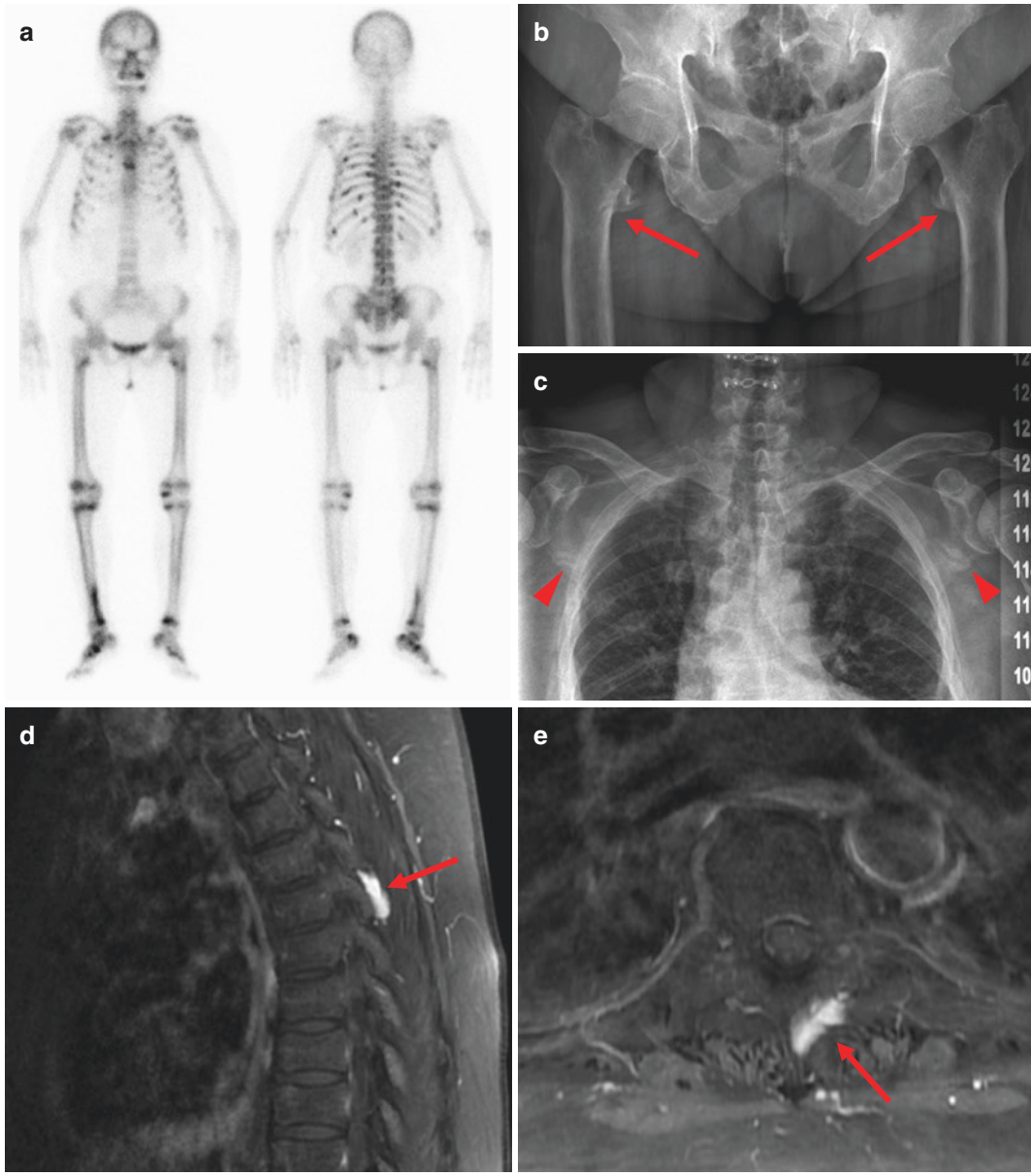

Fig. 13.9 Phosphaturic mesenchymal tumor/mixed connective tissue tumor (PMTMCT). Bone scan (**a**) shows multiple hot uptakes in the ribs, proximal femora, and distal tibiae, in keeping with insufficiency fracture due to osteomalacia. Radiographs (**b**, **c**) demonstrate symmetric transverse lucencies with sclerotic irregular margins in the medial cortex of the proximal femur (*arrows*) and lateral border of scapula (*arrowheads*), indicating looser zone. Postcontrast FS T1WIs (**d**, **e**) show a well-circumscribed enhancing soft tissue lesion (*arrows*) in the T5 left paraspinal muscle, which was histologically confirmed as PMTMCT

13.12.4 Epithelioid Sarcoma

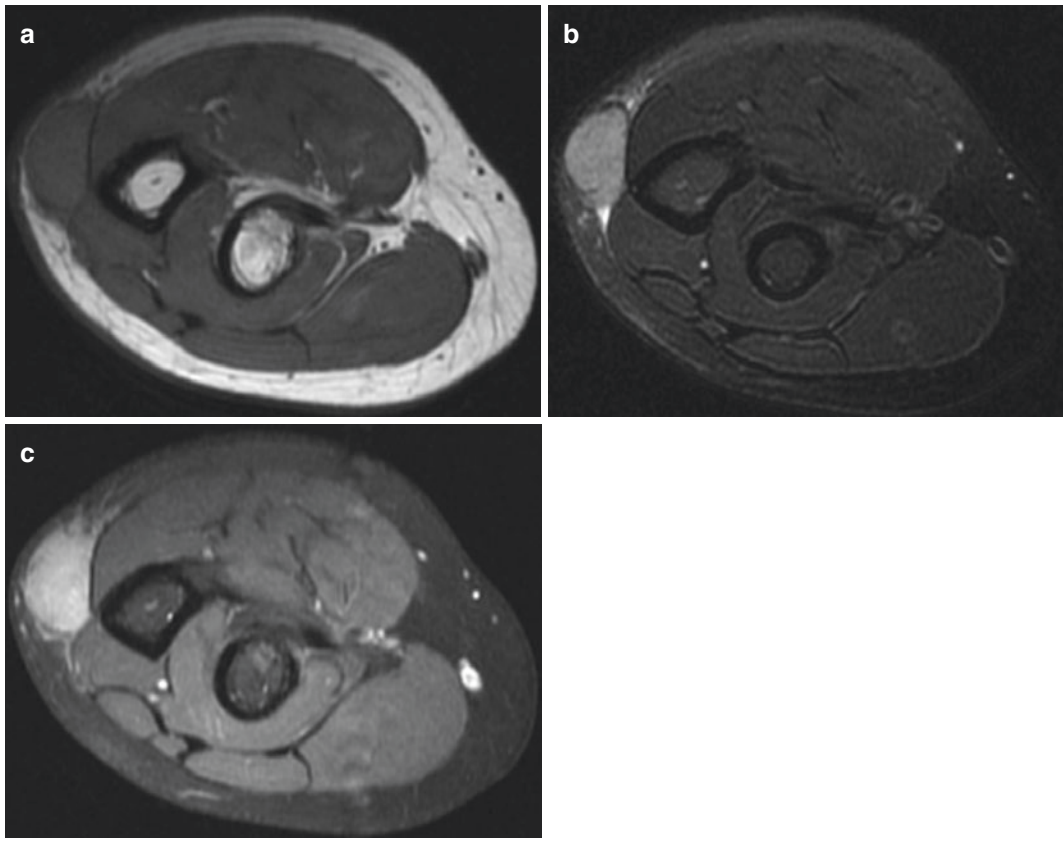

Fig. 13.10 Superficial epithelioid sarcoma. Axial T1WI (**a**) shows a subcutaneous mass with equal signal intensity to that of adjacent muscle. Axial FS T2WI (**b**) shows a superficial single nodular mass with a homogeneous hyperintense signal along the deep fascia of the right forearm. Axial postcontrast FS T1WI (**c**) exhibits homogeneous contrast enhancement with mild infiltrative margin

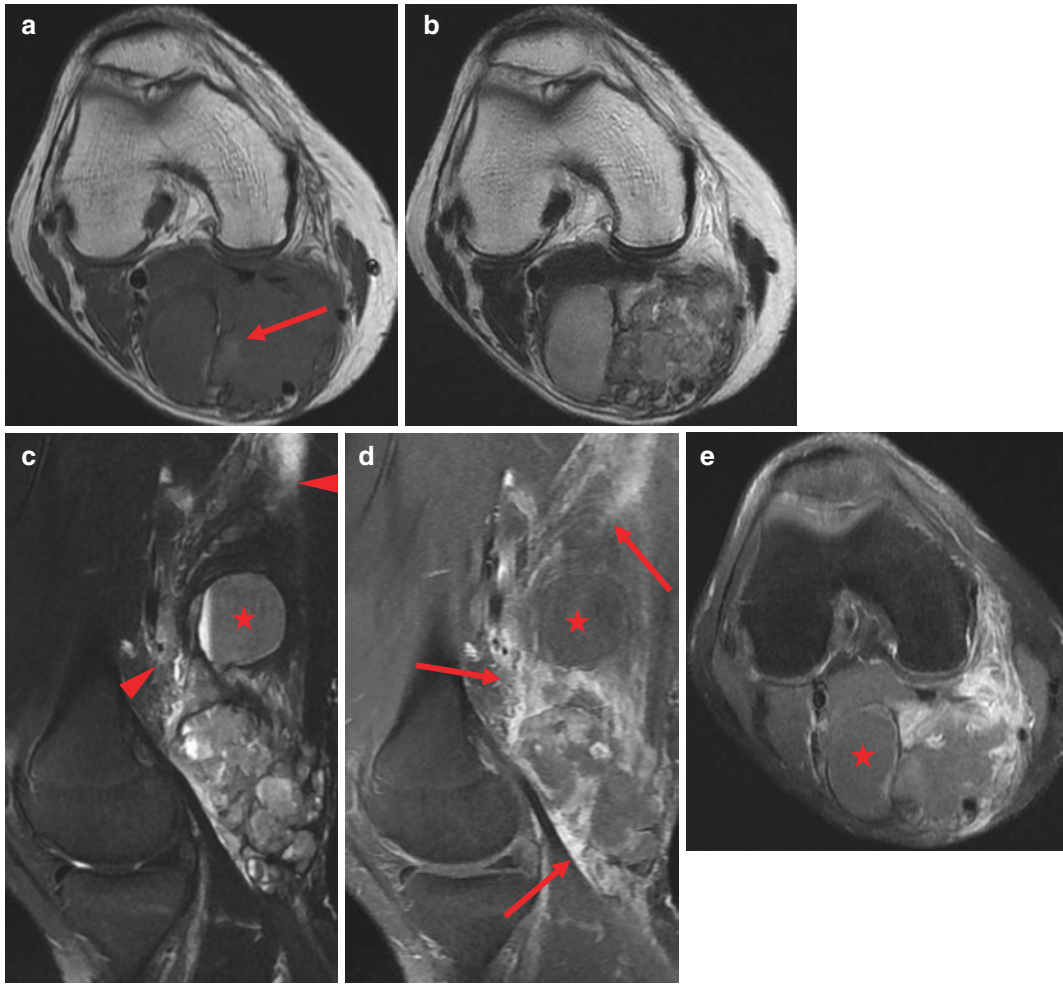

Fig. 13.11 Deep-seated epithelial sarcoma. Axial T1WI (**a**) shows a deep-seated infiltrative soft tissue mass involving the medial head of gastrocnemius muscle. An internal, increased signal intensity is seen, suggestive of hemorrhage (*arrow*). Axial and sagittal FS T2WIs (**b**, **c**) show a mass containing hemorrhagic changes with a fluid-fluid level (*star*) and a peritumoral edema-like signal (*arrowheads*). Axial and sagittal postcontrast FS T1WIs (**d**, **e**) reveal heterogeneous tumor enhancement with large hemorrhagic necrotic components (*stars*) and infiltrative, poorly defined margins (*arrows*)

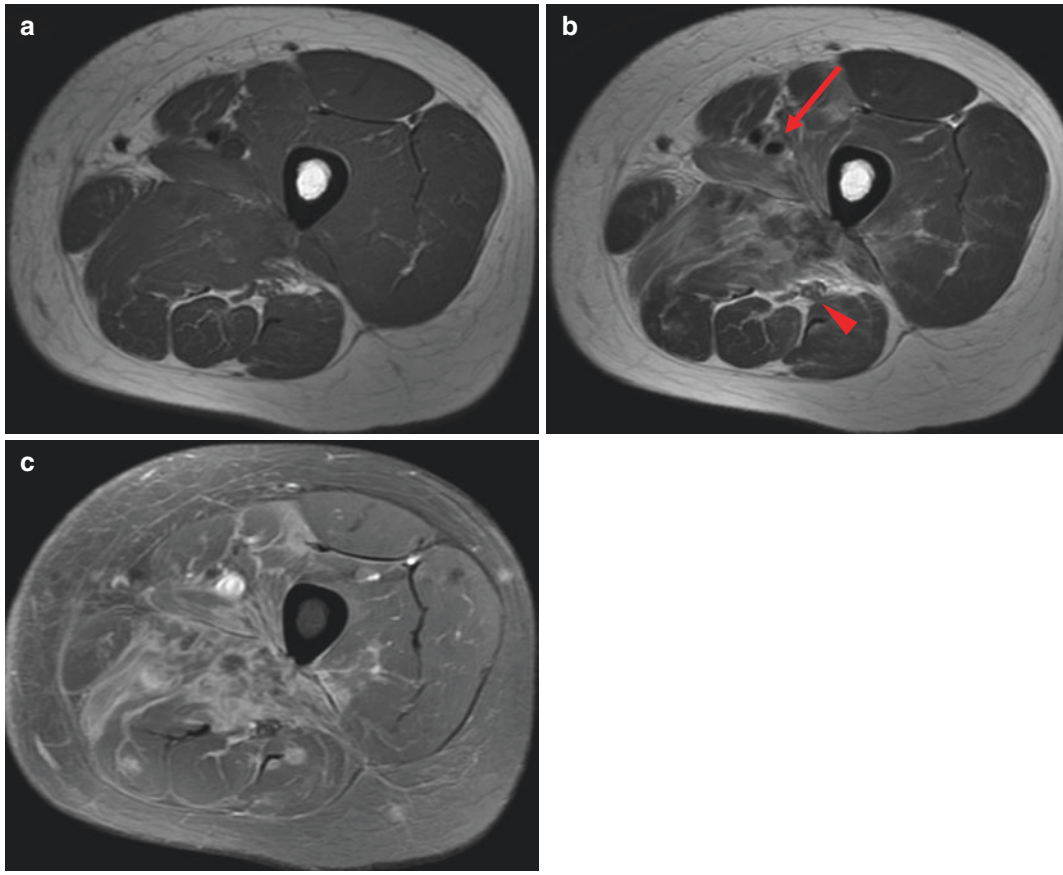

Fig. 13.12 Infiltrative epithelial sarcoma. Axial T1WI (**a**) reveals a deep-seated soft tissue mass wrapping around the medial thigh, showing a similar signal intensity to that of the adjacent muscle. Axial T2WI (**b**) shows heterogeneous signal intensities. The tumor encases the femoral neurovascular bundle (*arrow*) and closely abuts the sciatic nerve (*arrowhead*), with infiltrative margins. Axial post-contrast FS T1WI (**c**) demonstrates tumor enhancement with infiltrative, poorly defined margins extending to all compartments of the thigh

13.12.5 Angiosarcoma

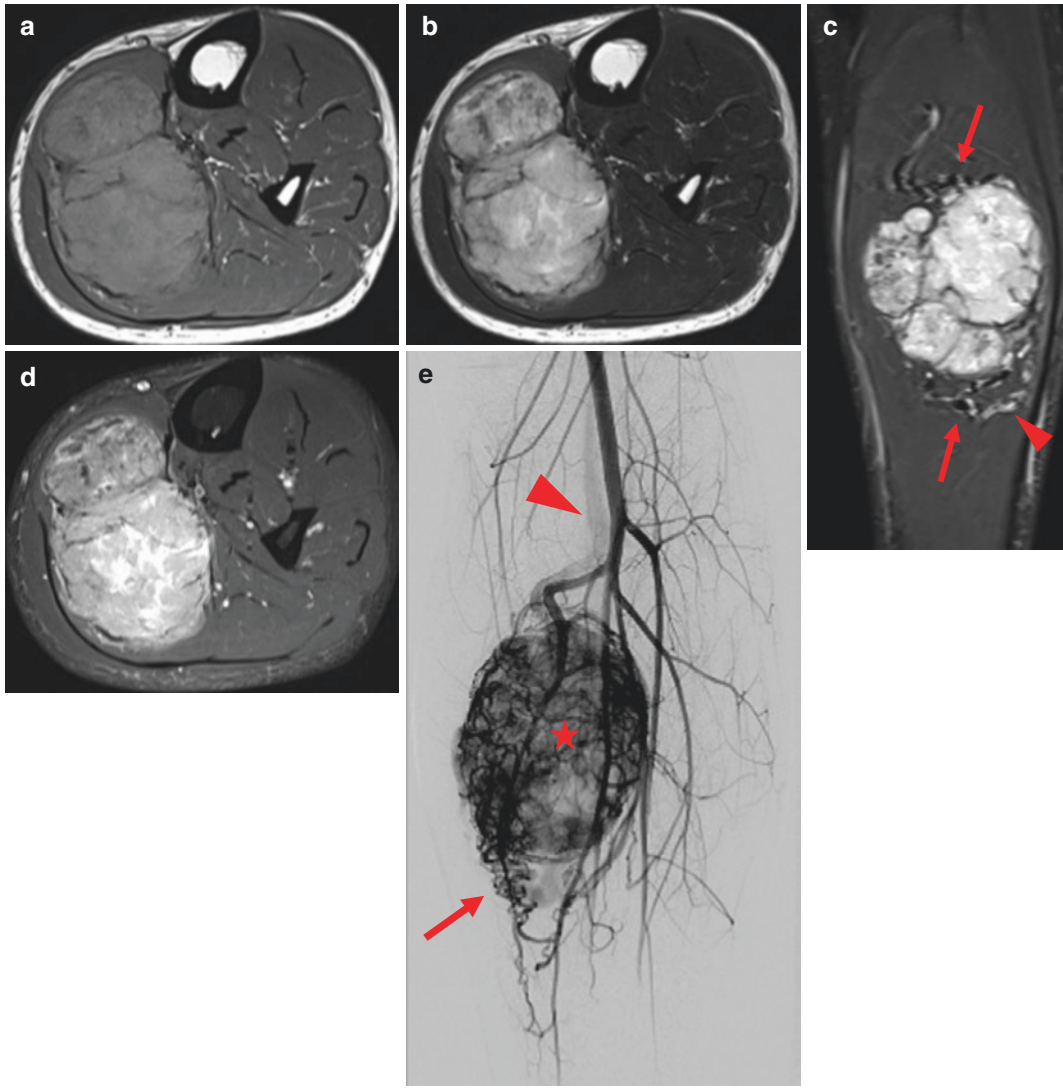

Fig. 13.13 Alveolar soft part sarcoma. Axial T1WI (**a**) reveals an intramuscular mass with a higher signal intensity compared with the adjacent muscles. Axial and coronal FS T2WIs (**b**, **c**) show a large soft tissue mass with a heterogeneous high signal intensity. Peritumoral feeding arteries (*arrows*) and draining veins (*arrowhead*) can be observed on coronal FS T2WI (**c**). Axial postcontrast FS T1WI (**d**) reveals intense enhancement with multiple flow voids around the mass, suggestive of prominent intra- and peritumoral vessels. Angiogram (**e**) demonstrates hypervascularity with prominent feeding arteries (*arrow*), prolonged capillary staining (*star*), and a draining vein (*arrowhead*)

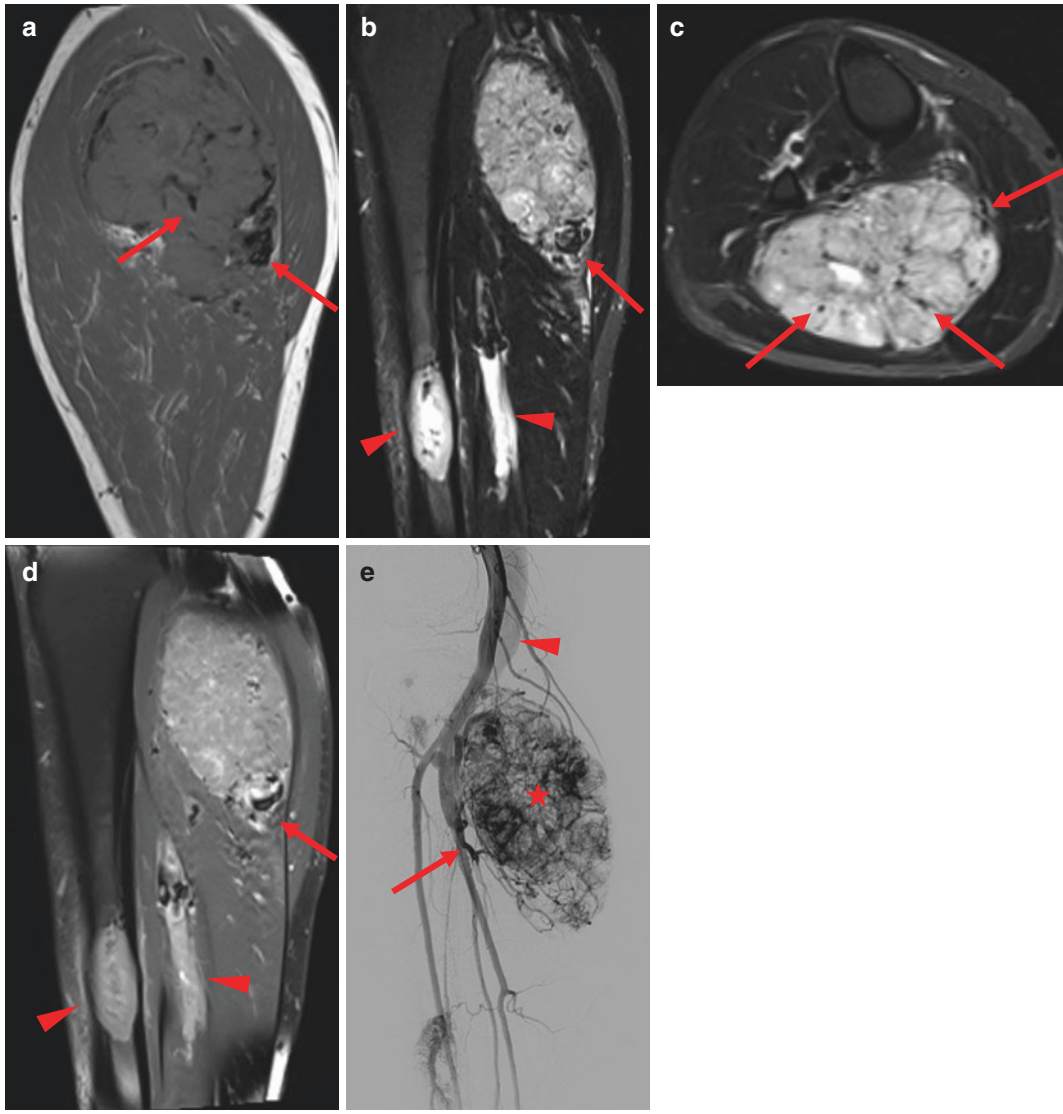

Fig. 13.14 Alveolar soft part sarcoma. Coronal T1WI (**a**) reveals an intramuscular mass in the soleus muscle, with multiple intra- and peritumor flow voids (*arrows*). Sagittal and axial FS T2WIs (**b**, **c**) show a heterogeneously hyperintense tumor with multiple flow voids (*arrows*). Metastatic masses (**b**) are also observed in the adjacent muscle and diaphysis of the tibia (*arrowheads*). Characteristic flow voids in and around the mass are observed. Sagittal postcontrast FS T1WI (**d**) demonstrates intense enhancement with multiple flow voids around the mass, suggestive of prominent intra- and peritumoral vessels (*arrow*). The metastatic masses also show intense enhancement (*arrowheads*). Angiogram (**e**) demonstrates hypervascularity with prominent feeding arteries (*arrow*), draining veins (*arrowhead*), and prolonged capillary staining (*star*)

13.12.6 Clear Cell Sarcoma

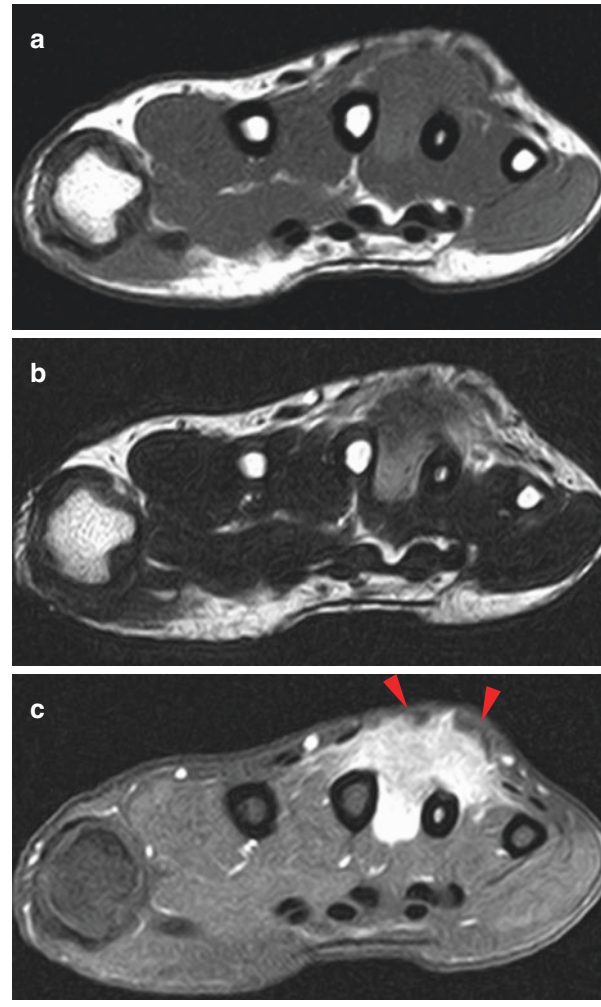

Fig. 13.15 Clear cell sarcoma. Axial T1WI (**a**) reveals a soft tissue mass in the dorsal aspect of third inter-metacarpal space, which abuts the third and fourth metacarpal bones, adjacent to the extensor tendons. The mass is slightly hyperintense to the adjacent muscle, corresponding to the presence of intralesional melanin. Axial T2WI (**b**) shows a mass with low to intermediate signal intensity. Axial postcontrast FS T1WI (**c**) demonstrates intense and homogeneous enhancement enveloping the third and fourth extensor tendons (*arrowheads*)

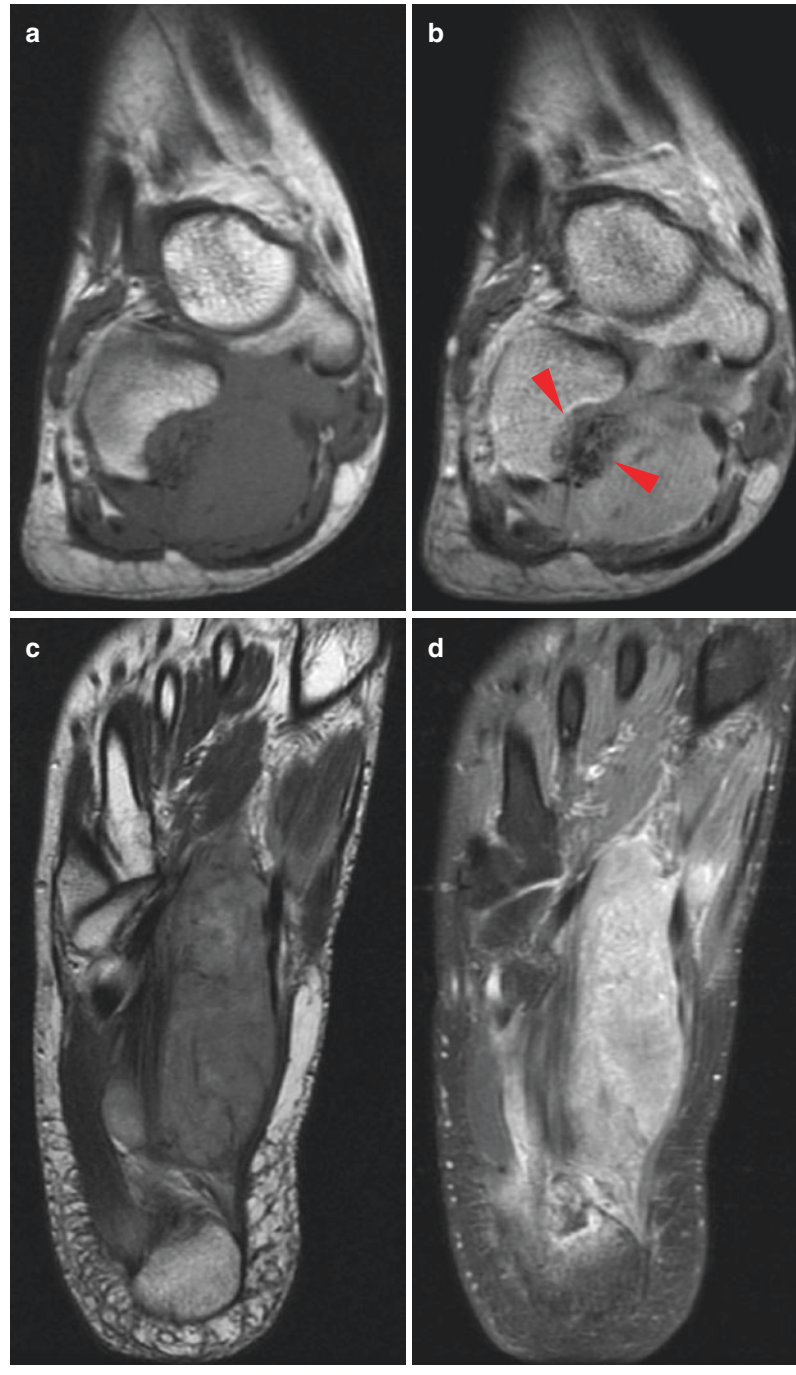

Fig. 13.16 Clear cell sarcoma. Axial T1WI (**a**) reveals a soft tissue mass in the sole. The tumor has a slightly higher signal intensity compared with muscle on T1WI. Axial and coronal T2WIs (**b**, **c**) show intermediate signal intensity with internal low signal foci. The mass encases plantar intrinsic ligament (*arrowheads* in **b**) and displaces the flexor tendons. Coronal postcontrast FS T1WI (**d**) demonstrates intense enhancement

13.12.7 Extraskeletal Myxoid Chondrosarcoma

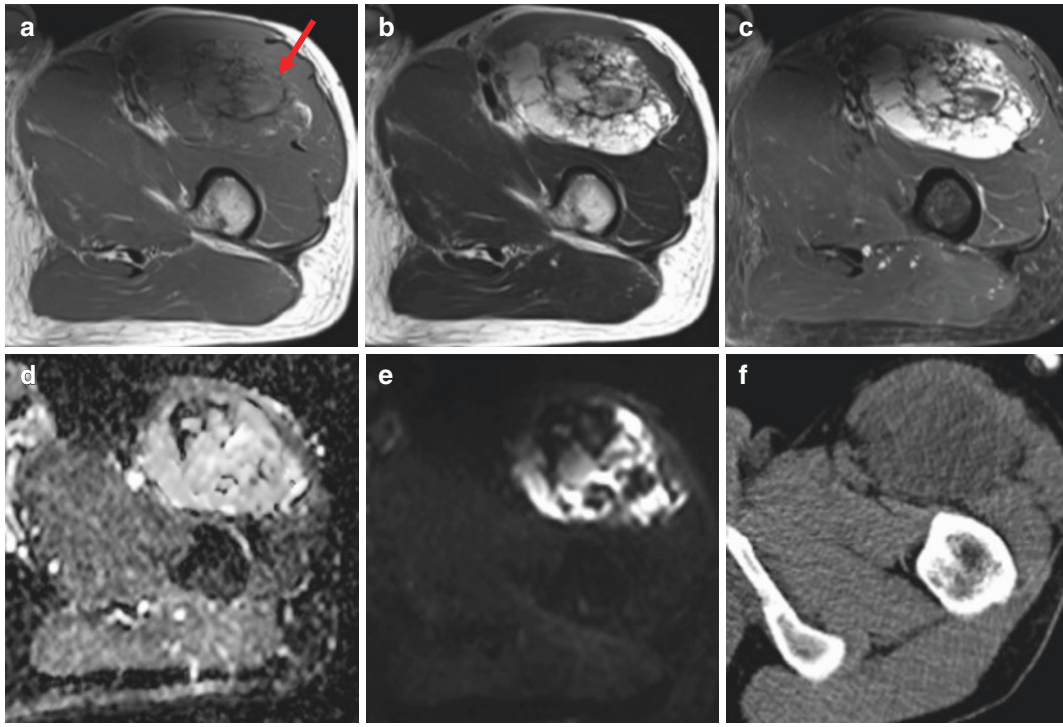

Fig. 13.17 Extraskeletal myxoid chondrosarcoma. Axial T1WI (**a**) reveals a multilobulated intramuscular mass in the anterior thigh. The lesion shows hyperintense foci corresponding to hemorrhagic changes within the tumor (*arrow*). Axial T2WI (**b**) shows a mass with high signal intense lobules defined by thin fibrous septa of low signal intensity. Axial postcontrast FS T1WI (**c**) reveals heterogeneous but prominent enhancement (except a small hemorrhagic portion), indicating a highly myxoid tumor. DWI (**d**) and ADC map (**e**) show nonrestricted diffusion due to the characteristic nature of the chondroid matrix, which has a high fluid content. CT (**f**) reveals a well-defined and low-attenuated mass without calcification or bone formation

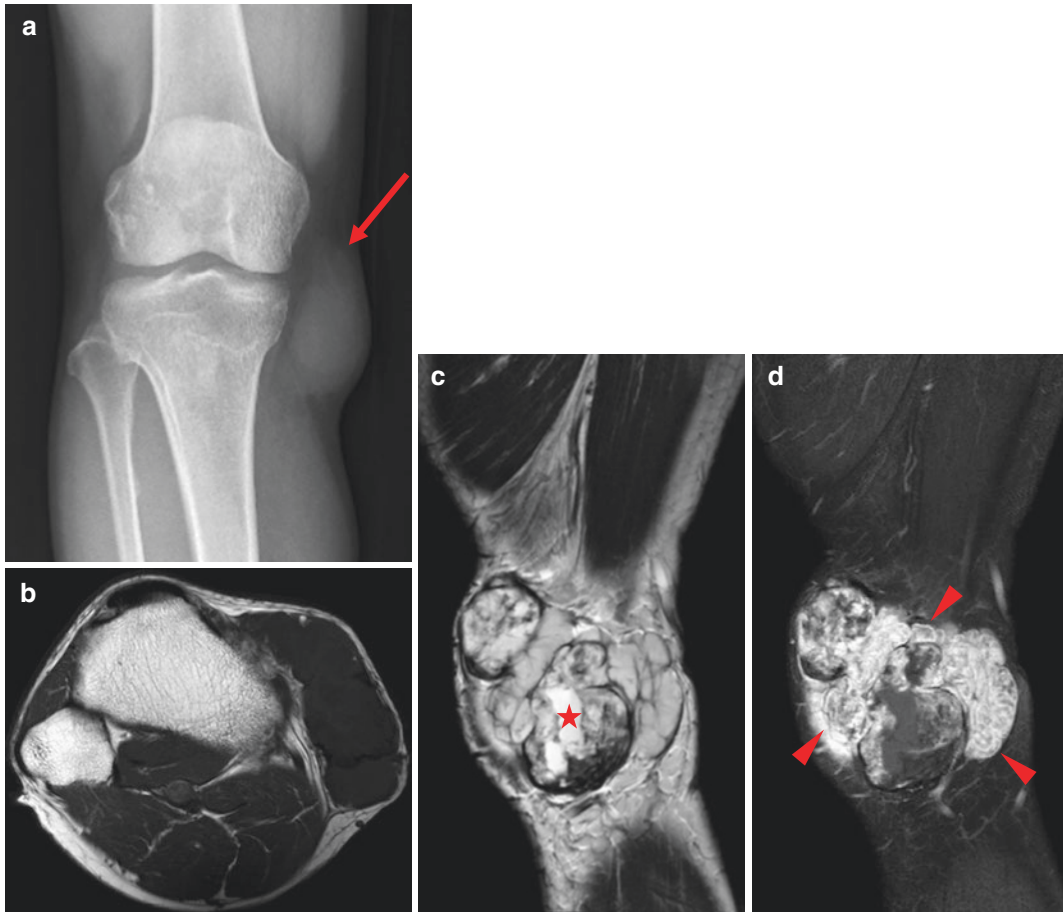

Fig. 13.18 Extraskeletal myxoid chondrosarcoma. AP radiograph of the knee (**a**) shows nonspecific soft tissue mass (*arrow*) in the medial knee that does not contain calcifications or exhibits bone formation. Axial T1WI (**b**) reveals a subcutaneous mass in the medial aspect of the proximal tibia. The tumor is isointense to the adjacent muscle. Sagittal T2WI (**c**) shows a high signal mass with thin fibrous septa of low signal intensity. There is a small area of necrotic change (*star*). Sagittal postcontrast FS T1WI (**d**) shows prominent enhancement with a peripheral/septal enhancement pattern (*arrowheads*)

13.12.8 Extraskeletal Ewing Sarcoma

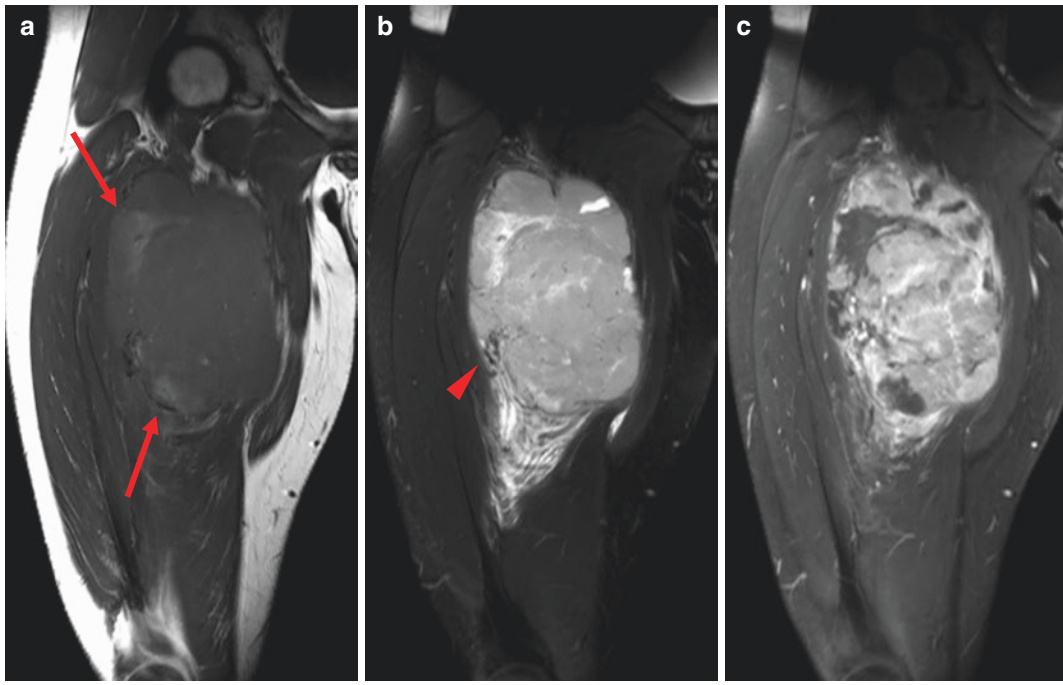

Fig. 13.19 Extraskeletal Ewing sarcoma. Coronal T1WI (**a**) reveals a large intramuscular mass in the medial aspect of the proximal thigh. The mass shows heterogeneous signal intensity that is similar to that of muscle, with small, hyperintense hemorrhagic foci (*arrows*). Coronal T2WI (**b**) shows a mass with intermediate to high signal intensity due to the high cellularity of the mass. The mass has low signal intensity (*arrowhead*) on all pulse sequences, suggestive of the presence of high-flow vascular channels, which is an additional image feature of extraskeletal Ewing sarcoma. Coronal postcontrast FS T1WI (**c**) shows prominent enhancement with non-enhancing hemorrhagic changes

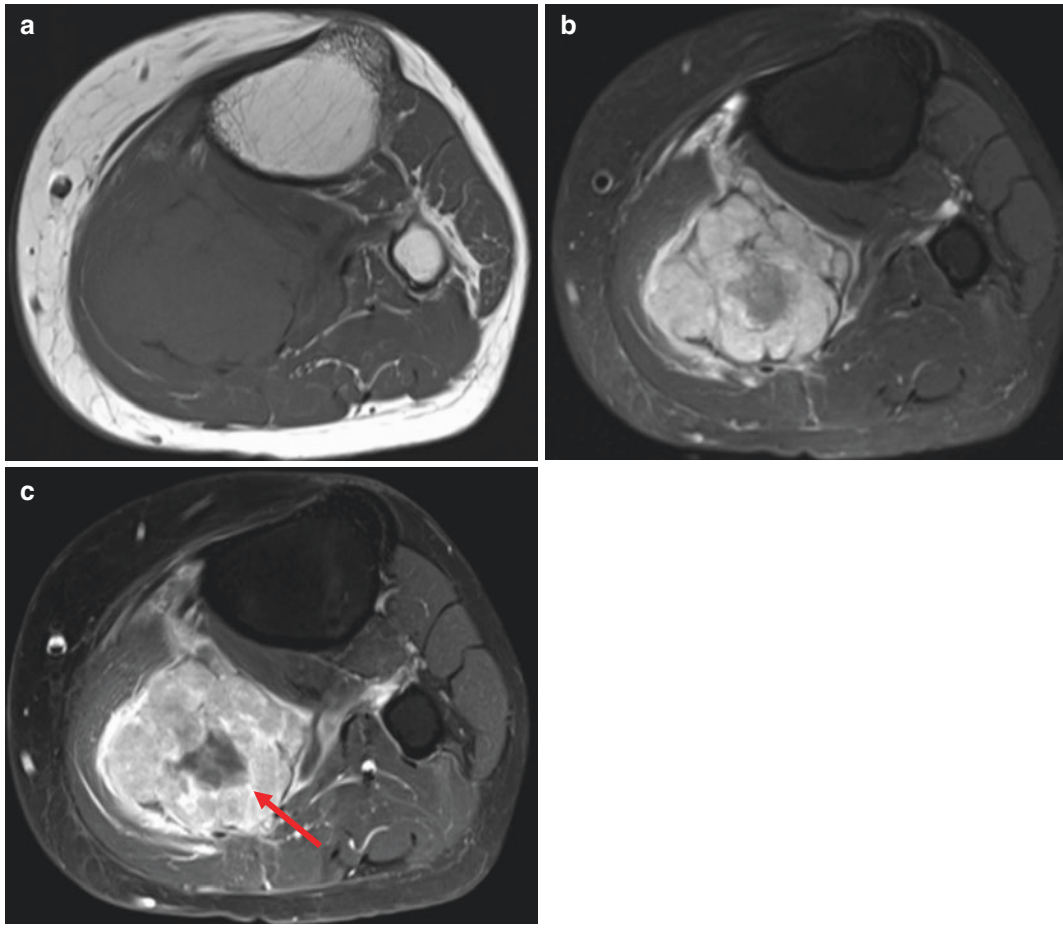

Fig. 13.20 Extraskeletal Ewing sarcoma. Axial T1WI (**a**) reveals an intramuscular mass in the calf. The mass is isointense to the adjacent muscle. Axial T2WI (**b**) shows a heterogeneously hyperintense tumor with a central hypointense necrotic area. Axial postcontrast FS T1WI (**c**) shows prominent enhancement, except in the central necrotic area (*arrow*)

13.12.9 Extrarenal Rhabdoid Tumor

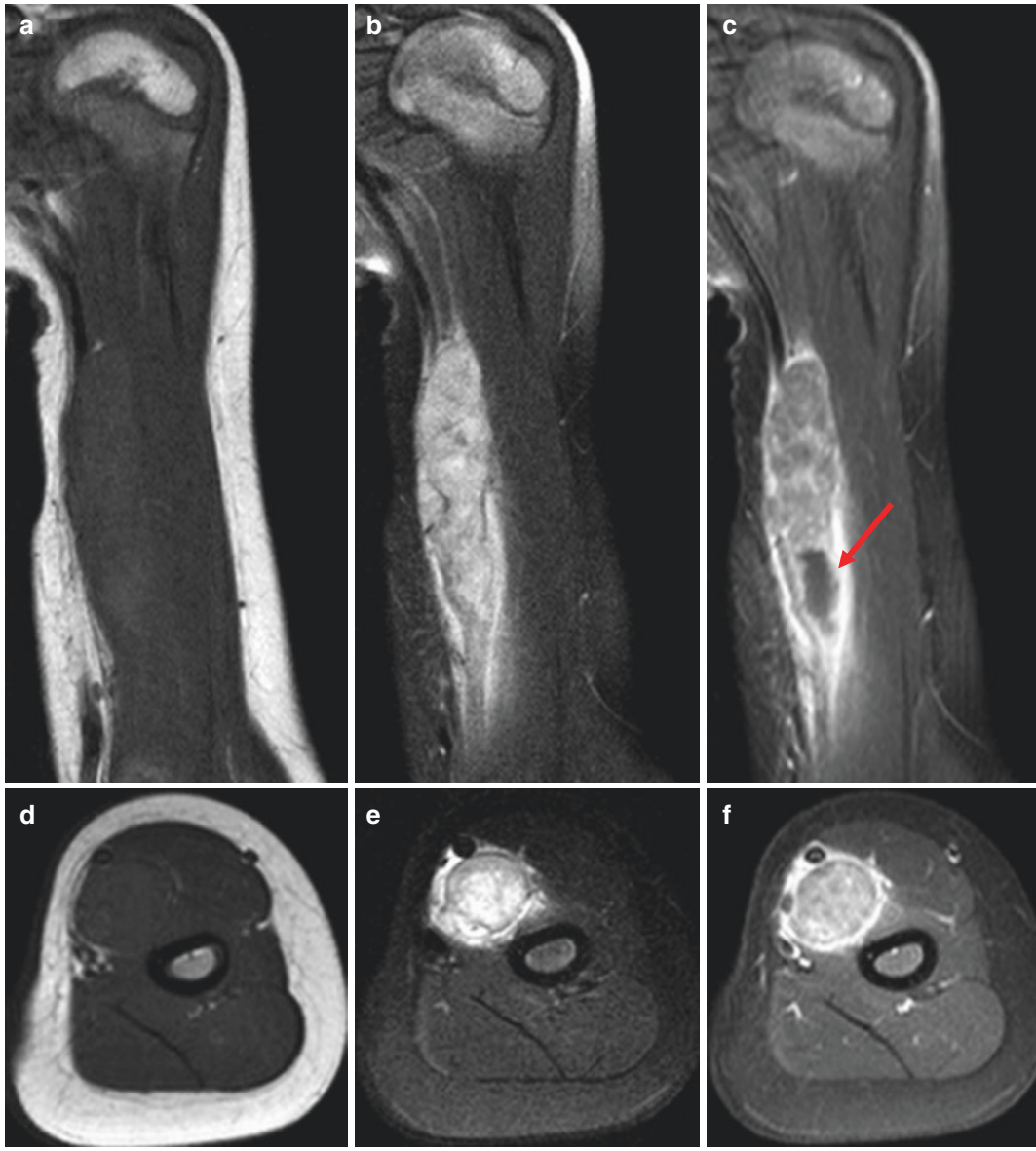

Fig. 13.21 Extrarenal rhabdoid tumor. T1WIs (**a**, **d**) show an intramuscular mass in the medial upper arm. The signal intensity of the mass is equal to that of the adjacent muscle. T2WIs (**b**, **e**) show a lobulated hyperintense mass with an ill-defined margin at the inferior portion of the tumor. There is peritumoral edema in the adjacent muscle. Postcontrast FS T1WIs (**c**, **f**) demonstrate heterogeneous enhancement, with a non-enhancing necrotic portion in the lower part of the mass (*arrow*)

13.12.10 Myoepithelioma

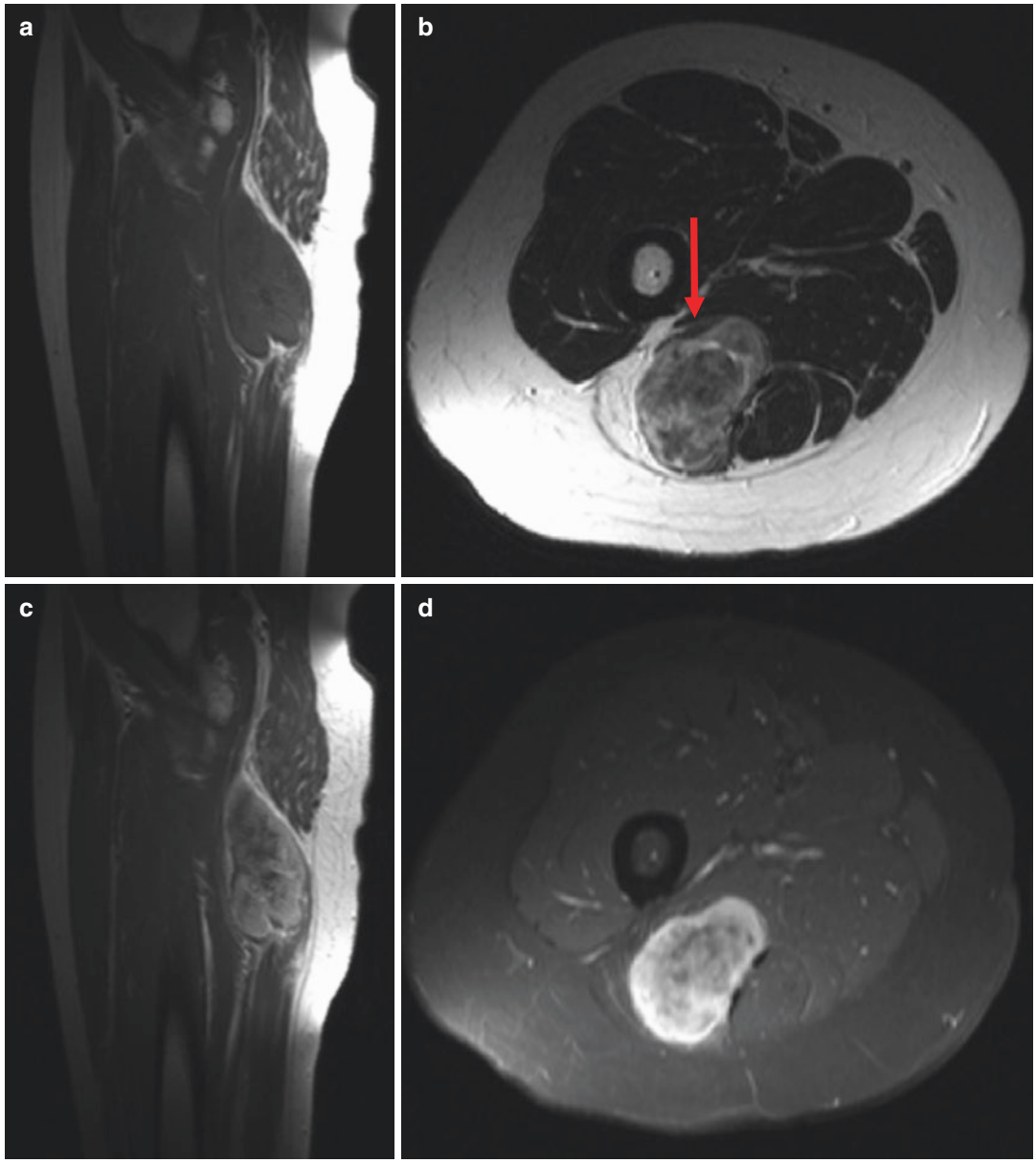

Fig. 13.22 Malignant myoepithelioma. Sagittal T1WI (**a**) and axial T2WI (**b**) reveal a deeply situated intermuscular soft tissue mass adjacent to the sciatic nerve in the posterior compartment of the right proximal thigh. The mass is heterogeneously isointense on T1WI (**a**) and intermediate to hyperintense to the adjacent muscle on T2WI (**b**, **c**). The sciatic nerve is anterolaterally displaced (*arrow* in **b**). Axial postcontrast FS T1WI (**d**) shows heterogeneous enhancement

13.12.11 Pleomorphic Hyalinizing Angiectatic Tumor of Soft Part

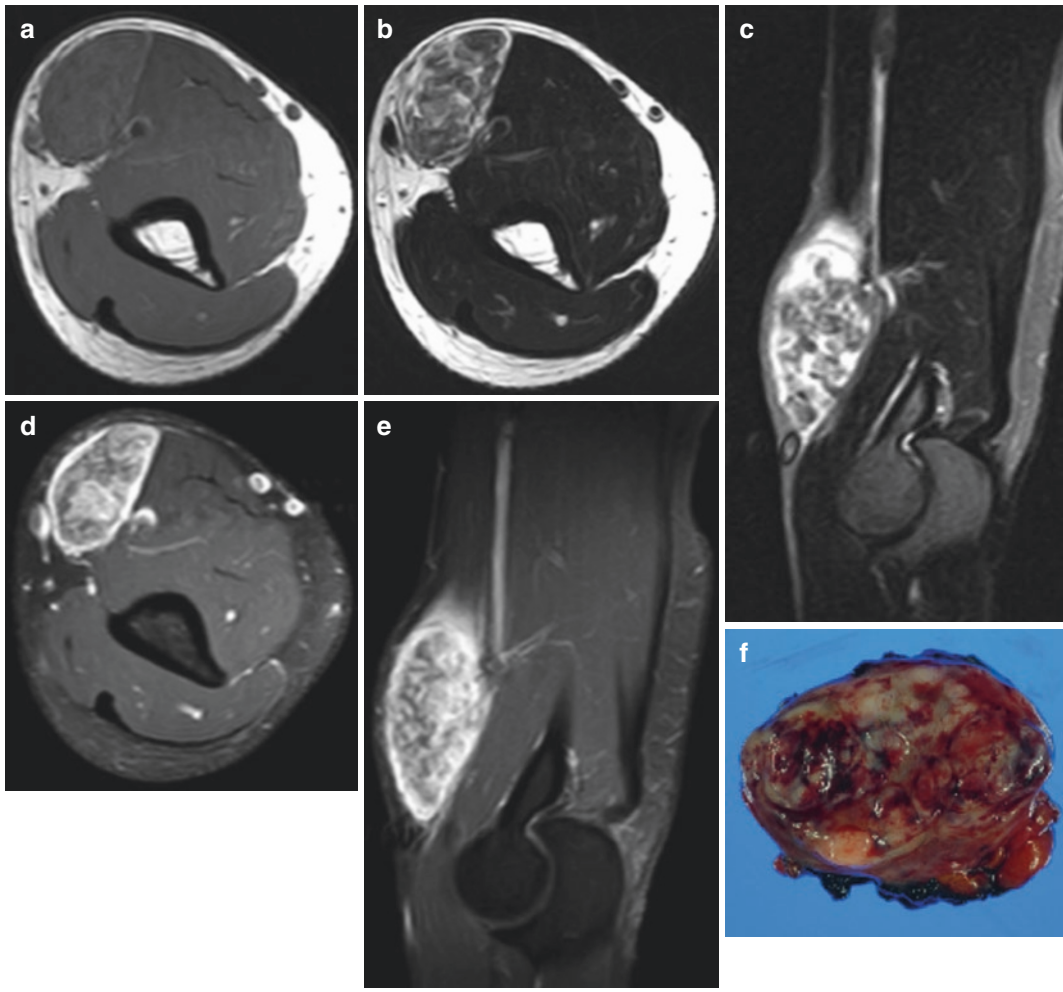

Fig. 13.23 Pleomorphic hyalinizing angiectatic tumor of soft part. Axial T1WI (**a**) shows a well-circumscribed intramuscular mass within the biceps brachii muscle. The mass is heterogeneously isointense to the adjacent muscle. Axial and sagittal T2WIs (**b**, **c**) show a heterogeneously hyperintense soft tissue mass with internal low signal foci and a peripheral high signal rim. Axial and sagittal postcontrast FS T1WIs (**d**, **e**) show heterogeneous enhancement. The central portion of the mass is less enhanced, but the peripheral portion of the T2 hyperintensity is well enhanced. Surgical specimen (**f**) reveals heterogeneous mass

References

Abbes I, Sassi S, Mrad K, et al. A myoepithelial tumour of the soft tissue of the thigh: a case report. Pathology. 2008;40(5):541–2. doi:10.1080/00313020802198085.

Abdullah A, Patel Y, Lewis TJ, Elsamaloty H, Strobel S. Extrarenal malignant rhabdoid tumors: radiologic findings with histopathologic correlation. Cancer Imaging. 2010;10:97–101. doi:10.1102/1470-7330.2010.0010.

Ali S, Leng B, Reinus WR, Khilko N, Khurana JS. Parachordoma/myoepithelioma. Skeletal Radiol. 2013;42(3):431, 457–38. doi:10.1007/s00256-012-1413-6.

Anderson ME, Hornicek FJ, Gebhardt MC, Raskin KA, Mankin HJ. Alveolar soft part sarcoma: a rare and enigmatic entity. Clin Orthop Relat Res. 2005;438:144–8.

Bakri A, Shinagare AB, Krajewski KM, et al. Synovial sarcoma: imaging features of common and uncommon primary sites, metastatic patterns, and treatment response. Am J Roentgenol. 2012;199(2):W208–15. doi:10.2214/ajr.11.8039.

Bancroft LW, Kransdorf MJ, Menke DM, O'Connor MI, Foster WC. Intramuscular myxoma: characteristic MR imaging features. AJR Am J Roentgenol. 2002;178(5):1255–9. doi:10.2214/ajr.178.5.1781255.

Casanova M, Ferrari A, Bisogno G, et al. Alveolar soft part sarcoma in children and adolescents: a report from the Soft-Tissue Sarcoma Italian Cooperative Group. Ann Oncol. 2000;11(11):1445–9.

Chase DR, Enzinger FM. Epithelioid sarcoma. Diagnosis, prognostic indicators, and treatment. Am J Surg Pathol. 1985;9(4):241–63.

Chbani L, Guillou L, Terrier P, et al. Epithelioid sarcoma: a clinicopathologic and immunohistochemical analysis of 106 cases from the French sarcoma group. Am J Clin Pathol. 2009;131(2):222–7. doi:10.1309/AJCPU98ABIPVJAIV.

Christopherson WM, Foote Jr FW, Stewart FW. Alveolar soft-part sarcomas; structurally characteristic tumors of uncertain histogenesis. Cancer. 1952;5(1):100–11.

Chung EB, Enzinger FM. Malignant melanoma of soft parts. A reassessment of clear cell sarcoma. Am J Surg Pathol. 1983;7(5):405–13.

Clabeaux J, Hojnowski L, Valente A, Damron TA. Case report: parachordoma of soft tissues of the arm. Clin Orthop Relat Res. 2008;466(5):1251–6. doi:10.1007/s11999-008-0125-7.

De Beuckeleer LH, De Schepper AM, Vandevenne JE, et al. MR imaging of clear cell sarcoma (malignant melanoma of the soft parts): a multicenter correlative MRI-pathology study of 21 cases and literature review. Skeletal Radiol. 2000;29(4):187–95.

Delabrousse E, Couvreur M, Bartholomot B, Lucas X, Kastler B. Mazabraud syndrome: a case diagnosed with MRI. J Radiol. 2001;82(2):165–7.

Drilon AD, Popat S, Bhuchar G, et al. Extraskeletal myxoid chondrosarcoma: a retrospective review from 2 referral centers emphasizing long-term outcomes with surgery and chemotherapy. Cancer. 2008;113(12):3364–71. doi:10.1002/cncr.23978.

Enzinger FM, Shiraki M. Extraskeletal myxoid chondrosarcoma. An analysis of 34 cases. Hum Pathol. 1972;3(3):421–35.

Fisher C, Miettinen M. Parachordoma: a clinicopathologic and immunohistochemical study of four cases of an unusual soft tissue neoplasm. Ann Diagn Pathol. 1997;1(1):3–10.

Fletcher C, Bridge JA, Hogendoorn P, Mertens F. WHO classification of tumors of soft tissue and bone. Lyon, France: IARC Press; 2013.

Folpe AL, Weiss SW. Pleomorphic hyalinizing angiectatic tumor: analysis of 41 cases supporting evolution from a distinctive precursor lesion. Am J Surg Pathol. 2004;28(11):1417–25.

Folpe AL, Fanburg-Smith JC, Billings SD, et al. Most osteomalacia-associated mesenchymal tumors are a single histopathologic entity: an analysis of 32 cases and a comprehensive review of the literature. Am J Surg Pathol. 2004;28(1):1–30.

Garces-Inigo EF, Leung R, Sebire NJ, McHugh K. Extrarenal rhabdoid tumours outside the central nervous system in infancy. Pediatr Radiol. 2009;39(8):817–22. doi:10.1007/s00247-009-1288-4.

Gebhardt MC, Parekh SG, Rosenberg AE, Rosenthal DI. Extraskeletal myxoid chondrosarcoma of the knee. Skeletal Radiol. 1999;28(6):354–8.

Girish G, Jamadar DA, Landry D, et al. Sonography of intramuscular myxomas: the bright rim and bright cap signs. J Ultrasound Med. 2006;25(7):865–9. quiz 870–861

Goldblum JR, Weiss SW, Folpe AL. Enzinger and Weiss's soft tissue tumors. 6th ed. Philadelphia: Saunders; 2014.

Graadt van Roggen JF, Mooi WJ, Hogendoorn PC. Clear cell sarcoma of tendons and aponeuroses (malignant melanoma of soft parts) and cutaneous melanoma: exploring the histogenetic relationship between these two clinicopathological entities. J Pathol. 1998;186(1):3–7. doi:10.1002/(SICI)1096-9896(199809)186:1<3::AID-PATH153>3.0.CO;2-V.

Guillou L, Wadden C, Coindre JM, Krausz T, Fletcher CD. "Proximal-type" epithelioid sarcoma, a distinctive aggressive neoplasm showing rhabdoid features. Clinicopathologic, immunohistochemical, and ultrastructural study of a series. Am J Surg Pathol. 1997;21(2):130–46.

Hanna SL, Kaste S, Jenkins JJ, et al. Epithelioid sarcoma: clinical, MR imaging and pathologic findings. Skeletal Radiol. 2002;31(7):400–12. doi:10.1007/s00256-002-0509-9.

Hourani M, Khoury N, Mourany B, Shabb NS. MR appearance of clear cell sarcoma of tendons and aponeuroses (malignant melanoma of soft parts): radiologic-pathologic correlation. Skeletal Radiol. 2005;34(9):543–6. doi:10.1007/s00256-005-0893-z.

Javery O, Krajewski K, O'Regan K, et al. A to Z of extraskeletal Ewing sarcoma family of tumors in adults: imaging features of primary disease, metastatic patterns, and treatment responses. AJR Am

J Roentgenol. 2011;197(6):W1015–22. doi:10.2214/AJR.11.6667.

Jones BC, Sundaram M, Kransdorf MJ. Synovial sarcoma: MR imaging findings in 34 patients. Am J Roentgenol. 1993;161(4):827–30. doi:10.2214/ajr.161.4.8396848.

Kabukcuoglu F, Kabukcuoglu Y, Yilmaz B, Erdem Y, Evren I. Mazabraud's syndrome: intramuscular myxoma associated with fibrous dysplasia. Pathol Oncol Res. 2004;10(2):121–3. doi:PAOR.2004.10.2.0121.

Kapoor N, Shinagare AB, Jagannathan JP, et al. Clinical and radiologic features of extraskeletal myxoid chondrosarcoma including initial presentation, local recurrence, and metastases. Radiol Oncol. 2014;48(3):235–42. doi:10.2478/raon-2014-0005.

Kempson R, Fletcher C, Evans H. Tumors of uncertain differentiation and those in which differentiation is nonmesenchymal. In: Goldblum JR, editor. Tumors of the soft tissues, vol. 3. Bethesda, MD: Armed Forces Institute of Pathology; 2001. p. 419–501.

Kim SJ. Sonographic appearance of an intramuscular myxoma of the pectoralis major muscle. J Clin Ultrasound. 2014;42(8):505–8. doi:10.1002/jcu.22149.

Kodet R, Newton Jr WA, Sachs N, et al. Rhabdoid tumors of soft tissues: a clinicopathologic study of 26 cases enrolled on the Intergroup Rhabdomyosarcoma Study. Hum Pathol. 1991;22(7):674–84.

Kransdorf MJ. Malignant soft-tissue tumors in a large referral population: distribution of diagnoses by age, sex, and location. Am J Roentgenol. 1995;164(1):129–34. doi:10.2214/ajr.164.1.7998525.

Kransdorf MJ, Meis JM. From the archives of the AFIP. Extraskeletal osseous and cartilaginous tumors of the extremities. Radiographics. 1993;13(4):853–84. doi:10.1148/radiographics.13.4.8356273.

Kransdorf MJ, Murphey MD. Imaging of soft tissue tumors. 3rd ed. Philadelphia: Lippincott Williams & Wilkins; 2014.

Langezaal SM, Graadt van Roggen JF, Cleton-Jansen AM, Baelde JJ, Hogendoorn PC. Malignant melanoma is genetically distinct from clear cell sarcoma of tendons and aponeurosis (malignant melanoma of soft parts). Br J Cancer. 2001;84(4):535–8. doi:10.1054/bjoc.2000.1628.

Lieberman PH, Foote Jr FW, Stewart FW, Berg JW. Alveolar soft-part sarcoma. JAMA. 1966;198(10):1047–51.

Lieberman PH, Brennan MF, Kimmel M, et al. Alveolar soft-part sarcoma. A clinico-pathologic study of half a century. Cancer. 1989;63(1):1–13.

Lo HH, Kalisher L, Faix JD. Epithelioid sarcoma:radiologic and pathologic manifestations. AJR Am J Roentgenol. 1977;128(6):1017–20. doi:10.2214/ajr.128.6.1017.

Lorigan JG, O'Keeffe FN, Evans HL, Wallace S. The radiologic manifestations of alveolar soft-part sarcoma. AJR Am J Roentgenol. 1989;153(2):335–9. doi:10.2214/ajr.153.2.335.

Lucas DR, Nascimento AG, Sim FH. Clear cell sarcoma of soft tissues. Mayo Clinic experience with 35 cases. Am J Surg Pathol. 1992;16(12):1197–204.

Luna A, Martinez S, Bossen E. Magnetic resonance imaging of intramuscular myxoma with histological comparison and a review of the literature. Skeletal Radiol. 2005;34(1):19–28. doi:10.1007/s00256-004-0848-9.

McCarville MB, Muzzafar S, Kao SC, et al. Imaging features of alveolar soft-part sarcoma: a report from Children's Oncology Group Study ARST0332. AJR Am J Roentgenol. 2014;203(6):1345–52. doi:10.2214/AJR.14.12462.

Murphey MD, Kransdorf MJ, Smith SE. Imaging of soft tissue neoplasms in the adult: malignant tumors. Semin Musculoskelet Radiol. 1999;3(1):39–58. doi:10.1055/s-2008-1080050.

Murphey MD, McRae GA, Fanburg-Smith JC, et al. Imaging of soft-tissue myxoma with emphasis on CT and MR and comparison of radiologic and pathologic findings. Radiology. 2002;225(1):215–24. doi:10.1148/radiol.2251011627.

Murphey MD, Gibson MS, Jennings BT, et al. From the archives of the AFIP: imaging of synovial sarcoma with radiologic-pathologic correlation. Radiographics. 2006;26(5):1543–65. doi:10.1148/rg.265065084.

Murphey MD, Senchak LT, Mambalam PK, et al. From the radiologic pathology archives: Ewing sarcoma family of tumors: radiologic-pathologic correlation. Radiographics. 2013;33(3):803–31. doi:10.1148/rg.333135005.

Oda Y, Tsuneyoshi M. Extrarenal rhabdoid tumors of soft tissue: clinicopathological and molecular genetic review and distinction from other soft-tissue sarcomas with rhabdoid features. Pathol Int. 2006;56(6):287–95. doi:10.1111/j.1440-1827.2006.01962.x.

Ogose A, Hotta T, Emura I, et al. Recurrent malignant variant of phosphaturic mesenchymal tumor with oncogenic osteomalacia. Skeletal Radiol. 2001;30(2):99–103.

Orbach D, Brennan B, Casanova M, et al. Paediatric and adolescent alveolar soft part sarcoma: a joint series from European cooperative groups. Pediatr Blood Cancer. 2013;60(11):1826–32. doi:10.1002/pbc.24683.

Pennacchioli E, Fiore M, Collini P, et al. Alveolar soft part sarcoma: clinical presentation, treatment, and outcome in a series of 33 patients at a single institution. Ann Surg Oncol. 2010;17(12):3229–33. doi:10.1245/s10434-010-1186-x.

Perez Sanchez P, Gonzalez Llorente J. Mazabraud's syndrome, an uncommon association of intramuscular myxoma with fibrous dysplasia. Radiologia. 2014;56(3):281–3. doi:10.1016/j.rx.2012.06.006.

Portera Jr CA, Ho V, Patel SR, et al. Alveolar soft part sarcoma: clinical course and patterns of metastasis in 70 patients treated at a single institution. Cancer. 2001;91(3):585–91.

Reeves BR, Fletcher CD, Gusterson BA. Translocation t(12;22)(q13;q13) is a nonrandom rearrangement in clear cell sarcoma. Cancer Genet Cytogenet. 1992;64(2):101–3.

Rodriguez E, Sreekantaiah C, Reuter VE, Motzer RJ, Chaganti RS. t(12;22)(q13;q13) and trisomy 8 are nonrandom aberrations in clear-cell sarcoma. Cancer Genet Cytogenet. 1992;64(2):107–10.

Segal NH, Pavlidis P, Noble WS, et al. Classification of clear-cell sarcoma as a subtype of melanoma by genomic profiling. J Clin Oncol. 2003;21(9):1775–81. doi:10.1200/JCO.2003.10.108.

Smith ME, Fisher C, Weiss SW. Pleomorphic hyalinizing angiectatic tumor of soft parts. A low-grade neoplasm resembling neurilemoma. Am J Surg Pathol. 1996;20(1):21–9.

Subhawong TK, Subhawong AP, Montgomery EA, Fayad LM. Pleomorphic hyalinizing angiectatic tumor: imaging findings. Skeletal Radiol. 2012;41(12):1621–6. doi:10.1007/s00256-012-1443-0.

Suh JS, Cho J, Lee SH, et al. Alveolar soft part sarcoma: MR and angiographic findings. Skeletal Radiol. 2000;29(12):680–9.

Suzuki K, Yasuda T, Hori T, et al. Pleomorphic hyalinizing angiectatic tumor arising in the thigh: a case report. Oncol Lett. 2014;7(4):1249–52. doi:10.3892/ol.2014.1883.

Tateishi U, Hasegawa T, Kusumoto M, Yokoyama R, Moriyama N. Radiologic manifestations of proximal-type epithelioid sarcoma of the soft tissues. AJR Am J Roentgenol. 2002;179(4):973–7. doi:10.2214/ajr.179.4.1790973.

Tateishi U, Hasegawa T, Beppu Y, Satake M, Moriyama N. Synovial sarcoma of the soft tissues: prognostic significance of imaging features. J Comput Assist Tomogr. 2004;28(1):140–8.

Tateishi U, Hasegawa T, Nojima T, Takegami T, Arai Y. MRI features of extraskeletal myxoid chondrosarcoma. Skeletal Radiol. 2006;35(1):27–33. doi:10.1007/s00256-005-0021-0.

Tian L, Cui CY, Lu SY, et al. Clinical presentation and CT/MRI findings of alveolar soft part sarcoma: a retrospective single-center analysis of 14 cases. Acta Radiol. 2016;57(4):475–80. doi:10.1177/0284185115597720.

Van Rijswijk C, Hogendoorn P, Taminiau A, Bloem J. Synovial sarcoma: dynamic contrast-enhanced MR imaging features. Skeletal Radiol. 2001;30(1):25–30.

Vliet M, Kliffen M, Krestin GP, Dijke CF. Soft tissue sarcomas at a glance: clinical, histological, and MR imaging features of malignant extremity soft tissue tumors. Eur Radiol. 2009;19(6):1499–511. doi:10.1007/s00330-008-1292-3.

Weidner N, Santa Cruz D. Phosphaturic mesenchymal tumors. A polymorphous group causing osteomalacia or rickets. Cancer. 1987;59(8):1442–54.

Yao MS, Chen CY, Chin-Wei Chien J, Chen CL, Chan WP. Magnetic resonance imaging of gluteal intramuscular myxoma. Clin Imaging. 2007;31(3):214–6. doi:10.1016/j.clinimag.2007.01.010.

Zou LY, Brown DA, Li AC. Intramuscular myxoma. Ultrasound Q. 2013;29(3):255–6. doi:10.1097/RUQ.0b013e3182a25746.

Undifferentiated/Unclassified Sarcoma

14

Malignant fibrous histiocytoma (MFH), the malignant counterpart of the so-called fibrohistiocytic tumors, was first described in 1963 and is generally accepted as one of the most common types of soft tissue sarcoma in the extremities of elderly patients (Weiss and Enzinger 1978; Gibbs et al. 2001). The concept and classification of MFH have changed over the past five decades. With recent advances in immunohistochemistry, cytogenetic, and molecular genetic studies, many tumors labeled 'MFH' could be subclassified as lineage-specific sarcoma after reassessment and close scrutiny. The World Health Organization (WHO) significantly reorganized the nomenclature of MFH in 2002. The term 'MFH' was removed, and the lesions are now included in the quite separate and new category of undifferentiated/unclassified sarcomas. The myxoid variant of MFH was renamed 'myxofibrosarcoma' and moved into the fibroblastic/myofibroblastic tumor section. These lesions show no definable line of differentiation using currently available technologies. Dedifferentiated types of specific sarcomas are not included in this category. Such undifferentiated tumors may have spindle cell, pleomorphic, round cell or epithelioid cytomorphologies. A significant subset of radiation-associated sarcomas is included in this category (Rosenberg 2013; Fletcher 2014; Goldblum 2014; Doyle 2014).

14.1 Undifferentiated Pleomorphic Sarcoma

Undifferentiated pleomorphic sarcoma (UPS) was used synonymously with 'MFH', the outdated terminology, in the past. UPS still accounts for a significant proportion of sarcomas occurring in late adult life between the ages of 50 and 70 years. The tumor occurs most frequently in the lower extremities, especially the thigh, followed by the upper extremities. It usually manifests as a painless, slowly enlarging mass (Goldblum 2014). The vast majority of UPS are high-grade lesions, having a local recurrence rate that ranges from 19% to 31%, a metastatic rate from 31% to 35%, and a 5-year survival rate from 65% to 70% (Le Doussal et al. 1996; Zagars et al. 1996; Salo et al. 1999; Engellau et al. 2004).

Microscopically, UPS manifests a highly variable histologic appearance, although it shows frequent transitions from storiform to pleomorphic areas (Matushansky et al. 2009; Goldblum 2014). Therefore, UPS is a diagnosis of exclusion. The diagnosis of UPS is made after exclusion of a specific type of pleomorphic sarcoma (e.g., pleomorphic leiomyosarcoma, pleomorphic liposarcoma), dedifferentiated liposarcoma, and sarcomatoid carcinoma.

The imaging features of UPS are quite nonspecific. On CT imaging, the tumor appears as

H.S. Kang et al., *Oncologic Imaging: Soft Tissue Tumors*, DOI 10.1007/978-981-287-718-5_14

a heterogeneous enhancing mass, with similar attenuation to the adjacent muscle. Depending on the cellularity and presence of hemorrhage, necrosis, and/or calcification, the tumor shows low to intermediate signal intensity on T1-weighted images and heterogeneous high signal intensity on T2-weighted images. The lesion usually exhibits contrast enhancement, which may be heterogeneous if areas of necrosis or hemorrhage are present. An infiltrative growth pattern or tail-like spread of the tumor along deep fascia is frequently observed in superficial UPS, a feature that is described as a 'tail-sign' on MR imaging. Several studies describe the 'tail-sign' as a tail-like, multidirectional, and extensive spread along the fascial plane on T2-weighted images. On contrast-enhanced T1-weighted images, a tapered fascial enhancement more than 2 mm thick is observed extending from the tumor margin. Recently, the 'tail-sign' has become recognized as an important risk factor for postoperative positive margins and local recurrence (Lefkowitz et al. 2013; Iwata et al. 2014; Yoo et al. 2014; Imanishi et al. 2016). However, this sign is not specific for UPS and is frequently observed in myxofibrosarcoma or nodular fasciitis.

14.2 Undifferentiated Round Cell and Spindle Cell Sarcoma

These lesions show round cell or spindle cell morphology but cannot be classified into any other category. The subclassification of round cell and spindle cell sarcomas is important because it can provide optimal treatment options and well-defined chemotherapeutic regimens in certain subsets of round cell (e.g., Ewing sarcoma/PNET, rhabdomyosarcoma) and spindle cell sarcomas (e.g., synovial sarcoma). If tumors appear to be undifferentiated by whatever techniques are applied, they remain in this category. However, at least within the round cell category, new genetic markers are beginning to be recognized for a subset of undifferentiated round cell (non-Ewing) sarcomas, specifically those that harbor CIC-DUX4, BCOR-CCNB3, or BCOR-MAML3 fusion genes. The identification of these markers suggests that some undifferentiated/unclassified sarcomas will eventually be recognized as genetically distinct tumor types (Doyle 2014; Fletcher 2014; Specht et al. 2016; Fletcher 2008).

14.3 Illustrations: Undifferentiated/Unclassified Sarcoma

14.3.1 Undifferentiated Pleomorphic Sarcoma

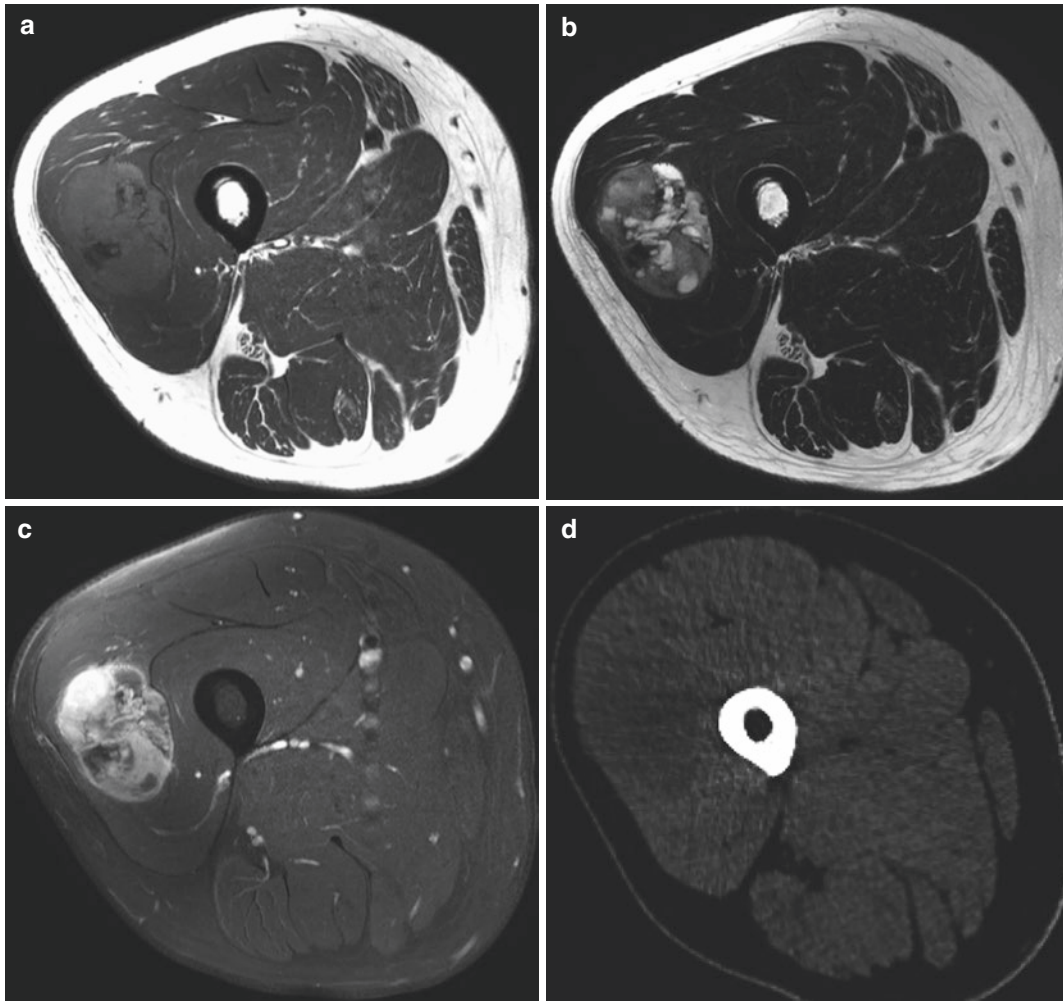

Fig. 14.1 Undifferentiated pleomorphic sarcoma. Axial T1WI (**a**) and T2WI (**b**) show an intramuscular mass with heterogeneous and mixed signal intensities. The mass appears to be heterogeneously enhanced on axial postcontrast FS T1WI (**c**). There is no intratumoral mineralization on CT (**d**)

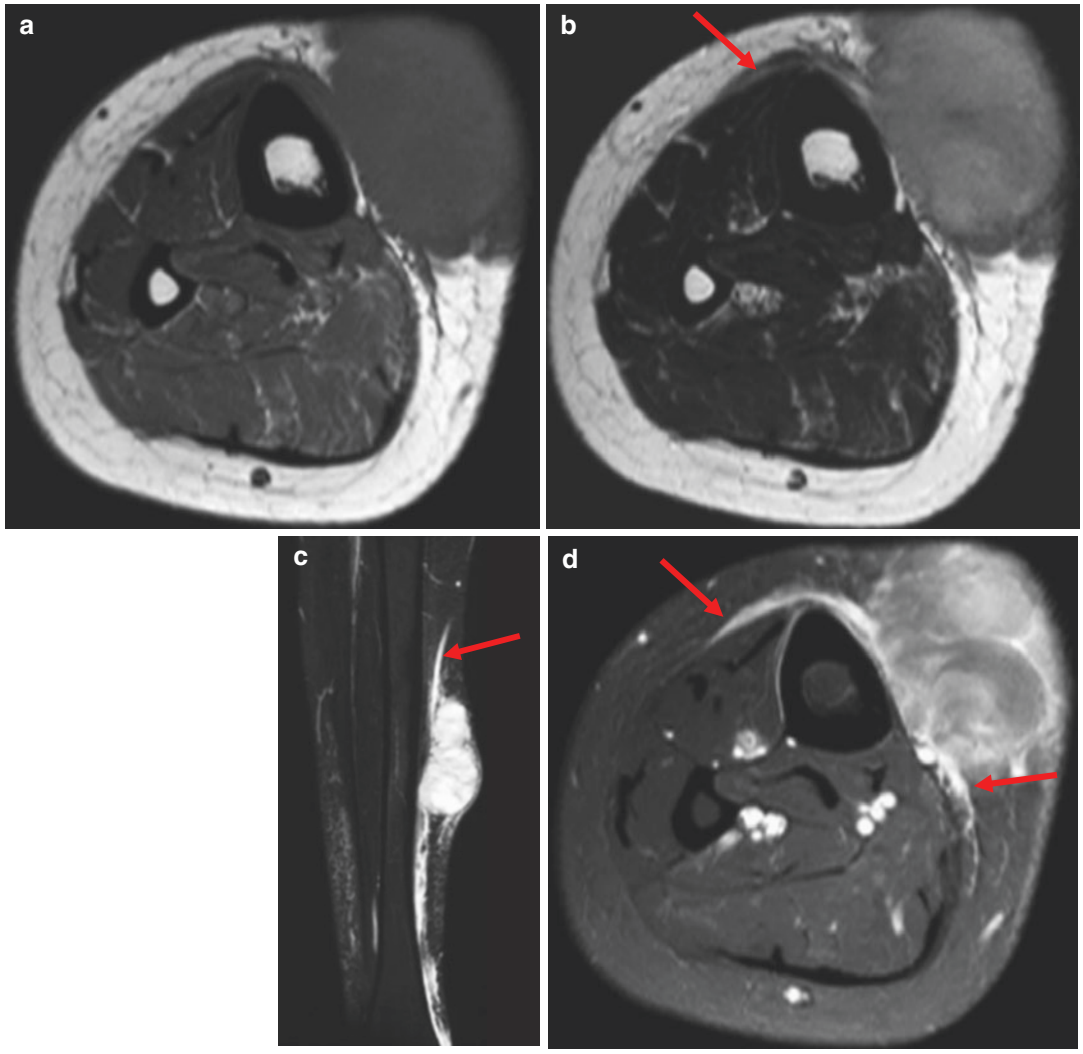

Fig. 14.2 Undifferentiated pleomorphic sarcoma. Axial T1WI (**a**) shows a nonspecific subcutaneous soft tissue mass. Axial and coronal T2WIs (**b**, **c**) demonstrate hyperintense mass. There is tapered fascial thickening along the crural fascia, extending from the subcutaneous mass (*arrows*). Axial postcontrast FS T1WI (**d**) demonstrates heterogeneous enhancement in the mass and reveals a tail-like contrast enhancement spreading from the mass, indicating a tail-sign (*arrows*). Three years after wide excision of the mass, localized periosteal thickening (*arrows*) was found on follow-up MR image (**e**–**g**), likely indicating a local tumor recurrence. US (**h**) also shows localized periosteal soft tissue thickening (*arrow*), histologically confirmed as recurred tumor

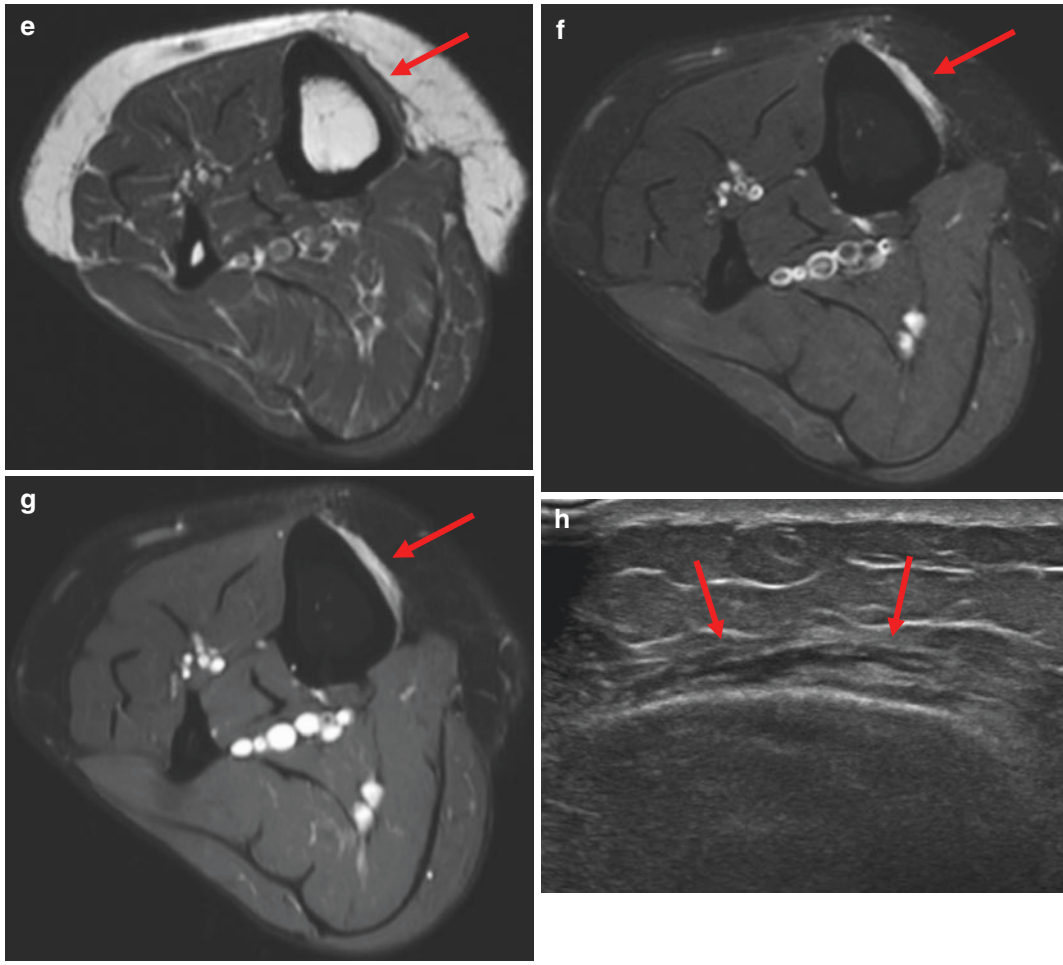

Fig. 14.2 (continued)

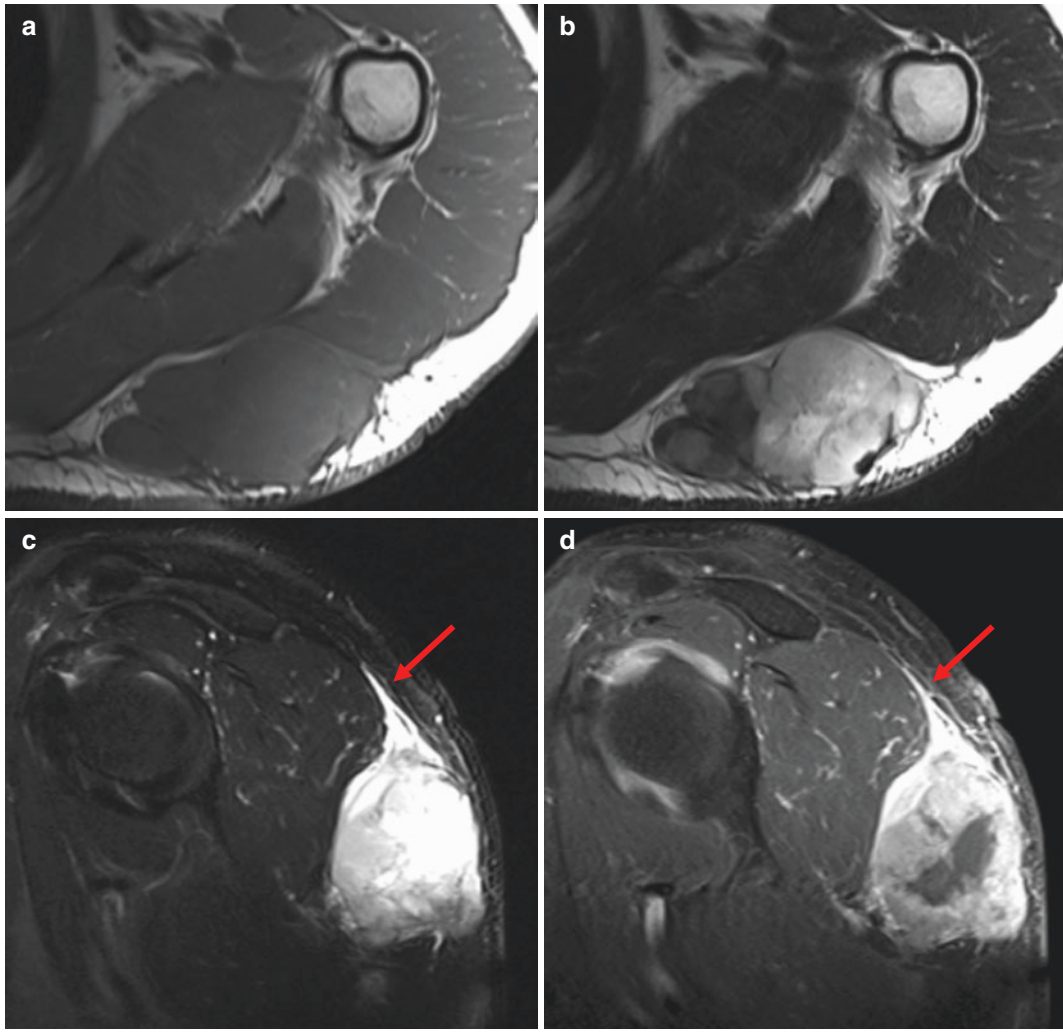

Fig. 14.3 Undifferentiated pleomorphic sarcoma. Axial T1WI (**a**) and T2WI (**b**) show a nonspecific subcutaneous soft tissue mass in the posterior shoulder. The mass is isointense on T1WI (**a**) and heterogeneously hypo- to hyperintense on T2WI (**b**). Sagittal FS T2WIs (**c**) demonstrate a perifascial extension of signal abnormalities spreading from the main mass, suggestive of the tail-sign (*arrow*). Sagittal postcontrast FS T1WI (**d**) also shows heterogeneous enhancement with central necrosis and a tail-sign (*arrow*) along the adjacent deep fascia

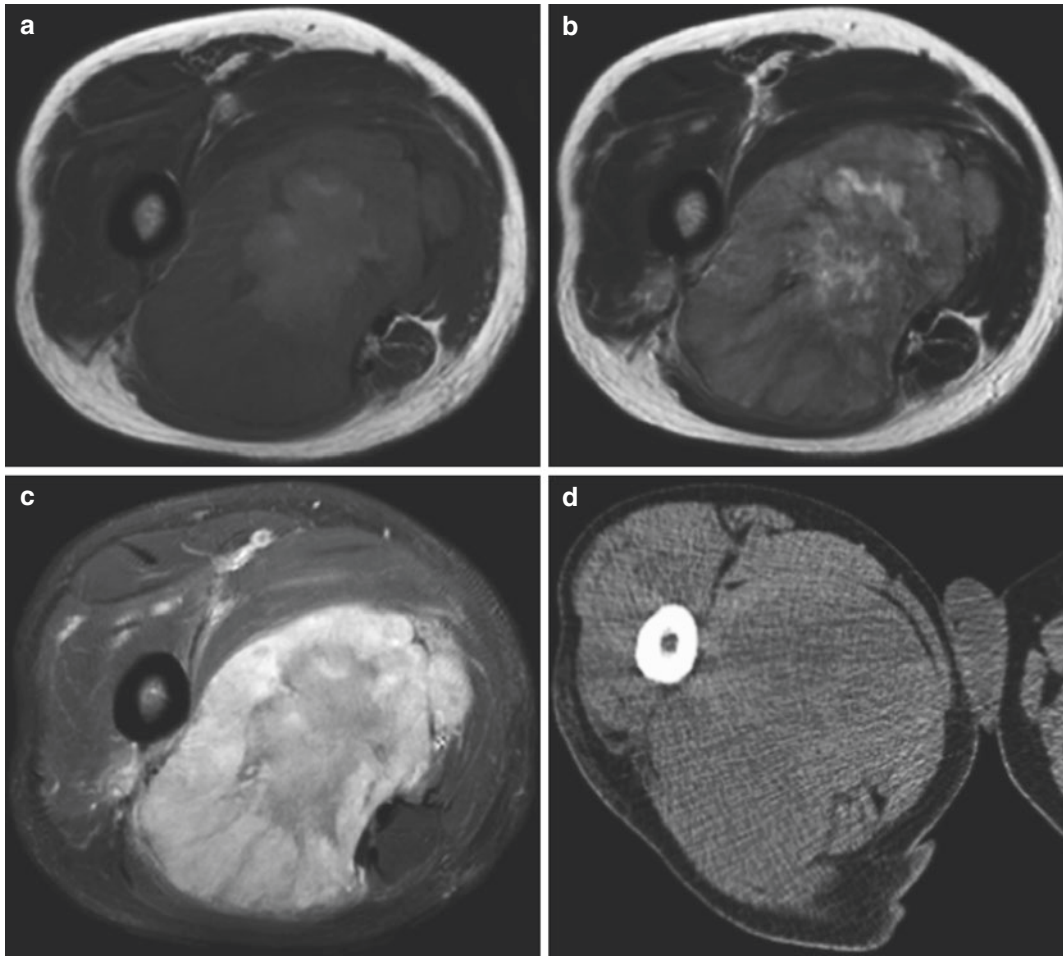

Fig. 14.4 Undifferentiated pleomorphic sarcoma. Axial T1WI (**a**) shows a large intramuscular mass of slightly higher signal intensity than the surrounding muscle. Axial T2WI (**b**) shows heterogeneous intermediate to high signal intensity. Axial postcontrast FS T1WI (**c**) reveals heterogeneous enhancement. Non-contrast CT (**d**) shows a nonspecific intramuscular mass without calcification

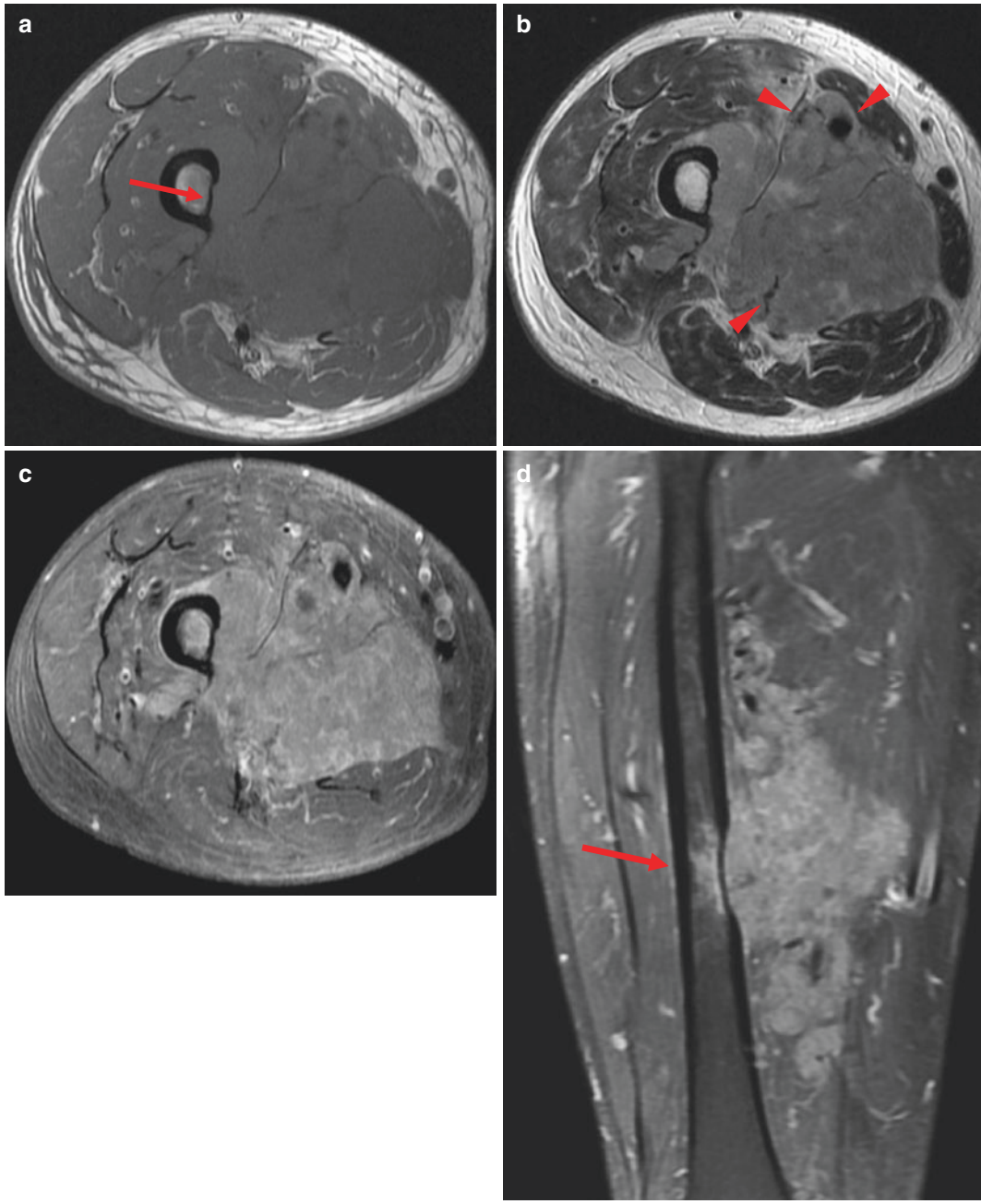

Fig. 14.5 Undifferentiated pleomorphic sarcoma. Axial T1WI (**a**) shows a poorly defined intramuscular mass involving the adjacent femur cortex (*arrow*). Axial T2WI (**b**) reveals an infiltrative soft tissue mass of intermediate to high signal intensity encasing the neurovascular bundle (*arrowheads*). Axial (**c**) and coronal (**d**) postcontrast FS T1WIs reveal diffuse contrast enhancement of the mass. Direct bone invasion (*arrow*) is observed in the medial cortex of the femur, with adjacent bone marrow enhancement

14.3.2 CIC-DUX4 Fusion Positive Undifferentiated Round Cell Sarcoma

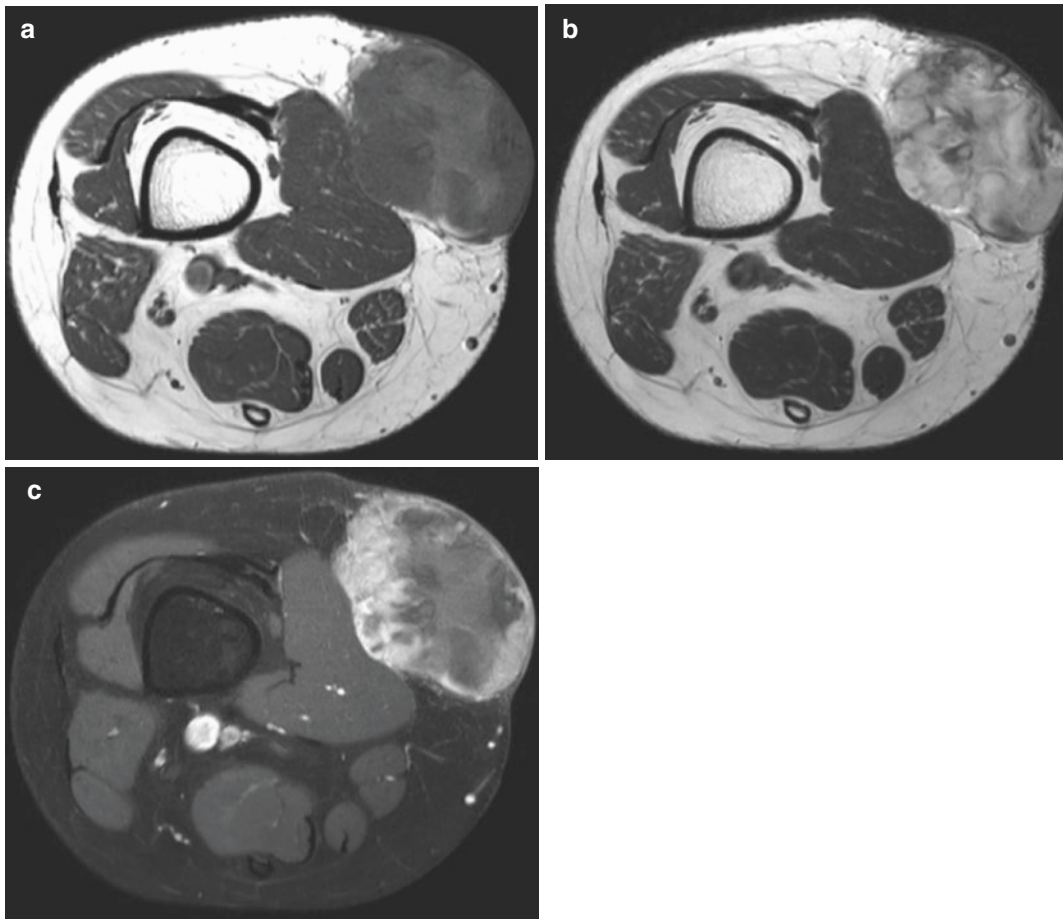

Fig. 14.6 CIC-DUX4 fusion positive undifferentiated round cell sarcoma. Axial T1WI (**a**) and T2WI (**b**) show a subcutaneous mass of heterogeneous signal intensity. Axial postcontrast FS TWI (**c**) shows central necrosis and peripheral enhancement

References

Doyle LA. Sarcoma classification: an update based on the 2013 world health organization classification of tumors of soft tissue and bone. Cancer. 2014;120(12):1763–74. doi:10.1002/cncr.28657.

Engellau J, Anderson H, Rydholm A, et al. Time dependence of prognostic factors for patients with soft tissue sarcoma: a Scandinavian Sarcoma Group study of 338 malignant fibrous histiocytomas. Cancer. 2004;100(10):2233–9. doi:10.1002/cncr.20254.

Fletcher CD. Undifferentiated sarcomas: what to do? And does it matter? A surgical pathology perspective. Ultrastruct Pathol. 2008;32(2):31–6. doi:10.1080/01913120801896945.

Fletcher CD. The evolving classification of soft tissue tumours—an update based on the new 2013 WHO classification. Histopathology. 2014;64(1):2–11. doi:10.1111/his.12267.

Gibbs JF, Huang PP, Lee RJ, et al. Malignant fibrous histiocytoma: an institutional review. Cancer Investig. 2001;19(1):23–7.

Goldblum JR. An approach to pleomorphic sarcomas: can we subclassify, and does it matter? Mod Pathol. 2014;27(Suppl 1):S39–46. doi:10.1038/modpathol.2013.174.

Imanishi J, Slavin J, Pianta M, et al. Tail of superficial myxofibrosarcoma and undifferentiated pleomorphic sarcoma after preoperative radiotherapy. Anticancer Res. 2016;36(5):2339–44.

Iwata S, Yonemoto T, Araki A, et al. Impact of infiltrative growth on the outcome of patients with undifferentiated pleomorphic sarcoma and myxofibrosarcoma. J Surg Oncol. 2014;110(6):707–11. doi:10.1002/jso.23708.

Le Doussal V, Coindre JM, Leroux A, et al. Prognostic factors for patients with localized primary malignant fibrous histiocytoma: a multicenter study of 216 patients with multivariate analysis. Cancer. 1996;77(9):1823–30. doi:10.1002/(SICI)1097-0142(19960501)77:9<1823::AID-CNCR10>3.0.CO;2-1.

Lefkowitz RA, Landa J, Hwang S, et al. Myxofibrosarcoma: prevalence and diagnostic value of the "tail sign" on magnetic resonance imaging. Skelet Radiol. 2013;42(6):809–18. doi:10.1007/s00256-012-1563-6.

Matushansky I, Charytonowicz E, Mills J, et al. MFH classification: differentiating undifferentiated pleomorphic sarcoma in the 21st century. Expert Rev Anticancer Ther. 2009;9(8):1135–44. doi:10.1586/era.09.76.

Rosenberg AE. WHO classification of soft tissue and bone, fourth edition: summary and commentary. Curr Opin Oncol. 2013;25(5):571–3. doi:10.1097/01.cco.0000432522.16734.2d.

Salo JC, Lewis JJ, Woodruff JM, Leung DH, Brennan MF. Malignant fibrous histiocytoma of the extremity. Cancer. 1999;85(8):1765–72.

Specht K, Zhang L, Sung YS, et al. Novel BCOR-MAML3 and ZC3H7B-BCOR gene fusions in undifferentiated small blue round cell sarcomas. Am J Surg Pathol. 2016;40(4):433–42. doi:10.1097/PAS.0000000000000591.

Weiss SW, Enzinger FM. Malignant fibrous histiocytoma: an analysis of 200 cases. Cancer. 1978;41(6):2250–66.

Yoo HJ, Hong SH, Kang Y, et al. MR imaging of myxofibrosarcoma and undifferentiated sarcoma with emphasis on tail sign; diagnostic and prognostic value. Eur Radiol. 2014;24(8):1749–57. doi:10.1007/s00330-014-3181-2.

Zagars GK, Mullen JR, Pollack A. Malignant fibrous histiocytoma: outcome and prognostic factors following conservation surgery and radiotherapy. Int J Radiat Oncol Biol Phys. 1996;34(5):983–94.

Superficial Soft Tissue Masses 15

15.1 Epidermal Inclusion Cyst

Epidermal inclusion cyst is a benign lesion derived from the focal proliferation of dermal squamous epithelium. This tumor is also referred to as sebaceous, epidermoid, epidermal, infundibular, or keratin cysts (Kim et al. 2011a). Epidermal inclusion cysts are lined with stratified squamous epithelium and filled with a white, cheesy material, reflecting layers of keratin and cholesterol-rich debris (Hong et al. 2006). The cyst may be a congenital lesion developed from the subcutaneous implantation of keratinizing epithelial cells during embryogenesis. Epidermal inclusion cysts can also be a result of downward growth of epithelial cells after occlusion of the hair follicle and the growth of implanted epithelial elements after trauma or surgery (Hong et al. 2006; Huang et al. 2011; Kim et al. 2011a). Clinically, epidermal inclusion cysts present as slow-growing dermal or subcutaneous cysts. These cysts usually occur in the hair-bearing areas of the body, such as the scalp, face, neck, trunk, and back (Kim et al. 2011a). Moreover, they usually remain asymptomatic unless they become infected or rupture into the adjacent soft tissues.

On US, the cyst is a well-circumscribed, ovoid, and hypoechoic mass containing variable echogenic foci. Associated internal debris includes internal linear echogenic reflections, filiform anechoic areas, or alternating layers of hyper- and hypoechoic rings (an 'onion ring' or 'bull's eye' appearance has been described for the testis). Histologically, the floating linear echogenic reflections are created by sporadically distributed cholesterol, sebaceous foci, or calcifications, while the dark clefts occur in areas containing scattered fragments of packed lamellae of keratin (Lee et al. 2001; Huang et al. 2011). The internal debris is mobile, showing a 'swirling' appearance when pressed with the probe (Kim et al. 2011a). The cyst exhibits posterior acoustic enhancement and a small extension into the dermis, corresponding to its communication with the skin (i.e., dermal attachment) (Lee et al. 2001). Color Doppler study usually shows no vascular flow signal, but this can be observed in ruptured cysts.

On MR imaging, the lesion is a well-demarcated oval-shaped mass of high signal intensity on T2-weighted image. Moderate linear dark debris can be observed in the nondependent portion of the mass and can be best visualized on T2-weighted image. On T1-weighted image, the internal signal intensity is either hyper- or isointense to that of adjacent muscles due to its proteinaceous content. After contrast administration, the mass shows thin peripheral enhancement. However, ruptured epidermal cysts usually contain septa and show thick and irregular rim enhancement, with fuzzy adjacent soft tissue enhancement on postcontrast images. These imaging features of a ruptured epidermal cyst could mimic a mass of infectious or neoplastic origin. (Hong et al. 2006).

H.S. Kang et al., *Oncologic Imaging: Soft Tissue Tumors*, DOI 10.1007/978-981-287-718-5_15

15.2 Pilomatricoma

Pilomatricoma is a benign superficial tumor of the hair follicle. It frequently occurs in the dermal or subcutaneous layer of the neck, head, and face (including the periorbital, preauricular, cheek, and scalp areas), followed by the upper extremity. However, pilomatricoma can occur in any hair-bearing skin, usually within the first two decades of life. Clinically, this tumor appears as an asymptomatic palpable mass with a rock-hard consistency. Histologically, the tumor is composed of epithelial cells surrounded by a connective tissue capsule. There are basaloid cells in the peripheral regions of the tumor, whereas the central region contains mummified ghost cells. These cells have lost their nuclei and are filled with keratin and often calcium deposits. The stroma is composed of collagen and contains blood vessels. Calcification is observed in approximately 85% of lesions (Hwang et al. 2005; Lim et al. 2007; Garioni et al. 2008; De Beuckeleer et al. 1996).

Little is known about the ultrasonographic features of pilomatricoma despite its frequent occurrence because this entity is usually excised without imaging studies. On US, pilomatricoma usually appears to be an oval hyperechoic or isoechoic mass with well-defined margin. Most cases have internal echogenic foci that represent calcifications and posterior acoustic shadowing behind these calcifications. Occasionally, it presents as a calcification only or as an irregular hyperechoic lesion with an obscured margin due to posterior acoustic shadowing. A hypoechoic rim is also frequently found, representing a connective tissue capsule that surrounds the tumor histopathologically. Color Doppler flows are commonly found in the peripheral region only (Hwang et al. 2005). On CT, pilomatricoma is a well-defined mass of soft tissue density showing varying levels of calcification and variable enhancement (Lim et al. 2007). Lim et al. reported findings of cystic degeneration and peritumoral changes. On MR imaging, pilomatricoma shows a homogeneous intermediate signal intensity on T1-weighted image and heterogeneous low to intermediate signal intensity on T2-weighted image, which may be related to the large amount of collagen within the lesion (De Beuckeleer et al. 1996). Pilomatricoma has an internal reticulation and patchy areas on T2-weighted image and post-contrast T1-weighted image, which corresponded to the distribution of the intercellular stroma on pathologic specimens (Lim et al. 2007). Peritumoral hyperechogenicity on US and peritumoral strands on CT and MR imaging can be found if pilomatricoma is accompanied by chronic inflammation with foreign body reaction. The radiologic differential diagnosis of pilomatricomas includes calcified lymph nodes, ossifying hematoma, hemangioma with phlebolith, granuloma annulare, and dermatofibrosarcoma.

15.3 Fat Necrosis

Fat necrosis infrequently presents as a soft tissue mass and usually located over a pressure point or bony protuberance. Clinically, the patient may be asymptomatic or may present with pain, skin induration, ecchymosis, skin retraction, or skin thickening. Numerous etiologies of fat necrosis have been reported, including trauma, cold exposure, iatrogenic injections, collagen vascular disease, sickle cell disease, and vasculitis. The end result has been described as vascular impairment or saponification of fat by lipase originating from blood (Walsh et al. 2008). Fat necrosis can be a finding in lobular panniculitis, which is an inflammation in the fat lobules of subcutaneous fat (Fernando et al. 2003). Histologic examination reveals nonviable adipose tissue with chronic and focal inflammation, frequently surrounded by a reactive fibrous capsule (Chan et al. 2003; Fernando et al. 2003; Walsh et al. 2008). It has variable appearances that range from nonspecific soft tissue stranding to mimicking lipoma or liposarcoma.

The radiologic appearance of fat necrosis in the extremities has not been well described, while its sonographic and mammographic appearances in the breast are better documented (Fernando et al. 2003). Fernando et al. and Walsh et al. reported fat necrosis may have two different

sonographic appearances, either appearing as a poorly defined hyperechoic region within the more hypoechoic subcutaneous fat, or a well-defined isoechoic mass with a hypoechoic halo (Fernando et al. 2003; Walsh et al. 2008). The signal characteristics of subcutaneous fat necrosis on MR imaging are not clearly defined. Lopez et al. described fat necrosis in the extremities as a small, linear spiculated lesion with either a globular T1 hyperintense area (corresponding to fat necrosis) or a T2 hypointense laminar component (representing reactive fibrous tissue) (López et al. 1997). Tsai et al. described the MR features of subcutaneous fat necrosis as a lack of a discrete mass, linear hypointensity on T1-weighted images, and mixed hyper- or hypointensity on T2-weighted images. The variability of linear signal intensities is most likely related to the variable stages of necrosis, edema, hemorrhage, and fibrosis that are associated with fat necrosis after trauma over time (Tsai et al. 1997). In cases of poorly defined hyperechoic regions on US, Walsh et al. described fat necrosis on MR imaging as an ill-defined mass with intermediate signal intensity and either diffuse or ring enhancement after contrast administration (Walsh et al. 2008).

15.4 Rheumatoid Nodule

Rheumatoid nodules are uncommon but well-known extra-articular manifestations of rheumatoid arthritis, commonly occurring at sites of repetitive mechanical irritation, such as the extensor surfaces of the hand, feet, elbow, and the ischial tuberosities (Veys and De Keyser 1993).

Radiographs show nonspecific soft tissue mass that is uncommonly calcified. On MR imaging, rheumatoid nodule appears as an ill-defined solid mass or a predominantly cystic mass. The solid mass shows a low signal intensity on T1-weighted image, low to intermediate signal intensity on T2-weighted image and is well enhanced after contrast administration. These findings are correlated with predominantly chronic inflammatory tissue observed on microscopic examination (El-Noueam et al. 1997). The predominantly cystic mass has a central area of necrosis surrounded by chronic inflammatory cells and palisading fibroblasts (Sanders et al. 1998). US shows a moderately well-circumscribed, ovoid, hypoechoic, heterogeneous lesion with a paucity of lesional vascularity on color Doppler study. F-18 FDG PET/CT can show moderate uptake (SUV max 4.2) mimicking malignant soft tissue tumor (Strobel et al. 2009).

15.5 Morel-Lavallee Lesion

Morel-Lavallee lesion is a traumatic lesion pattern that has been termed ‘closed degloving injury’ because it is the result of abrupt separation of the subcutaneous fatty tissue from the underlying fascia (Parra et al. 1997; Mellado et al. 2004; Neal et al. 2008). Disruption of the rich lymphatic and vascular plexus occurs upon separation from the adjacent fascia; accumulation of blood and lymph can therefore be observed (Parra et al. 1997). Long-standing lesions are typically encapsulated with serosanguinous fluid containing blood and lymph (Mellado et al. 2004). The lesion typically is observed in the proximal thigh and trochanteric region.

On MR imaging, the lesions show some expansive effects, generating a palpable bulge or compressive deformity on the adjacent muscles. The MR signal intensities of the lesions may be variable depending on the composition and stage of development (Mellado et al. 2004). Long-standing lesions may present fluid-like MR signal characteristics with a hypointense peripheral rim, a finding that is correlated with a fibrous capsule. Morel-Lavallee lesions may also show a homogeneous high signal intensity on both T1- and T2-weighted images, indicating the presence of methemoglobin in a subacute hematoma. The third MR signal intensity pattern is heterogeneous hyperintensity on T2-weighted image, which reflects hemosiderin deposition, granulation tissue, necrotic debris, fibrin, and blood clots, which are characteristics of chronic organizing hematoma. The hypointense peripheral ring can represent a hemosiderin-laden fibrous capsule with mild inflammatory infiltrate. Patchy

internal enhancement and peripheral enhancement may also be present (Mellado et al. 2004). US also shows a variable appearance, being more homogeneous and flat or fusiform in shape, with well-defined margins in older lesions. All Morel-Lavallee lesions are hypoechoic or anechoic, compressible, and located between the deep fat and overlying fascia (Neal et al. 2008).

15.6 Malignant Melanoma

Malignant melanoma is a malignant neoplasm of melanocytes, most frequently arising from the skin as a growing pigmented lesion. However, it can also appear pink, tan, or even white (http://www.cancer.org/cancer/skincancer-melanoma/detailedguide/melanoma-skin-cancer-what-is--melanoma). Primary tumors most frequently present in Caucasian women on the leg, whereas most melanomas most commonly occur on the trunk in men (Kalkman and Baxter 2004; Catalano et al. 2010a). Melanoma can be cured in its early stages with a 99% survival rate, but it is likely to spread to other parts of the body if it is not detected early (Kalkman and Baxter 2004; Catalano et al. 2010a). At initial diagnosis, cross-sectional imaging modalities, such as CT, MR imaging, PET, and PET/CT, may help assess patients with cutaneous malignant melanomas for locoregional and distant metastases (Choi and Gershenwald 2007; Veit-Haibach et al. 2009; Catalano et al. 2010a).

On US, a primary tumor appears as a hypoechoic lesion bordered by a thin and echoic epidermal surface. The thickness of the primary lesion is an important parameter in management and prognosis of cutaneous melanoma (Choi and Gershenwald 2007; Veit-Haibach et al. 2009; Catalano et al. 2010a; Catalano and Siani 2010). US is also helpful in assessing locoregional metastasis. Satellite metastasis is defined when a metastatic nodule is found 2–3 cm from the primary tumor. In-transit metastasis is reported if the lesion develops along the lymphatic course toward the locoregional lymph node basin (Meier et al. 2002; Catalano et al. 2010a). Metastatic nodules present as subcutaneous hypoechoic nodules, often with low-level internal echoes due to the poor beam reflection of melanin (Catalano et al. 2010a; Catalano and Siani 2010; Catalano et al. 2010b). Typical metastatic lymph nodes show a round or broad oval shape, with macrolobulated or microlobulated borders and a complete or partial loss of the internal echoic hilum (Catalano et al. 2010a; Catalano et al. 2010b). Color Doppler US may be helpful in differentiating the metastatic lymph node from reactive lymph node hyperplasia. On MR imaging, melanoma usually appears as a hyperintense lesion on T1-weighted image, which is a characteristic signal pattern produced by melanin. The tumor shows diffusion restriction on diffusion-weighted imaging (DWI) and intense enhancement after contrast agent administration (Choi and Gershenwald 2007; Juan et al. 2014). PET/CT represents the newest imaging modality used in the staging of melanoma, exhibiting between 95% and 100% sensitivity, specificity, and accuracy for N- and M-staging (Veit-Haibach et al. 2009). PET can provide added value for detecting in-transit or satellite metastatic lesions (Veit-Haibach et al. 2009).

15.7 Lymphoma (Cutaneous and Subcutaneous)

Cutaneous T-cell lymphomas (CTCLs) represent a heterogeneous group of neoplasms that originate from skin-homing T cells (Willemze and Meijer 2006). CTCL is the most common type of cutaneous lymphoma and typically presents with dry skin, itching, a red rash, and thick plaques that often mimic eczema or chronic dermatitis. The disease affects men more than women and usually occurs in men in their 50s and 60s. Subcutaneous T-cell lymphoma is also known as a panniculitis-like T-cell lymphoma, which infiltrates the subcutaneous fat but does not involve the skin. This disease most commonly presents in young adults with subcutaneous nodules, primarily located on the trunk, extremities, and face (Willemze and Meijer

Table 15.1 WHO-EORTC classification of cutaneous lymphomas with primary cutaneous manifestations

Cutaneous T-cell and NK cell lymphomas
Mycosis fungoides
MF variants and subtypes
Folliculotropic MF
Pagetoid reticulosis
Granulomatous slack skin
Sézary syndrome
Adult T-cell leukemia/lymphoma
Primary cutaneous CD 30+ lymphoproliferative disorders
Primary cutaneous anaplastic large cell lymphoma
Lymphomatoid papulosis
Subcutaneous panniculitis-like T-cell lymphoma
Extranodal NK/T-cell lymphoma, nasal type
Primary cutaneous aggressive epidermotropic CD8-positive cytotoxic T-cell lymphoma (provisional entity)
Cutaneous g/d T-cell lymphoma (provisional entity)
Primary cutaneous CD4-positive small/medium-sized pleomorphic T-cell lymphoma (provisional entity)
Primary cutaneous peripheral T-cell lymphoma, unspecified
Cutaneous B-cell lymphoma
Primary cutaneous marginal zone B-cell lymphoma
Primary cutaneous follicle center lymphoma
Primary cutaneous diffuse large B-cell lymphoma, leg type
Primary cutaneous diffuse large B-cell lymphoma, other
Anaplastic or plasmablastic subtypes
T-cell/histiocyte rich large B-cell lymphoma
Intravascular large B-cell lymphoma

2006; Kim et al. 2011b; Jang et al. 2012; Juan et al. 2014). Cutaneous B-cell lymphomas (CBCLs) are the less common version of cutaneous lymphomas, constituting approximately 20–25% of all primary cutaneous lymphomas. The disease presents in the skin, without evidence of extracutaneous disease at the time of diagnosis (Willemze and Meijer 2006). The detection of extracutaneous involvement by imaging is crucial for staging and therapeutic planning for lymphoma (Juan et al. 2014). The World Health Organization (WHO)-European Organization for Research and Treatment of Cancer (EORTC) classification of cutaneous lymphomas is summarized in Table 15.1. Clinically, subcutaneous lymphomas are often confused with inflammatory panniculitis associated with connective tissue disease. Most cutaneous lymphomas typically fall into the category of indolent lymphomas and respond well to mild treatments. In contrast, cutaneous diffuse large B-cell lymphomas are characterized by an aggressive clinical course and have a more unfavorable prognosis than other groups of cutaneous lymphomas (Zinzani et al. 2006; Willemze 2006). Subcutaneous B-cell lymphomas have rarely been reported and seem to be characterized by rapid growth (Alaibac et al. 2008).

On US, subcutaneous lymphomas show a poorly defined hyperechogenicity, with or without central hypoechoic areas in the subcutaneous fat layer (Kang et al. 2007; Kim et al. 2011b). The hyperechogenicity of the tumors reflects the difference in acoustic impedance between adipose cells and lymphocyte clusters. The central hypoechoic areas result from the decrease in acoustic impedance due to the dense accumulation of lymphocytes, and lymphocytoid cells in the central portion of the mass reflect its hypoechoic appearance (Fujii et al. 2004). Color Doppler US demonstrates relative hypervascularity with a low resistive index. (Kang et al. 2007). On CT, lymphomas appear as enhancing nodules and infiltrative cutaneous and subcutaneous masses. The tumors show nonspecific imaging features on MR imaging, appearing as a discrete mass or thickening of the skin and subcutaneous tissue, with T1 hypo- and T2 hyper-intense signal intensities. Enhancement is observed after contrast agent administration (Juan et al. 2014). PET/CT is more accurate than CT in the staging and assessment of the treatment response of cutaneous lymphoma because these tumors are typically FDG avid. Measuring the maximum SUV can be a useful parameter to assess the aggressiveness of the lymphoma. (Juan et al. 2014; Kim et al. 2011b).

However, there are no specific imaging features of cutaneous/subcutaneous lymphomas. For this reason, the differential diagnoses should include panniculitis, subcutaneous edema, hemorrhage, cellulitis, and lipoma (Kang et al. 2007). Moreover, the clinical findings are important, and the biopsy must be recommended with a high index of clinical suspicion.

15.8 Soft Tissue Metastasis

Soft tissue metastasis is a relatively uncommon cause of soft tissue masses. The primary tumor of origin of soft tissue metastasis is the skin, lung, and breast, followed by the kidney, colon, and rectum. However, metastases may spread from any primary tumor location (Beaman et al. 2007). Sarcomas are an uncommon cause of metastases to the soft tissues. Soft tissue metastasis may be misidentified as primary soft tissue sarcomas or inflammatory lesions based on the physical findings and imaging studies. A multiplicity of lesions and known primary tumors may help in diagnosing soft tissue metastases.

Metastases to the skeletal muscle have been generally considered rare, but recent investigations show that they are more common than previously suggested (Haygood et al. 2012). These metastases usually occur in the abdominal wall, back/ periscapular region, thigh, and chest wall. Metastases distal to the knee and elbow are extremely rare (Gottlieb and Schermer 1970).

Metastasis to the skin occurs in 0.7–9% of all patients with cancer (Damron and Heiner 2000; Beaman et al. 2007; Plaza et al. 2008). There are several mechanisms of cutaneous metastasis, including distant organ metastasis, local invasion, locoregional lymphatic dissemination, and local iatrogenic cancer cell contamination in the surgical scar (Kovács et al. 2013). If melanoma is excluded, lung cancer is the most frequent source of cutaneous metastasis in men, with breast carcinoma being the most common source in women (Alcaraz et al. 2012). However, gastric, hepatic, and pancreatic cancers have a lower probability of spreading into the skin (Kovács et al. 2013). Common sites of cutaneous metastases are variable depending on their primary tumor type and locations. Generally, lower gastrointestinal and genitourinary cancers prefer infradiaphragmatic skin regions, unlike upper gastrointestinal cancers, whereas lung and kidney cancers prefer supradiaphragmatic regions. Cutaneous metastases generally arise in a late stage of cancer with a poor prognosis but may also be the first clinical manifestation of an asymptomatically progressing cancer (Kovács et al. 2013).

On CT, soft tissue metastasis generally appears as an area of decreased attenuation. On MR imaging, soft tissue metastases often present as a nonspecific soft tissue mass. In some cases, they appear as abscess-like lesions with rim enhancement (Surov et al. 2010). They may present with multiple intramuscular calcifications, which have been described sporadically in gastric cancer, esophageal, and colonic adenocarcinoma (Surov et al. 2010). In metastases of mucinous adenocarcinoma of the colon or pancreas, marked hypointensity is observed on T2-weighted image as a consequence of the high ratio between nuclei and cytoplasm and limited extracellular space (Damron and Heiner 2000).

15.9 Illustrations: Superficial Soft Tissue Masses

15.9.1 Epidermal Inclusion Cyst

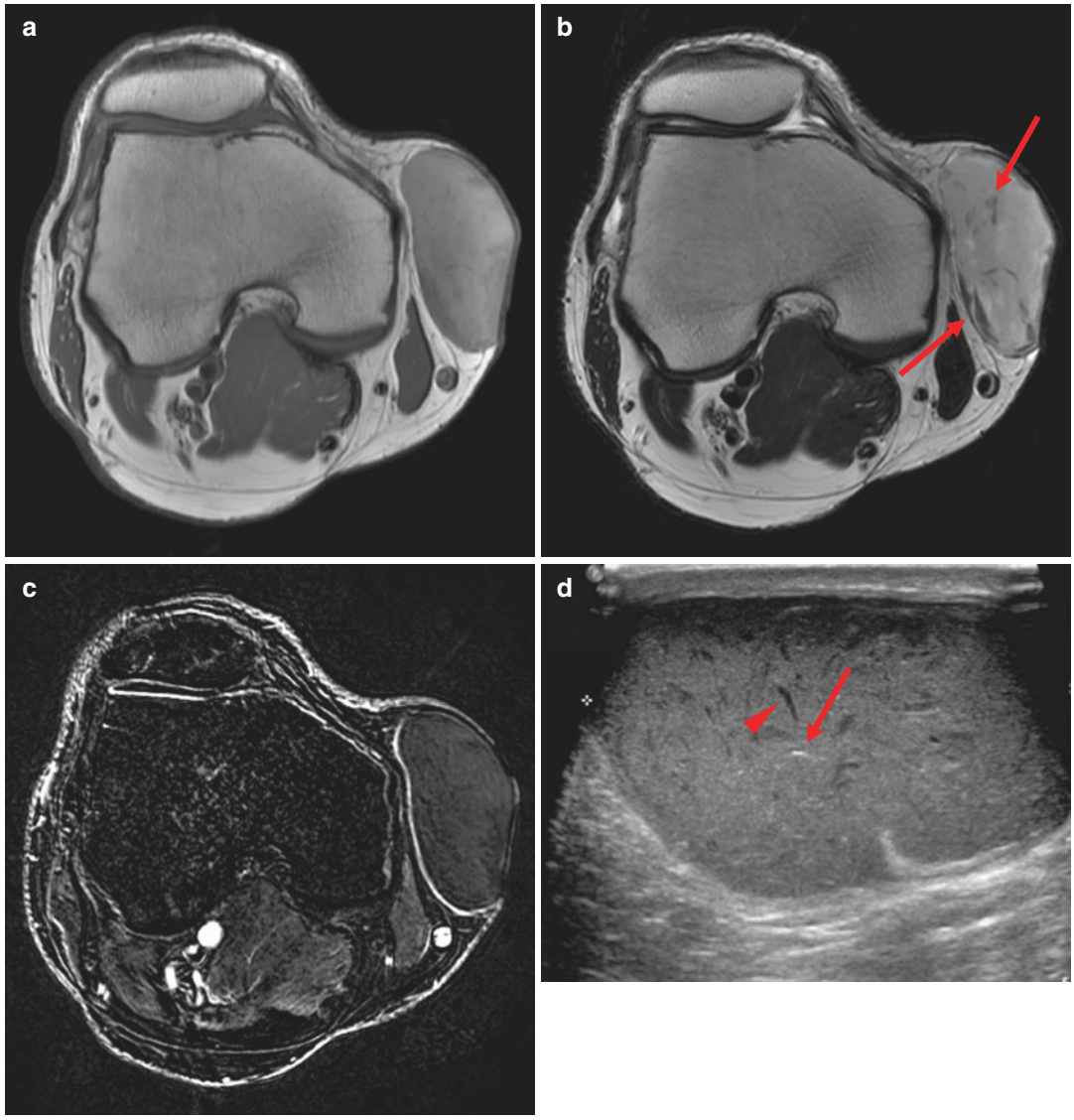

Fig. 15.1 Epidermal inclusion cyst. Axial T1WI (**a**) shows a subcutaneous mass in the medial knee, with slightly higher signal intensity compared to the muscle. Axial T2WI (**b**) shows a hyperintense mass with internal hypointense debris (*arrows*). Axial postcontrast FS T1WI (**c**) demonstrates only thin peripheral rim enhancement. US (**d**) shows a heterogeneously hyperechoic mass with scattered internal linear echogenic reflections (*arrow*), dark clefts (*arrowhead*), and increased posterior acoustic enhancement

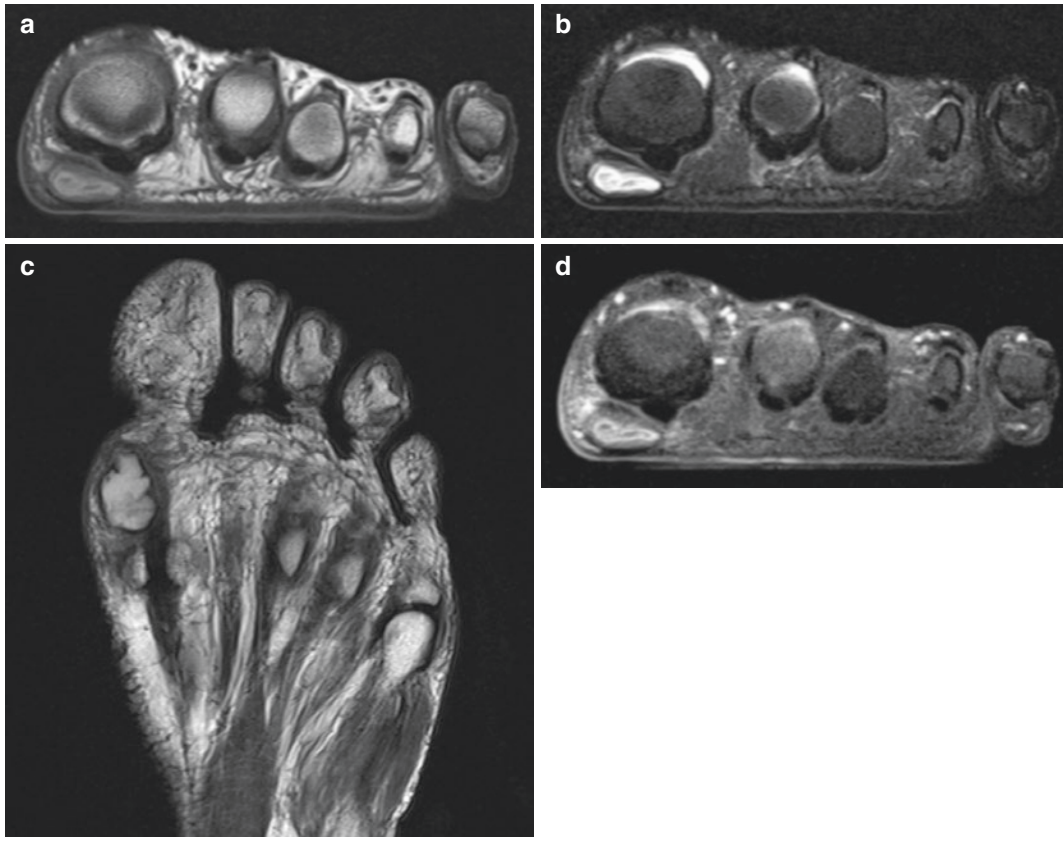

Fig. 15.2 Epidermal inclusion cyst. Axial T1WI (**a**) shows a subcutaneous, hyperintense mass in the plantar aspect of first toe. Axial and coronal T2WIs (**b**, **c**) reveal a hyperintense mass with a peripheral hypointense fibrotic rim. Mild peri-lesional edema is observed. The mass shows irregular rim enhancement with fuzzy adjacent soft-tissue enhancement on axial postcontrast FS T1WI (**d**)

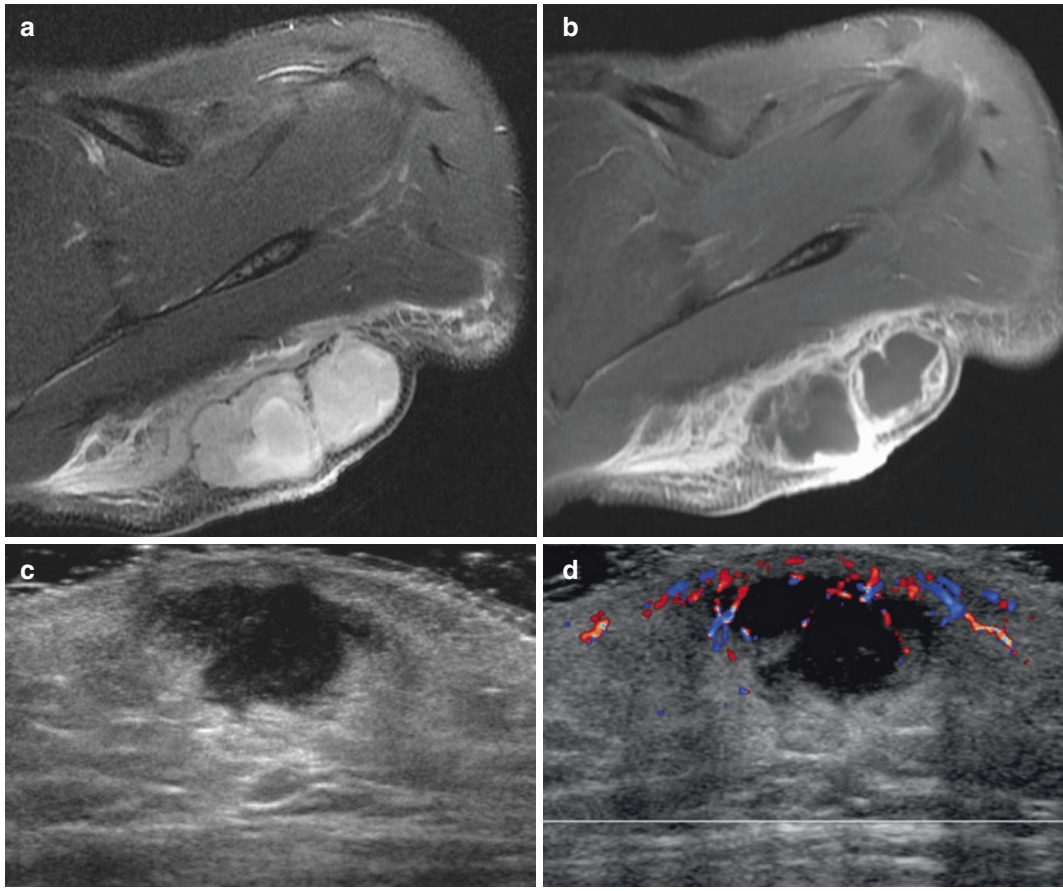

Fig. 15.3 Ruptured epidermal inclusion cyst. Axial T2WI (**a**) shows a subcutaneous mass with irregular contours and extensive peri-lesional edema in the left posterior shoulder. The mass contains septa and shows thick and irregular rim enhancement with fuzzy adjacent soft-tissue enhancement on axial postcontrast FS T1WI (**b**). US images (**c**, **d**) also shows irregular margins and peri-lesional hypervascularity, indicating a ruptured epidermal cyst. These imaging features of a ruptured epidermal cyst could mimic a mass of infectious or neoplastic origin

15.9.2 Pilomatricoma

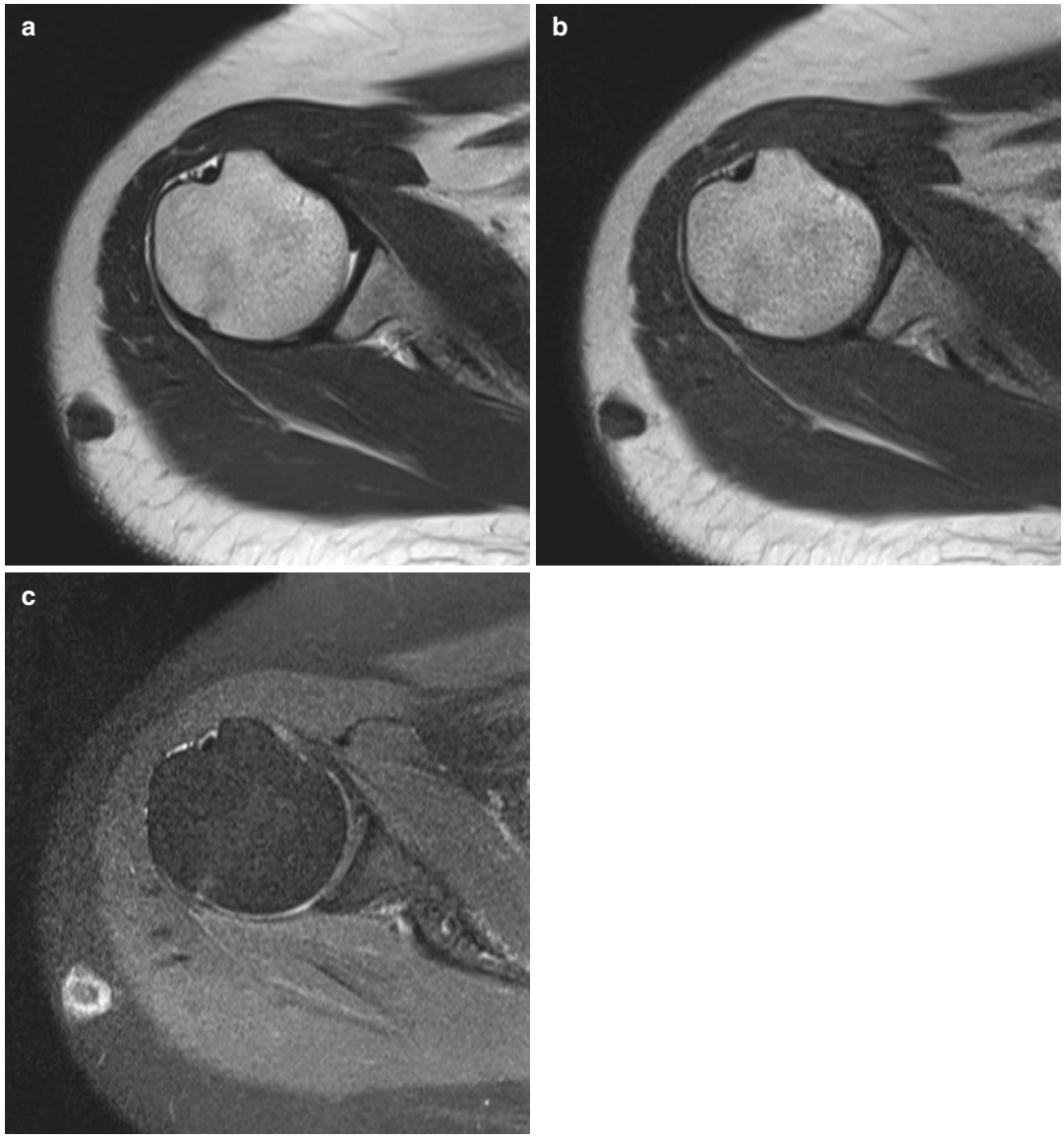

Fig. 15.4 Pilomatricoma. Axial T1WI (**a**) and T2WI (**b**) show a small, well-demarcated, subcutaneous mass with low signal intensity. Axial postcontrast FS T1WI (**c**) shows peripheral thick rim enhancement with central non-enhancement

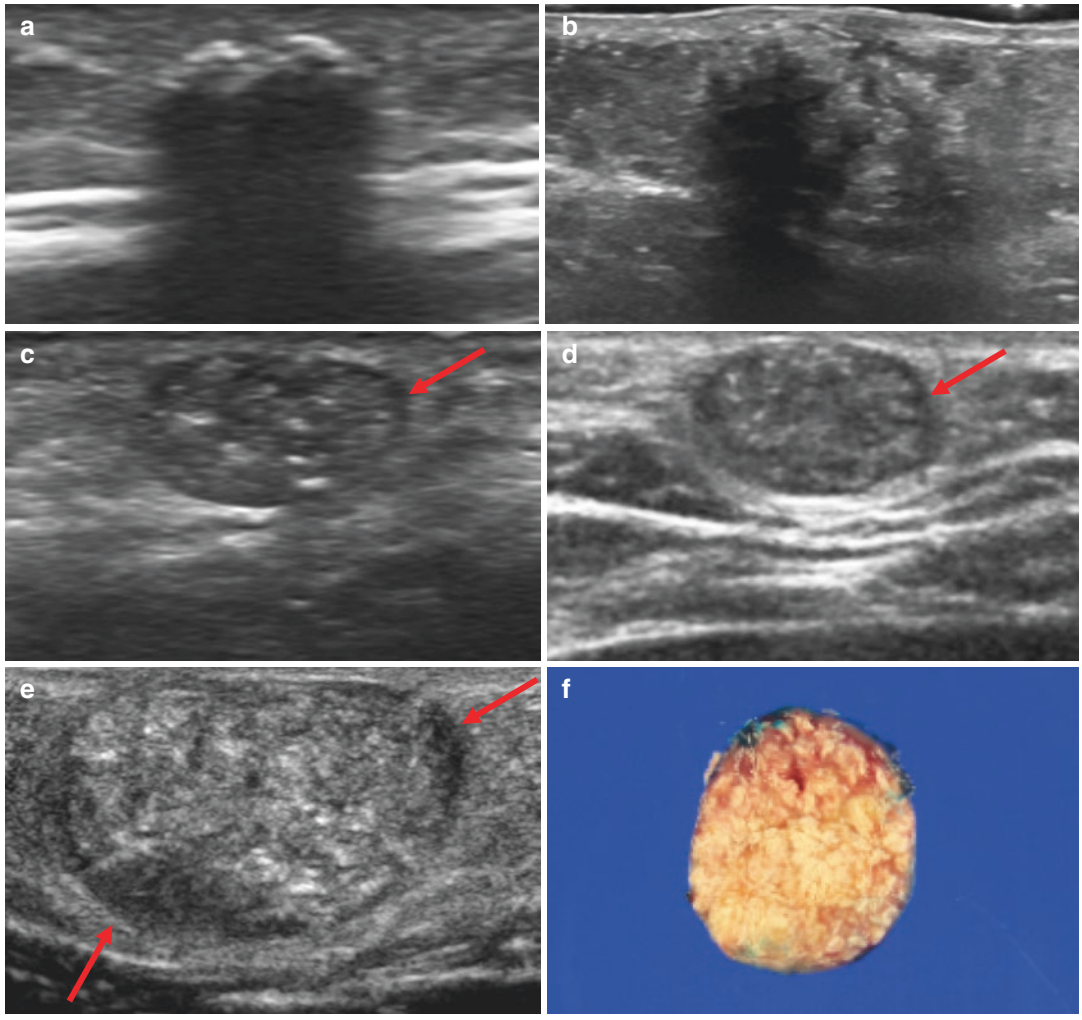

Fig. 15.5 Pilomatricoma. Variable sonographic appearances of pilomatricoma. Completely calcified pilomatricoma with posterior acoustic shadowing artifact (**a**). Irregular hyperechoic lesion with an obscured margin due to posterior acoustic shadowing (**b**). Well-defined iso- to hyperechoic masses with variable internal echogenic foci in the superficial subcutaneous tissue (**c**–**e**). A hypoechoic rim (*arrows*) is also frequently found, which represents a connective tissue capsule surrounding the tumor. (**f**) The surgical specimen reveals a nodulocystic tan-colored mass containing irregularly shaped, lobulated islands of cells surrounded by a fibrous capsule

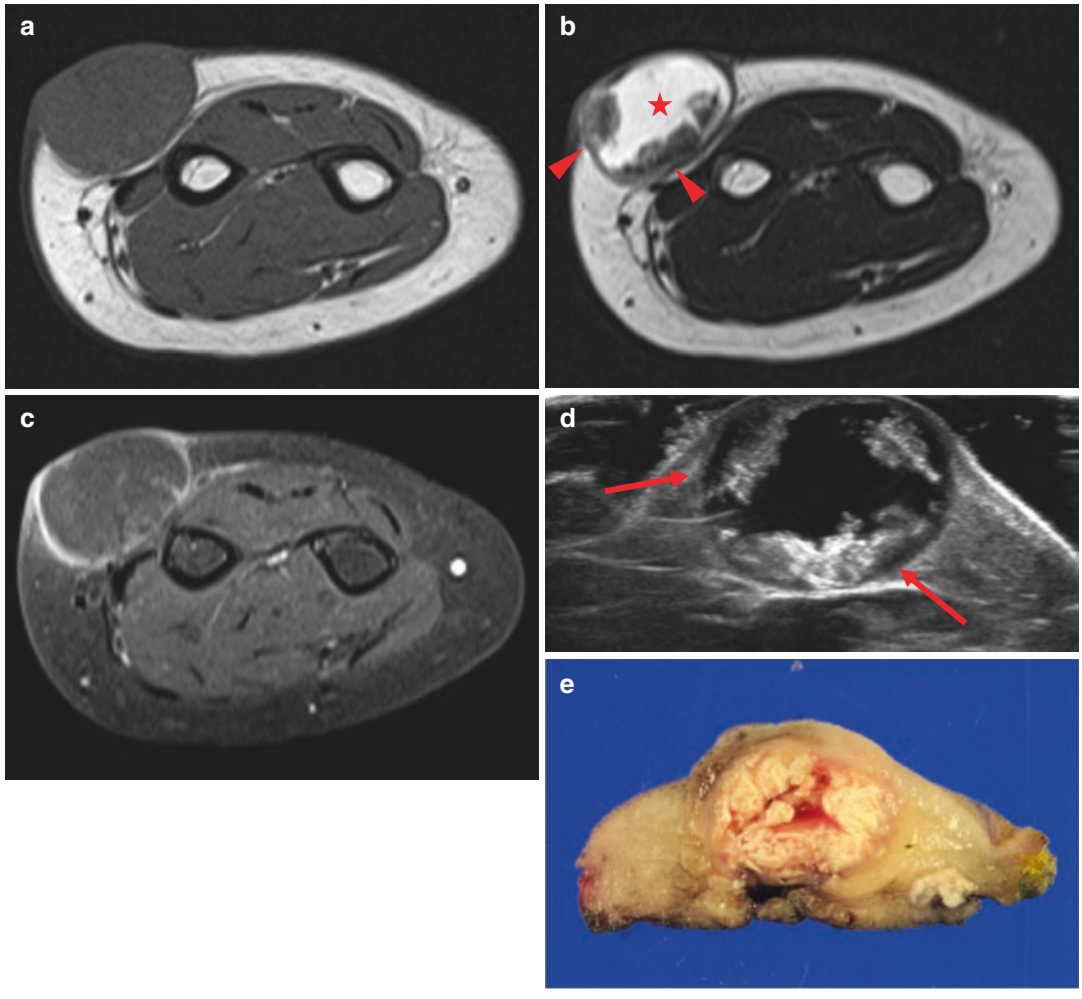

Fig. 15.6 Pilomatricoma. Cystic variant of pilomatricoma is observed on MR imaging. Axial T1WI (**a**) and T2WI (**b**) reveal a solid-cystic mass with a hypointense nodular portion (*arrowheads*) associated with a T2 hyperintense fluid-filled cystic component (*star*). Axial post-contrast FS T1WI (**c**) shows thin peripheral rim enhancement. US (**d**) shows fluid-containing cyst with a hyperechoic peripheral solid portion surrounded by a hypoechoic rim (*arrows*). The surgical specimen (**e**) shows a well-demarcated solid mass with a central cleft

15.9.3 Fat Necrosis

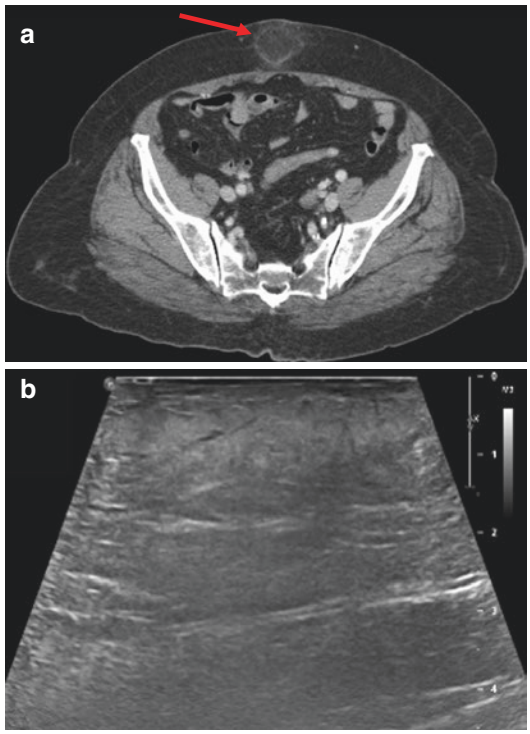

Fig. 15.7 Fat necrosis. Axial contrast-enhanced CT (**a**) scan of an abdomen shows a hypodense lesion in the subcutaneous tissue. Rim enhancement (*arrow*) and perilesional stranding can be seen. US (**b**) shows a hyperechoic, heterogeneous poorly defined region

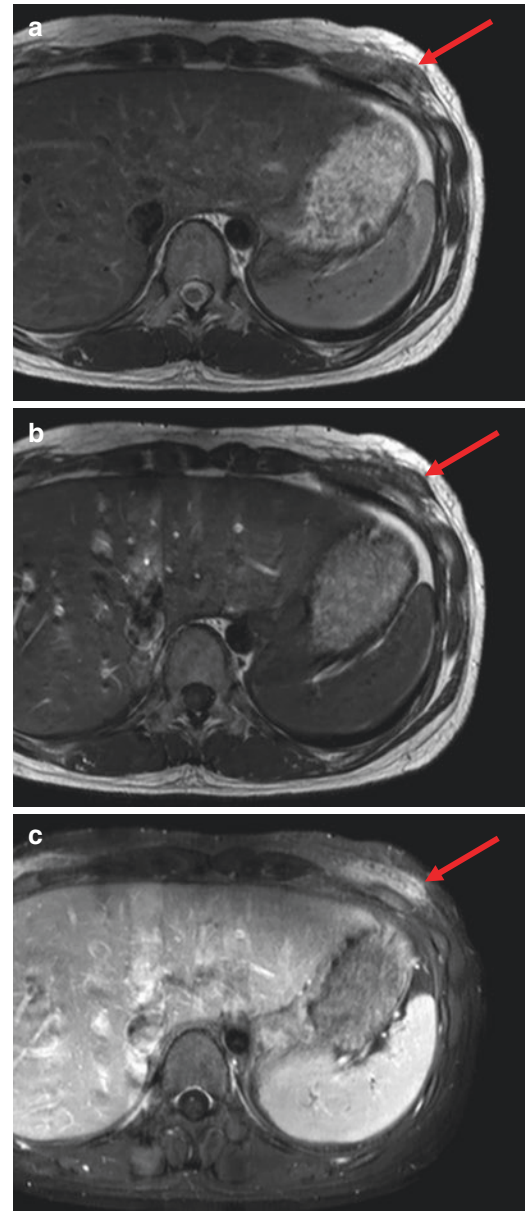

Fig. 15.8 Fat necrosis. Axial T1WI (**a**) and T2WI (**b**) show a left chest wall lesion with low signal intensity and infiltrative margin (*arrows*). Axial postcontrast FS T1WI (**c**) shows diffuse enhancement of the mass

15.9.4 Rheumatoid Nodule

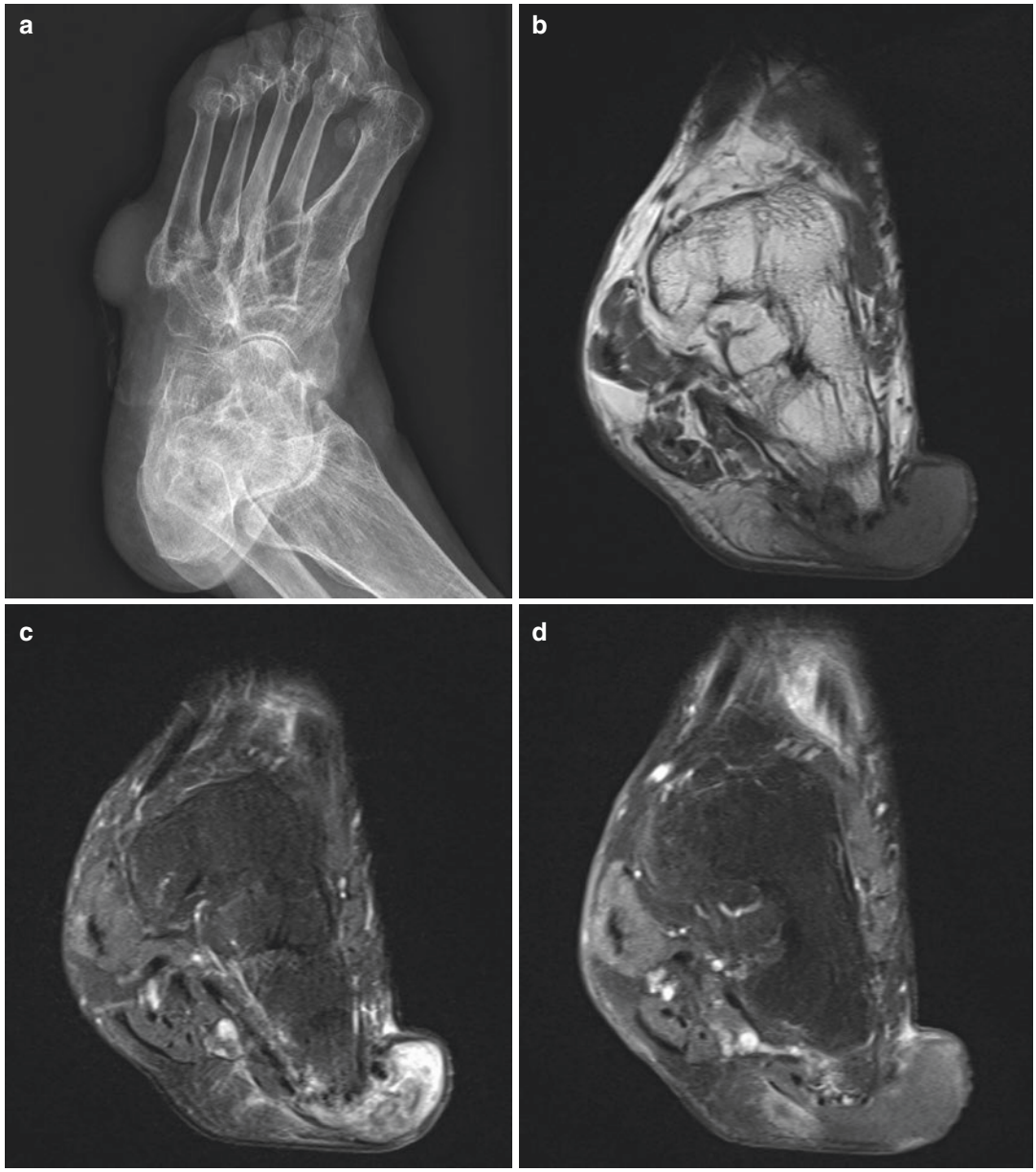

Fig. 15.9 Rheumatoid nodule. AP oblique radiograph of the foot (**a**) shows a bulging soft tissue density over the peroneal tuberosity in the lateral foot. Axial T1WI (**b**) reveals a subcutaneous soft tissue mass with bulging contours. The solid mass shows a low signal intensity on T1WI (**b**) and low to intermediate signal intensity on T2WI (**c**). Axial postcontrast FS T1WI (**d**) reveals rim enhancement surrounding the non-enhancing central necrotic tissue

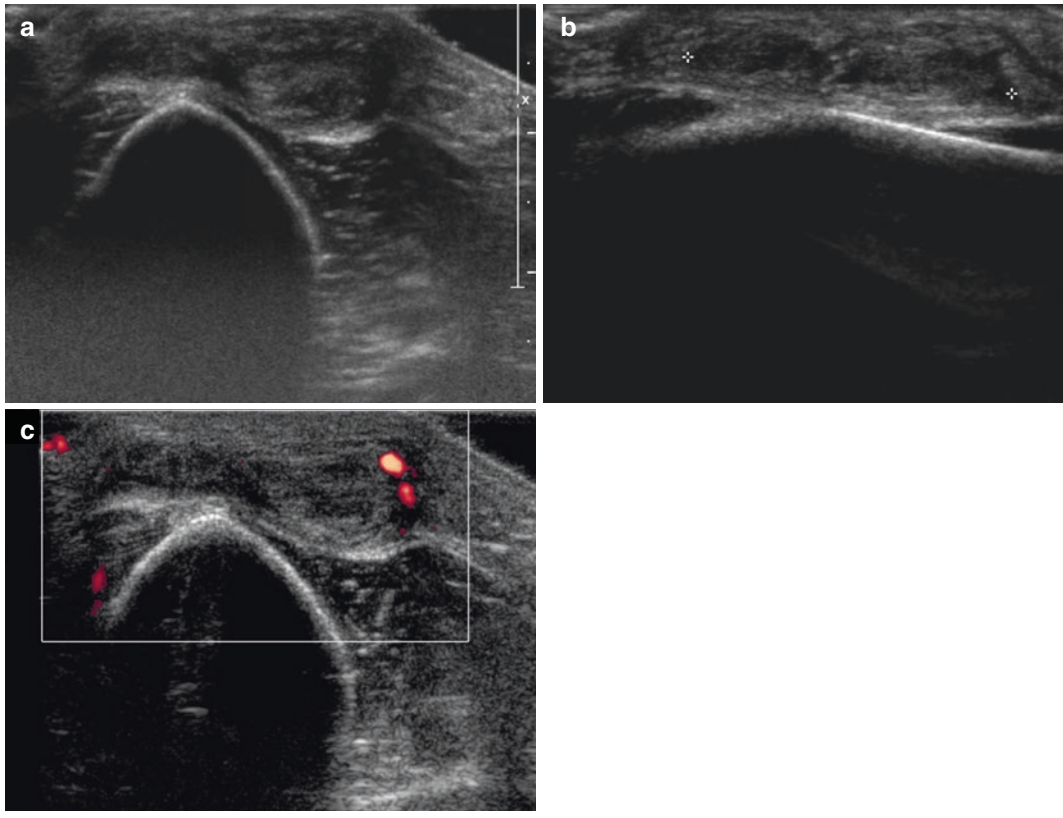

Fig. 15.10 Rheumatoid nodule. Transverse (**a**) and longitudinal (**b**) US images reveal a heterogeneous, predominantly hypoechoic mass over the extensor surface of the elbow. Color Doppler study (**c**) shows limited peripheral vascularity

15.9.5 Morel-Lavallee Lesion

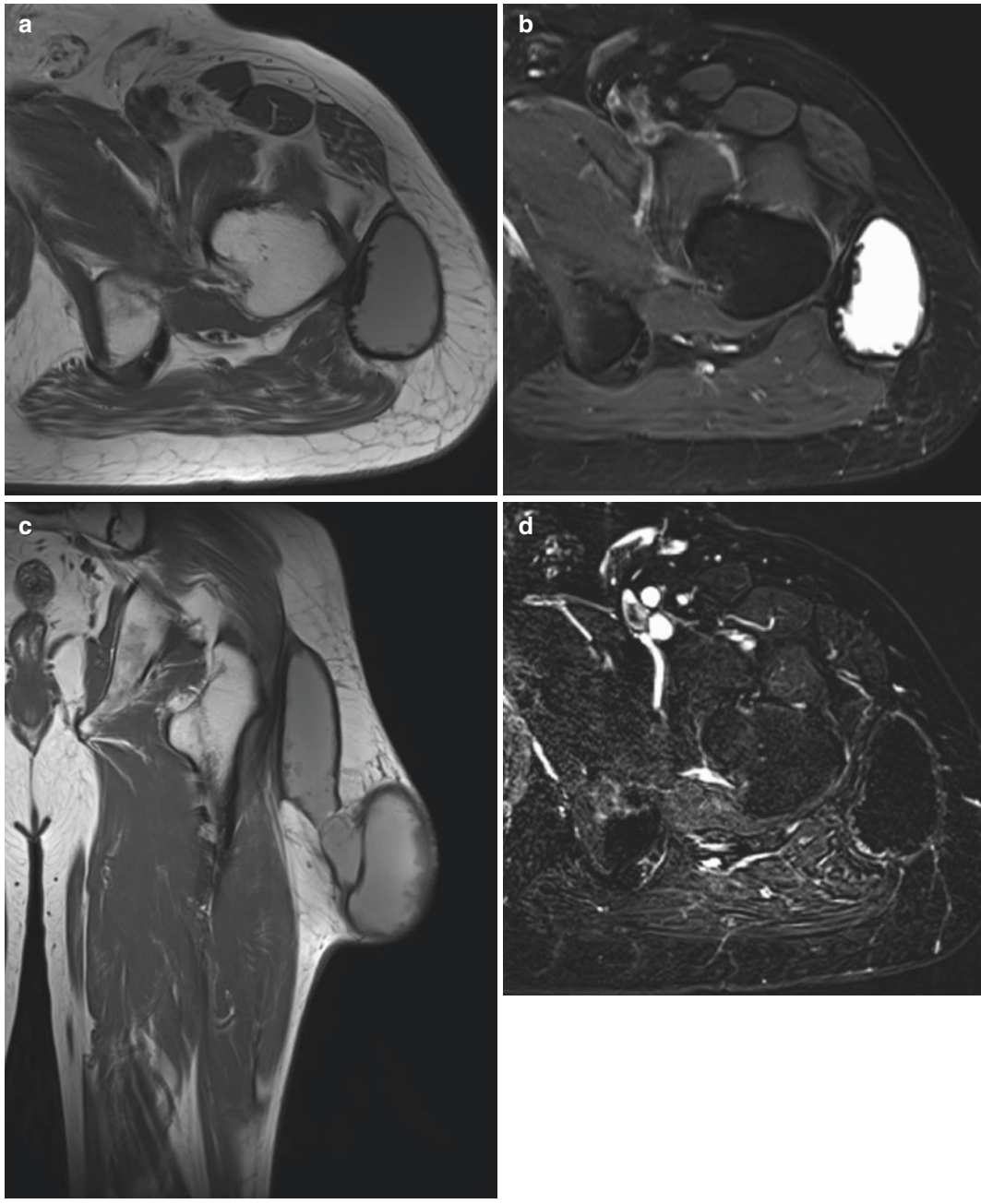

Fig. 15.11 Morel-Lavallee lesion. Axial T1WI (**a**) shows a large lobulated cystic mass of high signal intensity in the lateral aspect of the lateral thigh. Axial T2WI (**b**) shows markedly increased signal intensity with a dark signal rim. Coronal T1WI (**c**) shows that the mass abuts the deep fascia with inferolateral extension, resulting in a bulging mass. Axial postcontrast FS T1WI (**d**) shows no enhancement, except thin peripheral rim enhancement

15.9.6 Malignant Melanoma

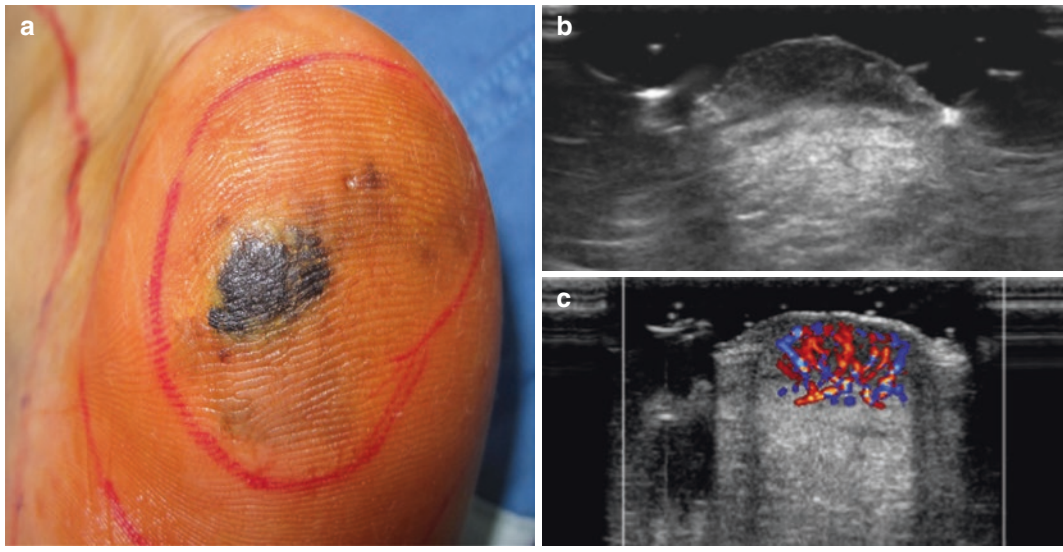

Fig. 15.12 Malignant melanoma. Clinical photograph (**a**) shows a dark black, asymmetric, and irregularly bordered skin lesion in the heel. US images (**b**, **c**) shows hypoechoic skin mass with marked vascularity

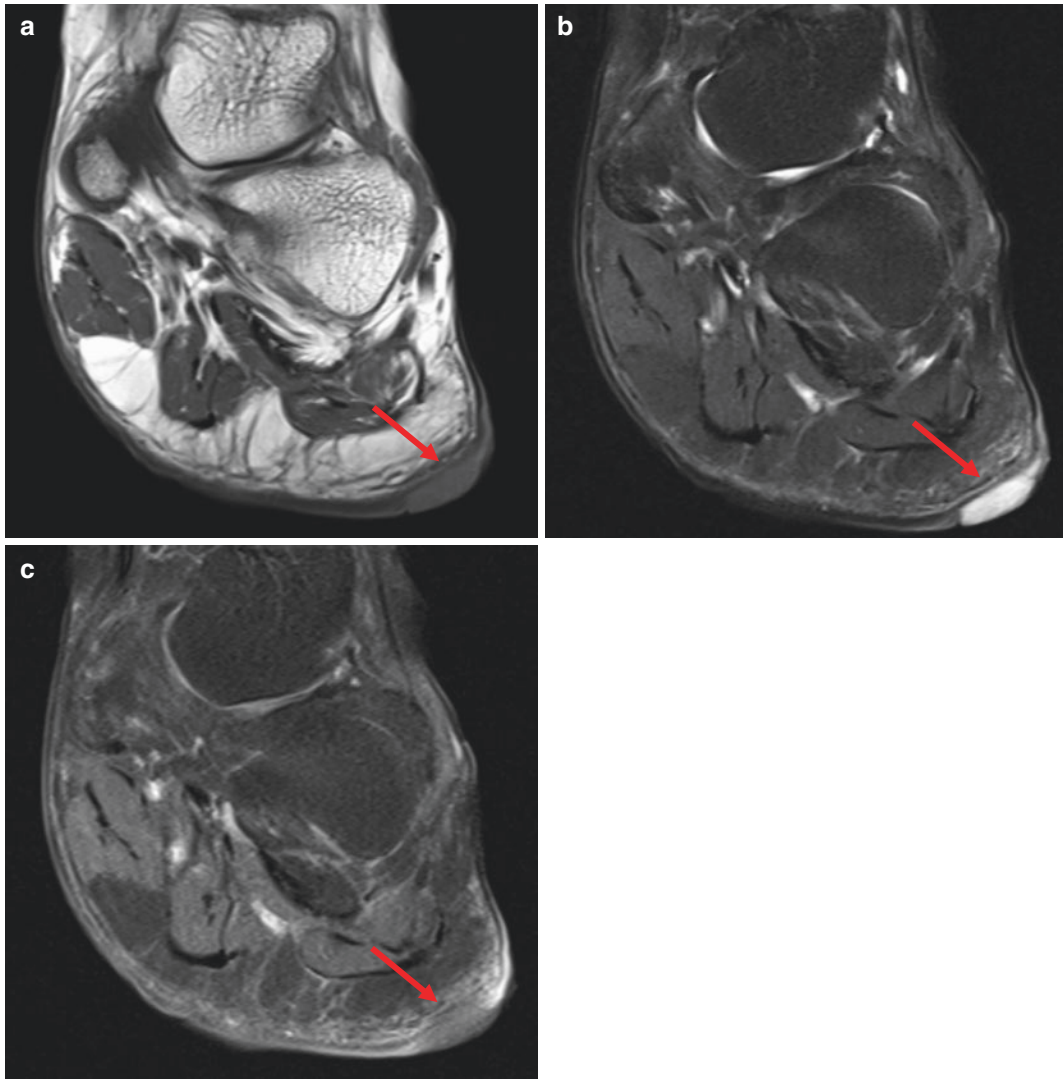

Fig. 15.13 Malignant melanoma. On MR imaging, a fungating skin lesion (*arrows*) is observed on the lateral aspect of the sole at the level of the calcaneocuboidal joint. The mass exhibits hyperintensity on both T1WI (**a**) and FS T2WI (**b**), which is a characteristic of signal intensity produced by melanin, and is mildly enhanced after gadolinium administration (**c**)

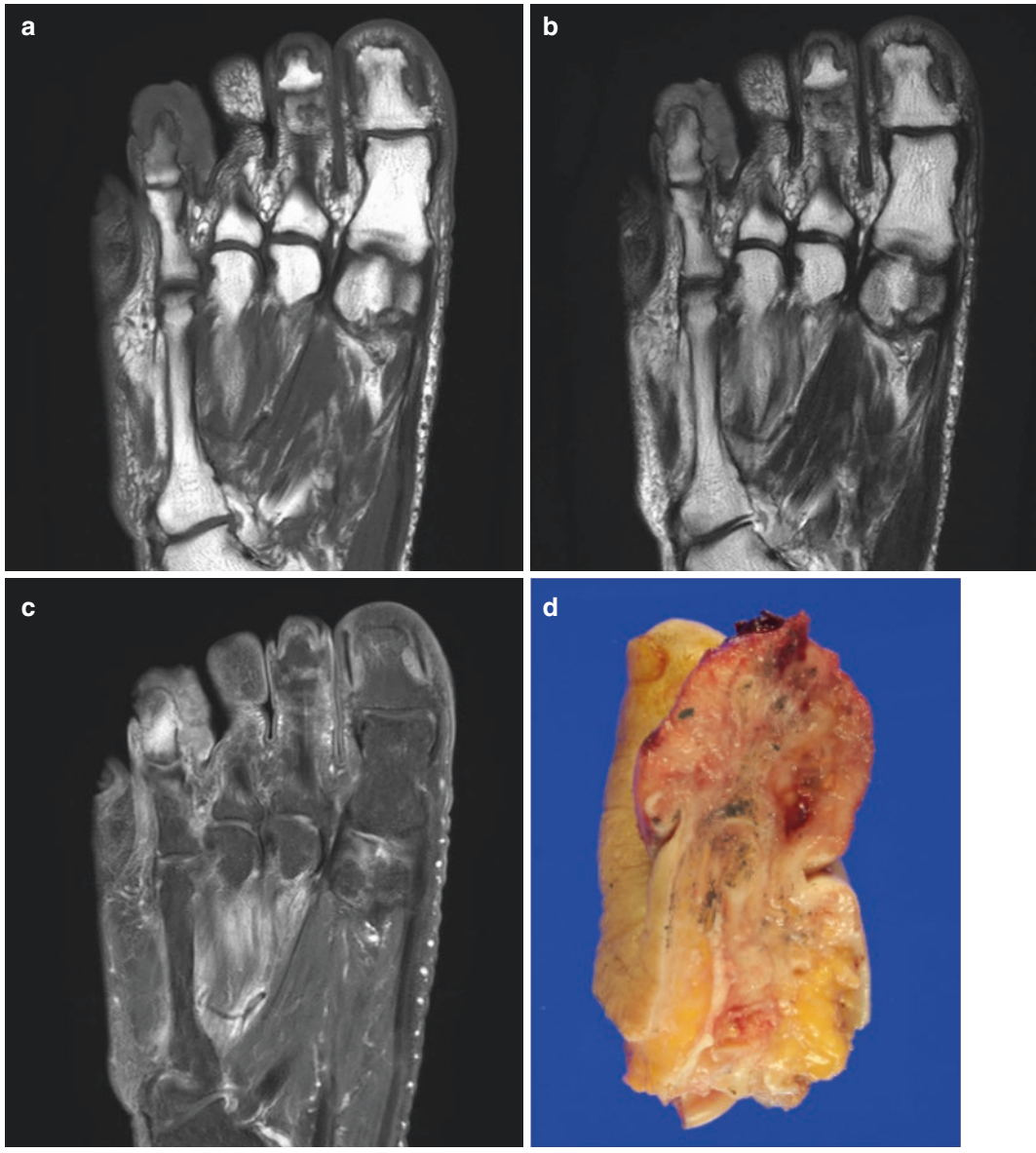

Fig. 15.14 Malignant melanoma. There is soft tissue thickening in the fourth toe. The mass shows mild hyperintensity compared to adjacent muscle on both T1WI and T2WI (**a**, **b**). The mass is mildly enhanced on postcontrast FS T1WI (**c**). Surgical specimen also shows soft tissue thickening in the distal phalanx of the fourth toe (**d**)

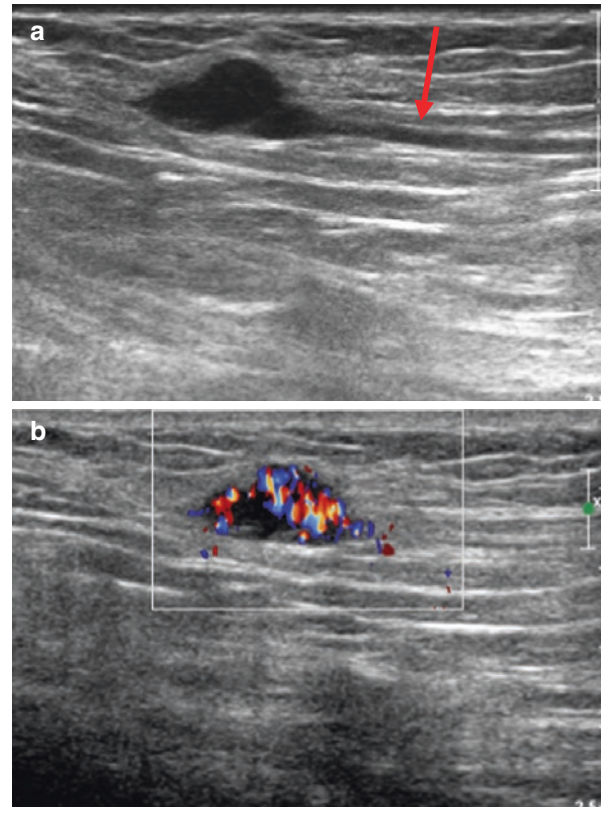

Fig. 15.15 In-transit metastasis of malignant melanoma. US (**a**) of patient with a history of malignant melanoma reveals a subcutaneous hypoechoic nodule along the dilated lymphatic course (*arrow*) toward the locoregional lymph node basin, consistent with in-transit metastasis. The nodule shows marked hypervascularity on color Doppler study (**b**)

15.9.7 Lymphoma (Cutaneous and Subcutaneous)

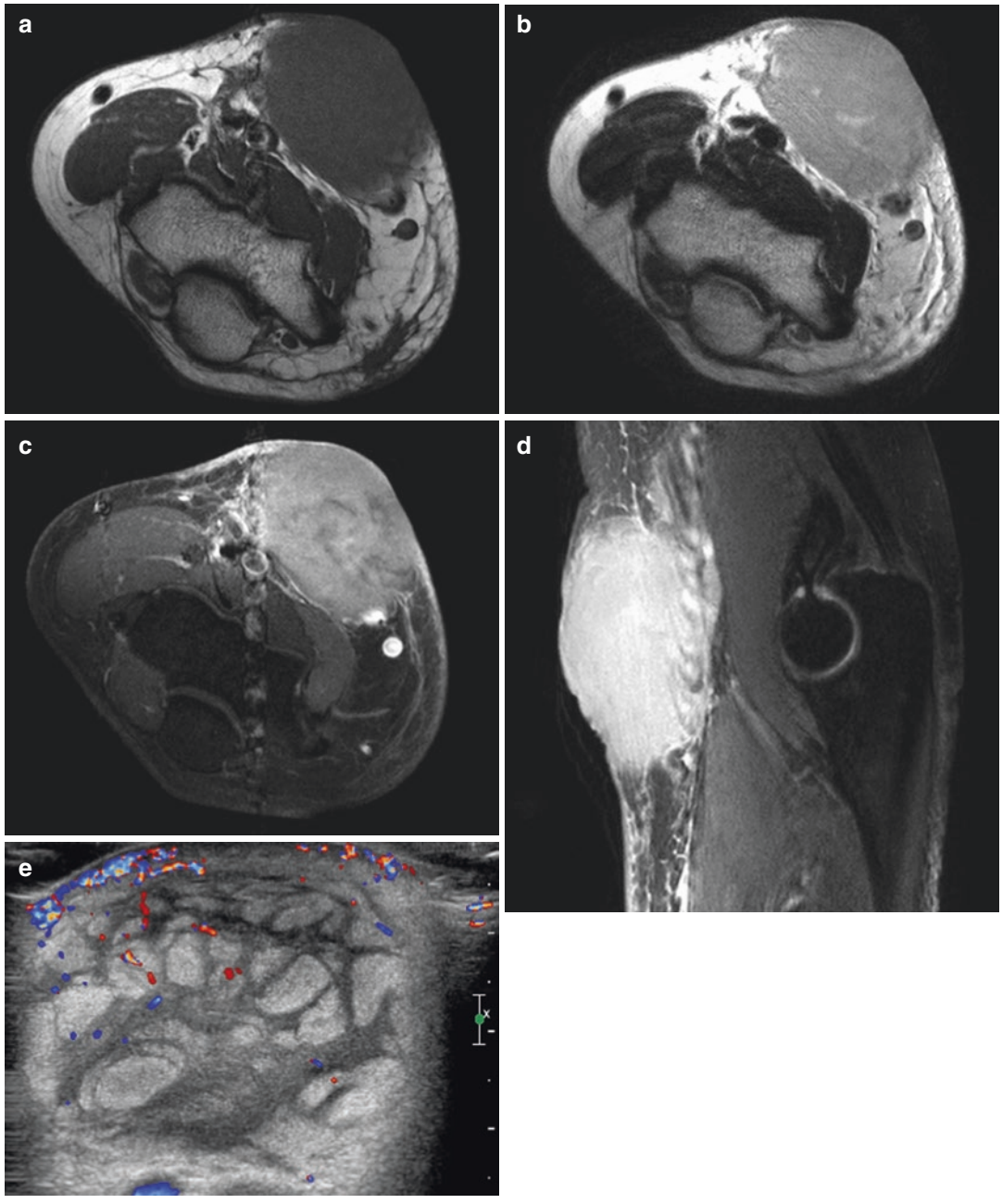

Fig. 15.16 Peripheral T-cell lymphoma. Axial T1WI (**a**) and T2WI (**b**) show ill-defined subcutaneous soft tissue mass and perilesional fat stranding in the anterior aspect of the elbow. Axial (**c**) and sagittal (**d**) postcontrast FS T1WIs show diffuse and intense enhancement. Color Doppler study (**e**) reveals hyperechoic mass with branching hypoechoic structures in the subcutaneous fat layer and relative hypervascularity

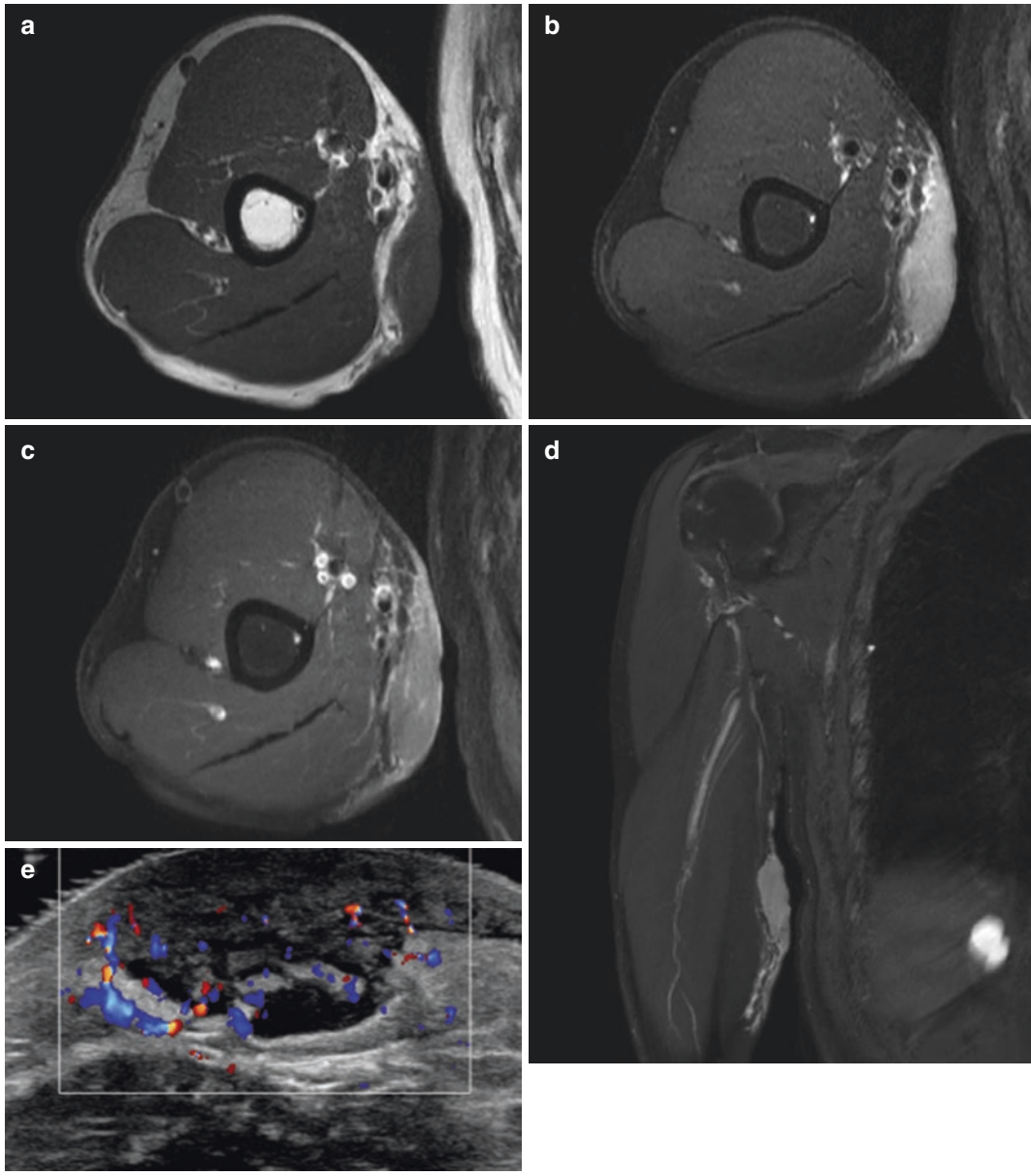

Fig. 15.17 Diffuse large B-cell lymphoma. Axial T1WI (**a**) and FS T2WI (**b**) show a large tumor involving the ulnar side of the right upper arm. The tumor involves the skin and subcutaneous tissue with hypointensity on axial T1WI (**a**). On axial FS T2WI (**b**), the mass is hyperintense to adjacent muscle. Axial (**c**) and sagittal (**d**) postcontrast FS T1WIs reveal that the mass has diffused and intense enhancement. Color Doppler study (**e**) reveals heterogeneous echoic mass with branching hypoechoic structures in the subcutaneous layer and relative hypervascularity

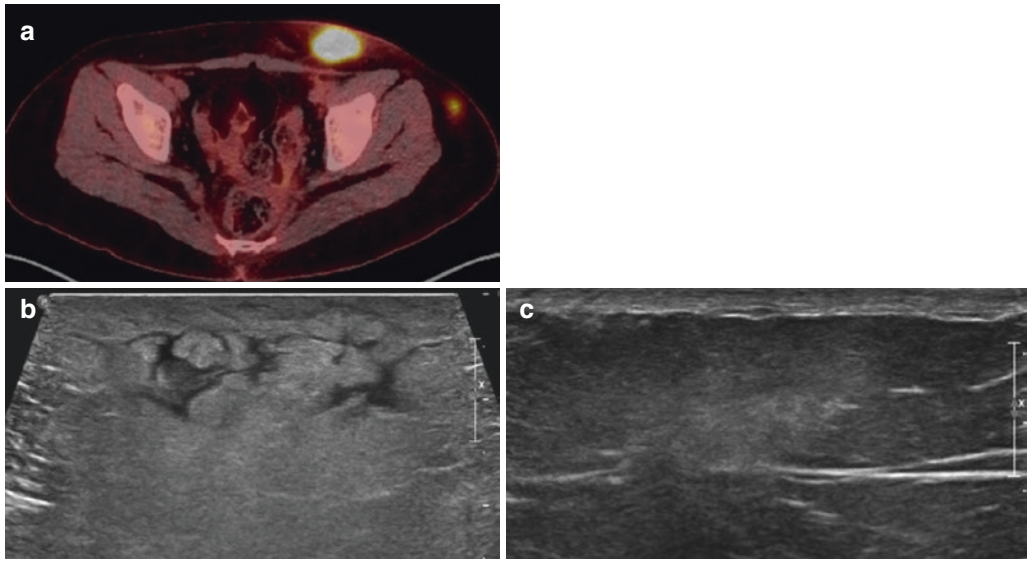

Fig. 15.18 Panniculitis-like T-cell lymphoma. PET-CT image (**a**) shows two subcutaneous masses with intense FDG uptake in the abdominal wall. The corresponding US obtained in the left anterior abdominal wall (**b**) reveals a poorly defined hyperechogenicity with multiple, linear hypoechoic areas in the central portion. US obtained in the left lateral buttock (**c**) shows ill-defined hyperechoic infiltration in the subcutaneous fat layer

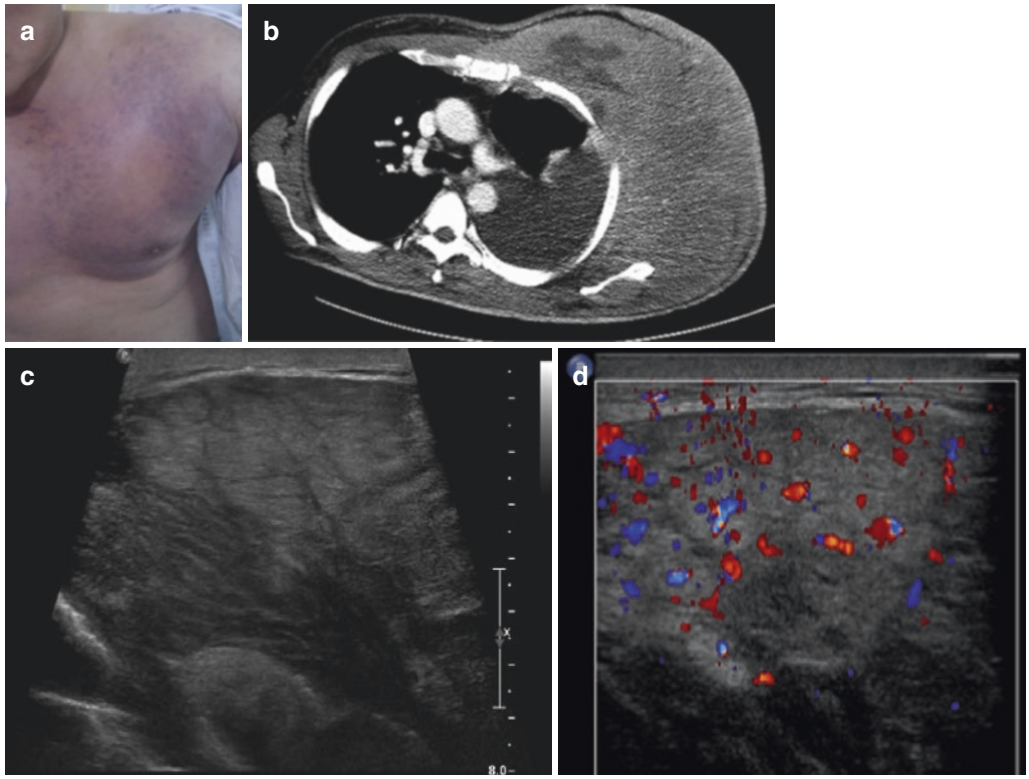

Fig. 15.19 Diffuse large B-cell lymphoma. The patient presents with a rapidly growing chest wall mass and skin color change (**a**). Contrast-enhanced chest CT (**b**) shows diffuse soft tissue and skin thickening. The corresponding US (**c**) reveals diffuse thickening of chest wall muscles and intervening hypoechoic linear structures, indicating preservation of muscle fascicular structures. Color Doppler study (**d**) reveals hypervascularity of the mass

15.9.8 Soft Tissue Metastasis

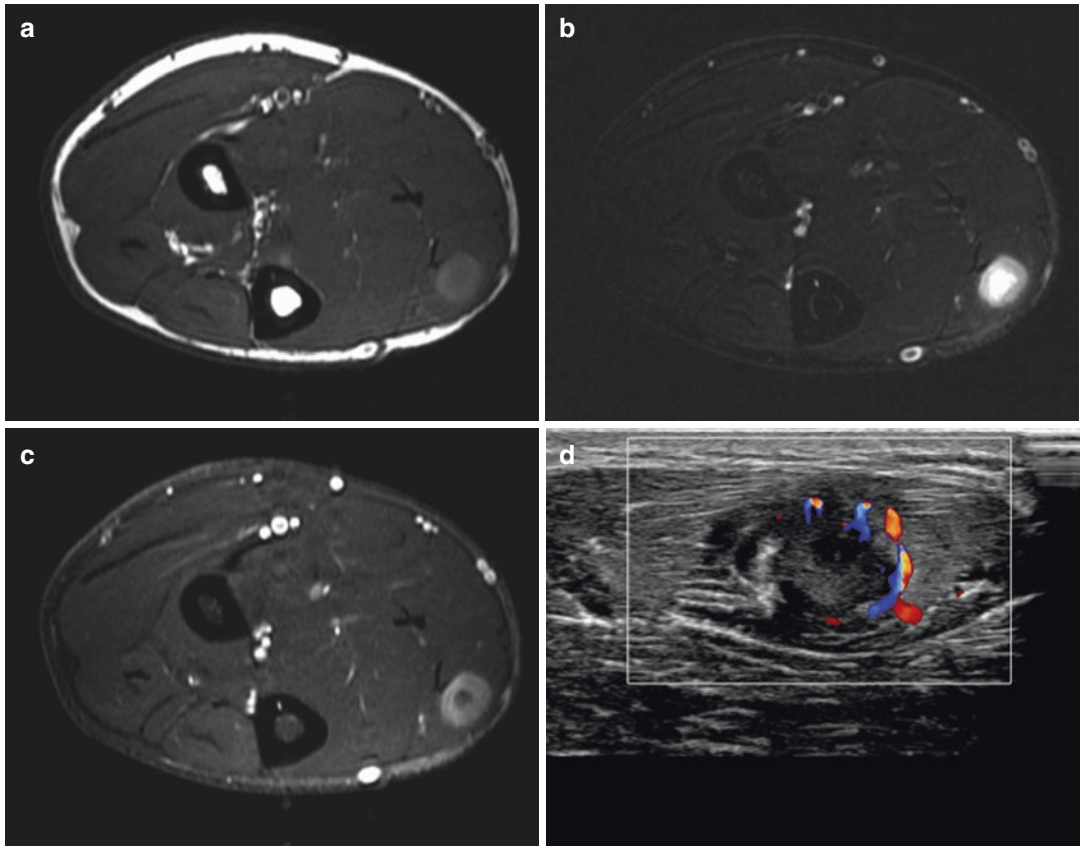

Fig. 15.20 Intramuscular metastasis of rhabdomyosarcoma. Axial T1WI (**a**) shows a nonspecific soft tissue mass in the flexor carpi ulnaris muscle. The mass is isointense to the adjacent skeletal muscle. Axial FS T2WI (**b**) reveals hyperintense mass with a small central cystic portion. Axial postcontrast FS T1WI (**c**) demonstrates thick peripheral enhancement. Prominent vascularity is found on color Doppler study (**d**)

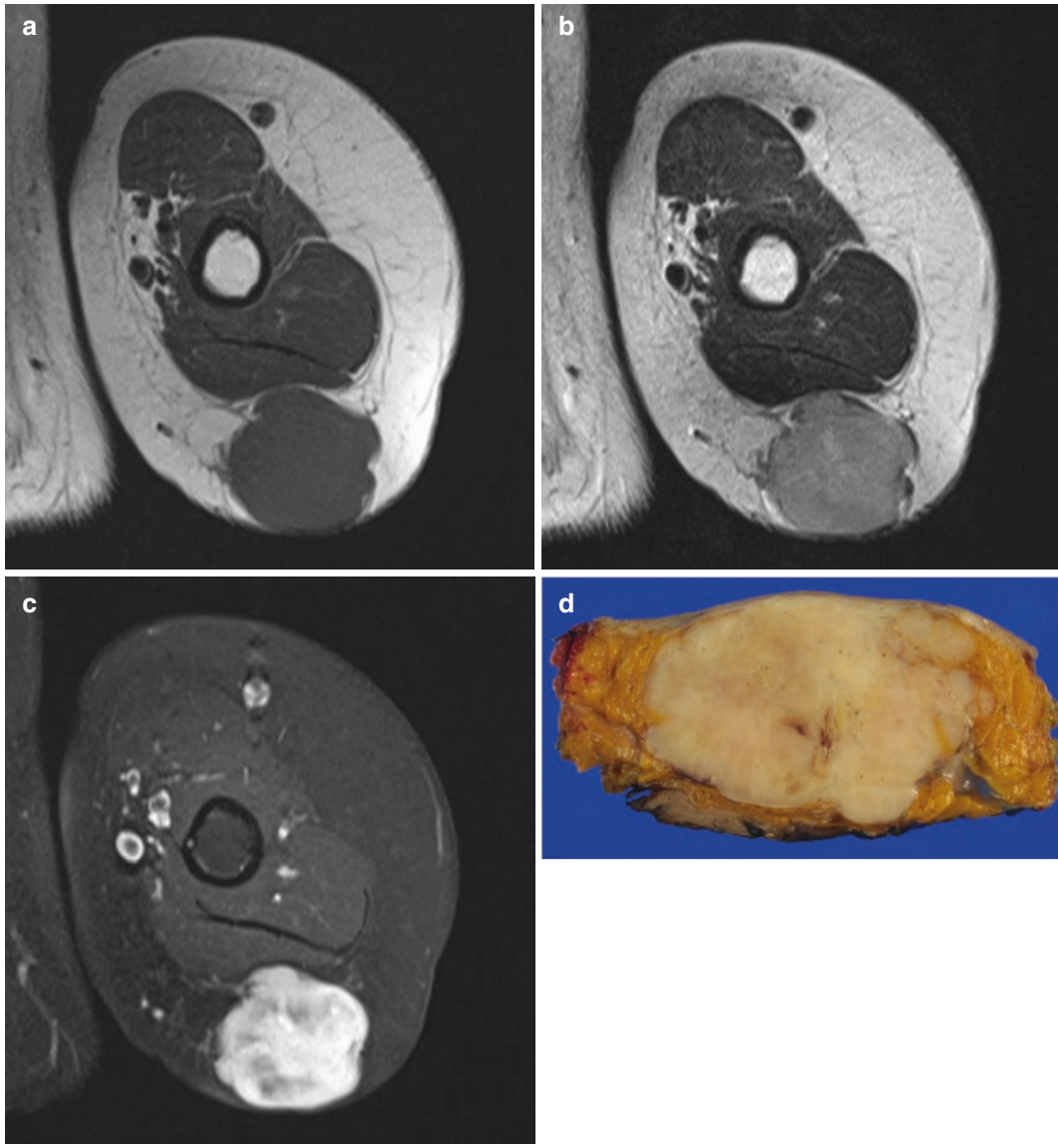

Fig. 15.21 Subcutaneous metastasis of malignant phyllodes tumor from the breast. Axial T1WI (**a**) shows a nonspecific soft tissue mass in the subcutaneous layer of the left upper arm. Axial T1WI and T2WI (**b**) reveal nonspecific signal intensity. Axial postcontrast FS T1WI (**c**) shows diffuse and intense contrast enhancement. Surgical specimen (**d**) shows multilobulated solid mass

References

Alaibac M, Bordignon M, Pennelli N, et al. Primary subcutaneous B-cell lymphoma: case report and literature review. Acta Derm Venereol. 2008;88(2):151–4. doi:10.2340/00015555-0373.

Alcaraz I, Cerroni L, Rutten A, Kutzner H, Requena L. Cutaneous metastases from internal malignancies: a clinicopathologic and immunohistochemical review. Am J Dermatopathol. 2012;34(4):347–93. doi:10.1097/DAD.0b013e31823069cf.

Beaman FD, Kransdorf MJ, Andrews TR, et al. Superficial soft-tissue masses: analysis, diagnosis, and differential considerations. Radiographics. 2007;27(2):509–23. doi:10.1148/rg.272065082.

Catalano O, Siani A. Cutaneous melanoma: role of ultrasound in the assessment of locoregional spread. Curr

Probl Diagn Radiol. 2010;39(1):30–6. doi:10.1067/j.cpradiol.2009.04.001.
Catalano O, Caraco C, Mozzillo N, Siani A. Locoregional spread of cutaneous melanoma: sonography findings. AJR Am J Roentgenol. 2010a;194(3):735–45. doi:10.2214/AJR.09.2422.
Catalano O, Setola SV, Vallone P, Raso MM, D'Errico AG. Sonography for locoregional staging and follow-up of cutaneous melanoma: how we do it. J Ultrasound Med. 2010b;29(5):791–802.
Chan LP, Gee R, Keogh C, Munk PL. Imaging features of fat necrosis. Am J Roentgenol. 2003;181(4):955–9. doi:10.2214/ajr.181.4.1810955.
Choi EA, Gershenwald JE. Imaging studies in patients with melanoma. Surg Oncol Clin N Am. 2007;16(2):403–30. doi:10.1016/j.soc.2007.03.004.
Damron TA, Heiner J. Distant soft tissue metastases: a series of 30 new patients and 91 cases from the literature. Ann Surg Oncol. 2000;7(7):526–34.
De Beuckeleer LHL, De Schepper AMA, Neetens I. Magnetic resonance imaging of pilomatricoma. Eur Radiol. 1996;6(1):72–5. doi:10.1007/bf00619959.
El-Noueam KI, Giuliano V, Schweitzer ME, O'Hara BJ. Rheumatoid nodules: MR/pathological correlation. J Comput Assist Tomogr. 1997;21(5):796–9.
Fernando RA, Somers S, Edmonson RD, Sidhu PS. Subcutaneous fat necrosis: hypoechoic appearance on sonography. J Ultrasound Med. 2003;22(12):1387–90.
Fujii Y, Shinozaki T, Koibuchi H, et al. Primary peripheral T-cell lymphoma in subcutaneous tissue: sonographic findings. J Clin Ultrasound. 2004;32(7):361–4. doi:10.1002/jcu.20045.
Garioni E, Danesino GM, Madonia L. Pilomatricoma: sonographic features. J Ultrasound. 2008;11(2):76–8. doi:10.1016/j.jus.2008.03.001.
Gottlieb JA, Schermer DR. Cutaneous metastases from carcinoma of the colon. JAMA. 1970;213(12):2083. doi:10.1001/jama.1970.03170380057025.
Haygood TM, Wong J, Lin JC, et al. Skeletal muscle metastases: a three-part study of a not-so-rare entity. Skelet Radiol. 2012;41(8):899–909. doi:10.1007/s00256-011-1319-8.
Hong SH, Chung HW, Choi J-Y, et al. MRI findings of subcutaneous epidermal cysts: emphasis on the presence of rupture. Am J Roentgenol. 2006;186(4):961–6. doi:10.2214/AJR.05.0044.
Huang C-C, Ko S-F, Huang H-Y, et al. Epidermal cysts in the superficial soft tissue: sonographic features with an emphasis on the Pseudotestis pattern. J Ultrasound Med. 2011;30(1):11–7.
Hwang JY, Lee SW, Lee SM. The common ultrasonographic features of pilomatricoma. J Ultrasound Med. 2005;24(10):1397–402.
Jang MS, Baek JW, Kang DY, et al. Subcutaneous panniculitis-like T-cell lymphoma: successful treatment with systemic steroid alone. J Dermatol. 2012;39(1):96–9. doi:10.1111/j.1346-8138.2011.01291.x.
Juan Y-H, Saboo SS, Tirumani SH, et al. Malignant skin and subcutaneous neoplasms in adults: multimodality imaging with CT, MRI, and 18F-FDG PET/CT. Am J Roentgenol. 2014;202(5):W422–38. doi:10.2214/AJR.13.11424.
Kalkman E, Baxter G. Melanoma. Clin Radiol. 2004;59(4):313–26. doi:10.1016/j.crad.2003.09.020.
Kang BS, Choi SH, Cha HJ, et al. Subcutaneous panniculitis-like T-cell lymphoma: US and CT findings in three patients. Skelet Radiol. 2007;36(Suppl 1):S67–71. doi:10.1007/s00256-006-0173-6.
Kim HK, Kim SM, Lee SH, Racadio JM, Shin MJ. Subcutaneous epidermal inclusion cysts: ultrasound (US) and MR imaging findings. Skelet Radiol.2011a;40(11):1415–9.doi:10.1007/s00256-010-1072-4.
Kim JW, Chae EJ, Park YS, et al. Radiological and clinical features of subcutaneous panniculitis-like T-cell lymphoma. J Comput Assist Tomogr. 2011b;35(3):394–401. doi:10.1097/RCT.0b013e3182106585.
Kovács KA, Kenessey I, Tímár J. Skin metastasis of internal cancers: a single institution experience. Pathol Oncol Res. 2013;19(3):515–20. doi:10.1007/s12253-013-9611-7.
Lee HS, Joo KB, Song HT, et al. Relationship between sonographic and pathologic findings in epidermal inclusion cysts. J Clin Ultrasound. 2001;29(7):374–83.
Lim HW, Im SA, Lim G-Y, et al. Pilomatricomas in children: imaging characteristics with pathologic correlation. Pediatr Radiol. 2007;37(6):549–55. doi:10.1007/s00247-007-0461-x.
López JA, Saez F, Larena JA, et al. MRI diagnosis and follow-up of subcutaneous fat necrosis. J Magn Reson Imaging. 1997;7(5):929–32. doi:10.1002/jmri.1880070523.
Meier F, Will S, Ellwanger U, et al. Metastatic pathways and time courses in the orderly progression of cutaneous melanoma. Br J Dermatol. 2002;147(1):62–70.
Mellado JM, del Palomar LP, Díaz L, Ramos A, Saurí A. Long-standing Morel-Lavallée lesions of the trochanteric region and proximal thigh: MRI features in five patients. Am J Roentgenol. 2004;182(5):1289–94. doi:10.2214/ajr.182.5.1821289.
Neal C, Jacobson JA, Brandon C, et al. Sonography of Morel-Lavallée lesions. J Ultrasound Med. 2008;27(7):1077–81.
Parra JA, Fernandez MA, Encinas B, Rico M. Morel-Lavallee effusions in the thigh. Skelet Radiol. 1997;26(4):239–41.
Plaza JA, Perez-Montiel D, Mayerson J, Morrison C, Suster S. Metastases to soft tissue: a review of 118 cases over a 30-year period. Cancer. 2008;112(1):193–203. doi:10.1002/cncr.23151.
Sanders TG, Linares R, Su A. Rheumatoid nodule of the foot: MRI appearances mimicking an indeterminate soft tissue mass. Skelet Radiol. 1998;27(8):457–60.
Strobel K, Arthur R, Exner UG. FDG uptake in a rheumatoid nodule with imaging appearance similar to a malignant soft tissue tumor. Clin Nucl Med. 2009;34(10):691–2.
Surov A, Hainz M, Holzhausen HJ, et al. Skeletal muscle metastases: primary tumours, prevalence, and radio-

logical features. Eur Radiol. 2010;20(3):649–58. doi:10.1007/s00330-009-1577-1.

Tsai TS, Evans HA, Donnelly LF, Bisset GS, Emery KH. Fat necrosis after trauma: a benign cause of palpable lumps in children. Am J Roentgenol. 1997;169(6):1623–6. doi:10.2214/ajr.169.6.9393177.

Veit-Haibach P, Vogt FM, Jablonka R, et al. Diagnostic accuracy of contrast-enhanced FDG-PET/CT in primary staging of cutaneous malignant melanoma. Eur J Nucl Med Mol Imaging. 2009;36(6):910–8. doi:10.1007/s00259-008-1049-x.

Veys EM, De Keyser F. Rheumatoid nodules: differential diagnosis and immunohistological findings. Ann Rheum Dis. 1993;52(9):625–6.

Walsh M, Jacobson JA, Kim SM, et al. Sonography of fat necrosis involving the extremity and torso with magnetic resonance imaging and histologic correlation. J Ultrasound Med. 2008;27(12):1751–7.

Willemze R. Primary cutaneous B-cell lymphoma: classification and treatment. Curr Opin Oncol. 2006;18(5):425–31. doi:10.1097/01.cco.0000239879.31463.42.

Willemze R, Meijer CJ. Classification of cutaneous T-cell lymphoma: from Alibert to WHO-EORTC. J Cutan Pathol. 2006;33(Suppl 1):18–26. doi:10.1111/j.0303-6987.2006.00494.x.

Zinzani PL, Quaglino P, Pimpinelli N, et al. Prognostic factors in primary cutaneous B-cell lymphoma: the Italian Study Group for Cutaneous Lymphomas. J Clin Oncol. 2006;24(9):1376–82. doi:10.1200/JCO.2005.03.6285.

Masses That May Mimic Soft Tissue Tumors

16

16.1 Ganglion

Ganglion is a benign cystic mass containing a gelatinous fluid rich in hyaluronic acid and other mucopolysaccharides, with a fibrous capsule without synovial lining (McCarthy and McNally 2004). The mass arises from the joint capsule, ligaments, tendon sheaths, bursae, or subchondral bone (Bermejo et al. 2013). Ganglion is usually found in the periarticular soft tissues in areas under repetitive stress, with or without communication with joint spaces. Occasionally, they can occur far from a joint or even in an intramuscular location. The origin of the fluid has been postulated to arise from one of following three mechanisms. First, it may be pumped into the cyst from the joint by motion of the wrist. Second, it may result from an extra-articular degenerative process, cyst formation, and subsequent communication with the joint. Lastly, it may be the result of excessive mucin production by mesenchymal cells within the wall (Gude and Morelli 2008). Intraneural ganglion cysts are rarely found. The common peroneal nerve is most frequently involved, and other affected nerves are often located near articular spaces. The cystic lesion is located within the epineurium, causing an eccentric displacement of the nerve fascicles. The proposed pathogenesis of intraneural ganglion cyst is a dissection of synovial joint fluid into the epineurium of an articular branch nerve supplying a joint, with subsequent centripetal dissection into the parent nerve (Spinner et al. 2007a, b).

On US, ganglion is usually an anechoic mass with posterior acoustic enhancement, but small cysts (less than 10 mm in the largest dimension) may have echogenic foci without posterior acoustic enhancement. Larger ganglion cysts are more likely to have well-defined borders and multiple lobulations (Wang et al. 2007).

On MR imaging, ganglion typically presents as well-defined rounded or lobulated fluid collections with sharply defined internal septations ('bunch of grapes' appearance) (Perdikakis and Skiadas 2013; McCarthy and McNally 2004). These cysts show a homogeneous high signal intensity on T2-weighted image but may have a more heterogeneous appearance. On T1-weighted image, the signal intensity of ganglion depends on its protein concentration and the presence of hemorrhagic contents. Complication, including bleeding or inflammatory changes may also be present (Bermejo et al. 2013). Complicated ganglion may have a more heterogeneous appearance, with a thick peripheral rim or internal septa in cases of infectious or inflammatory changes. However, they should not demonstrate internal enhancement after contrast administration (Bermejo et al. 2013).

16.2 Vascular Lesion

Aneurysms or pseudoaneurysms may be erroneously diagnosed as a soft tissue tumor in the extremities. True aneurysms contain all three

H.S. Kang et al., *Oncologic Imaging: Soft Tissue Tumors*, DOI 10.1007/978-981-287-718-5_16

layers of the arterial wall (intima, media, and adventitia). In contrast, pseudoaneurysms contain only adventitia and is considered to be a hematoma between the arterial wall and surrounding parenchyma, lined by inflammatory cells and fibroblasts, analogous to an intramural hematoma (Kransdorf and Murphey 2014; Anderson et al. 2003). The popliteal artery is the most frequently affected by peripheral aneurysm. Patients are generally older men in the fifth or sixth decades. Pseudoaneurysms may be associated with a history of a single direct trauma or, more commonly, chronic blunt trauma (Anderson et al. 2003). The lesions may remain stable for years, and symptoms may relate to the overall size of the lesion. Clinical clues to the diagnosis include pulsatility and bruit in close proximity to an artery in a patient with a history of trauma. In these cases, it is important to make the diagnosis prospectively and to avoid biopsy (Wu and Hochman 2009). The hypothenar hammer syndrome is a rare clinical entity associated with thrombosed pseudoaneurysm in the ulnar artery. This syndrome describes signs and symptoms associated with ischemia of the hand and fingers resulting from blunt repetitive injury of the ulnar artery and superficial volar arch against the hook of hamate (Anderson et al. 2003).

Aneurysms or pseudoaneurysms can be recognized on MR imaging with characteristic imaging features. Aneurysms present as well-defined round to elliptical masses with a persistent flow signal void. On T1- and T2-weighted images, they have a complex signal intensity caused by blood products of varying ages: signal void in regions of flowing blood, hyperintensity on T1- and T2-weighted images due to subacute hemorrhage, and hypointensity caused by hemosiderin deposits (Stacy and Kapur 2011). Moreover, MR images reveal a characteristic flow-related artifact in the direction of the phase encoding gradient (Sundaram and Sharafuddin 1995). The imaging distinction between an aneurysm with extensive thrombus and a pseudoaneurysm may be difficult.

16.3 Gout

Gout is characterized by the inflammatory response that results from the deposition of monosodium urate crystals in soft tissues and joints (Desai et al. 2011). Tophaceous gout represents the chronic phase of the disease process. Pathologically, gouty tophi are aggregations of urate crystals and a proteinaceous matrix, surrounded by an intense inflammatory reaction. The development of a tophus in the absence of prior episodes of gouty arthritis is unusual (Yu et al. 1997). Rarely, a soft tissue tophus may occur in the absence of articular disease, which may result in a misdiagnosis of infection or neoplasm (Yu et al. 1997). Gouty tophus may be observed around joints and have a predilection for the olecranon and prepatellar regions.

Radiographs of gouty tophus usually demonstrate a juxta-articular soft tissue mass. Calcification of the mass may be observed but is uncommon. On T1-weighted image, a tophus shows an intermediate signal intensity. The signal intensity on T2-weighted image is variable, from low to high signal intensity, depending on the extent and distribution of calcification, whether the calcification is hydrated, and whether there is associated edema or inflammatory reaction (Yu et al. 1997). However, a heterogeneous intermediate to low signal intensity is the most common pattern on T2-weighted image, resulting from the presence of urate crystals and fibrous tissue (Narváez et al. 2003). After gadolinium administration, intense enhancement may be seen, reflecting the surrounding granulation tissue and increased vascularity of the affected synovium (Narváez et al. 2003). Recently, dual-energy CT has been introduced to differentiate urate crystals from calcium using specific attenuation characteristics. Dual-energy CT may be used in patients with an unclear diagnosis or for excluding gout and a volumetric analysis of tophi in patients with confirmed gout. Dual-energy CT promises to be a unique and clinically relevant modality in the diagnosis and management of gout (Desai et al. 2011).

16.4 Sarcoidosis

Sarcoidosis is a systemic granulomatous disorder which can affect multiple organs (Moore and Teirstein 2003; Koyama et al. 2004). Musculoskeletal involvement in sarcoidosis usually occurs in patients with generalized disease (Koyama et al. 2004).

In skeletal muscles, sarcoidosis can occur in the following two different forms: myopathic or nodular type involvement. The nodular type often causes solitary or multiple nodules; therefore, the most common clinical presentation is a palpable mass without pain or with mild tenderness. The myopathic type involves muscles symmetrically and diffusely and does not form a mass. Slowly progressive myalgia, weakness, and atrophy are usually observed (Otake 1994; Moore and Teirstein 2003). Nodular type muscular sarcoidosis has a characteristic appearance at MR imaging that may allow accurate diagnosis (Koyama et al. 2004). On axial T2-weighted image, the nodule has a star-shaped central region of low signal intensity, surrounded by a bright rim (i.e., 'dark star' sign). Only the peripheral hyperintense rim shows intense enhancement after gadolinium administration. Histologically, a star-shaped hypointense center corresponds to fibrous tissue, and the peripheral hyperintense rim is believed to reflect active inflammatory granulomas and edema (Otake 1994; Moore and Teirstein 2003; Koyama et al. 2004). The peripheral areas of the nodules show increased signal intensity on T1-weighted image due to the high cellularity of granulomas (Otake 1994). Coronal and sagittal images may show the 'three stripes' sign, consisting of a hypointense inner stripe and hyperintense outer stripes. Gallium-67 scintigraphy shows increased uptake in the nodules but is otherwise nonspecific (Otake 1994). US also demonstrates the star-shaped central lesion and the three stripes. However, the locations of black and white on the US are reversed from their locations on MR images (Otake 1994). In myopathic type involvement, the involved muscle has nonspecific high signal intensity on T2-weighted images.

Cutaneous involvement is observed in 25% of cases, typically at the time of diagnosis (Newman et al. 1997; Ahmed and Harshad 2006). Among these cases, subcutaneous sarcoidosis is the least common subset of cutaneous lesions, with a 1.4–6% of incidence in patients with systemic sarcoidosis (Chen et al. 2009). Subcutaneous involvement is diagnosed by identifying noninfectious sarcoidal or epithelioid granulomas with minimal lymphocytic inflammation that predominantly involves the panniculus. Ahmed and Harstad reported 21 cases of subcutaneous sarcoidosis (Ahmed and Harshad 2006). These authors reported that subcutaneous sarcoidosis is characterized by a peak incidence during the fourth decade, female predisposition, slightly tender subcutaneous lesions that typically involve the upper extremities, cutaneous lesional multiplicity and clustering, a strong association with a systemic disease component at the outset of disease, and, notably, bilateral hilar adenopathy (Ahmed and Harshad 2006). On MR imaging, sarcoidal subcutaneous granulomatous infiltration, skin nodules, and soft tissue masses associated with lymphadenopathy may be detected. These lesions show increased signal intensity on T2-weighted image, low signal intensity on T1-weighted image, and enhancement after gadolinium administration (Moore and Teirstein 2003). US demonstrates irregularly thickened subcutaneous tissue with several hyperechoic plaque-like lesions. Histologically, the hypoechoic portion corresponds to the noncaseating granulomas, and the hyperechoic portion corresponds to the surrounding inflammatory infiltrates (Chen et al. 2009). Color Doppler study reveals mild hypervascularity.

16.5 Morton's Neuroma

Morton's neuroma is a common cause of forefoot pain. The term was popularized after the description of this condition by Thomas G. Morton in 1876 (Bencardino et al. 2000; Murphey et al. 1999). Although the exact cause is controversial,

Morton's neuroma most likely represents an entrapment neuropathy by the overlying transverse intermetatarsal ligament, causing perineural fibrosis, nerve degeneration, leukocyte infiltration, and epineural and endoneural vascular hyalinization, resulting in a significantly thicker intermetatarsal nerve (Bencardino et al. 2000). Patients classically experience sharp pain, a burning sensation, and paresthesias during weight bearing in the region of the intermetatarsal spaces, which can be relieved by rest. The third intermetatarsal space is the most frequently involved (Torres-Claramunt et al. 2012).

Morton's neuroma is identified by US as a focal hypoechoic nodule replacing the normally hyperechoic fat of the web spaces of the forefoot at the level of the metatarsal heads. In the longitudinal plane, Morton's neuroma appears as a fusiform hypoechoic mass, with its long axis oriented obliquely to the metatarsals. To further increase diagnostic confidence and overall accuracy, pressure can be applied to the medial and lateral aspects of the forefoot. When the metatarsal heads are squeezed together, Morton's neuroma abruptly displaces toward the plantar surface of the foot, causing a palpable click, which is the so-called sonographic Mulder sign (Torriani and Kattapuram 2003). MR imaging typically demonstrates a well-defined teardrop-shaped mass with intermediate-to-low signal intensity on T1- and T2-weighted images because of its predominantly fibrous composition. Lesions can show variable enhancement. T2-weighted image could be useful in the evaluation of other diagnostic possibilities, including intermetatarsal bursitis and ganglion cyst. Plantar extension of the lesion further below the level of the metatarsal head is frequently observed. In general, MR imaging shows higher sensitivity (76–100%) than that of US in confirmation of the diagnosis (Zanetti et al. 1999; Torres-Claramunt et al. 2012).

There is doubt as to the necessity of imaging evidence to make this diagnosis because Morton's neuroma is frequently found on MR imaging in asymptomatic patients. Previous studies have demonstrated that larger (> 5 mm in transverse diameter) Morton's neuromas are more commonly symptomatic than are smaller ones, but significant overlap was noted between the two groups (Zanetti et al. 1999; Bencardino et al. 2000). Therefore, careful correlation between clinical and MR imaging findings is mandatory before Morton's neuroma is considered clinically relevant (Bencardino et al. 2000). The information provided by MR imaging may have a major effect on the diagnostic and therapeutic decisions of orthopedic surgeons when Morton's neuroma is suspected (Zanetti et al. 1999).

16.6 Traumatic Neuroma

Neuroma is a nonneoplastic, insufficient, and reparative proliferation of nerve tissue, the purpose of which is to regain axonal continuity at the end of an injured nerve. Neuroma is usually observed 1–12 months after amputation (Singson et al. 1987; Murphey et al. 1999; Henrot et al. 2000). Typically, neuroma is associated with trauma or amputation. There are two types of traumatic neuromas based on the anatomic location of the regenerating axonal mass with respect to the proximal nerve end (Singson et al. 1987; Murphey et al. 1999; Henrot et al. 2000; Kransdorf and Murphey 2014). Spindle neuroma is a focal, fusiform swelling of the nerve away from the severed nerve ending and represents the response of a peripheral nerve subjected to chronic friction or irritation (Henrot et al. 2000). Terminal neuroma originates at the end of the severed nerve and is usually due to the multidirectional proliferation of axons without the support of Schwann cells. This lesion has a bulbous-end morphology and is continuous proximally with the normal nerve (Murphey et al. 1999; Henrot et al. 2000). On histological analysis, traumatic neuroma shows disorganization of the neurogenic tissue, which allows it to be distinguished from neurofibroma (Murphey et al. 1999).

On US, terminal neuroma appears as a small hypoechoic mass in continuity with the opposite edges of the severed nerve. Usually, the neuroma is slightly larger than the axial diameter of the nerve. Typically, spindle neuroma appears as a

fusiform mass with an entering and exiting nerve. The margins of neuromas are often well-defined, although some irregularity can be observed due to multidirectional cell proliferation (Murphey et al. 1999). On MR imaging, neuroma shows nonspecific signal characteristics and variable enhancement. However, MR imaging is the optimal imaging modality to identify the direct relationship of the nerve to the lesion (Henrot et al. 2000).

16.7 Xanthoma

Xanthomas are nonneoplastic lesions characterized by a local concentration of lipid-laden macrophages, giant cells, and other inflammatory cells in response to cholesterol deposition in tissues. Xanthomas most frequently involve the skin (eruptive xanthomas) and subcutaneous tissue (tuberous xanthomas). However, the tendon, synovium, and, rarely, bone can also be affected (Kransdorf and Murphey (2014)). Xanthomas usually involve the extensor tendons of the hands, both Achilles tendons, and patellar ligaments (tendon xanthomas) (Fernandes et al. 2015). The extent of involvement is usually directly related to the degree and duration of increased cholesterol levels. Histologically, these lesions are characterized by sheets of lipid-filled foamy histiocytes, extracellular cholesterol (cholesterol clefts), giant cells, and some inflammatory cells. Focal cystic and degenerative change with calcification can also be observed (Bude et al. 1994).

On radiography, tendon xanthomas are shown either as an abnormal tendon thickening or soft tissue masses without calcification (Fernandes et al. 2015). US demonstrates single or multiple focal, hypoechoic lesions, reflecting tendon xanthomas or a diffusely enlarged heterogeneous tendon (Bude et al. 1994). On MR imaging, a speckled or reticulated appearance is observed on both T1- and T2-weighted images, which differs from acute or chronic tears (Liem et al. 1992; Fernandes et al. 2015). Although xanthomas are composed of lipids, T1 signal intensities obtained from xanthomas are much lower than those of fat. Those MR signal characteristics are produced by free cholesterol and cholesterol ester (the major lipid components of xanthomas), which do not produce a measurable MR signal. Focal areas with a high signal on T1- and T2-weighted images can be observed when a component of interfascicular edema or inflammation is present in response to the infiltrative cholesterol deposition. (Liem et al. 1992; Bude et al. 1994).

16.8 Illustrations: Masses That May Mimic Soft Tissue Tumors

16.8.1 Ganglion

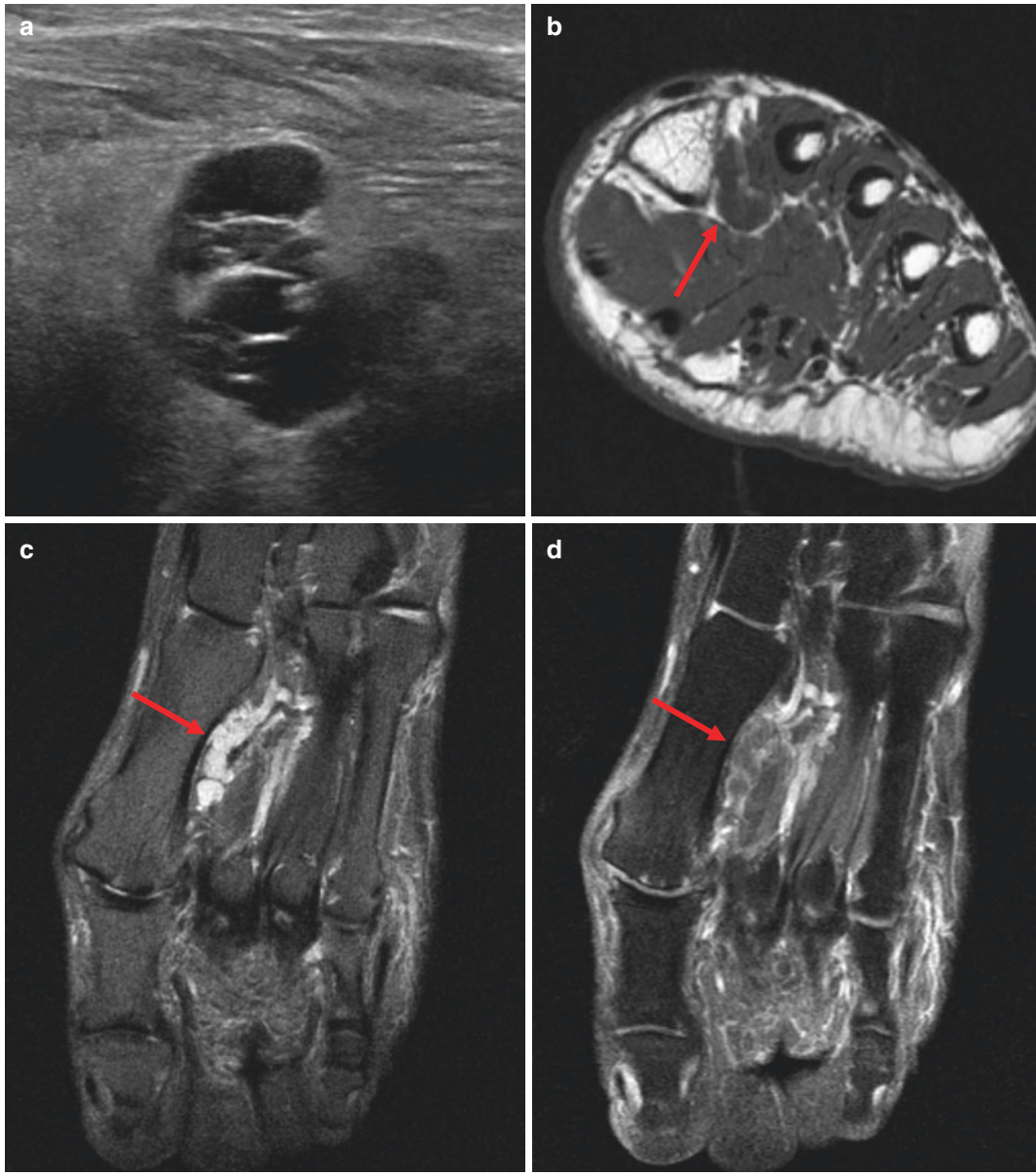

Fig. 16.1 Ganglion. US (**a**) reveals a multilobulated anechoic mass with multiple internal septa (*bunch of grapes appearance*) and mild posterior acoustic enhancement. The multilobulated, elongated mass is located in the first intermetatarsal space, with low signal intensity on axial T1WI (**b**) and high signal intensity on coronal T2WI (**c**). Coronal postcontrast FS T1WI (**d**) shows thin peripheral rim enhancement

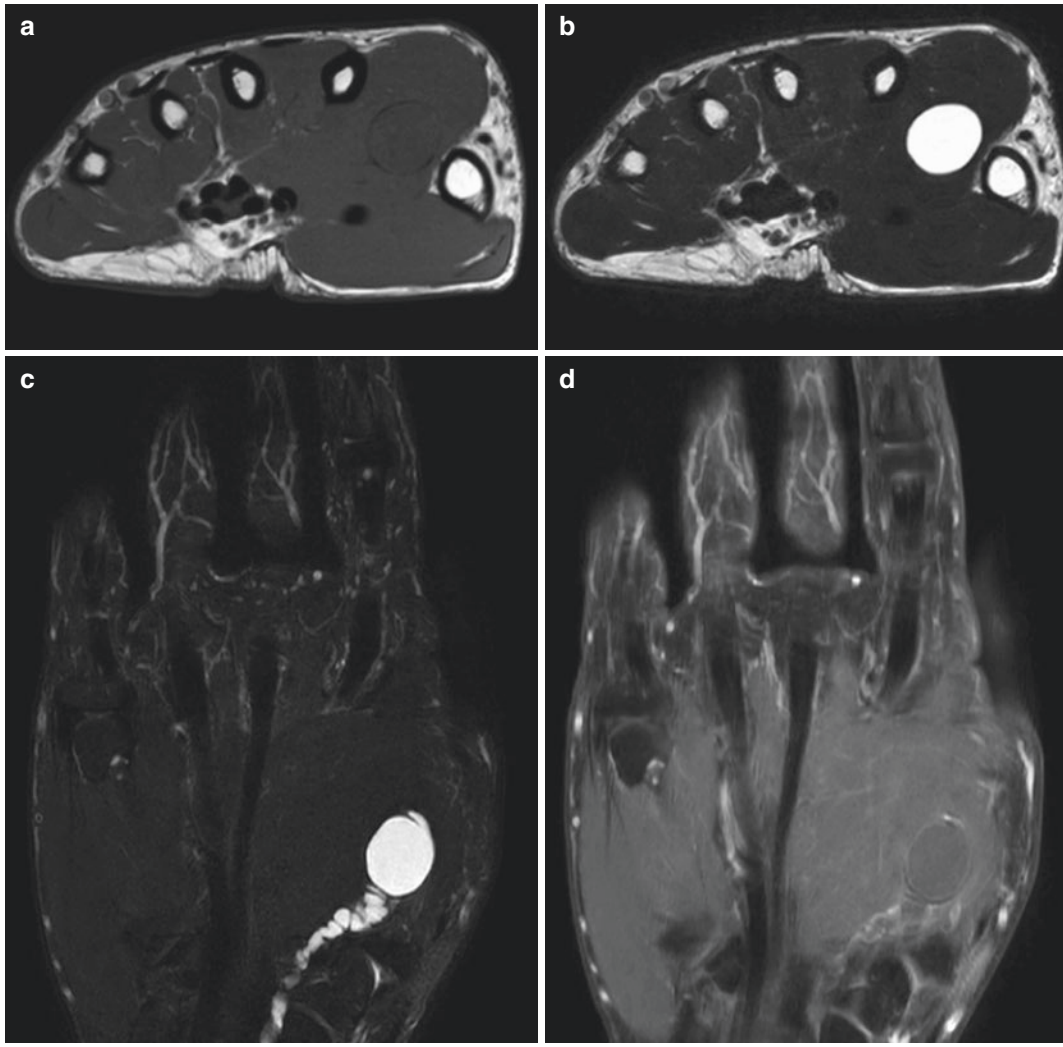

Fig. 16.2 Ganglion. Axial T1WI (**a**) shows a well-defined round mass with isointensity to adjacent skeletal muscle. On axial (**b**) and coronal (**c**) T2WIs, the mass appears with bright, high signal intensity, consistent with the characteristic MR signal intensities of ganglion. Coronal postcontrast FS T1WI (**d**) shows thin peripheral enhancement

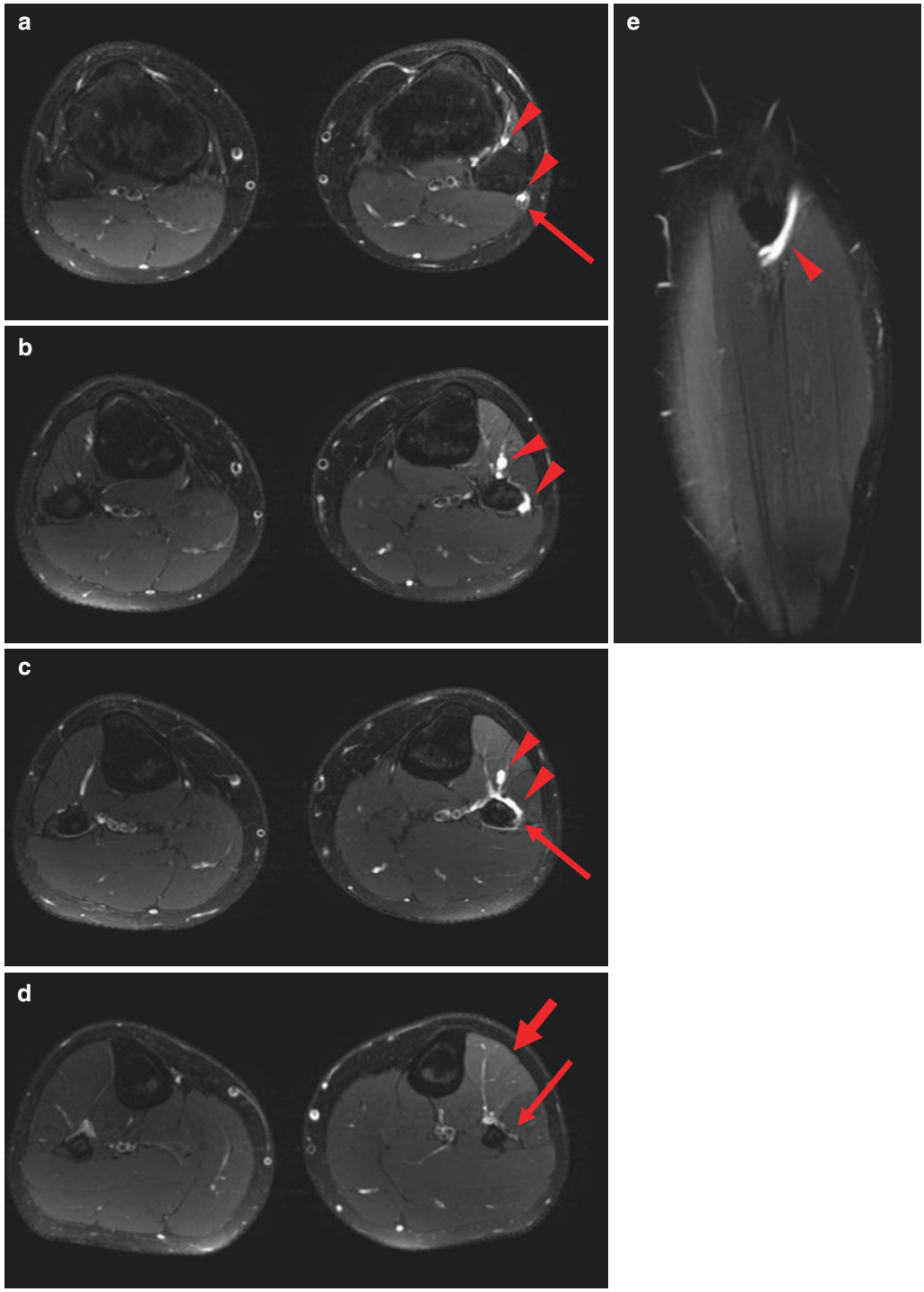

Fig. 16.3 Common peroneal nerve sheath ganglion cyst. Axial and sagittal FS T2WIs (**a**–**e**) show a multilobulated cystic lesion (*arrowheads*) around the left fibula head. The lesion extends along the course of the common peroneal nerve (*arrows*), with a channel projecting anteriorly towards proximal tibiofibular joint. Compared to contralateral nerve, the affected nerve shows mild swelling and increased signal intensity (*arrows*). There is mildly increased signal intensity in anterior compartment muscles (**d**, *thick arrow*), suggestive of early denervation muscle change

16.8.2 Vascular Lesion

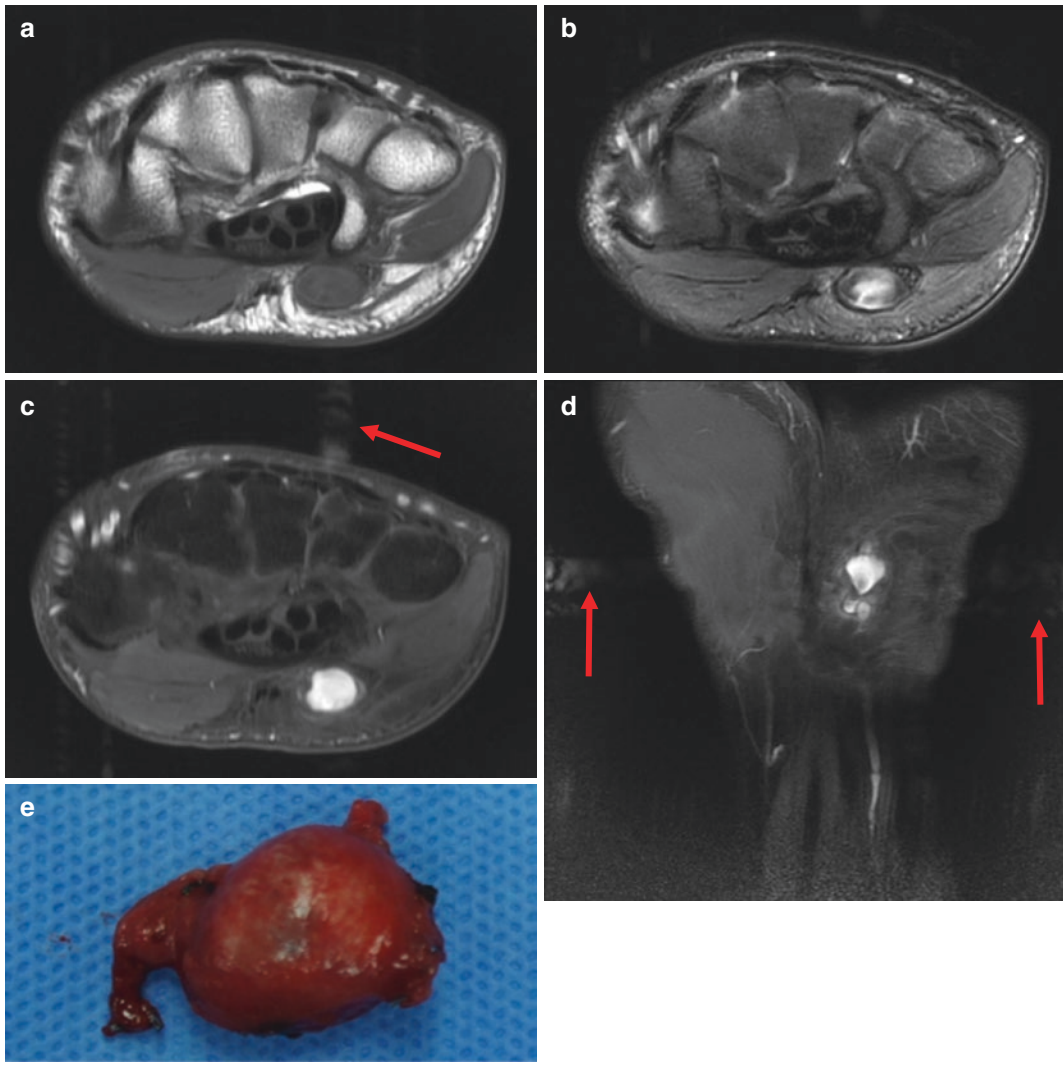

Fig. 16.4 Aneurysm. Axial T1WI (**a**) shows a slightly hyperintense mass that is closely related to the ulnar neurovascular bundle. Axial T2WI (**b**) shows that the mass has central high and peripheral low signal intensity. Postcontrast FS T1WIs (**c**, **d**) reveals diffuse, intense enhancement of the mass, showing a characteristic flow-related artifact (*arrows*) in the direction of the phase encoding gradient. The surgical specimen shows an enlarged mass connected with the ulnar artery (**e**)

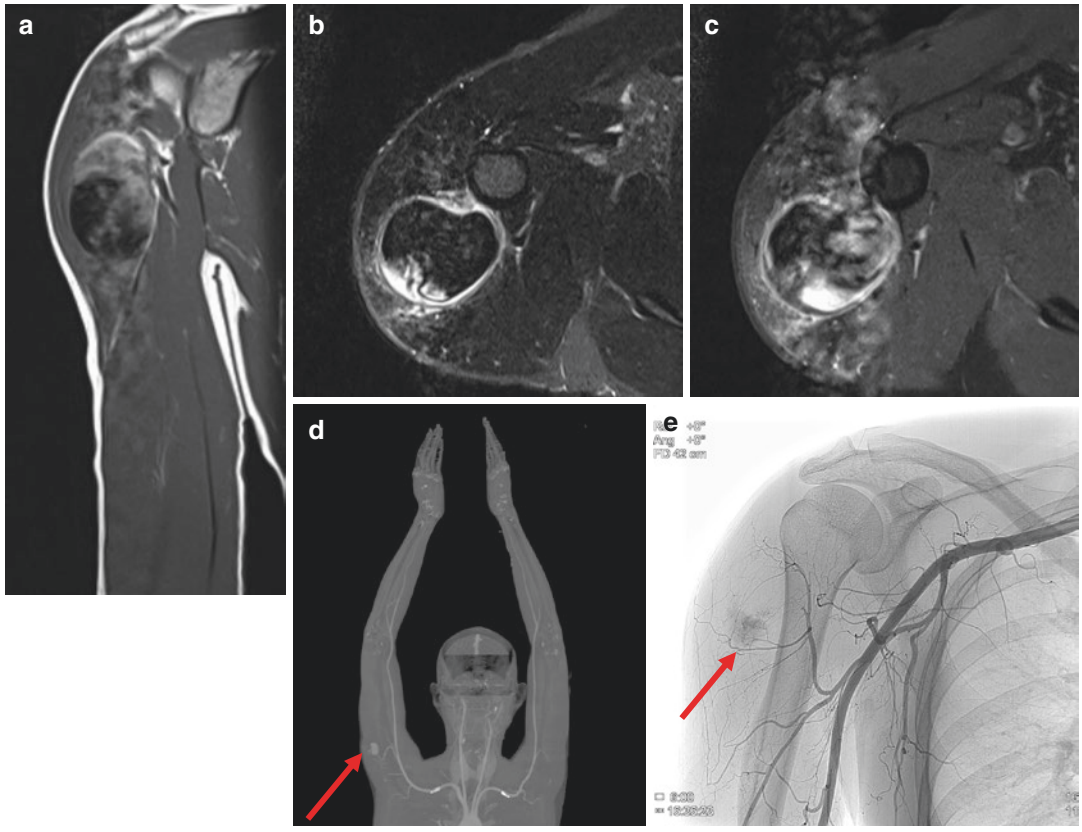

Fig. 16.5 Pseudoaneurysm. Coronal T1WI (**a**) shows a well demarcated ovoid mass-like lesion in the right deltoid muscle. Coronal T1WI (**a**) and axial FS T2WI (**b**) show a signal void and prominent pulsation artifact in the direction of the phase encoding gradient. Axial postcontrast FS T1WI (**c**) shows focal enhancement and a prominent pulsation artifact. CT maximum intensity projection image (**d**) shows a pseudoaneurysm (*arrow*) in the right deltoid muscle, likely supplied by the right anterior circumflex artery. Digital subtraction angiogram (**e**) reveals extravasation of contrast (*arrow*) from the right anterior circumflex artery

16.8.3 Gout

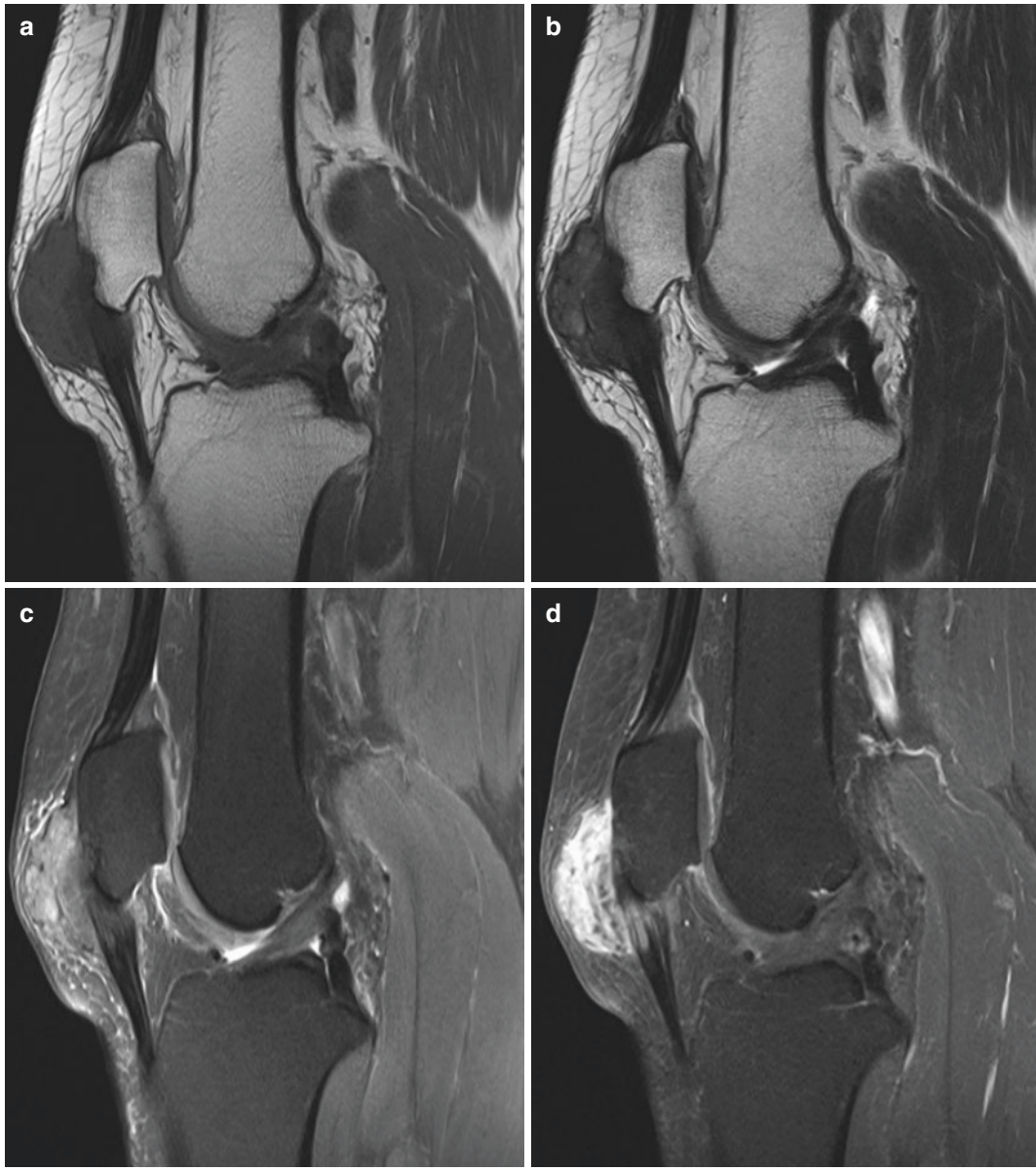

Fig. 16.6 Gout. There is juxta-articular soft tissue mass with close proximity to the anterior cortex of the patella and involving the proximal patellar ligament (**a**–**d**). Sagittal T1WI (**a**) and T2WI (**b**) show a mass with heterogeneous intermediate to low signal intensity in the prepatellar region, involving the patellar ligament. On FS T2WI (**c**), the mass shows heterogeneous signal intensity, predominantly intermediate to low, with overlying subcutaneous fat infiltration. The mass is heterogeneously enhanced after gadolinium administration (**d**)

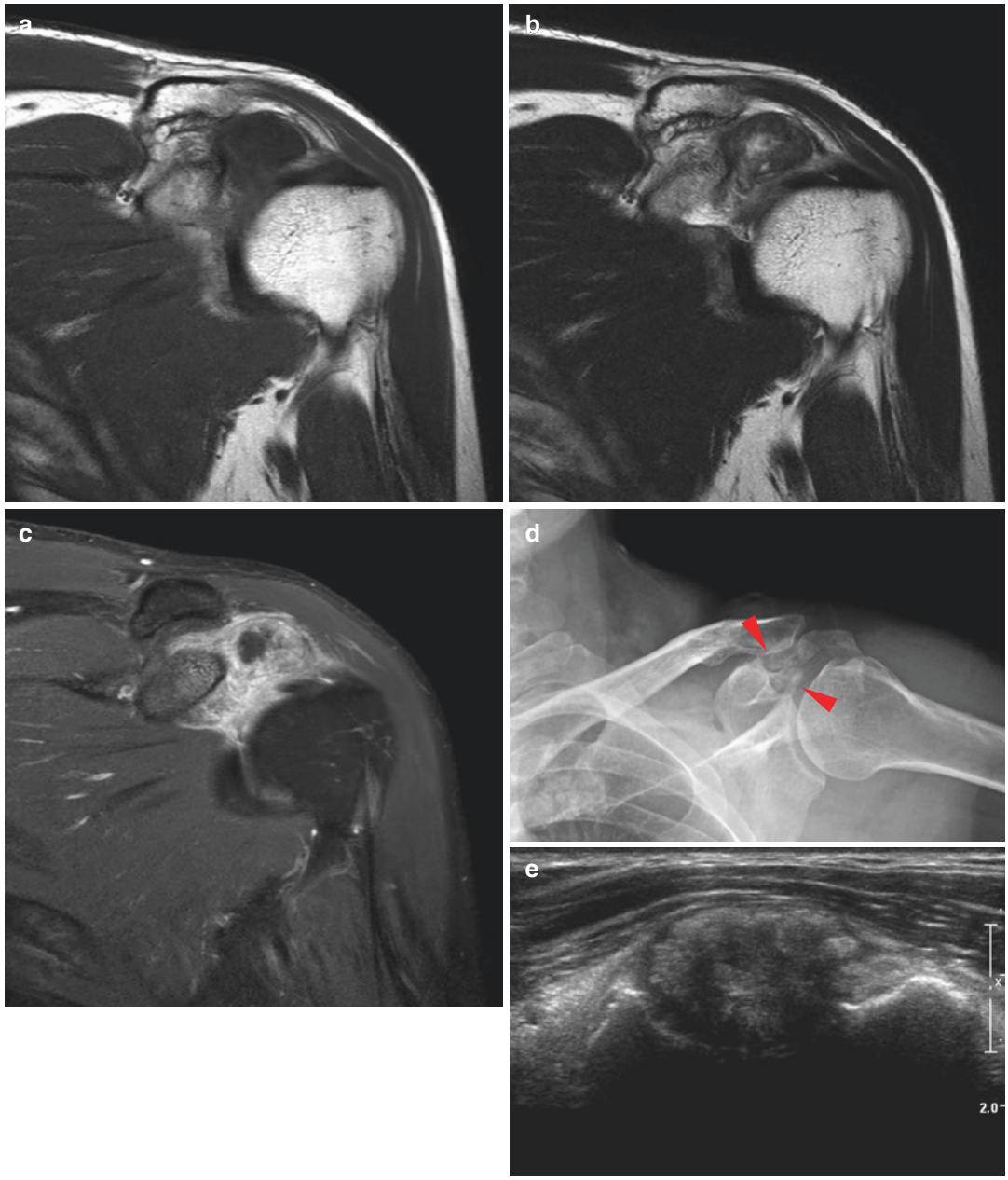

Fig. 16.7 Gout. MR images (**a**–**c**) shows a mass in the left shoulder. On coronal T2WI (**b**), the mass shows heterogeneous signal intensity, predominantly intermediate to low. The mass demonstrates heterogeneous enhancement with central cavitation on postcontrast FS T1WI (**c**). Radiograph of the left shoulder (**d**) reveals mineralization in SASD space (*arrowheads*). US (**e**) shows a hyperechoic mass with posterior shadowing, in keeping with crystal deposition

16.8.4 Sarcoidosis

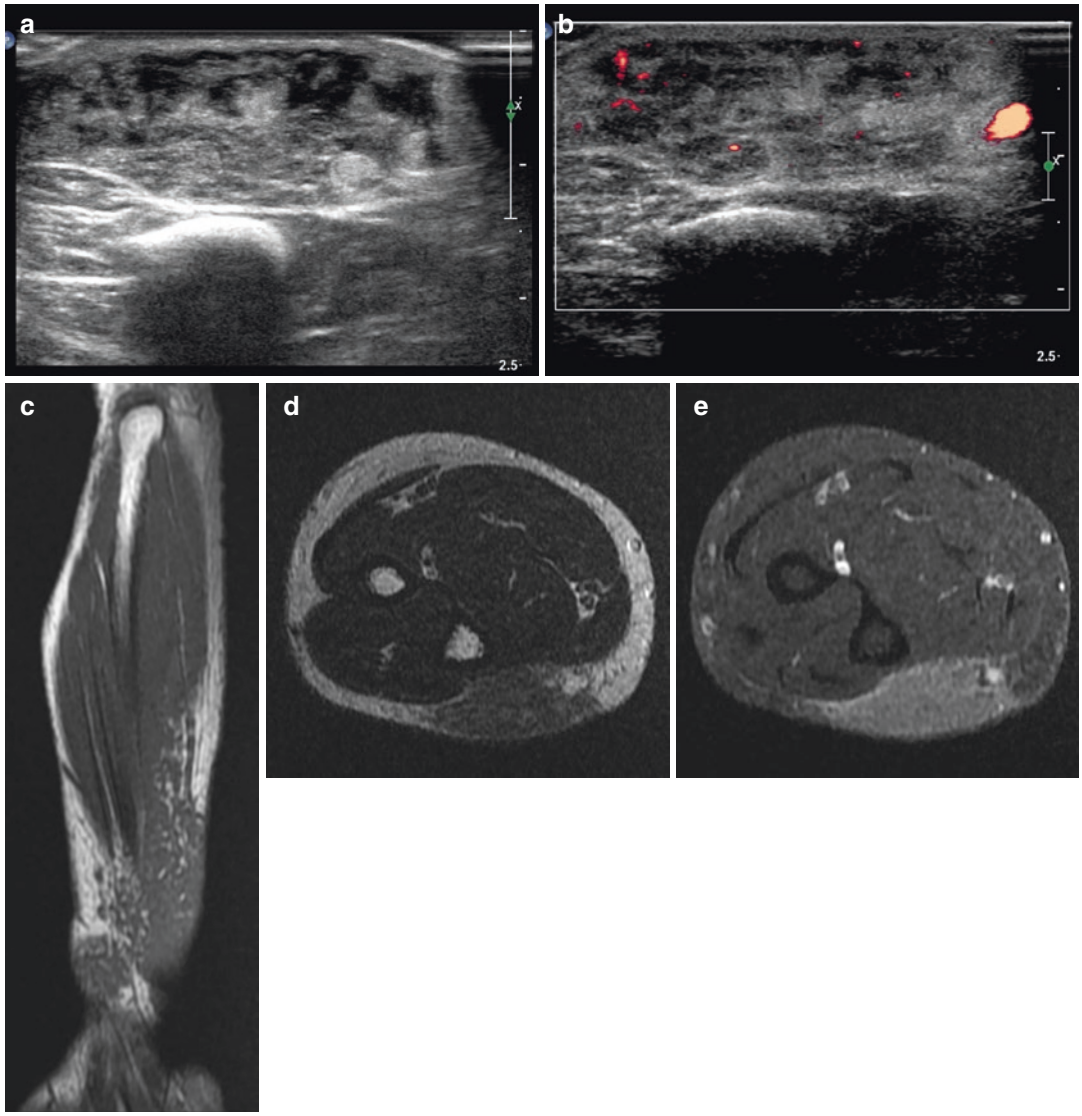

Fig. 16.8 Subcutaneous sarcoidosis. Transverse US (**a**) of the forearm shows a heterogeneous echoic mass in the thickened subcutaneous tissue. Color Doppler study (**b**) reveals several Doppler signals within the subcutaneous mass. Coronal T1WI (**c**) shows poorly defined subcutaneous infiltration with low signal intensity in the ulnar aspect of the forearm. Axial T2WI (**d**) shows a mass of intermediate signal intensity. Axial postcontrast FS T1WI (**e**) shows that the mass has diffuse contrast enhancement

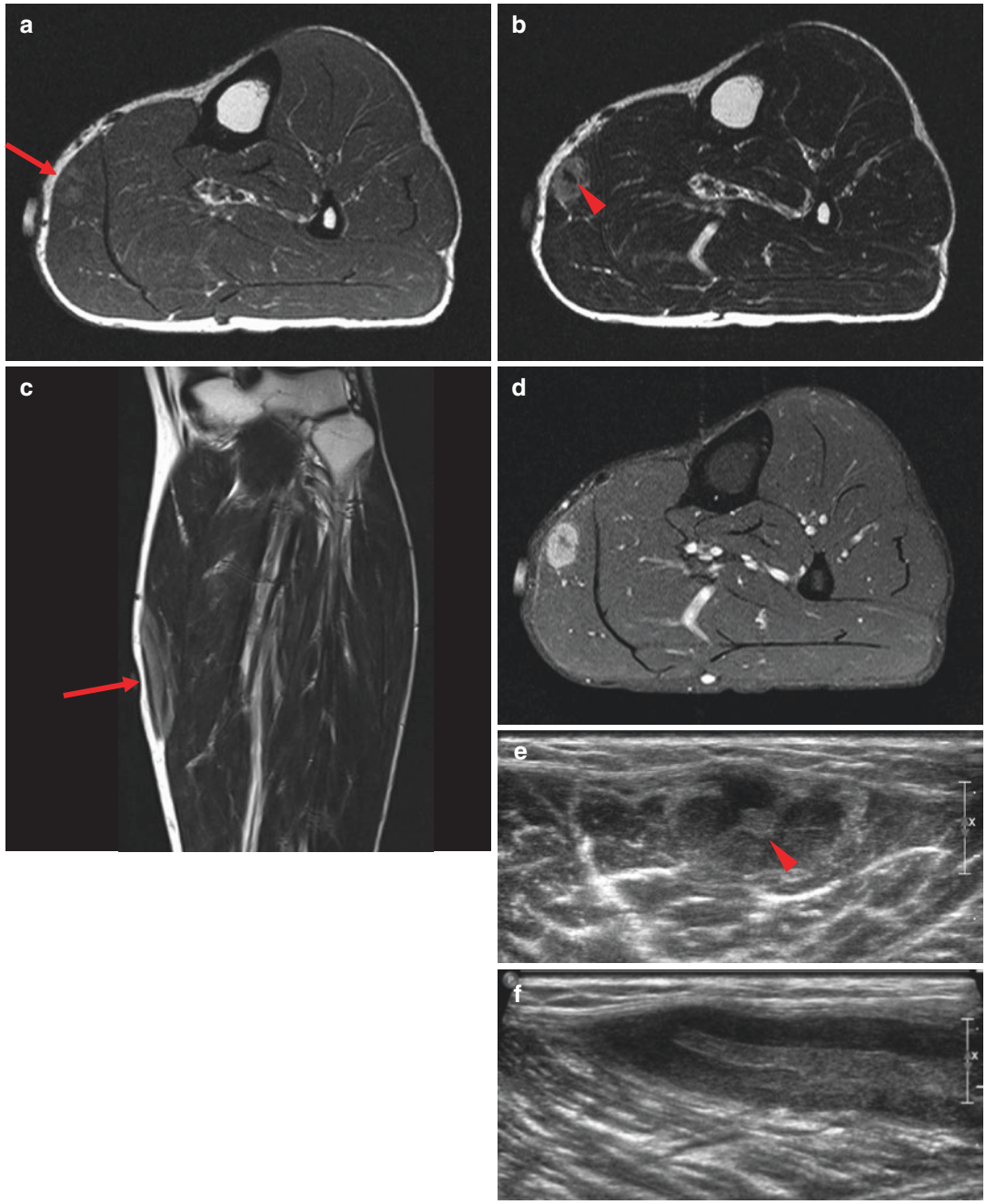

Fig. 16.9 Muscular sarcoidosis. Axial T1WI (**a**) and T2WI (**b**) show a slightly hyperintense nodule (*arrow*). Axial T2WI (**b**) shows the star-shaped central structure with dark signal intensity in the nodule (*arrowhead*, 'dark star sign'). Coronal T2WI (**c**) shows three strips (*arrow*): an inner stripe of low signal intensity and outer stripes of high signal intensity. Axial postcontrast FS T1WI (**d**) reveals intense enhancement except central dark structure. US also demonstrates the star-shaped central lesion (**e**, *arrowhead*) and the three stripes (**f**). However, the locations of black and white on the US are reversed relative to the MR images

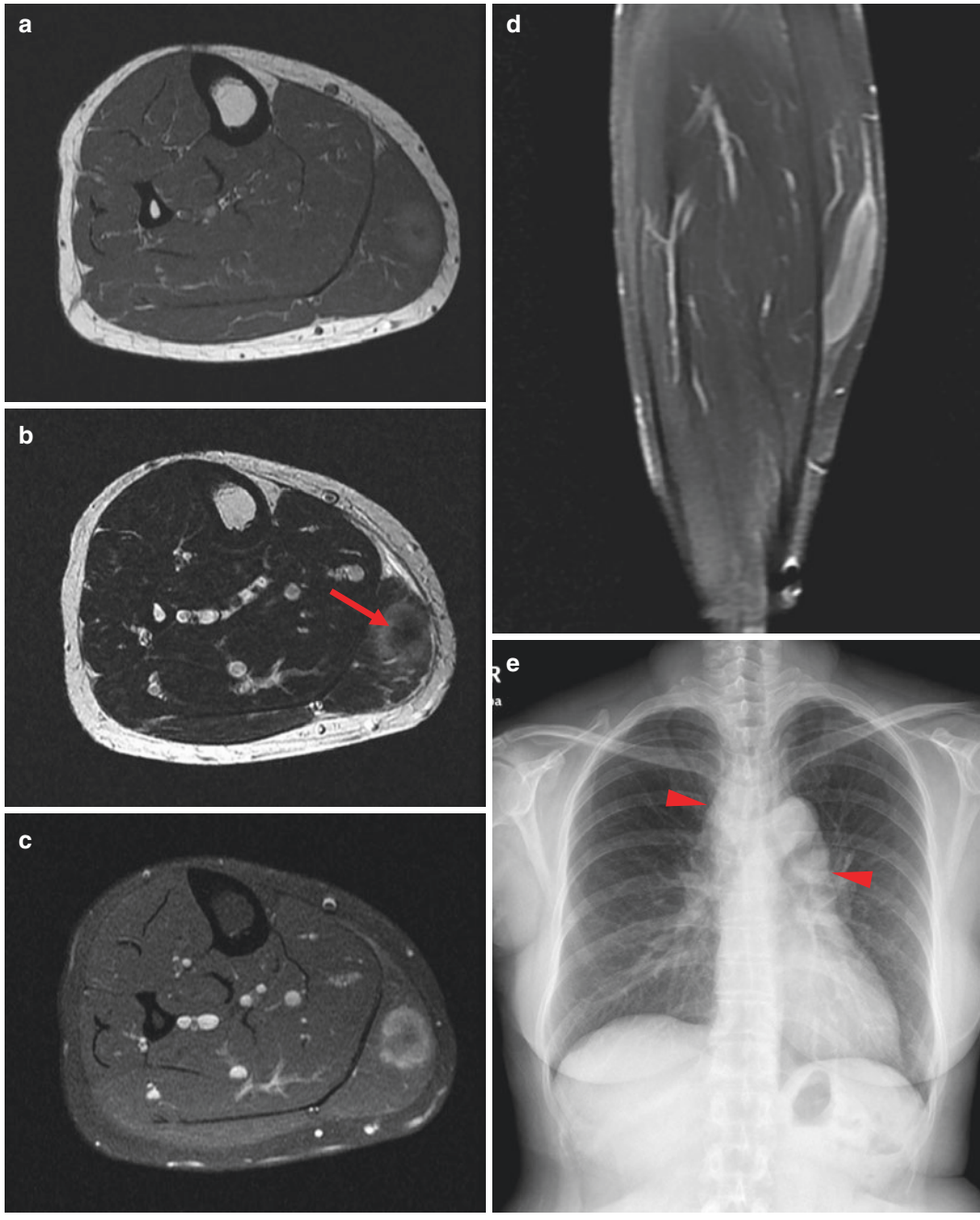

Fig. 16.10 Muscular sarcoidosis. Axial T1WI (**a**) shows a nodule of slightly increased signal intensity. Axial T2WI (**b**) shows a hyperintense nodule with a central hypointense region, exhibiting a dark star appearance. On axial (**c**) and sagittal (**d**) postcontrast FS T1WIs, a thick peripheral hyperintense rim and outer stripes show intense enhancement. Chest PA (**e**) demonstrates typical bilateral hilar adenopathy (*arrowheads*)

16.8.5 Morton's Neuroma

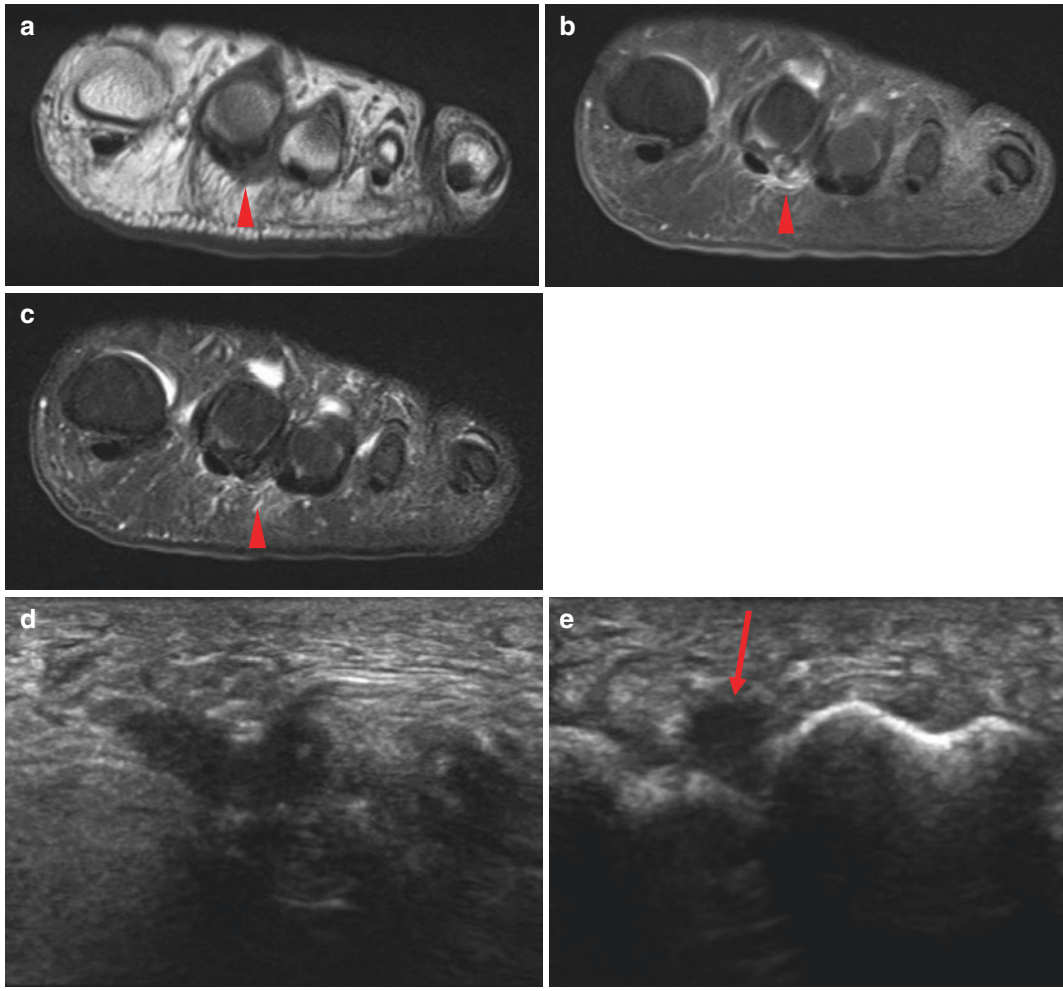

Fig. 16.11 Morton's neuroma. Axial T1WI (**a**) obtained perpendicular to the metatarsal bones reveals a nodular mass with plantar extension (*arrowhead*). On axial FS T2WI (**b**), the lesion (*arrowhead*) shows lower signal intensity compared to that of adjacent fat tissue. The mass is not enhanced (*arrowhead*) on axial postcontrast FS T1WI (**c**). On the longitudinal plane, US (**d**) shows teardrop-shaped hypoechoic lesion in the second intermetatarsal space with its long axis oriented obliquely to the metatarsals. When squeezing the foot, transverse US (**e**) demonstrates abrupt displacement of the mass (*arrow*) toward the plantar surface (sonographic Mulder sign)

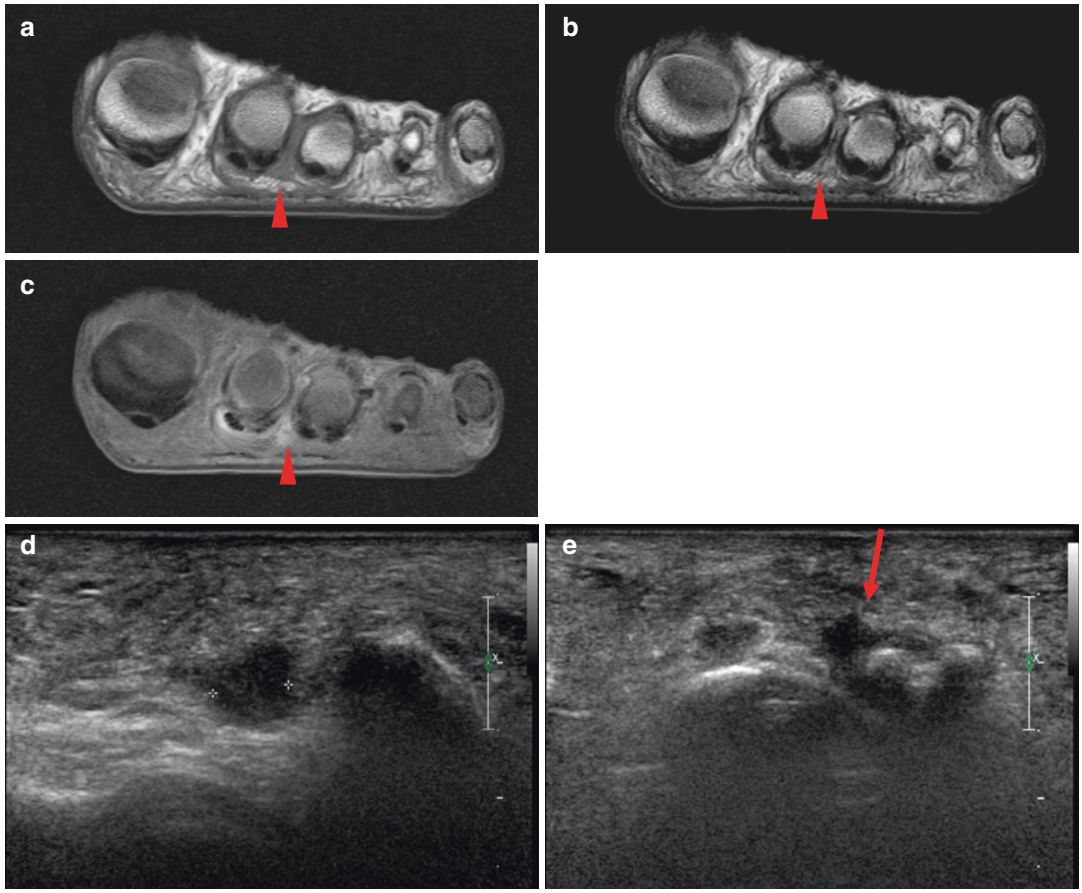

Fig. 16.12 Morton's neuroma. Axial T1WI (**a**) obtained perpendicular to the metatarsal bones reveals a nodular mass with plantar extension (*arrowhead*). On axial T2WI (**b**), the lesion shows a lower signal intensity compared to that of the adjacent fat tissue (*arrowhead*). The mass shows subtle enhancement (*arrowhead*) on postcontrast FS T1WI (**c**). Longitudinal (**d**) and transverse (**e**) US show a hypoechoic nodule (*arrow*) in the second web space, replacing the normal intermetatarsal fat tissue

16.8.6 Traumatic Neuroma

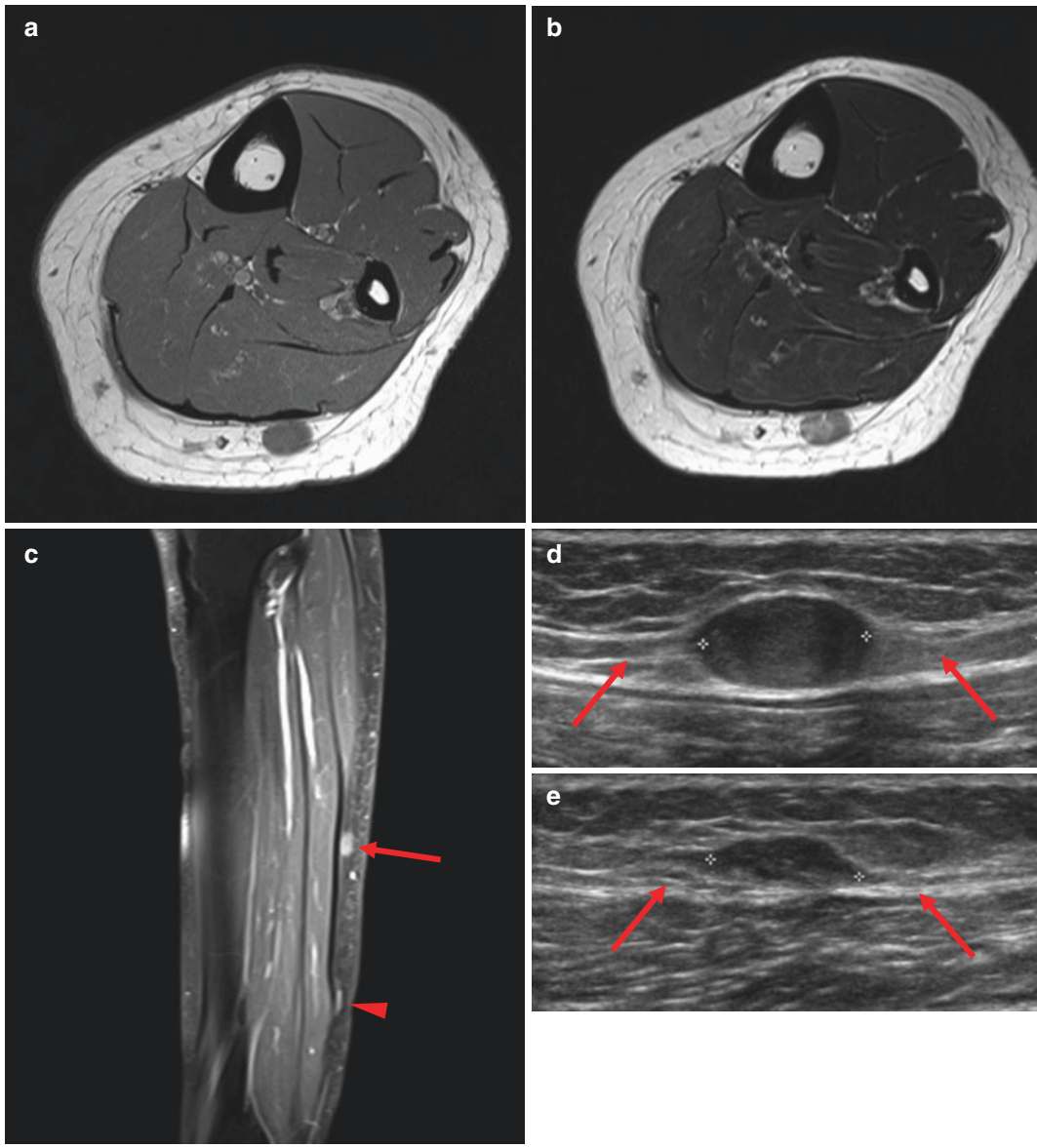

Fig. 16.13 Spindle neuroma. Axial T1WI (**a**) and T2WI (**b**) show a small nodule in the subcutaneous tissue of the calf. Sagittal postcontrast FS T1WI (**c**) shows another nodule (*arrowhead*) in the distal calf, below the aforementioned nodule (*arrow*). Longitudinal US images (**d**, **e**) reveal fusiform or spindle-shaped lesions with an entering and exiting nerve (*arrows*)

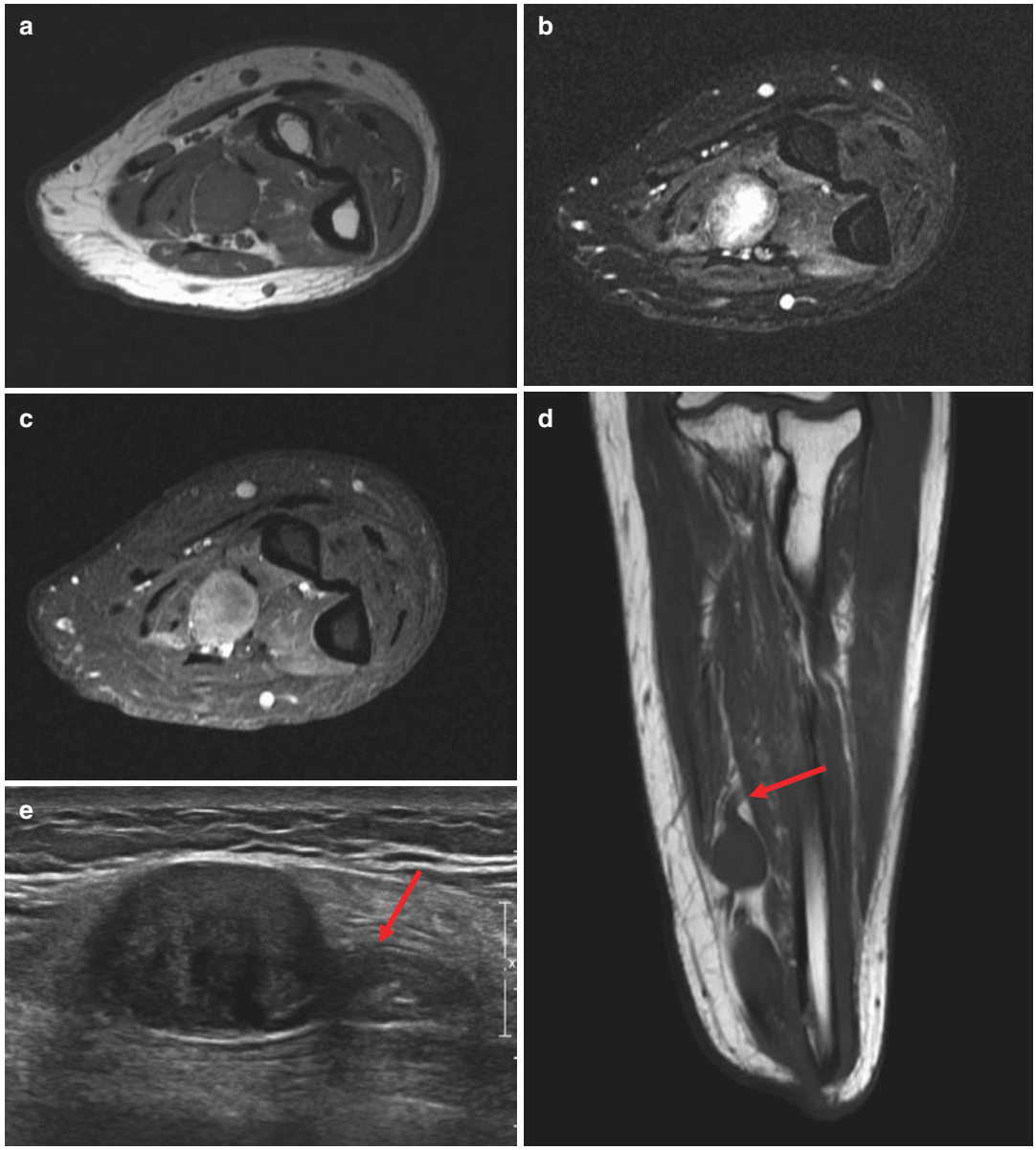

Fig. 16.14 Terminal neuroma. Axial T1WI (**a**) and FS T2WI (**b**) show an ovoid mass in the distal forearm of a patient who underwent a hand amputation. The mass is well enhanced after gadolinium administration (**c**). Coronal T1WI (**d**) reveals an ovoid mass at the end of the severed median nerve (*arrow*). US (**e**) reveals a hypoechoic mass in continuity with the end of the severed nerve (*arrow*)

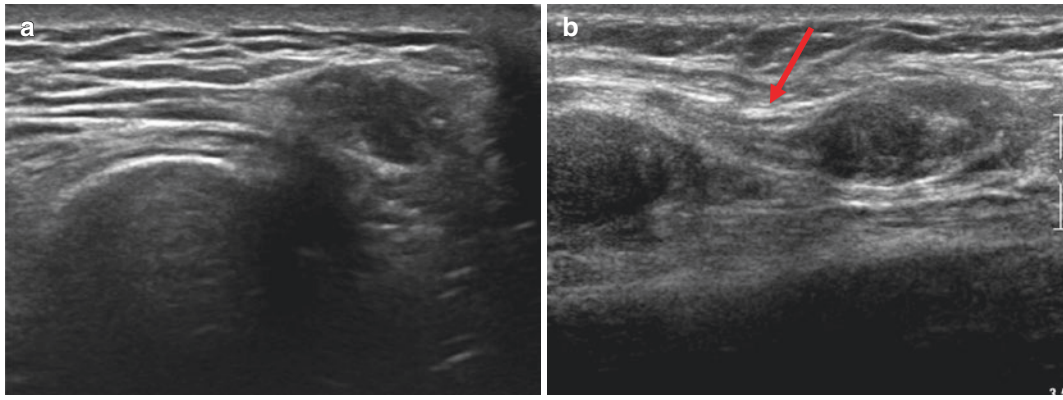

Fig. 16.15 Terminal neuroma. Transverse US (**a**) shows hypoechoic terminal neuroma with a poorly defined margin, indicating multidirectional proliferation of axons without the support of the Schwann cells. Longitudinal US (**b**) reveals hypoechoic fusiform terminal neuroma in continuity with the end of the severed nerve (*arrow*)

16.8.7 Xanthoma

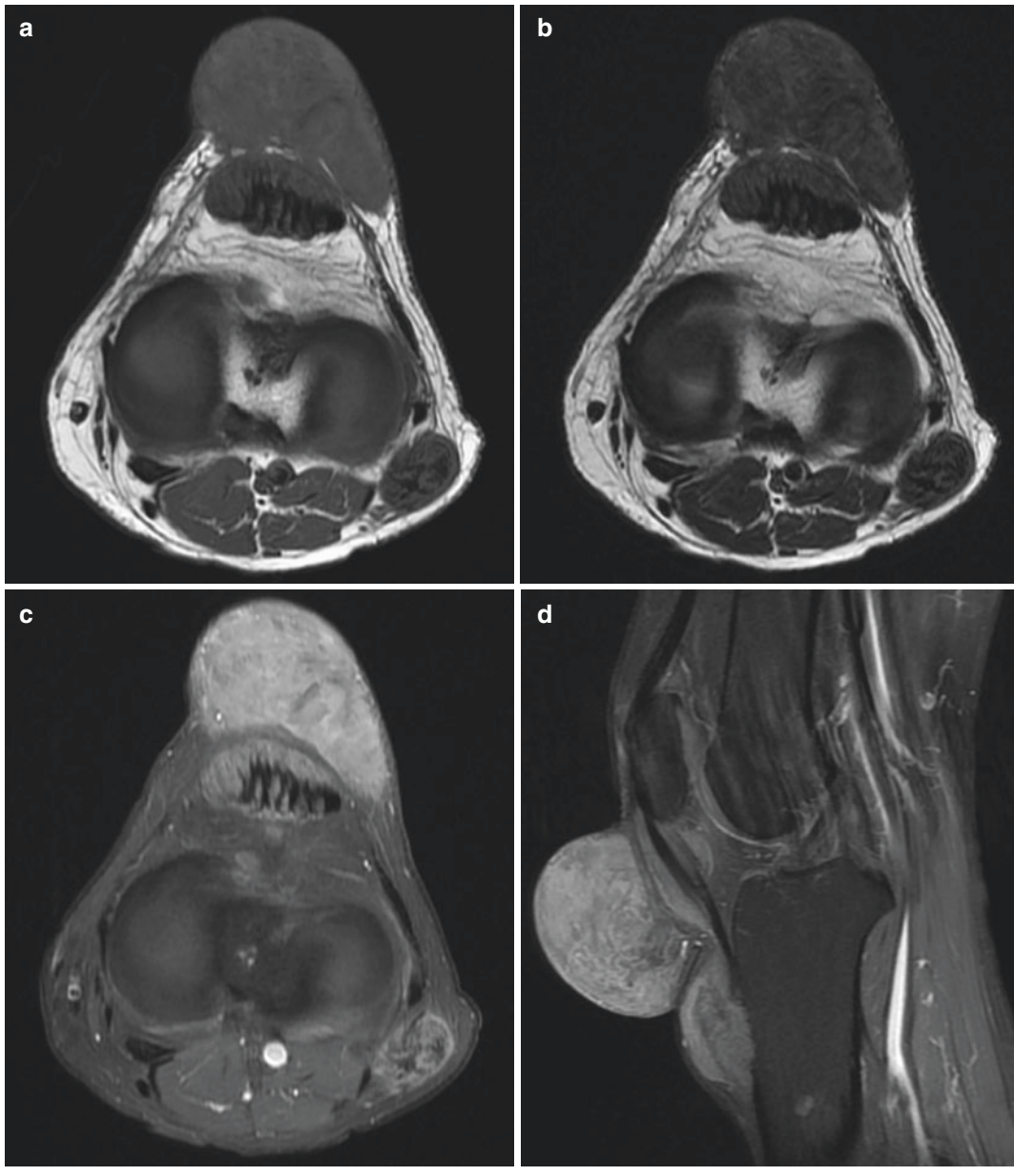

Fig. 16.16 Xanthoma. MR images (**a**–**c**) show diffuse thickening of the patellar ligament and distal biceps femoris tendon. The affected tendons have a speckled appearance, with an inner low signal intensity on axial T1WI (**a**) and T2WI (**b**). There is a large prepatellar mass involving skin and subcutaneous fat tissue. Axial and sagittal post-contrast FS T1WIs (**c**, **d**) demonstrate diffuse contrast enhancement of tendinous and subcutaneous masses

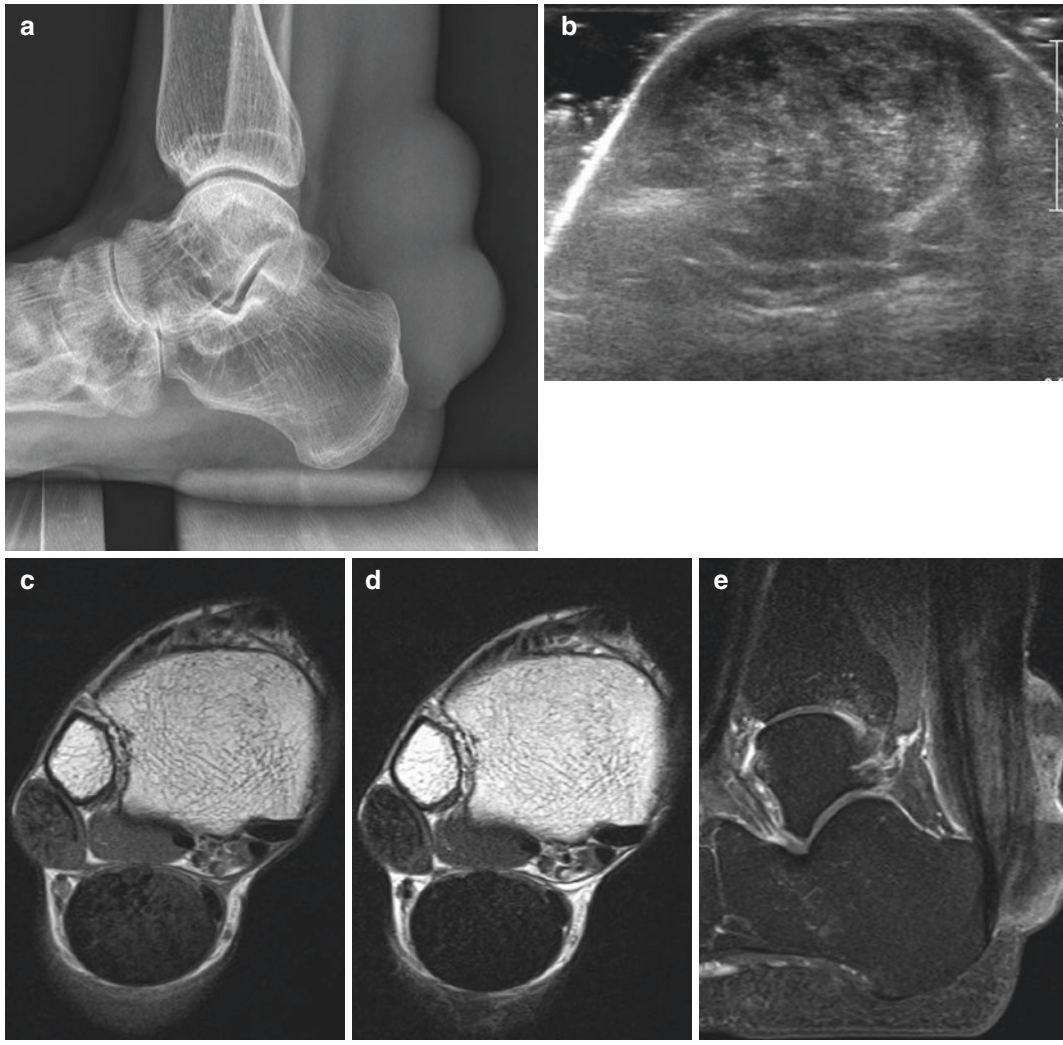

Fig. 16.17 Xanthoma. Lateral radiograph of the ankle (**a**) shows a lobulated bulging soft tissue contour in the posterior aspect of the ankle. Transverse US (**b**) demonstrates marked diffuse thickening of the Achilles tendon, with a diffuse heterogeneity. Confluent hypoechoic areas and thin hyperechoic foci are observed within the tendon, causing a loss of the fibrillary pattern of tendon. MR images (**c**, **d**) show diffuse thickening of Achilles tendon with speckled inner low signal intensity on T1WI and T2WI, suggestive of cholesterol deposition. The ventral margin of the tendon has a convex outline on axial images (**c**, **d**). Sagittal postcontrast FS T1WIs (**e**) demonstrate mild contrast enhancement of tendinous mass

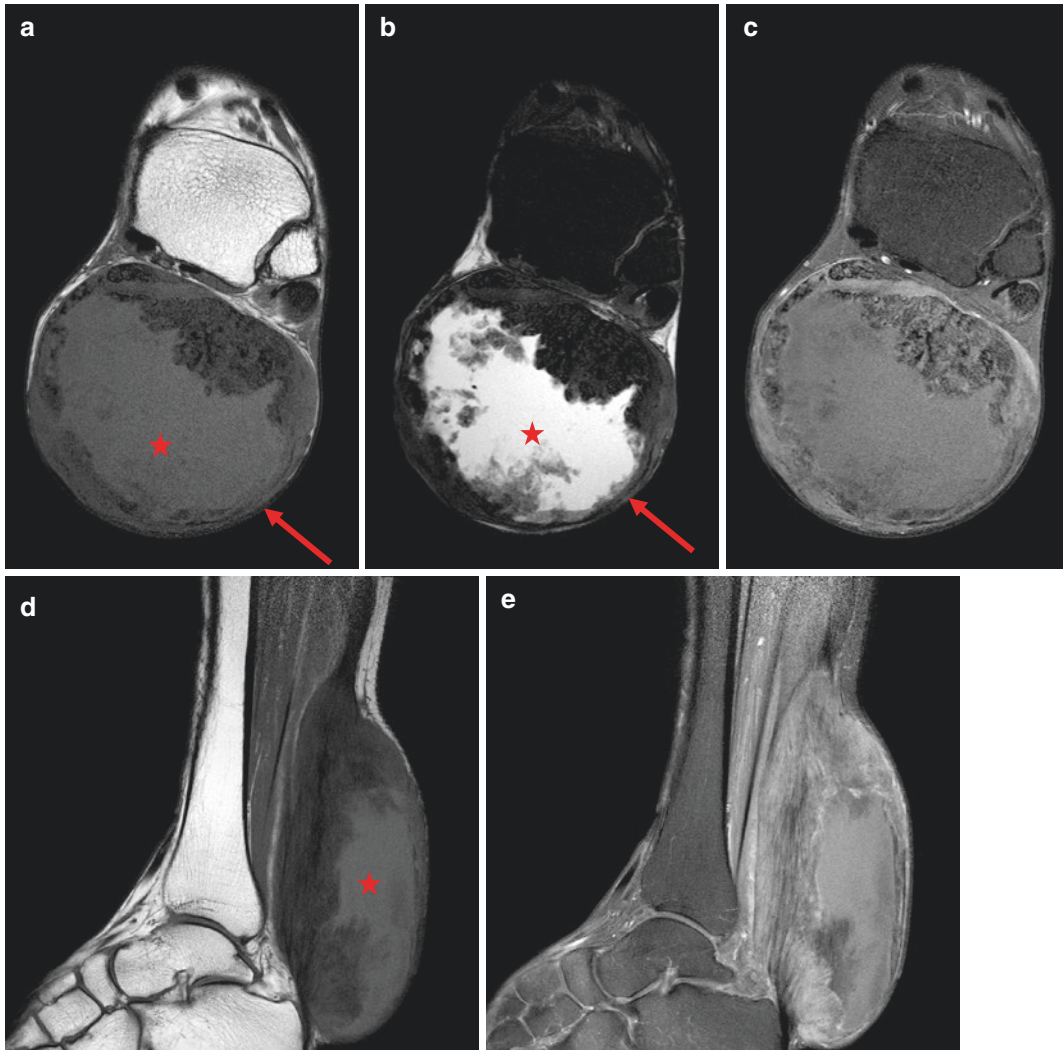

Fig. 16.18 Xanthoma. MR images (**a**–**e**) demonstrate a thickened Achilles tendon and a large bilobed mass. The mass arises from the Achilles tendon and extends from the heel to the mid-calf level. A thin rim of low signal intensity (*arrows*) is observed on T1WI (**a**, **d**) and FS T2WI (**b**). The inner portion (*stars*) of the mass displays heterogeneous signal intensity on T1WI (**a**, **d**) and FS T2WI (**b**), findings which are related to hemorrhagic and necrotic debris within the masses. Axial (**c**) and sagittal (**e**) post-contrast FS T1WIs demonstrate mild contrast enhancement of tendinous mass

References

Ahmed I, Harshad SR. Subcutaneous sarcoidosis: is it a specific subset of cutaneous sarcoidosis frequently associated with systemic disease? J Am Acad Dermatol. 2006;54(1):55–60. doi:10.1016/j.jaad.2005.10.001.

Anderson SE, De Monaco D, Buechler U, et al. Imaging features of pseudoaneurysms of the hand in children and adults. Am J Roentgenol. 2003;180(3):659–64. doi:10.2214/ajr.180.3.1800659.

Bencardino J, Rosenberg ZS, Beltran J, Liu X, Marty-Delfaut E. Morton's neuroma: is it always symptomatic? AJR Am J Roentgenol. 2000;175(3):649–53. doi:10.2214/ajr.175.3.1750649.

Bermejo A, Bustamante TDD, Martinez A, et al. MR imaging in the evaluation of cystic-appearing soft-tissue masses of the extremities. Radiographics. 2013;33(3):833–55. doi:10.1148/rg.333115062.

Bude RO, Adler RS, Bassett DR. Diagnosis of Achilles tendon xanthoma in patients with heterozygous familial hypercholesterolemia: MR vs sonography. Am J Roentgenol. 1994;162(4):913–7. doi:10.2214/ajr.162.4.8141017.

Chen HH, Chen YM, Lan HH, Lee CH, Chen DY. Sonographic appearance of subcutaneous sarcoidosis. J Ultrasound Med. 2009;28(6):813–6.

Desai MA, Peterson JJ, Garner HW, Kransdorf MJ. Clinical utility of dual-energy CT for evaluation of tophaceous gout. Radiographics. 2011;31(5):1365–75. doi:10.1148/rg.315115510.

Fernandes EÁ, Santos EHS, Tucunduva TCM, AJL F, Fernandes ARC. Achilles tendon xanthoma imaging on ultrasound and magnetic resonance imaging. Rev Bras Reumatol. 2015;55(3):313–6. doi:10.1016/j.rbre.2013.12.003.

Gude W, Morelli V. Ganglion cysts of the wrist: pathophysiology, clinical picture, and management. Curr Rev Muscoskelet Med. 2008;1(3–4):205–11. doi:10.1007/s12178-008-9033-4.

Henrot P, Stines J, Walter F et al. Imaging of the painful lower limb stump. Radiographics. 2000;20 Suppl 1:S219–S235. doi:10.1148/radiographics.20.suppl_1.g00oc14s219

Koyama T, Ueda H, Togashi K, et al. Radiologic manifestations of sarcoidosis in various organs. Radiographics. 2004;24(1):87–104. doi:10.1148/rg.241035076.

Kransdorf MJ, Murphey MD. Imaging of soft tissue tumors. 3rd ed. Philadelphia: Lippincott Williams & Wilkins; 2014.

Liem MSL, Leuven JAG, Bloem JL, Schipper J. Magnetic resonance imaging of Achilles tendon xanthomas in familial hypercholesterolemia. Skelet Radiol. 1992;21(7):453–7. doi:10.1007/bf00190990.

McCarthy CL, McNally EG. The MRI appearance of cystic lesions around the knee. Skelet Radiol. 2004;33(4):187–209. doi:10.1007/s00256-003-0741-y.

Moore SL, Teirstein AE. Musculoskeletal sarcoidosis: Spectrum of appearances at MR imaging. Radiographics. 2003;23(6):1389–99. doi:10.1148/rg.236025172.

Murphey MD, Smith WS, Smith SE, Kransdorf MJ, Temple HT. From the archives of the AFIP. Imaging of musculoskeletal neurogenic tumors: radiologic-pathologic correlation. Radiographics. 1999;19(5):1253–80. doi:10.1148/radiographics.19.5.g99se101253.

Narváez JA, Narváez J, Ortega R, et al. Hypointense synovial lesions on T2-weighted images: differential diagnosis with pathologic correlation. Am J Roentgenol. 2003;181(3):761–9. doi:10.2214/ajr.181.3.1810761.

Newman LS, Rose CS, Maier LA. Sarcoidosis. N Engl J Med. 1997;336(17):1224–34. doi:10.1056/NEJM199704243361706.

Otake S. Sarcoidosis involving skeletal muscle: imaging findings and relative value of imaging procedures. Am J Roentgenol. 1994;162(2):369–75. doi:10.2214/ajr.162.2.8310929.

Perdikakis E, Skiadas V. MRI characteristics of cysts and "cyst-like" lesions in and around the knee: what the radiologist needs to know. Insights Imaging. 2013;4(3):257–72. doi:10.1007/s13244-013-0240-1.

Singson RD, Feldman F, Slipman CW, et al. Postamputation neuromas and other symptomatic stump abnormalities: detection with CT. Radiology. 1987;162(3):743–5. doi:10.1148/radiology.162.3.3809488.

Spinner RJ, Amrami KK, Angius D, Wang H, Carmichael SW. Peroneal and tibial intraneural ganglia: correlation between intraepineurial compartments observed on magnetic resonance images and the potential importance of these compartments. Neurosurg Focus. 2007a;22(6):E17.

Spinner RJ, Amrami KK, Wolanskyj AP, et al. Dynamic phases of peroneal and tibial intraneural ganglia formation: a new dimension added to the unifying articular theory. J Neurosurg. 2007b;107(2):296–307. doi:10.3171/JNS-07/08/0296.

Stacy GS, Kapur A. Mimics of bone and soft tissue neoplasms. Radiol Clin N Am. 2011;49(6):1261–86. vii doi:10.1016/j.rcl.2011.07.009.

Sundaram M, Sharafuddin MJ. MR imaging of benign soft-tissue masses. Magn Reson Imaging Clin N Am. 1995;3(4):609–27.

Torres-Claramunt R, Ginés A, Pidemunt G, Puig L, de Zabala S. MRI and ultrasonography in Morton's neuroma: diagnostic accuracy and correlation. Indian J Orthop. 2012;46(3):321–5. doi:10.4103/0019-5413.96390.

Torriani M, Kattapuram SV. Technical innovation. Dynamic sonography of the forefoot: the sonographic Mulder sign. AJR Am J Roentgenol. 2003;180(4):1121–3. doi:10.2214/ajr.180.4.1801121.

Wang G, Jacobson JA, Feng FY, et al. Sonography of wrist ganglion cysts: variable and noncystic appearances. J Ultrasound Med. 2007;26(10):1323–8.

Wu JS, Hochman MG. Soft-tissue tumors and tumorlike lesions: a systematic imaging approach. Radiology. 2009;253(2):297–316. doi:10.1148/radiol.2532081199.

Yu JS, Chung C, Recht M, Dailiana T, Jurdi R. MR imaging of tophaceous gout. Am J Roentgenol. 1997;168(2):523–7. doi:10.2214/ajr.168.2.9016240.

Zanetti M, Strehle JK, Kundert H-P, Zollinger H, Hodler J. Morton neuroma: effect of MR imaging findings on diagnostic thinking and therapeutic decisions. Radiology. 1999;213(2):583–8. doi:10.1148/radiology.213.2.r99nv06583.

Part III

Practical Pearls in Diagnosis of Soft Tissue Tumors

Lesion Characterization Based on MR Signal Intensities

17

Most soft tissue tumors exhibit nonspecific signal intensity on MR imaging: low signal intensity on T1-weighted images and high signal intensity on T2-weighted images. When a soft tissue tumor has a different combination of signal intensities, it can aid in specific diagnosis and differential diagnosis of soft tissue tumors. Tumors with high signal intensity on T1-weighted images may contain fat, subacute hemorrhage, high proteinaceous fluid, or melanin (Table 17.1). Fat-suppression techniques can be used to distinguish fat from the other T1-hyperintense components. Intratumoral low signal intensity on T2-weighted images can also be a clue to the diagnosis (Table 17.2). Soft tissue tumors with collagenous fibrous tissue, mineralization, hemosiderin, and vascular signal void structures can be included in the differential diagnosis of the T2 hypointense lesions. Occasionally, soft tissue masses have very high signal intensity similar to fluid on T2-weighted images (Table 17.3). These lesions include fluid cysts, bursitis, myxoid tumors, chondroid tumors, vascular tumors, and vascular malformations. Contrast-enhanced MR images allow differentiation between truly cystic and solid masses.

Table 17.1 T1 hyperintense lesions

Lesion containing fat	Lipoma Lipoblastoma Hibernoma Elastofibroma Fibrous hamartoma of infancy Hemangioma Liposarcoma
Lesion containing methemoglobin	Morel-Lavallee lesion (subacute hematoma) Aneurysm, pseudoaneurysm Hemangioma
Lesion containing proteinaceous material	Ganglion Epidermal inclusion cyst
Lesion containing melanin	Malignant melanoma Clear cell sarcoma

H.S. Kang et al., *Oncologic Imaging: Soft Tissue Tumors*, DOI 10.1007/978-981-287-718-5_17

Table 17.2 T2 hypointense lesions

Lesion containing fibrous tissue	Calcifying aponeurotic fibroma Desmoplastic fibroblastoma Fibroma of tendon sheath Traumatic neuroma/Morton's neuroma Granular cell tumor Fibromatosis Solitary fibrous tumor Low-grade fibromyxoid sarcoma Sclerosing epithelioid fibrosarcoma Rheumatoid nodule Sarcoidosis
Lesion containing mineralization	Myositis ossification Hemangioma (phlebolith) Hemangioma (ossifying) Pilomatricoma Soft tissue chondroma Extraskeletal osteosarcoma Gout
Lesion containing hemosiderin	Tenosynovial GCT Hemangioma (thrombus)
Lesion containing cholesterol	Xanthoma
Lesion containing high-flow vessels	Hibernoma Solitary fibrous tumor Vascular lesions including arteriovenous malformation and hemangioendothelioma Alveolar soft part sarcoma Aneurysm, pseudoaneurysm

Table 17.3 T2 Fluid-equivalent hyperintense lesions

Lesion containing fluid	Ganglion Bursa Epidermal inclusion cyst Morel-Lavallee lesion (fluid-like)
Lesion containing myxoid tissue	Intramuscular myxoma Peripheral nerve sheath tumor Myxoid liposarcoma Myxofibrosarcoma Extraskeletal myxoid chondrosarcoma
Vascular lesion	Hemangioma Lymphangioma Glomus tumor
Lesion containing cartilage	Soft tissue chondroma

17.1 T1 Hyperintense Lesions

17.1.1 Lesion Containing Fat

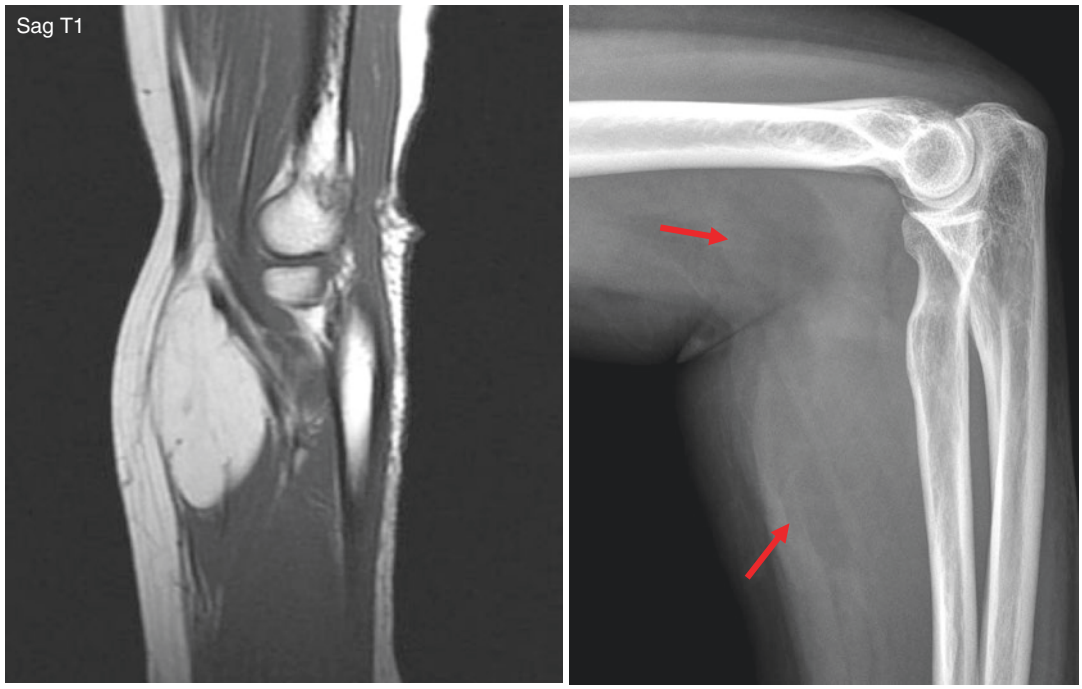

Fig. 17.1 Lipoma

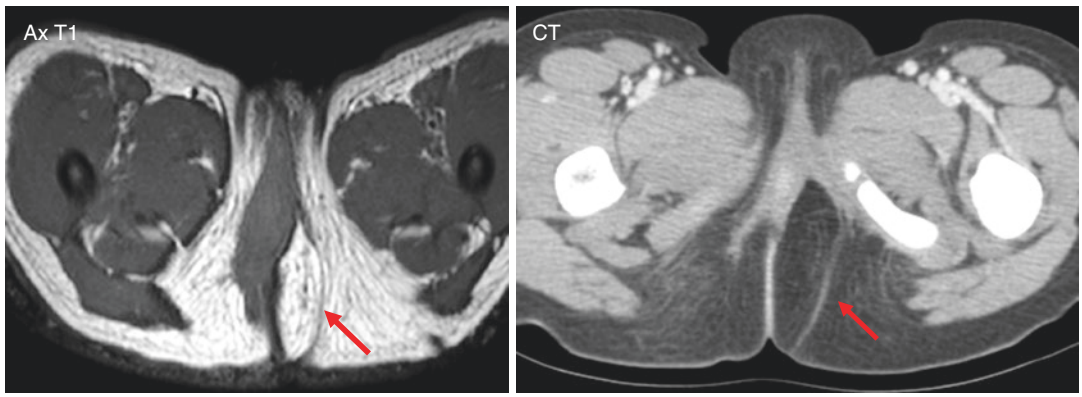

Fig. 17.2 Lipoblastoma

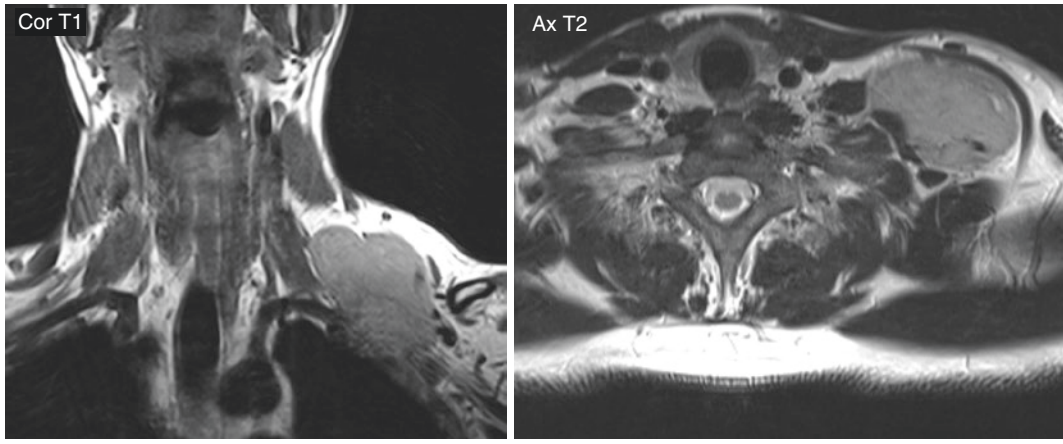

Fig. 17.3 Hibernoma

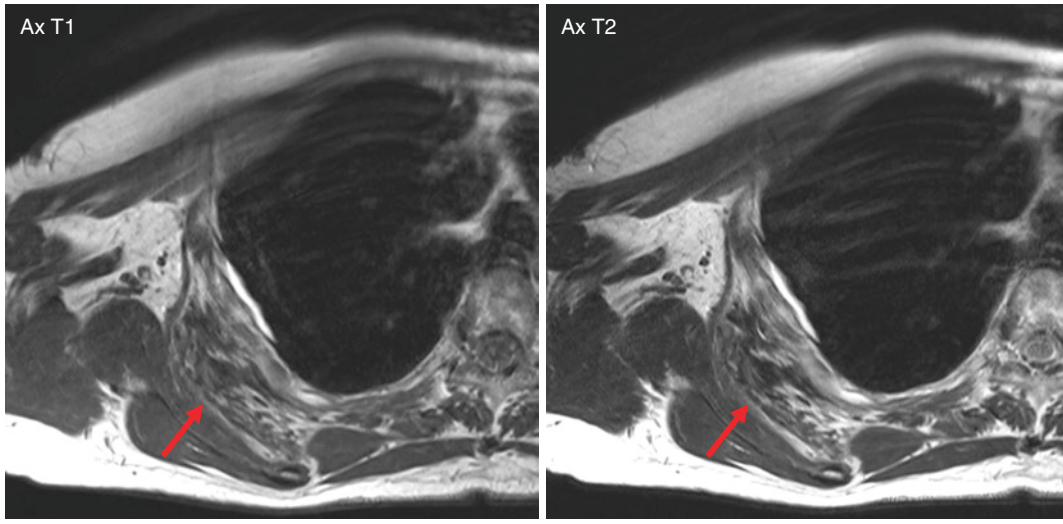

Fig. 17.4 Elastofibroma

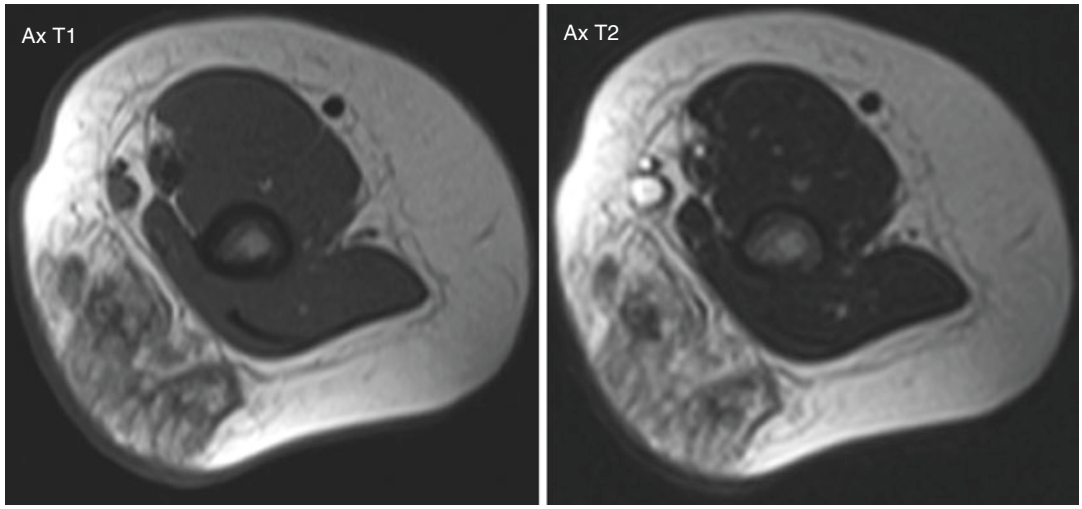

Fig. 17.5 Fibrous hamartoma of infancy

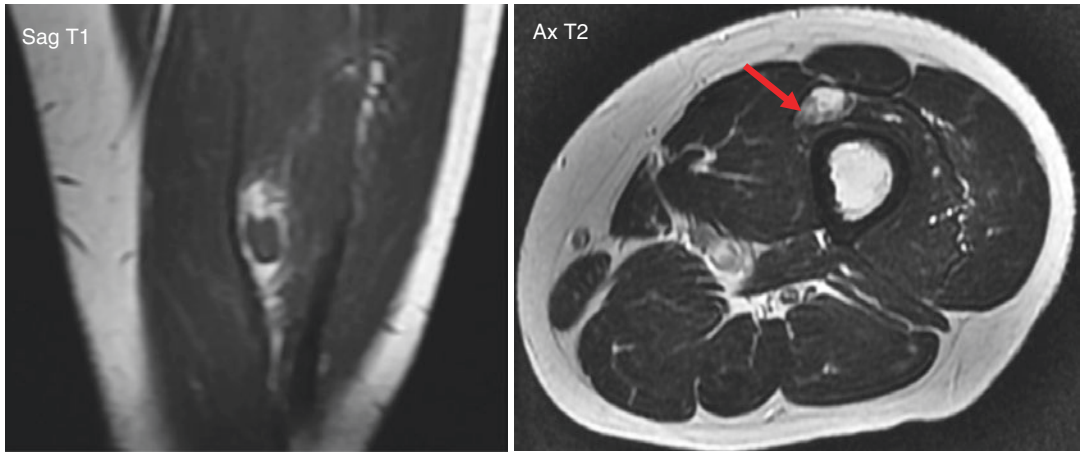

Fig. 17.6 Hemangioma

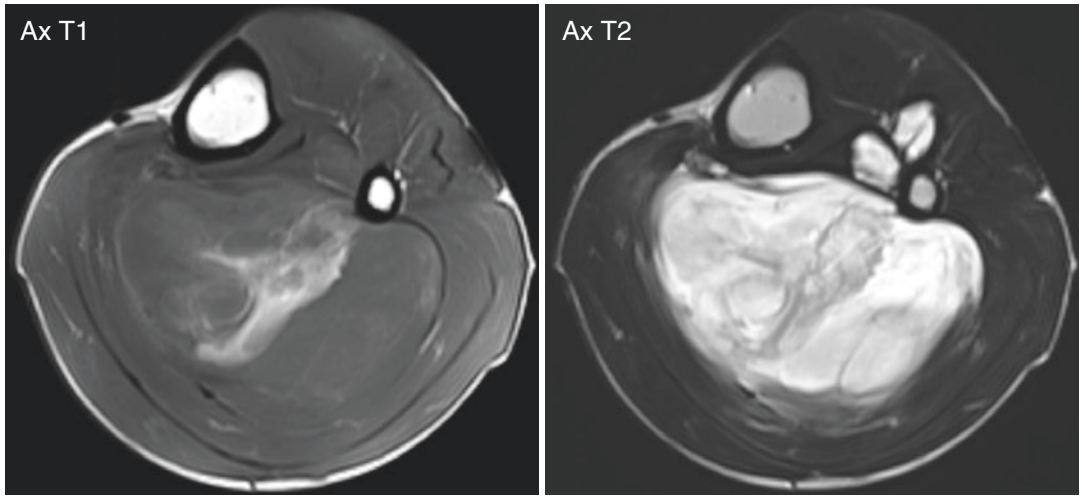

Fig. 17.7 Liposarcoma

17.1.2 Lesion Containing Methemoglobin

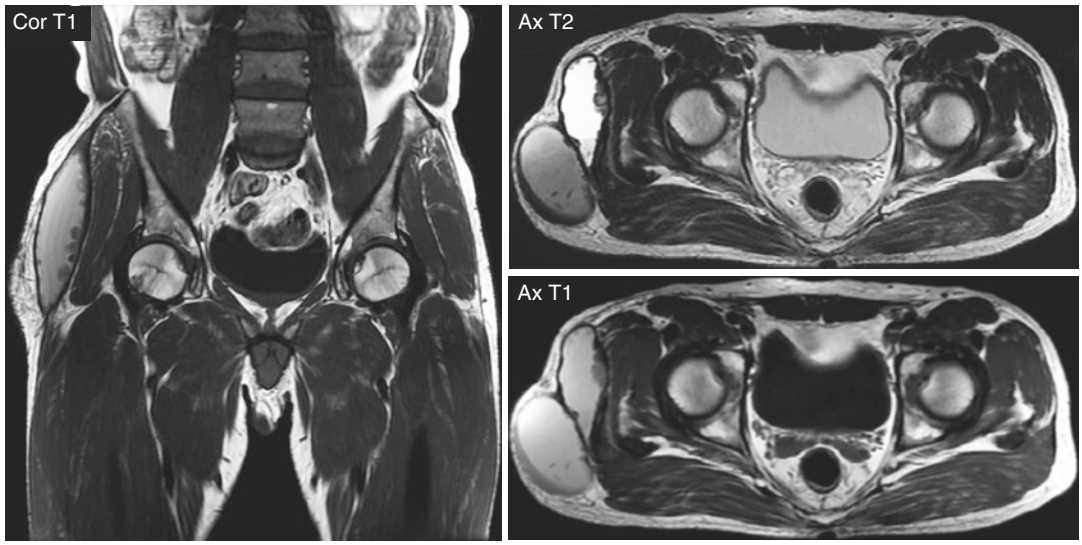

Fig. 17.8 Morel-Lavallee lesion (hematoma)

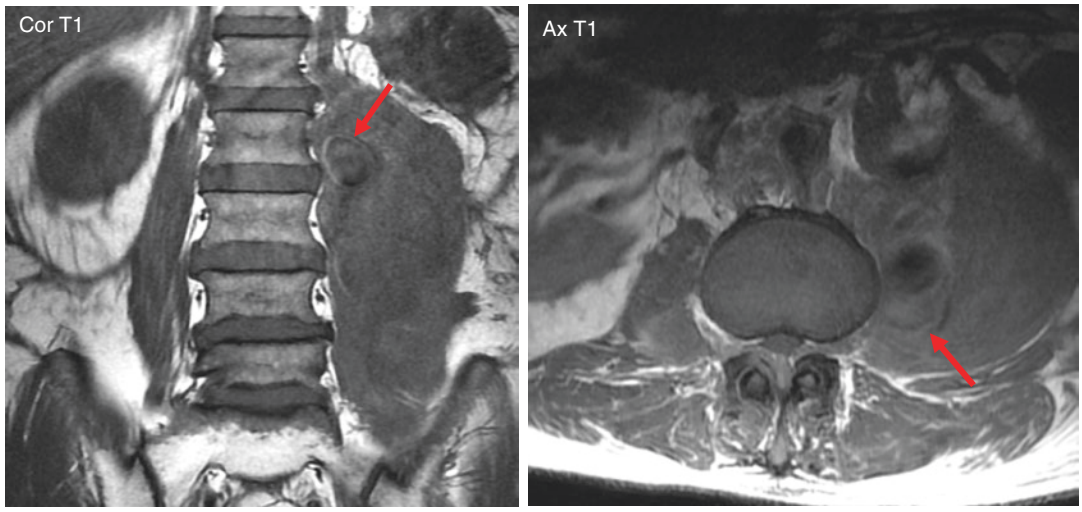

Fig. 17.9 Aneurysm, pseudoaneurysm

17.1.3 Lesion Containing Proteinaceous Material

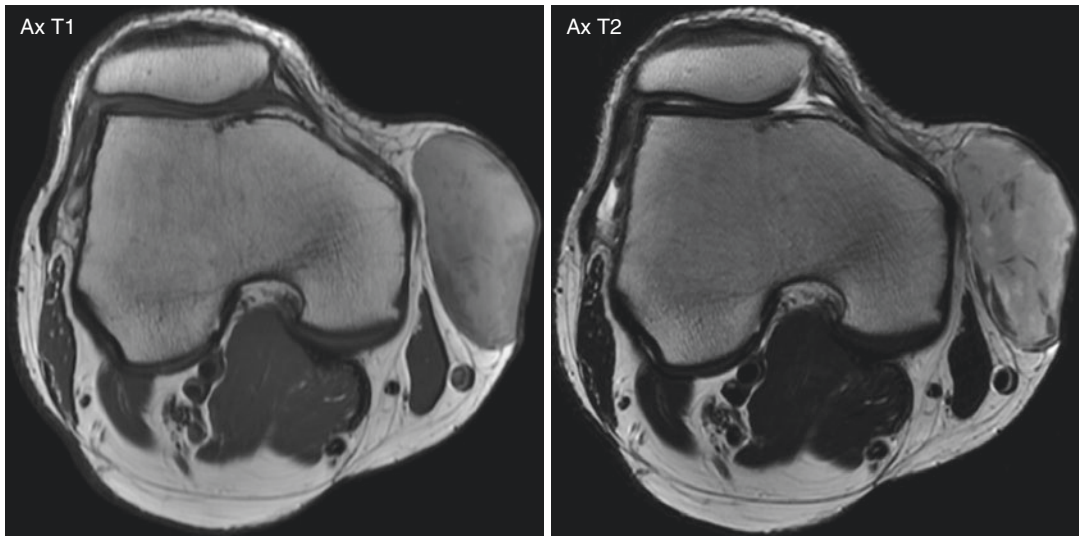

Fig. 17.10 Epidermal inclusion cyst

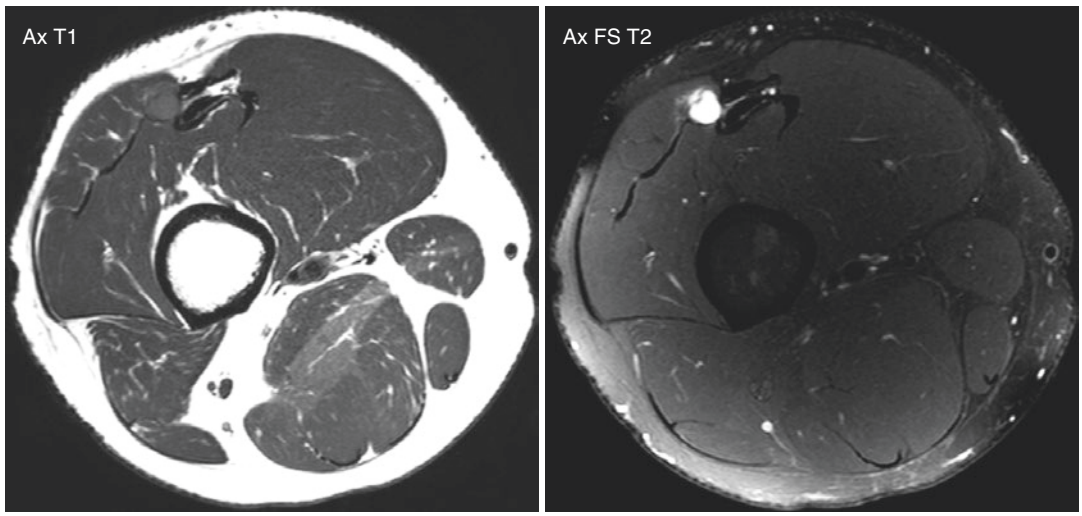

Fig. 17.11 Ganglion

17.1.4 Lesion Containing Melanin

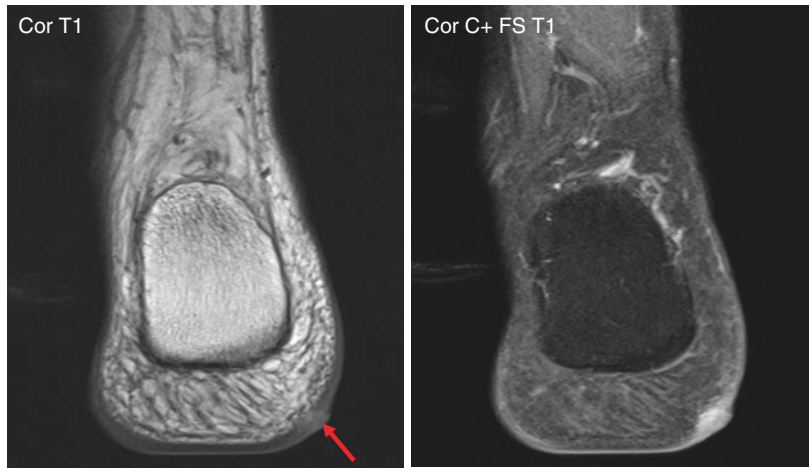

Fig. 17.12 Malignant melanoma

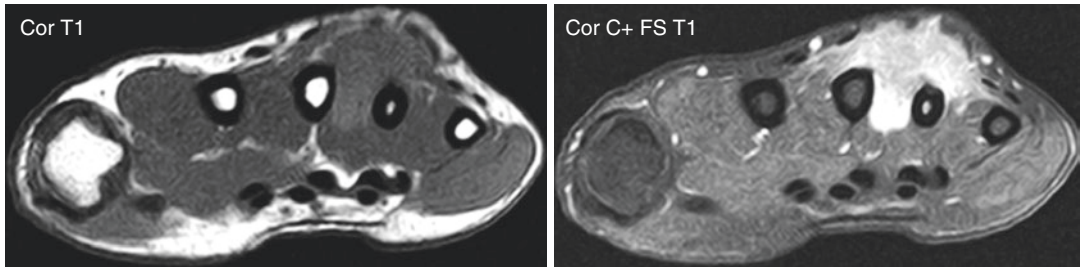

Fig. 17.13 Clear cell sarcoma

17.2 T2 Hypointense Lesions

17.2.1 Lesion Containing Fibrous Tissue

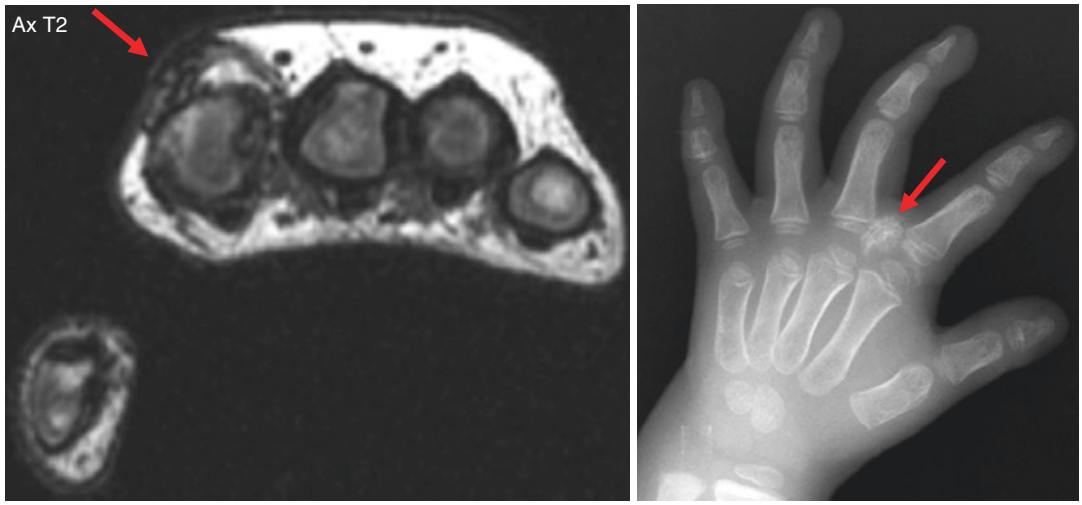

Fig. 17.14 Calcifying aponeurotic fibroma

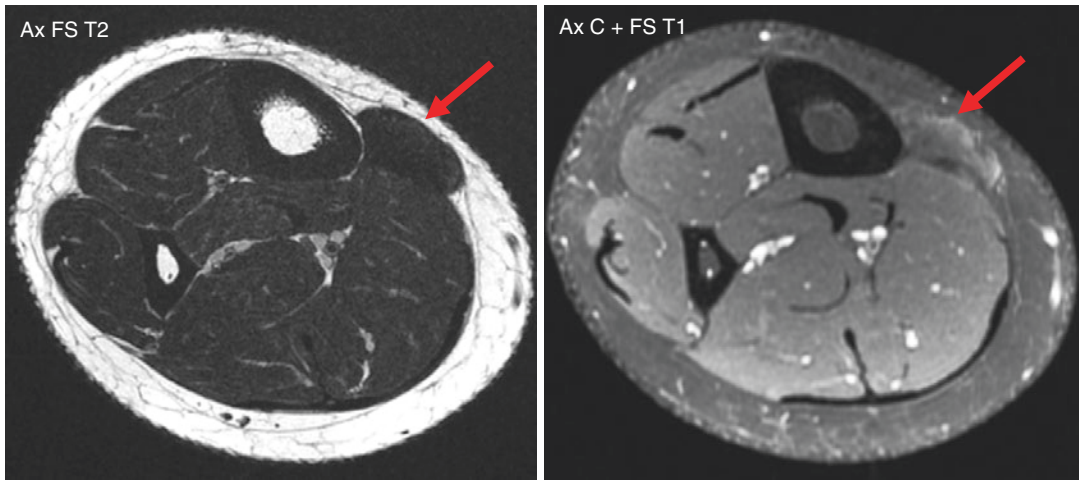

Fig. 17.15 Desmoplastic fibroblastoma

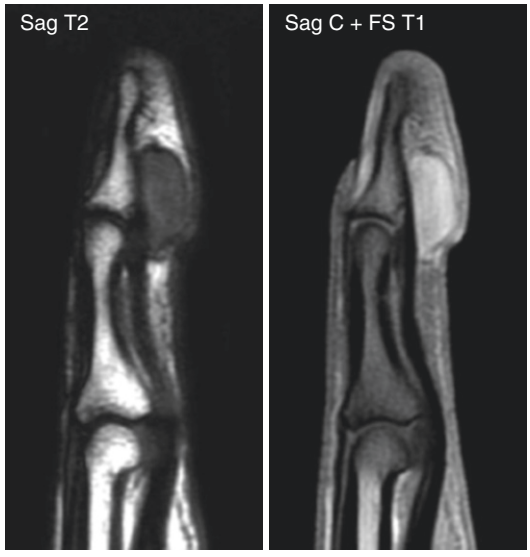

Fig. 17.16 Fibroma of tendon sheath

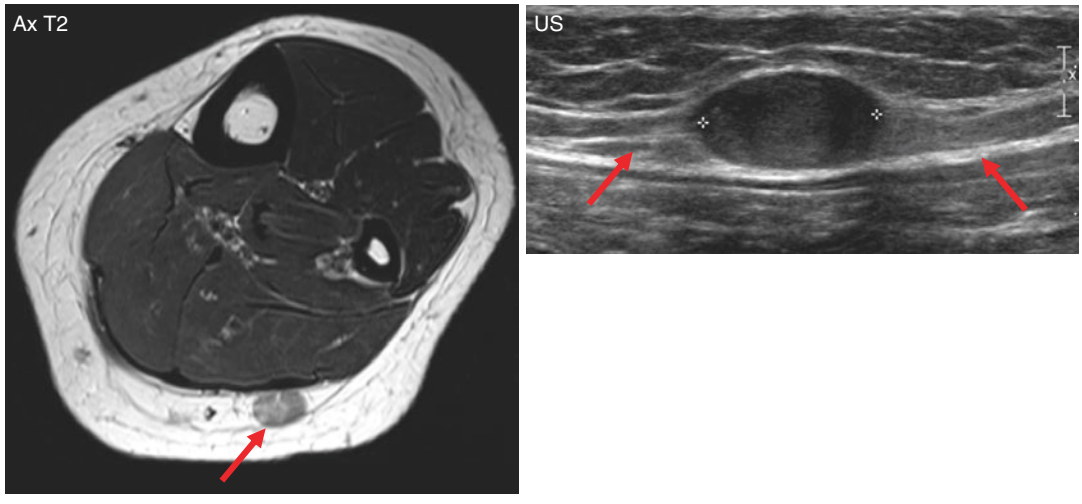

Fig. 17.17 Traumatic neuroma/Morton's neuroma

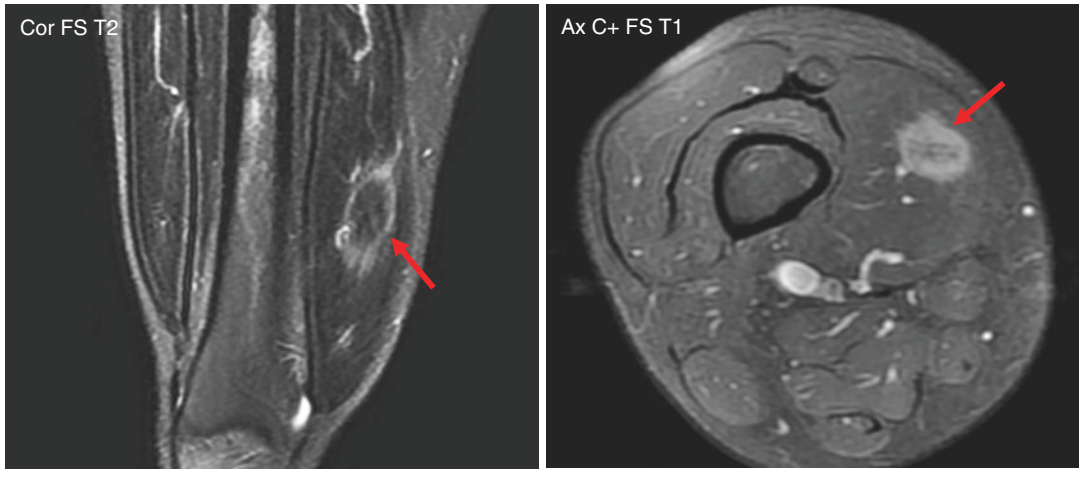

Fig. 17.18 Granular cell tumor

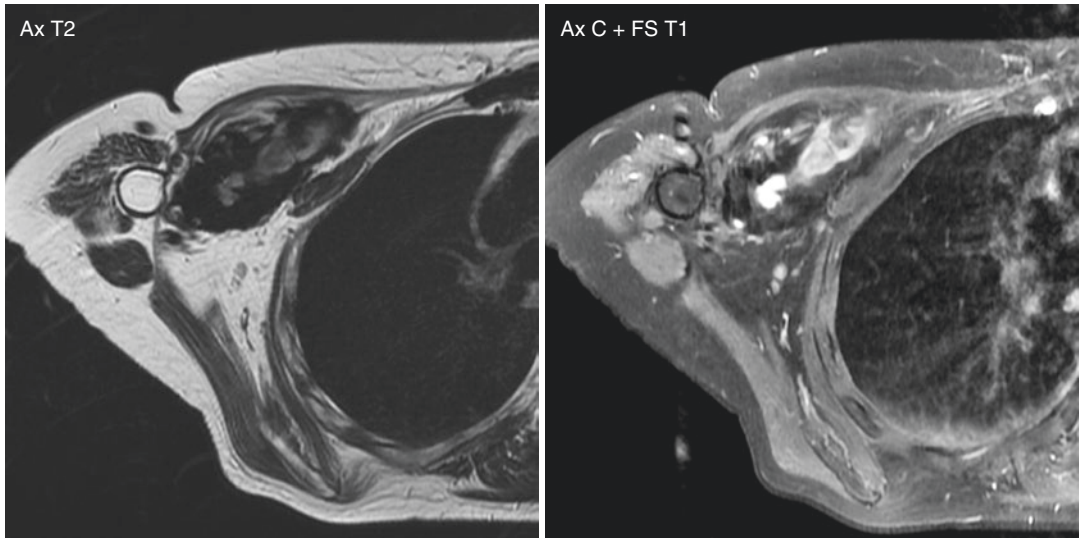

Fig. 17.19 Fibromatosis

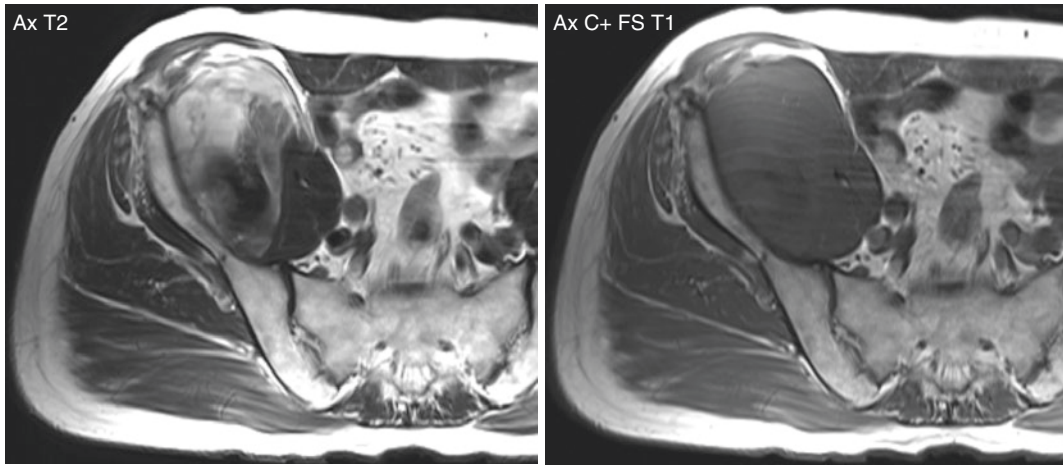

Fig. 17.20 Solitary fibrous tumor

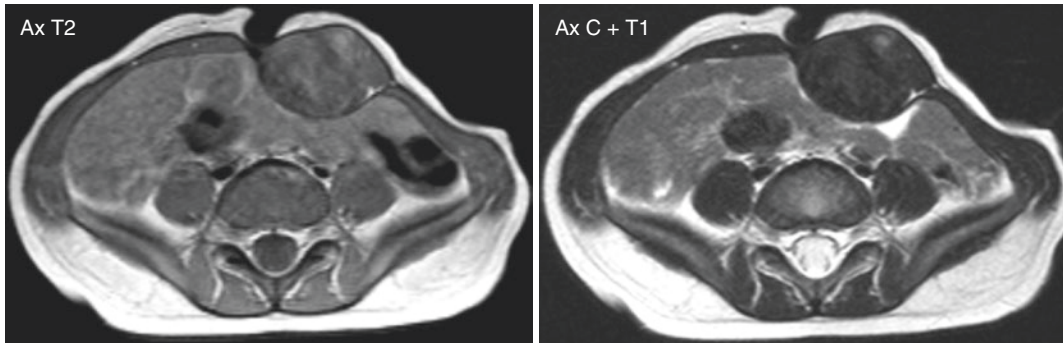

Fig. 17.21 Low-grade fibromyxoid tumor

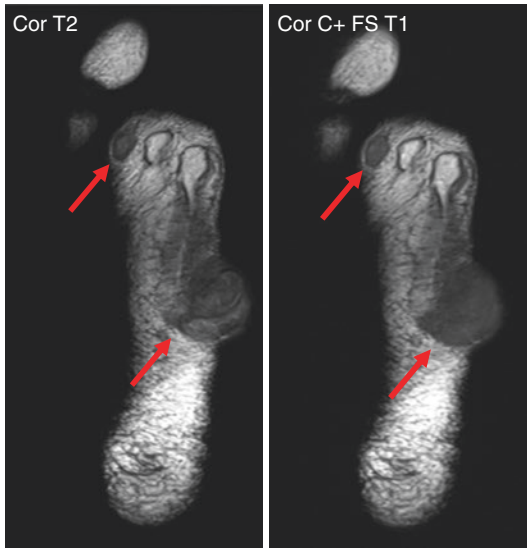

Fig. 17.22 Rheumatoid nodule

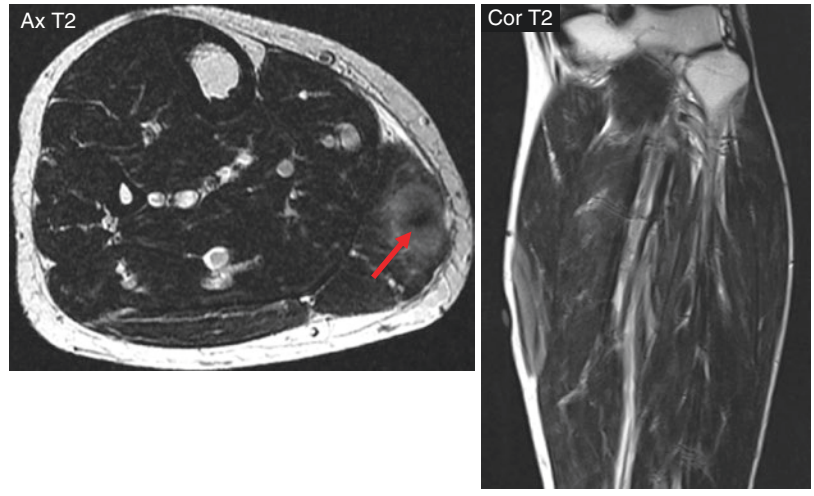

Fig. 17.23 Sarcoidosis

17.2.2 Lesion Containing Mineralization

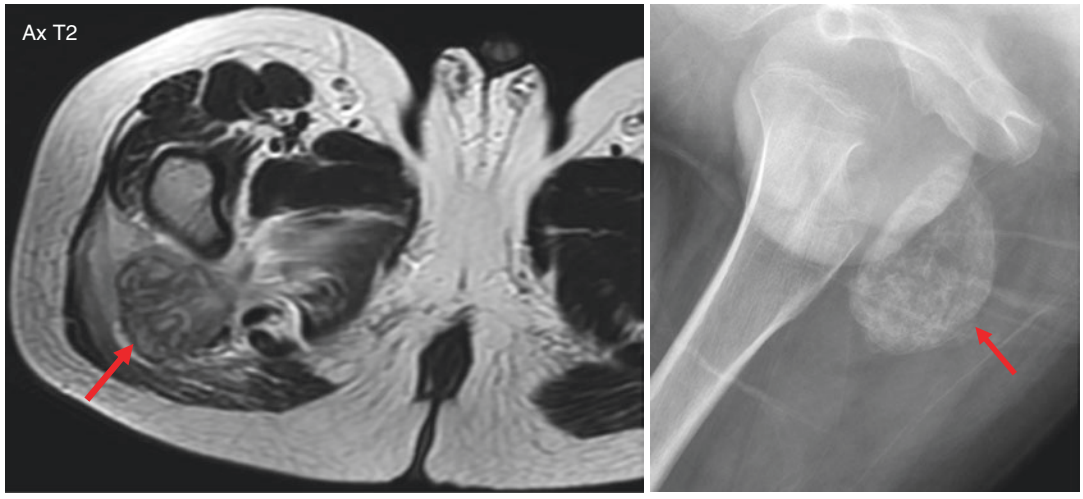

Fig. 17.24 Myositis ossification

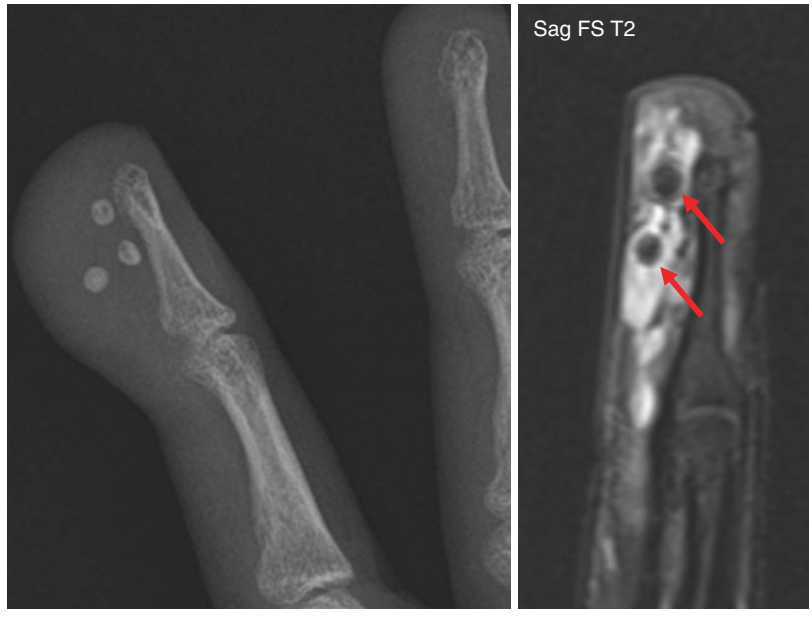

Fig. 17.25 Hemangioma (phlebolith)

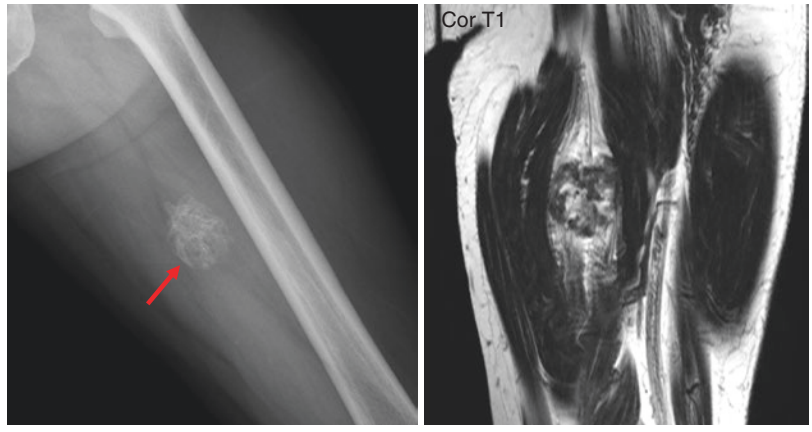

Fig. 17.26 Ossifying hemangioma

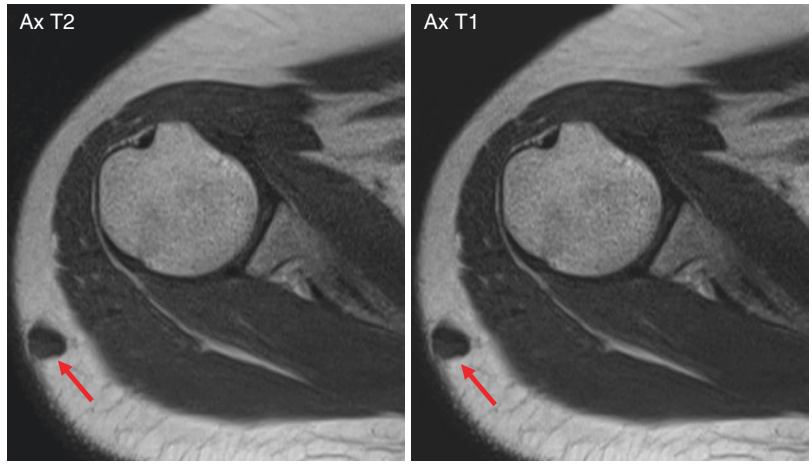

Fig. 17.27 Pilomatricoma

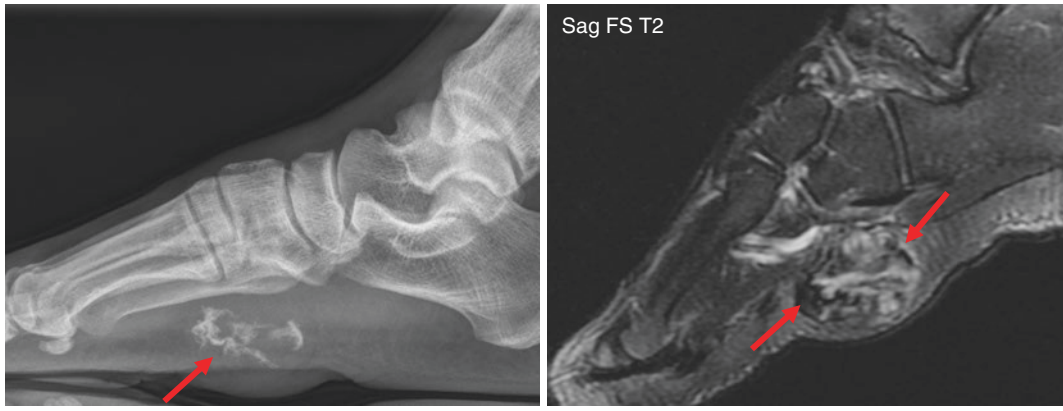

Fig. 17.28 Soft tissue chondroma

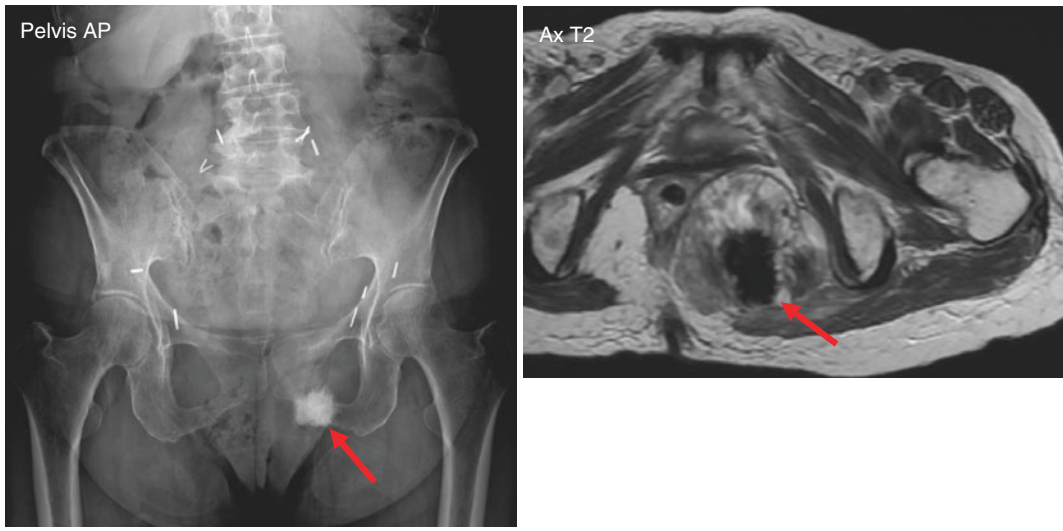

Fig. 17.29 Extraskeletal osteosarcoma

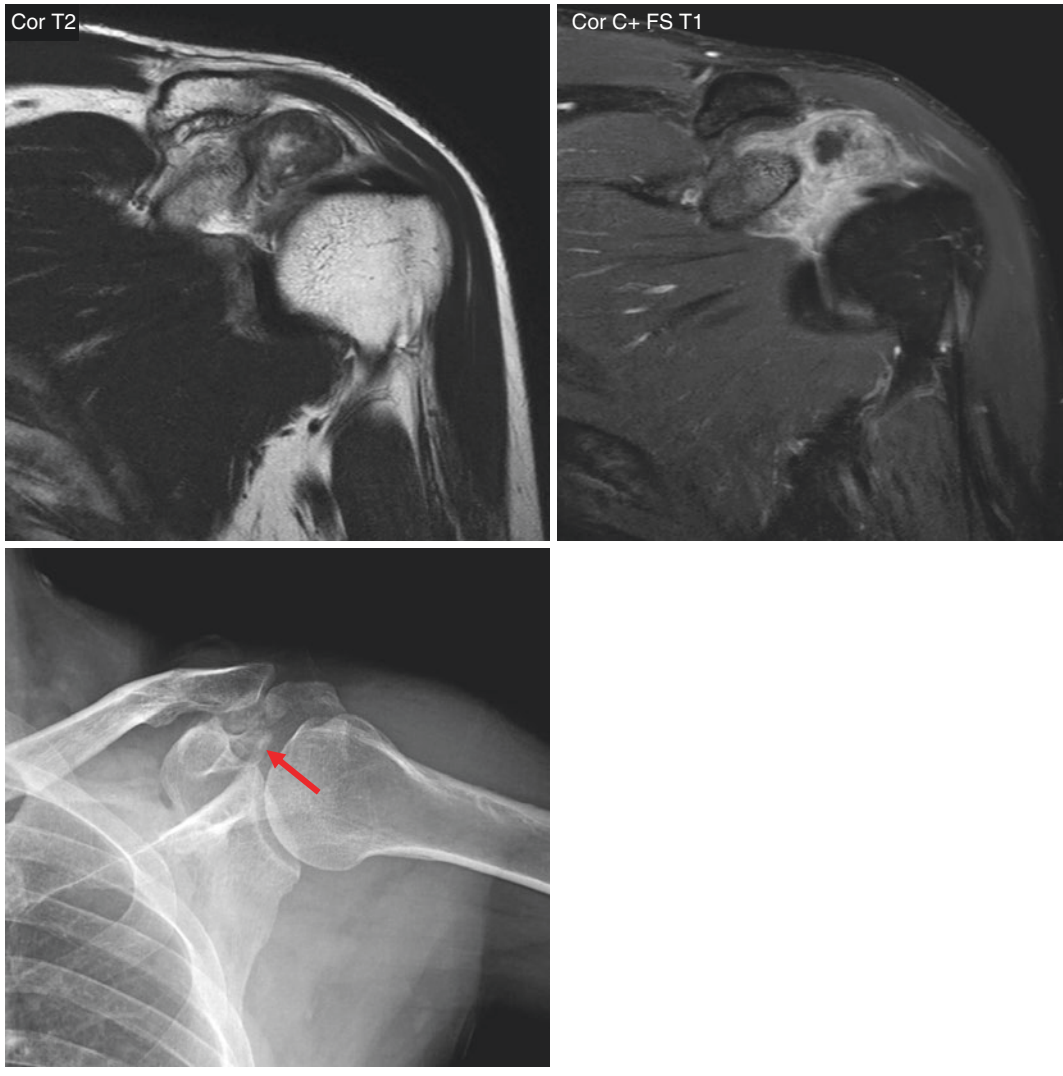

Fig. 17.30 Gout

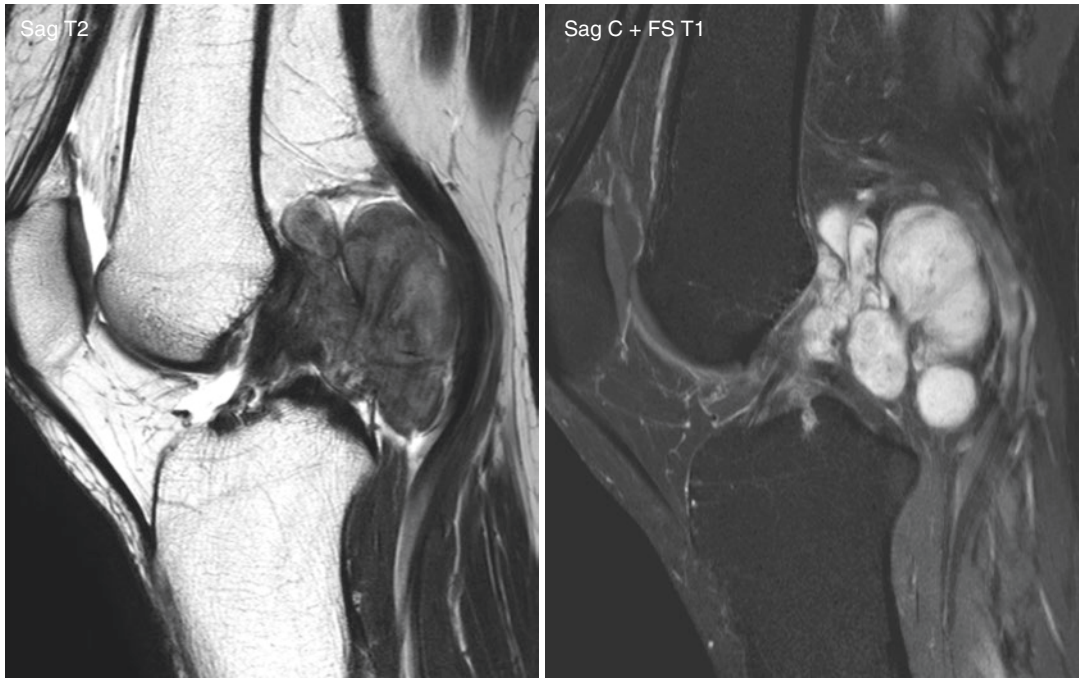

Fig. 17.31 Tenosynovial GCT

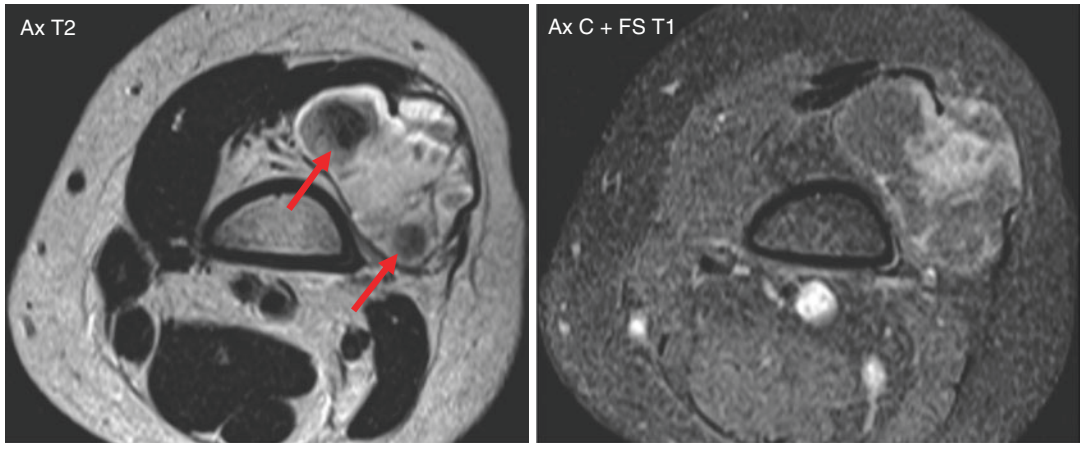

Fig. 17.32 Hemangioma (thrombus)

17.2.3 Lesion Containing Free Cholesterol

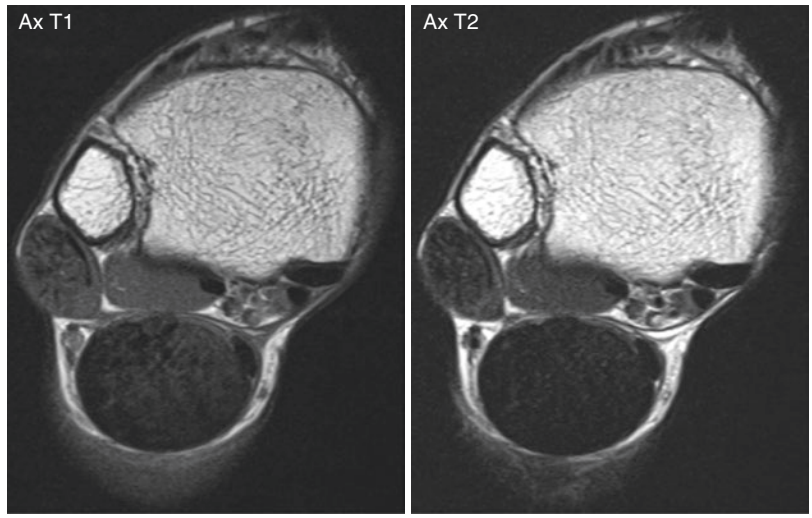

Fig. 17.33 Xanthoma

17.2.4 Lesion Containing High-Flow Vessels

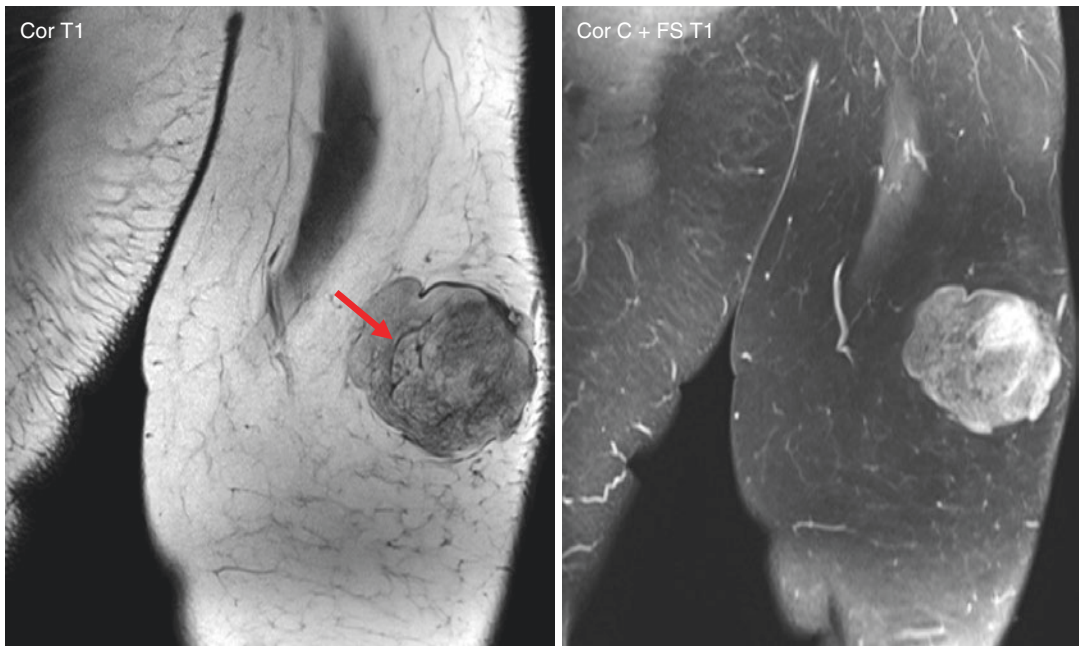

Fig. 17.34 Hibernoma

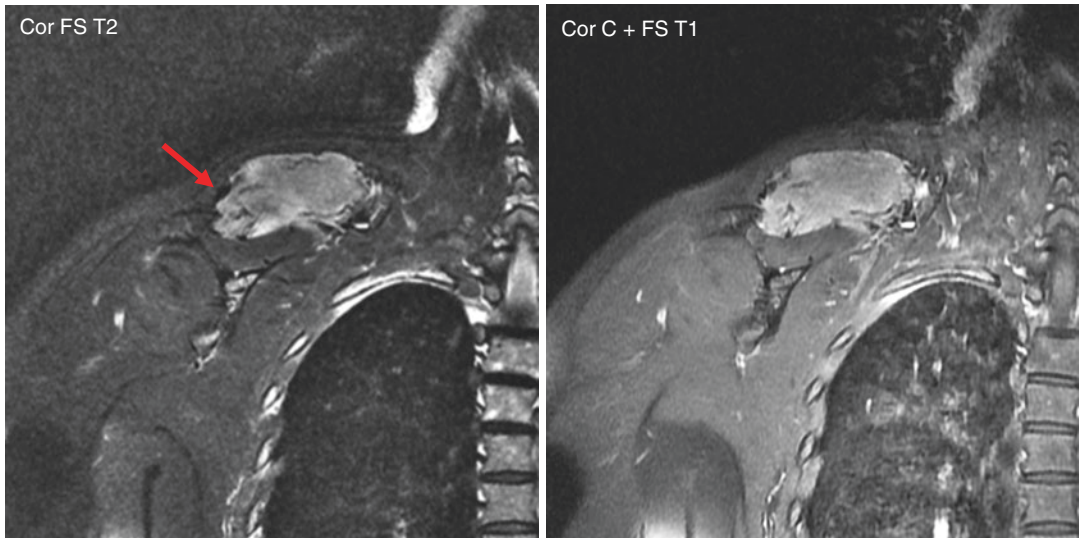

Fig. 17.35 Solitary fibrous tumor

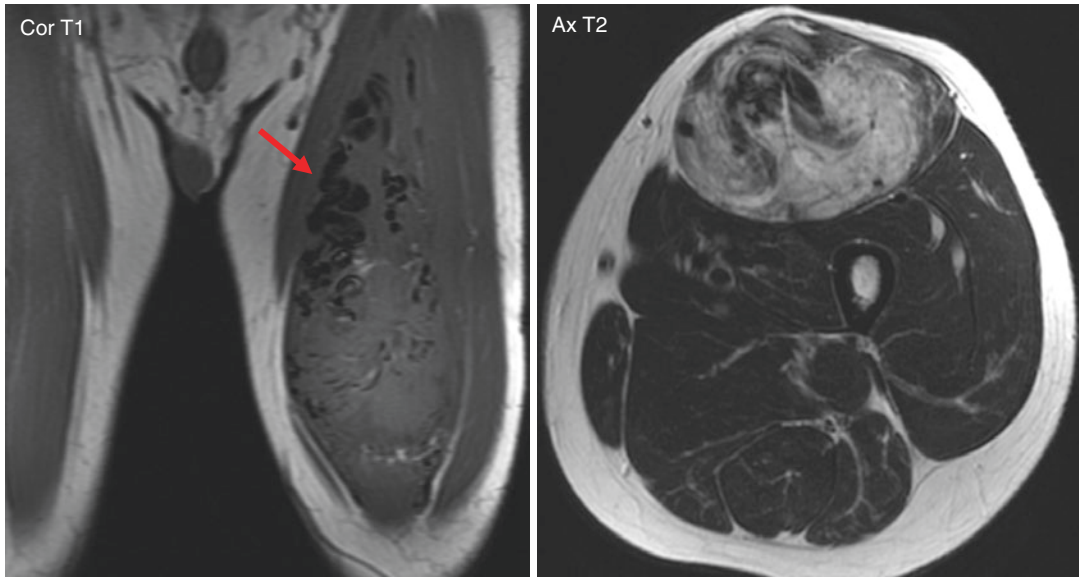

Fig. 17.36 Vascular lesions including arteriovenous malformation and hemangioendothelioma

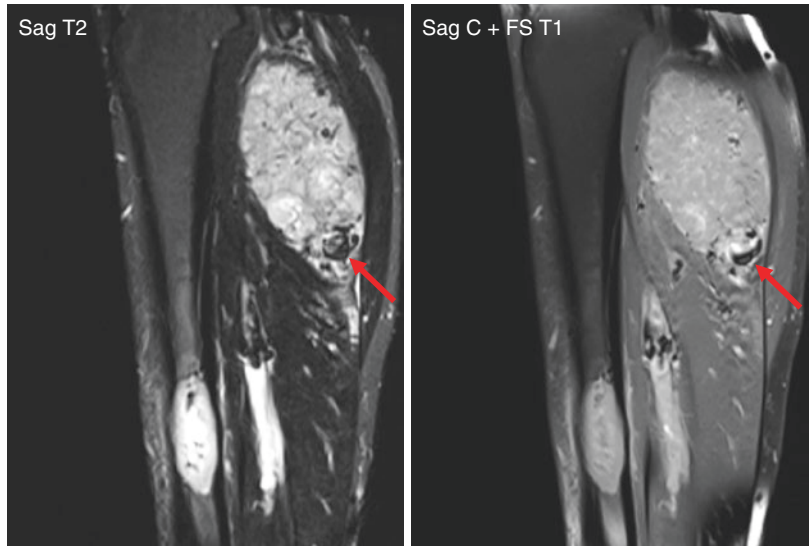

Fig. 17.37 Alveolar soft part sarcoma

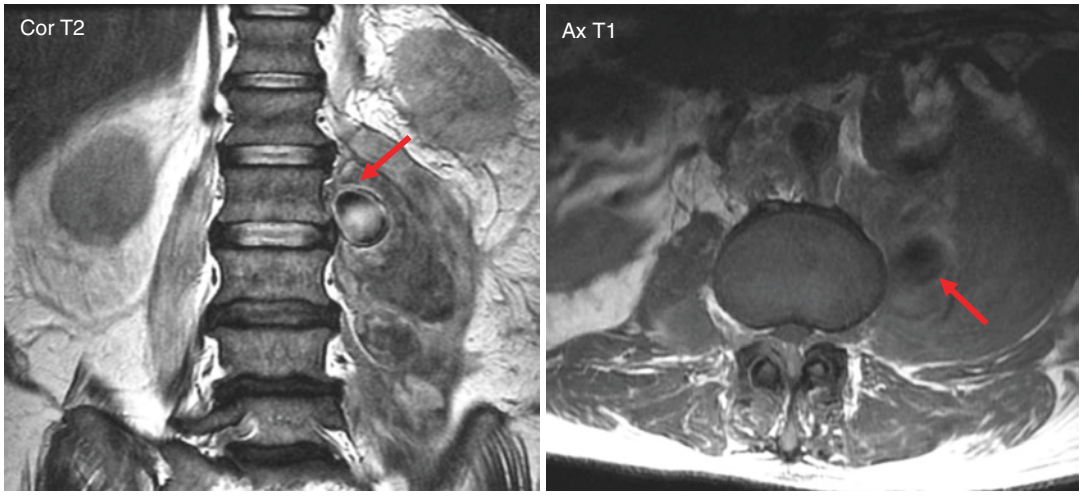

Fig. 17.38 Aneurysm, pseudoaneurysm

17.3 T2 Fluid-Equivalent Hyperintense Lesions

17.3.1 Lesion Containing Fluid

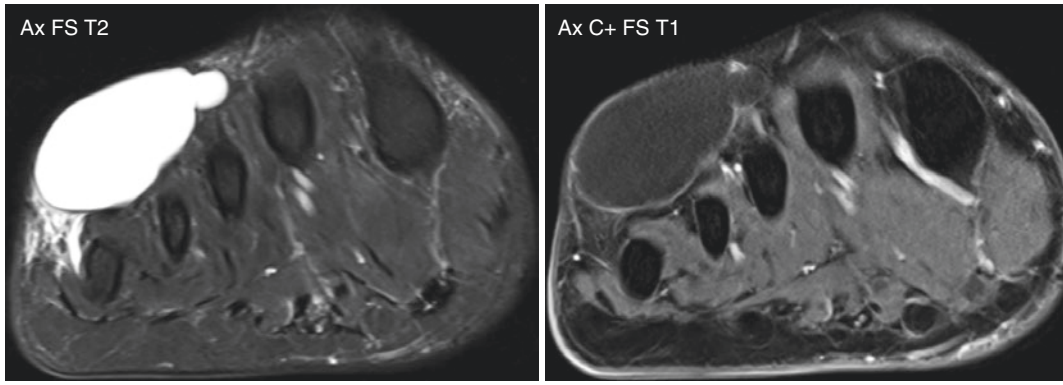

Fig. 17.39 Ganglion

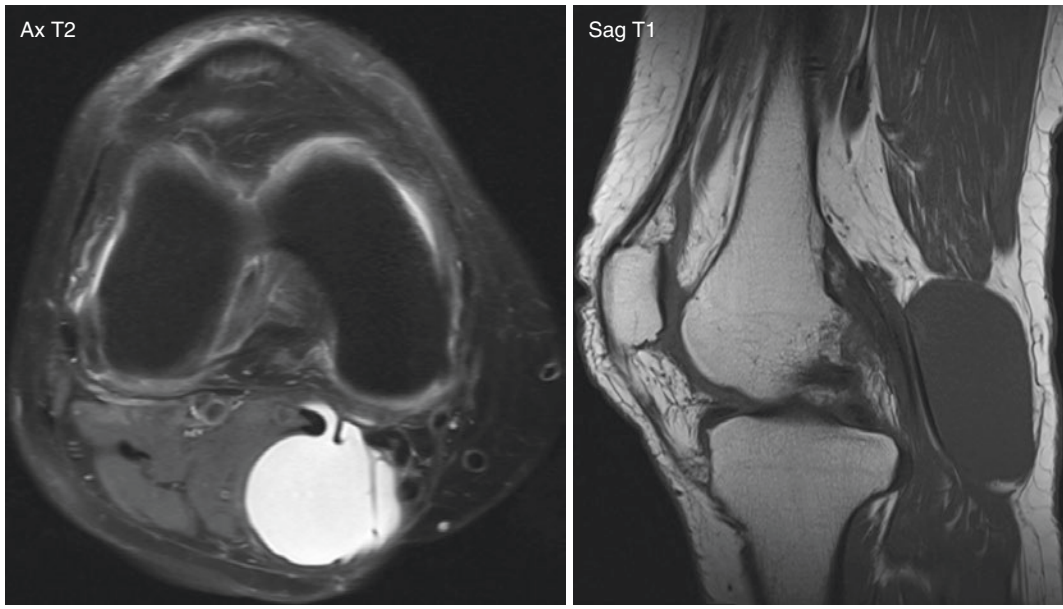

Fig. 17.40 Bursitis

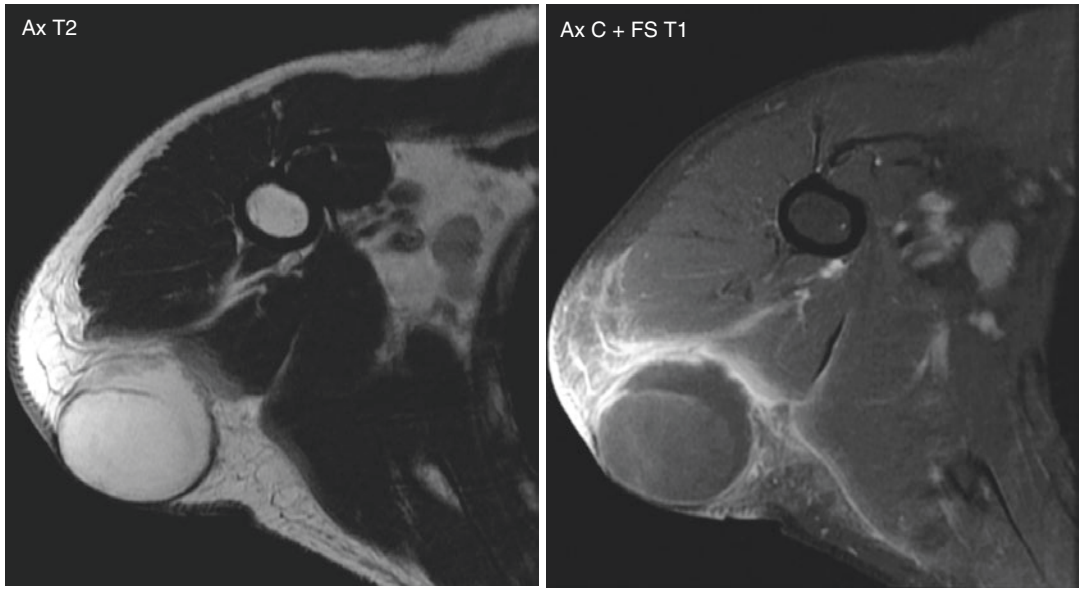

Fig. 17.41 Epidermal inclusion cyst

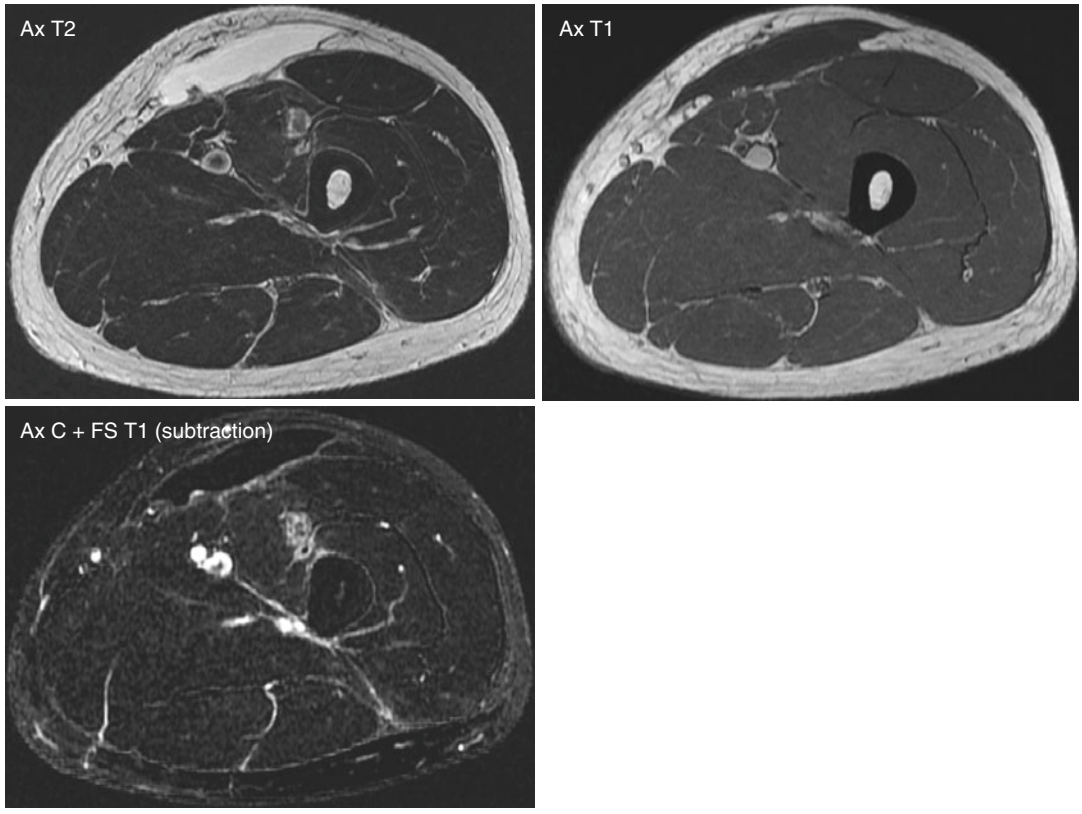

Fig. 17.42 Morel-Lavallee lesion (fluid-like)

17.3.2 Lesion Containing Myxoid Tissue

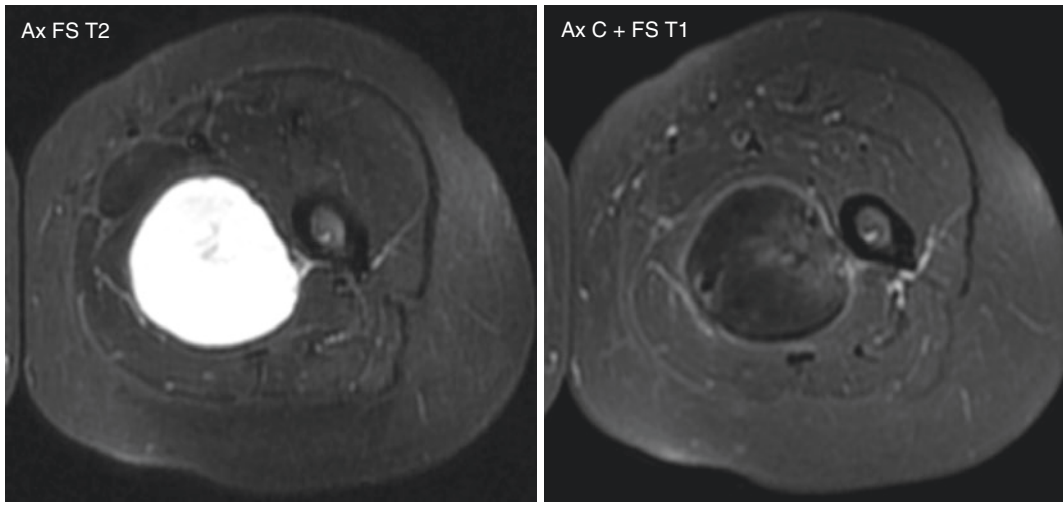

Fig. 17.43 Intramuscular myxoma

Fig. 17.44 Peripheral nerve sheath tumor

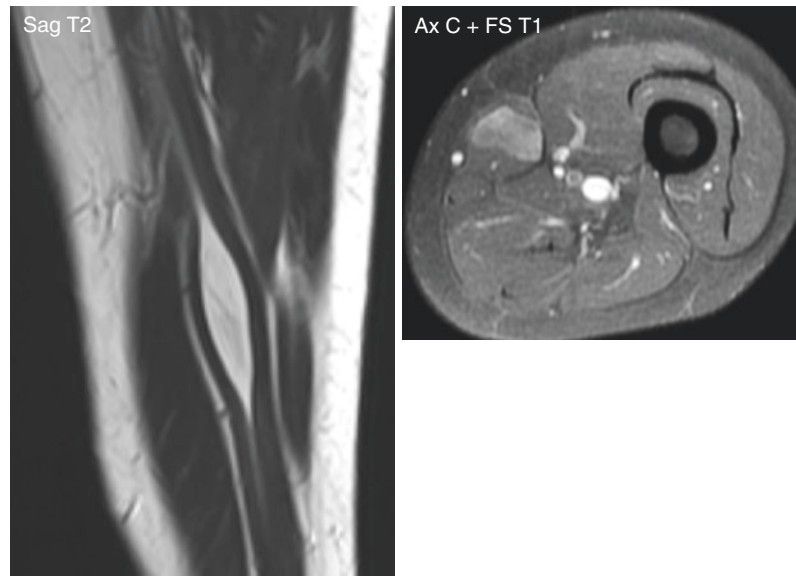

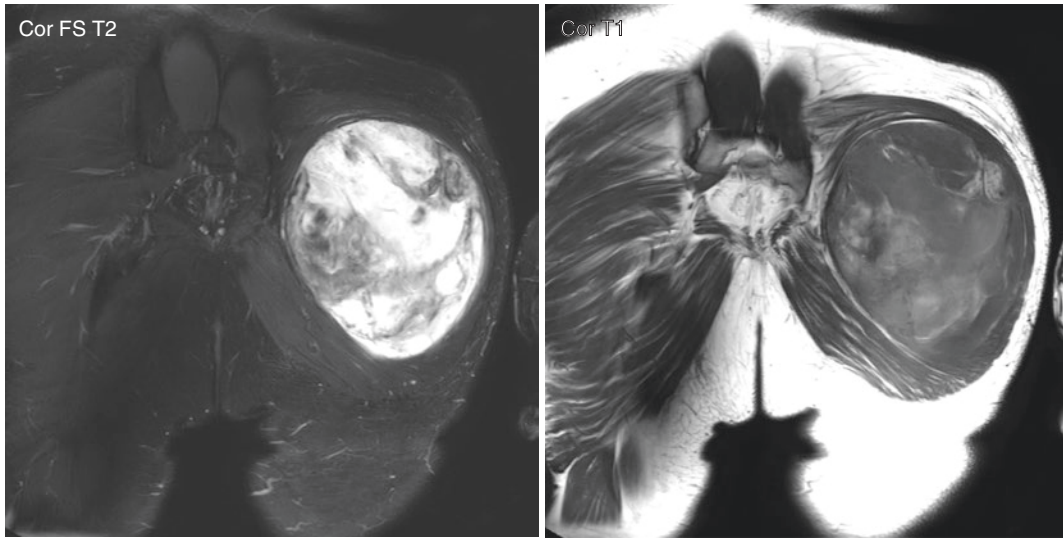

Fig. 17.45 Myxoid liposarcoma

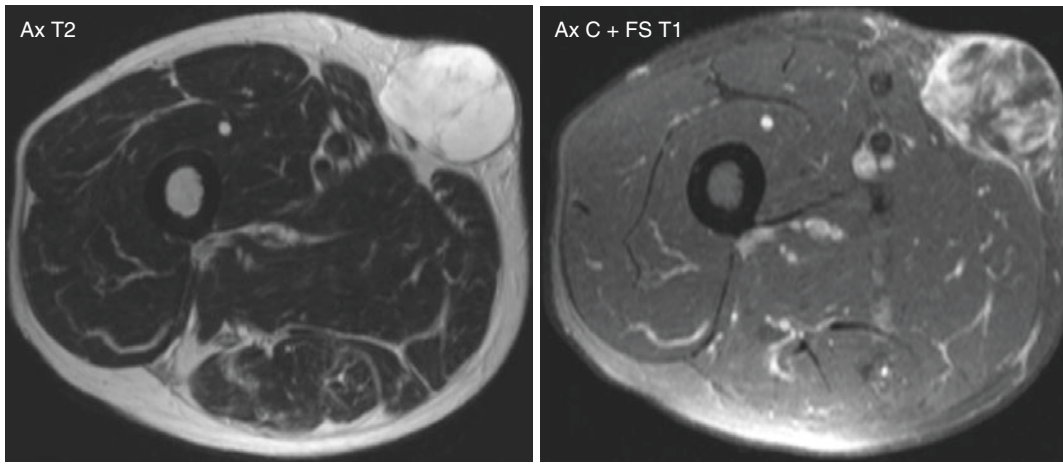

Fig. 17.46 Myxofibrosarcoma

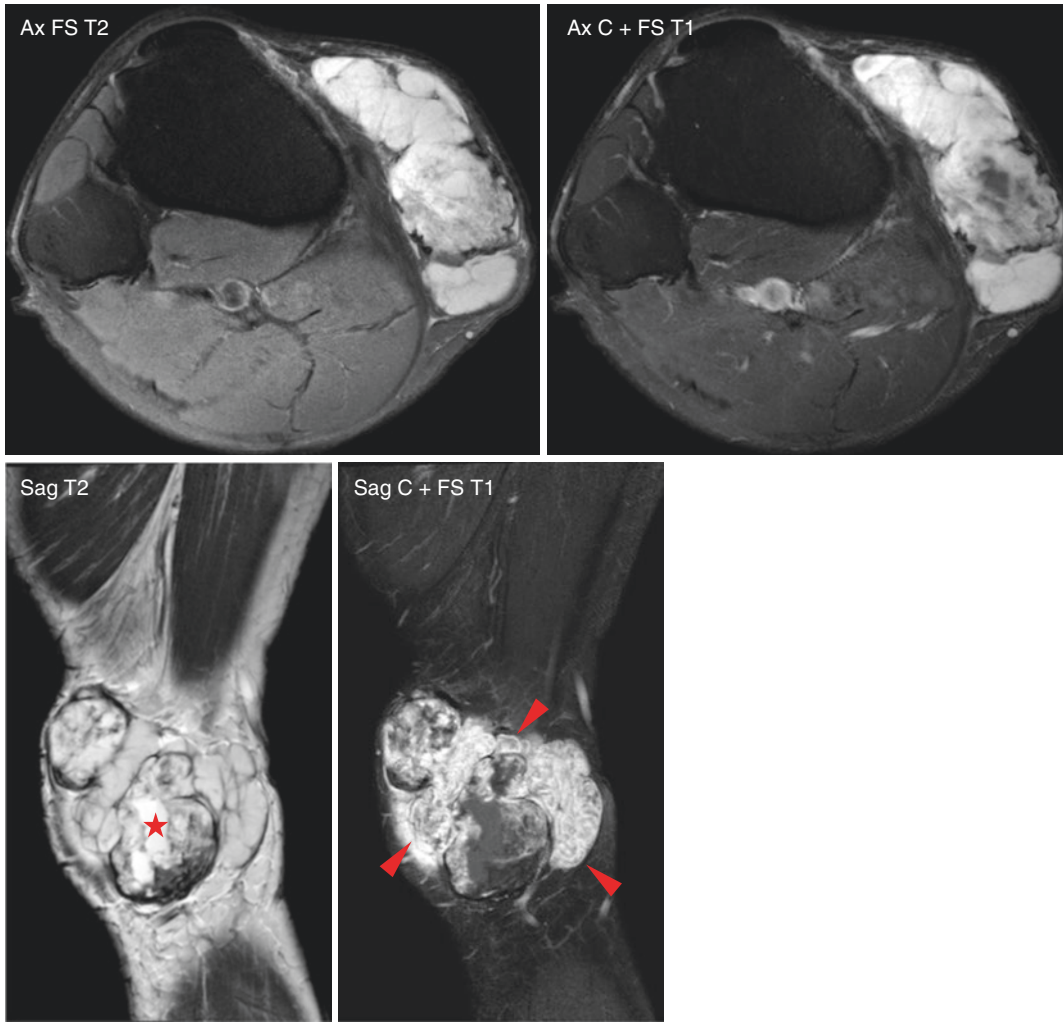

Fig. 17.47 Extraskeletal myxoid chondrosarcoma

17.3.3 Vascular Lesion

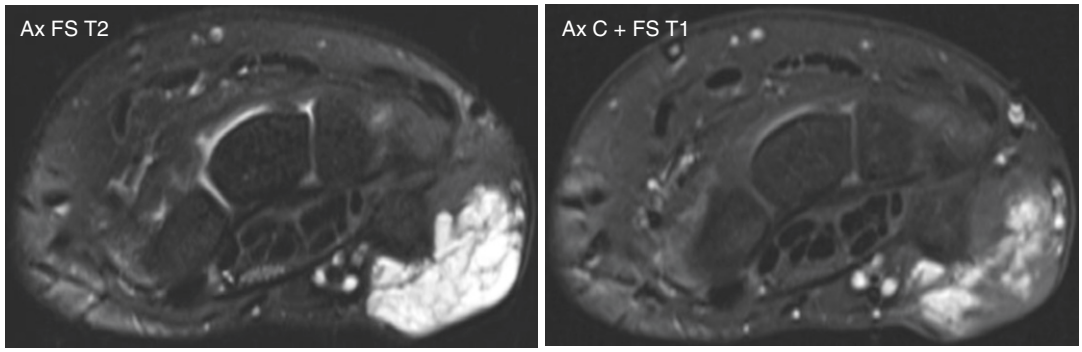

Fig. 17.48 Hemangioma

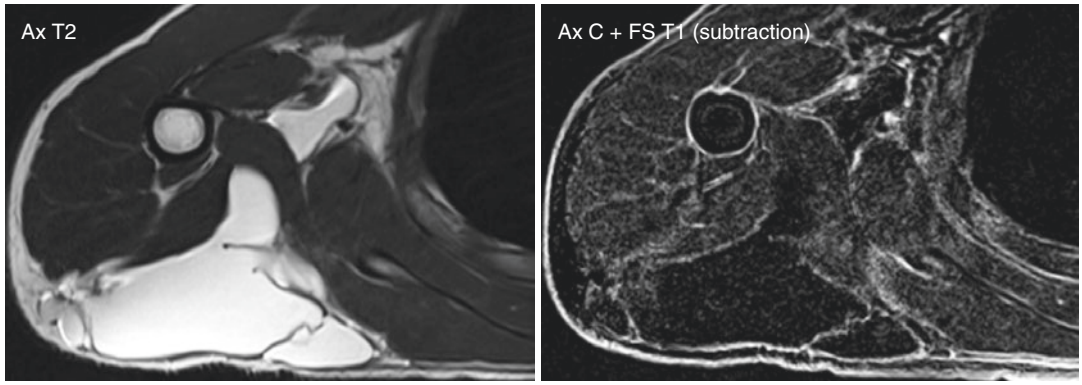

Fig. 17.49 Lymphangioma

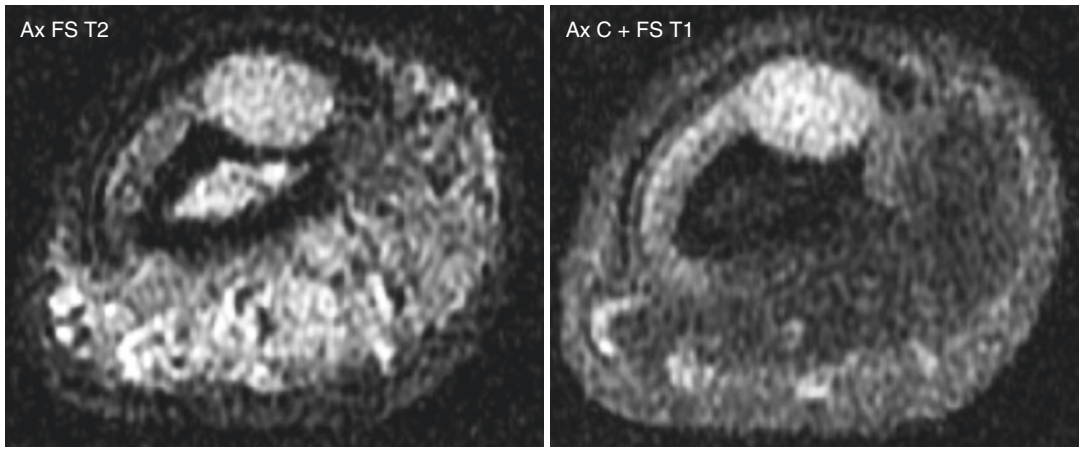

Fig. 17.50 Glomus tumor

17.3.4 Lesions Containing Cartilage

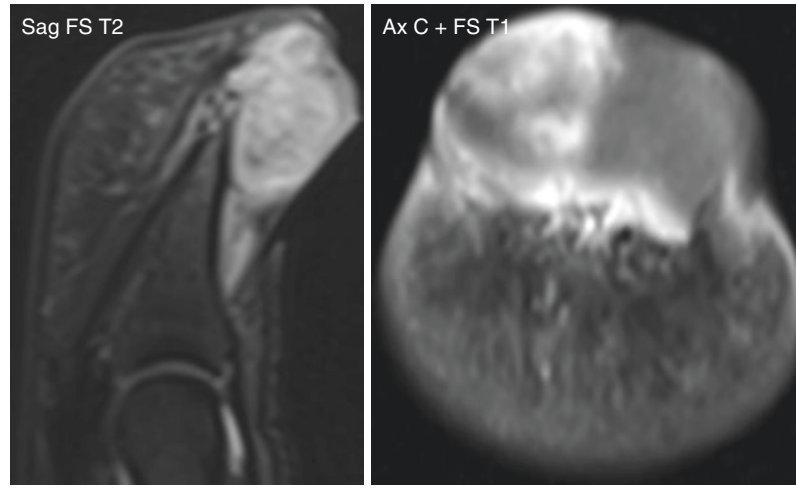

Fig. 17.51 Soft tissue chondroma

Diagnostic Signs

18

18.1 Bowl of Grapes Sign

- Heterogeneous signal intensity
- Multilocular mass with fluid–fluid levels
- Seen in synovial sarcoma

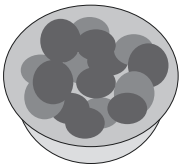

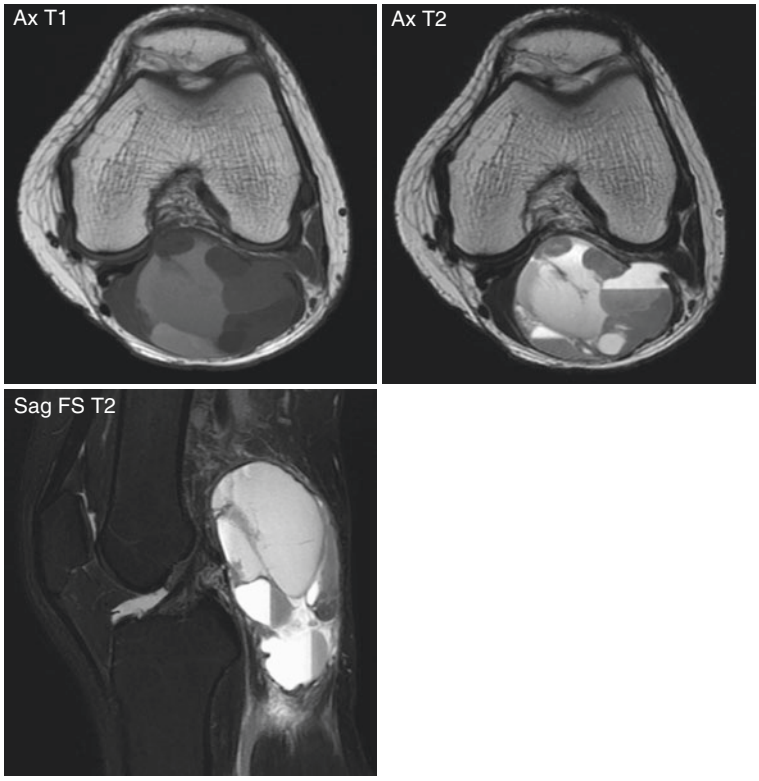

Fig. 18.1

H.S. Kang et al., *Oncologic Imaging: Soft Tissue Tumors*, DOI 10.1007/978-981-287-718-5_18

18.2 Bunch of Grapes Appearance

- Multilobulated anechoic mass with multiple internal septa on US
- Seen in ganglion

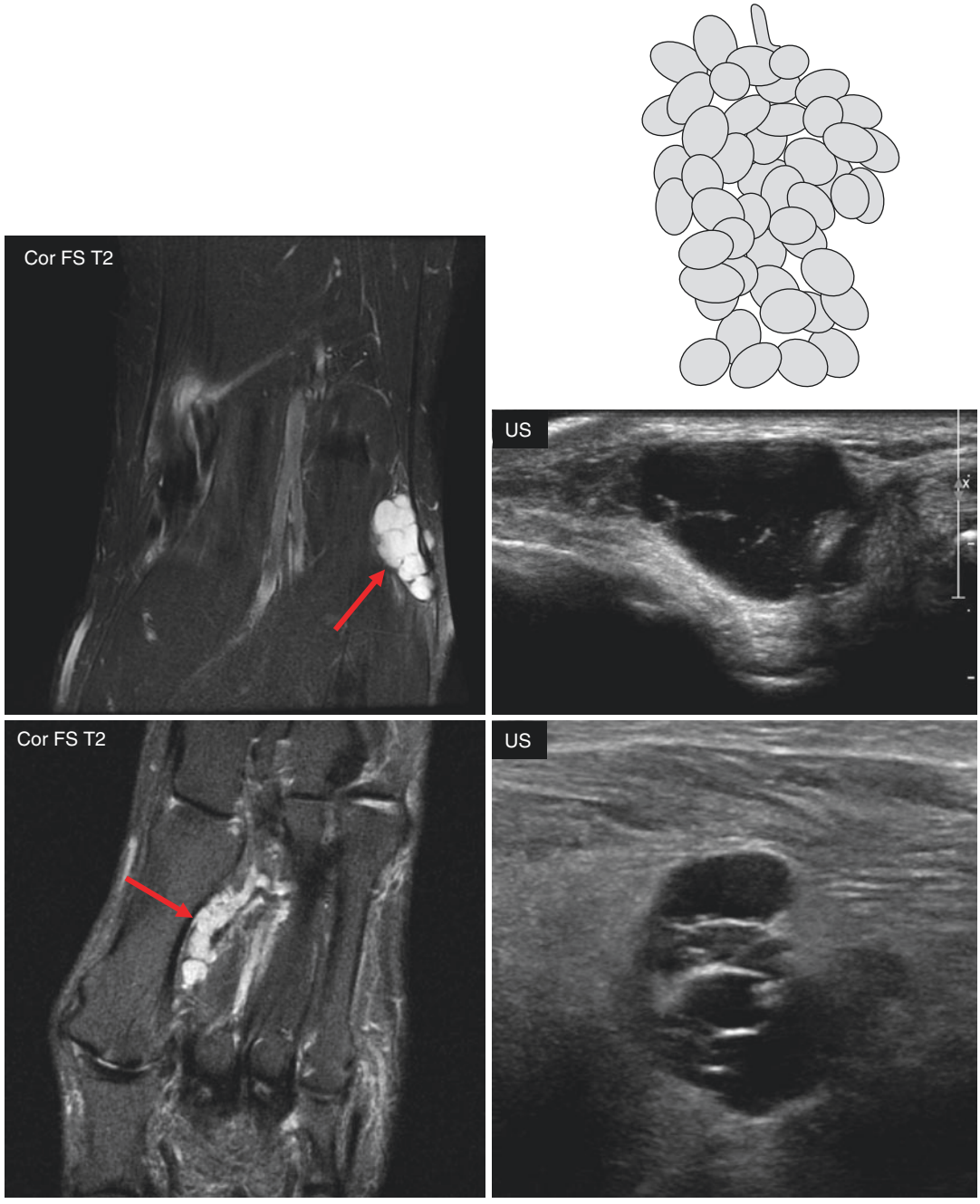

Fig. 18.2

18.3 Checkerboard Appearance

- Checkerboard pattern resembling dry, cracked mud
- Hyperintense strands between hypointense muscle fascicles on T2WI and postcontrast T1WI
- Seen in proliferative myositis

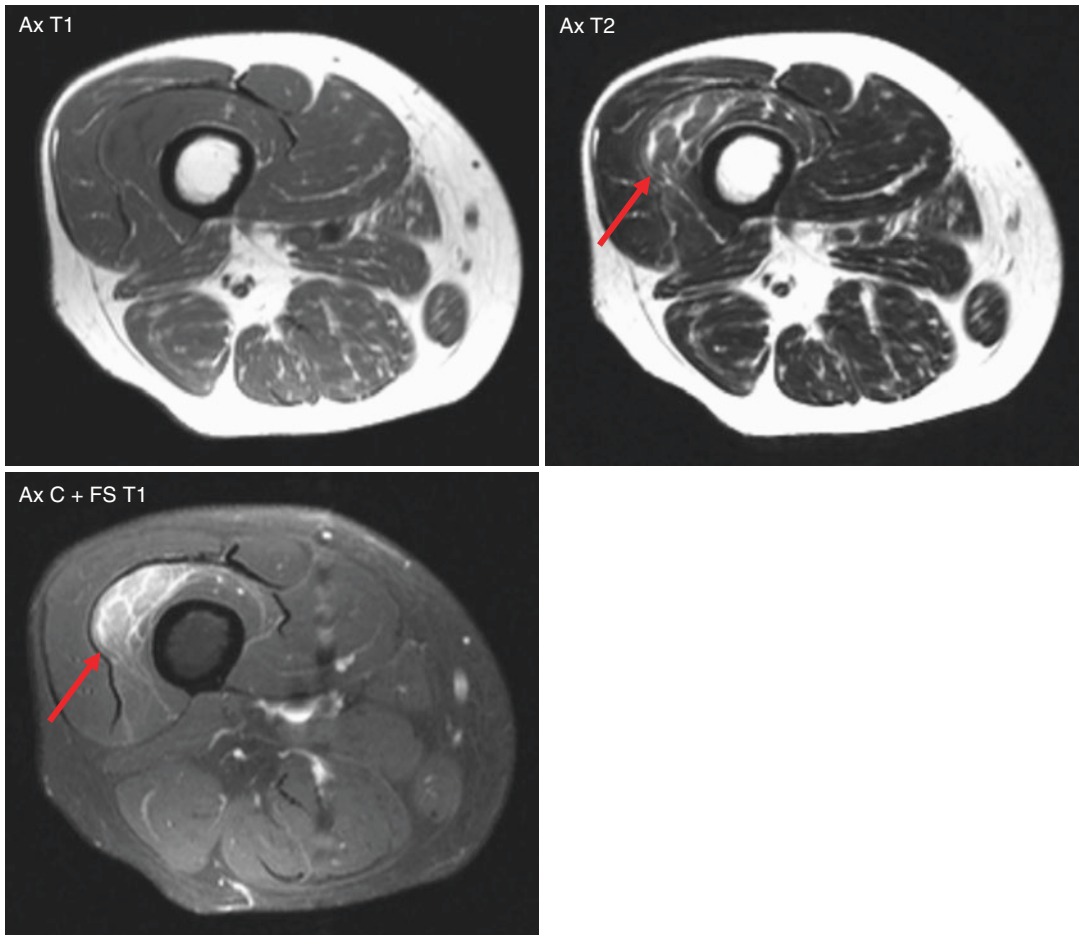

Fig. 18.3

18.4 Coaxial Cable-Like Appearance

- Serpentine nerve fascicles embedded within fatty tissue
- Seen in lipomatosis of nerve in axial MRI

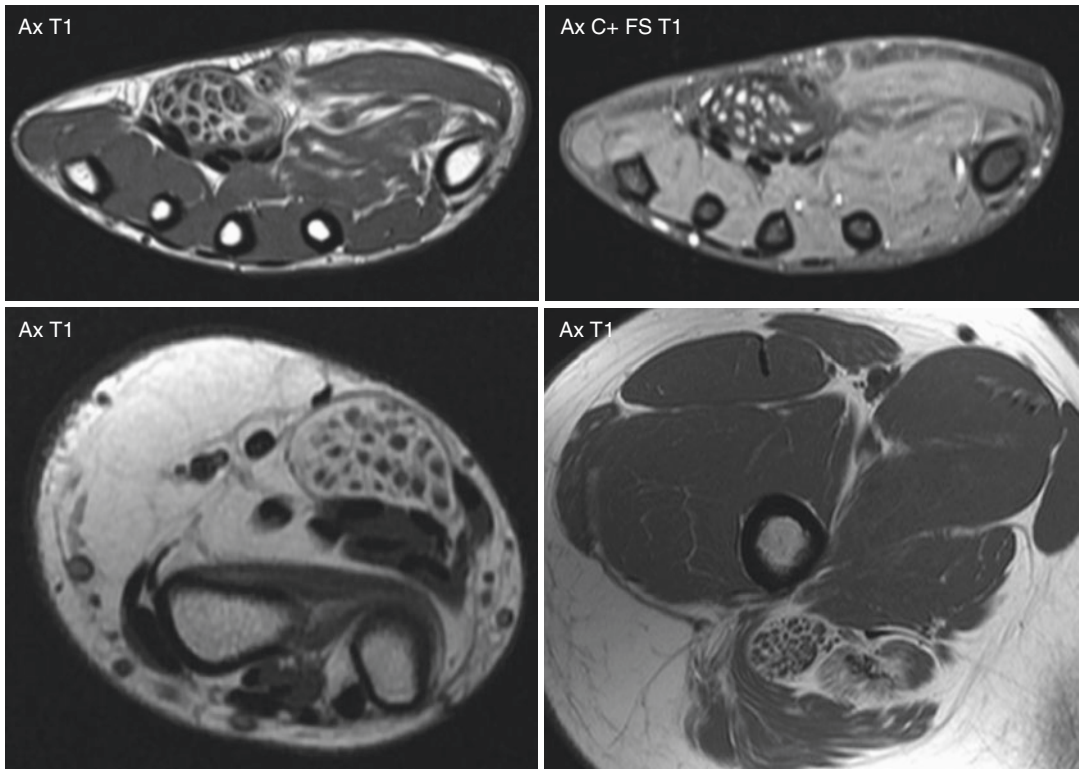

Fig. 18.4

18.5 Dark Star Sign

- Star-shaped central structure with low signal intensity on MRI
- Star-shaped central structure with increased echotexture on US
- Seen in sarcoidosis

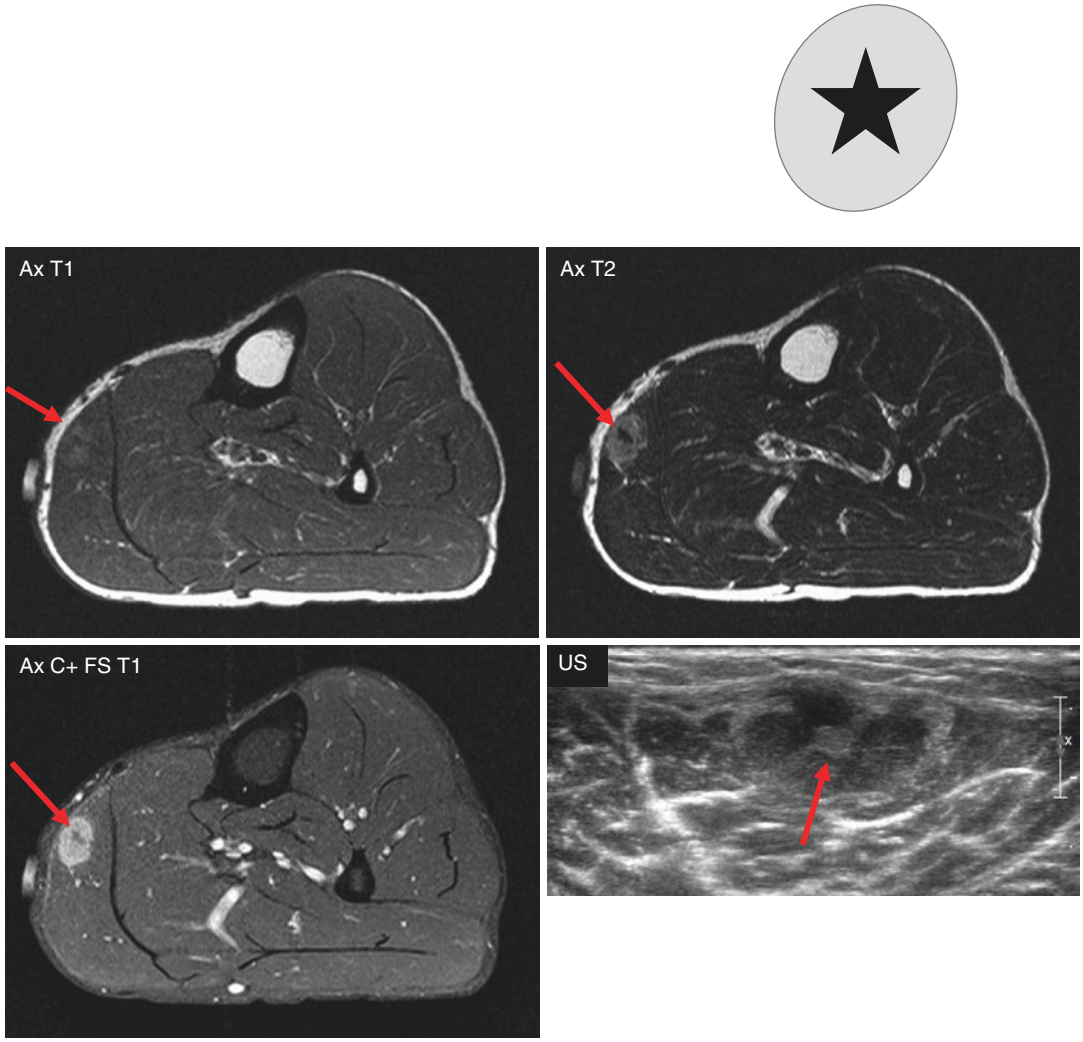

Fig. 18.5

18.6 Fascicular Sign

- Multiple small hypointense ringlike structures within the hyperintense area on T2WI
- Reflecting the fascicular bundles within the nerves seen histologically
- Found in peripheral nerve sheath tumors (neurofibroma, schwannoma)

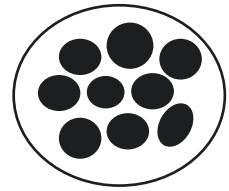

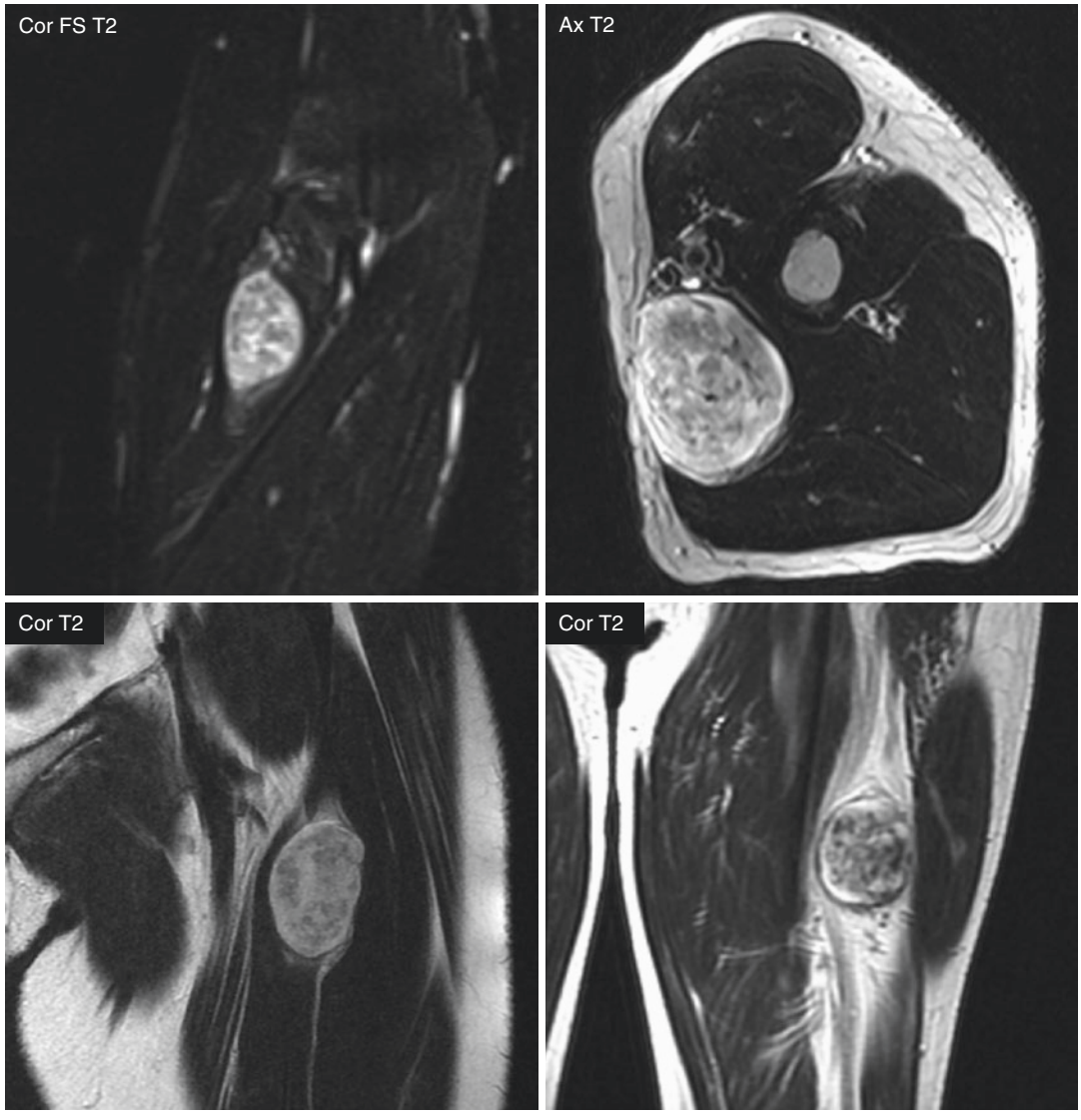

Fig. 18.6

18.7 Inverted Target Sign

- Central T2 hyperintensity and peripheral T2 hypointensity
- Non-enhancing central area on postcontrast T1WI
- Seen in nodular fasciitis

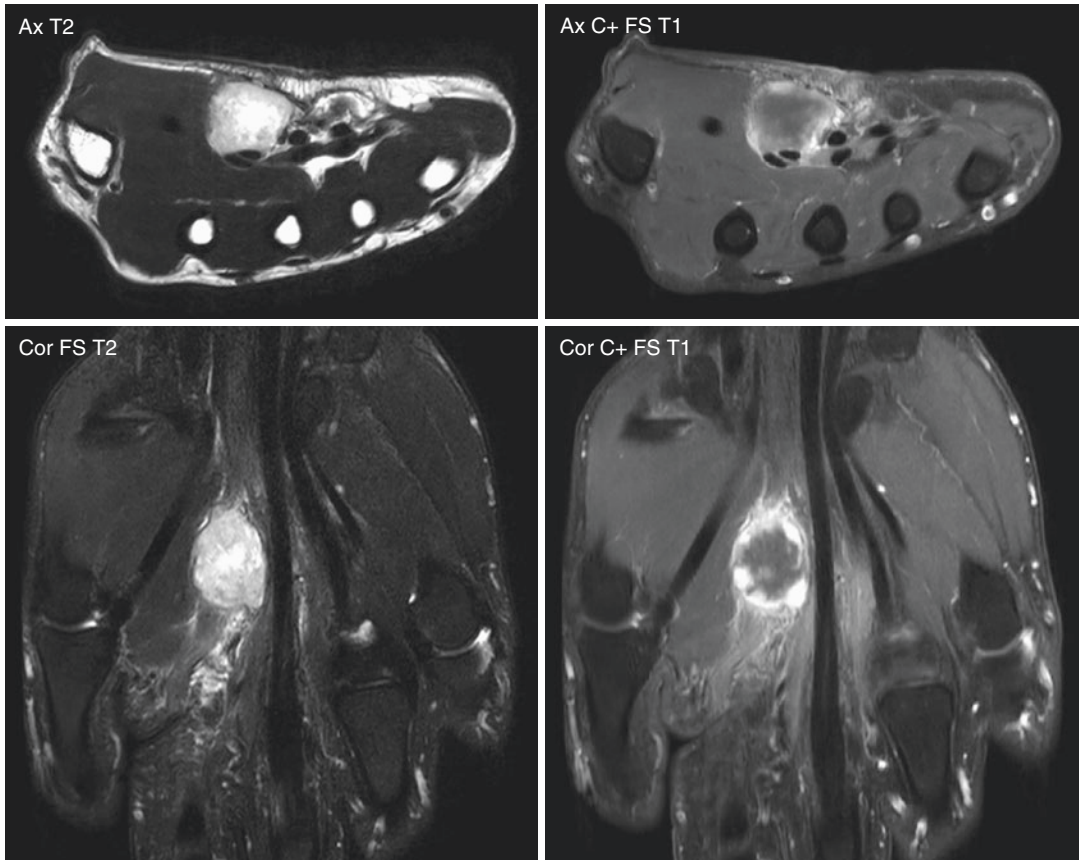

Fig. 18.7

18.8 Gyriform Pattern

- Multiple folded layers mimicking brain gyri
- Low to iso-signal intensity on fluid-sensitive sequences
- Seen in low-grade fibromyxoid sarcoma

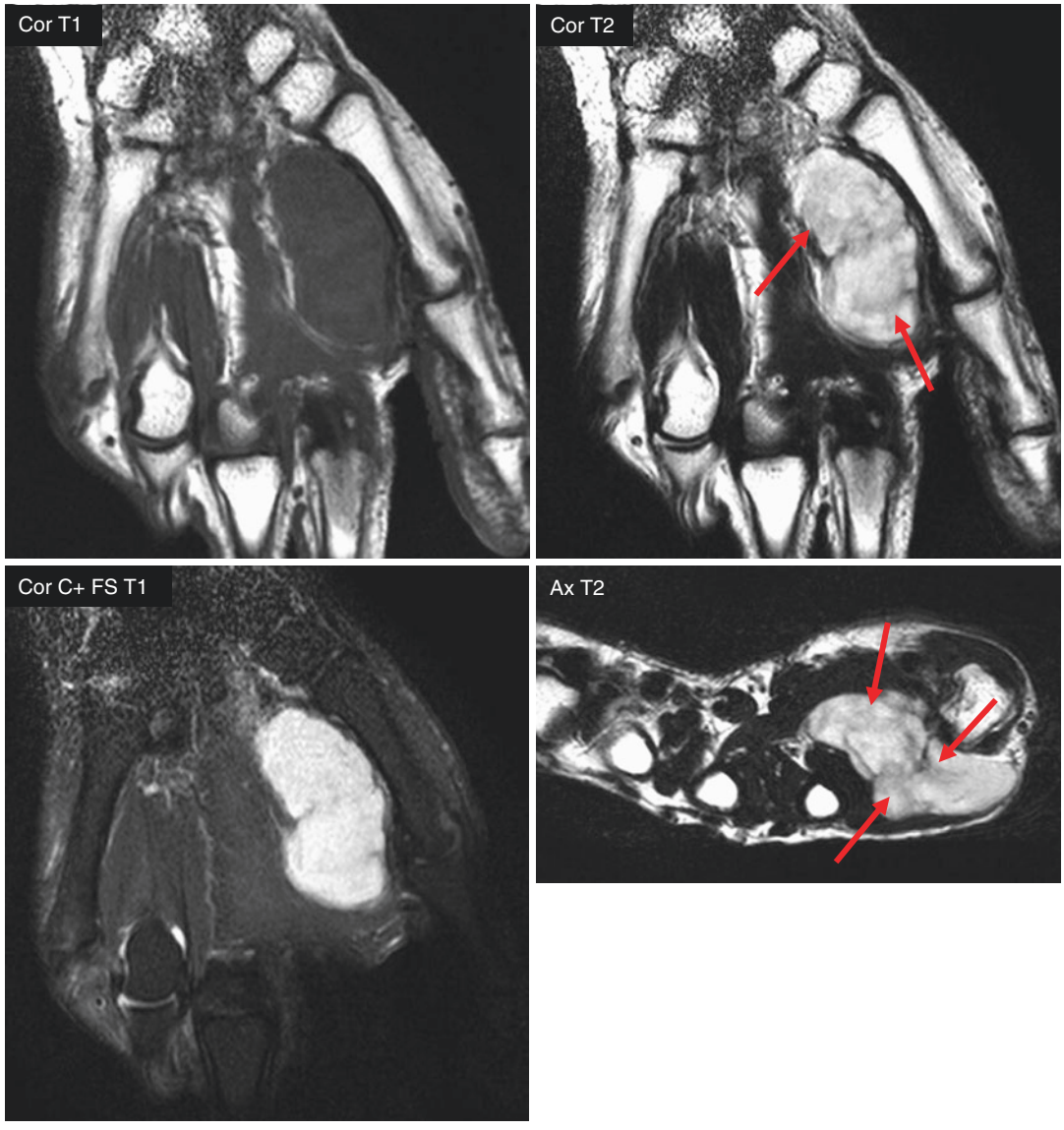

Fig. 18.8

18.9 Reverse Target Sign

- Enhancement of the central fibrous component and a relative lack of enhancement of the surrounding myxoid component on postcontrast T1WI
- Seen in peripheral nerve sheath tumors (neurofibroma, schwannoma)

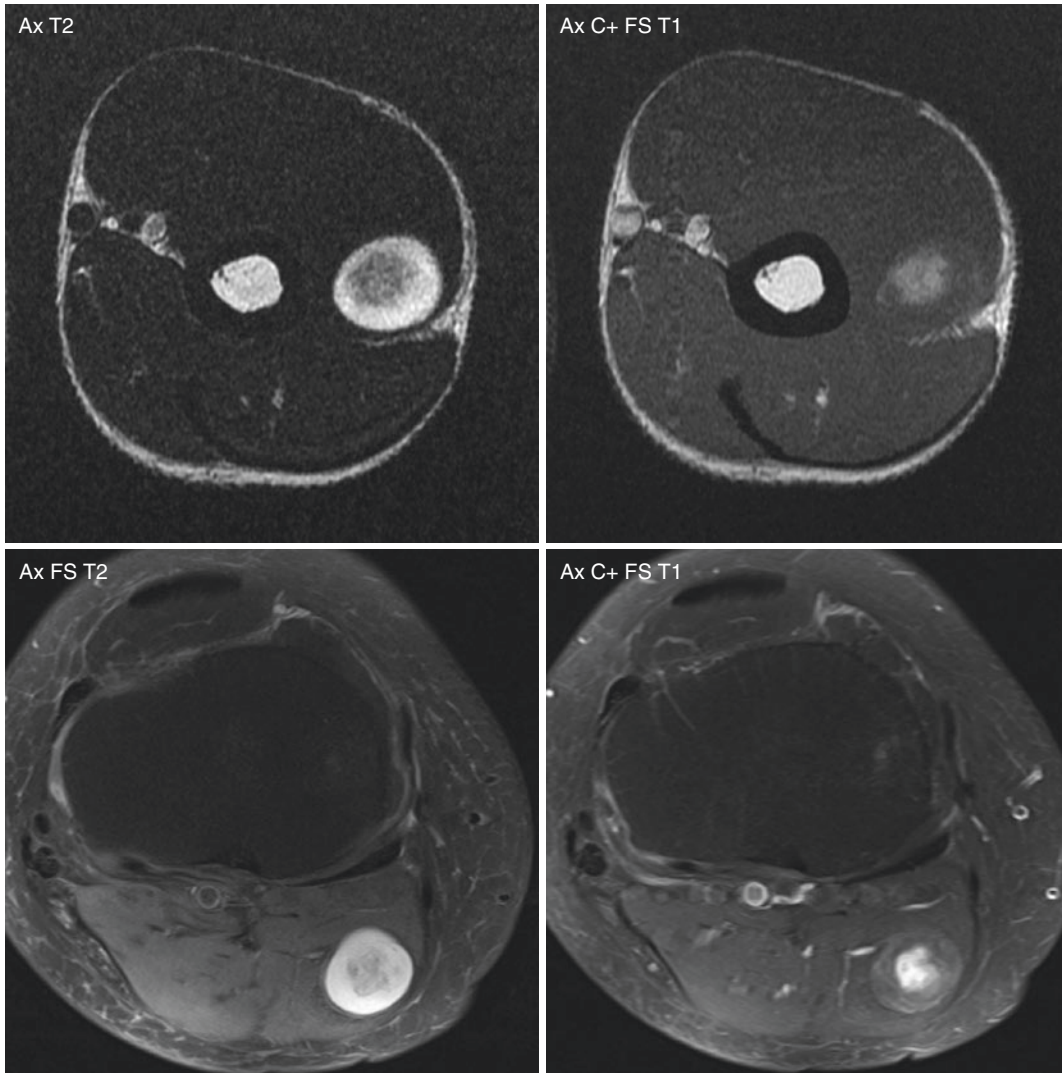

Fig. 18.9

18.10 Reverse Zoning Phenomenon

- Central location of the osteoid in the lesion
- The densest ossification (*arrow*) in the center of the lesion and the least ossification at the periphery
- Pathological findings of a "reverse zoning phenomenon": central deposition of osteoid material and atypical spindle cell proliferation at the periphery
- Found in extraskeletal osteosarcoma

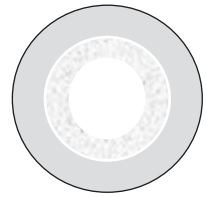

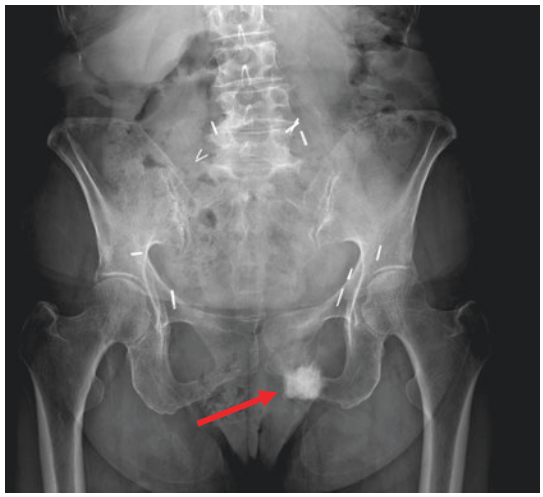

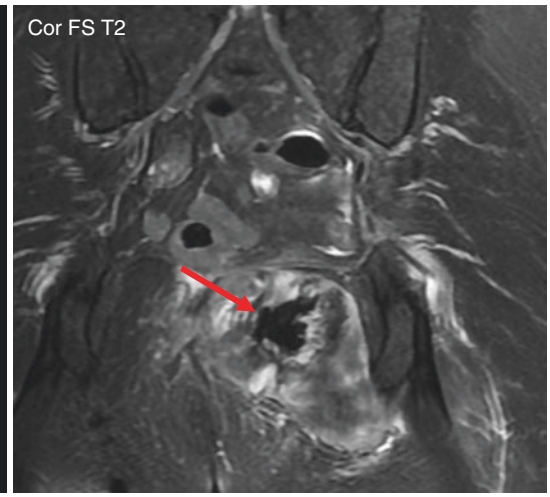

Fig. 18.10

18.11 Spaghetti-Like Appearance

- Serpentine nerve fascicles embedded within fatty tissue
- Seen in lipomatosis of nerve on longitudinal MRI

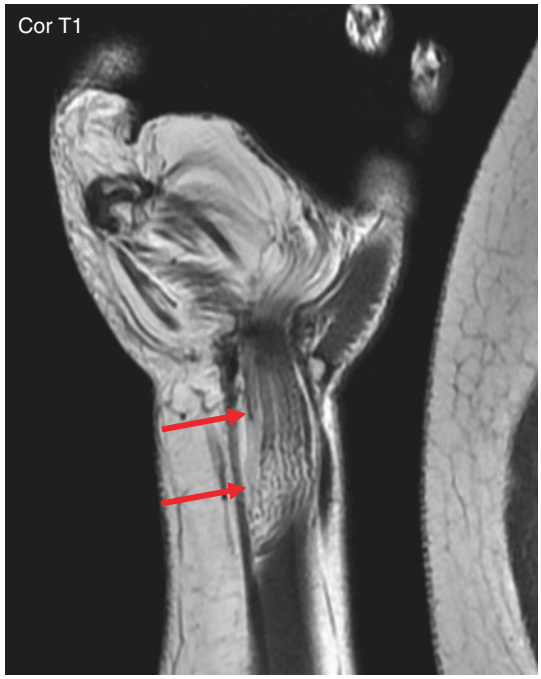

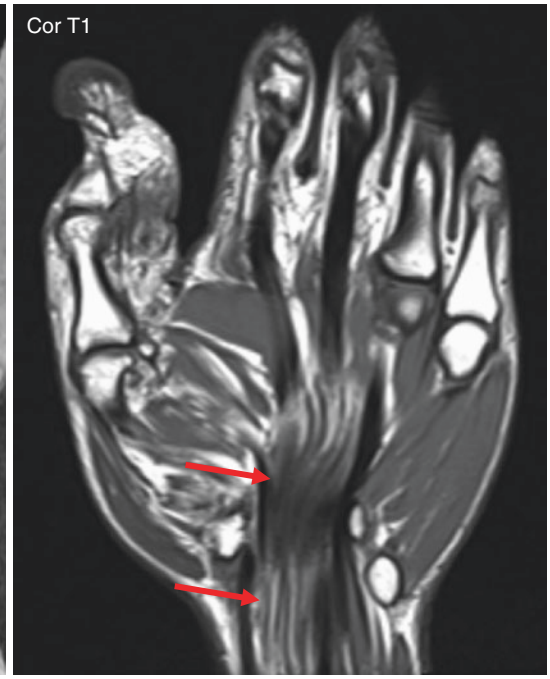

Fig. 18.11

18.12 Split Fat Sign

- Tapered rim of fat at the upper and lower poles of a lesion or fine rind of the fat around the lesion
- Best seen on T1WI
- Observed in peripheral nerve sheath tumors and other soft tissue tumors in intermuscular location

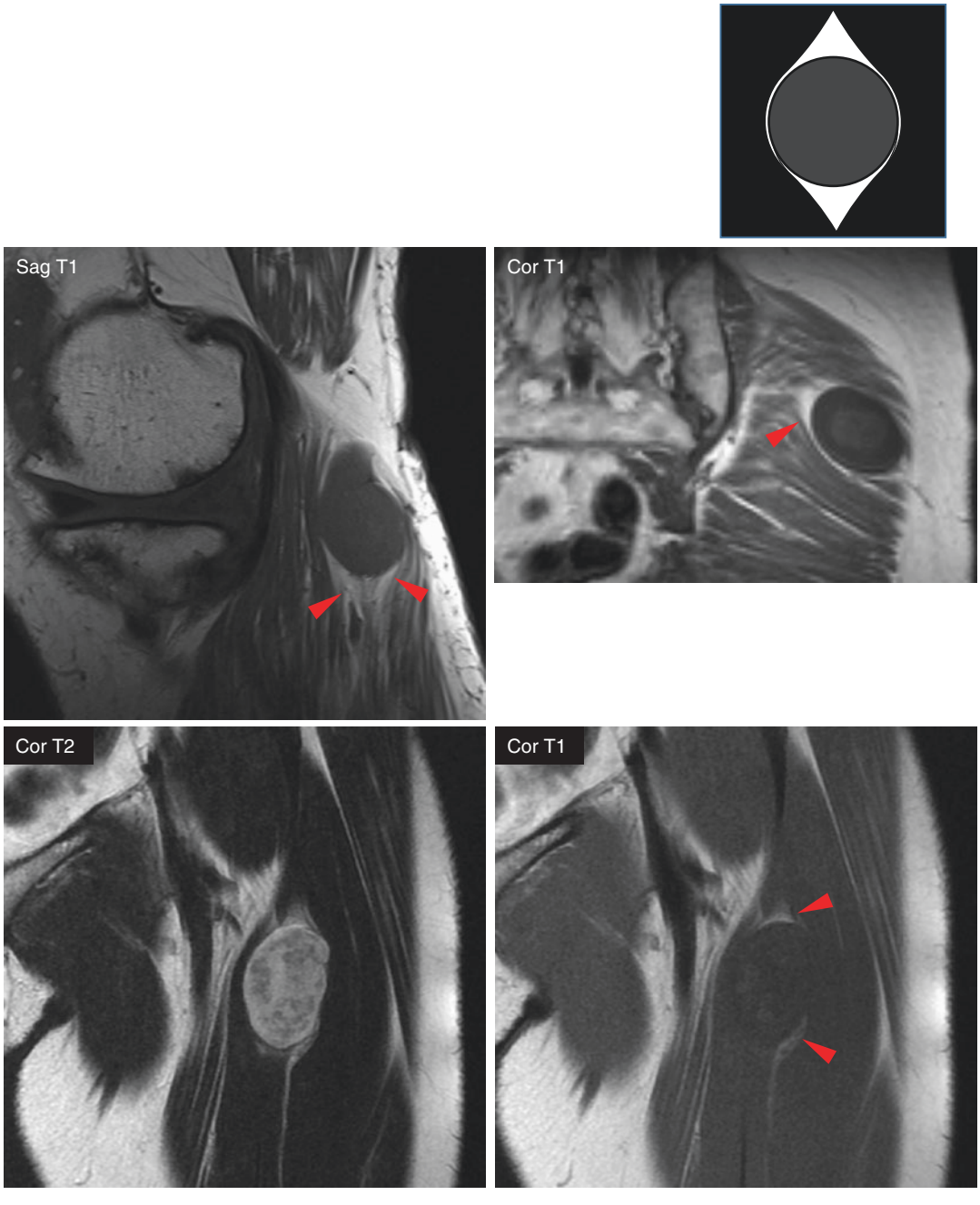

Fig. 18.12

18.13 String Sign

- On US and MRI
- Delineation of the entering and exiting nerve in a lesion, affecting large, deep nerves
- Seen in peripheral nerve sheath tumor

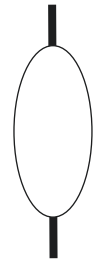

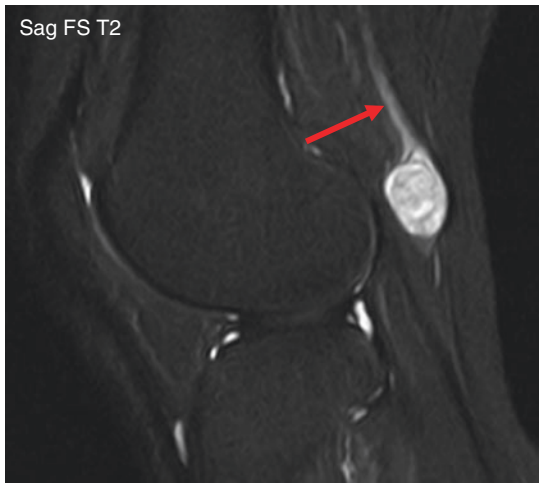

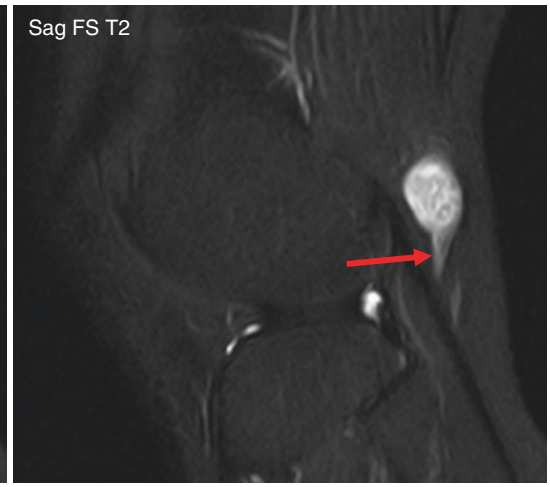

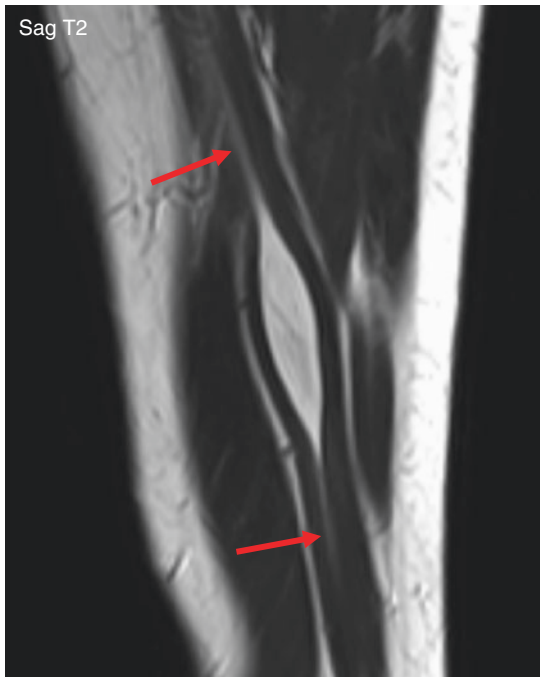

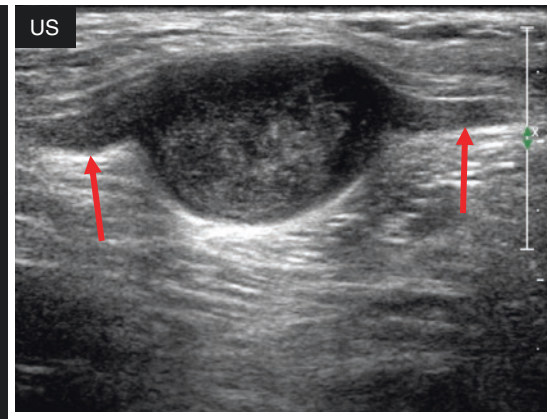

Fig. 18.13

18.14 Stripe Sign

- On US and MRI
- Intralesional hypointense lines continuous with the adjacent muscle fibers at the craniocaudal portion of the mass, representing the preservation of the adjacent muscle fibers
- Described in granular cell tumor

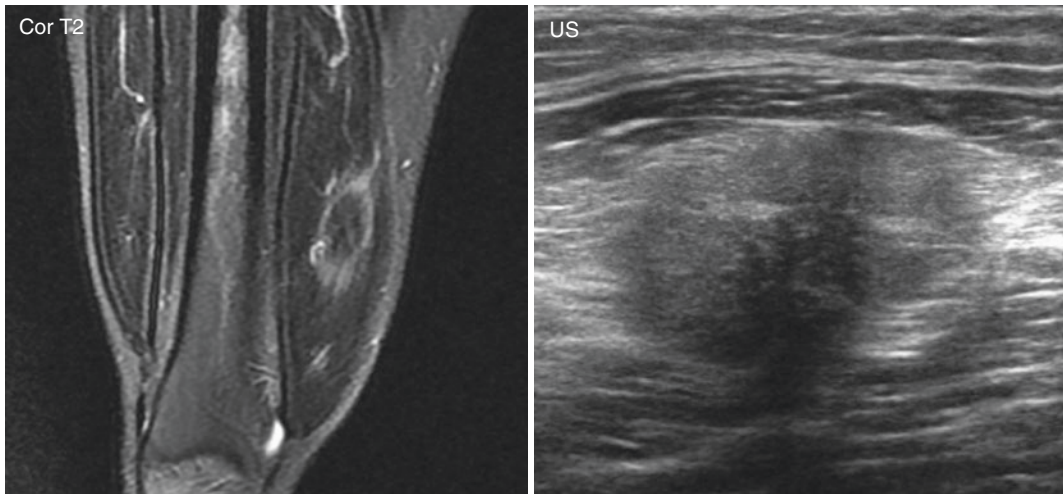

Fig. 18.14

18.15 Swiss Cheese Appearance

- X-ray: multiple rings and arc-like ossification with a coarse trabecular pattern
- MRI: non-enhanced, spotted, or irregular shaped areas of very low signal intensity both on T1WI and T2WI, corresponding to the ossification
- Seen in ossifying hemangioma
- Different from zonal phenomenon in myositis ossificans

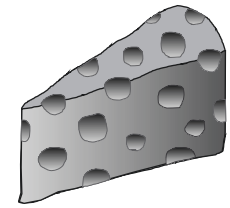

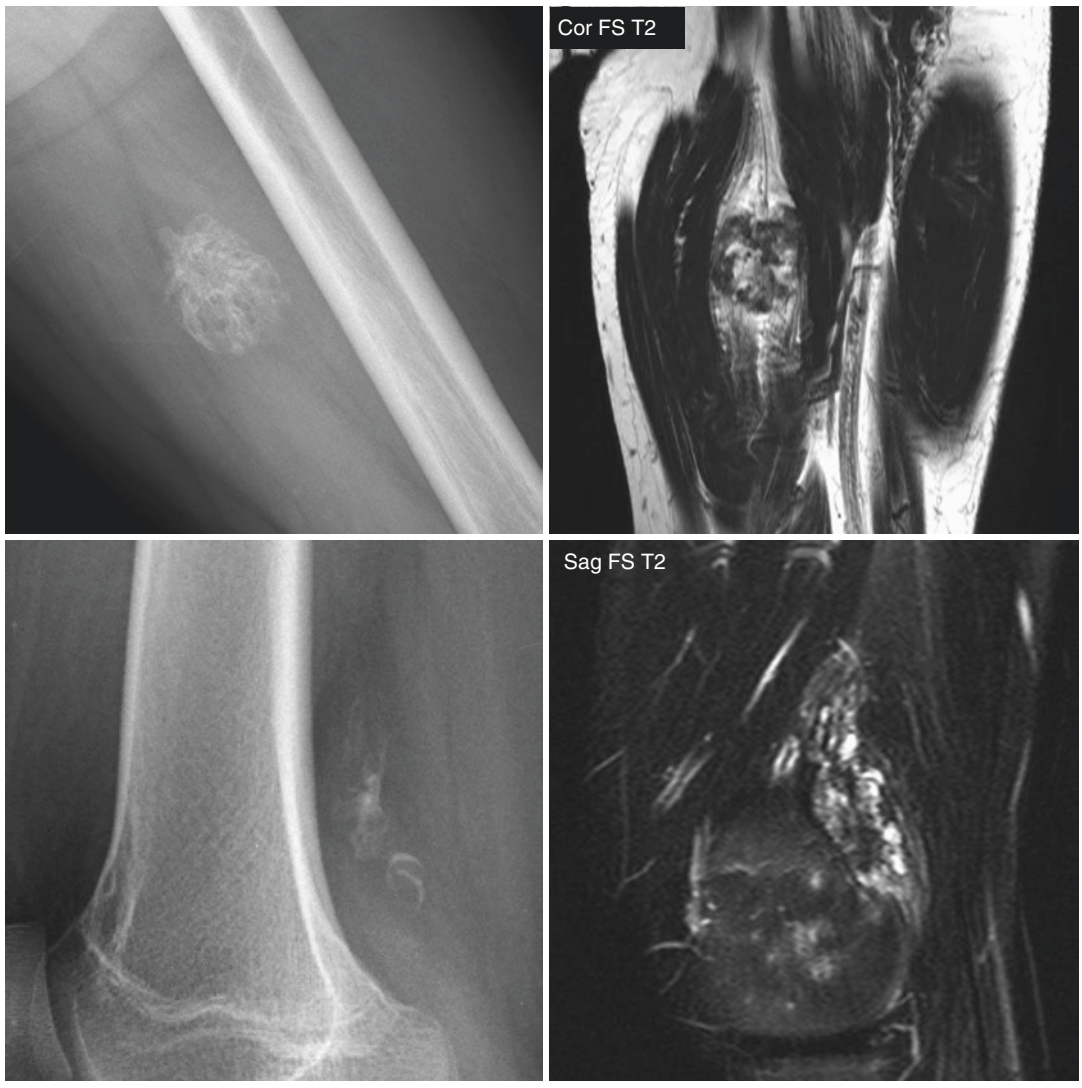

Fig. 18.15

18.16 Tail Sign

- Tail-like multidirectional spread along the fascial plane on T2WI
- Tapered fascial enhancement extending from the tumor margin with more than 2 mm thickness on postcontrast T1WI
- Observed in undifferentiated pleomorphic sarcoma, myxofibrosarcoma, and nodular fasciitis

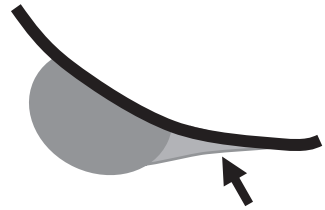

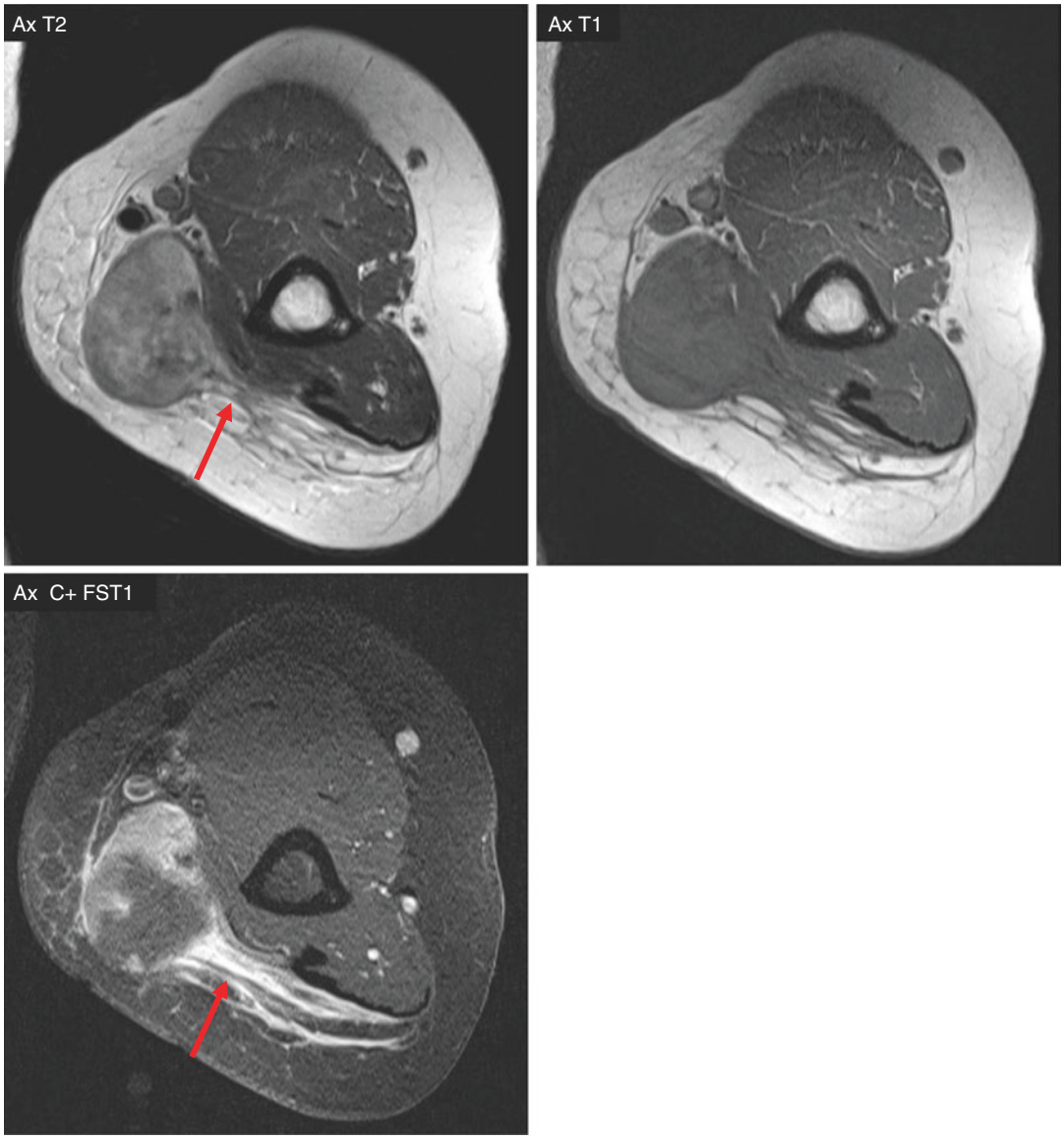

Fig. 18.16

18.17 Target Sign

- On T2WI
- Central area of low signal intensity: histologically fibrocollagenous tissue in the tumor's core
- Surrounding area of high signal intensity: more myxomatous tissue
- Seen in peripheral nerve sheath tumors (neurofibroma, schwannoma)

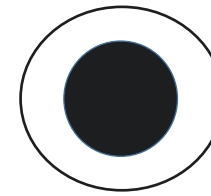

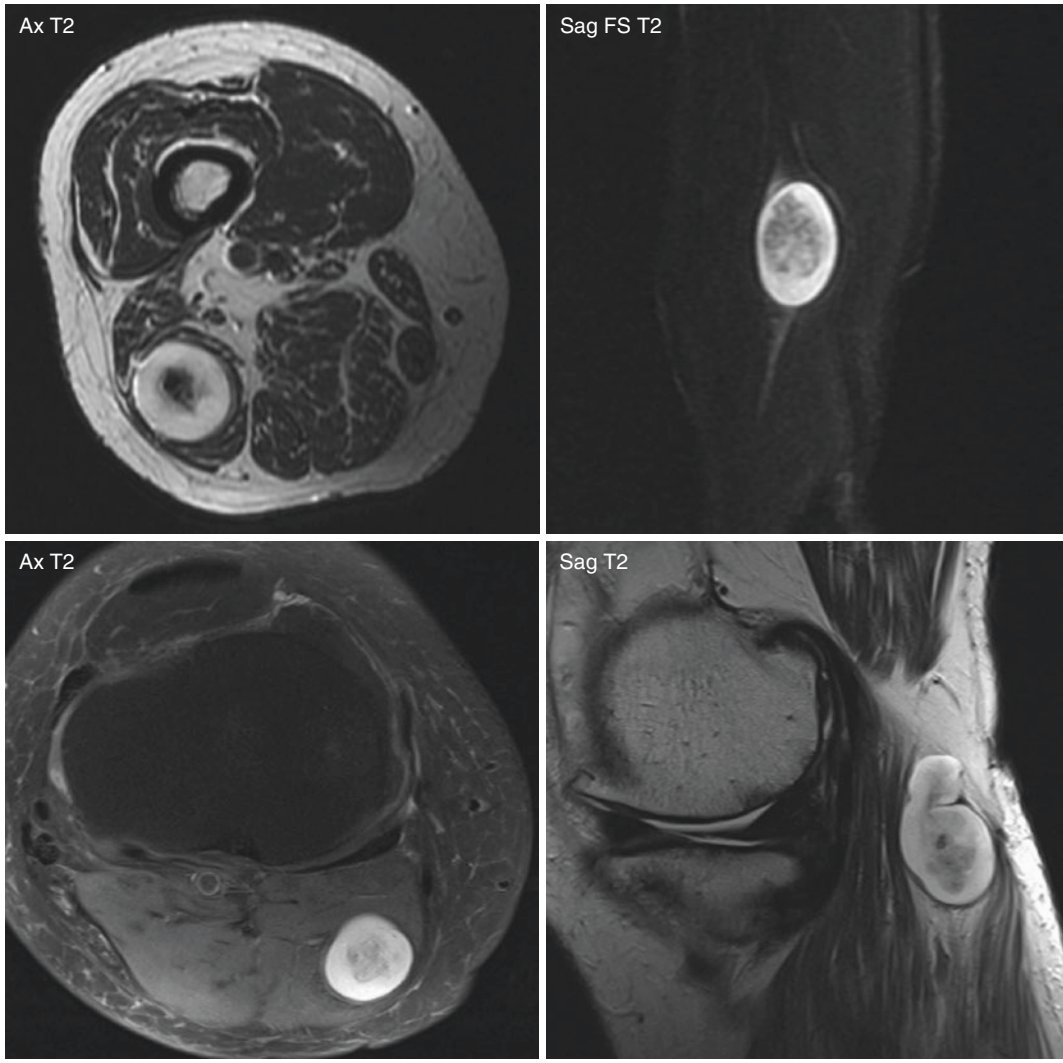

Fig. 18.17

18.18 Three Stripes Sign

- Three strips, an inner stripe of low signal intensity and outer stripes of high signal intensity on T2WI and postcontrast FS T1WI
- Reversed locations of black and white on US
- Seen in sarcoidosis

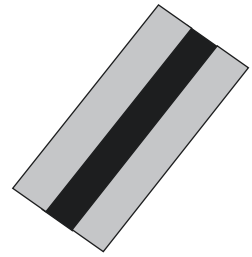

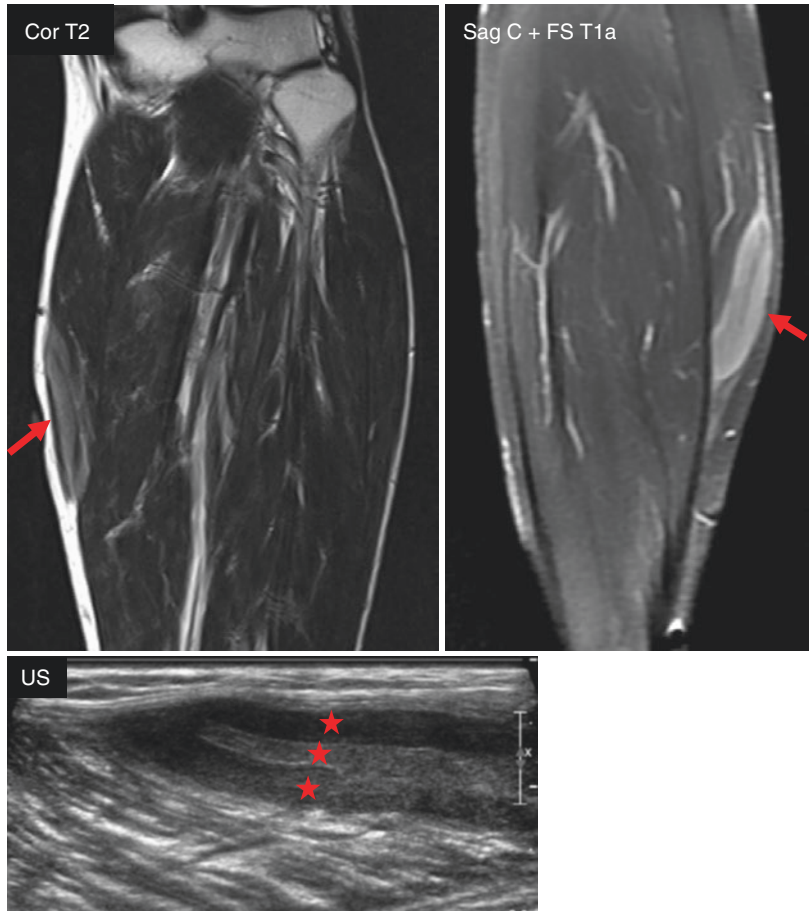

Fig. 18.18

18.19 Triple Signal Sign

- Areas of high, intermediate, and low signal intensity (SI) on T2WIs
- Low SI: calcified, hemorrhagic, or fibrotic collagenized regions
- Intermediate SI: solid cellular elements
- High SI: hemorrhage or necrosis
- Seen in synovial sarcoma

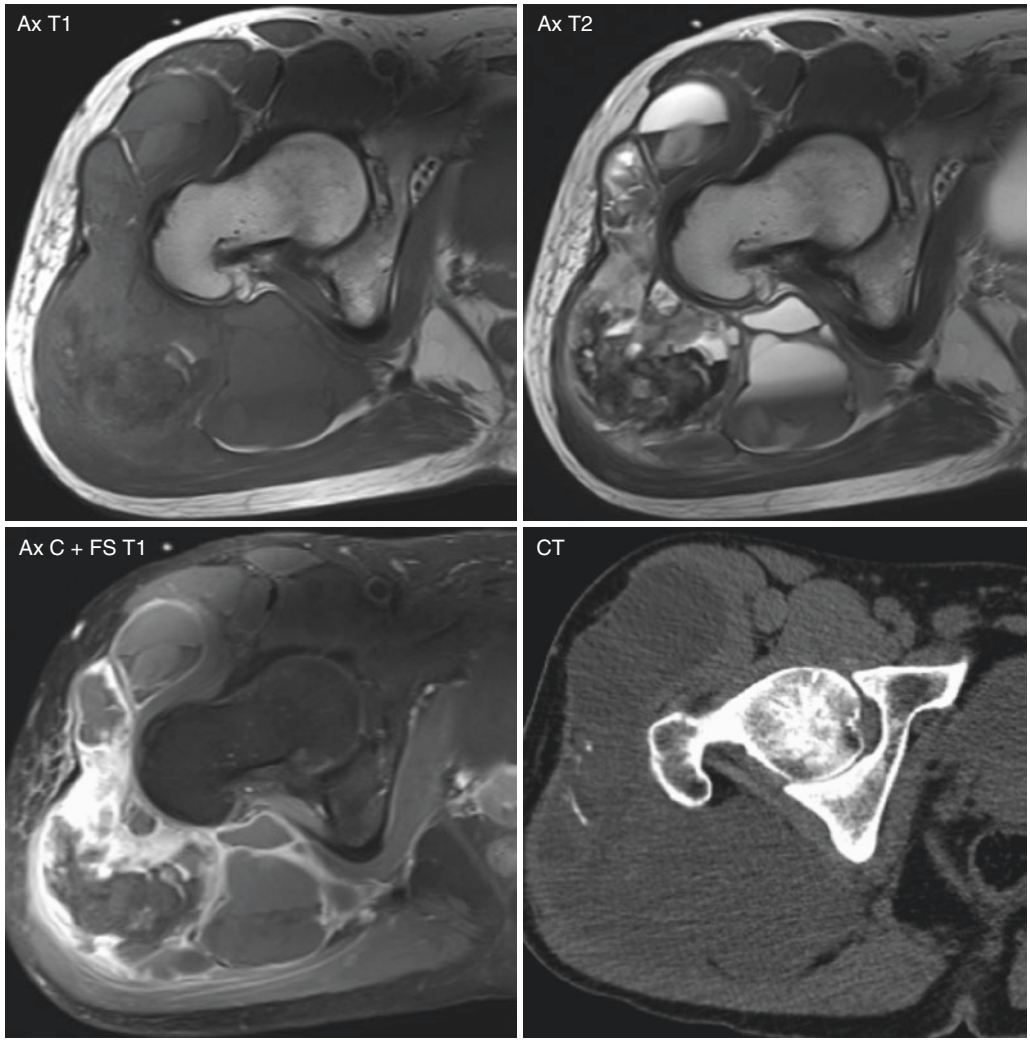

Fig. 18.19

18.20 Zonal Phenomenon

- Peripheral mineralization and non-mineralized center
- Can be better appreciated on CT than MRI
- Seen in myositis ossificans

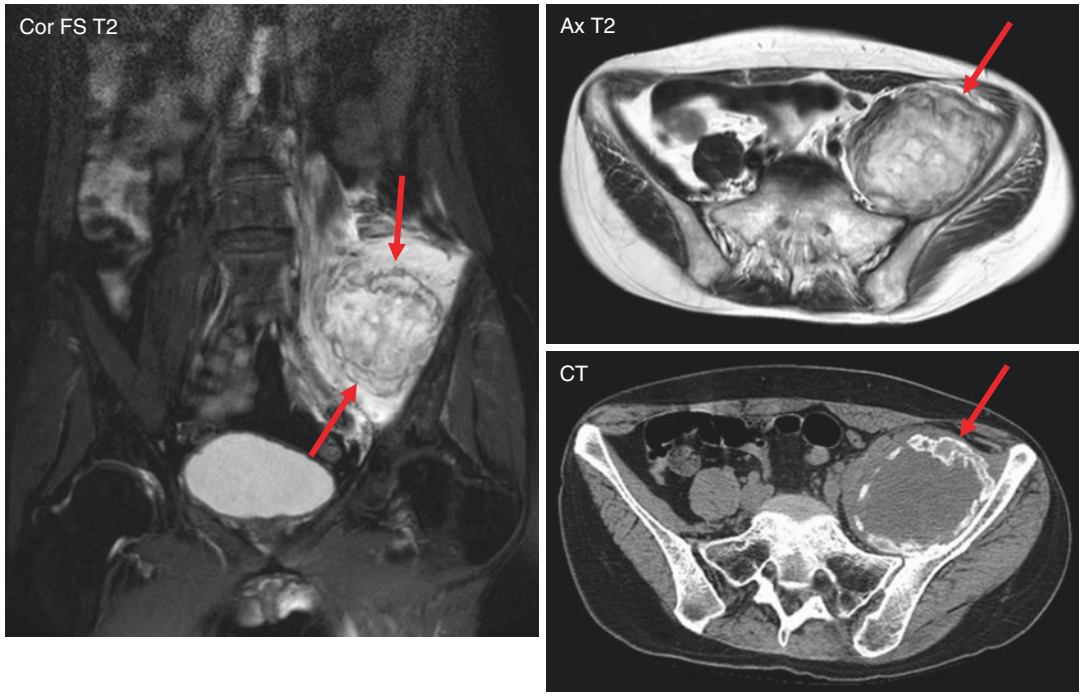

Fig. 18.20

Syndrome-Associated Soft Tissue Tumors

19

Soft tissue neoplasms may be associated with a variety of genetic disorders and malformation syndromes, especially when they arise in children, adolescents, and early adulthood. A summary of syndromes, associated soft tissue tumors, which are uncommon, but not rare, is shown in Table 19.1.

Table 19.1 Syndromes and associated soft tissue tumors

Syndrome	Soft tissue tumors	Principal features
Kasabach-Merritt syndrome	Kaposiform hemangioendothelioma Infantile hemangioma Tuft angioma	Microangiopathic hemolytic anemia Thrombocytopenia
Maffucci syndrome	Hemangioma Lymphangioma Epithelioid hemangioendothelioma	Enchondromas Chondrosarcoma
Klippel-Trenaunay syndrome	Venous or lymphatic malformation	Nevus inflammeus Hypertrophy of associated bone and soft tissue
Mazabraud syndrome	Intramuscular myxoma	Fibrous dysplasia
Neurofibromatosis type 1	Neurofibromas MPNST	Café au lait spots Lisch nodules
Neurofibromatosis type 2	Schwannoma Neurofibroma Rarely perineurioma	Meningioma Astrocytoma
Schwannomatosis	Schwannomas	Without vestibular nerve involvement
Carney complex	Melanotic schwannoma Myxoma	Involvement of multiple endocrine glands Pigmented lesions of the skin and mucosa
Familial hypercholesterolemia	Xanthomas	High cholesterol and LDL level

H.S. Kang et al., *Oncologic Imaging: Soft Tissue Tumors*, DOI 10.1007/978-981-287-718-5_19

19.1 Kasabach-Merritt Syndrome

- Rapidly growing vascular tumor: kaposiform hemangioendothelioma, infantile hemangioma, tuft angioma
- Thrombocytopenia
- Consumptive coagulopathy

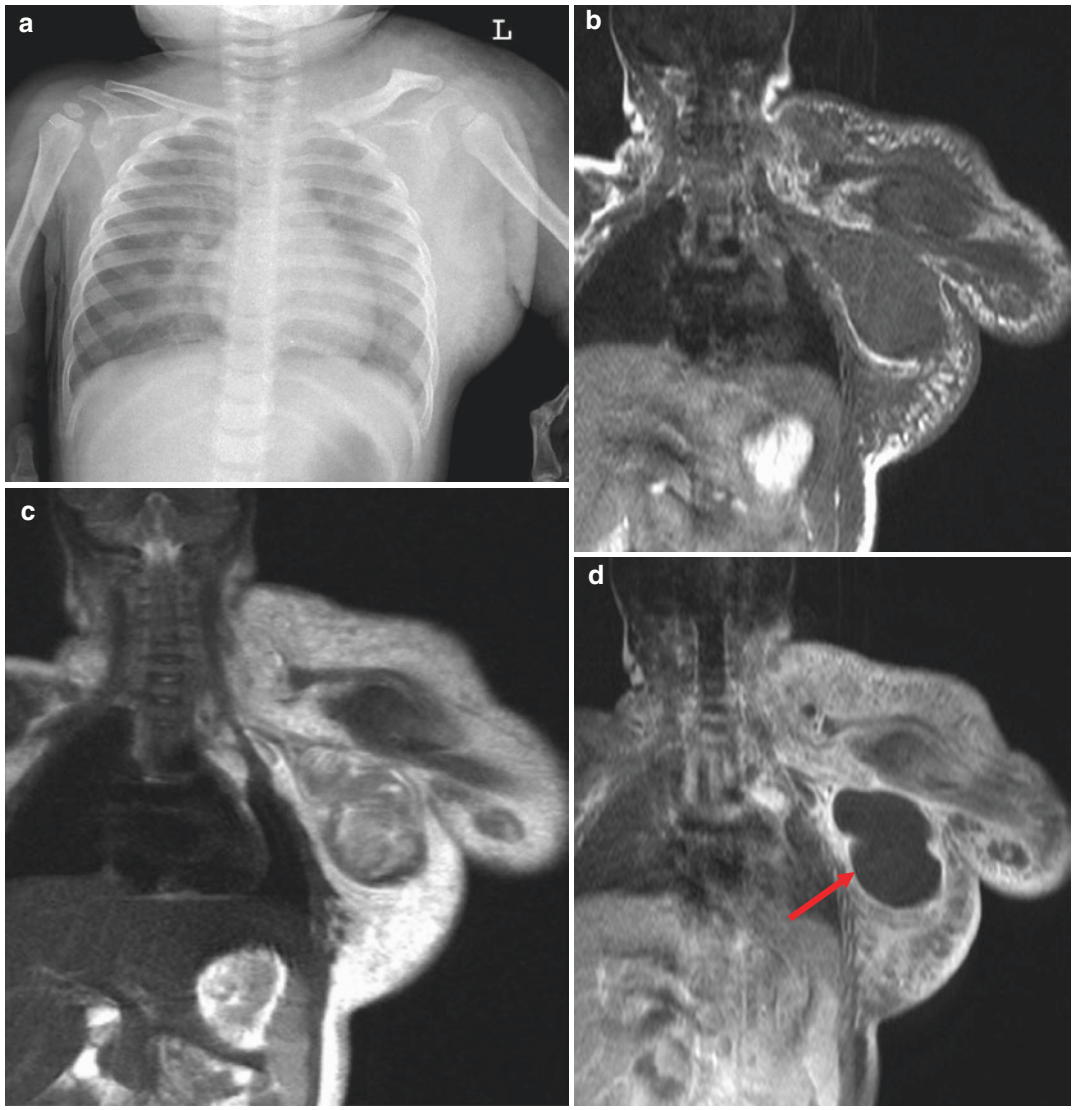

Fig. 19.1 Kasabach-Merritt syndrome. Infantogram (**a**) shows a huge soft tissue mass or hypertrophy in the left shoulder. Coronal T1WI (**b**), T2WI (**c**), and postcontrast FS T1WI (**d**) show diffuse hemangiomatous involvement of the soft tissues in the left shoulder, axilla, and upper arm. There is a non-enhancing component (*arrow* in **d**) consistent with lymphangioma in the left axilla. MR angiography (**e**) better demonstrates the extent of the enhancing hemangiomatous lesions (*arrows*). Seven years later, radiograph (**f**) and coronal postcontrast FS T1WI (**g**) show a marked decrease in extent of the soft tissue lesions. The patient had received radiation therapy

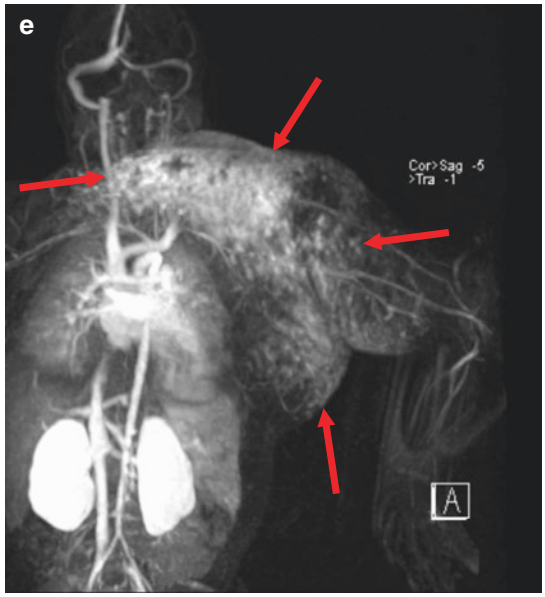

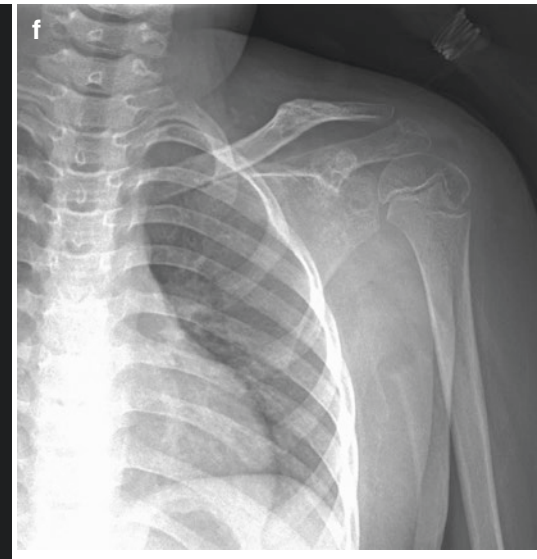

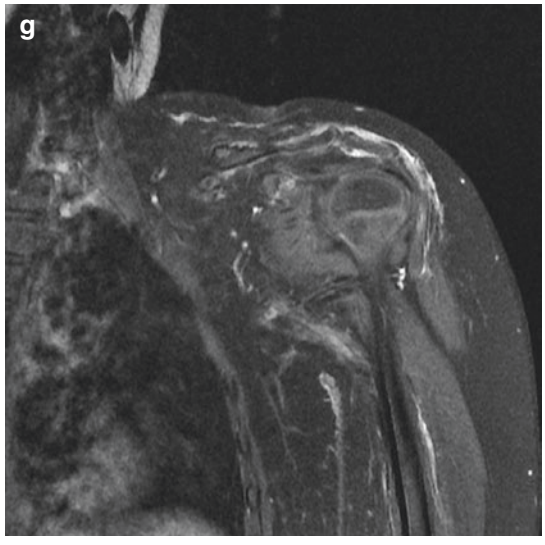

Fig. 19.1 (continued)

19.2 Maffucci Syndrome

- Congenital, nonhereditary mesodermal dysplasia
- Multiple enchondromas
- Soft tissue vascular lesions: cavernous or capillary hemangiomas, lymphangiomas, epithelioid hemangioendotheliomas

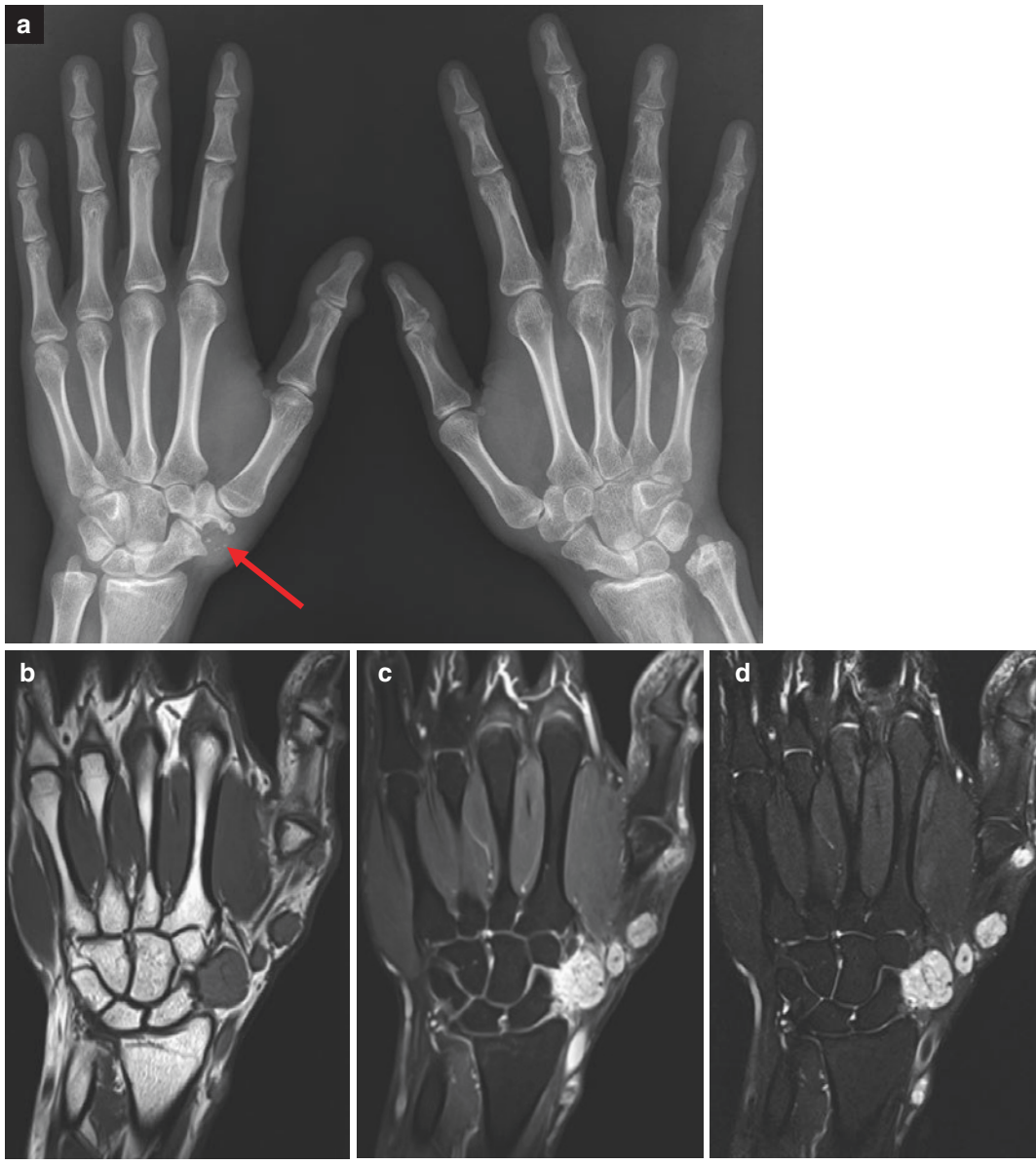

Fig. 19.2 Maffucci syndrome. AP radiograph of both hands (**a**) shows multiple enchondromas in the left 3rd–5th fingers and the left distal radius and ulna. There are multiple soft tissue masses in the right wrist and thumb, one (*arrow*) of which has multiple calcific foci and erodes the trapezium and scaphoid. Coronal T1WI (**b**), FS T2WI (**c**), and postcontrast FS T1WI (**d**) show multiple soft tissue hemangiomas in the right wrist and thumb. Lateral radiograph of the left knee (**e**) shows multiple channel-like enchondromas in the left femur and tibia. Sagittal (**f**) and coronal (**g**) FS T2WIs show multiple enchondromas of the bone and soft tissue hemangiomas (*arrows*)

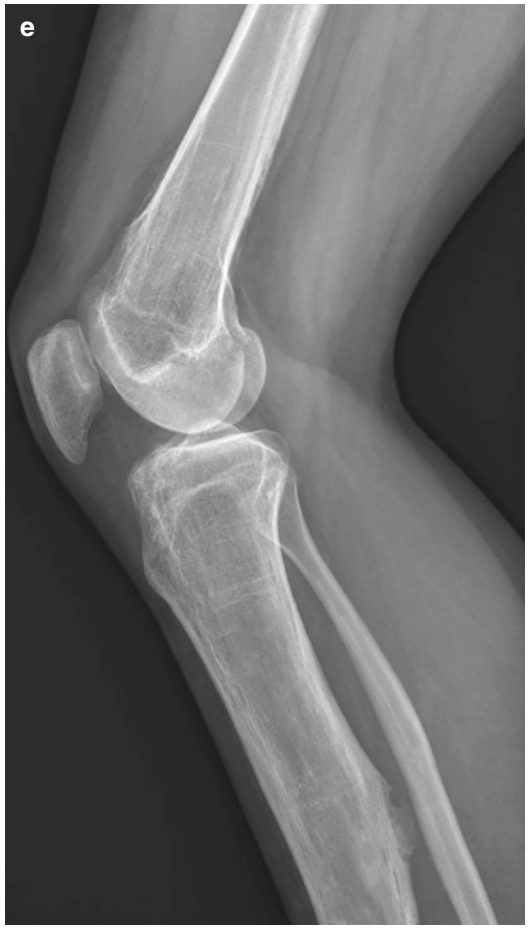

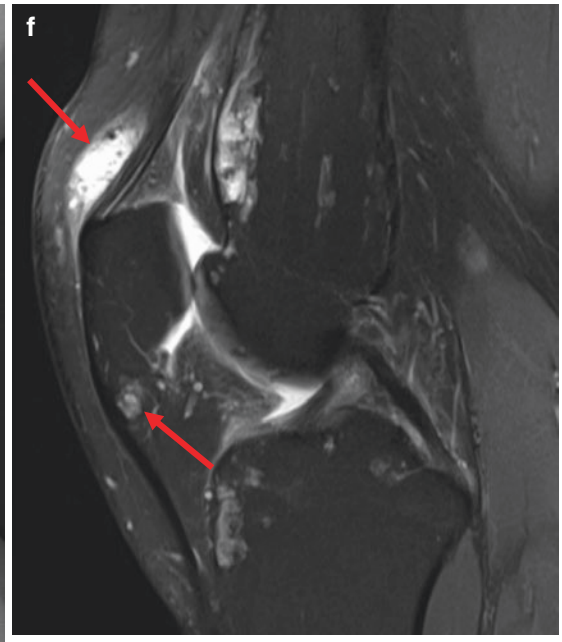

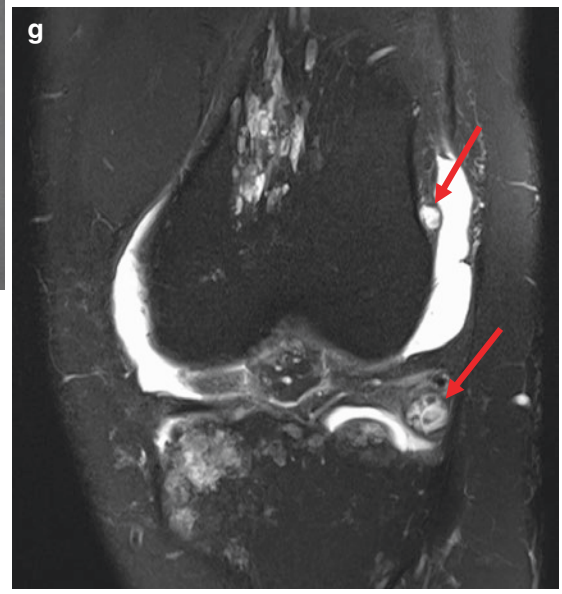

Fig. 19.2 (continued)

19.3 Klippel-Trenaunay Syndrome

- Nevus inflammeus
- Venous or lymphatic malformations
- Soft tissue hypertrophy

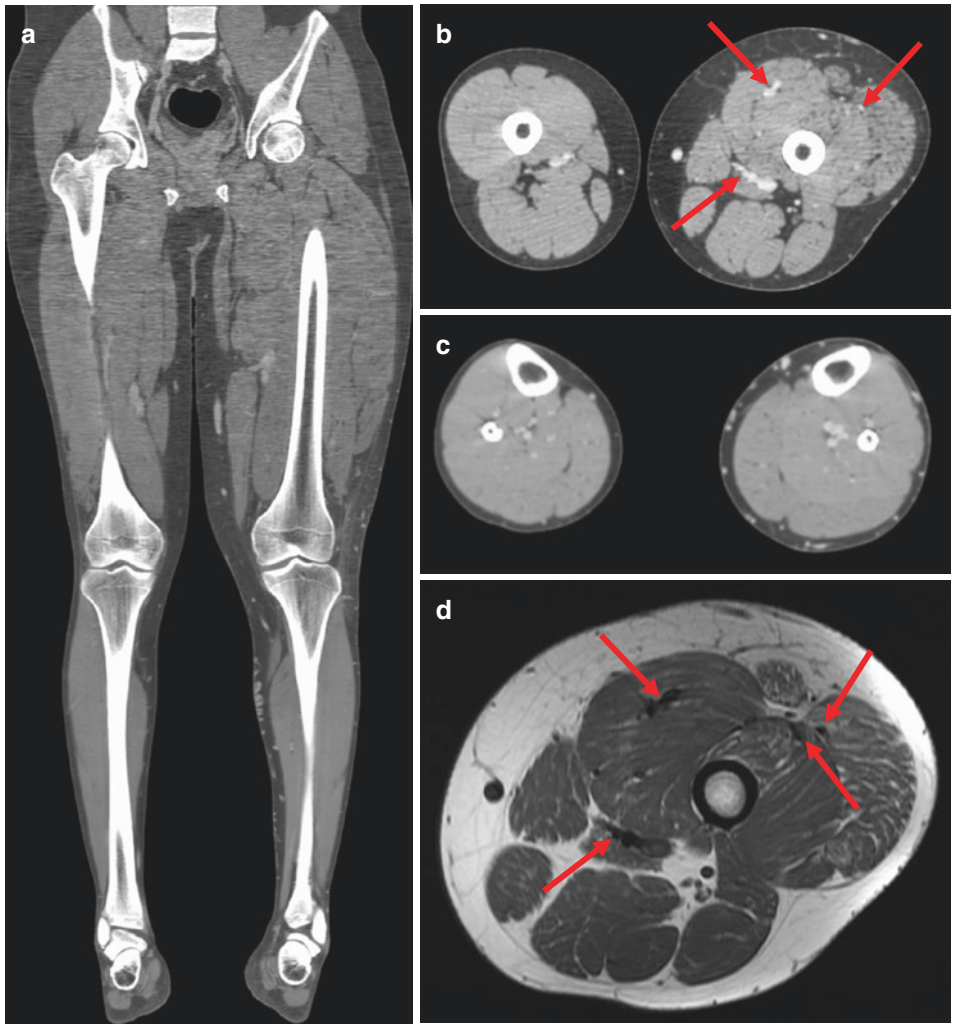

Fig. 19.3 Klippel-Trenaunay syndrome. Coronal (**a**) and axial (**b**, **c**) CT images show hypertrophied soft tissues in the left lower extremity. There are multiple varicose veins and intramuscular venous malformation (*arrows*) in the left lower extremity. Axial T1WI (**d**) demonstrates subcutaneous and muscular hypertrophies in the left thigh along with intramuscular venous malformation (*arrow*)

19.4 Mazabraud Syndrome

- Fibrous dysplasia (usually polyostotic)
- Multiple soft tissue myxomas

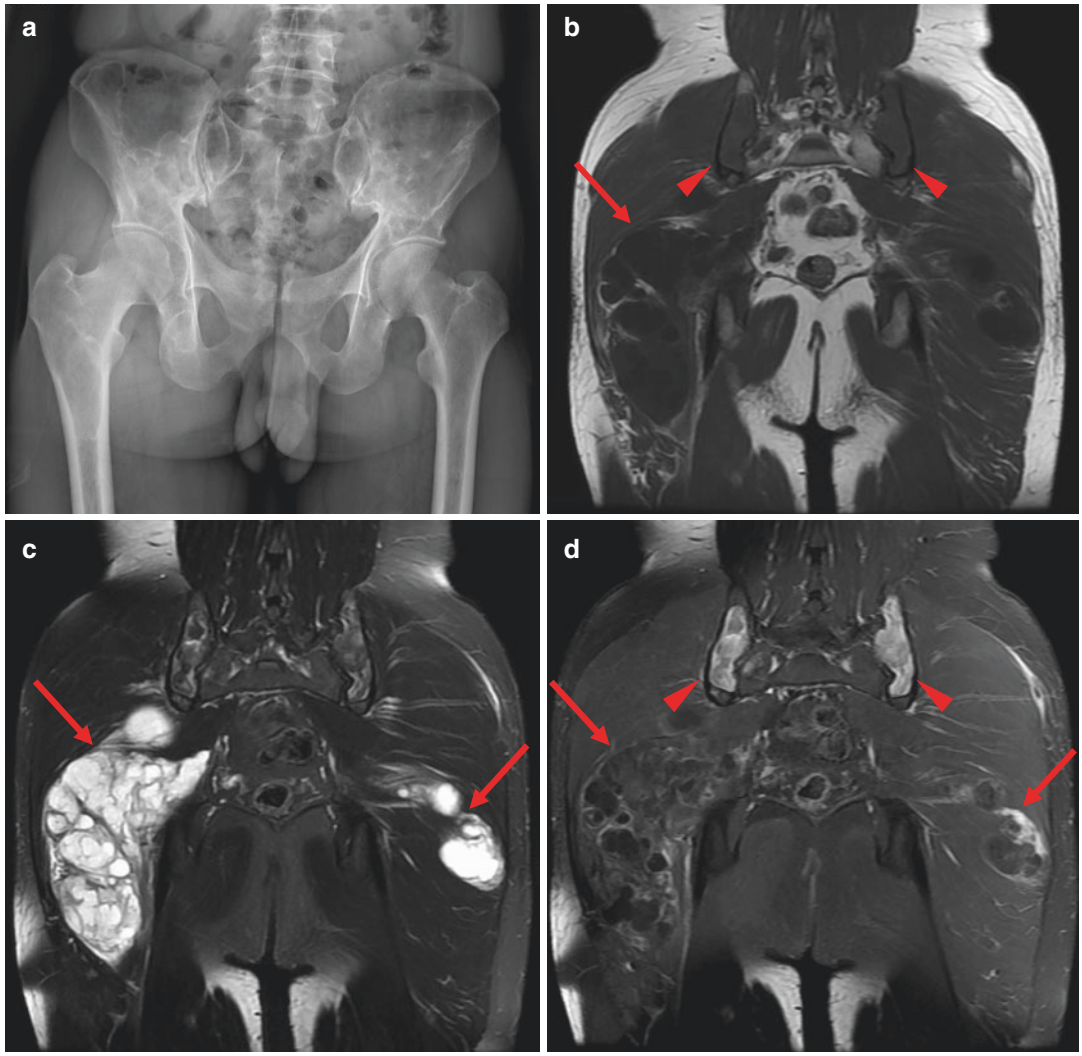

Fig. 19.4 Mazabraud syndrome. AP radiograph of the pelvis (**a**) shows multiple fibrous dysplasia in the pelvis and the right femur. Coronal T1WI (**b**), T2WI (**c**), and postcontrast FS T1WI (**d**) show multilobulated intramuscular myxomas in the both buttocks (*arrows*) and fibrous dysplasia in both ilia (*arrowheads*)

19.5 Neurofibromatosis Type 1

- Café au lait spots
- Iris hamartomas (Lisch nodules)
- Associated soft tissue tumors: neurofibomas with increased risk of MPNST (malignant peripheral nerve sheath tumor)
- Musculoskeletal manifestation
  - Plexiform neurofibromas
  - Kyphoscoliosis
  - Vertebral scalloping, enlarged neural foramina: due to dural ectasia or neurofibromas
  - Deural ectasia
  - Ribbon rib deformity, rib notching, and dysplasia
  - Cortical thinning, erosive defects, sclerosis, and periosteal proliferation due to extrinsic pressures
  - Pseudoarthrosis and bowing: related to mesodermal dysplasia

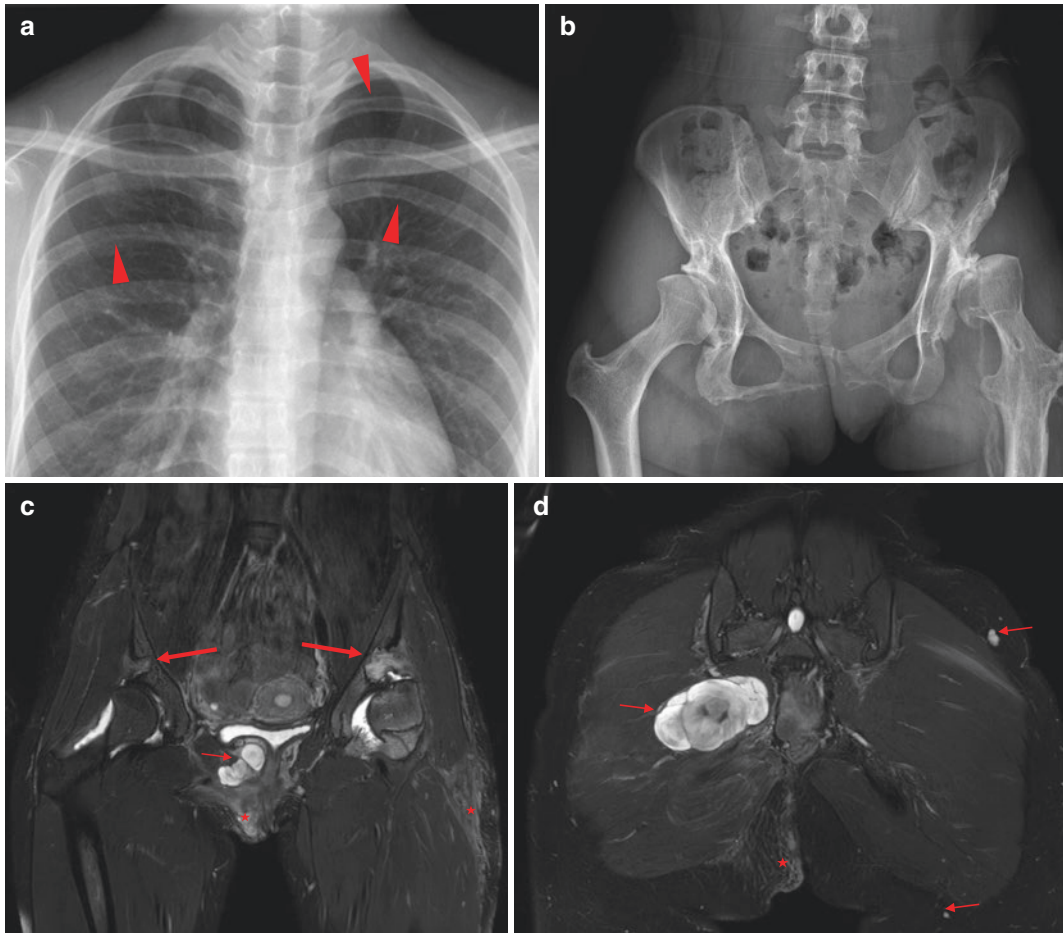

Fig. 19.5 Neurofibromatosis type 1. Chest radiograph (**a**) shows several rib notching or mild ribbon rib deformity (*arrowheads*). AP radiograph of the pelvis (**b**) demonstrates marked deformities of pelvic bones and both femora such as cortical thinning, erosive defects, sclerosis, and periosteal proliferation. Coronal FS T2WIs (**c**, **d**) show neurofibromas (*arrows*) with marked pressure erosions onto the neighboring iliac bones. Both femoral neck deformities are not associated with neurofibomas but related to the skeletal dysplasia. Multiple, variable-sized, circumscribed, localized neurofibromas (*thin arrows*) are noted in the subcutaneous tissue, muscle, and fascial planes. In addition, infiltrative, diffuse neurofibromas (*stars*) involving multicompartments are shown

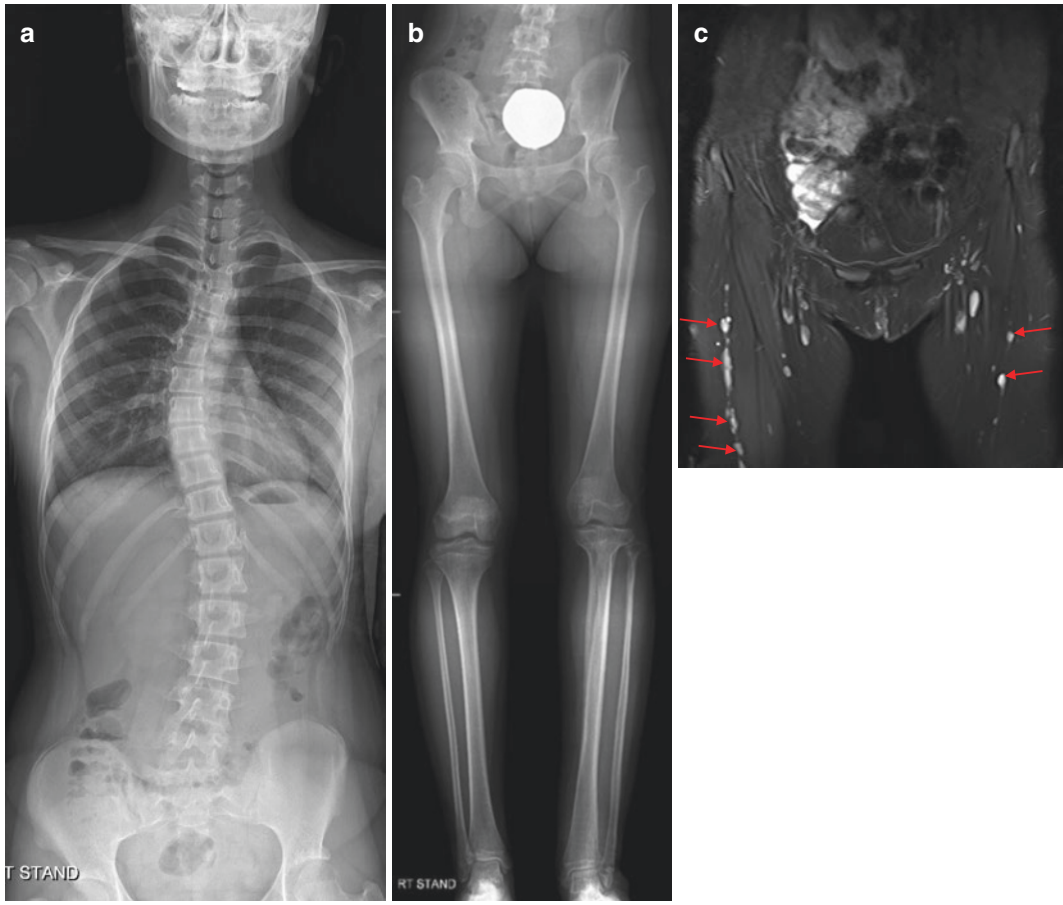

Fig. 19.6 Neurofibromatosis type 1. Whole spine standing AP radiograph (**a**) shows a thoracic scoliosis. Teleradiograph of the lower extremity (**b**) reveals dysplastic left proximal tibia with irregular thick cortex and widening of the affected tibia. Coronal FS T2WI (**c**) shows multiple, circumscribed, oval hyperintense soft tissue lesions (*thin arrows*) along the nerve courses in both thighs. Sagittal FS T2WI (**d**) of the lower leg shows a typical appearance, diffuse thickened nerve with nodularity, of plexiform neurofibroma affecting the common peroneal nerve and its branches. The target sign with low signal centrally and high signal intensity peripherally is seen in numerous lesions. Two years later, he complained of local pain and swelling at the proximal tibial level. Follow-up sagittal T2WI (**e**) shows interval development of a large subcutaneous mass (*star*). The mass has isointense to muscle on T1WI (**f**) and heterogeneous hyperintensity on T2WI (**g**) with inhomogeneous enhancement on postcontrast FS T1WI (**h**). These findings represent malignant transformation

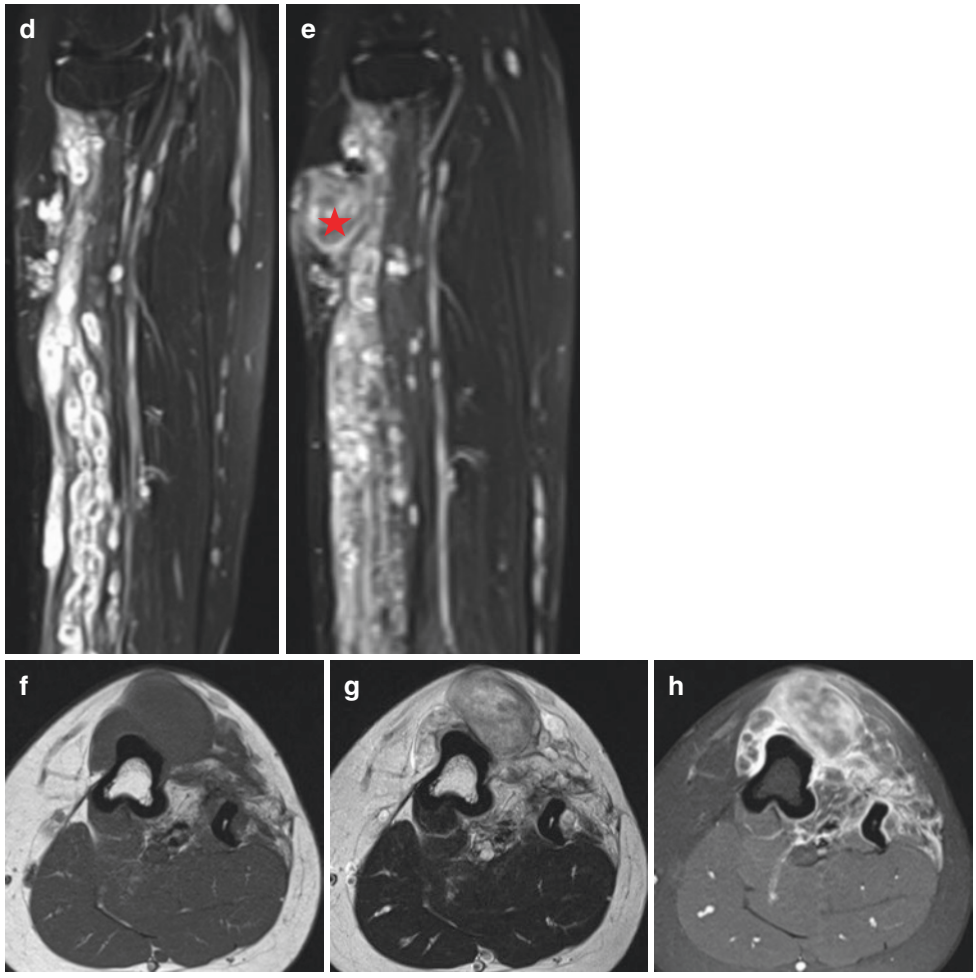

Fig. 19.6 (continued)

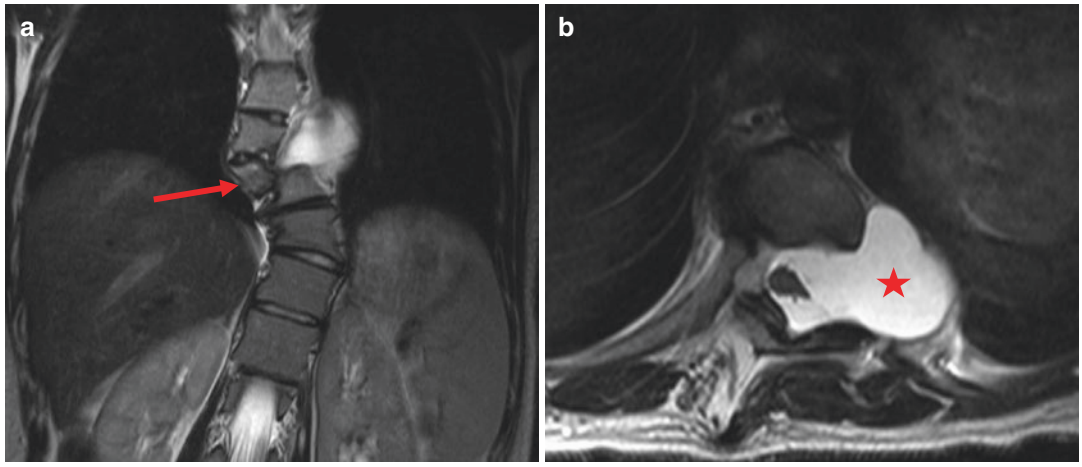

Fig. 19.7 Neurofibromatosis type 1. Coronal T2WI of the thoracic spine (**a**) shows the scoliosis with hemivertebra (*arrow*). Axial T2WI (**b**) demonstrates the dilated dural sac (dural ectasia) with direct extension into the paravertebral space (*star*) through the marked widened left neural foramen

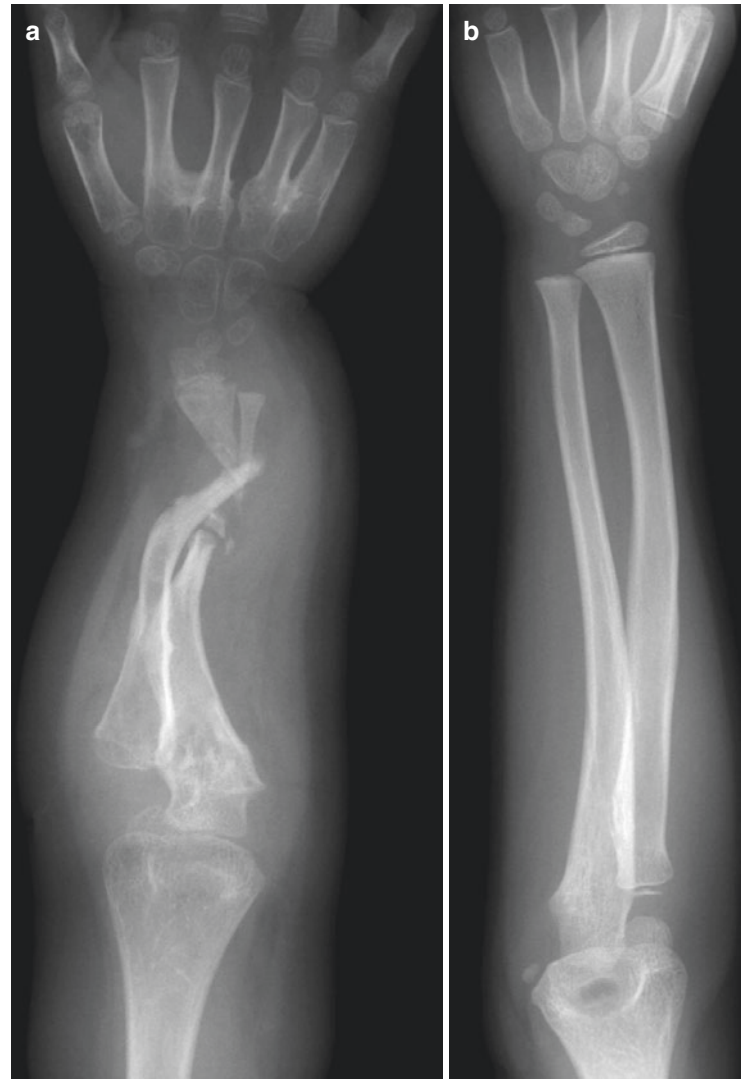

Fig. 19.8 Neurofibromatosis type 1. AP radiograph of the right forearm (**a**) shows a dysplastic appearance of the affected radius and ulna with narrowing, sclerosis, and obliteration of the medullary canal (pseudoarthrosis). AP radiograph of the left forearm (**b**) for comparison

19.6 Neurofibromatosis Type 2

- Bilateral acoustic schwannomas and other schwannomas
- Meningiomas and other CNS tumors

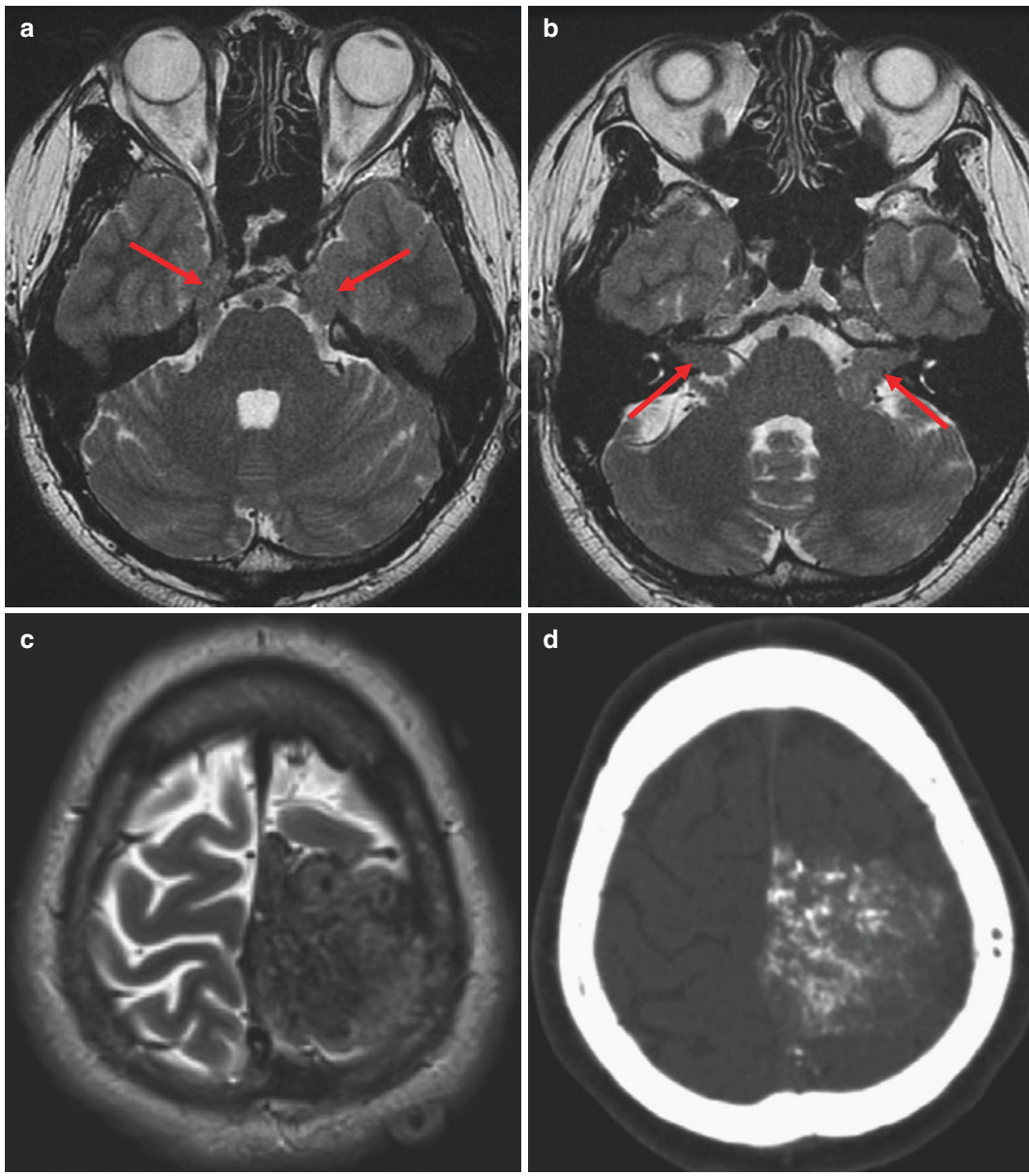

Fig. 19.9 Neurofibromatosis type 2. Axial T2WIs of the brain shows bilateral trigeminal (**a**) and acoustic (**b**) schwannomas (*arrows*). T2WI (**c**) and CT (**d**) show a large calcifying left meningioma abutting the falx. Sagittal (**e**) and axial (**h**) T2WIs demonstrate a extradural multilobulating, circumscribed soft tissue mass (*star*) with pressure erosions, and resultant neural foraminal widening, which represents a schwannoma. Sagittal (**f**, **g**) and axial (**i**) T2WIs reveal two dark signal intradural extramedullary masses (*arrows*) at the level of C1 and T1/2, respectively, which are pressing the spinal cord and keep in with calcified meningiomas. In addition, there are numerous tiny leptomeningeal nodules (*thin arrows*) along the cord surface and cauda equina, representing schwannomatosis

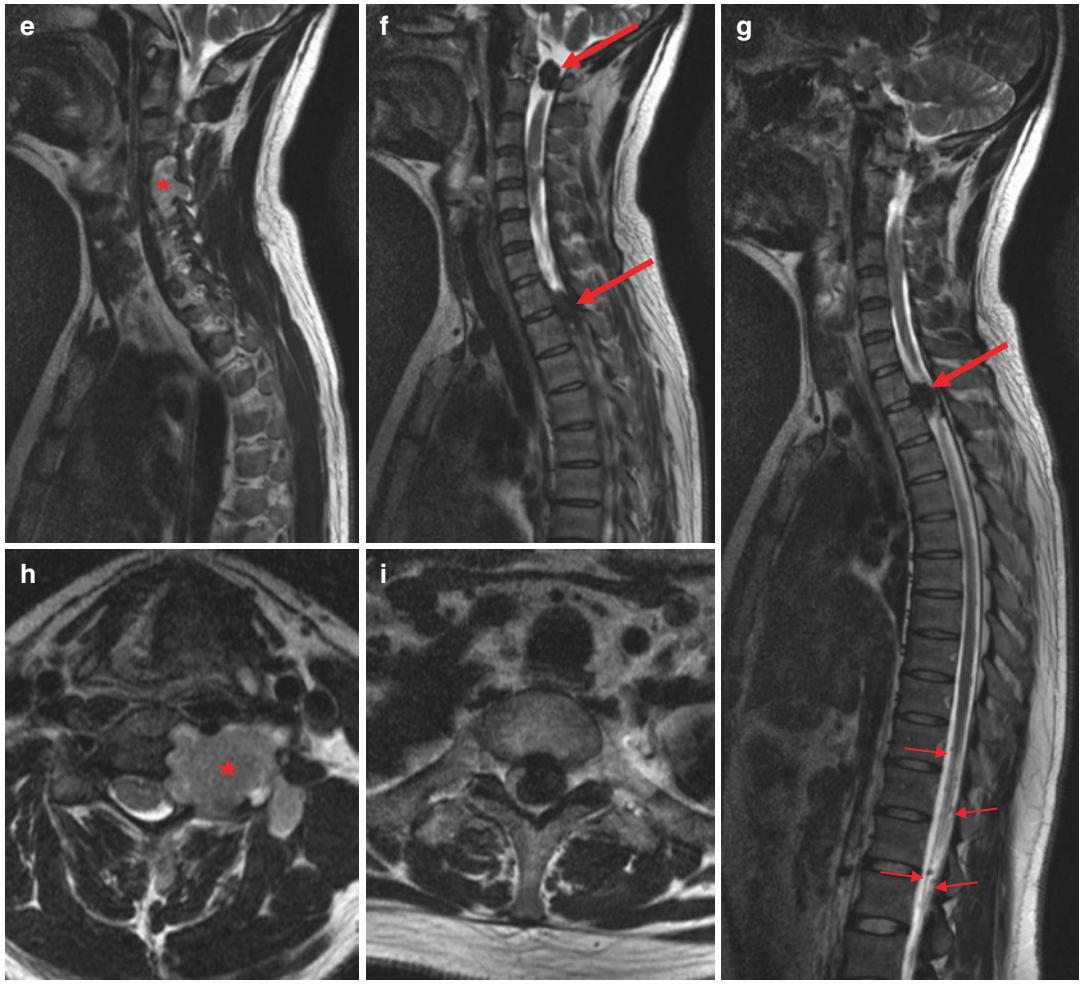

Fig. 19.9 (continued)

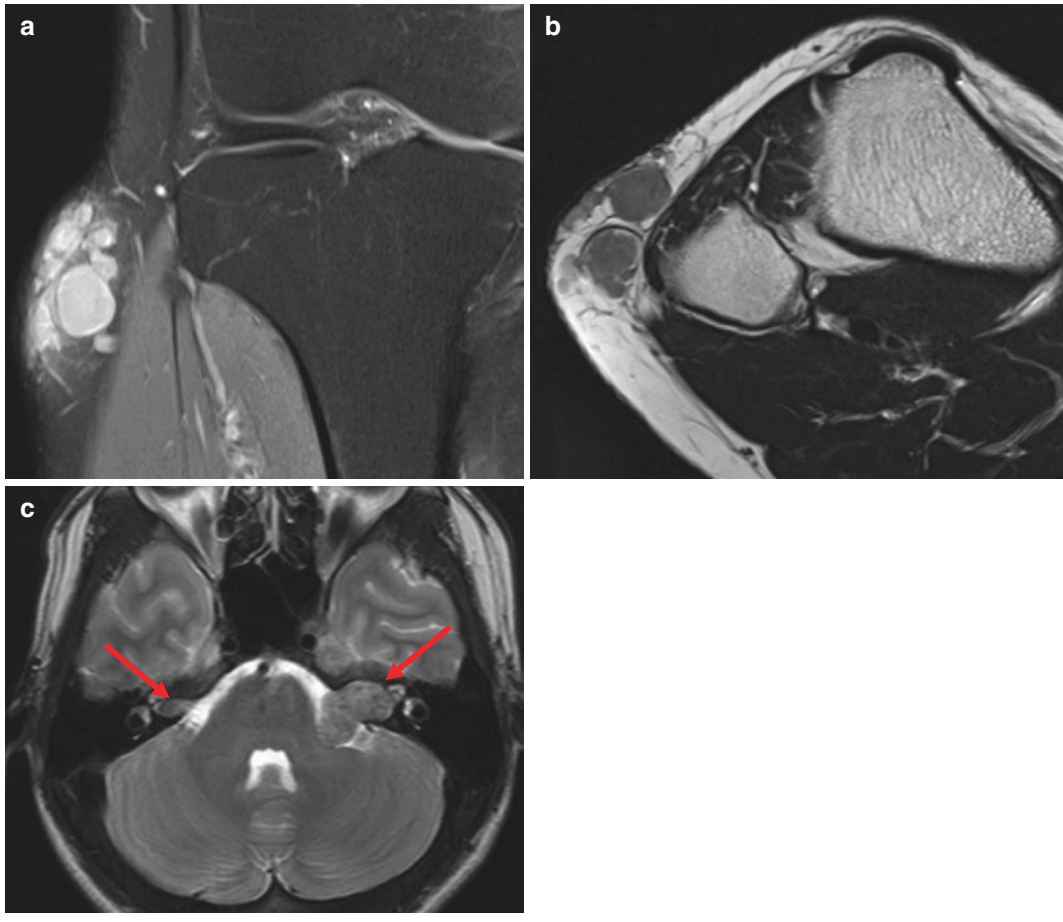

Fig. 19.10 Neurofibromatosis type 2. Coronal FS (**a**) and axial (**b**) T2WIs of the knee show aggregation of the variable-sized, circumscribed soft tissue lesions affecting the skin and subcutaneous tissue, which has central intermediate signal area and thin peripheral hyperintense rim, respectively. Brain MRI (**c**) of the same patient shows bilateral acoustic schwannomas (*arrows*)

19.7 Schwannomatosis

- Known as neurilemmomatosis
- Multiple schwannomas without vestibular nerve involvement or meningioma
- Only 15%: familial
- Recognized most often in people over the age of 30

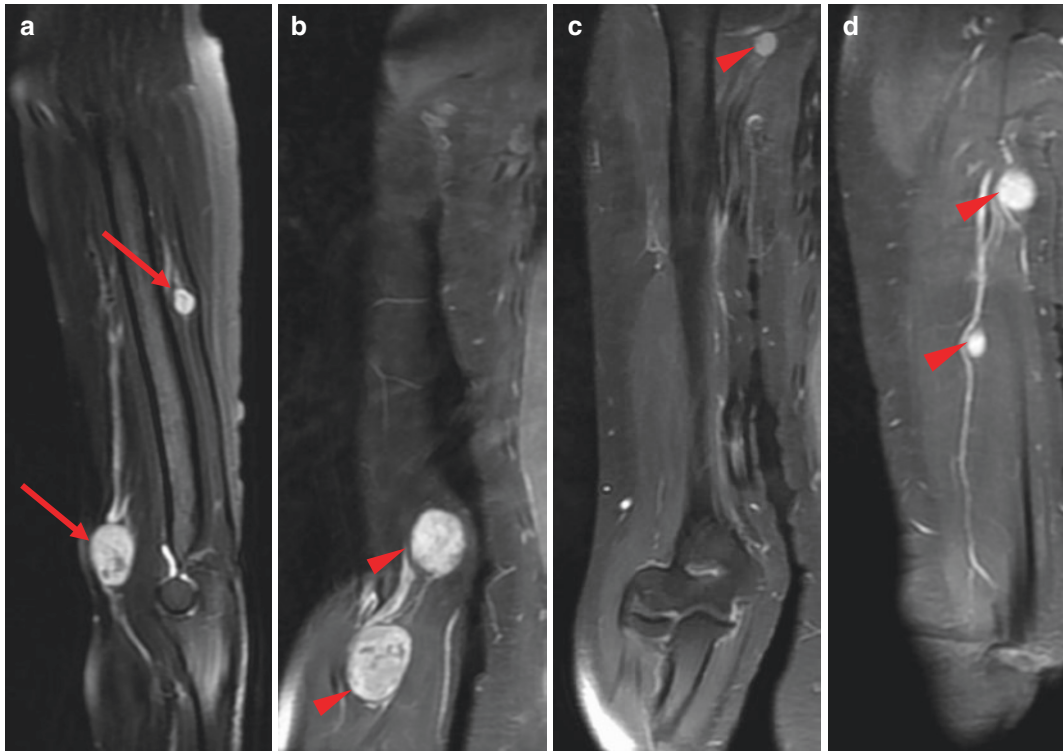

Fig. 19.11 Schwannomatosis. Sagittal FS T2WI (**a**) of right upper arm reveals two circumscribed oval soft tissue masses (*arrows*) with target and string signs. Coronal postcontrast FS T1WIs (**b**, **c**, **d**) show multiple inhomogeneous intense enhancing soft tissue lesions (*arrowheads*) along the nerve course. Two of those were surgically confirmed as schwannomas

19.8 Carney Complex

- Multiple neoplasia syndrome
- Involvement of multiple endocrine glands
- Pigmented lesions of the skin and mucosa
- Associated soft tissue tumors: melanotic schwannomas, myxomas

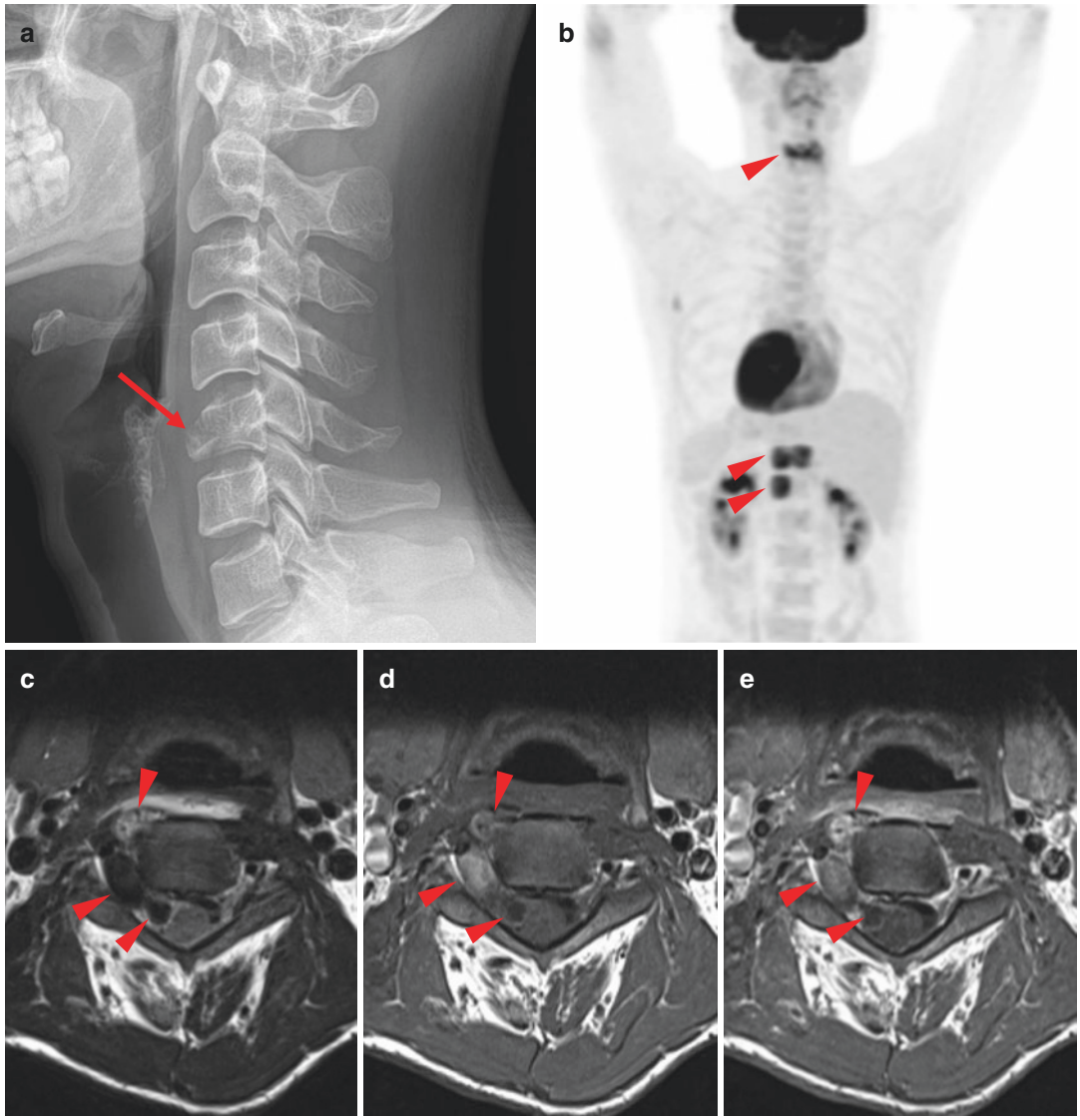

Fig. 19.12 Carney complex. A 33-year-old male has the history of Cushing syndrome, s/p adrenalectomy, and cardiac myxoma. Lateral radiograph of the cervical spine (**a**) reveals an osteolytic lesion (*arrow*) affecting C5 vertebral body with pathologic fracture. PET (**b**) demonstrates several hypermetabolic bony lesions (*arrowheads*) at the cervical and thoracolumbar junction, suggesting bone metastases. Axial MRI of the cervical spine shows a multilobulating soft tissue mass (*arrowheads*) C3/4 right neural foramen with direct extension into intradural space and mild cord compression, which has dark signal intensity on T2WI (**c**), hyperintensity on T1WI (**d**), and mild heterogeneous enhancement such as rim enhancement on postcontrast FS T1WI (**e**). Hyperintensity on T1WI represents melanin deposition. Sagittal MRI shows the C5 lesion to have the same signal characteristics as the above soft tissue mass. Note a smaller intraosseous lesion (*thin arrows*) in C3 spinous process, which shows mildly hypointensity on T2WI (**f**) and T1WI (**g**), and diffuse enhancement on postcontrast FS T1WI (**h**). Reactive prevertebral soft tissue edema (*star*) is shown. CT-guided bone biopsy was performed for T12 vertebral lesion, and then melanotic schwannoma was confirmed. Finally, melanotic schwannoma (*arrowheads*) C3/4 right neural foramen and multiple bone metastases were diagnosed

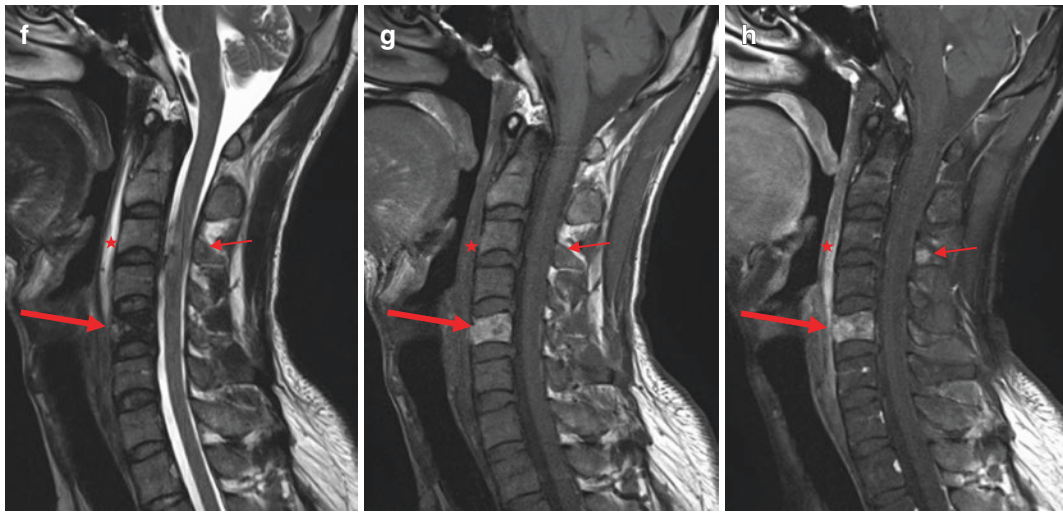

Fig. 19.12 (continued)

19.9 Familial Hypercholesterolemia

- High cholesterol levels, specifically very high levels of low-density lipoprotein (LDL), in the blood
- Yellow deposits of cholesterol-rich fat in the skin, and tendons, particularly the Achilles tendon

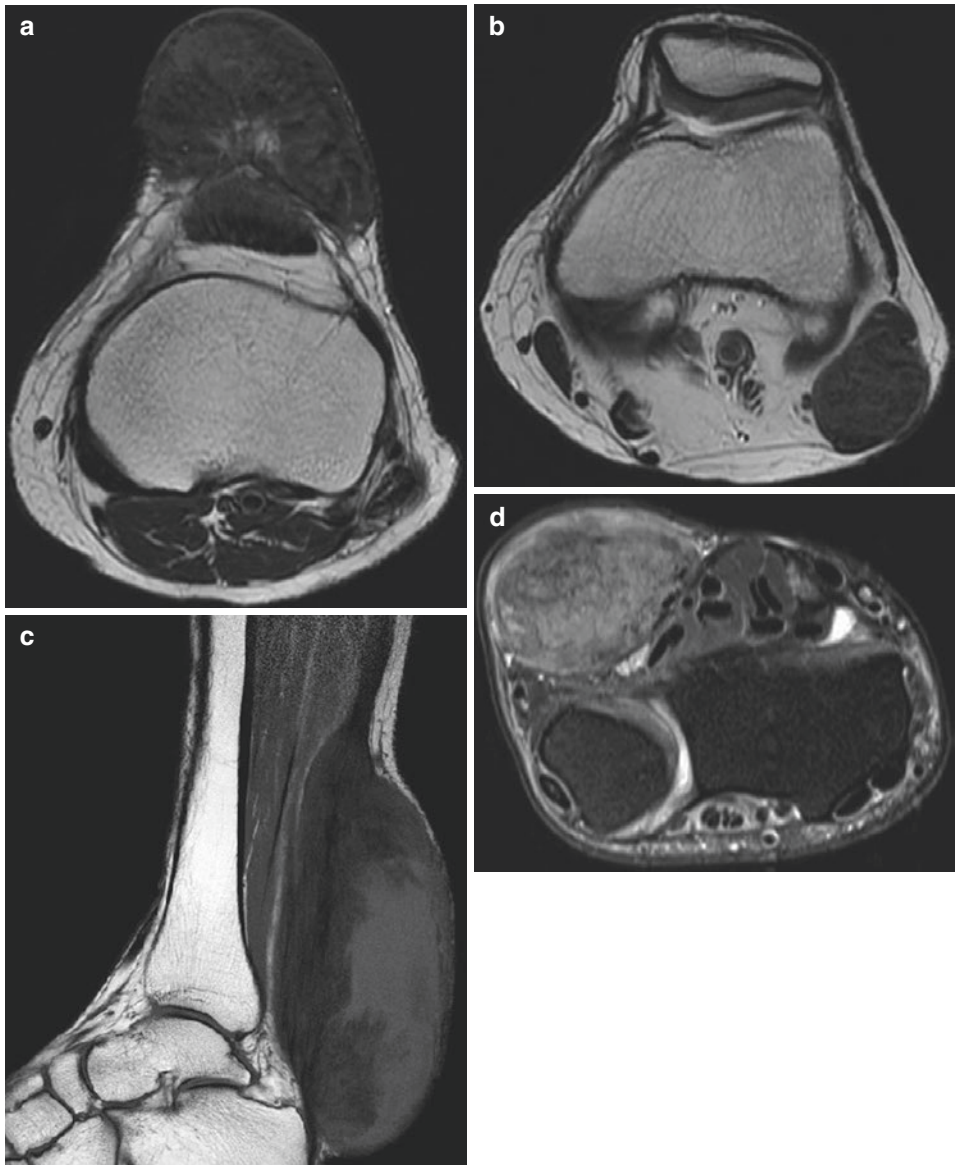

Fig. 19.13 Familial hypercholesterolemia. MR images show hypointense soft tissue masses (tendinous xanthomas) in patellar ligament (**a**), biceps femoris tendon (**b**), Achilles tendon (**c**), and flexor carpi ulnaris (**d**). Axial T2WI (**a**) and US (**e**–**g**) also demonstrate skin and subcutaneous masses (tuberous xanthomas) on the extensor surface of knee (**a**), elbow (**e**), distal forearm (**f**), and finger (**g**)

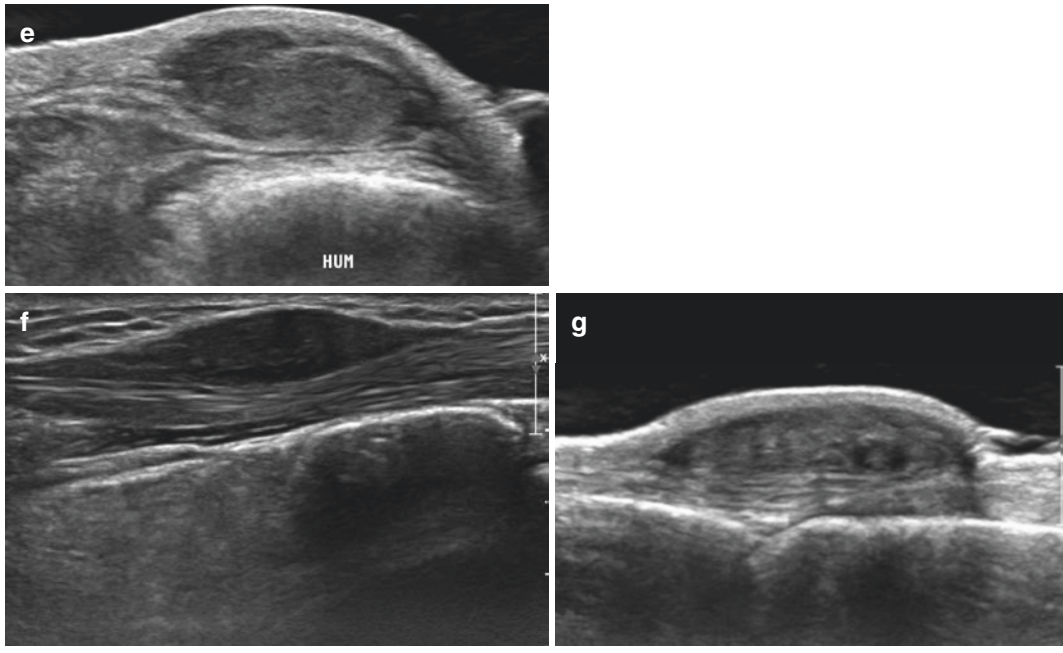

Fig. 19.13 (continued)

Part IV

Drill and Practice

Image Interpretation Session 20

H.S. Kang et al., *Oncologic Imaging: Soft Tissue Tumors*, DOI 10.1007/978-981-287-718-5_20

20.1 Quiz

A 54-year-old male, left posterior upper arm mass

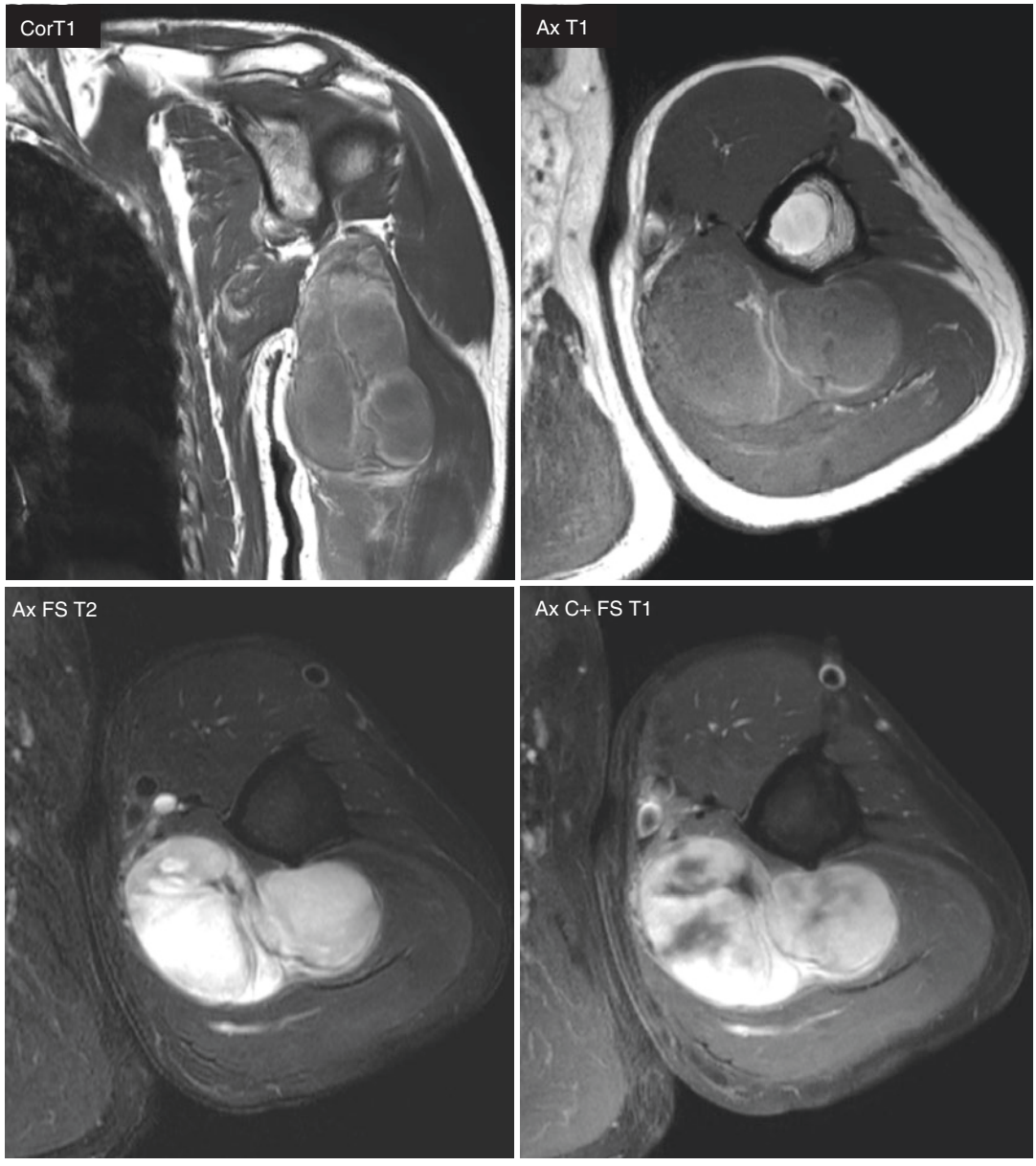

Fig. 20.1

20.1 Answer

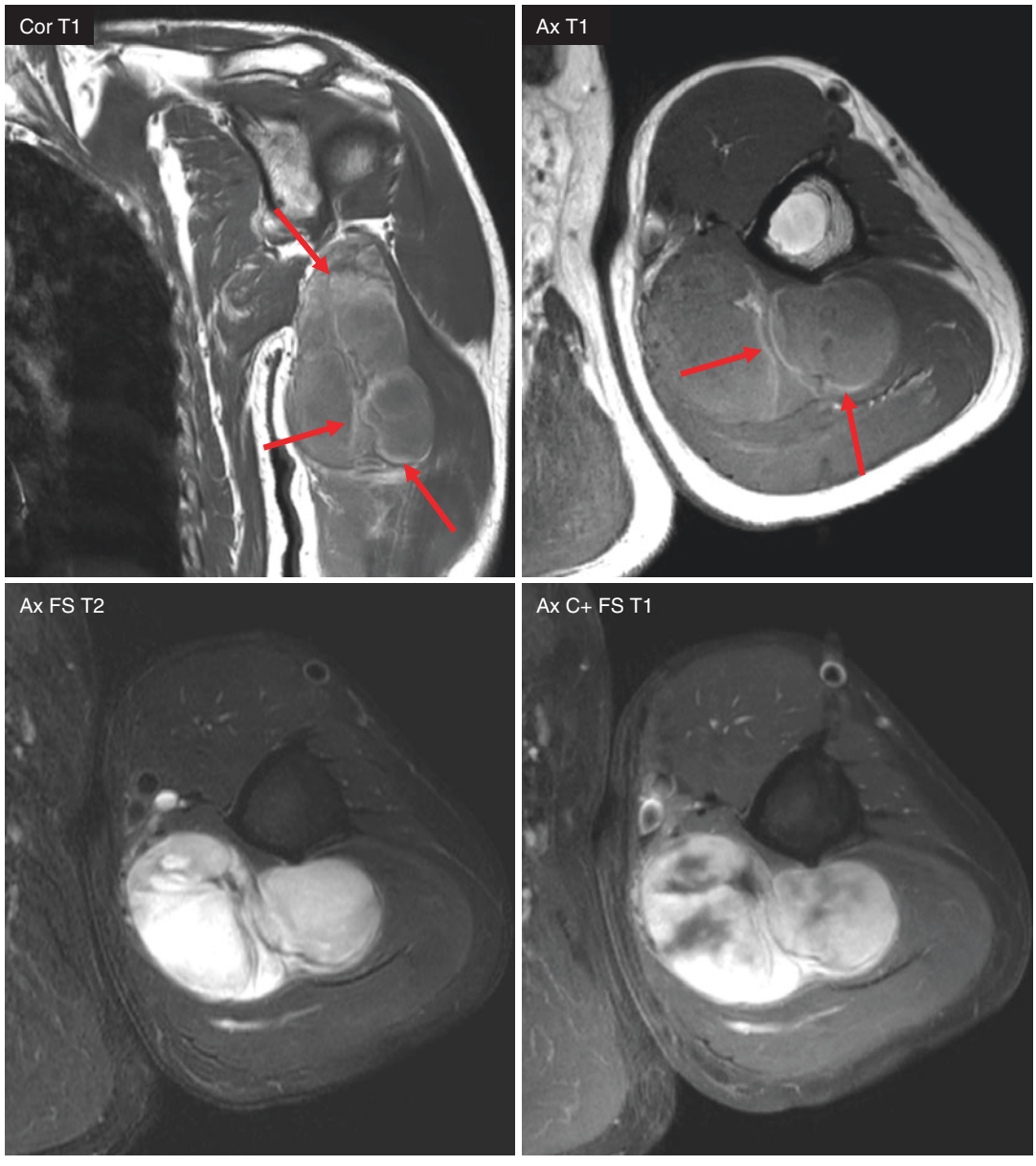

Myxoid liposarcoma (Chap. 4)

- Small amount of fat in septa (*arrows*)
- Marked hyperintensity on T2WI
- "Myxoid-pattern" enhancement

20.2 Quiz

A 83-year-old female, left upper arm palpable mass

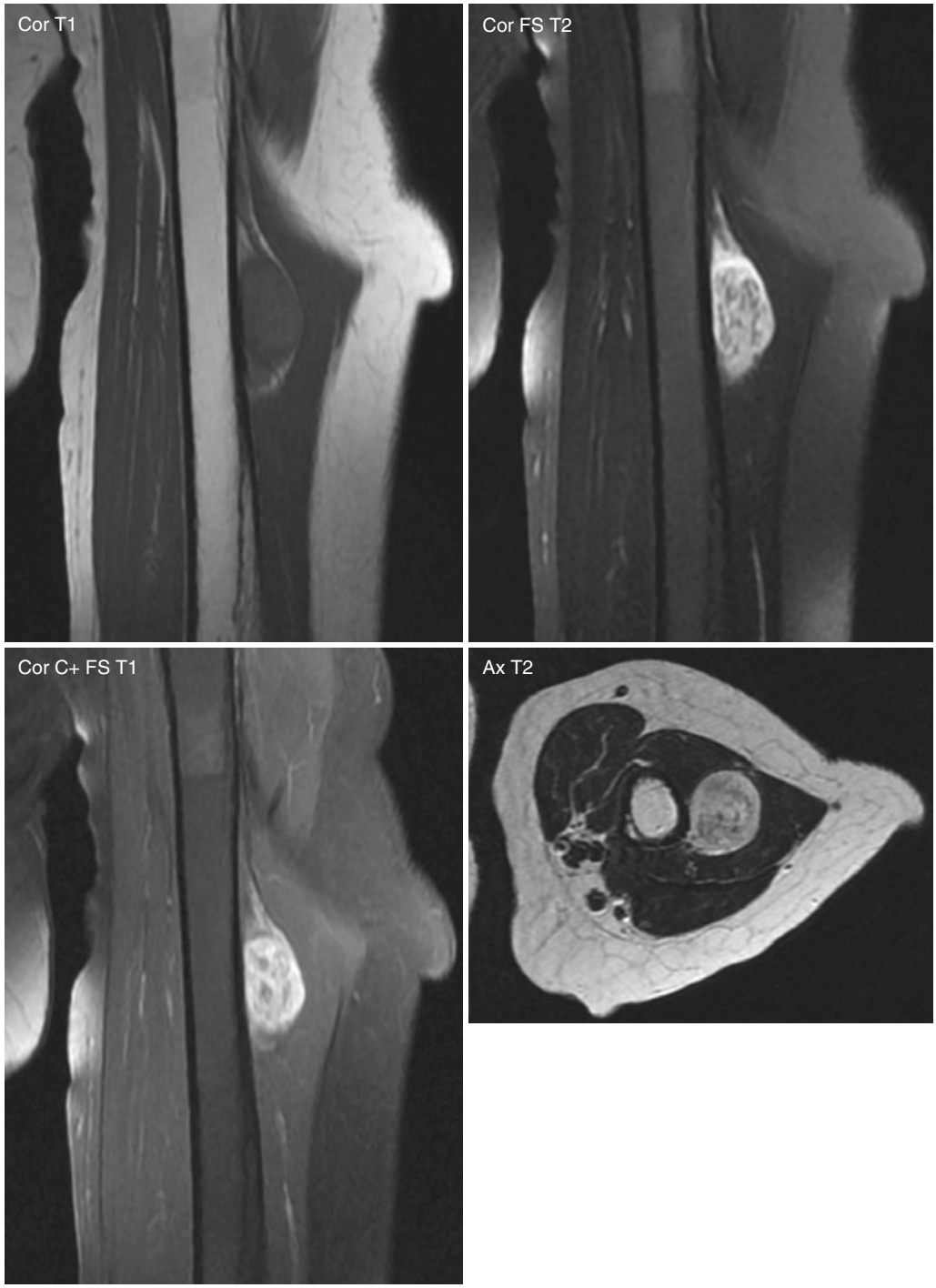

Fig. 20.2

20.2 Answer

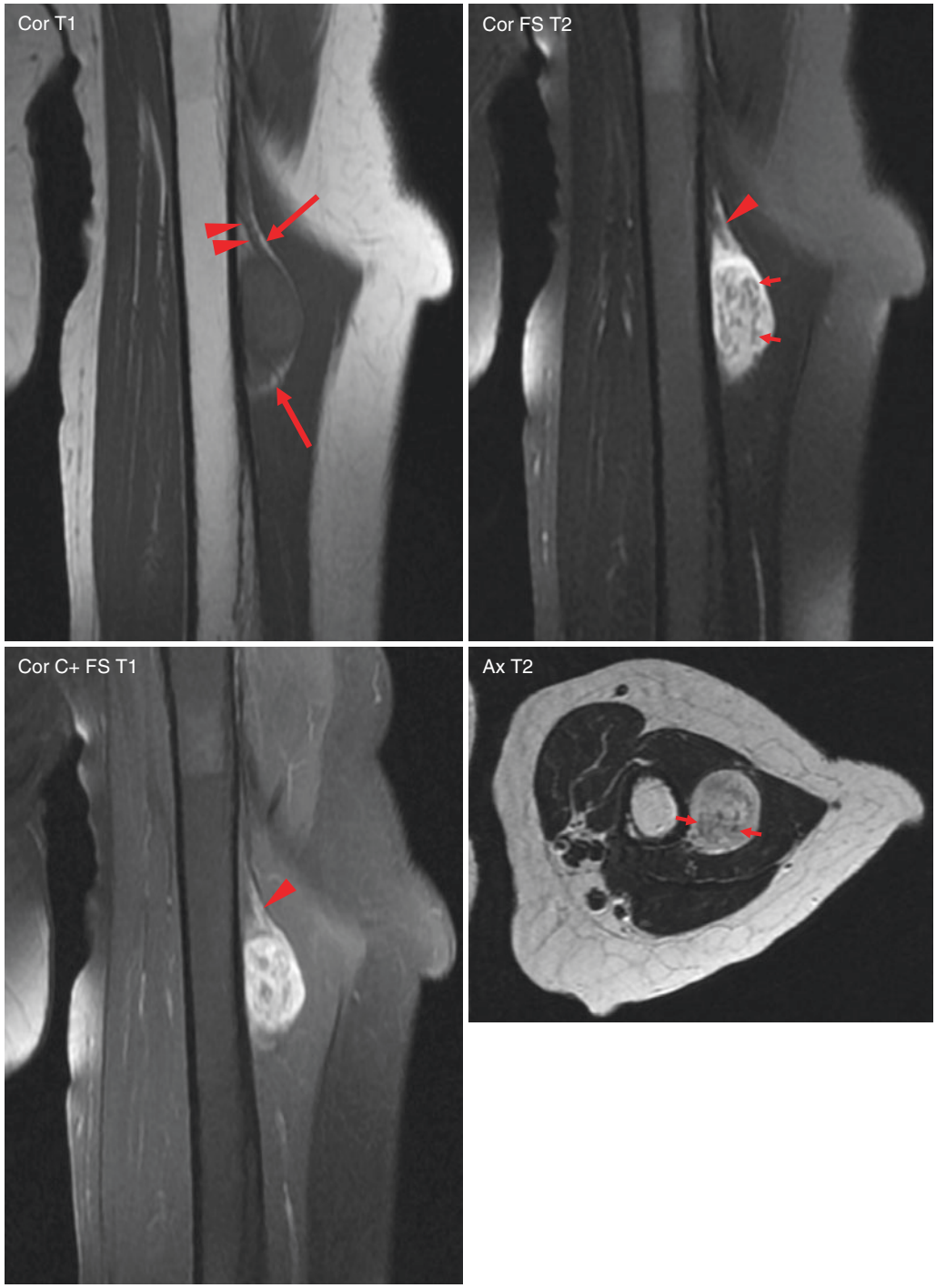

Schwannoma (Chap. 12)

- Entering radial nerve (*arrowhead*)
- Fascicular sign on T2WI (*small arrows*)
- Split-fat sign on T1WI (*arrows*)

20.3 Quiz

A 58-year-old female, right knee painful mass

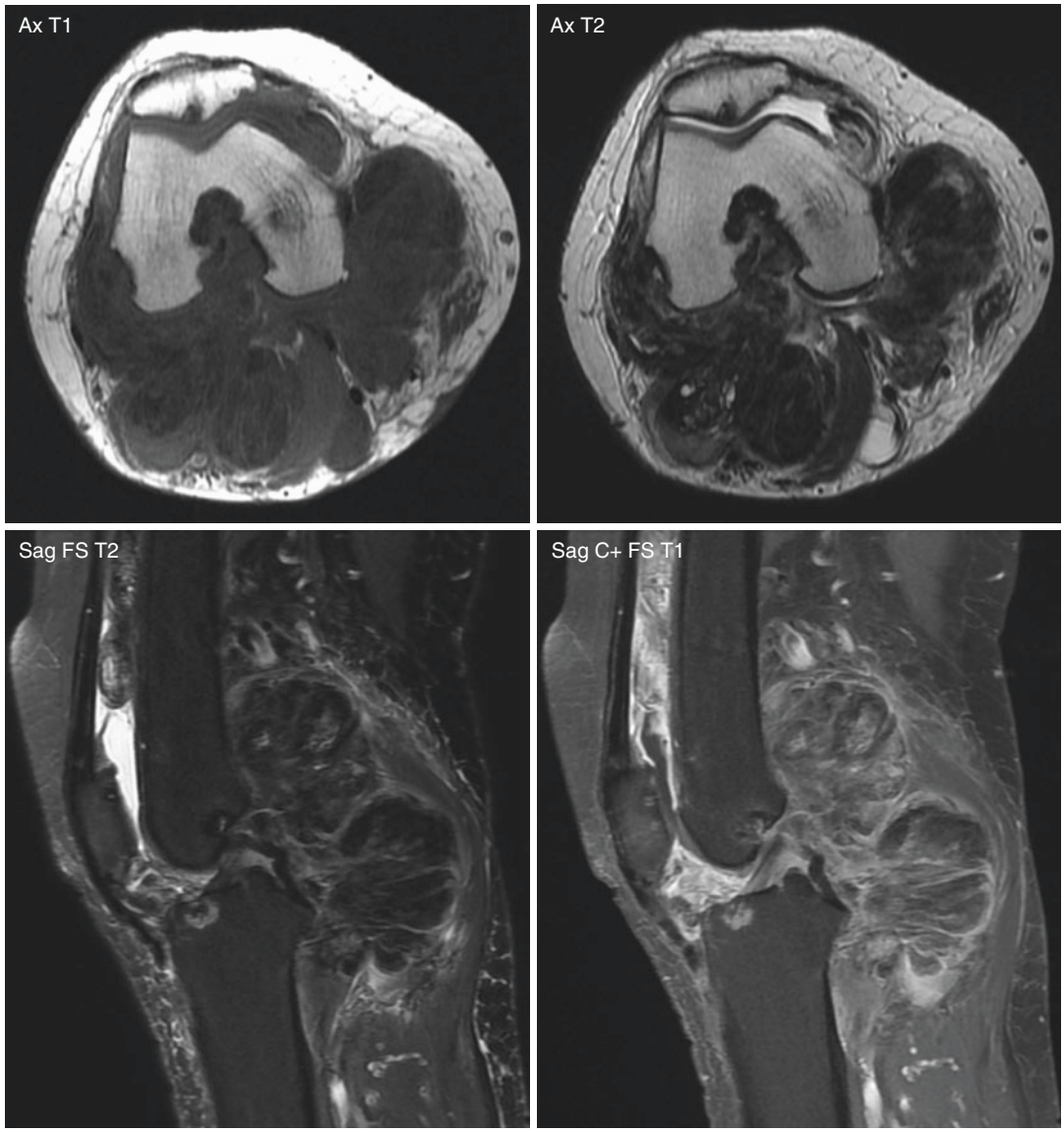

Fig. 20.3

20.3 Answer

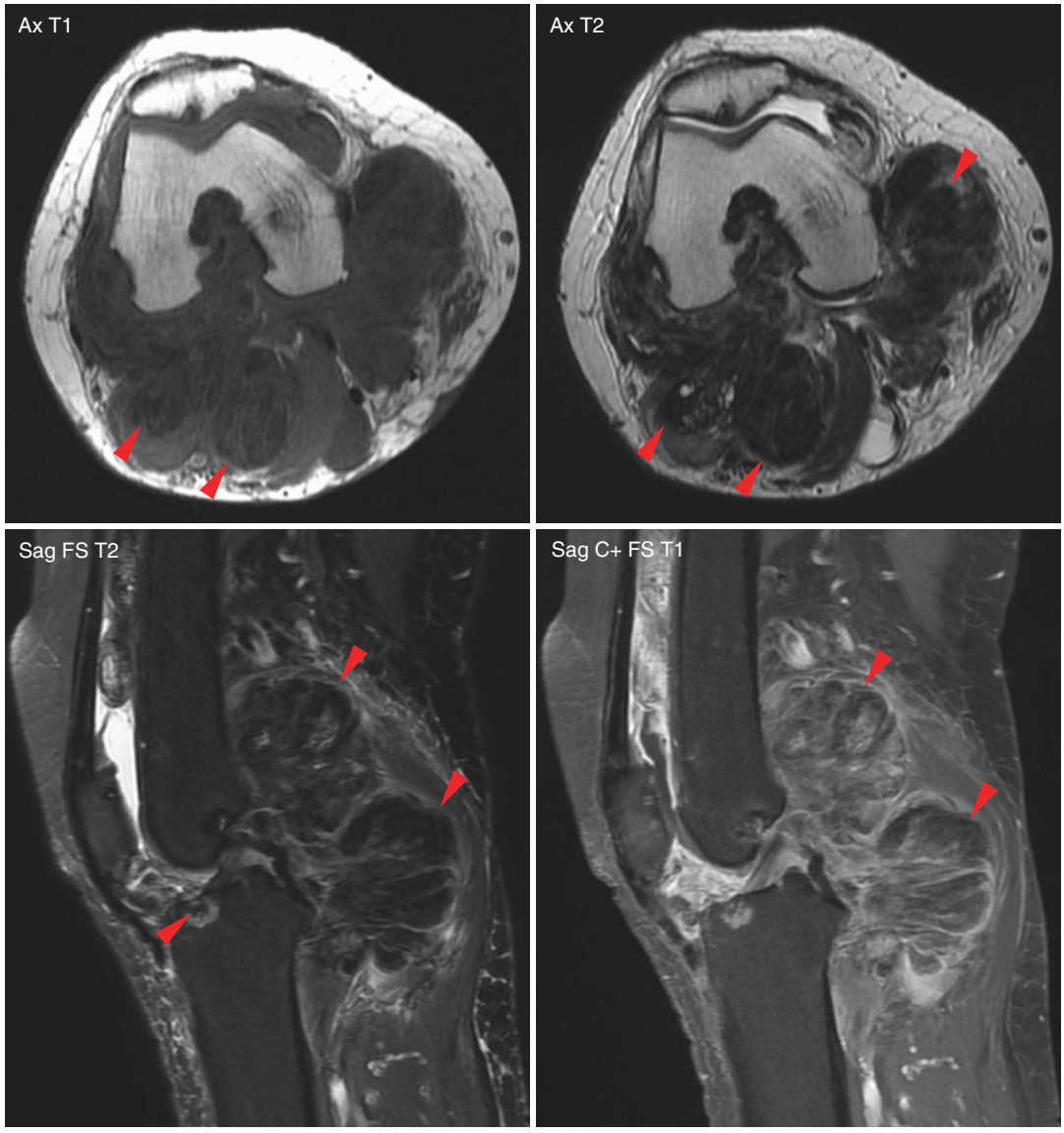

Tenosynovial giant cell tumor, diffuse type (Chap. 6)

- Intra-articular lesion location
- Very low signal regions (*arrowheads*) in the lesion on all sequences, reflecting hemosiderin depositions

20.4 Quiz

An 11-year-old male, right pubic mass

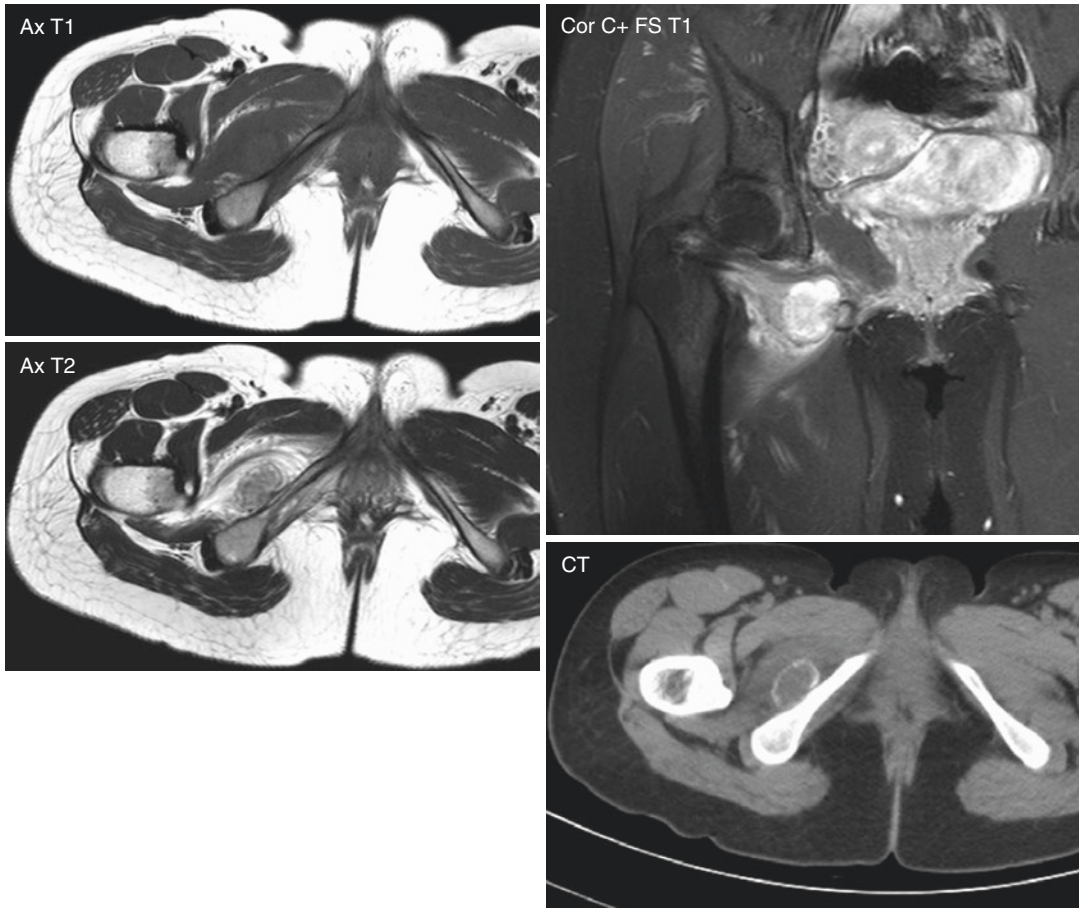

Fig. 20.4

20.4 Answer

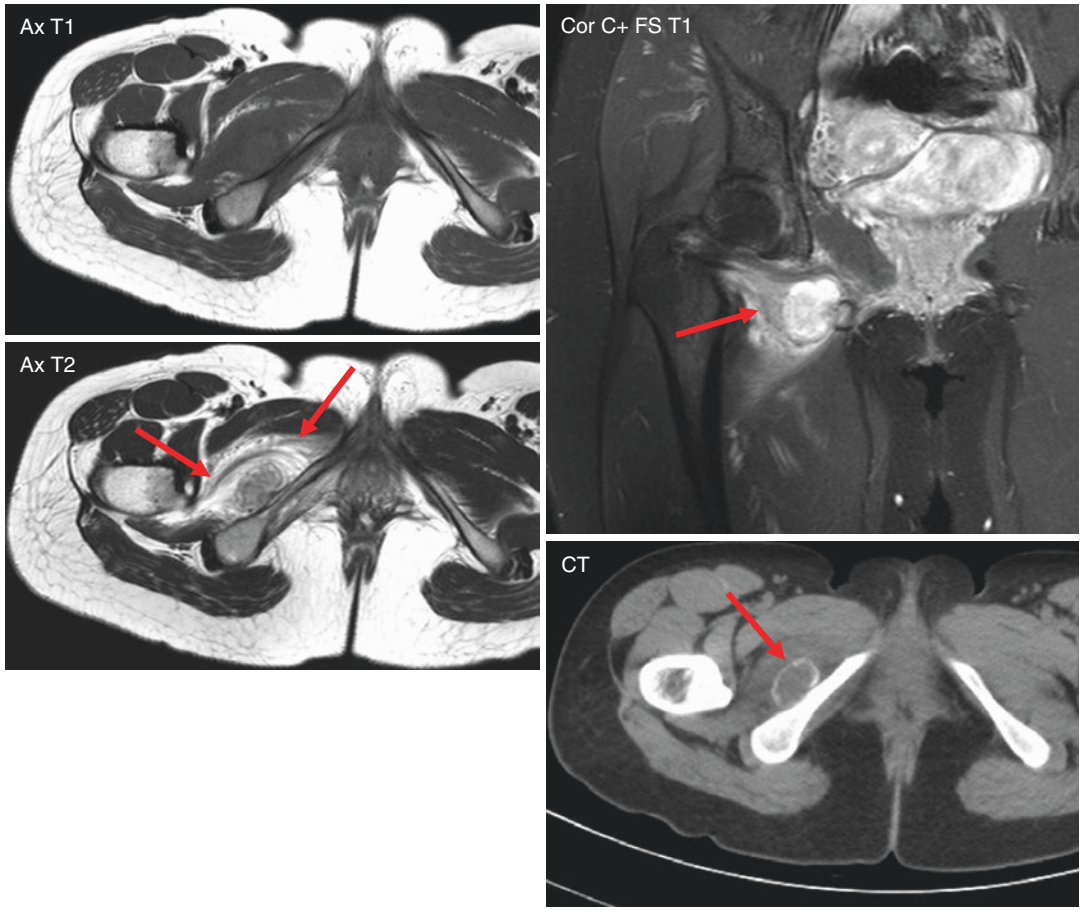

Myositis ossificans (Chap. 5)

- Slightly T1 hyperintense mass
- Surrounding soft tissue edema and enhancement (*arrows*) on T2WI and postcontrast T1WI
- Zonal phenomenon of calcification (*arrow*) on CT

20.5 Quiz

A 47-year-old female, left wrist mass

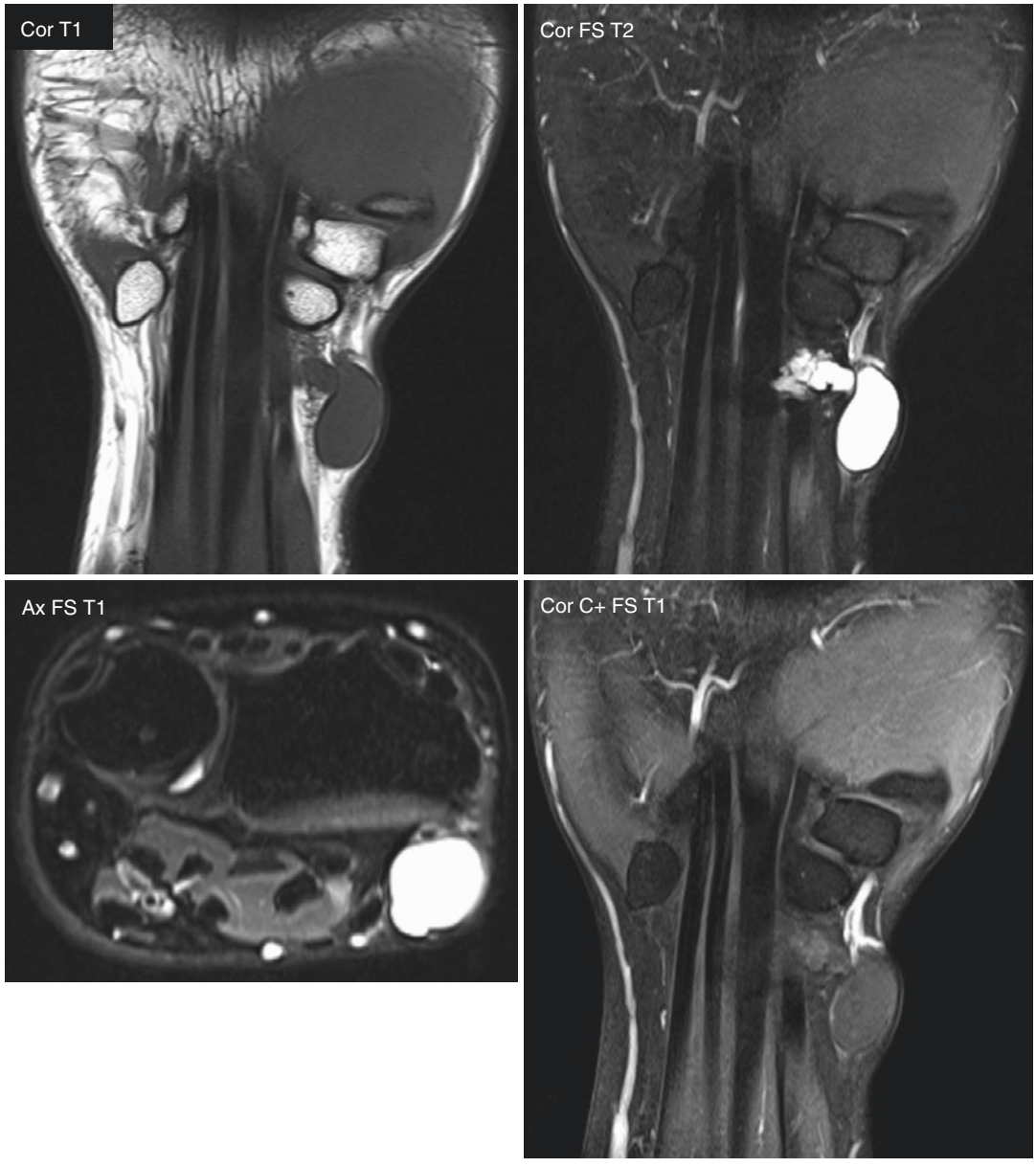

Fig. 20.5

20.5 Answer

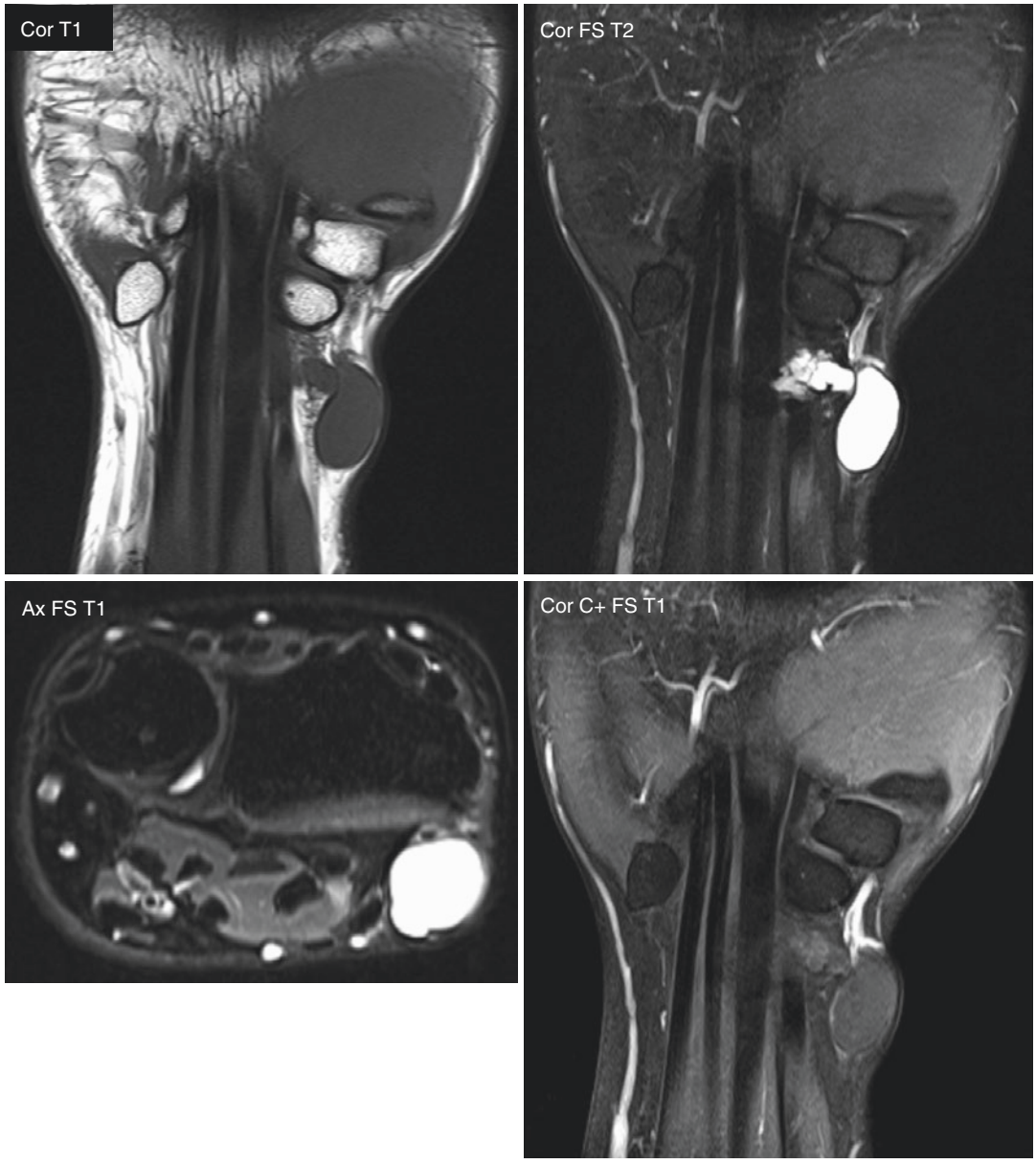

Ganglion (Chap. 16)

- Fluid-like high signal intensity on T2WI
- Multilobulated and elongated appearance on T2WI
- No contrast enhancement

20.6 Quiz

A 67-year-old male, right upper arm mass

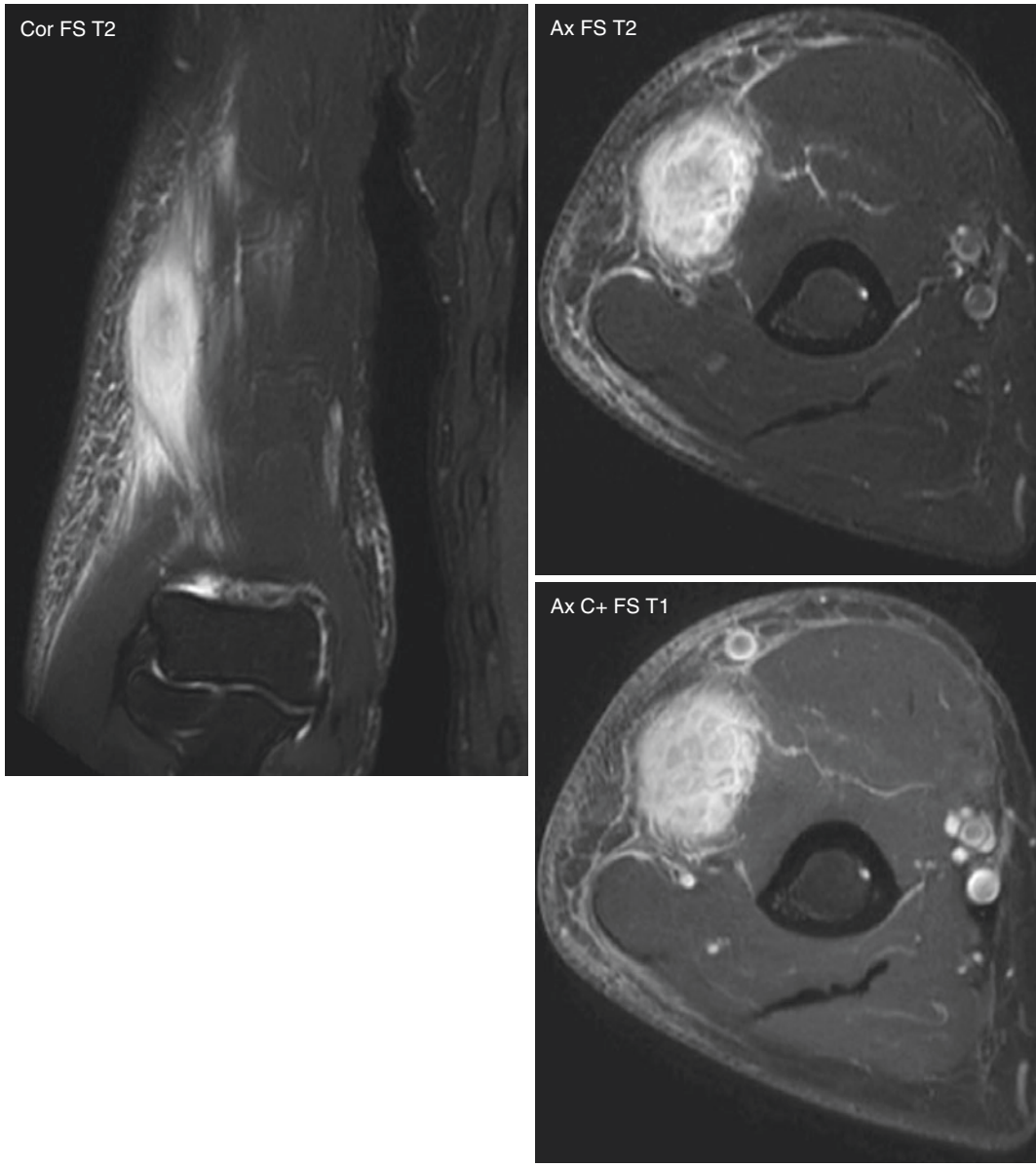

Fig. 20.6

20.6 Answer

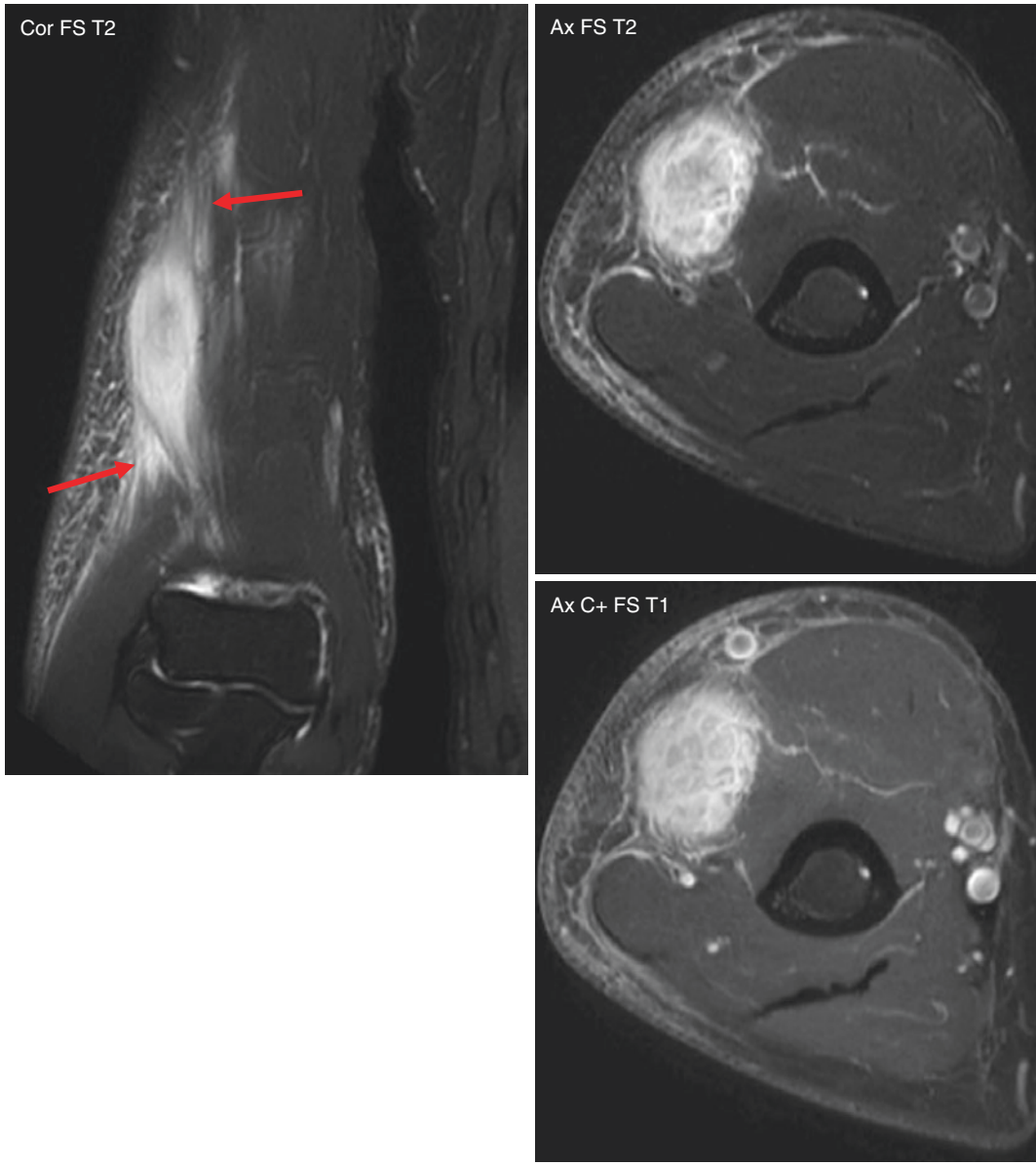

Proliferative myositis (Chap. 5)

- Expansile muscle mass with preserved fascicles
- Extensive perilesional edema (*arrows*)
- Checkerboard appearance on axial T2WI and postcontrast T1WI

20.7 Quiz

A 48-year-old female, right thigh mass

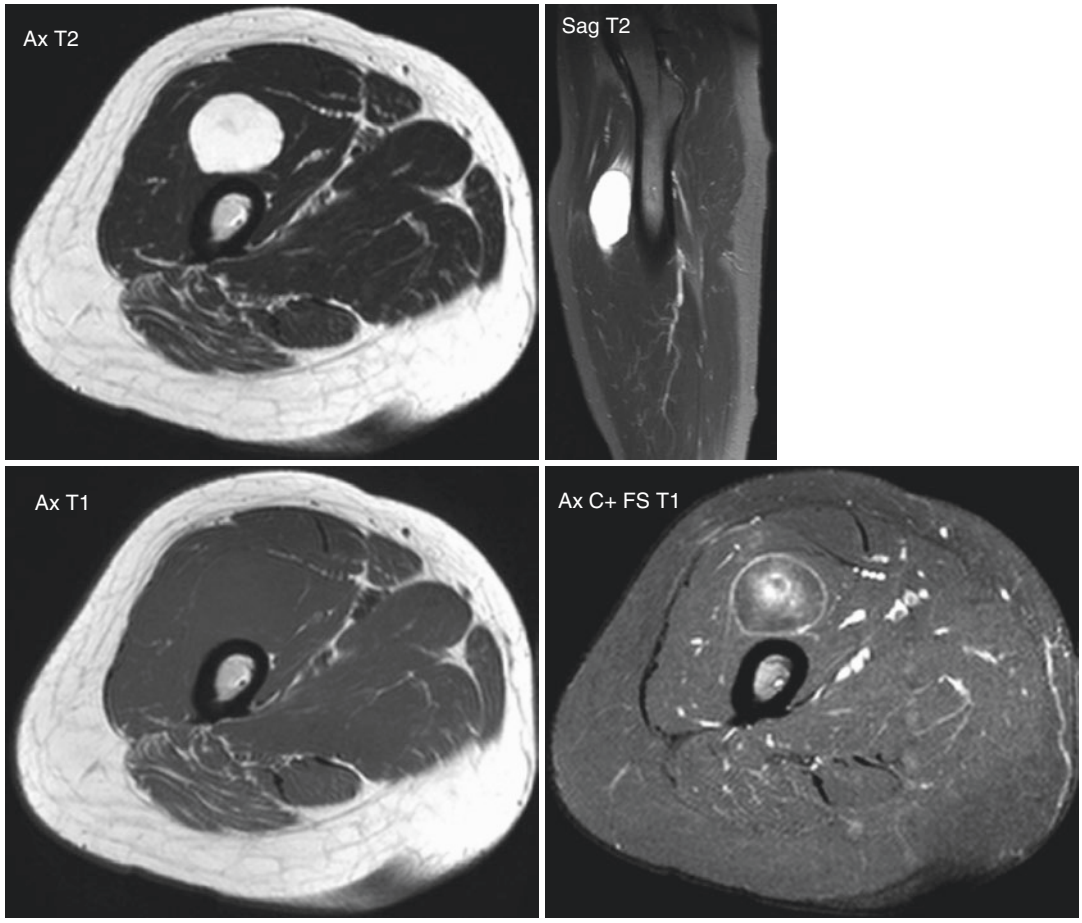

Fig. 20.7

20.7 Answer

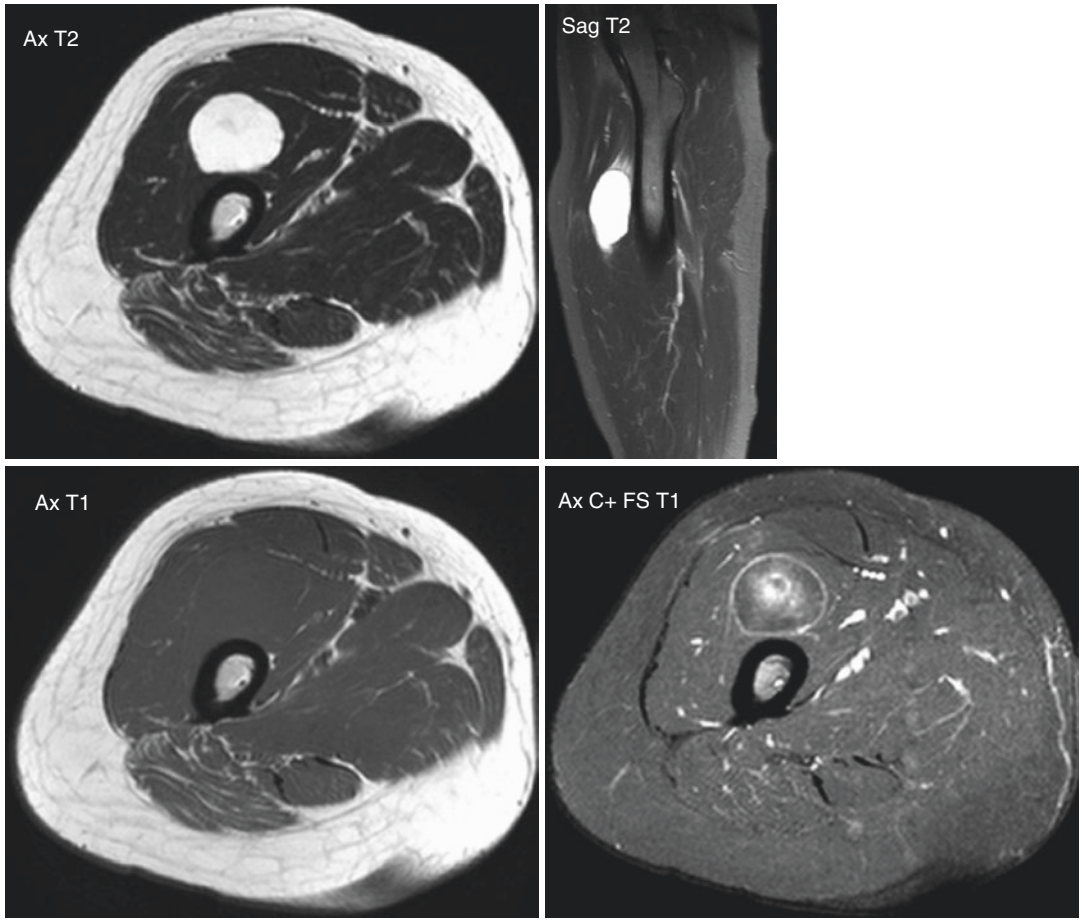

Intramuscular myxoma (Chap. 13)

- Fluid-like bright high signal intensity on T2WI
- Fuzzy and mild contrast enhancement

20.8 Quiz

A 47-year-old female, left wrist mass

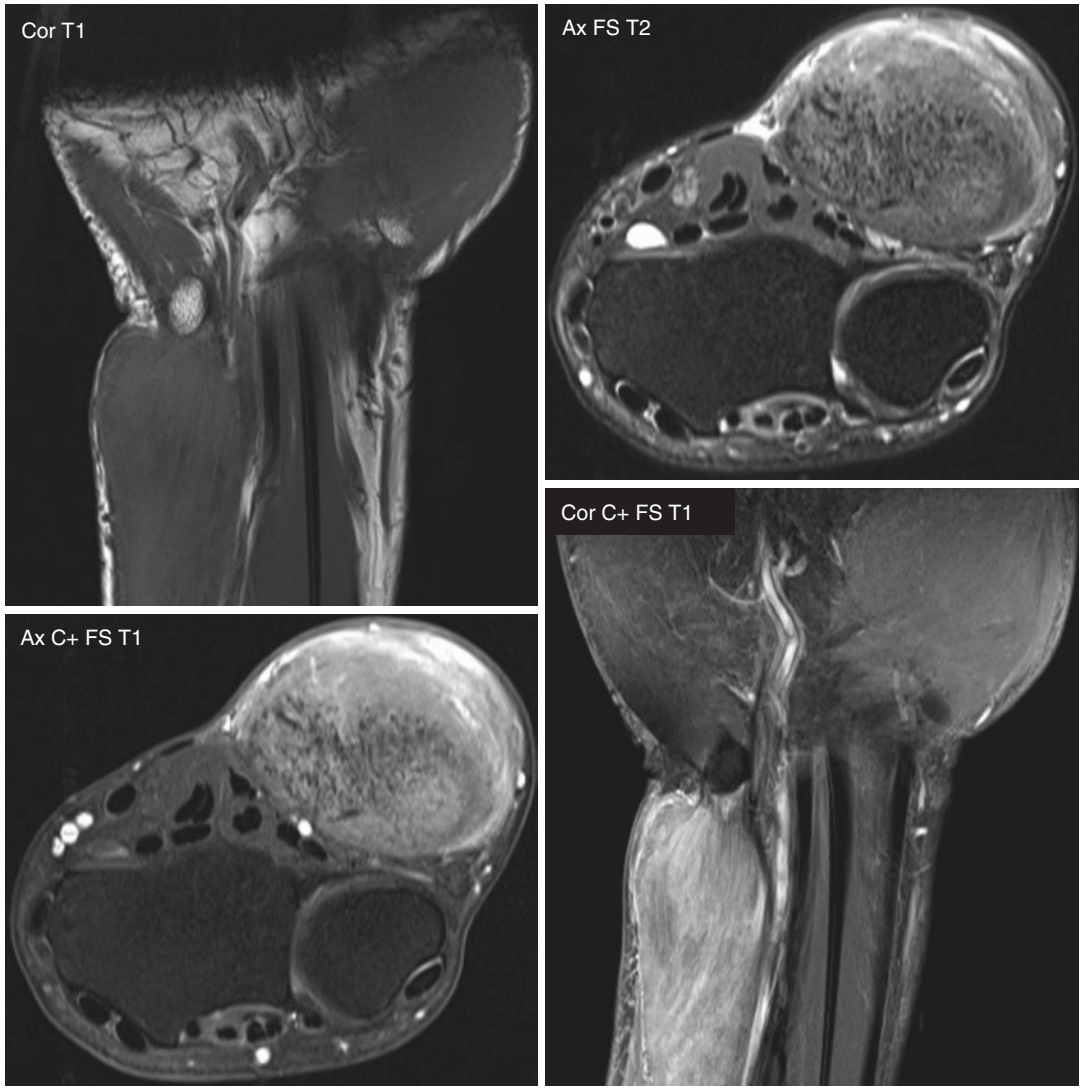

Fig. 20.8

20.8 Answer

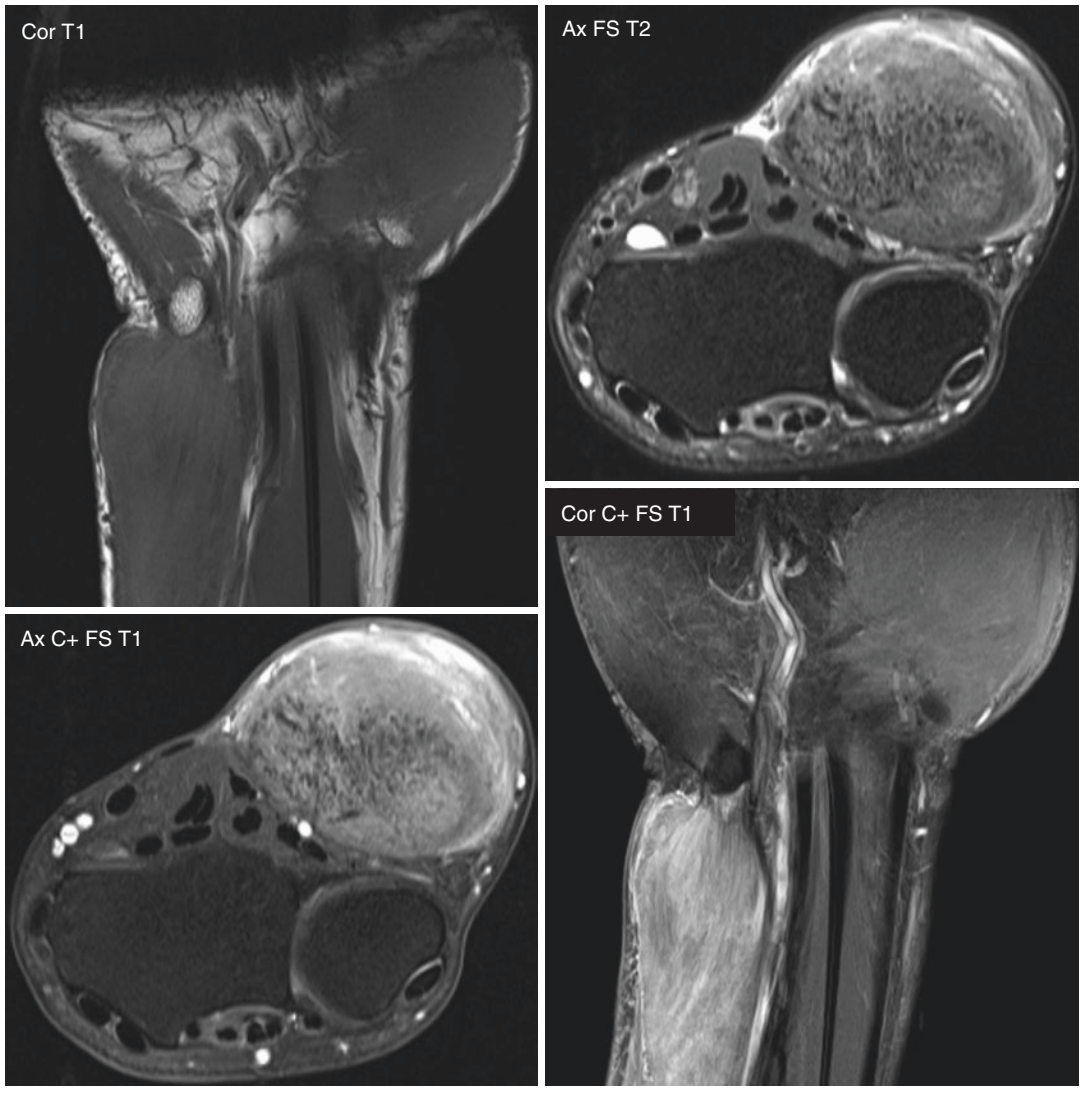

Tendinous xanthoma (Chap. 16)

- Enlargement of flexor carpi ulnaris tendon with speckled inner low signal intensity on T1- and T2WI
- Diffuse contrast enhancement

20.9 Quiz

A 43-year-old male, finger mass 1 year ago

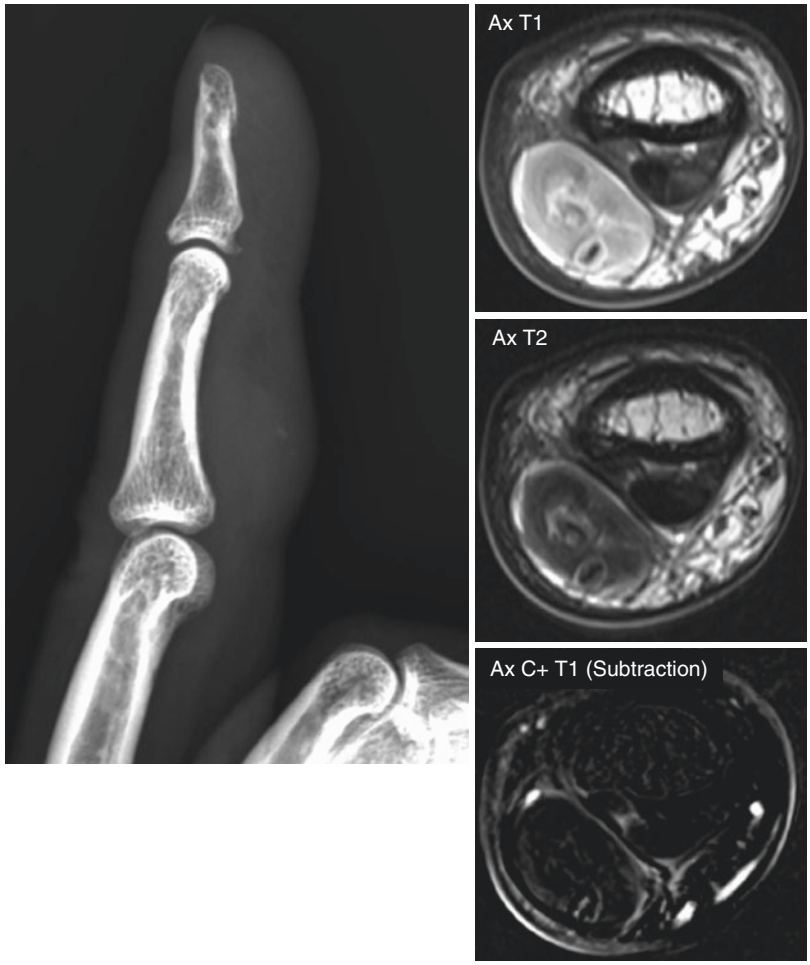

Fig. 20.9

20.9 Answer

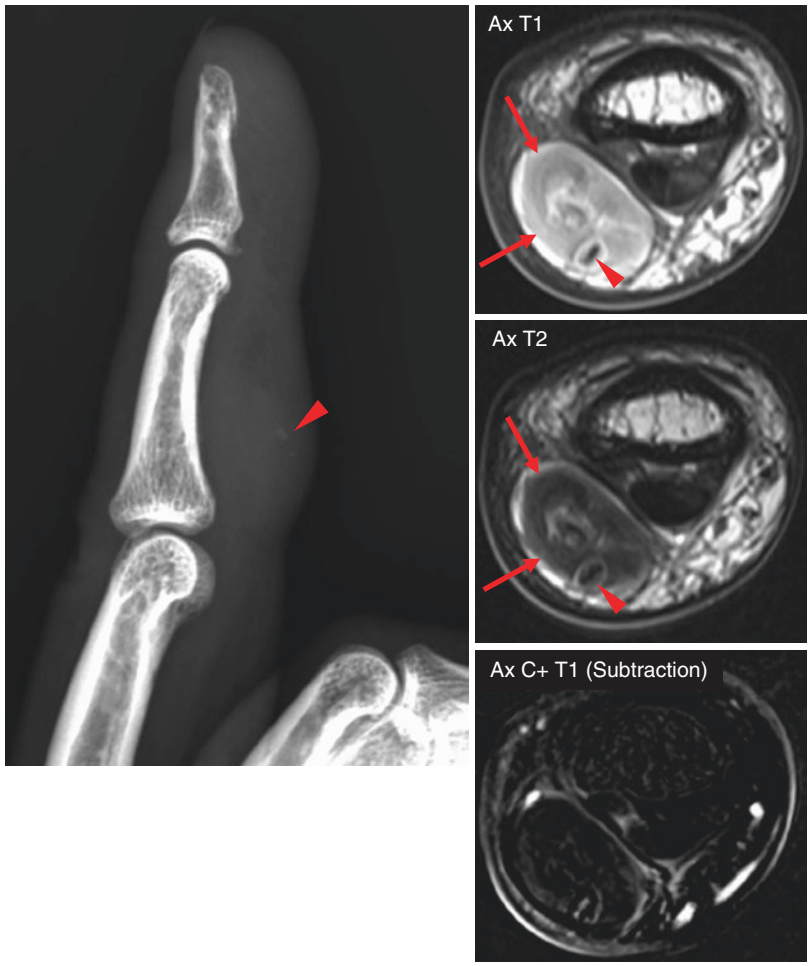

Thrombosed hemangioma (Chap. 10)

- Phleboliths (*arrowheads*)
- Diffuse intralesional hyperintensity on T1WI and hypointensity on T2WI, representing thrombi (*arrows*)
- No demonstrable contrast enhancement on the subtracted postcontrast T1WI

20.10 Quiz

A 66-year-old female, right subdeltoid bursa lesion

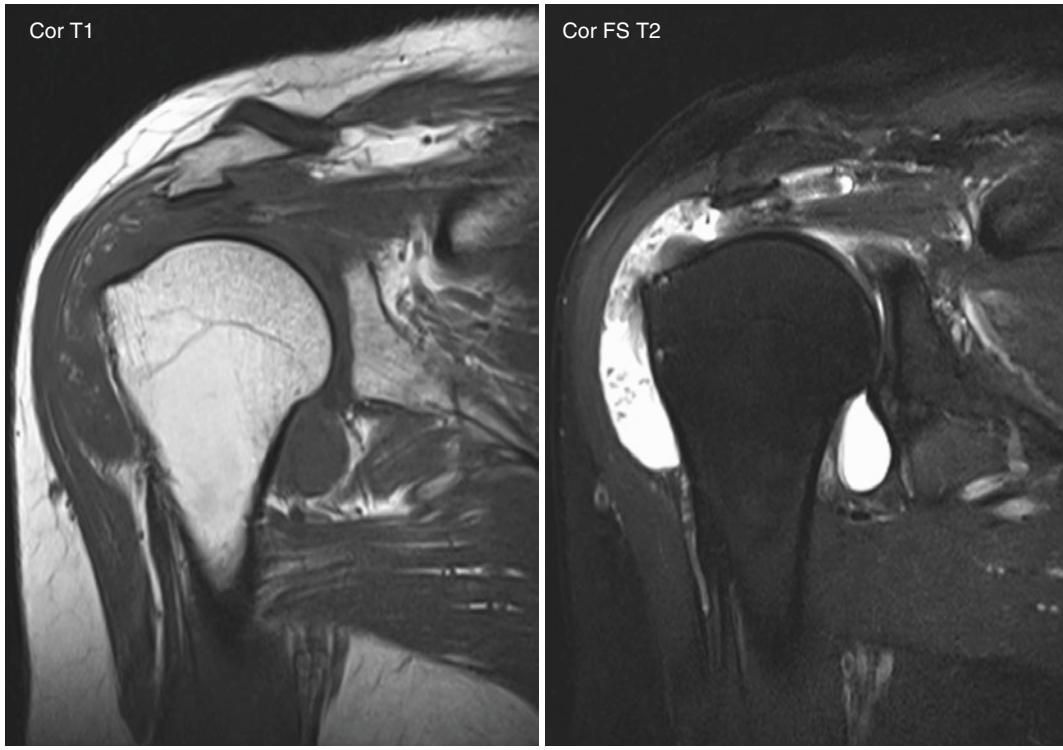

Fig. 20.10

20.10 Answer

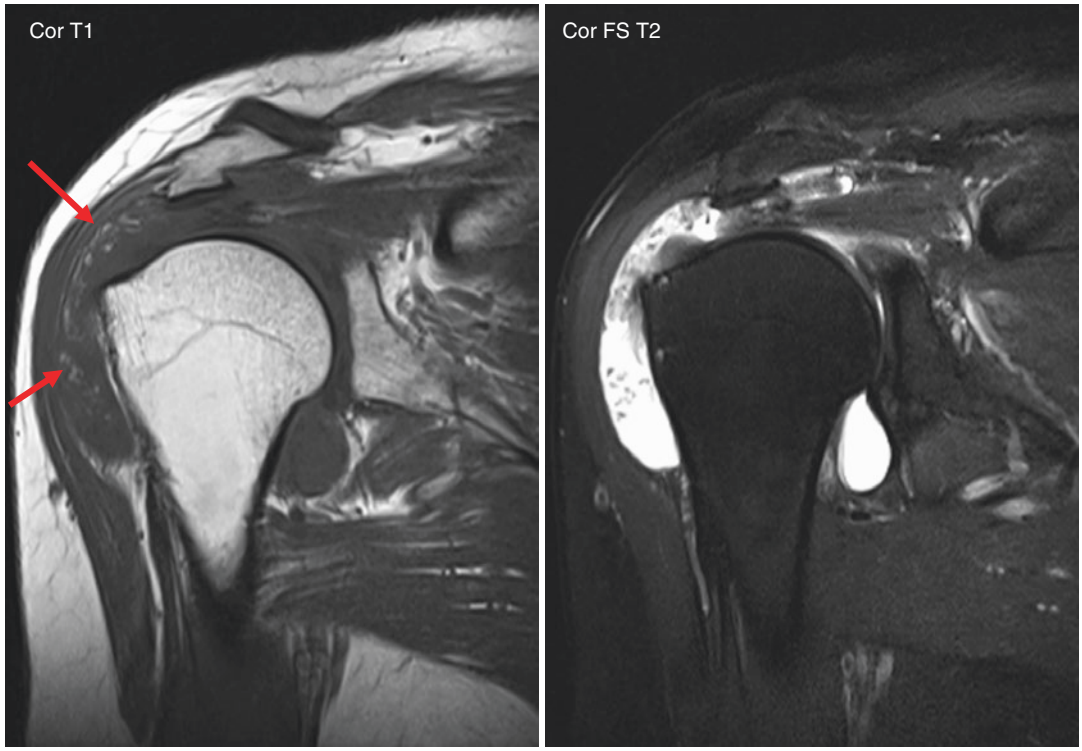

Lipoma arborescens (Chap. 4)

- Frond-like synovial mass
- Isointense (*arrows*) to fat on T1WI
- Suppressed signal on fat suppression sequence

20.11 Quiz

A 70-year-old male, right lower leg mass

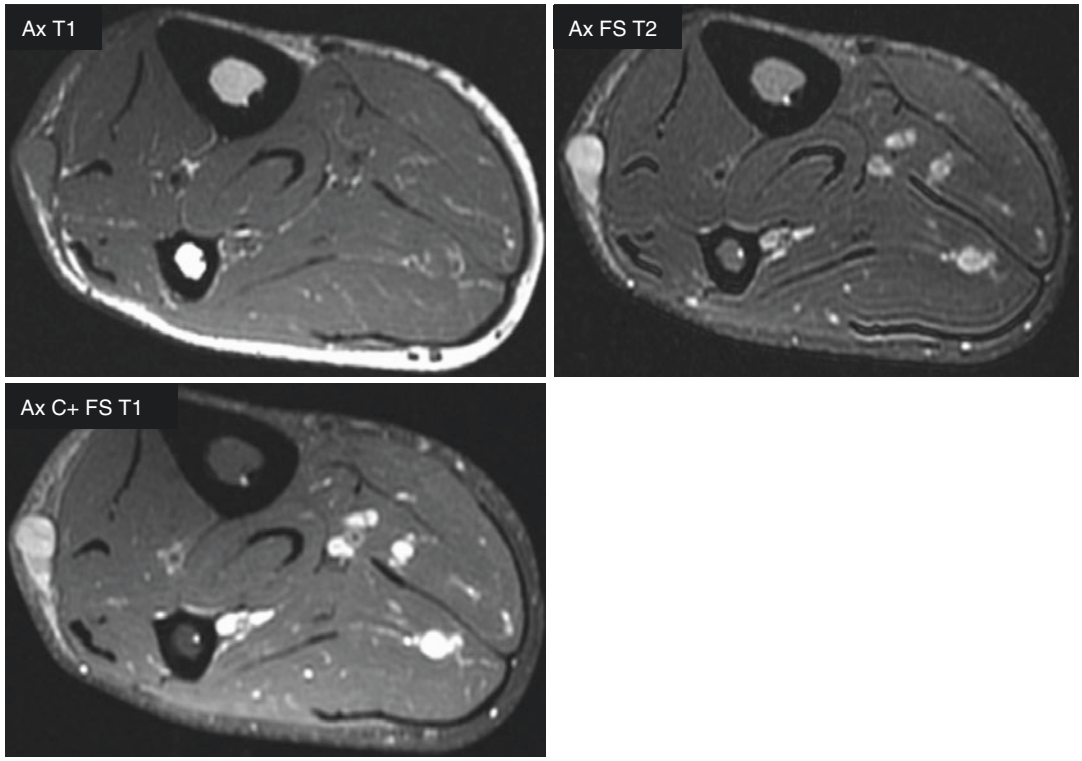

Fig. 20.11

20.11 Answer

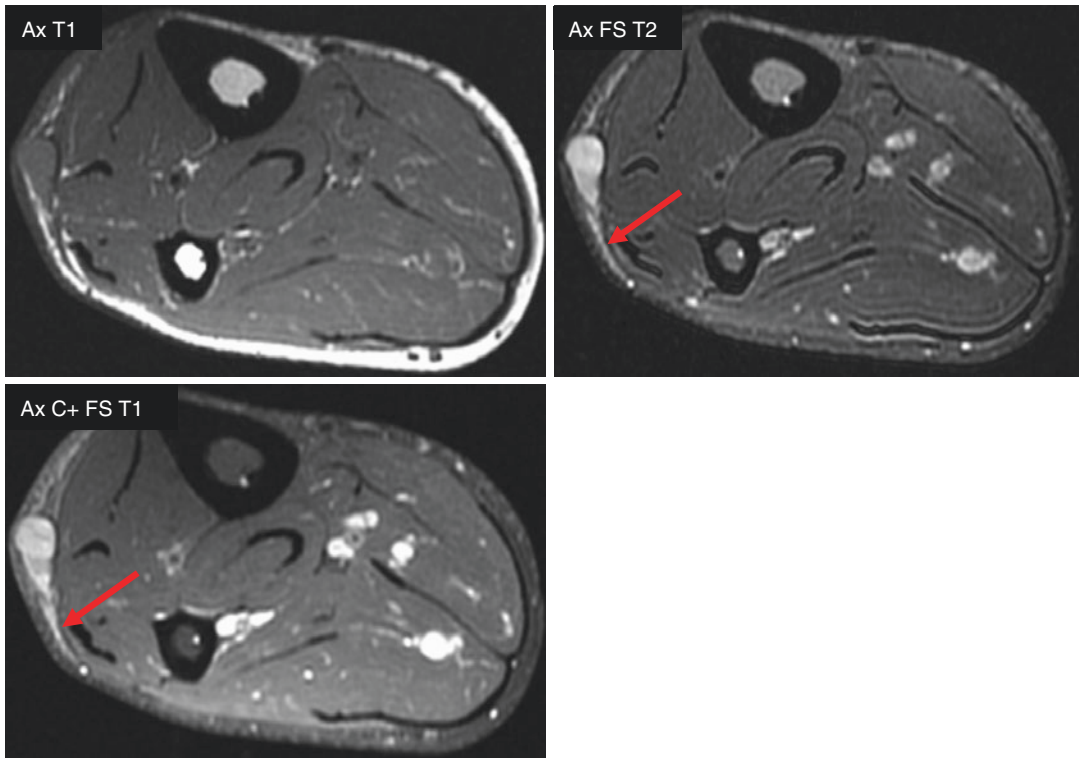

Myxofibrosarcoma (Chap. 5)

- Perifascial mass with infiltrative margin
- Curvilinear projection along fascial plane, "tail sign" (*arrows*)

20.12 Quiz

A 2-year-old boy, right arm mass

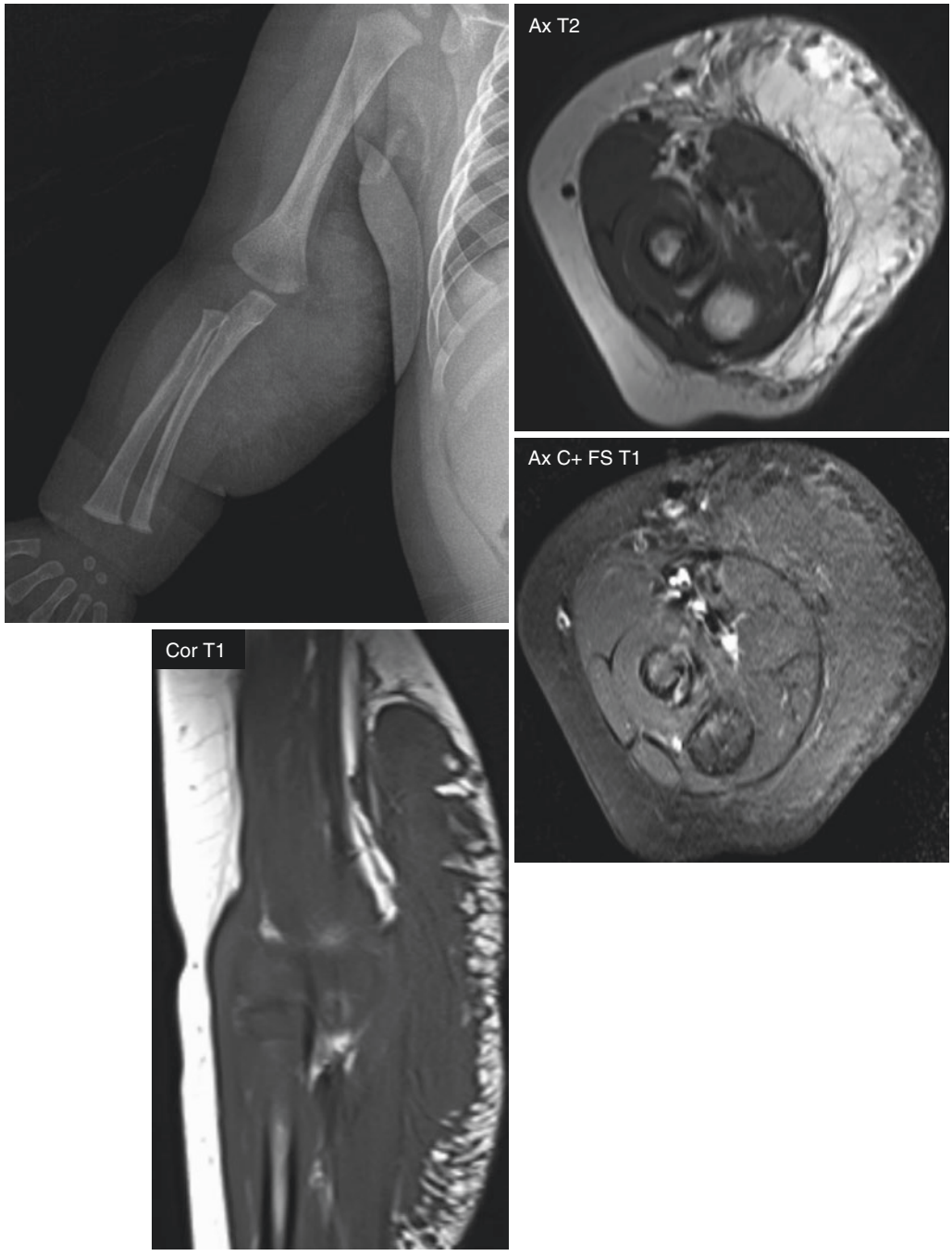

Fig. 20.12

20.12 Answer

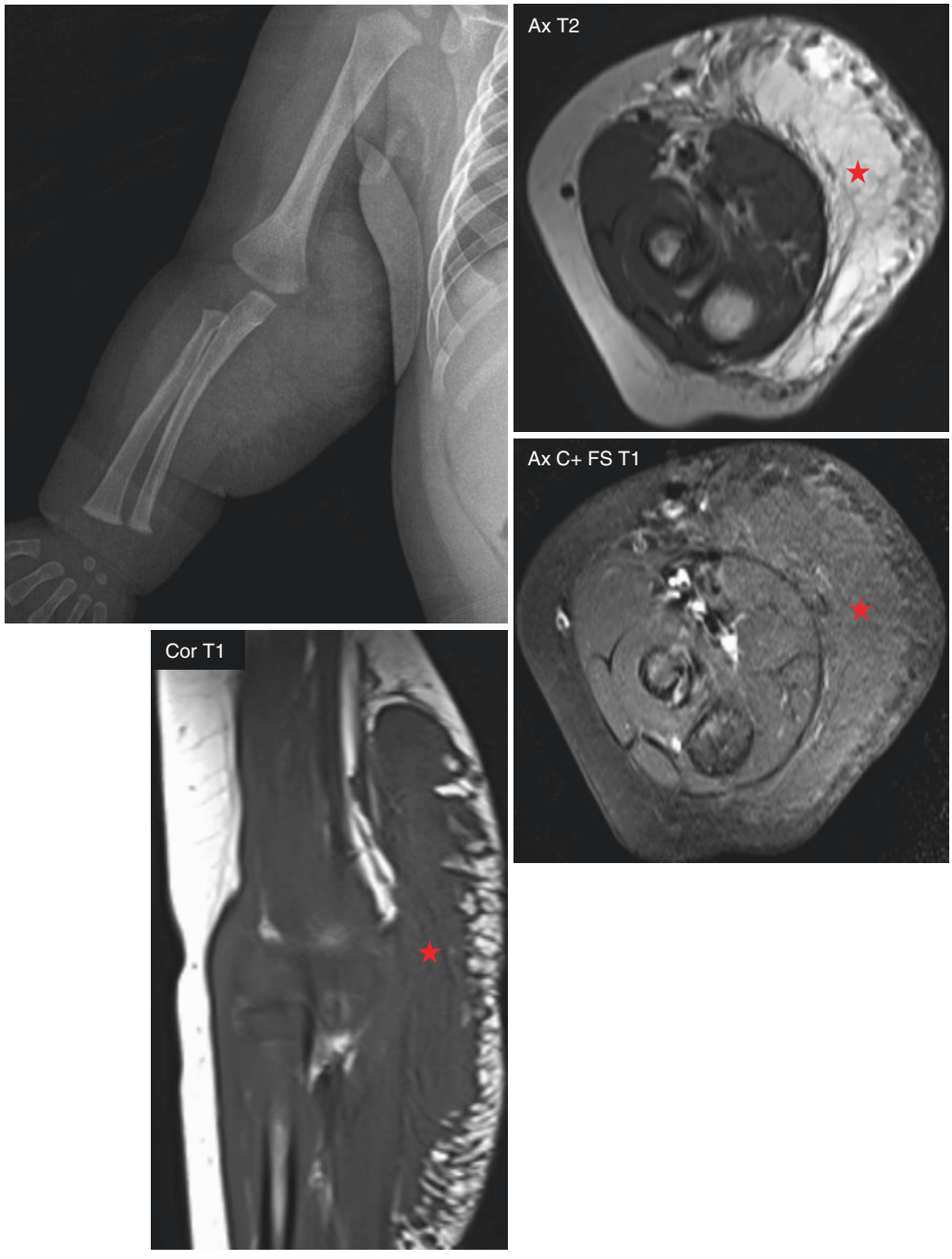

Lymphangioma (Chap. 10)

- Child
- Huge subcutaneous non-enhanced cystic mass (*stars*)

20.13 Quiz

A 37-year-old male, right thigh mass

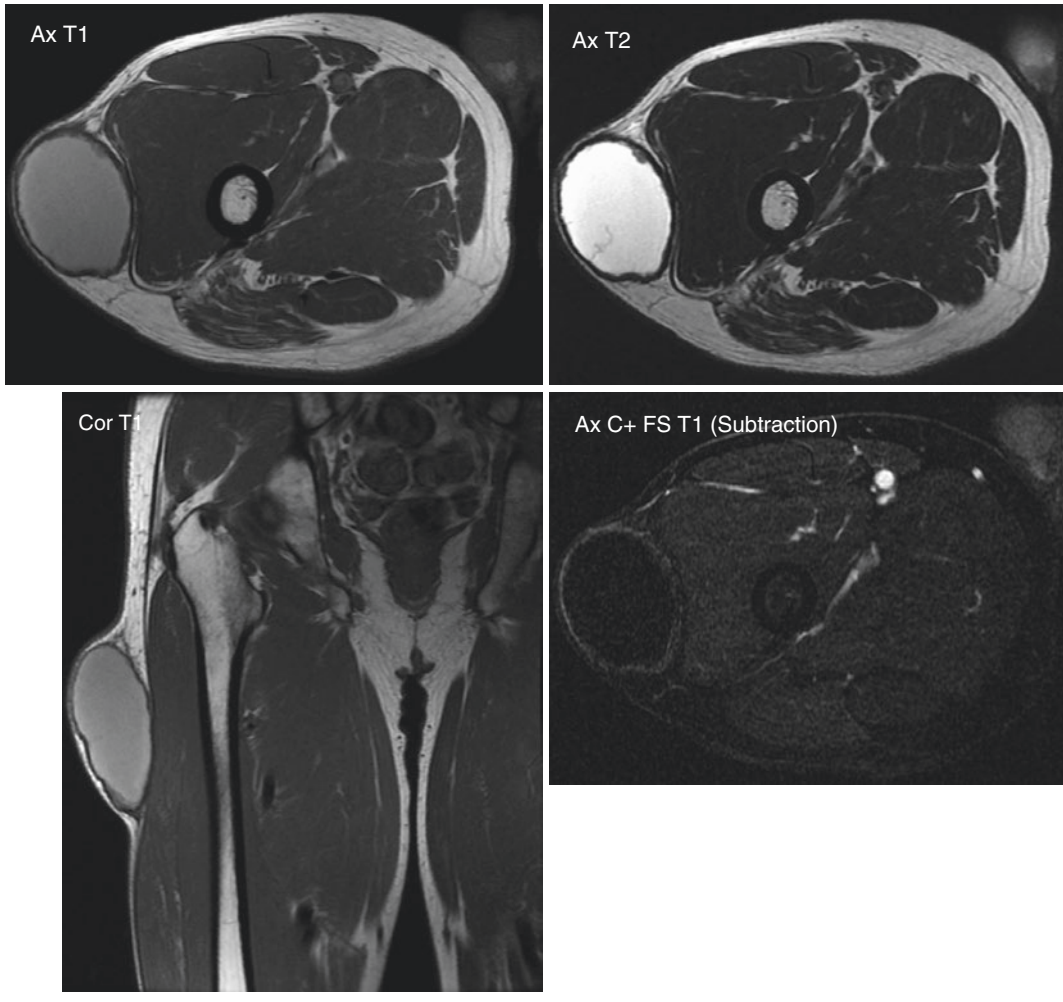

Fig. 20.13

20.13 Answer

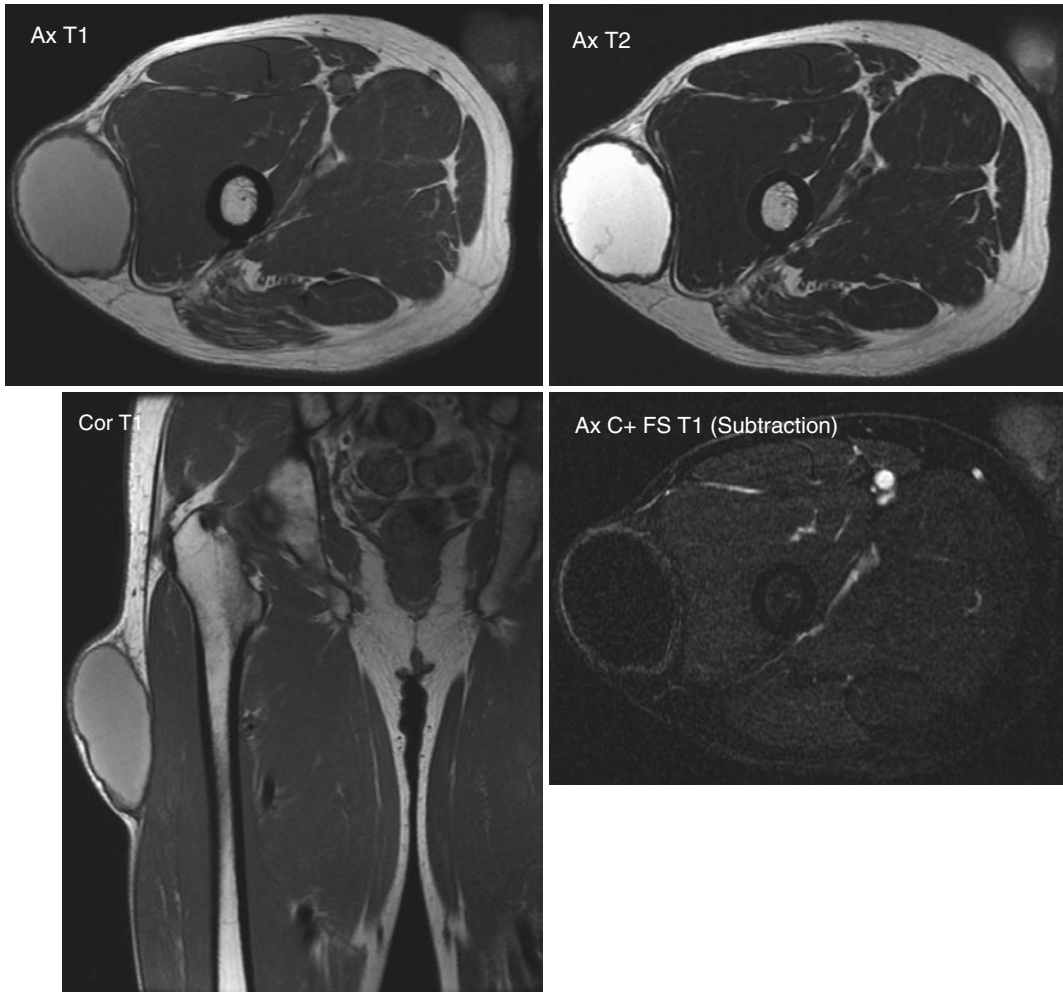

Morel-Lavallee lesion (Chap. 15)

- High signal intensity on T1WI
- Dark signal rim on T2WI
- No contrast enhancement except peripheral thin wall on postcontrast FS T1

20.14 Quiz

A 55-year-old female, right posterior shoulder mass

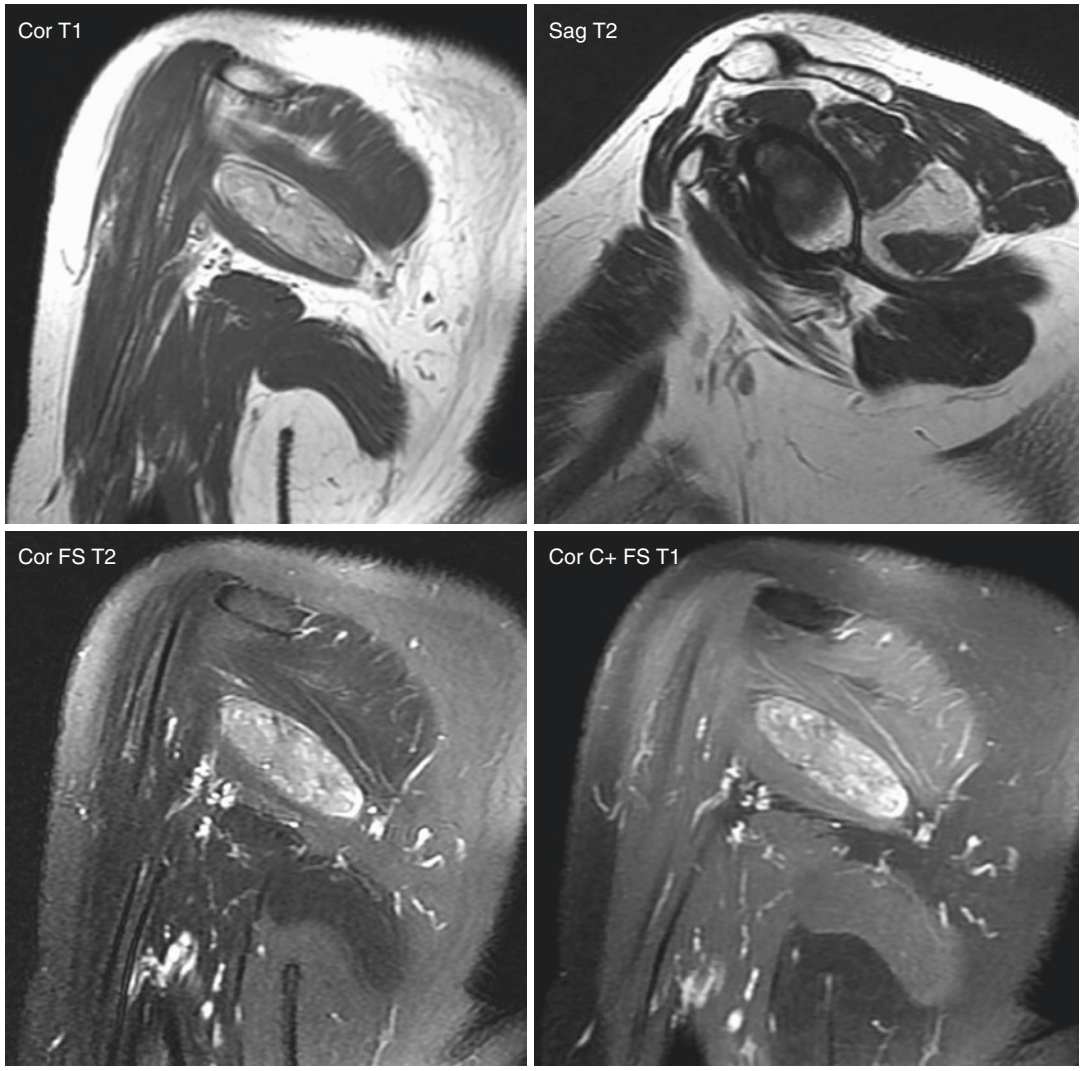

Fig. 20.14

20.14 Answer

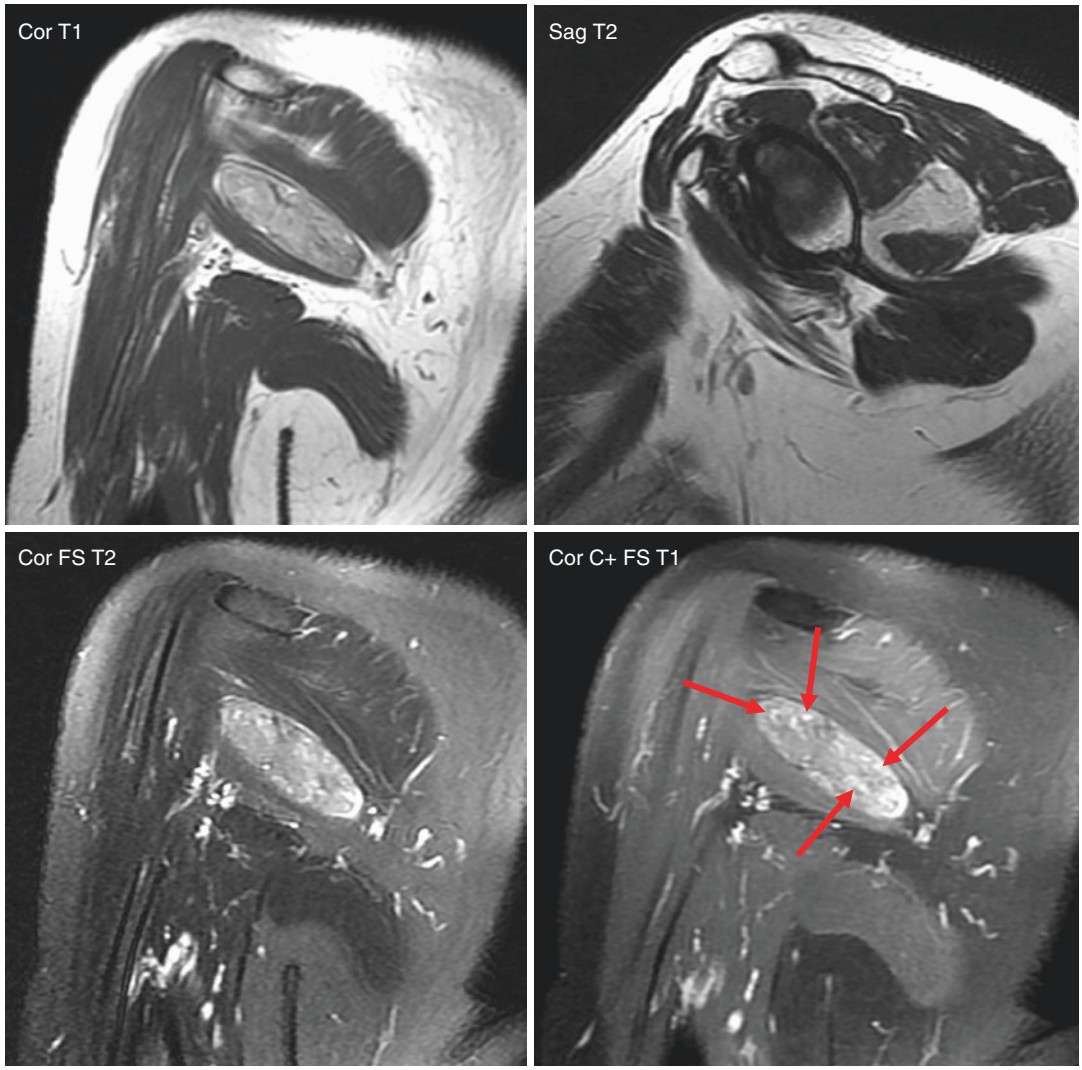

Hibernoma (Chap. 4)

- Slightly hypointense relative to fat on T1WI
- Incomplete signal suppression on FS T2WI
- Prominent internal vascularity (*arrows*)

20.15 Quiz

A 36-year-old male, left anterior elbow mass

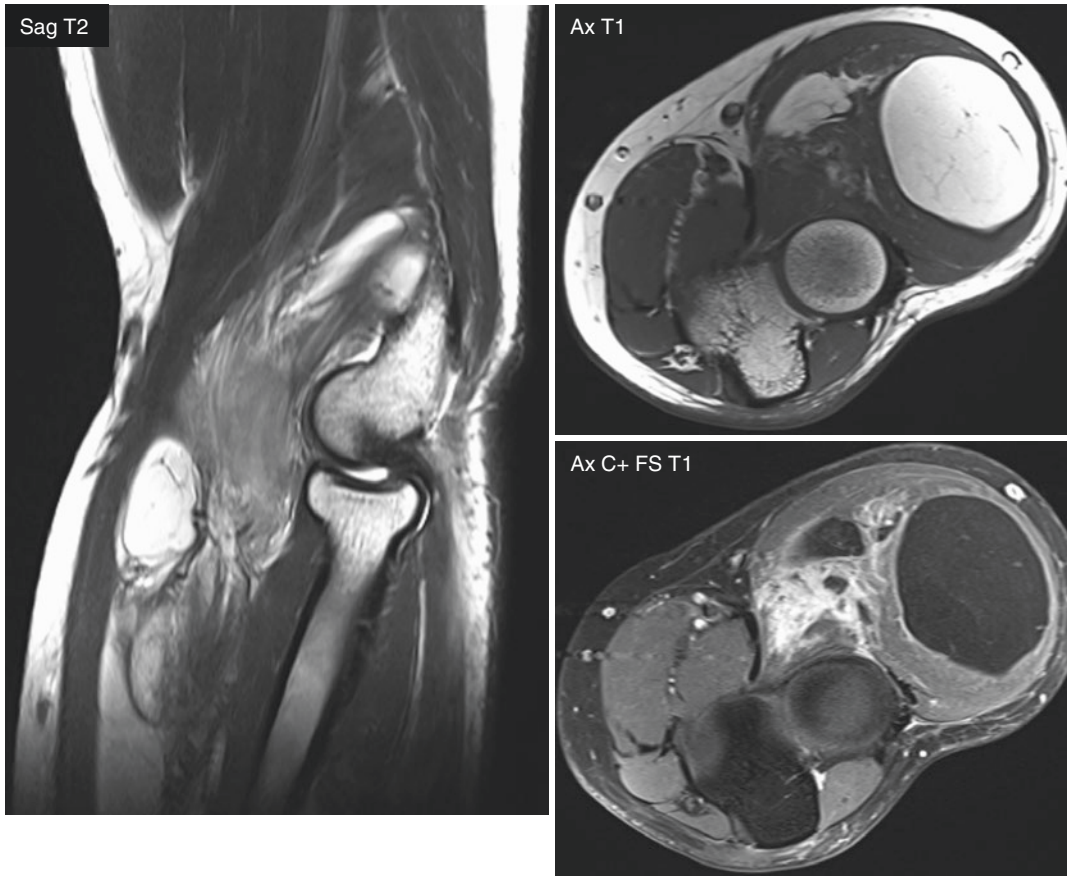

Fig. 20.15

20.15 Answer

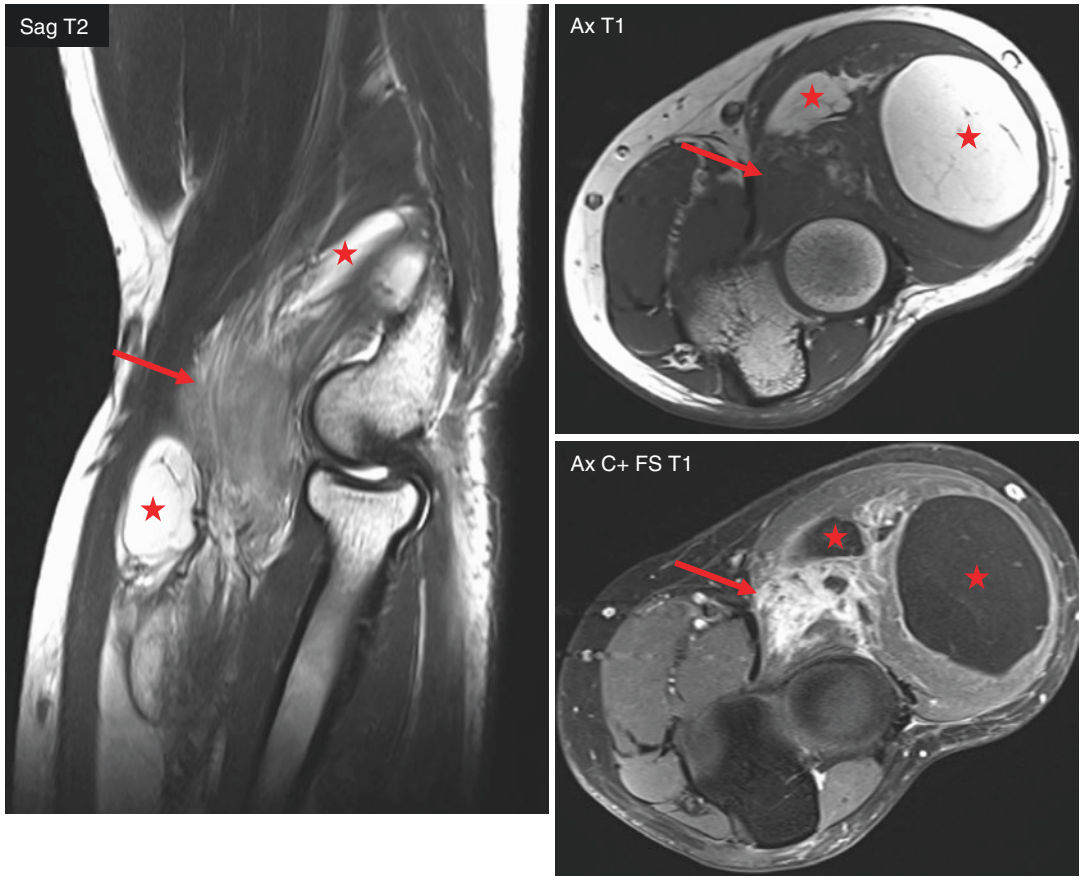

Dedifferentiated liposarcoma (Chap. 4)

- Well-differentiated liposarcoma-type component (*stars*)
- Enhancing nonlipomatous mass (*arrow*)

20.16 Quiz

A 79-year-old male, right medial foot pain

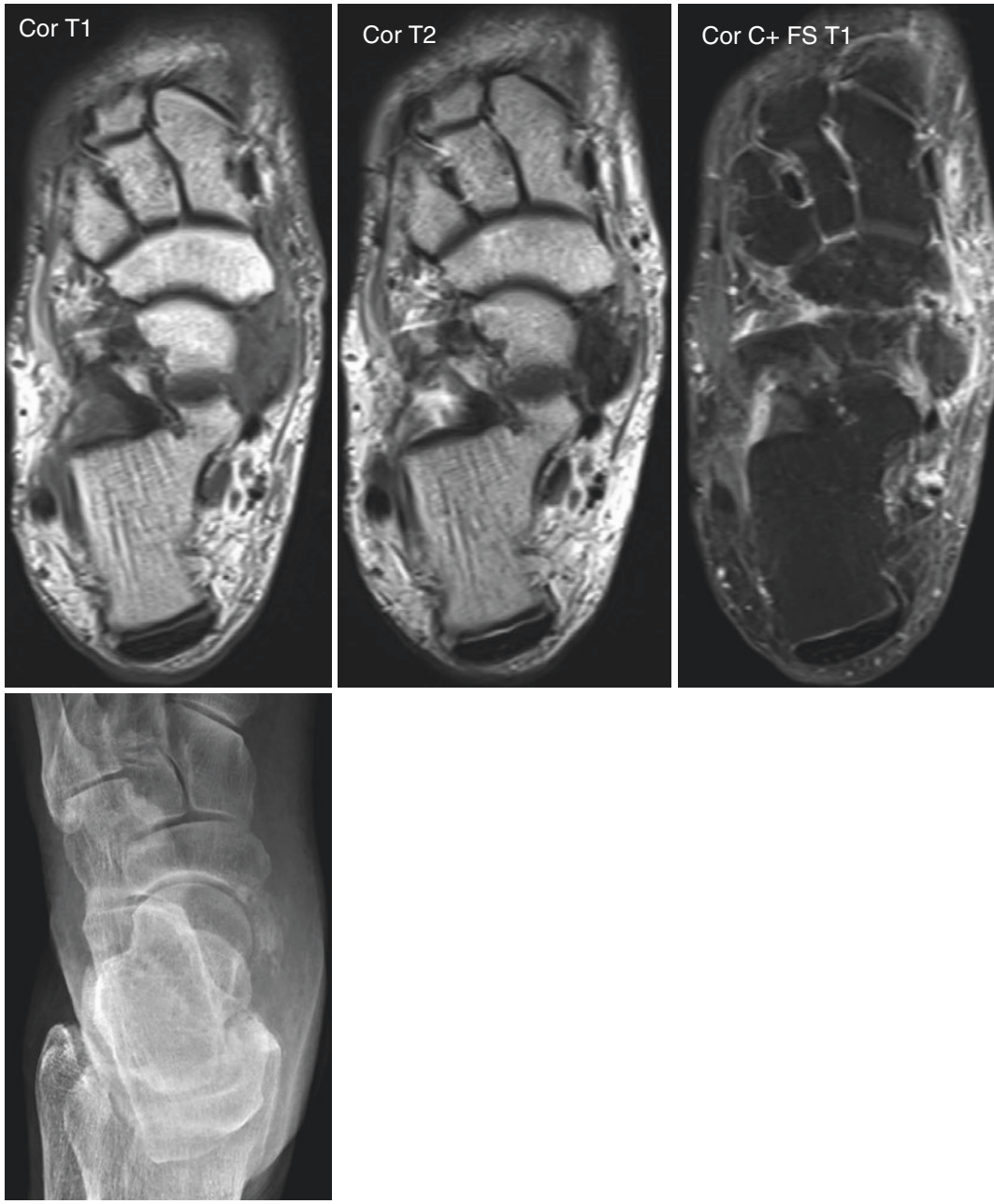

Fig. 20.16

20.16 Answer

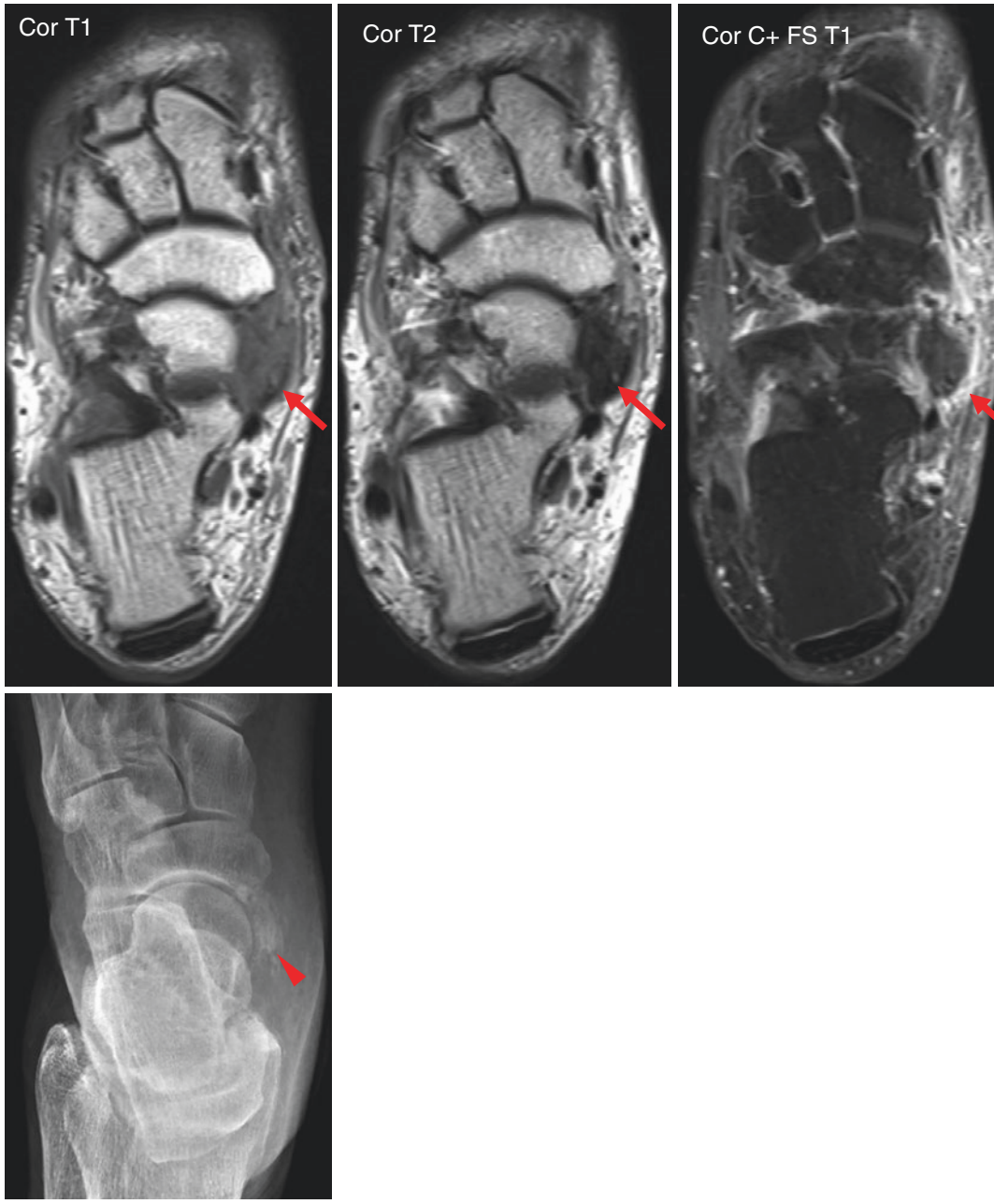

Chronic tophi in gout (Chap. 16)

- Low signal intensity on T1WI and T2WIs (*arrows*)
- Only peripheral enhancement
- Calcific deposit (*arrowhead*)

20.17 Quiz

A 19-year-old female, left medial thigh mass

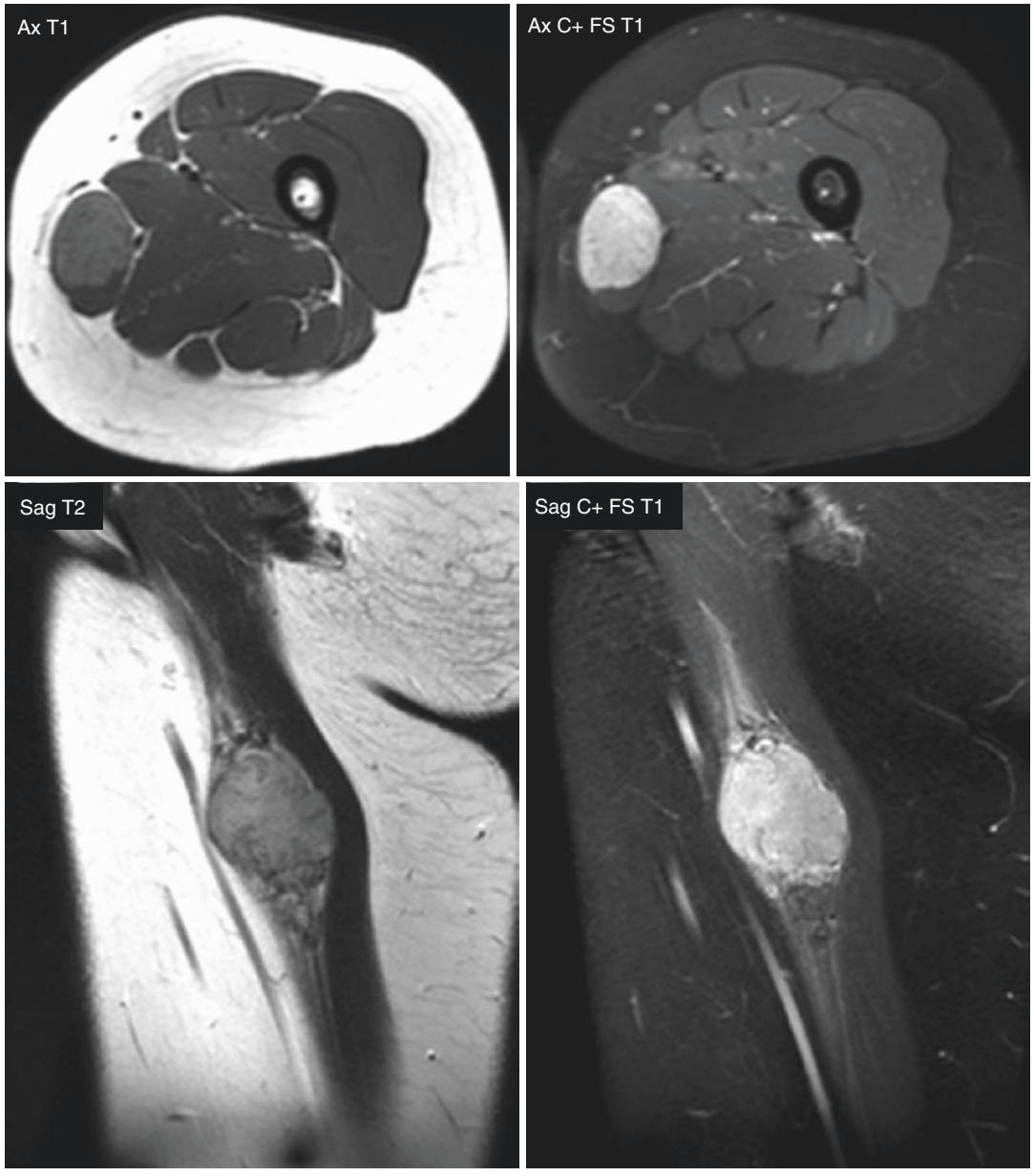

Fig. 20.17

20.17 Answer

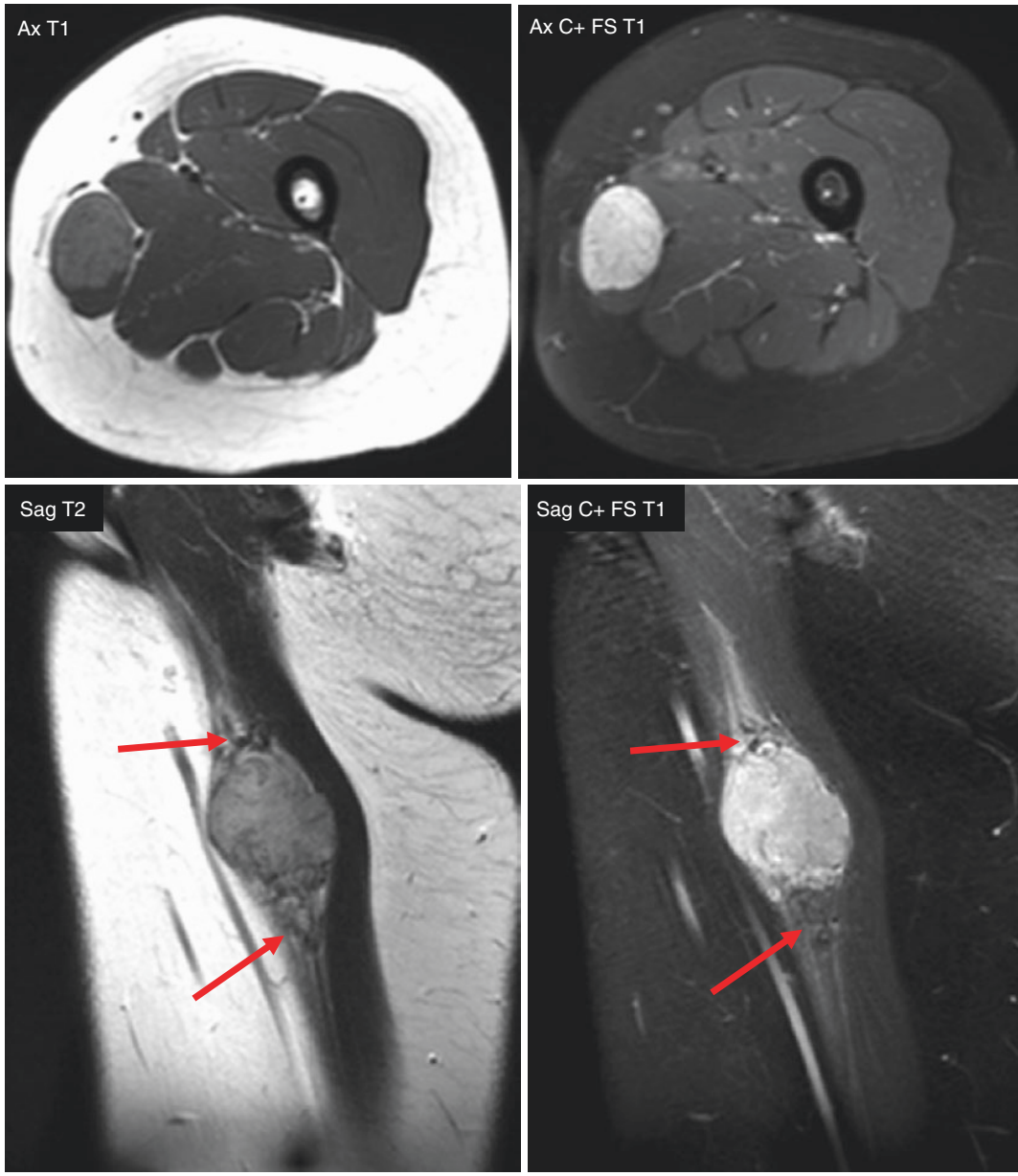

Alveolar soft part sarcoma (Chap. 13)

- High signal intensity on T1WI
- Multiple signal voids in and around the mass on T2WI (*arrows*)
- Strong enhancement with surrounding signal voids

20.18 Quiz

A 56-year-old female, left posterior thigh mass

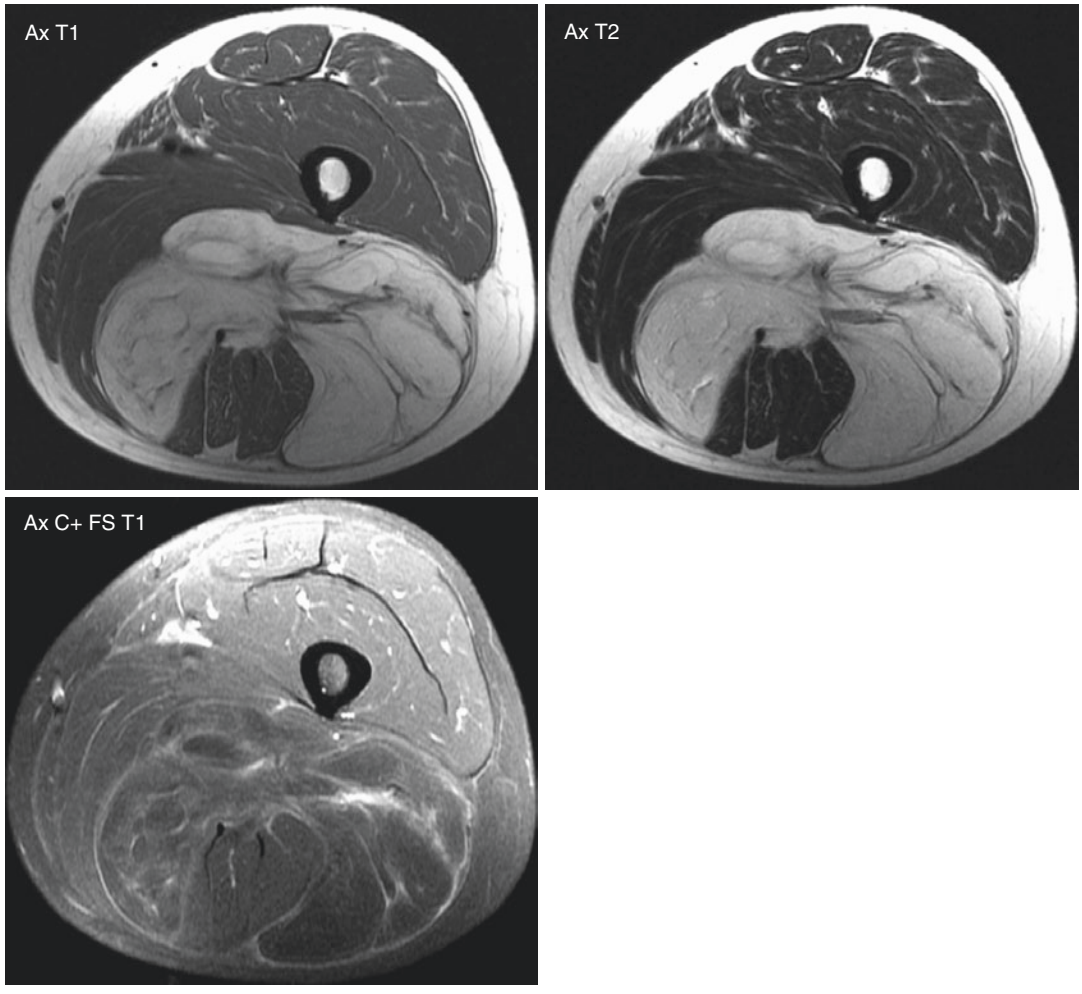

Fig. 20.18

20.18 Answer

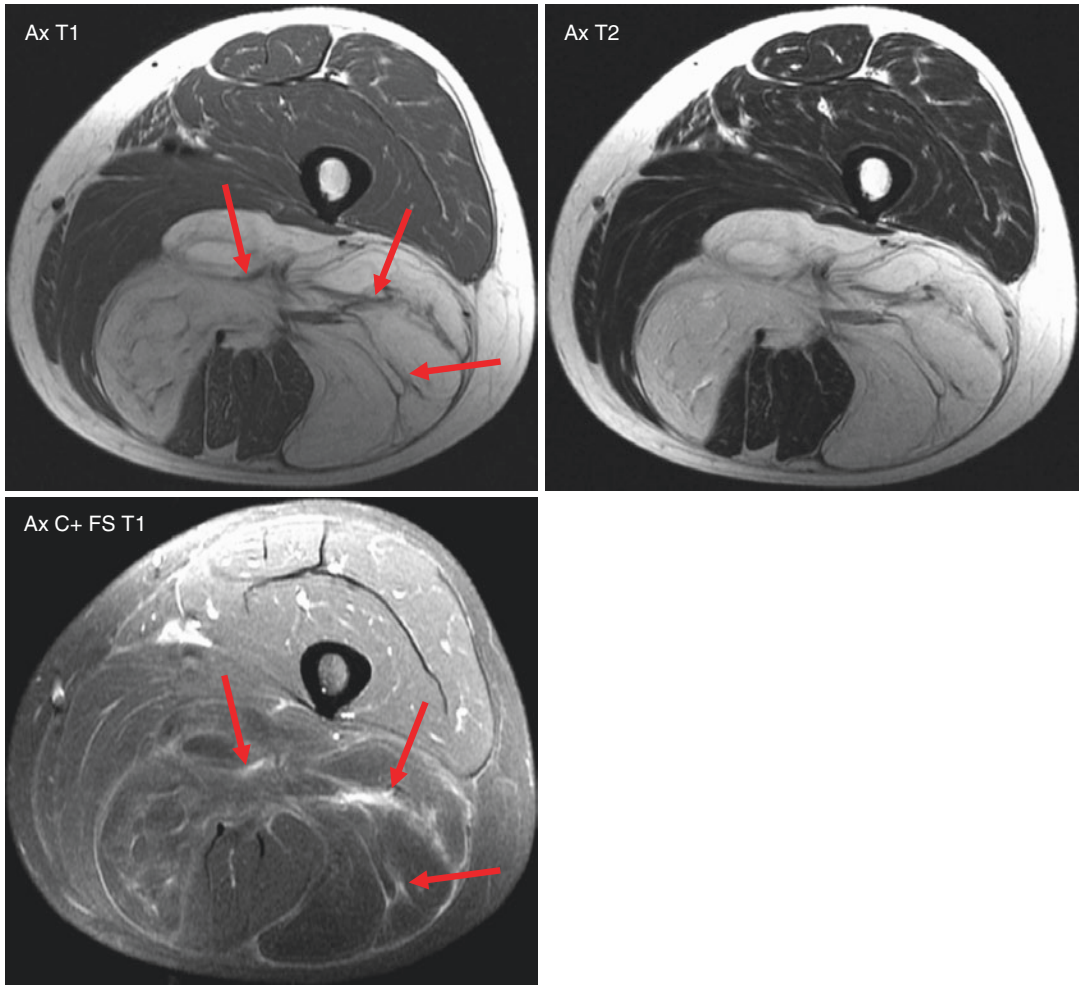

Well-differentiated liposarcoma (Chap. 4)

- Large fatty mass
- Multiple thick and enhancing septa (*arrows*)
- No significant nonlipomatous component

20.19 Quiz

A 27-year-old male with neurofibromatosis type 1, growing painful lower leg mass

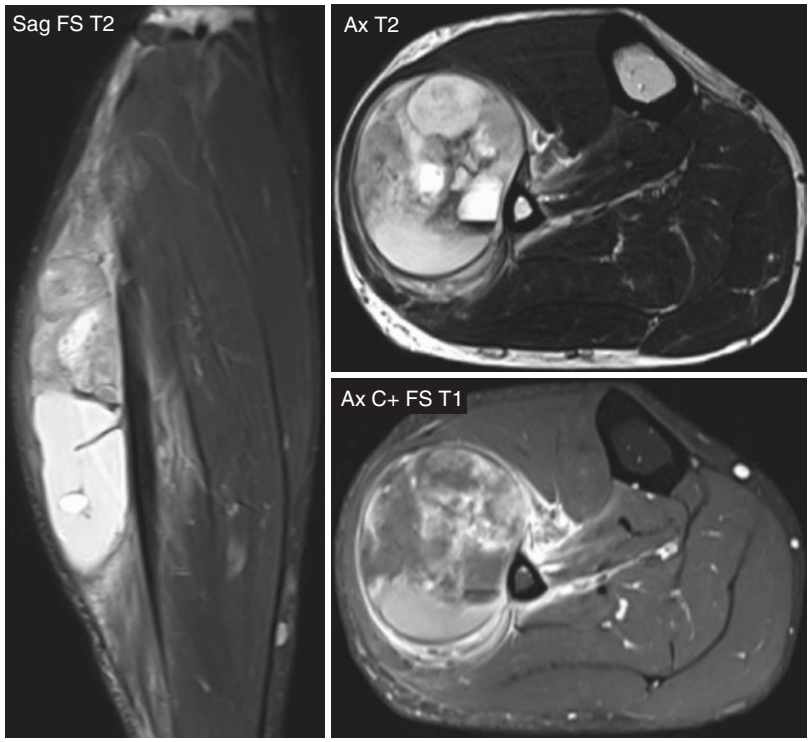

Fig. 20.19

20.19 Answer

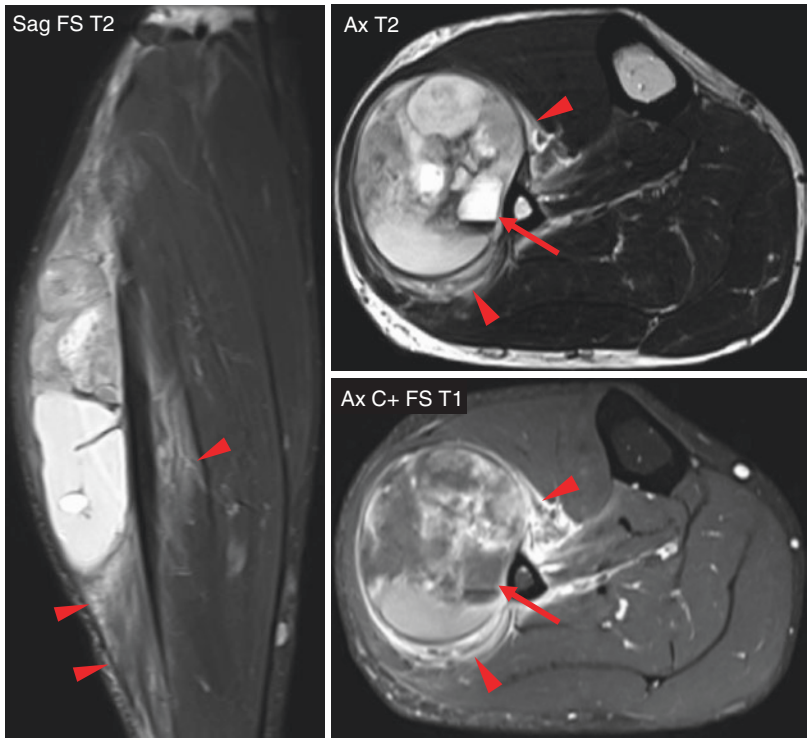

Malignant peripheral nerve sheath tumor (Chap. 12)

- Neurofibromatosis patient
- Large size of the lesion
- Intralesional hemorrhagic necrosis (*arrows*)
- Extensive surrounding perilesional edema (*arrowheads*)

20.20 Quiz

A 71-year-old male, right chest wall swelling

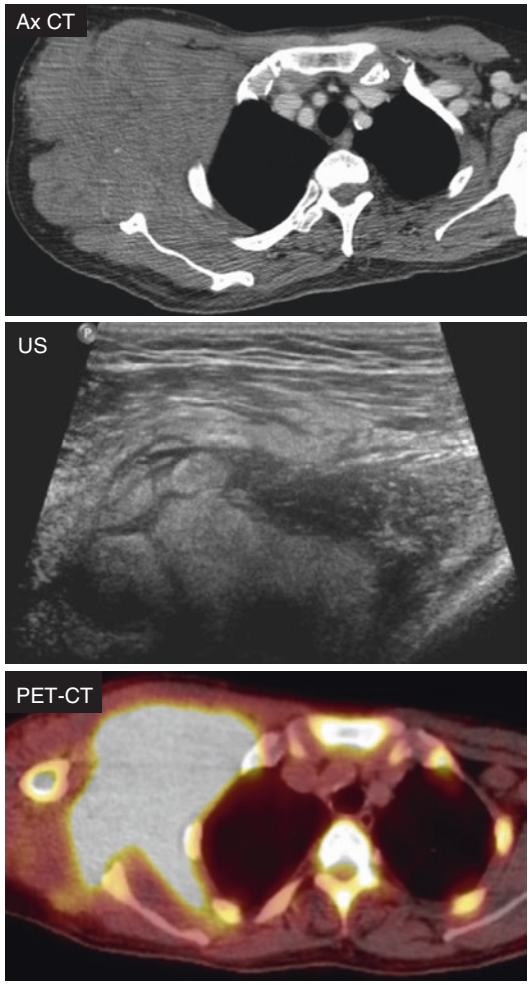

Fig. 20.20

20.20 Answer

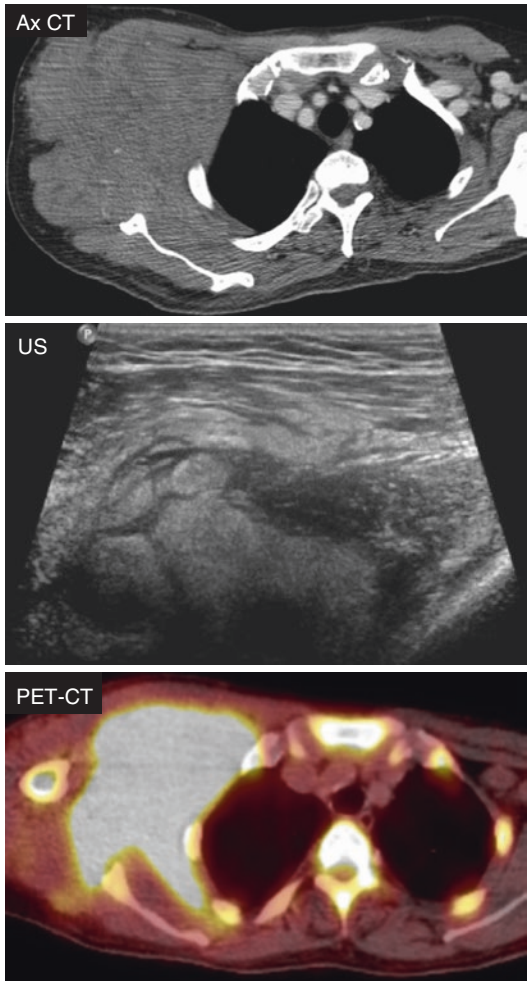

Lymphoma (Chap. 15)

- Diffuse muscle swelling on CT and US
- Strong FDG uptake on PET-CT

20.21 Quiz

A 39-year-old male, left hand mass

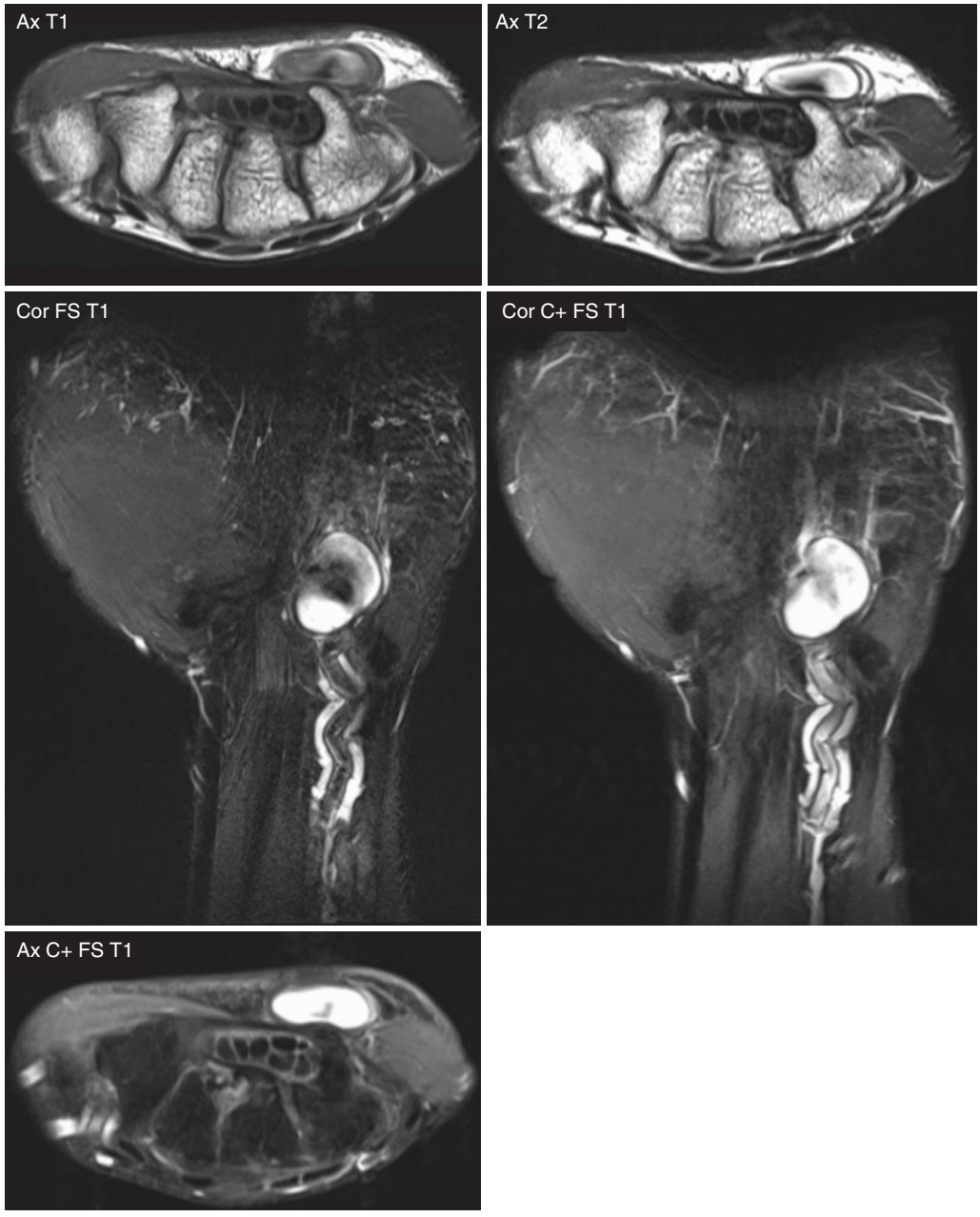

Fig. 20.21

20.21 Answer

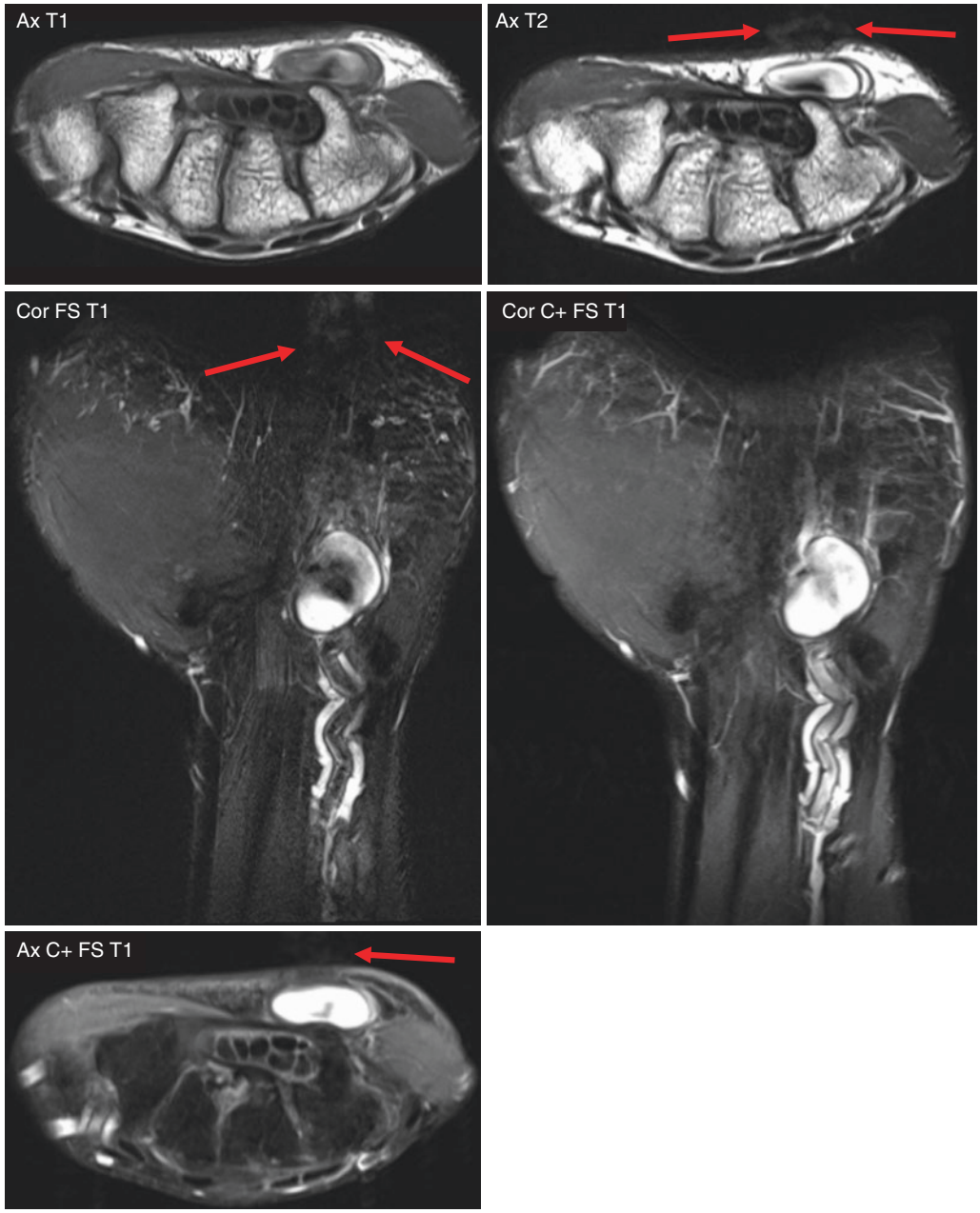

Aneurysm (Chap. 16)

- High signal intensity on T1WI
- Internal dark signal portion on T2WI
- Prominent pulsation artifact (*arrows*) around the mass on phase-encoding direction

20.22 Quiz

A 22-year-old male, right elbow mass

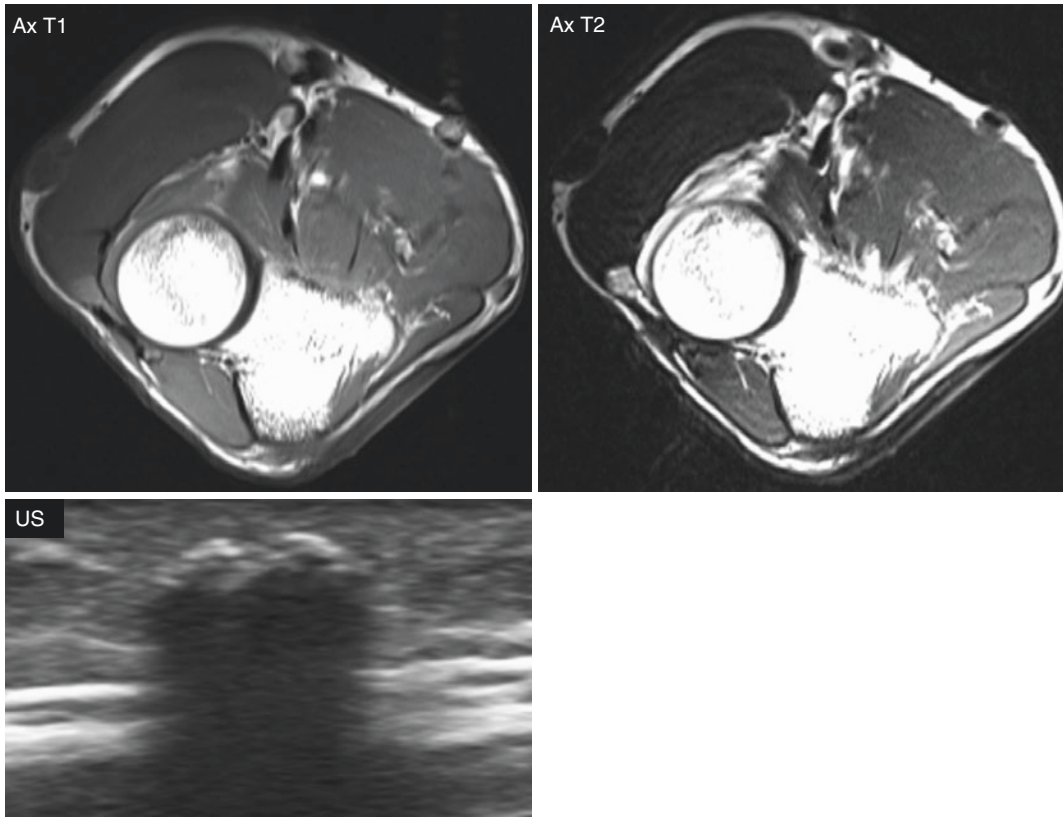

Fig. 20.22

20.22 Answer

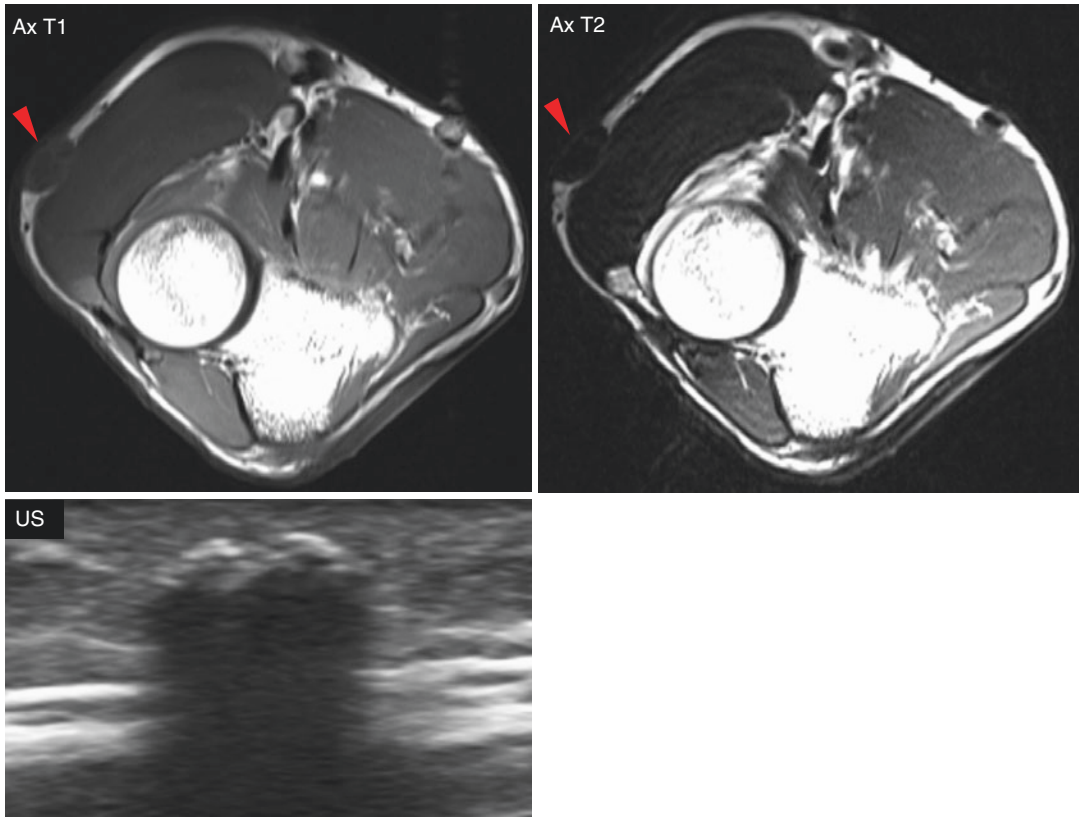

Pilomatricoma (Chap. 15)

- Low signal intensity on T1- and T2WIs (*arrowheads*)
- Linear hyperechoic lesion with posterior shadowing on US

20.23 Quiz

A 69-year-old female, slowly growing thigh mass

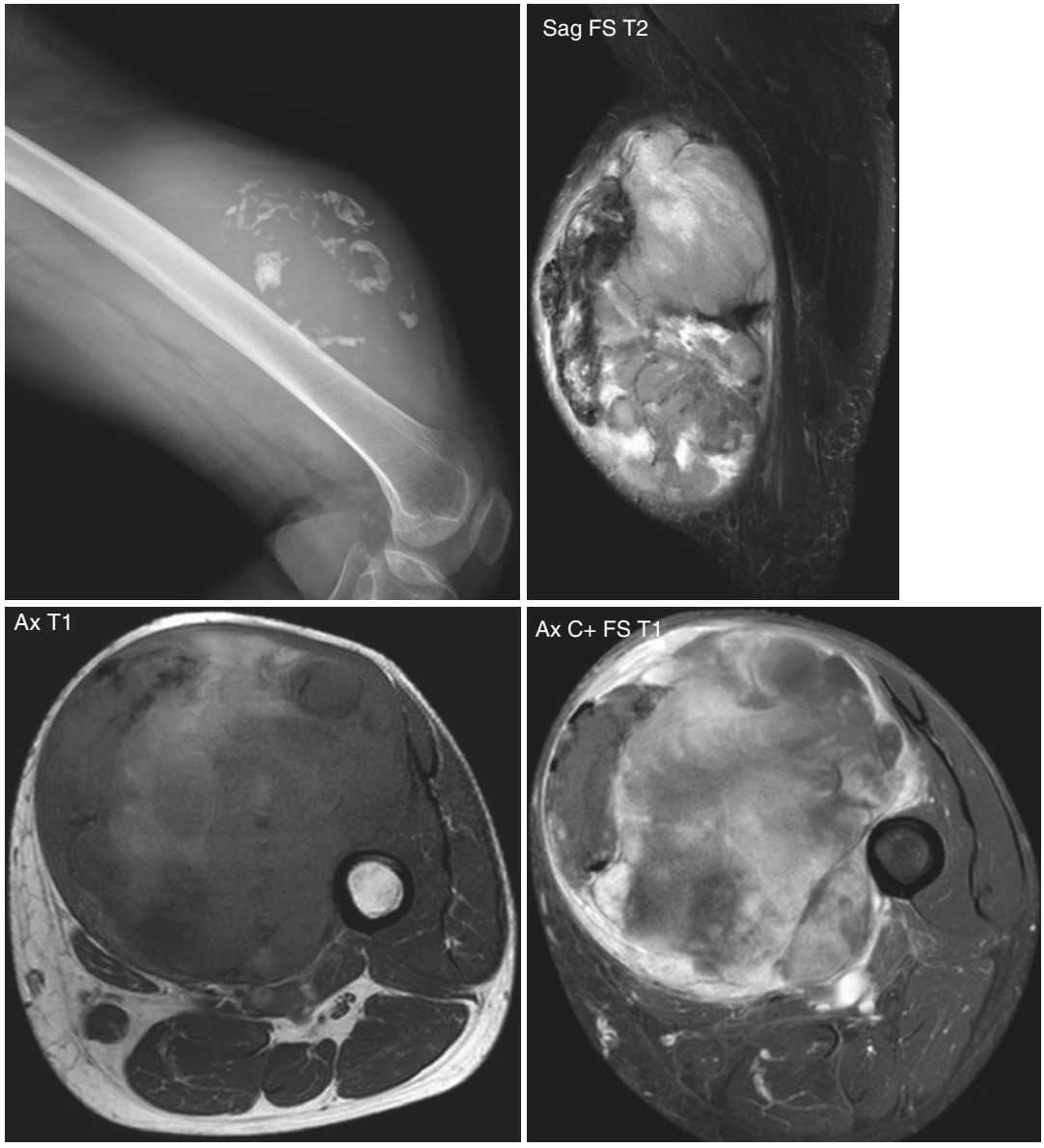

Fig. 20.23

20.23 Answer

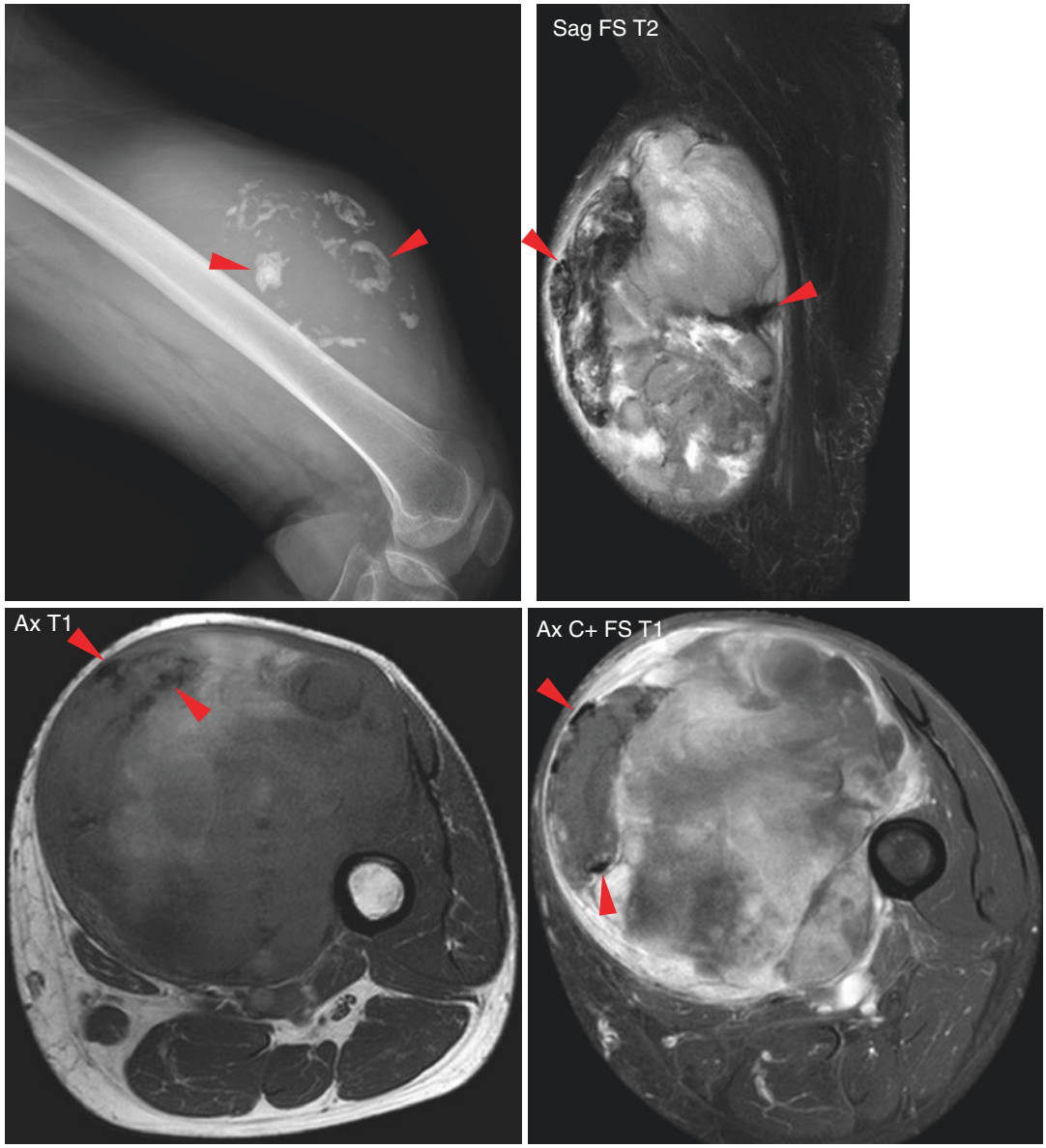

Extraskeletal osteosarcoma (Chap. 11)

- Intralesional haphazard osteoid mineralization (*arrowheads*)

20.24 Quiz

A 65-year-old male, left posterior shoulder mass

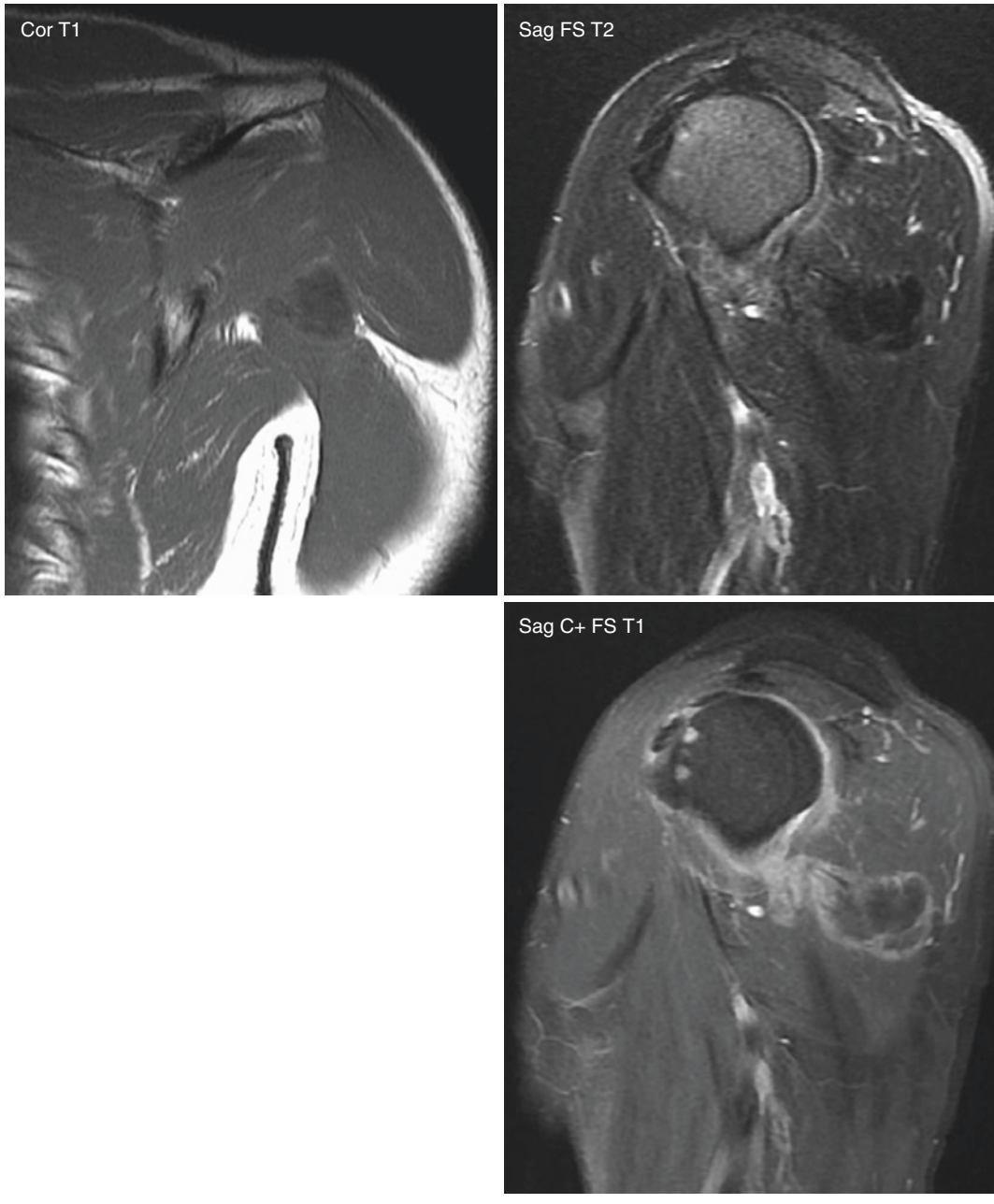

Fig. 20.24

20.24 Answer

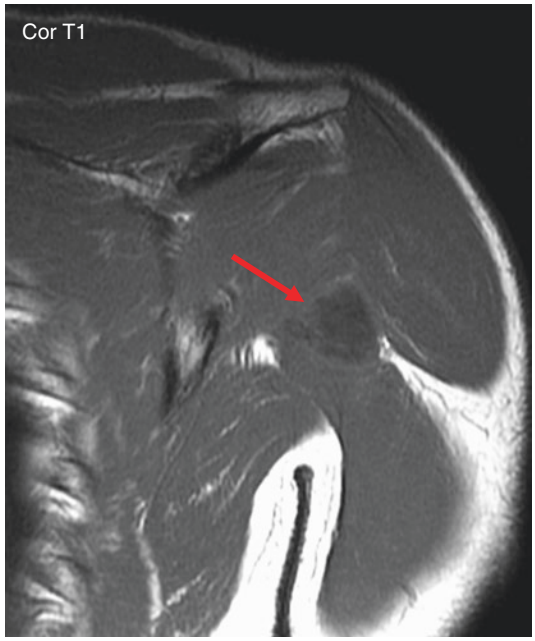

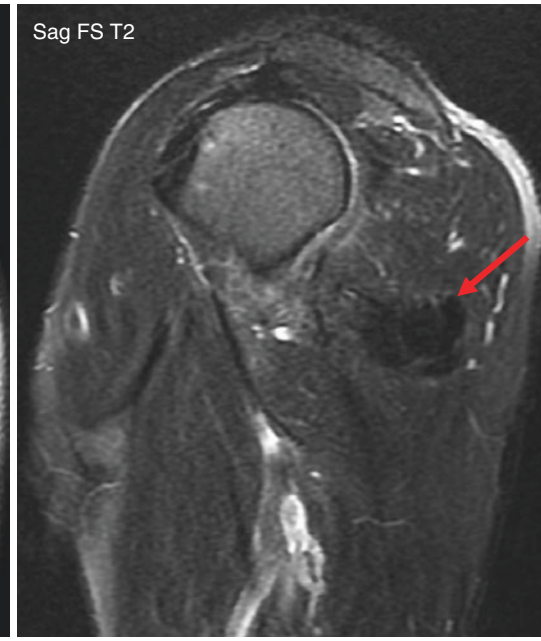

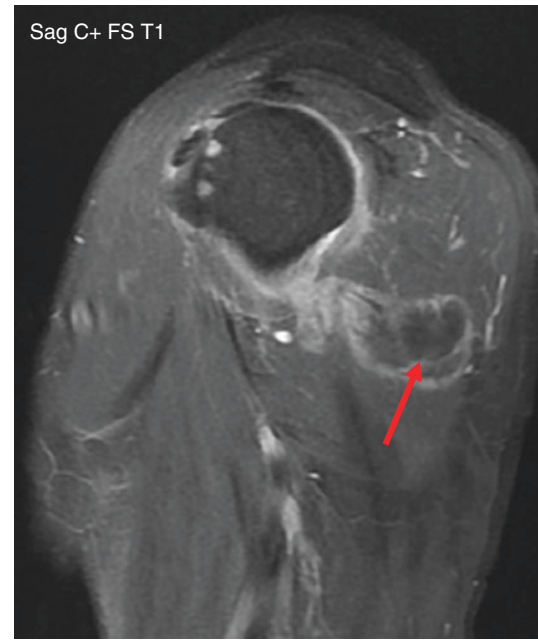

Desmoplastic fibroblastoma (Chap. 5)

- Predominantly low signal on T1- and T2WIs (*arrow*)
- Non-enhancing collagenous components (*arrow*)

20.25 Quiz

A 7-year-old boy, right lateral knee mass

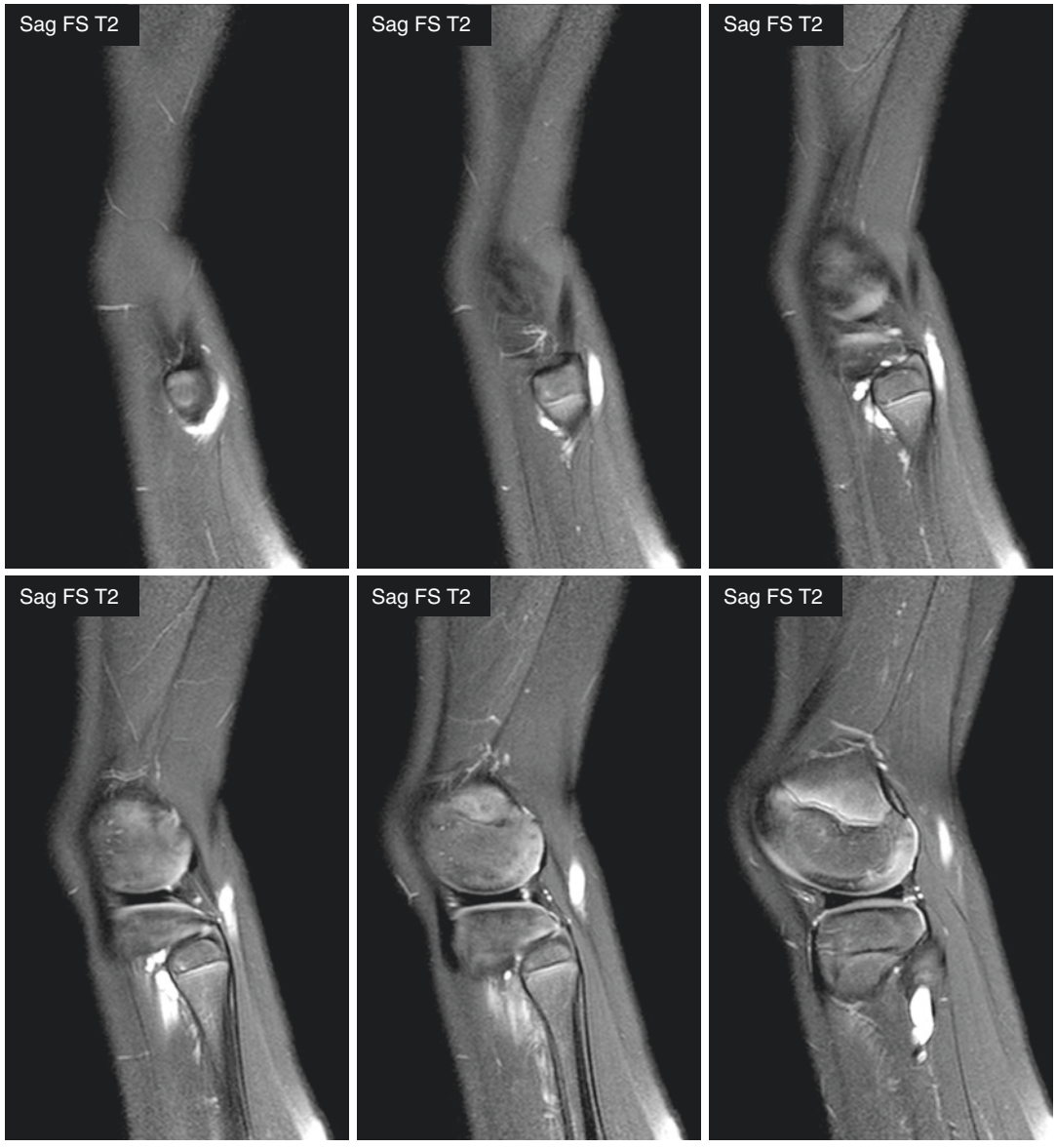

Fig. 20.25

20.25 Answer

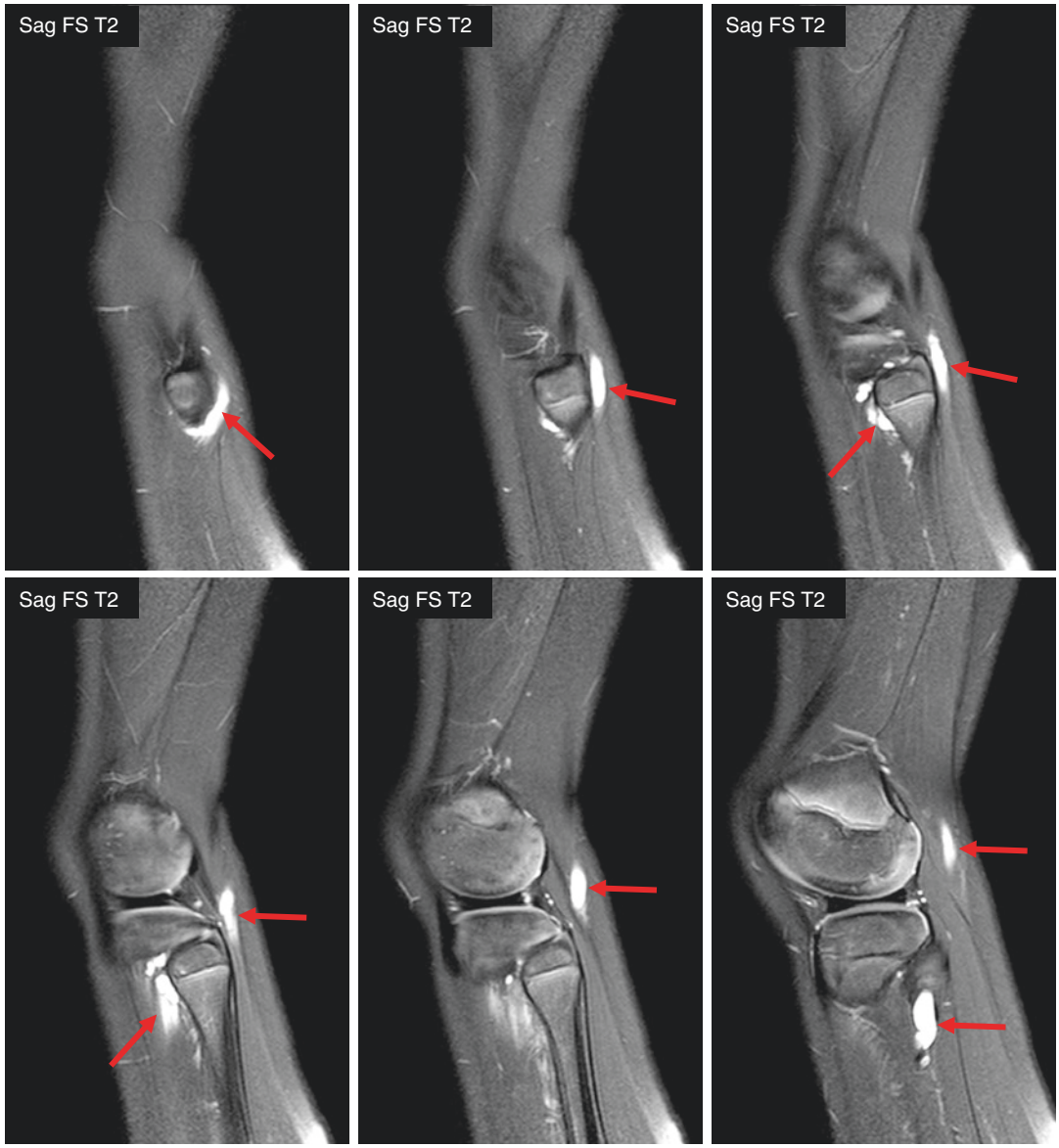

Intraneural ganglion (Chap. 16)

- Elongated mass along the common peroneal nerve with fluid-like high signal intensity on T2WI (*arrows*)

20.26 Quiz

A 60-year-old male, right shoulder mass

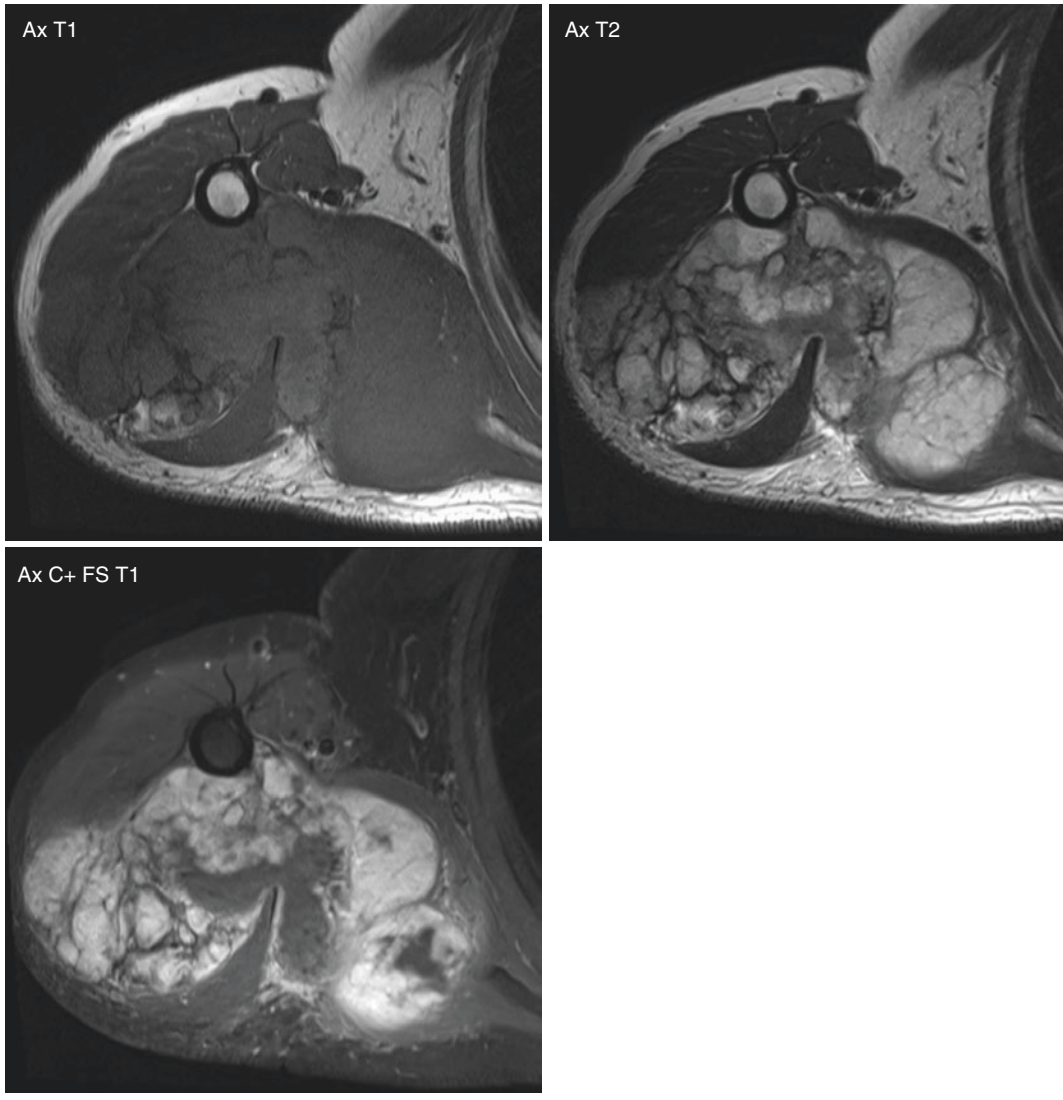

Fig. 20.26

20.26 Answer

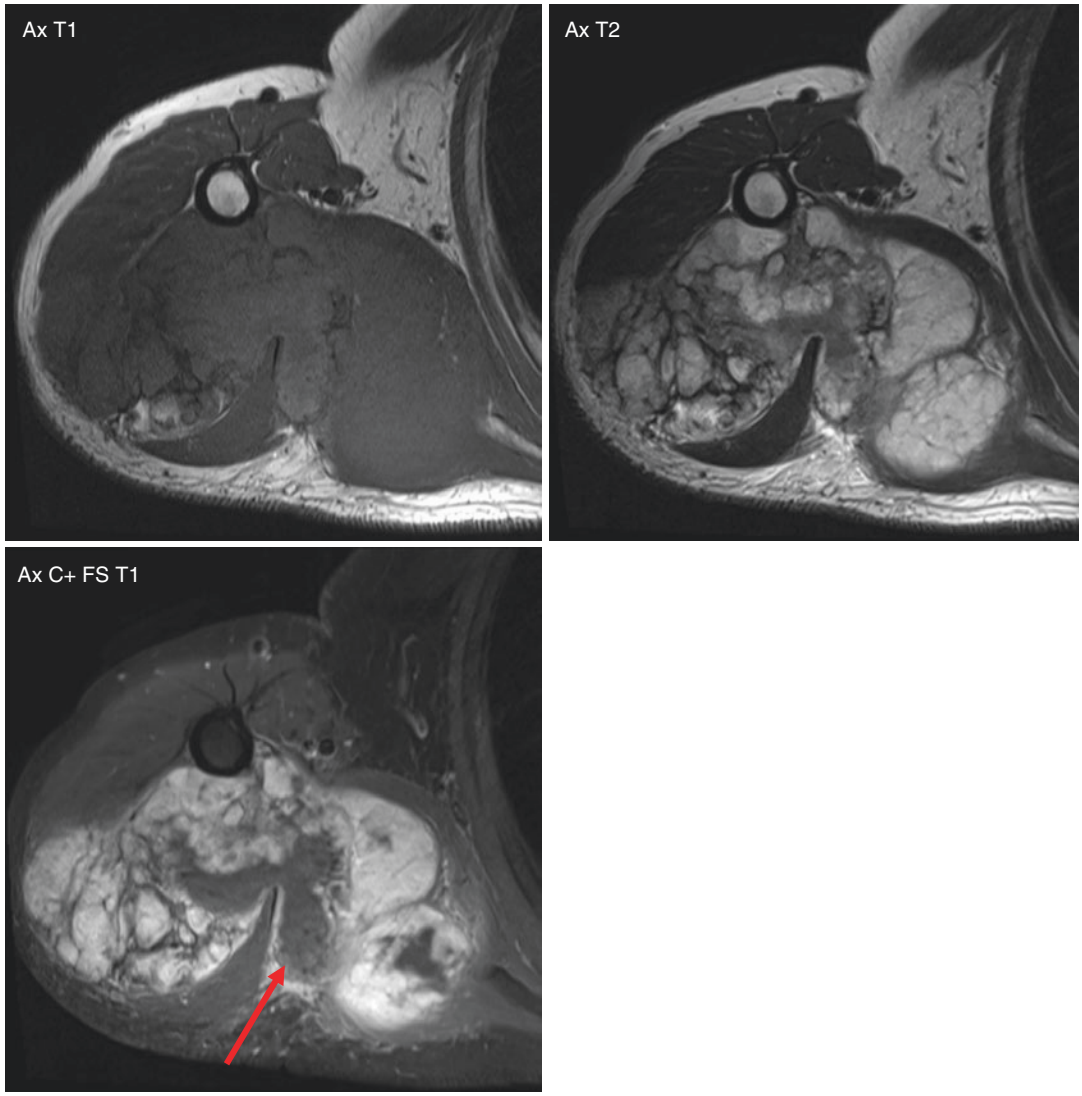

Extraskeletal myxoid chondrosarcoma (Chap. 13)

- High signal intensity with thin fibrous septa of low signal intensity on T2WI
- An area of necrotic change (*arrow*)
- Prominent enhancement with peripheral/septal enhancement pattern

20.27 Quiz

A 31-year-old male, left thigh palpable mass

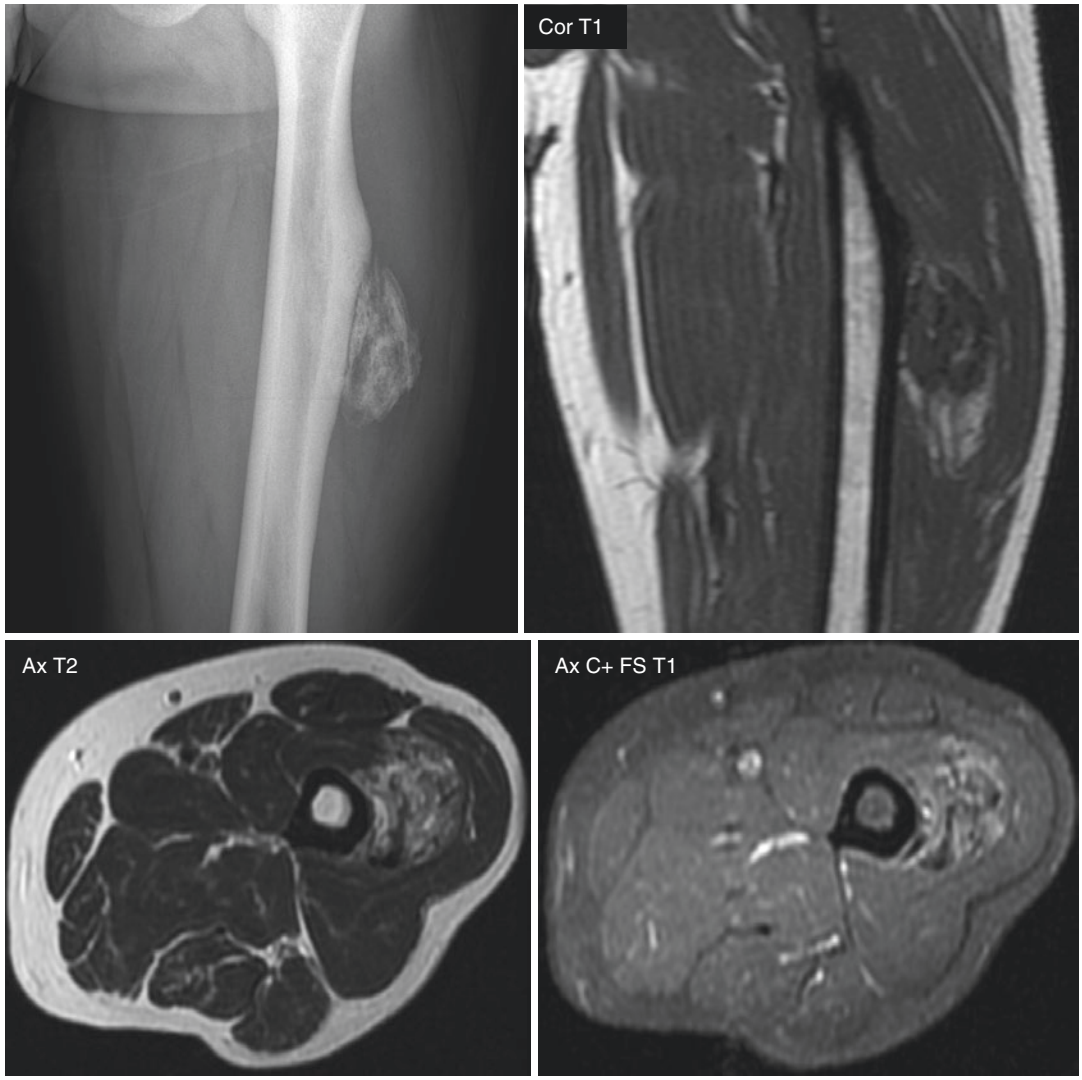

Fig. 20.27

20.27 Answer

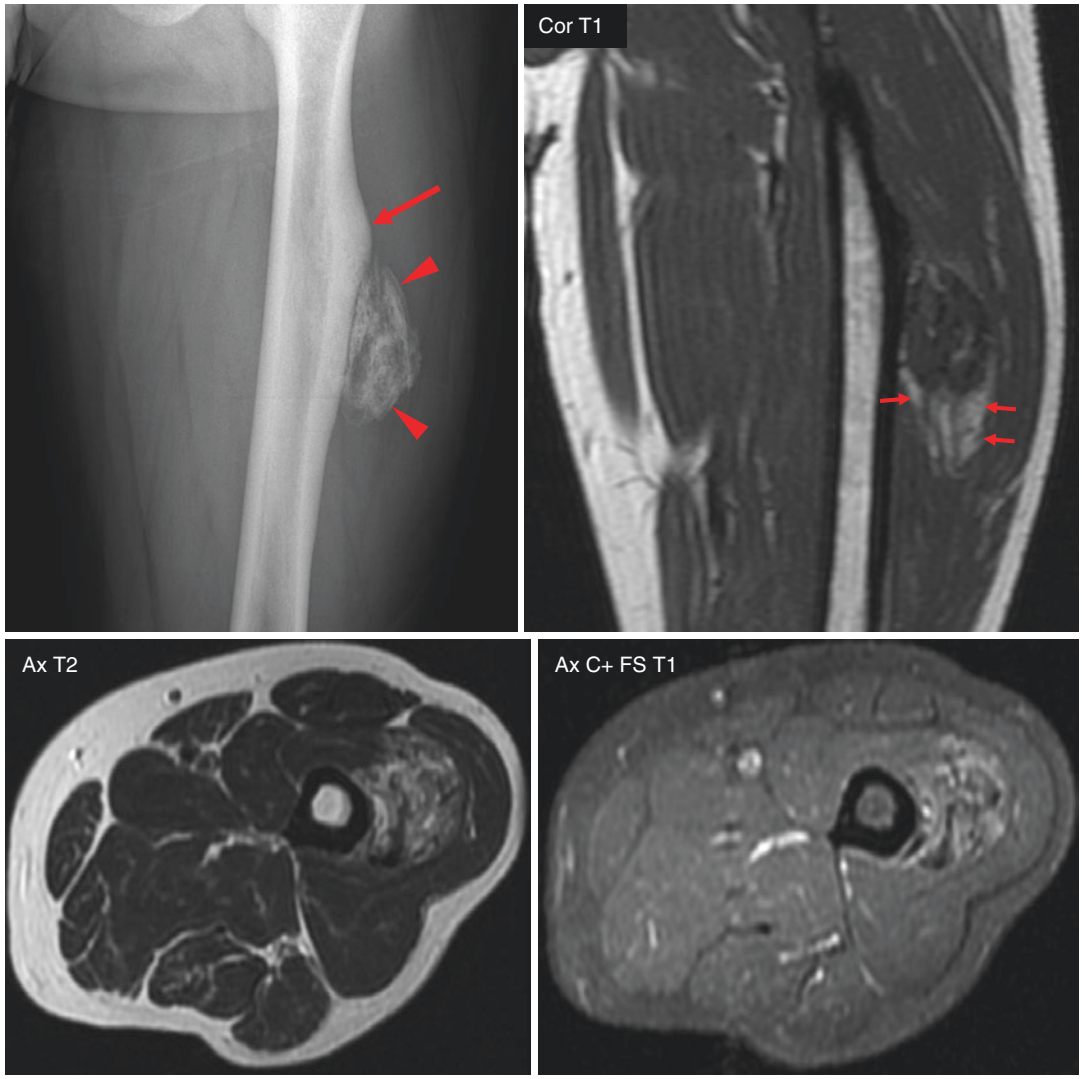

Ossifying hemangioma (Chap. 10)

- "Swiss cheese" appearance of intralesional mineralization (*arrowheads*)
- Periosteal cortical hypertrophy (*arrow*)
- Peripheral fat overgrowth (*small arrows*)

20.28 Quiz

A 65-year-old male, right thigh mass

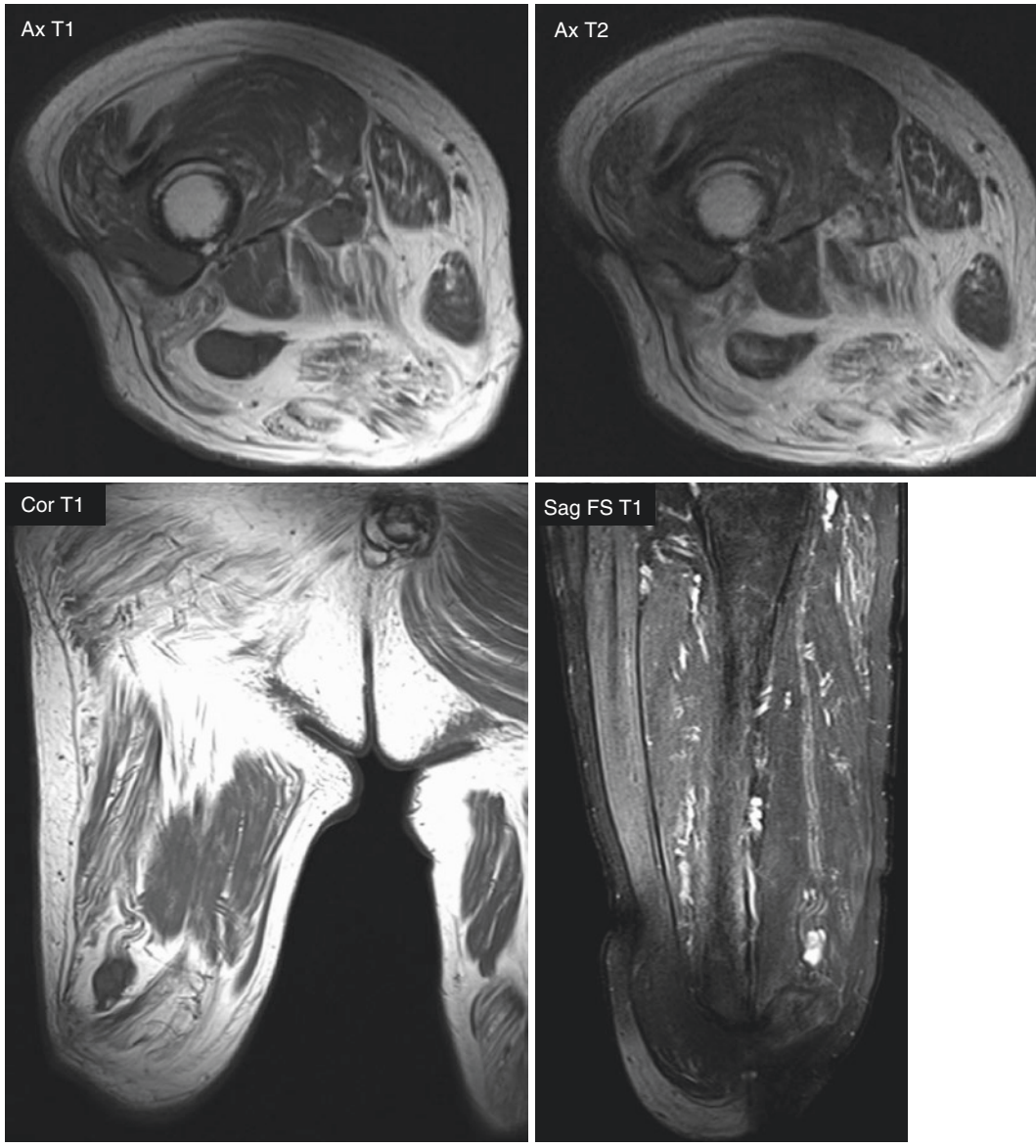

Fig. 20.28

20.28 Answer

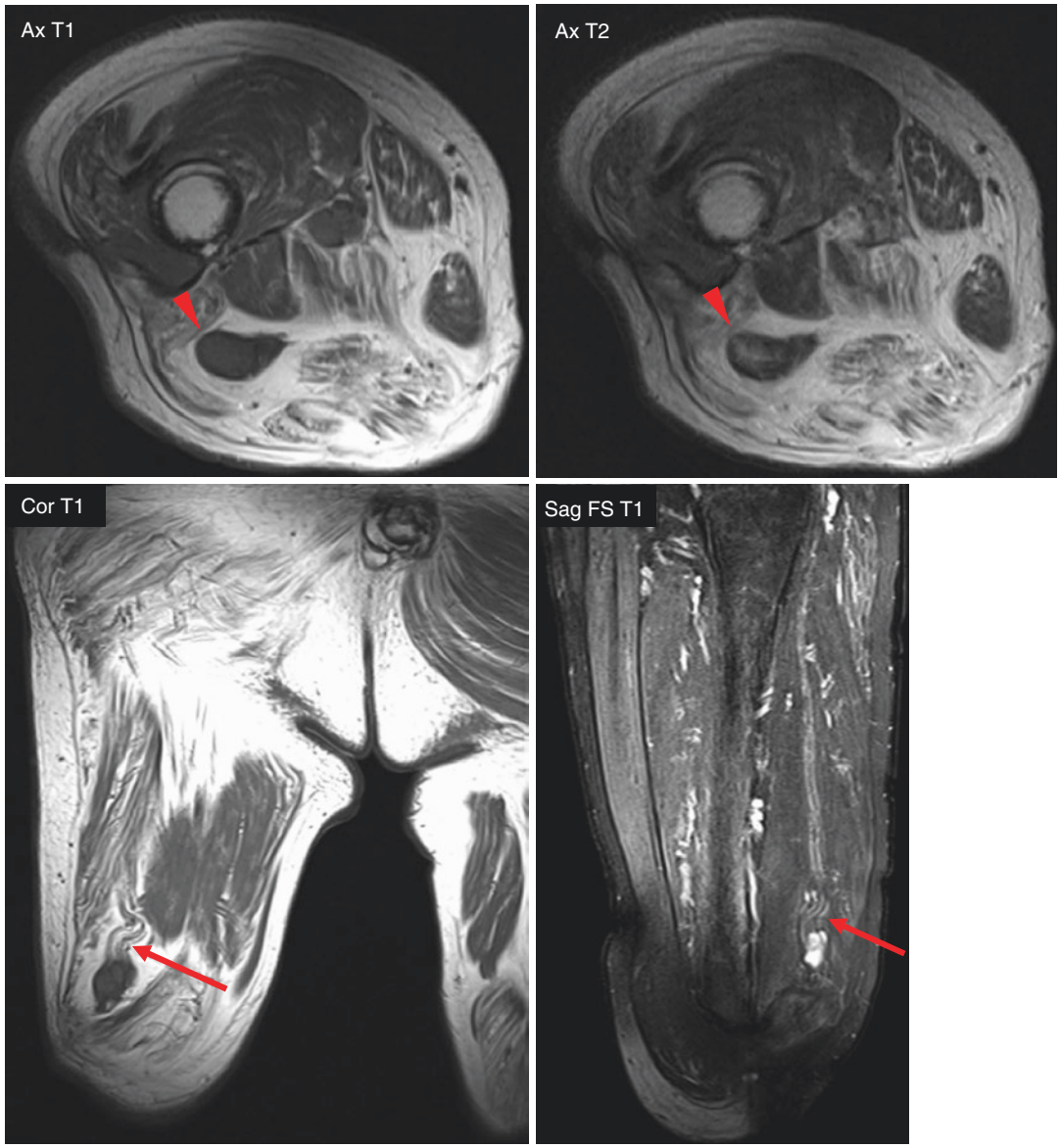

Terminal neuroma (Chap. 16)

- Hypointense mass (*arrowheads*) on T1- and T2WIs
- A mass in continuity with the end of the severed sciatic nerve (*arrows*)

20.29 Quiz

A 12-year-old girl, slowly growing foot mass

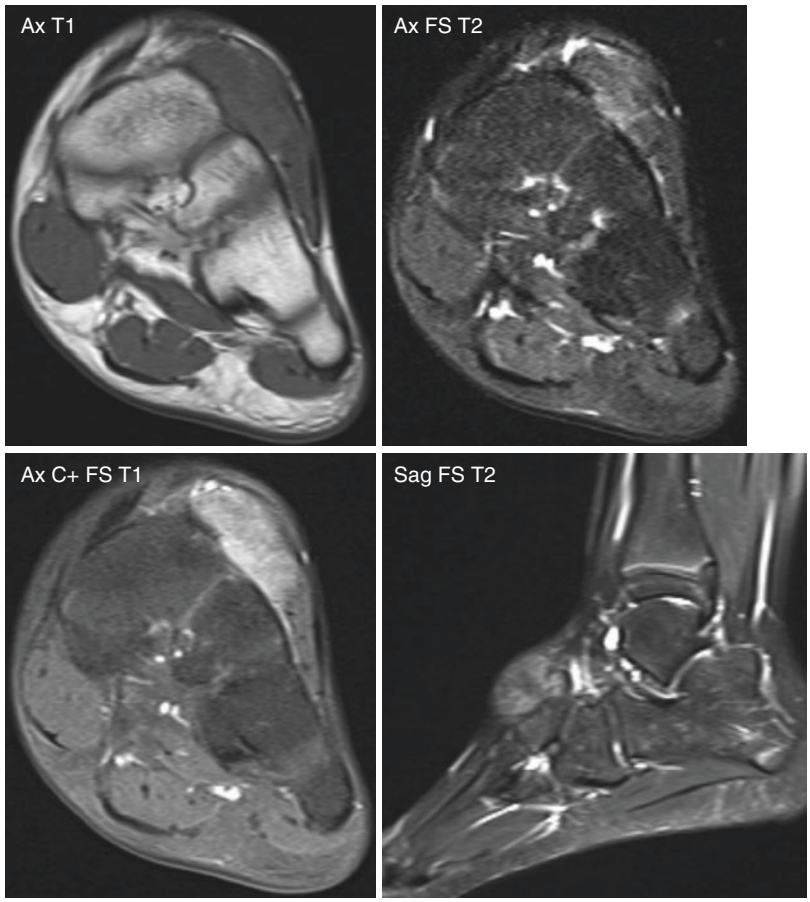

Fig. 20.29

20.29 Answer

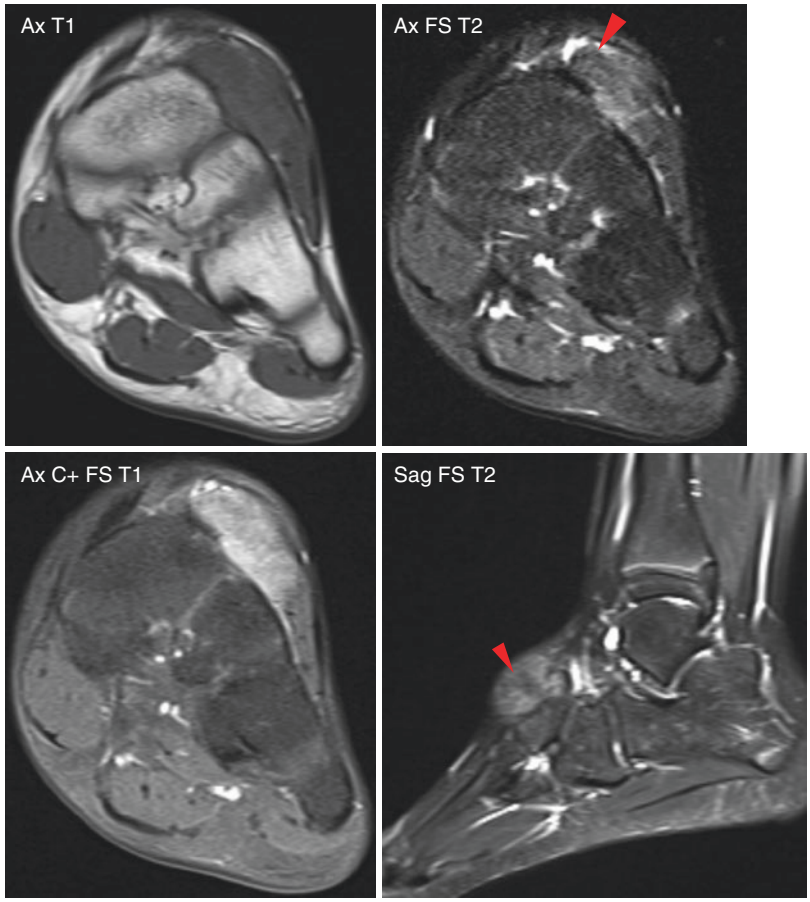

Tenosynovial giant cell tumor, localized type (Chap. 6)

- Very low signal regions (*arrowheads*) within the lesion on T2WI, reflecting hemosiderin depositions

20.30 Quiz

A 32-year-old female, pain and cold sensitivity

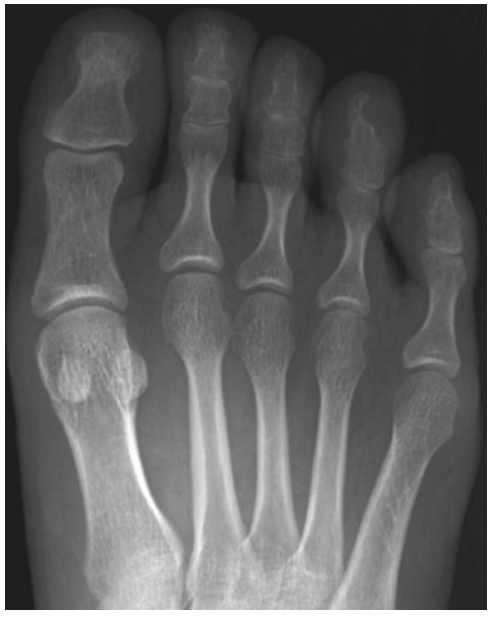
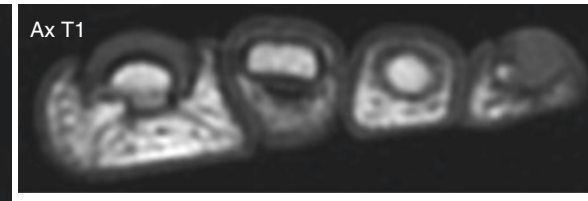

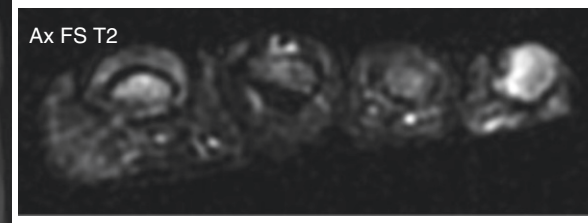

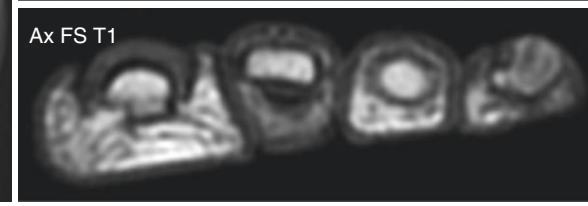

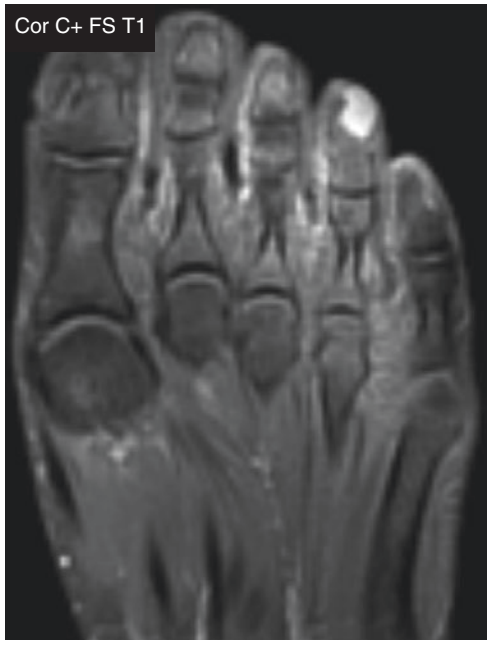

Fig. 20.30

20.30 Answer

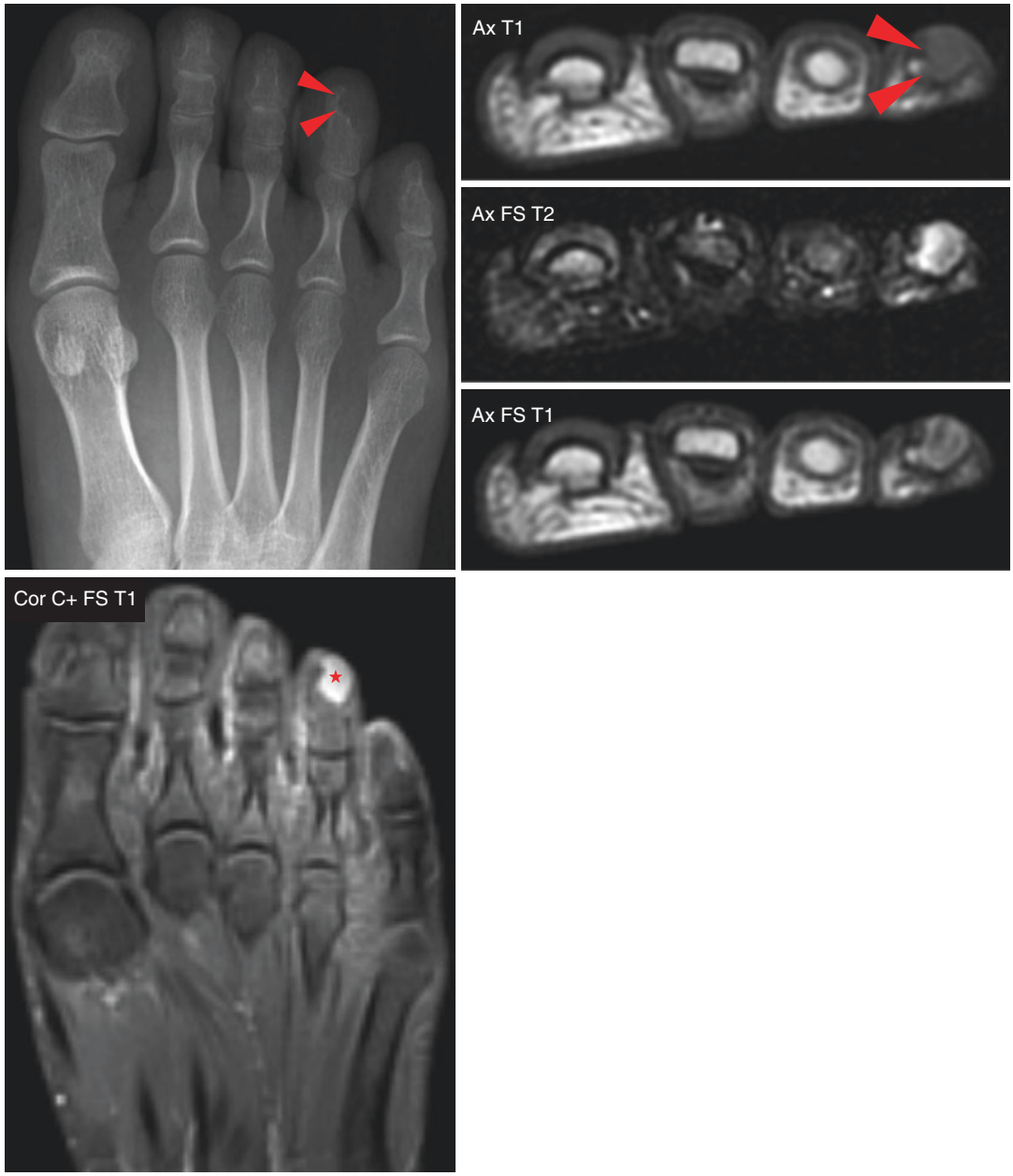

Glomus tumor (Chap. 8)

- Located in the nail bed
- Present neighboring bone erosion (*arrowheads*)
- Intense contrast enhancement due to hypervascularity (*star*)

20.31 Quiz

A 25-year-old male, neurofibromatosis type 1

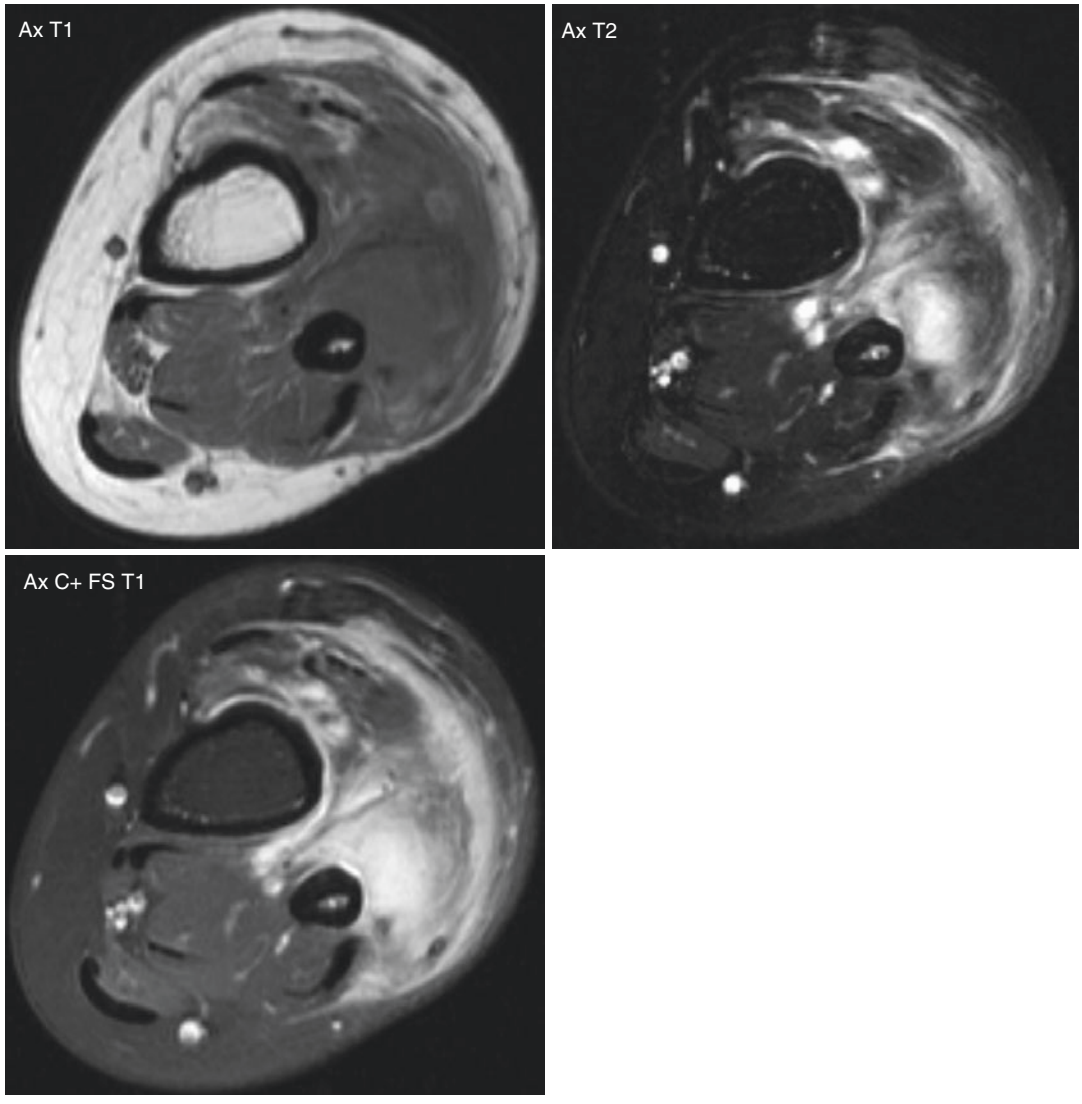

Fig. 20.31

20.31 Answer

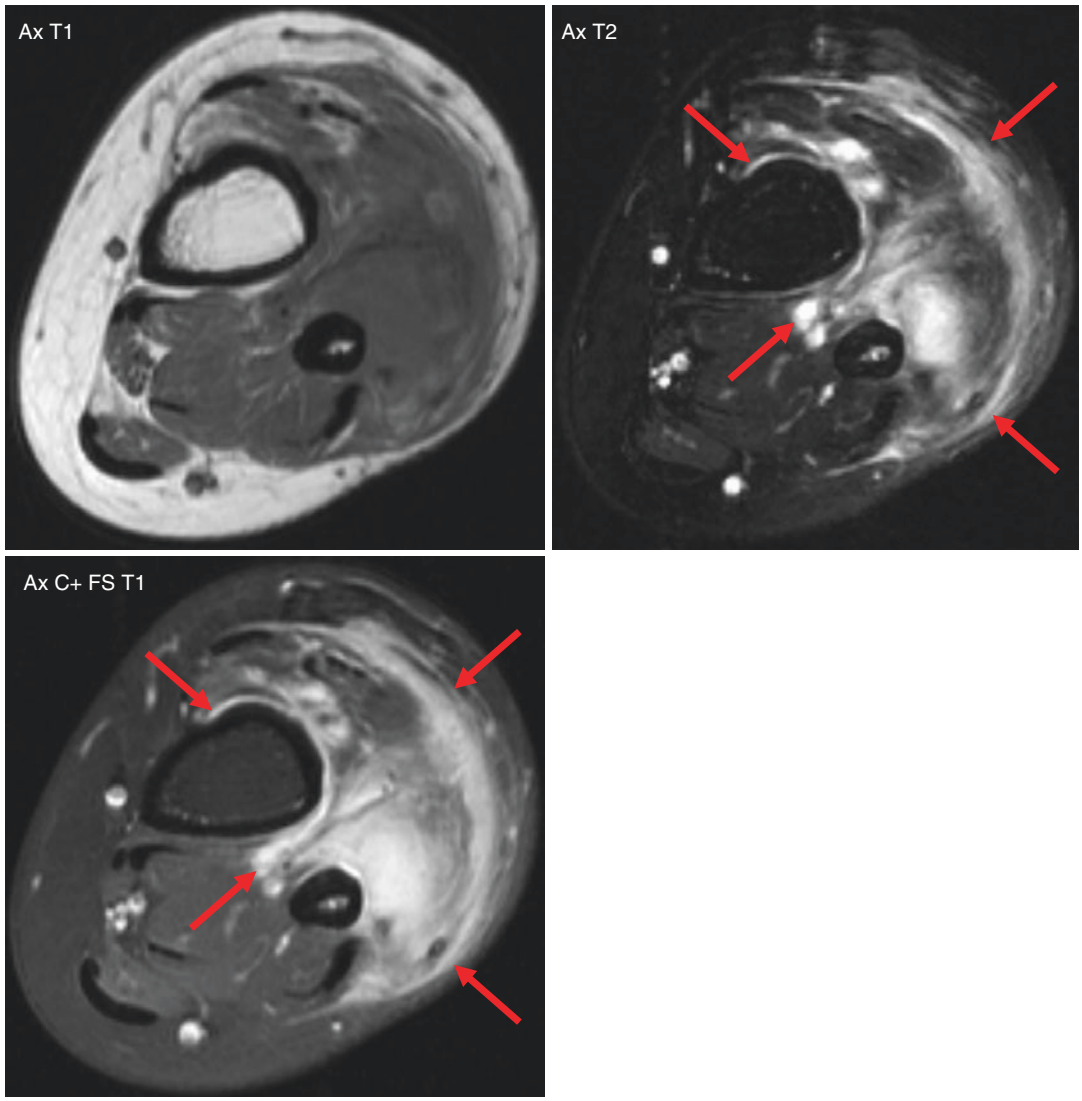

Neurofibroma, diffuse type (Chap. 12)

- Neurofibromatosis type 1
- Infiltrative soft tissue mass affecting multiple tissue planes (*arrows*)

20.32 Quiz

A 42-year-old male, left posterior elbow mass

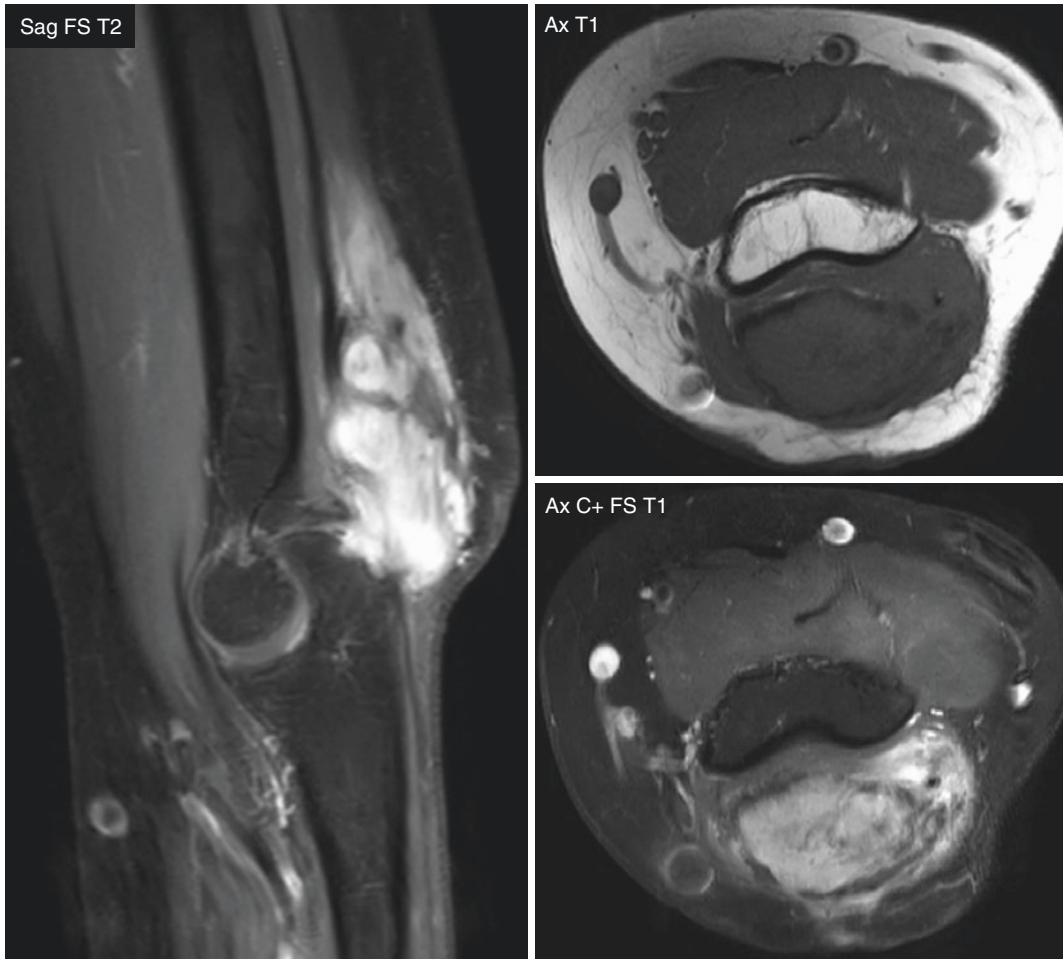

Fig. 20.32

20.32 Answer

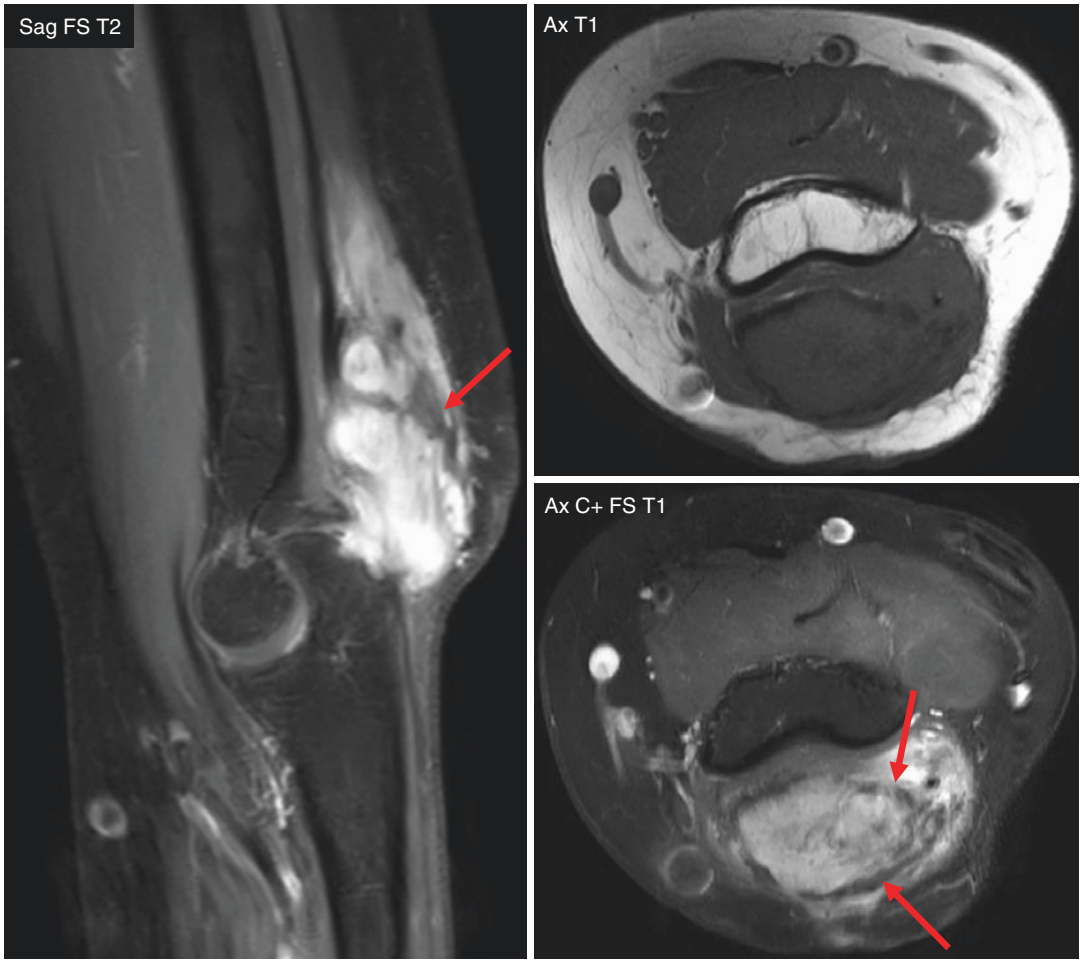

Fibromatosis (Chap. 5)

- Infiltrative soft tissue mass
- Marked contrast enhancement
- T2 hypointense, non-enhancing band-like components (*arrows*)

20.33 Quiz

An 1-year-old boy, left thigh mass

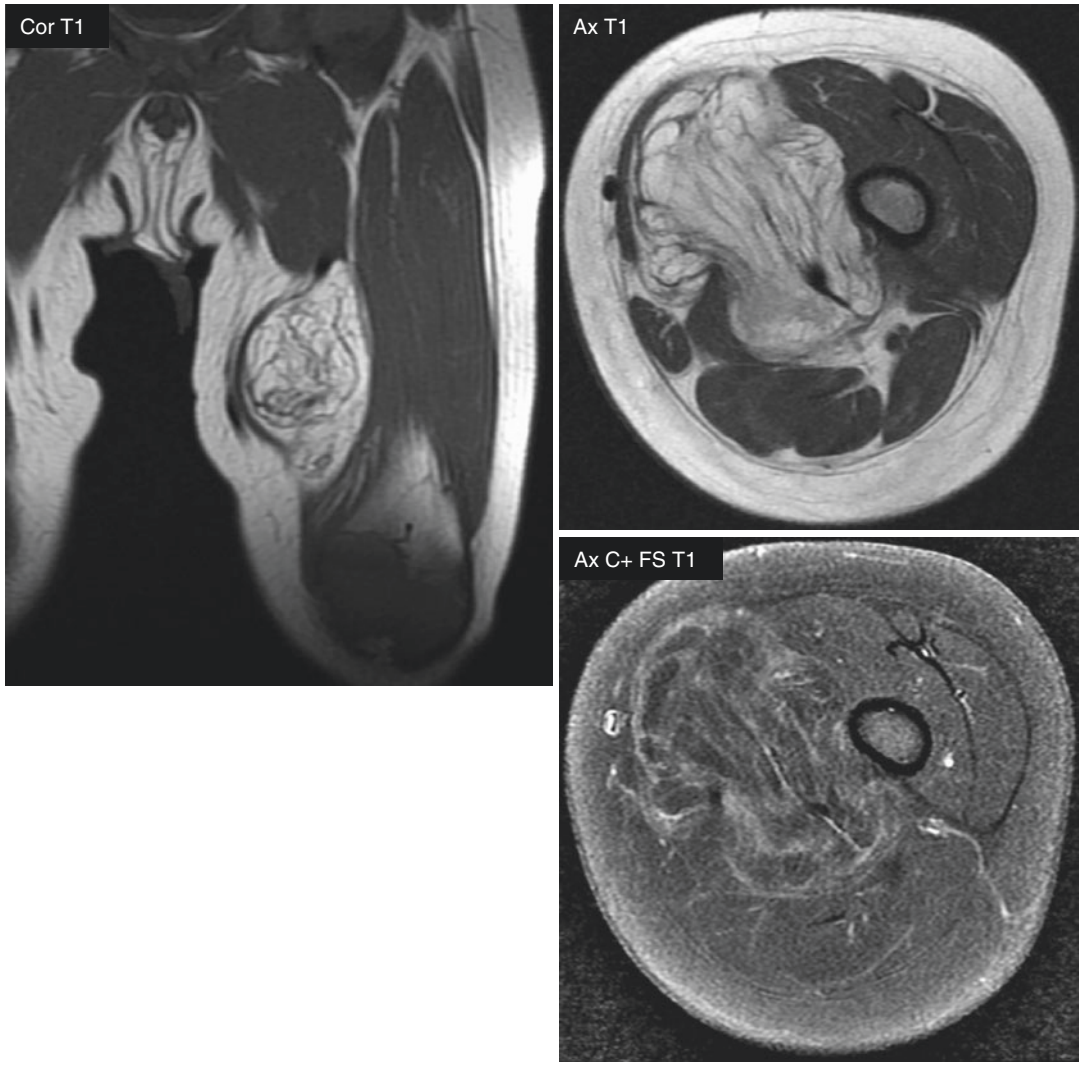

Fig. 20.33

20.33 Answer

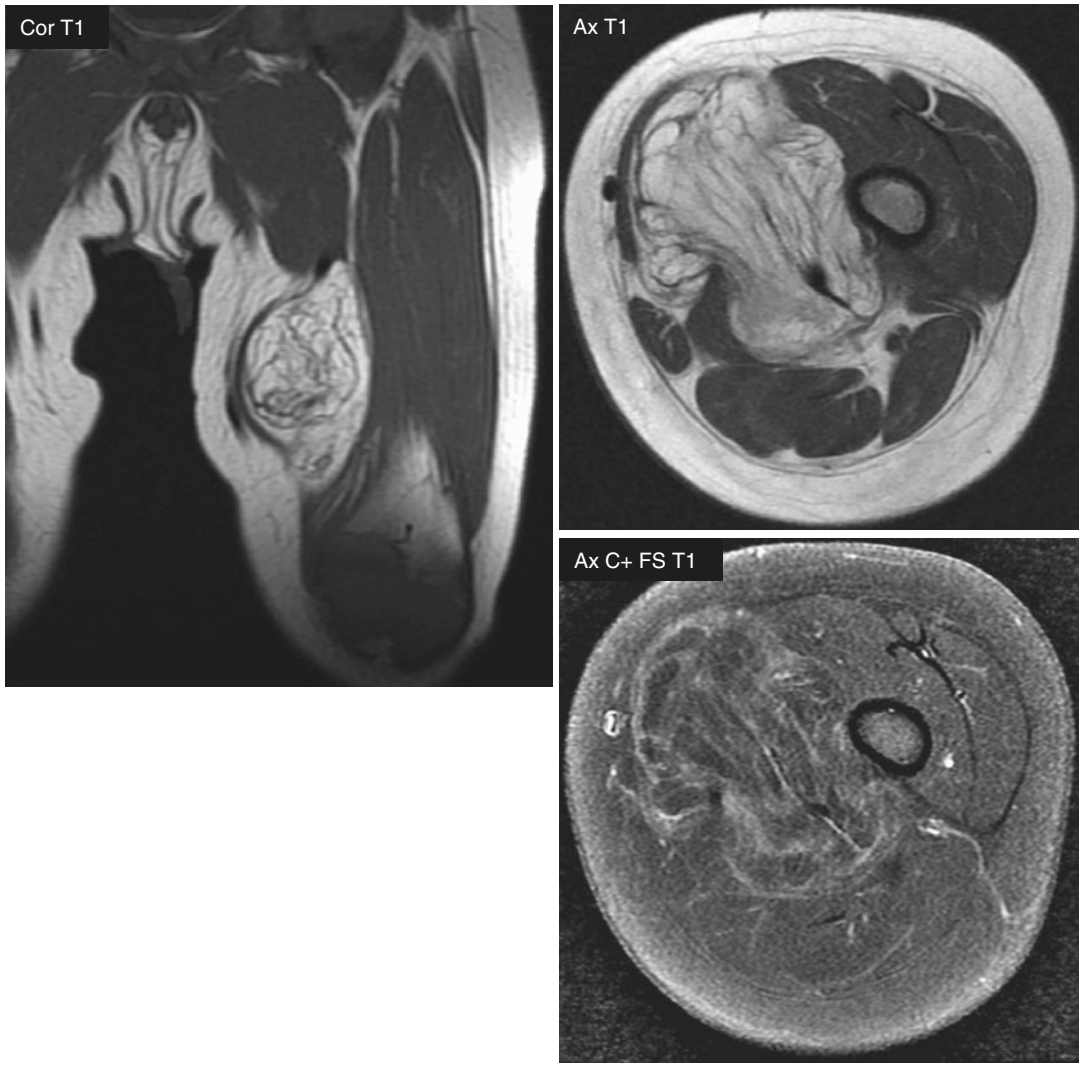

Lipoblastoma (Chap. 4)

- Child
- Predominantly fatty mass
- Multiple enhancing septa